Large scale roll-to-roll produced organic photovoltaic devices: manufacturing, lifetime and environmental impact

Benatto, Gisele Alves dos Reis

Publication date:
2017

Document Version
Publisher's PDF, also known as Version of record

Technical University of Denmark

Large Scale Roll-to-Roll Produced Organic Photovoltaic Devices: Manufacturing, Lifetime and Environmental Impact

Gisele Benatto
Department of Energy Conversion and Storage
Ph.D. Thesis, January 2017

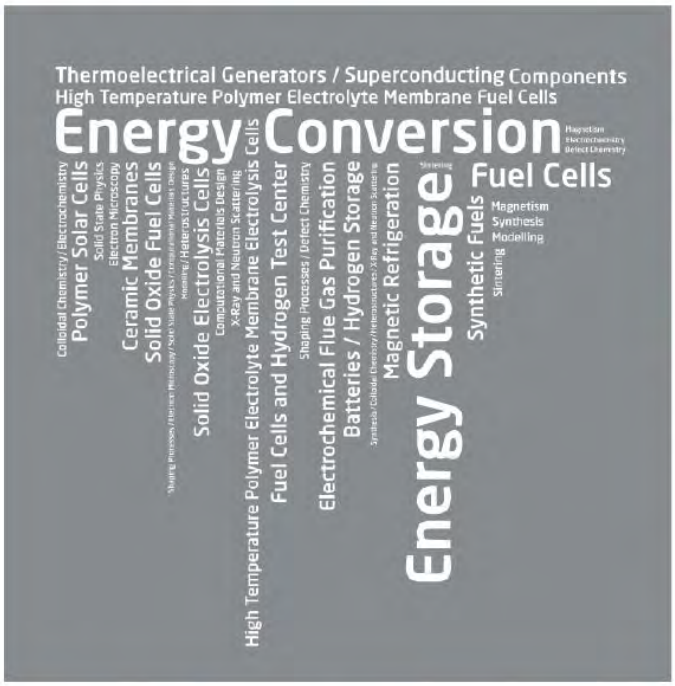

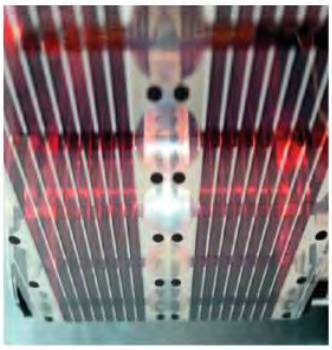

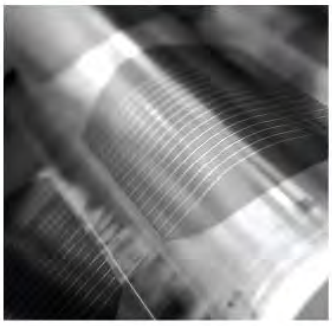

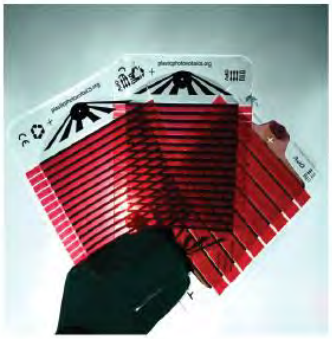

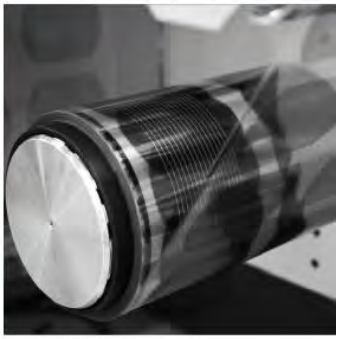

DTU Energy
Department of Energy Conversion and Storage

TECHNICAL UNIVERSITY OF DENMARK

LARGE SCALE ROLL-TO-ROLL PRODUCED ORGANIC PHOTOVOLTAIC DEVICES:

MANUFACTURING, LIFETIME AND ENVIRONMENTAL IMPACT

PH.D. THESIS

GISELE ALVES DOS REIS BENATTO

JANUARY 2017

Author:
Gisele Alves dos Reis Benatto

Title:
Large Scale Roll-to-roll Produced Organic Photovoltaics Devices: Manufacturing, Lifetime and Environmental Impact

Supervisor:
Professor Frederik Christian Krebs

Co-supervisor:
Dr. Nieves Espinosa Martinez

Assessment committee
Professor Jens Wenzel Andreasen, Technical University of Denmark
Professor David M. Tanenbaum, Pomona College, CA, USA
Associate Professor Ergang Wang, Chalmers University of Technology, Sweden

Date of defence:
9 March 2017

Sponsorship:
Energinet.dk. Grant Number: 12144
Danish Ministry of Science, Innovation and Higher Education. Grant Number: DFF-1335-00037A

ISBN: 978-87-92986-60-3.

DTU Energy
Department of Energy Conversion and Storage
Technical University of Denmark

OEM - Organic Energy Materials
Risø Campus
Frederiksberg 399
4000 Roskilde, Denmark
garb@dtu.dk
http://www.energy.dtu.dk/

“The first and last thing which is required of genius is the love of truth.”
Johann Wolfgang von Goethe

Preface

The present Ph.D. Thesis contains the main results obtained during the three years of Ph.D. studies at the Technical University of Denmark (DTU), from 15th January 2014 to 14th January 2017. The vast majority of the work was carried out at the Organic Energy Materials (OEM) section in the Department of Energy Conversion and Storage (DTU Energy), located at Risø Campus, Roskilde, Denmark. During this period, collaborations with the School of Electronic Engineering in Bangor University and University of Applied Sciences and Arts Northwestern Switzerland (FHNW) in Basel, Switzerland where performed. While the former corresponded to 5 months external stay. This work was funded by the Danish Ministry of Science, Innovation and Higher Education grant number: DFF-1335-00037A, and Energinet.dk grant number: 12144.

The structure of the thesis

This thesis is focused on large scale manufacture, operational lifetime and environmental impact assessment of organic photovoltaics (OPV). This is done by using established methodologies and also developing new setups. A brief introduction to energy demand, resources, solar energy, and photovoltaics generations is given in Chapter 1; along with a general description the OPV technology, research challenges, and contributions to the literature. The following chapter describes printing and coating techniques for large scale OPV production and the statistics of four different OPV devices in the size of postcards. Such OPV modules were based on carbon electrodes, and Chapter 3 presents the life-cycle assessment methodology applied to evaluate such modules environmental performance in comparison to OPV with metal-based electrodes. Environmentally friendly OPV modules can use the strategy of using no metals at all or use lower amounts of it. OPV modules using both these strategies have their operational lifetime tested in Chapter 4, including eight different OPV technologies. To verify if a new technology is truly green, outdoor leaching setups were developed simulating real outdoor use phase and disposal in a landfill. Such experiments and their outcomes are described in Chapter 5. Chapter 6 describes a full product which includes an OPV panel, compared with 2 other similar products already established in the market. Lastly, the overall conclusions and outlook are presented in Chapter 7. The total contribution of this work to the literature comprises so far of 13 peer-reviewed publications. 12 of them are included in the appendix, as they are better connected to this Ph.D. thesis.

Acknowledgements

I still remember that, seven years ago when I was reading Frederik's publications, how it would be to work in DTU with him, in such productive group. Today I know that the research that comes from his group goes far beyond anything I could imagine and that the environment is better than I had ever idealized. I thank Frederik Krebs immensely, for giving me the opportunity to be supervised by him. In these three years he was always available when I needed, always good natured, and with the mind full of amazing ideas that inspired me immensely and still does. I thank also Eva for calling me and give the news that I was selected for the PhD position, and for this great time in OEM, for her help and smiles. I thank Mikkel for being permanently helpful among his fascinating and fruitful work.

In the beginning when you first come to a new place, and later, there are so many things to solve. For this I thank hugely Bente and Birgit for all the careful assistance in all kinds of paper work and documentation. Birgit especially, for the essential help with the abstract translation and frequent willingness for helping. I hugely thank also Nieves, for her close and continuous help, guidance and friendship. Her intelligence and open attitude motivated me every time during these three years. I thank also greatly for the fast and super-efficient help from Kristian, Torben and Martin. Ole and June for the Danish conversation practice. And for the breakfast club members for such nice time every Friday morning.

I would like to especially thank Morten and Markus for the proof reading of several chapters of this thesis. I thank Nieves again for her time dedicated in these last writing months. I thank Suren, Roar, Thue, Ilona, and Tiago as well for the help with corrections.

From the people I had the pleasure to know in my stay in Basel, Switzerland, I thank Markus Lenz for the valuable and dedicated guidance; Yannick Zimmerman for the real high quality training, teaching, countless help and great time; and finally Éva Ujaczki and Karen Viacava for the kind and sincere friendship.

Thank you all my amazing colleagues: Michael, Bérenger, Francesco Livi, Dechan, Francesco Pastorelli, Michail, Lea, Emil, Mariana, Tiago, Jacob and Henrik, Jon and Martin, Markus, Thue, Morten, Suren, and Rafael; for the funniest talks, high level talks, scientific discussions, and the highly motivating conversations.

Thank you Ilona for such special and tight friendship! So many stories told, lived, experimental problems being solved and scientific discussions all in between. These whole three years and even more this last year, have been unique for me because of her.

I finally thank my husband Herick for his strong confidence in what is possible, for his company and endless laughing times, and his intense belief in me and my capacity that were essential for the development of the PhD studies. Finally, I thank my parents Nelson and Helena, more than anything, for my existence.

Risø campus, 14th January 2017.

Gisele Benatto.

Abstract

The world energy production has risen intensely during the last decades bringing human development until the point that our current society cannot function without it. Two-thirds of global greenhouse gas emissions, along with other releases which can be highly harmful to humans and the ecosystem come from electricity production. Consequentially, the need for clean, renewable and sustainable ways of energy production rises up, due to pollutants and the finite nature of fossil fuels. Solar energy is by far the most abundant renewable resource available and fulfils the requirements of a truly green energy resource. The most efficient form of harvesting energy from the sun is through photovoltaics (PV) devices, for which the most used technology require high amounts of materials and energy, and brings several drawbacks to overall solar energy production such as high price and long energy payback times (EPBT). The development of new PV technologies brought a new horizon to the PV industry in terms of cost and applications. Organic photovoltaics (OPV) has the shortest EPBT and can avoid the use of high energy demanding processes and hazardous elements, with low environmental impacts over its entire life cycle of the system, i.e., from its manufacturing through its deployment and operation up to its final disposal.

As OPV comes about as an emerging technology just about to be commercialised, this thesis demonstrates the reproducible production of vacuum-, indium tin oxide (ITO)-, and silver-free OPV. The fast roll-to-roll (R2R) processing of these devices can bring such low costs to OPV that it balances its lower efficiencies and lifetime compared with other PV technologies. Such silver-free devices use carbon as electrode material instead and represent a potential truly green technology. To evaluate the truly environmental friendliness of OPVs, four electrodes alternatives have been assessed using the life-cycle assessment (LCA) methodology, indicating that metal based electrodes are the major contributors to the environmental burden of the OPV modules.

One of the main challenges for OPV relies on the short operational lifetime. Two OPV technologies using electrodes with the lower energy demand and metal content (carbon and silver nanowires) in a total of eight different OPV structures have their stability behaviour analysed in a total of seven standard conditions. Some outdoor tests lasted for more than 700 days. Many of them presented outstanding operational lifetimes compared with the most recent reports. Such lifetimes are already compatible with applications such as in seasonal greenhouses and electronic devices.

The challenges associated with end-of-life management of large scale installation of OPV must be addressed as the technology comes closer and closer to reality. OPV modules with and without silver installed outdoors had their emission of silver and zinc to the aqueous environment (rain, fog, dew) measured and quantified in a rain runoff setup simulating their use phase. Such studies included intact and deliberately damaged OPV modules exposed to natural weather conditions in Denmark for six months. End-of-life management was assessed simulating a landfill, or an uncontrolled disposal, at the end-of-life. The setup consisted of buried intact and shredded OPV modules in soil columns simulating best and worst case, respectively. The results revealed the recycling of silver in the disposal is mandatory from an environmental point of view for silver containing OPV.

Finally, the LCA was also used as a tool to quantitatively compare the potential environmental advantage of a product over another. A power bank product including a portable OPV panel brings the possibility of the battery to be charged from the sun and not only from the grid. The environmental burden of this and two other well-established power banks products are assessed through LCA. One of them also

includes a solar panel (made of amorphous silicon – a-Si) and the other is a regular power bank without it. The results point out the advantages in charging the battery using the sun instead of the grid, differences between the products when they are used and disposed in Denmark or in China, and indicate improvements focused on the products ecodesign. Even though the OPV based product is still at a pilot production scale and have a much more detailed inventory with primary data collection, it scores lower than the a-Si based in some impact categories. Such products with portable solar panels have also the advantage of giving the power of lowering the environmental impact in the hands of the user, and for OPV it is a first step as a commercially available technology contributing to clean and sustainable energy production.

Resumé

Verdens energiproduktion er steget voldsomt i løbet af de seneste årtier. Det har bragt den menneskelige udvikling til et punkt, hvor vores nuværende samfund ikke kan fungere uden en stigende energiproduktion. To tredjedele af de globale drivhusgasemissioner sammen med andre udledninger, som kan være yderst skadelige for mennesker og økosystemer, kommer fra energiproduktion. På grund af disse forureningskilder og de fossile energikilders begrænsede omfang er behovet for rene, vedvarende og bæredygtige former for energiproduktion voksende. Solenergi er den vedvarende energiressource med det langt største potentiale som vi har til rådighed, og den opfylder kravene til en ægte grøn energiressource. Den mest effektive metode til at indvinde energi fra solen, er gennem solceller (PV). Den mest anvendte solcelle teknologi kræver dog store mængder af materialer og energi ved fremstillingen, og den medfører flere ulemper til den samlede solenergiproduktion såsom høj pris og lang energi tilbagebetalingstid (EPBT). Udviklingen af nye PV-teknologier bragte nye perspektiver til PV industrien med hensyn til omkostninger og anvendelser. Organiske solceller (OPV) har den korteste EPBT og indebærer ikke energikrævende processer og skadelige stoffer. Derfor medfører OPV en begrænset miljøpåvirkning gennem hele solcellens livscyklus, dvs. fra produktionen gennem implementering og drift til den endelige bortskaffelse.

Da OPV er en ny teknologi, der først lige er ved at blive komme på markedet, viser denne afhandling en reproducerbar produktion af vakuum-, indiumtinoxid (ITO)-, og sølv-fri OPV. Den hurtige rulle-til-rulle (R2R) fremstilling af disse solceller medfører, at de lave produktionsomkostninger balancerer med en lavere effektivitet og levetid i forhold til konventionelle PV-teknologier. Sølv-fri solceller bruger kul som erstatning for sølv til elektrodemateriale og udgøre en potentiel ægte grøn teknologi. For at evaluere OPV-enhedernes miljøvenlighed er fire elektrode alternativer blevet vurderet ved hjælp af livscyklusanalyser (LCA). LCA indikerer, at metal elektroder er de vigtigste bidragydere til miljøbelastningen af OPV-moduler.

En af de vigtigste udfordringer for OPV er en kort operationel levetid. Ud af otte OPV-strukturer, hvis stabilitetsegenskaber er analyseret ud fra syv forskellige standardparametre, er to OPV-strukturer med elektroder af hhv. kul og nanotråde, som kræver ringe energiforbrug at producere og har lavt metalindhold, fundet. Nogle udendørs test varede i mere end 700 dage. Mange af dem viste en fremragende operationel levetid sammenlignet med resultater præsenteret i de seneste rapporter. Sådanne levetider er allerede kompatible med applikationer som i drivhuse og elektroniske apparater.

Udfordringerne forbundet med bortskaffelse af store OPV-installationer efter endt brug skal tages op efterhånden som sådanne installationer kommer tættere og tættere på at blive realiseret. OPV moduler installeret udendørs med og uden sølv blev undersøgt for udledning af sølv og zink til vandmiljøet (regn, tåge, dug), som blev som og kvantificeret i en regnafstrømningsopsætning, der simulerede brugsfasen. Sådanne undersøgelser omfattede intakte og bevidst beskadigede OPV-moduler eksponeret for naturlige vejrforhold i Danmark gennem seks måneder. Sluthåndteringen blev vurderet under forhold som på en losseplads eller ved ukontrolleret bortskaffelse ved slutningen af produktets levetid. Opsætningen bestod af nedgravede intakte og iturevne OPV-moduler i jordkolonner, der simulerede hhv. bedste og værste tilfælde. Resultaterne viste at genbrug af sølv ved bortskaffelsen er nødvendig ud fra et miljømæssigt synspunkt.

LCA er yderligere et vigtigt redskab til kvantitativt at sammenligne de potentielle miljømæssige fordele ved et produkt frem for et andet. Et powerbank-produkt i form af et bærbart OPV-panel bringer mulighed for at batteriet oplades fra solens energi, og ikke kun fra nettet. Den miljømæssige belastning af

denne og to andre veletablerede powerbank-produkter vurderes ved hjælp af LCA. En af disse omfatter også et solpanel (amorft silicium - a-Si), og den anden er en regulær powerbank uden solpanel. Resultaterne påviser fordele ved at oplade batteriet ved hjælp af solen i stedet for nettet, forskelle mellem produkter når de bruges og bortskaffes i hhv. Danmark og Kina og indikerer yderligere forbedringer på grundlag af produktets økodesign. Selvom det OPV-baserede produkt stadig er på pilotprojekt-stadiet og indeholder et meget mere detaljeret primært dataindsamlingssystem, scorede det lavere end det a-Si-baserede produkt på visse påvirkningsfaktorer. Sådanne produkter med bærbare solpaneler har også den fordel, at de lægger muligheden for at sænke miljøbelastningen i hænderne på brugeren, og for OPV er det et første skridt som kommercielt tilgængelig teknologi, der bidrager til ren og bæredygtig energiproduktion.

Table of Contents

List of Abbreviations

Ag	Silver
AgNP	Silver nanoparticles
AgNW	Silver nanowires
Al	Aluminium
AM	Air mass
a-Si	Amorphous silicon
BHJ	Bulk heterojunction
C	Carbon
CB	Chlorobenzene
CdTe	Cadmium Telluride
CED	Cumulative Energy Demand
CIGS	Copper indium gallium diselenide
CN	China
c-Si	Crystalline silicon
Cu	Copper
DfD	Design for disassembly/dismantling
DIY	Do it yourself
DK	Denmark
E_g	Gap energy
EOL	End-of-life
EPBT	Energy payback time
ETL	Electron transporting layer
F1	Barrier foil prone to form bubbles
F2	Barrier foil bubbles-free
FF	Fill factor
FL	Flexo printing or flexography
freeOPV	Freely available organic photovoltaics
FU	Functional unit
HOMO	Highest occupied molecular orbital
HTL	Hole transporting layer
ICBA	1',1'',4',4''-Tetrahydro-di[1,4]methanonaphthaleno[1,2:2',3',56,60:2'',3'']][5,6]fullerene-C60
ICP-MS	Inductively coupled plasma mass spectrometry
ILCD	International Reference Life Cycle Data System
IR	Infrared
I_{SC}	Short circuit current
ISOS	International Summit on Organic and Hybrid Solar Cells Stability
ITO	Indium tin oxide
IV	Current-voltage
kWh	Kilowatt hour
LB	Low band gap

LBIC	Laser Beam Induced Current
LCA	Life cycle assessment
LDS	Luminescent down-shifting material
LOD	Limit of detection
LUMO	Lowest unoccupied molecular orbital
mAh	Miliampere hour
ODCB	Ortho-chlorobenzene
OPV	Organic photovoltaics
P3HT	Poly(3-hexylthiophene)
PBDTTTz-4	Low band gap polymer based on hexylthiophene, thiazolo[5,4-*d*]thiazole and benzodithiophene
PCBM	[6,6]-phenyl-C61-butyric acid methyl ester
PCE	Power conversion efficiency
PEDOT:PSS	Poly(3,4-ethylenedioxythiophene):polystyrene sulfonate
PET	Polyethylene terephthalate
P_{IN}	Incident light power
P_{max}	Maximum power point
PT	Polythiophene
PV	Photovoltaics
R2R	Roll-to-roll
SD	Slot-die coating
SP	Screen printing
TFPV	Thin-film photovoltaic
TWh	Terawatt hour
TWy	Terawatt year
V_{OC}	Open circuit voltage
Zn	Zinc
ZnO	Zinc oxide

Chapter 1

Introduction

This first chapter is dedicated to show a short background of the current energy production and the available energy resources. Furthermore, a brief overview of the solar energy status and solar cell background is presented, followed by the working principles and structures detail of organic photovoltaics (OPV). Guidelines of the environmental impact point of view and life-cycle assessment methods are shown, as well as state-of-the-art of the OPV production and technologies. The final remarks present the structure of this thesis and relevant contributions made during the PhD study.

1.1.Energy production in a world in development

The global energy consumption is constantly increasing proportionally to the population and standard of living growth. Figure 1.1 shows the increasing profile of the energy production in the world throughout the years from 1900 until 2014 in terawatt years (TWy) [1–3]. The demand of energy increased continuously since the fifties, bringing higher human development and quality of life; until the point where our society simply cannot function without it. The share of highly pollutant fossil fuels, first the only accessible resource, is still very high. The more accelerated growth of the energy production in the last 15 years is related to the demand of emerging economies, led by China and India, which rely directly on the production of large amounts of low cost energy. This meant not only economic growth, but also moved millions of people out of poverty, while, more than a billion people still live without electricity around the world [4].

The energy consumption of an individual is directly related to the human development index (HDI), which is critically related to the increase of environmental footprint. Energy production is responsible for two-thirds of global greenhouse gas emissions, besides other releases which can be highly harmful to humans and the ecosystem [5–7]. Therefore, it is essential for both preserving the environment and human health to fulfil the energy demands with renewable energy production as much as possible.

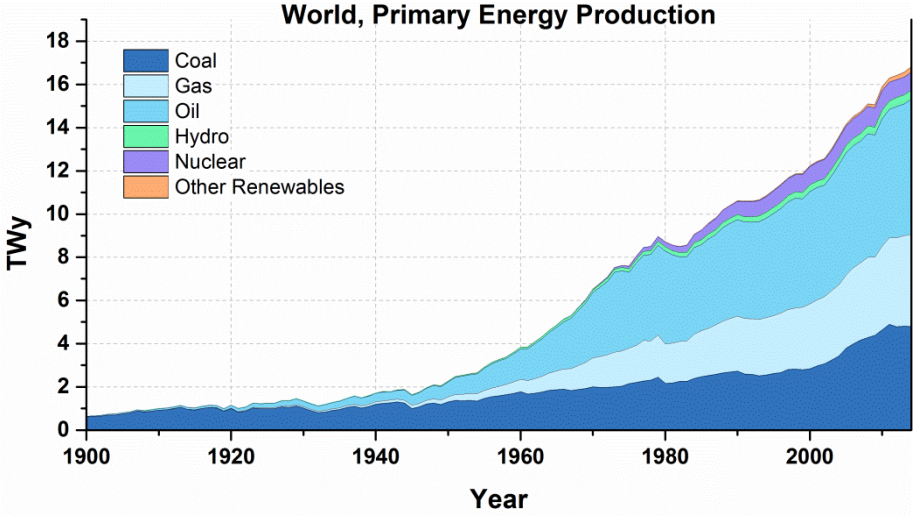

Figure 1.1 - World energy production by source from 1900 until 2014. Terawatt years (TWy) corresponds to 8766 terawatt hours (TWh). Data from [1–3].

The world energy consumption was 18.5 TWy during 2015 and by 2050 is expected to increase to 27 TWy [8]. Besides the drive backs of emissions to the environment, fossil fuels are also finite, generating increasing concern during the years. In this context, the need of clean, environmentally sustainable renewable resources, which often rely on the development of new technologies, is imperative. Currently the share of renewable energy remains small (2.8%), but it is in a strong growing process accounting for more than a third of the entire increase in global energy consumption. The recent improvements in technology brought down the prices of renewable energy production in general, which, together with policies, contributed significantly to this growth [5].

A vast number of renewable sources of energy are available in the planet. Figure 1.2 shows the estimated reserves (in TWy) together with the yearly potential of renewable sources (expressed in amount of energy per year - TWy/y) [9]. As the non-renewables are shown as total recoverable reserves, the concern through the years when compared with the world energy use, which increases every year, becomes clear. The yearly available energy from the sun is enormous, showing no restrictions in this sense to concentrate efforts in the development of technologies concerning solar energy.

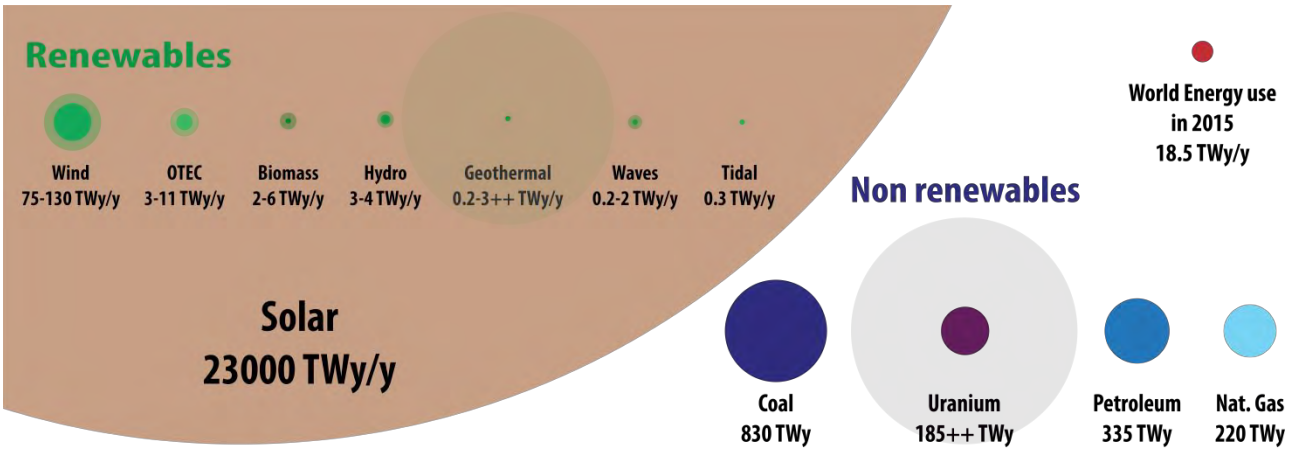

Figure 1.2 - Estimated finite reserves and renewable energy potential in TWy from 2015. Total recoverable reserves are shown for the finite resources. Yearly potential is shown for the renewables. OTEC stands for ocean thermal energy conversion. Data from [9].

1.2.Solar energy

The sun offers a clean, environmental friendly and extremely abundant source of energy. Considering the intermittent or localised renewable sources as wind, geothermal, hydro, etc., solar energy is also the most well spread resource in the world. The energy from the sun can be harvested using solar heating, concentrating solar thermal energy, photovoltaics, among others or even new technologies to come. The main employed technology today is photovoltaics (PV) [10,11].

Particularly photovoltaics have the advantages to be compact, can be acquired by single individuals, and are an excellent option for isolated localities. Solar panels have fast installation, no moving parts, no noise, and a relatively low first cost investment [12]. Figure 1.3 show the cumulative solar PV capacity and average prices trend (in USD) per watt in the world through the years from 2000 to 2015 [11,13]. The annual growth rate of solar PV supply is the highest between other renewables. The costs decrease by following the raw materials prices and production increase [14–16]. In sunny countries, roof-top PV can already compete when electricity prices are high, but in most markets solar electricity still need specific investments [15,17,18]. PV panels are the leading candidate for terawatt-scale electricity generation by 2050.

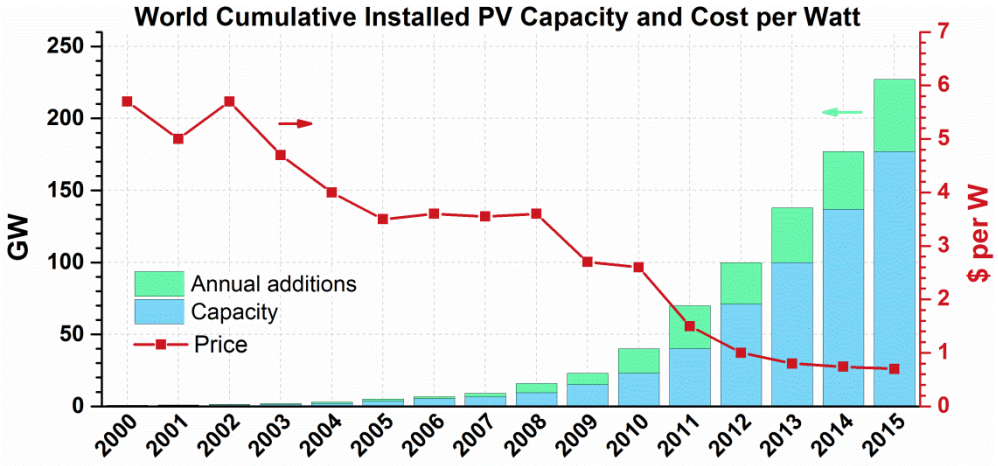

Figure 1.3 - World cumulative solar PV capacity and annual additions from 2000 to 2015. Data from [11,13,16].

1.2.1. Photovoltaic technologies: the three generations

The photovoltaic effect was for the first time described by Alexandre Edmond Becquerel in 1839. The first commercial solar panel was presented only in 1954 with efficiencies around 6% and for a long time used only in satellites and space applications due to the high production cost [19,20]. Today, many other PV technologies came about and they are usually divided into three main categories or generations [12,21,22]. Figure 1.4 shows some examples of modules corresponding to the three PV generations.

Wafer-based PVs are the so called 1st generation and include crystalline silicon solar cells (c-Si). They can be further classified as mono/single crystalline and poly/multi crystalline silicon PV and together they correspond more than 90% of the PV market today [23]. Their large scale efficiency records are 22.4% and 18.5% respectively and they present very good stability. c-Si PV modules have the limitation of an indirect bandgap [24], which demands that the device have thicknesses in the range of hundreds of micrometres in order to absorb enough light, limiting flexibility and requiring large amounts of material. They also rely on high purity silicon, which requires massive quantity of energy in the manufacturing. Such restrictions bring

up the price and the energy payback time (EPBT) of the modules, taking a long time for c-Si modules to pay back all the energy to the system, which was required for its fabrication.

In the attempt to get rid of such restrictions and energy demands faced by the c-Si PV technology, a 2nd generation of PV modules was developed, which consists of thin-film PV modules (TFPV). They include amorphous silicon (a-Si), Copper indium gallium diselenide (CIGS), and Cadmium telluride (CdTe) solar cells. The focus of these new technologies was the lower material usage, which allowed lighter weight, some flexibility, and lower prices. This was possible since CdTe, CIGS and (hydrogenated) a-Si absorb the solar spectrum much more efficiently than c-Si, allowing absorbing materials with thicknesses of a few micrometres. Today they account for approximately 8% of the PV market [23]. Their stability is good; efficiencies are in the range of 20% to 17% for CdTe and CIGS. Cadmium, tellurium, indium and gallium are very scarce elements, not mentioning their high toxicity, limiting the prices for such PV modules.

The 3rd PV generation goes even further in the progress for lower energy demands and EPBT, material usage, and prices. They are also TFPV technologies though include a number of different absorbing materials, architectures, and engineering strategies. Most of them are still under development and not yet in the market. Among others, such technologies include colloidal quantum dot photovoltaics (QDPV), dye-sensitized solar cells (DSSCs), perovskite solar cells, and organic photovoltaics (OPV). Some of those technologies allow even lower materials usage than the 2nd generation, with thicknesses in the order of nanometres. Energies for the production can be brought down in several orders of magnitude compared to the 1st generation, and EPBTs have possibilities to be down to one single day [25]. Furthermore, flexibility and transparency are possible, bringing up numerous new applications far beyond the limit of the 1st generation. OPV is the only 3rd generation PV technology that has a quick and inexpensive large scale production, can use no scarce or toxic materials, can be transparent, flexible, and are very light in weight altogether. The OPV efficiencies are, in the moment, lower than the average of previous generations. However, such low cost production brings the potential to compensate efficiency with larger installation areas. The interest in the commercial application of OPV is very high as companies such as Heliatek and infinityPV have been awarded in 2015 for their efforts in the OPV field by Technology Pioneer by World Economic Forum and the Royal Society of Chemistry, respectively [26,27].

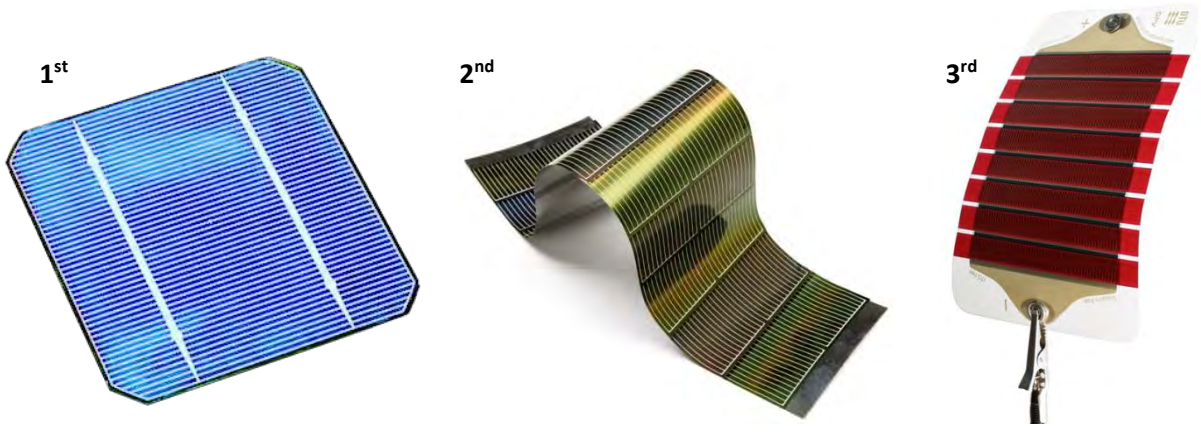

Figure 1.4 - Examples of photovoltaic devices from the first, second and third generation from left to right: c-Si [28], CIGS [29] and OPV.

1.3.Organic photovoltaics

As most of the photovoltaics technologies are named according to the characteristics for its absorbing material, OPVs have their active or absorbing material in the organic semiconductor, which can be small organic molecules or polymers. A semiconductor is a material where the light (or electromagnetic radiation) from the sun can be converted into electrical energy (a current and a voltage), defined as the photovoltaic effect. Unlike inorganic semiconductors, organic semiconductors can be solution processed and have improved mechanical proprieties. Following the same principle, but very differently in physical terms, OPV are built with an electron donor and electron acceptor materials, rather than semiconductor p-n junctions* as inorganic PV. At first, OPV were structured as a single or bilayer junctions, as a direct replacement for the inorganic semiconductors, presenting very low efficiencies [30,31]. Further approaches presented a bulk heterojunction (BHJ) of the donor and the acceptor materials together in a blend, making their interface, not planar as in a bilayer junction, but spatially distributed and with vastly higher interfacing area.

BHJ represent the state-of-the-art of OPV active layers and all samples in this thesis have such organic structure, which working principle is described in detail in the following section.

1.3.1. Working principle

In Figure 1.5 the band diagram and an illustration of photogenerated charges diffusing in a BHJ structure of an OPV device is shown. The photons from the irradiated light, which have higher energy than the band gap or gap energy (E_g) of a semiconductor, are absorbed and generate an exciton, i.e. an electron-hole pair, or a polaron pair in an organic material, as it is related to a distortion in the molecular structure. The E_g is defined by the separation in energy of the valence electrons and the nearest free electronic states; which is the difference in the energy of the highest occupied molecular orbital (HOMO) and the lowest unoccupied molecular orbital (LUMO). The BHJ is able to dissociate excitons very efficiently, as donor-acceptor interfaces are plentiful in the blend. In such interface, it can be more energetically preferable for the electron to be transferred to the acceptor material than to remain bounded to the hole by Coulomb forces. When dissociated, the exciton produces two free charge carriers (an electron and a hole). The OPV working mechanism can be also found in several exceptional reviews with different levels of depth [30–33], and as a whole, includes the following steps:

- A photon from irradiated light is mostly absorbed in the donor material. An electron is promoted to the LUMO level, at the same time that a hole remains in the HOMO.
- The exciton diffuses spatially in the donor until a donor-acceptor interface (Figure 1.5 right). In this stage, losses can occur, as charge carrier recombination or exciton decay.
- The exciton dissociates into free charges at donor-acceptor interface.
- Due to the work functions of the electrodes, the free charge carriers are separated by the internal electric field, which causes the band inclination shown in Figure 1.5 left.
- The electron is transported through the acceptor and collected at the cathode; the hole is transported through the donor and collected at the anode. In the process, trapped and moving charge carriers can recombine.

*p-n junctions are defined by two semiconductors, one rich in positive (p) and another in negative (n) charges interfacing each other, forming a diode.

As several losses can happen during the photogeneration process, a good control of the morphology of the BHJ is very important and this is one of the efforts pointed out in the research pursuit of highly efficient OPV devices.

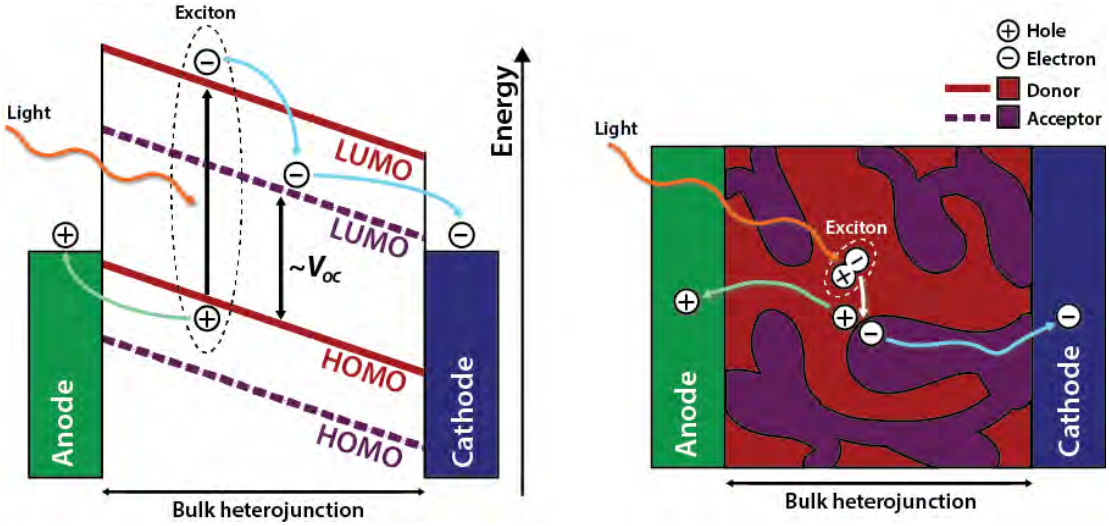

Figure 1.5 – Simplified energy diagram of a BHJ (left) and illustration of photogenerated charges spatial diffusion in a BHJ (right), both in an OPV device.

When the OPV device is not exposed to illumination, it behaves as a simple diode. Under illumination though, the generated photocurrent is added to the curve. Figure 1.6 shows the typical current-voltage curve (IV-curve) used to characterize electrically the PV devices and it is obtained by applying a voltage bias. The indicated key parameters will define the performance of the PV device: the maximum power (P_{max}) in Watts, voltage and current at the maximum power point (V_{Pmax} and I_{Pmax}) in Volts and Amperes, respectively, open circuit voltage (V_{OC}) in Volts, and short circuit current (I_{SC}) in Amperes. Moreover, the fill factor (FF) is a parameter defined by equation below, i.e. the ratio between the area of the grey and the white rectangles from Figure 1.6. The FF parameter consequently describes the ratio between PV produced power and the theoretic ideal.

$$FF = \frac{I_{Pmax} \,.\, V_{Pmax}}{I_{SC} \,.\, V_{OC}}$$

The efficiency or the power conversion efficiency (PCE) of a PV device is defined by the ratio of maximum power (P_{max}) in relation to the power of the incident light (P_{IN}) in Watts per square metres (W m^{-2}), on an area A in square metres, corresponding to the active area of the PV device. The PCE in the end will also be given as a percentage. Finally, the PCE can actually be given in terms of V_{OC}, I_{SC}, FF, incident light and the device active area.

$$PCE = \frac{P_{max}}{P_{IN} \,.\, A} = \frac{I_{Pmax} \,.\, V_{Pmax}}{P_{IN} \,.\, A} = FF \frac{I_{SC} \,.\, V_{OC}}{P_{IN} \,.\, A}$$

To increase efficiencies, the V_{OC}, I_{SC}, and FF, parameters should be as high as possible. FF is reliant on the series and shunt resistance of the device. The series resistance corresponds to the resistance

between every layer of the device, resistance of the layers themselves, and resistance between the cells in the case of a PV module. Therefore, it should be as low as possible. The shunt resistance is related to shunt defects in the layers and should be as high as possible. The state-of-the-art OPV have FF in the range of 60-70%. As pointed in Figure 1.5, the V_{OC} is proportional to the difference of the energy levels of donor and acceptor materials [34,35]. In this sense, the research in donor materials with lower HOMO levels is an important PCE improvement strategy.

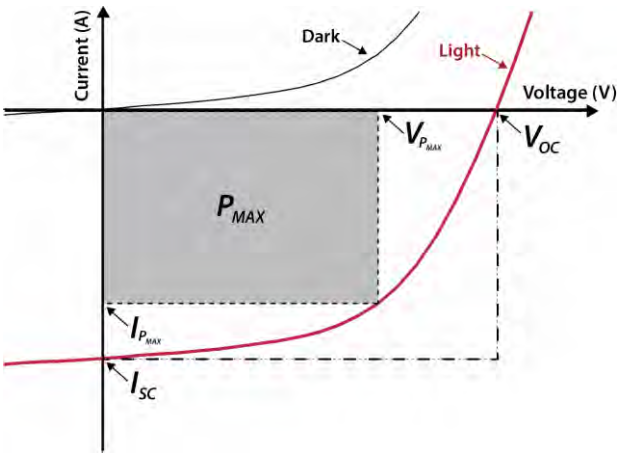

Figure 1.6 - Example IV-curve for a PV device with and without illumination. The key parameters of P_{max}, V_{Pmax} and I_{Pmax}, V_{OC} and I_{SC} are indicated on the curve acquired under illumination.

The light coming from the sun at normal incidence hits the atmosphere with a power of 1366 W m^{-2}. Before crossing it, the solar irradiance spectral distribution is called “air mass 0” or AM0. At the Earth surface, where PV panels are installed, the standard air-mass 1.5 global spectrum (AM1.5G) is adopted, corresponding to the solar spectrum at an angle of 44.2° from zenith, i.e. roughly 1.5 times the average thickness of the atmosphere including simulated diffuse light. AM1.5G designed for flat plate PV modules has an integrated power of 1000 W m^{-2} and such power input is called 1 sun. Figure 1.7 shows both AM0 and AM1.5 spectra for comparison.

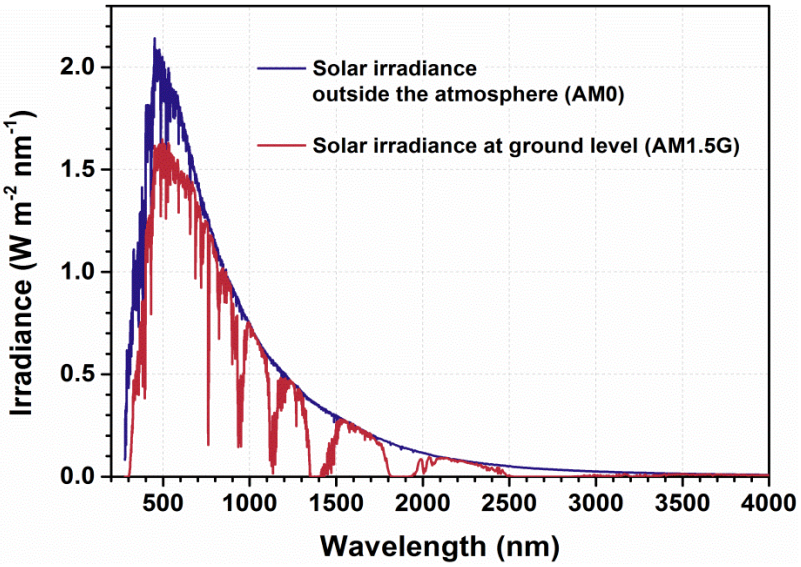

Figure 1.7 - Solar irradiance spectra outside the atmosphere AM0 and at ground level AM1.5G. Data from [36].

1.3.2. Architectures and materials

As shown before in Figure 1.5, the basic OPV structure comprises a light absorbing BHJ layer sandwiched between a positive (anode) and a negative (cathode) electrode, where at least one of the electrodes need to be transparent in order to let the light enter. The addition of selective charge transport layers, namely electron transporting layer (ETL) and hole transporting layer (HTL), between the BHJ and the electrodes improves the charge collection. Such layers need to be built on a substrate, which most commonly is glass or plastic as polyethylene terephthalate (PET). In practice, if the layers are built on top of the material where the light shines thought, this can be called, instead of substrate, a superstrate. As the materials of OPV can be sensitive to oxygen and humidity, they are often encapsulated specially for large scale and outdoor use.

The complete OPV layer stack can be distinguished as normal and inverted geometries, and are differentiated due to the direction of the charges flow in relation to the transparent electrode. Figure 1.8 illustrates such configurations. In the traditional normal geometry, the light passes through the anode, with the cathode functions as the back electrode. Such geometry includes the use of low work function materials as cathode, which can be more sensitive to degradation and/or cannot be solution processed. In the inverted geometry, the transparent front electrode is the cathode. This configuration allows the use of higher work function material as the back electrode, in this case the anode, which can be solution processed and have in addition a positive effect on the device lifetime [37,38].

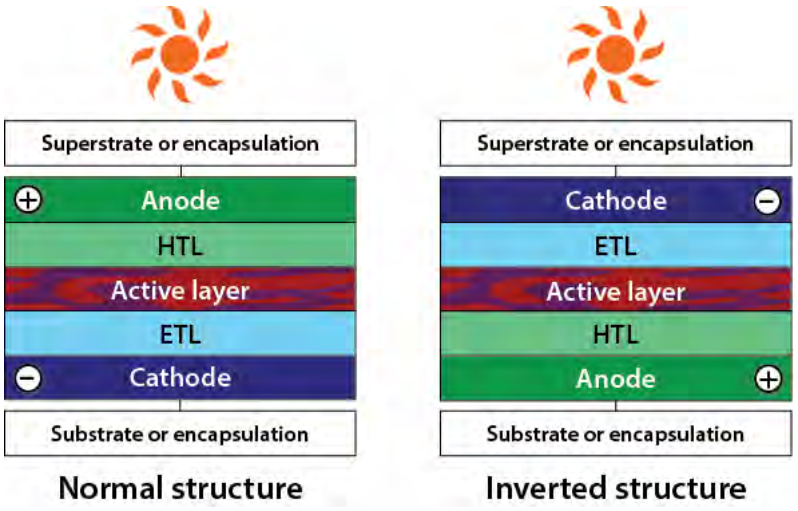

Figure 1.8 - Normal and inverted geometries of OPV

As mentioned before, the light absorbing active layer is a blend of two organic materials. The most used and well-studied combination include poly(3-hexylthiophene) (P3HT) as a donor and the fullerene derivative [6,6]-phenyl-C61-butyric acid methyl ester (PCBM) as acceptor, which molecular structures are presented in Figure 1.9. Nevertheless, the absorption from P3HT does not match the spectrum from the sun, making room to the research of new materials. Low band gap polymers, for instance, can harvest more light, therefore enable higher efficiencies [39,40]. In this work particularly, another fullerene derivative acceptor and a low band gap polymer donor are tested and presented in Chapter 2.

The transporting layers are chosen by their mobility proprieties towards electrons and holes, together with their energy level suitability in the whole device. Common hole transport materials in OPV include poly(3,4-ethylenedioxythiophene):polystyrene sulfonate (PEDOT:PSS) and metal oxides such as

molybdenum trioxide (MoO_3) and vanadium (V) oxide (V_2O_5). Electron transporting materials include calcium (Ca), lithium fluoride (LiF), and metal oxides such as zinc oxide (ZnO) and titanium oxide (TiO).

As transparent electrode, the most common material used in OPV is indium tin oxide (ITO). The indium scarcity, the ITO mechanical and deposition limitations lead though to efforts in its replacement, which is discussed further in Section 1.4 including the environmental point of view. Alternative for ITO-free OPV devices include highly conductive PEDOT:PSS, hybrid structures with PEDOT:PSS and metal grid, metal nanowires, carbon nanotubes, and graphene [41]. The back electrodes with convenient work functions include silver (Ag), aluminium (Al), and carbon (C) among others.

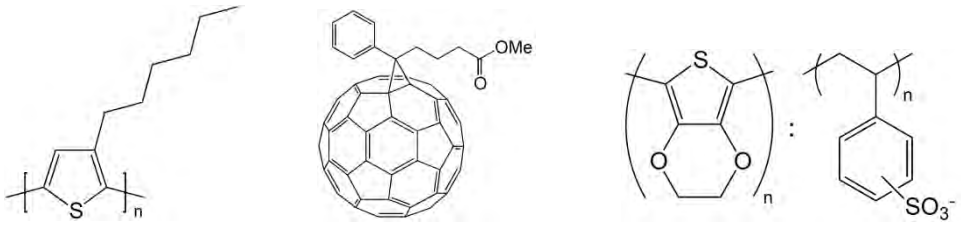

Figure 1.9 - Common organic compounds used in OPV (from left to right): P3HT, PCBM, PEDOT and PSS.

Although the above cited materials for the corresponding OPV functional layers are frequently used in research, many of them are not compatible with production in large quantities or are not solution processed. These among many other reasons can limit the OPV technology towards the PV market. Such challenges can be expressed in the unification of key important factors to the OPV development shown in Figure 1.10 [42,43]. Concerning processing, the OPV flexibility permits the use of very thin and light substrates, operable with well-known industrial roll-to-roll (R2R) technologies, which is even comparable to newspaper printing. Making the production fully solution processed and free of vacuum requirements lower immensely the OPV panels EPBT. Undoubtedly, it would be the least energy demanding PV panel in the market. Efficiency wise, the record for OPV is 13.2% [44], while in large modules this value is still much lower. Nevertheless, the technical development in the field has been very fast and estimated to reach its full potential before 2025 [15]. Stability outdoors for OPV is under important progress, with measured outdoor lifetimes of 2 years [45,46]. Cost of the energy produced by OPV is closely related with the former three factors. The levelised cost of electricity for OPV would be the same than the current c-Si panels with module efficiencies of 4% and lifetimes of 2 years [47].

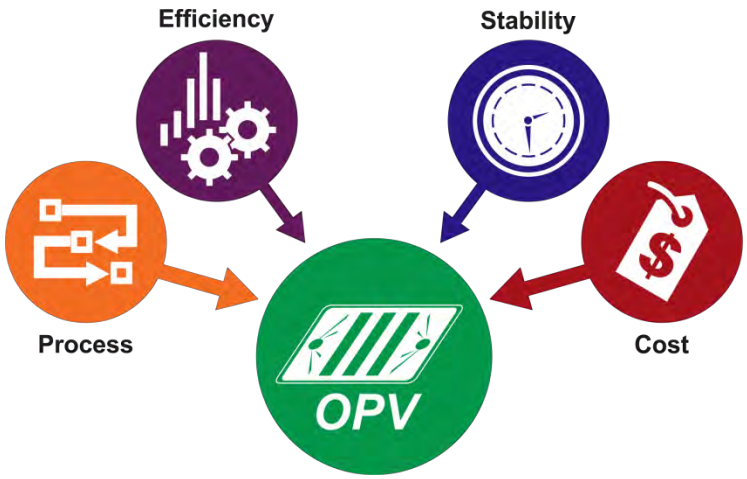

Figure 1.10 - The key factors unification challenge for OPV ingress in the PV market.

1.3.3. Freely available OPV

OPV devices have been basically unavailable physically to the public with maybe the exception of a few samples. The general availability in significant quantities certainly qualifies a new technology as a real future product. Figure 1.11 shows the freely available OPV (freeOPV) platform that consists of generic postcard sized OPV modules in an inverted geometry, fully solution processed and R2R manufactured using PET superstrate and encapsulation. Such a platform was conceived to enable the development of processing, reproducibility of large scale printing, testing of new materials, and also the free distribution of OPVs to anybody with an interest in the field of any kind [48–50]. OPVs have such low cost of materials that permitted concepts as the freeOPV platform to become true. The idea behind this program also includes the power of analysis linked to the amount of data and the feedback from any technical or scientific study regardless of its nature is highly encouraged.

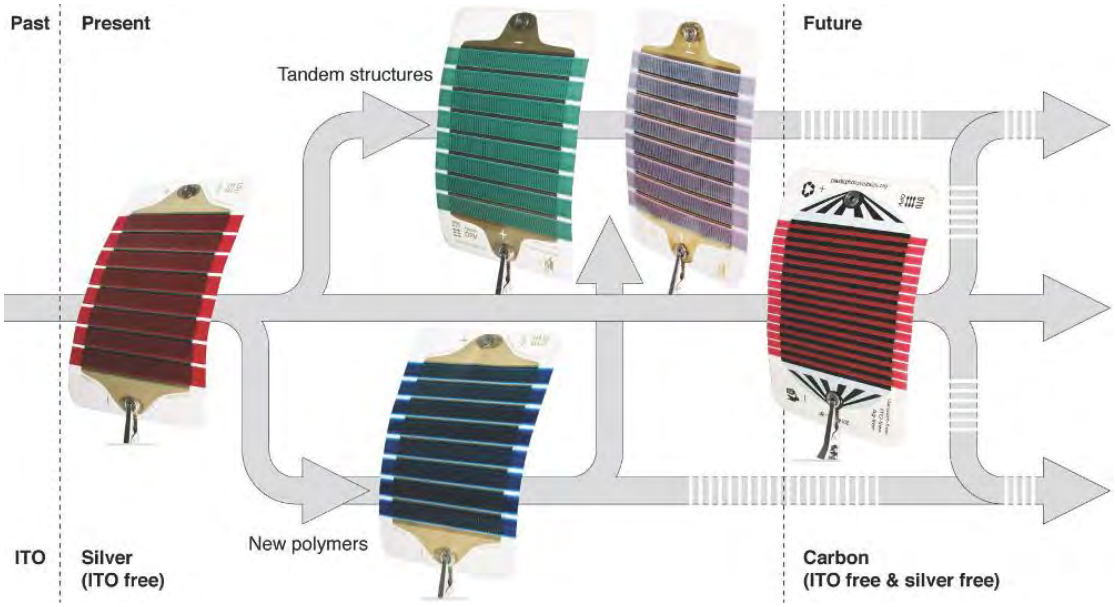

Figure 1.11 - Illustration of the evolution of the freeOPV platform from its initial form based on slanted Ag-grids and P3HT:PCBM as the active materials to encompass novel polymer active materials and present complex multilayer architectures such as the tandem freeOPV [48]. Reprinted with permission from [50].

The freeOPV platform is on its new generation. They are not only ITO-free but also Ag-free and built with carbon electrodes. Such modules are widely used in this thesis for the evaluation of new materials applied as active layers and electrodes; in the test of barriers and printing techniques; in stability performance, installation strategies, and outdoor leaching tests.

1.4.Life-cycle assessment

The environmental impact of an energy production also affects the cost of energy; hence, it is highly important to perform a careful life-cycle assessment (LCA) in an energy system. LCA is a powerful tool able to track all materials, energy demands, and pollutant flows of a system, from raw material extraction, manufacturing, use, and end-of-life (cradle-to-grave approach). It allows quantifying environmental

burdens, comparing to other energy technologies, and it can unveil bottlenecks and guide ecodesign, and generally helping the way towards more environmental friendly energy production [51].

The LCA framework (Figure 1.12) entails general steps according to the standards ISO 14040 and 14044 [52,53]. They comprise goal and scope definition, inventory analysis, impact assessment, and interpretation of the results. The goal and the scope define the first steps and boundaries of the assessment. The inventory analysis quantifies the material and energy inputs and outputs over each life-cycle stage. The impact assessment accounts for the emissions over the areas of protection: Human health, ecosystem health and resources. Lastly, the interpretation can drive changes in the previous steps, and final conclusions should indicate weaknesses and strengths of a system; provide feedback for environmental improvements; pinpoint bottlenecks if any; etc.

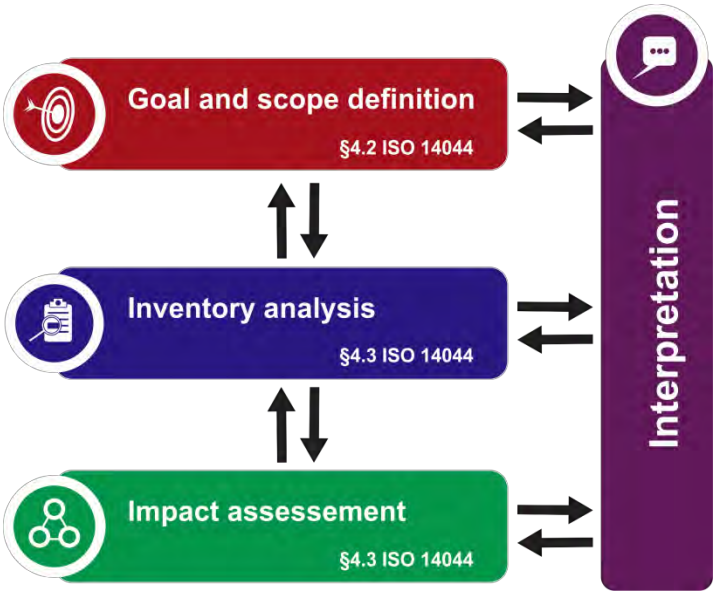

Figure 1.12 - LCA framework [52,53].

Several LCA studies showed that OPV environmental performance is considerably better when compared to other TFPV technologies and have been regarded as a truly green energy technology based on such results [25,54–56]. Compared to other TFPV technologies, OPV present the advantage of avoiding highly toxic and bioaccumulative elements such as cadmium, selenium or tellurium, and OPV release very minor and non-concerning amounts of metals to the environment in contrast to commercially available TFPV in laboratory experiments [57,58].

An important example of bottleneck identification made through LCA was the first detailed LCA of R2R processed OPV modules, when it was concluded that 90% of the total energy was embedded in the transparent electrode alone, as an imbalance in the inventory [54]. This was due to the indium scarcity, the large demand for energy in the ITO vacuum sputtering, and material waste as the process for OPV modules manufacture includes non-additive process (see Figure 1.13a). Furthermore, ITO was pointed out to dominate the materials cost as well [59].

Among a number of alternatives, three replacement options are shown in Figure 1.13 for ITO sputtered on PET. Patterned ITO (Figure 1.13a) requires the higher number of steps and involves subtractive etching processes with high material loss, slow process speed and specialized machinery for chemicals handling. The whole transparent electrode (cathode/ETL) using highly conductive PEDOT:PSS is

processed in just two steps (Figure 1.13b). As used in the first freeOPV modules (see Section 1.3.3), the steps for Ag nanoparticles (AgNP) grid and PEDOT:PSS as the cathode, plus the ZnO ETL is shown in Figure 1.13c. Ultimately process simplification is reached with a hybrid silver nanowires (AgNW)/ZnO which can be printed in a single printing step, with outside contact to improve device contacting. The printing and coating processes indicated in Figure 1.13 are presented in Chapter 2. Those three alternatives to ITO are employed throughout this thesis; mostly as freeOPV modules.

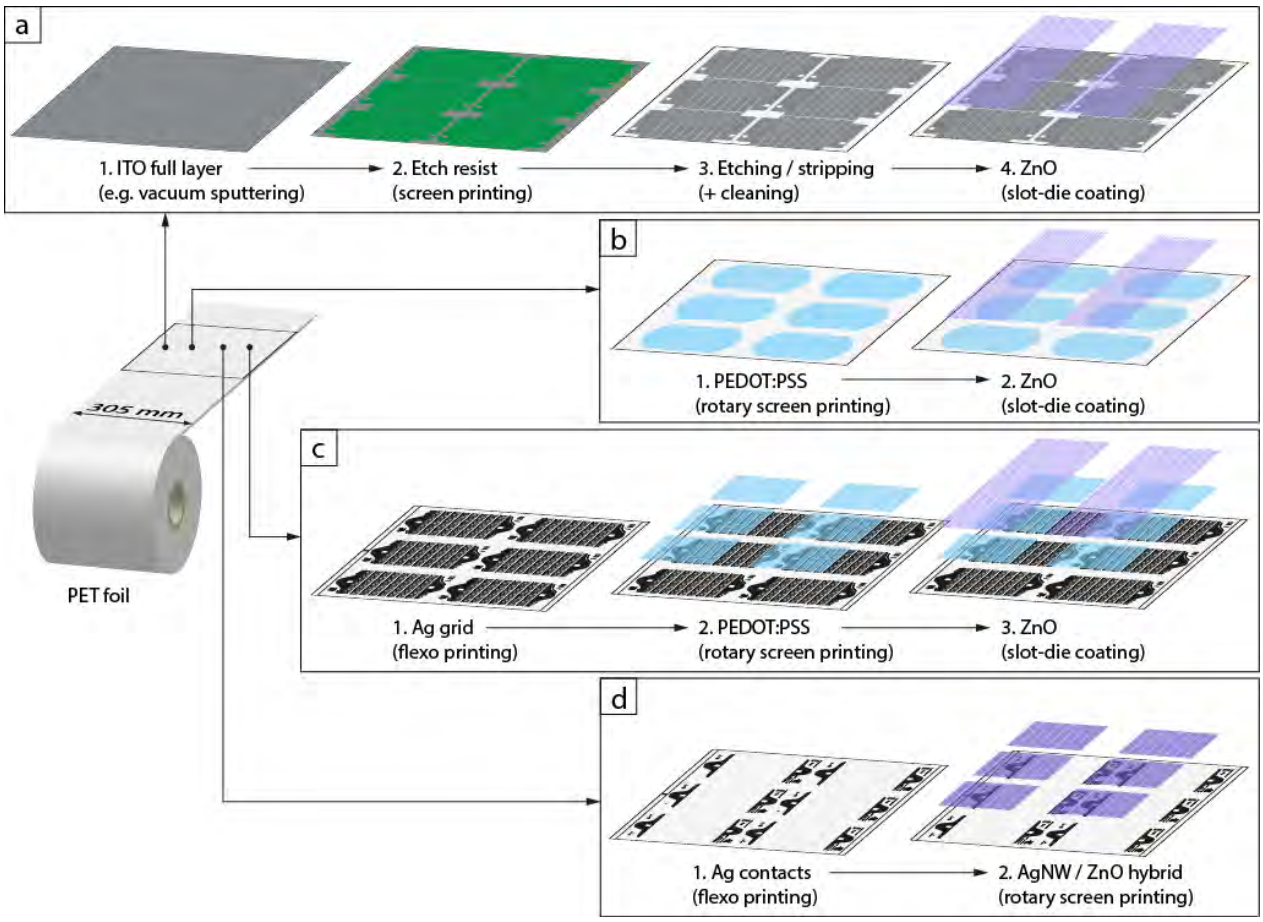

Figure 1.13 - Fabrication workflow of patterned cathode/ETL superstrates with a) ITO/ZnO, b) PEDOT:PSS/ZnO, c) Ag-grid/PEDOT:PSS/ZnO, and d) hybrid AgNW/ZnO. Adapted with permission from [41].

1.5.Thesis outline

The goals of this work include the evaluation of large scale produced OPV reproducibility, lifetime and their life-cycle assessment. All these subjects walk together, as efficient manufacture and longer lifetimes can directly lead to lower environmental burden of the energy produced by OPV panels. Additionally, the emissions coming from OPV when in use or at their disposal where quantified; tying up previous projects into a platform for maintenance and waste management of large-scale deployed OPV. At the end, the LCA of a full product with OPV is performed.

This thesis is divided in seven chapters including the above introduction and final conclusions.

Chapter 2 shows a short introduction of the printing and coating techniques followed by the testing of a large number of OPV modules and the built statistics. My contribution was specifically made on the final sample preparation step, which consisted of the electrical characterization under solar simulator, and

module preparation including labelling and laser cutting. I was also responsible for the organisation and shipping of a large amount of freeOPV during 2014 and 2015, until the exhaustion of samples.

Chapter 3 presents the LCA for evaluation of the environmental friendliness of OPV with different electrodes, including the carbon-based OPV which is essentially a metal-free module. This work was developed during my LCA methodology training and my contribution comprised the inventory information acquisition for manufacture of the carbon-based modules and their adaptation since Ag-based OPV LCA had been prepared before. I also contributed in the tests of the copper ink curing trials and inventory data; and in the final discussions during LCA interpretation.

Chapter 4 shows the lifetime of eight different OPV modules with different architectures. Four of them are C-OPV (presented in Chapter 2), and the other four are based on AgNW electrodes, which both contained the simplest processes for the front electrodes (see Figure 1.13). I particularly prepared, measured and analysed all samples in every ISOS condition presented.

Chapter 5 contains the work in collaboration with University of Applied Sciences and Arts Northwestern Switzerland (FHNW) where I spent my external stay and which corresponded to outdoor leaching experiments. The soil sequestration experiment started before I got involved in the project. Later on I participated in the planning and assembly of the rain runoff experiment and in the analysis of the water and soil samples using inductively coupled plasma mass spectrometry (ICP-MS). I also did the complete analysis of the data from the rain runoff results.

Chapter 6 describes the LCA of a full product based OPV, the HeLi-on power bank, compared with 2 other similar products already in the market. For this work, I did the research for inventory data for the 2 products based on manufacturer information and databases, adaptations of the OPV inventory and additional components of the power bank products. I also built the model for the acquisition of a consistent impact assessment and the interpretation was made under supervision of Dr. Nieves Espinosa.

Finally, Chapter 7 presents the overall conclusions and outlook; and the appendix includes a list of total contributions to the scientific community and attached papers related to the work presented in this thesis.

1.6.Contributions to the literature

During those three years of PhD studies, my work was concentrated on OPV device testing, stability performance and LCA. I participated in seven conferences, with three posters and five oral talks in total. Furthermore, many scientific papers were published in recognized peer-viewed journals, with several others submitted or close to submission including two first authored. The complete list can be found in the appendix. In the three first authored papers, my contribution was dominant and the contribution from the co-authors was essential. One of them is focused on reproducibility and in the freeOPV platform, and the other two were focused on stability tests of OPV postcard sized modules.

- **dos Reis Benatto, G. A.**; Corazza, M.; Roth, B.; Schütte, F.; Rengenstein, M.; Gevorgyan, S. A.; Krebs, F. C. Inside or Outside? Linking Outdoor and Indoor Lifetime Tests of ITO-Free Organic Photovoltaic Devices for Greenhouse Applications. *Energy Technol.* 2016, doi: 10.1002/ente.201600335.
- **dos Reis Benatto, G. A.**; Roth, B.; Corazza, M.; Søndergaard, R. R.; Gevorgyan, S. A.; Jørgensen, M.; Krebs, F. C. Roll-to-roll printed silver nanowires for increased stability of flexible ITO-free organic solar cell modules. *Nanoscale* 2016, *8*, 318–326.

- **dos Reis Benatto, G. A.**; Roth, B.; Madsen, M. V.; Hösel, M.; Søndergaard, R. R.; Jørgensen, M.; Krebs, F. C. Carbon: The Ultimate Electrode Choice for Widely Distributed Polymer Solar Cells. *Adv. Energy Mater.* 2014, *4*, 1400732.

In the following papers, my contribution was related to the performance and monitoring of stability tests in several ISOS conditions and data analysis, or contribution in scanning a large number of published papers with stability data.

- Roth, B. ; **dos Reis Benatto, G. A.**; Corazza, M.; Carlé, J. E.; Helgesen, M.; Gevorgyan, S. A.; Jørgensen, M.; Søndergaard, R. R.; Krebs, F. C. Improving the Operational Stability of PBDTTTz-4 Polymer Solar Cells Modules by Electrode Modification. *Adv. Eng. Mater.* 2016, *18*, 511–517.
- Roth, B.; **dos Reis Benatto, G. A.**; Corazza, M.; Søndergaard, R. R.; Gevorgyan, S. A.; Jørgensen, M.; Krebs, F. C. The Critical Choice of PEDOT:PSS Additives for Long Term Stability of Roll-to-Roll Processed OPVs. *Adv. Energy Mater.* 2015, *5*, 1401912.
- Gevorgyan, S. A.; Espinosa, N.; Ciammaruchi, L.; Roth, B.; Livi, F.; Tsopanidis, S.; Züfle, S.; Queirós, S.; Gregori, A.; **dos Reis Benatto, G. A.**; Corazza, M.; Madsen, M. V.; Hösel, M.; Beliatis, M. J.; Larsen-Olsen, T. T.; Pastorelli, F.; Castro, A.; Mingorance, A.; Lenzi, V.; Fluhr, D.; Roesch, R.; Maria Duarte Ramos, M.; Savva, A.; Hoppe, H.; Marques, L. S. A.; Burgués, I.; Georgiou, E.; Serrano-Luján, L.; Krebs, F. C. Baselines for Lifetime of Organic Solar Cells. *Adv. Energy Mater.* **2016**, 1600910.

In relation to LCA, two papers were published so far and one more is about to be finished (See list in the Appendix). In one of the published ones (at Adv. Eng. Mater) I contributed to the inventory metals profile and data collection. In the second one (published in Energy Environ. Sci.), I was responsible to the data collection whole final data analysis of the rain runoff experiment under the supervision of Dr. Yannick-Serge Zimmerman and Dr. Markus Lenz during my external stay in Basel, Switzerland.

- Espinosa, N.; Zimmermann, Y.-S.; **dos Reis Benatto, G. A.**; Lenz, M.; Krebs, F. C. Outdoor fate and environmental impact of polymer solar cells through leaching and emission to rainwater and soil. *Energy Environ. Sci.* 2016, *9*, 1674–1680.
- Espinosa, N.; Laurent, A.; **dos Reis Benatto, G. A.**; Hösel, M.; Krebs, F. C. Which Electrode Materials to Select for More Environmentally Friendly Organic Photovoltaics? *Adv. Eng. Mater.* 2016, *18*, 490–495.

Two publications were made in collaboration with the Prof. Jeff Kettle from Bangor University in Wales. My contribution in such papers was the electrical characterization under solar simulator; module preparation including labelling, organisation, and laser cutting; external quantum efficiency (EQE), and light beam induced current (LBIC) measurements.

- Kettle, J.; Bristow, N.; Sweet, T. K. N.; Jenkins, N.; **dos Reis Benatto, G. A.**; Jørgensen, M.; Krebs, F. C. Three dimensional corrugated organic photovoltaics for building integration ; improving the efficiency , oblique angle and diffuse performance of solar cells. *Energy Environ. Sci.* 2015, *8*, 3266–3273.
- Kettle, J.; Bristow, N.; Gethin, D. T.; Tehrani, Z.; Moudam, O.; Li, B.; Katz, E. A.; **dos Reis Benatto, G. A.**; Krebs, F. C. Printable luminescent down shifter for enhancing efficiency and stability of organic photovoltaics. *Sol. Energy Mater. Sol. Cells* 2016, *144*, 481–487.

My contribution in the following paper, which included the application of a low band gap polymer, was also module preparation including labelling, organisation, and laser cutting.

- Helgesen, M.; Carlé, J. E.; **dos Reis Benatto, G. A.**; Søndergaard, R. R.; Jørgensen, M.; Bundgaard, E.; Krebs, F. C. Making Ends Meet: Flow Synthesis as the Answer to Reproducible High-Performance Conjugated Polymers on the Scale that Roll-to-Roll Processing Demands. *Adv. Energy Mater.* 2015, *5*, 1401996.

In the following papers my contribution included the preparation of OPV samples in 1 cm^2 using the mini roll coater [60], either for the screening of several polymers or for testing a PEDOT:PSS/ZnO new front electrode (see Section 1.4).

- Bundgaard, E.; Livi, F.; Hagemann, O.; Carlé, J. E.; Helgesen, M.; Heckler, I. M.; Zawacka, N. K.; Angmo, D.; Larsen-Olsen, T. T.; **dos Reis Benatto, G. A.**; Roth, B.; Madsen, M. V.; Andersson, M. R.; Jørgensen, M.; Søndergaard, R. R.; Krebs, F. C. Matrix Organization and Merit Factor Evaluation as a Method to Address the Challenge of Finding a Polymer Material for Roll Coated Polymer Solar Cells. *Adv. Energy Mater.* 2015, *5*, 1402186.
- Hösel, M.; Angmo, D.; Søndergaard, R. R.; **dos Reis Benatto, G. A.**; Carlé, J. E.; Jørgensen, M.; Krebs, F. C. High-Volume Processed, ITO-Free Superstrates and Substrates for Roll-to-Roll Development of Organic Electronics. *Adv. Sci.* 2014, 1–12.

1.7.References

1. International Energy Statistics http://tonto.eia.doe.gov/cfapps/ipdbproject/IEDIndex3.cfm?tid=2&pid=2&aid=7 (accessed Dec 21, **2016**).

2. International Energy Agency Energy Statistics. *Statistics (Ber).* **2016**.

3. Etemad, B.; Luciani, J. *World energy production, 1800-1985 = Production mondiale d'énergie, 1800-1985*; Publicatio.; Librairie Droz: Genève, **1991**.

4. British Petroleum *BP Technology Outlook - Technology choices for a secure, affordable and sustainable energy future*; London, **2015**.

5. Dale, S. Energy in 2015: A year of plenty. **2016**.

6. Energy and Climate Change - World Energy Outlook Special Report **2015**.

7. Laurent, A.; Espinosa, N. Environmental impacts of electricity generation at global, regional and national scales in 1980–2011: what can we learn for future energy planning? *Energy Environ. Sci.* **2015**, *8*, 689.

8. Energy Technology Perspectives 2016. *Int. Energy Agency* **2016**.

9. Perez, R.; Perez, M. A Fundamental Look At Supply Side Energy Reserves For The Planet. *Int. Energy Agency SHC Program. Sol. Updat.* **2015**.

10. World Energy Outlook. *Int. Energy Agency* **2015**.

11. REN21 *Rerewable 2016 - Global status report - Key finding 2016*; **2016**.

12. Jean, J.; Brown, P. R.; Jaffe, R. L.; Buonassisi, T.; Bulovic, V. Pathways for solar photovoltaics. *Energy*

Environ. Sci. **2015**, *8*, 1200.

13. IEA Snapshot of Global PV Markets 2014. *Www.Iea-Pvps.Org* **2015**.

14. *Key Renewables Trends - Excerpt from Renewables Information (2016 edition)*; **2016**.

15. *Solar Photovoltaic Energy - Technology Roadmap*; **2014**.

16. Bloomberg, New Energy Finance https://www.bloomberg.com (accessed Dec 27, **2016**).

17. Sangster, A. J. Solar Photovoltaics. *Green Energy Technol.* **2014**, *194*, 145.

18. Masson, G.; Brunisholz, M. 2015 Snapshot of global photovoltaic markets - Photovoltaics Power Systems Programme. *Int. Energy Agency* **2016**.

19. Chapin, D. M.; Fuller, C. S.; Pearson, G. L. A new silicon p-n junction photocell for converting solar radiation into electrical power. *J. Appl. Phys.* **1954**, *25*, 676.

20. Spanggaard, H.; Krebs, F. C. A brief history of the development of organic and polymeric photovoltaics. *Sol. Energy Mater. Sol. Cells* **2004**, *83*, 125.

21. Kibria, M. T.; Ahammed, A.; Sony, S. M.; Hossain, F. A Review : Comparative studies on different generation solar cells technology. *Int. Conf. Environ. Asp. Bangladesh* **2014**, 51.

22. Bagnall, D. M.; Boreland, M. Photovoltaic technologies. *Energy Policy* **2008**, *36*, 4390.

23. Fraunhofer Institute for Solar Energy Systems - ISE Photovoltaics Report. **2016**.

24. Rosencher, E.; Vinter, B. Optoelectronics. *Cambridge Univ. Press* **2002**, 708.

25. Espinosa, N.; Hösel, M.; Angmo, D.; Krebs, F. C. Solar cells with one-day energy payback for the factories of the future. *Energy Environ. Sci.* **2012**, *5*, 5117.

26. sunflower-fp7.eu http://www.sunflower-fp7.eu/site/index.php/news/156-sunflower-wins-the-best-publicly-funded-demonstrator-award-in-the-2016-oe-a-competition (accessed Dec 28, **2016**).

27. Chemistry, R. S. of Emerging Technologies Competition: Previous winners http://www.rsc.org/competitions/emerging-technologies/previous-winners/#2015-winners (accessed Dec 28, **2016**).

28. Wikipedia Solar cell https://en.wikipedia.org/wiki/Solar_cell (accessed Dec 21, **2016**).

29. Building Power Distribution http://buildingpowerdistribution.com/green-news/zsw-sets-21-7-cigs-cell-record/ (accessed Dec 21, **2016**).

30. Deibel, C.; Dyakonov, V. Polymer-fullerene bulk heterojunction solar cells. *Reports Prog. Phys.* **2010**, *73*, 96401.

31. Nelson, J. Polymer: Fullerene bulk heterojunction solar cells. *Mater. Today* **2011**, *14*, 462.

32. Thompson, B. C.; Fréchet, J. M. J. Polymer-fullerene composite solar cells. *Angew. Chemie - Int. Ed.* **2008**, *47*, 58.

33. Bisquert, J.; Garcia-Belmonte, G. On Voltage, Photovoltage, and Photocurrent in Bulk Heterojunction Organic Solar Cells. *J. Phys. Chem. Lett.* **2011**, *2*, 1950.

34. Scharber, M. C.; Mühlbacher, D.; Koppe, M.; Denk, P.; Waldauf, C.; Heeger, A. J.; Brabec, C. J. Design rules for donors in bulk-heterojunction solar cells - Towards 10 % energy-conversion efficiency. *Adv. Mater.* **2006**, *18*, 789.

35. Qi, B.; Wang, J. Open-circuit voltage in organic solar cells. *J. Mater. Chem.* **2012**, *22*, 24315.

36. NREL Solar Spectral Irradiance: Air Mass 1.5 http://rredc.nrel.gov/solar/spectra/am1.5/ (accessed Dec

30, **2016**).

37. Jørgensen, M.; Norrman, K.; Krebs, F. C. Stability/degradation of polymer solar cells. *Sol. Energy Mater. Sol. Cells* **2008**, *92*, 686.

38. Gevorgyan, S. A.; Madsen, M. V.; Roth, B.; Corazza, M.; Hösel, M.; Søndergaard, R. R.; Jørgensen, M.; Krebs, F. C. Lifetime of Organic Photovoltaics: Status and Predictions. *Adv. Energy Mater.* **2015**, *6*, 1501208.

39. Bundgaard, E.; Krebs, F. C. Low-Band-Gap Conjugated Polymers Based on Thiophene , Benzothiadiazole , and Benzobis (thiadiazole). **2006**, 2823.

40. Helgesen, M.; Carlé, J. E.; Dos Reis Benatto, G. A.; Søndergaard, R. R.; Jørgensen, M.; Bundgaard, E.; Krebs, F. C. Making ends meet: Flow synthesis as the answer to reproducible high-performance conjugated polymers on the scale that roll-to-roll processing demands. *Adv. Energy Mater.* **2015**, *5*, 1401996.

41. Hösel, M.; Angmo, D.; Søndergaard, R. R.; dos Reis Benatto, G. A.; Carlé, J. E.; Jørgensen, M.; Krebs, F. C. High-Volume Processed, ITO-Free Superstrates and Substrates for Roll-to-Roll Development of Organic Electronics. *Adv. Sci.* **2014**, *1*, 1400002.

42. Krebs, F. C. Fabrication and processing of polymer solar cells: A review of printing and coating techniques. *Sol. Energy Mater. Sol. Cells* **2009**, *93*, 394.

43. Brabec, C. J. Organic photovoltaics: Technology and market. *Sol. Energy Mater. Sol. Cells* **2004**, *83*, 273.

44. Heliatek sets new Organic Photovoltaic world record efficiency of 13.2% - Heliatek – The future is light http://www.heliatek.com/en/press/press-releases/details/heliatek-sets-new-organic-photovoltaic-world-record-efficiency-of-13-2 (accessed Jan 2, **2017**).

45. Angmo, D.; Krebs, F. C. Over 2 Years of Outdoor Operational and Storage Stability of ITO-Free, Fully Roll-to-Roll Fabricated Polymer Solar Cell Modules. *Energy Technol.* **2015**, *3*, 774.

46. Gevorgyan, S. A.; Espinosa, N.; Ciammaruchi, L.; Roth, B.; Livi, F.; Tsopanidis, S.; Züfle, S.; Queirós, S.; Gregori, A.; dos Reis Benatto, G. A.; Corazza, M.; Madsen, M. V.; Hösel, M.; Beliatis, M. J.; Larsen-Olsen, T. T.; Pastorelli, F.; Castro, A.; Mingorance, A.; Lenzi, V.; Fluhr, D.; Roesch, R.; Maria Duarte Ramos, M.; Savva, A.; Hoppe, H.; Marques, L. S. A.; Burgués, I.; Georgiou, E.; Serrano-Luján, L.; Krebs, F. C. Baselines for Lifetime of Organic Solar Cells. *Adv. Energy Mater.* **2016**, 1600910.

47. Mulligan, C. J.; Bilen, C.; Zhou, X.; Belcher, W. J.; Dastoor, P. C. Levelised cost of electricity for organic photovoltaics. *Sol. Energy Mater. Sol. Cells* **2015**, *133*, 26.

48. Andersen, T. R.; Dam, H. F.; Hösel, M.; Helgesen, M.; Carle, J. E.; Larsen-Olsen, T. T.; Gevorgyan, S. a; Andreasen, J. W.; Adams, J.; Li, N.; Machui, F.; Spyropoulos, G. D.; Ameri, T.; Lemaitre, N.; Legros, M.; Scheel, A.; Gaiser, D.; Kreul, K.; Berny, S.; Lozman, O. R.; Nordman, S.; Valimaki, M.; Vilkman, M.; Sondergaard, R. R.; Jorgensen, M.; Brabec, C. J.; Krebs, F. C. Scalable, ambient atmosphere roll-to-roll manufacture of encapsulated large area, flexible organic tandem solar cell modules. *Energy Environ. Sci.* **2014**, *7*, 2925.

49. Krebs, F. C.; Hösel, M.; Corazza, M.; Roth, B.; Madsen, M. V.; Gevorgyan, S. A.; Søndergaard, R. R.; Karg, D.; Jørgensen, M. Freely available OPV-The fast way to progress. *Energy Technol.* **2013**, *1*, 378.

50. dos Reis Benatto, G. A.; Roth, B.; Madsen, M. V.; Hösel, M.; Søndergaard, R. R.; Jørgensen, M.; Krebs, F. C. Carbon: The Ultimate Electrode Choice for Widely Distributed Polymer Solar Cells. *Adv. Energy Mater.* **2014**, *4*, 1400732.

51. Espinosa, N.; Laurent, A.; dos Reis Benatto, G. A.; Hösel, M.; Krebs, F. C. Which Electrode Materials to Select for More Environmentally Friendly Organic Photovoltaics? *Adv. Eng. Mater.* **2016**, *18*, 490–495.

52. European Committee for Standardization ISO 14040:2006 - Environmental management - Life cycle

assessment - Principles and framework. **2006**.

53. European Committee for Standardization ISO 14044:2006 - Environmental management - Life cycle assessment - Requirements and guidelines. **2006**.

54. Espinosa, N.; García-Valverde, R.; Urbina, A.; Krebs, F. C. A life cycle analysis of polymer solar cell modules prepared using roll-to-roll methods under ambient conditions. *Sol. Energy Mater. Sol. Cells* **2011**, *95*, 1293.

55. Hengevoss, D., Zimmermann, Y.S., Brun, N., Hugi, C., Lenz, M., Corvini, P.F.X., Fent, K. Environmental aspects of printable and organic electronics (POE). In *Organic and Printed Electronics: Fundamentals and Applications.*; Ganz, S., Lupo, D., Nisato, G., Ed.; Pan Stanford Publishing Pte. Ltd.: Singapore, **2015**.

56. Espinosa, N.; Lenzmann, F. O.; Ryley, S.; Angmo, D.; Hösel, M.; Søndergaard, R. R.; Huss, D.; Dafinger, S.; Gritsch, S.; Kroon, J. M.; Jørgensen, M.; Krebs, F. C. OPV for mobile applications: an evaluation of roll-to-roll processed indium and silver free polymer solar cells through analysis of life cycle, cost and layer quality using inline optical and functional inspection tools. *J. Mater. Chem. A* **2013**, *1*, 7037.

57. Brun, N. R.; Wehrli, B.; Fent, K. Ecotoxicological assessment of solar cell leachates: Copper indium gallium selenide (CIGS) cells show higher activity than organic photovoltaic (OPV) cells. *Sci. Total Environ.* **2016**, *543*, 703.

58. Zimmermann, Y.-S.; Schäffer, A.; Corvini, P. F.-X.; Lenz, M. Thin-film photovoltaic cells: long-term metal(loid) leaching at their end-of-life. *Environ. Sci. Technol.* **2013**, *47*, 13151.

59. Azzopardi, B.; Emmott, C. J. M.; Urbina, A.; Krebs, F. C.; Mutale, J.; Nelson, J. Economic assessment of solar electricity production from organic-based photovoltaic modules in a domestic environment. *Energy Environ. Sci.* **2011**, *4*, 3741.

60. Hösel, M.; Dam, H. F.; Krebs, F. C. Development of Lab-to-Fab Production Equipment Across Several Length Scales for Printed Energy Technologies, Including Solar Cells. *Energy Technol.* **2015**, *3*, 293.

Chapter 2

Large scale production of environmentally friendly OPV

This chapter describes the details of the large scale manufacture of fully solution processed organic photovoltaics by means of roll-to-roll (R2R) techniques. Printing and coating processes performed are described, followed by the reproducibility report of carbon based OPV (C-OPV) postcard sized modules (freeOPV) with different active materials, and in its fully printed version. The use of carbon as electrode material instead of silver represents a potential truly green technology, since it doesn't contain significant amounts of metal and can even be disposed in the normal household waste for incineration or plastic recycling.

2.1.Roll-to-roll technique

In the production of solar cells, R2R is a very advantageous technique since the production can be made with high speed and by the meter instead of sheet to sheet. Other thin-film PV technologies can also be built on a flexible substrate that can be R2R manufactured as well. However, many materials need to be evaporated or sputtered under vacuum and are not solution processable. This matches with the processability issue for new sustainable PV technologies, since making a vacuum environment is a very energy demanding process. For OPV, it was possible to develop inks which do not require a vacuum environment do be deposited, and use printing and coating techniques, that are less energy demanding compared with evaporation and sputtering alone, besides the vacuum-free advantage [1,2].

As shown in Chapter 1, an OPV module is built out of various layers, with different materials, which may require different deposition techniques, intermediate treatments, drying times, or web speeds. The layer stack, in the case of this work, is built on top of a flexible thin PET-based barrier foil. Figure 2.1 shows the R2R printing machine located at DTU, used for the manufacture of the samples presented in this chapter and the whole thesis. It consists of 2 printing stations: flexographic printing (E) and rotary screen

printing units (H); and one coating station: slot-die coating (F). The whole machinery also includes an unwinder (A), edge guide (B), cleaning station (C), corona treatment (D), two ovens (G and I) and a rewinder (J). This setup can run with web speed up to 25 m min^{-1} and operates under full ambient conditions, without any clean-room needed. This machinery expresses the readiness for fully industrial production of OPV with integrated R2R processing on a single factory line. For this, several mechanic automatizations need to be developed in order to optimise a number of varying requirements for each printing/coating step.

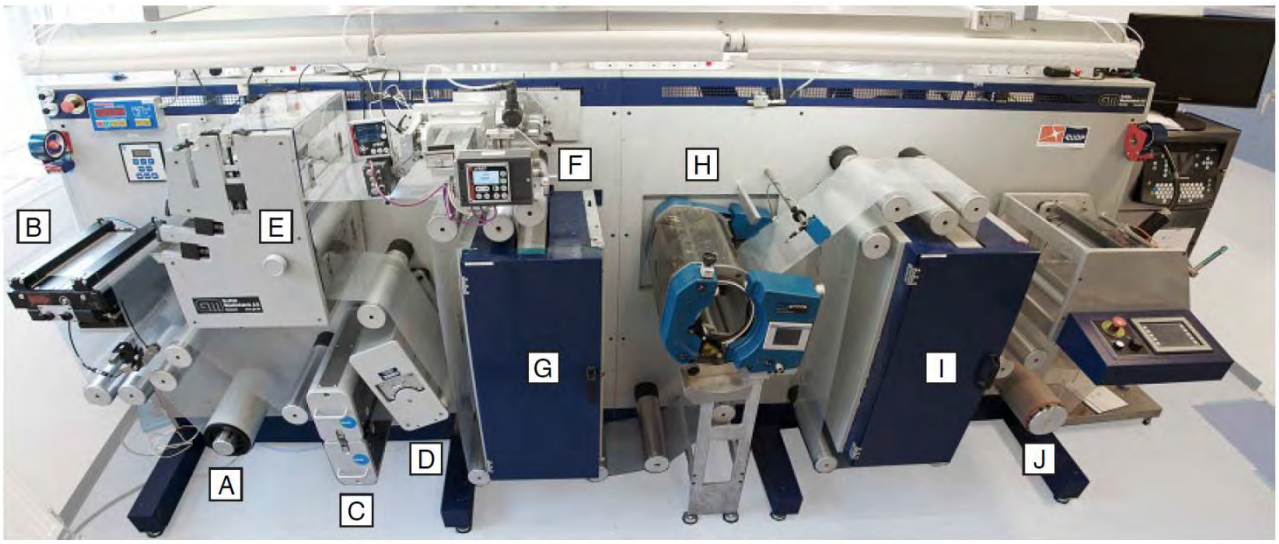

Figure 2.1 - R2R printing and coating machine for organic solar cells with (A) unwinder, (B) edge guide, (C) web cleaning, (D) corona treatment, (E) flexo printing unit, (F) slot-die station, (G) hot-air dryer, (H) rotary screen printing unit, (I) hot-air dryer, and (J) rewinder. Reprinted with permission from [2].

2.1.1. Printing and coating techniques

OPV particularly needs to have very thin layers, most of them even in the nanometre scale, to work well (in the case of the active layer for instance) and keep its flexibility, semitransparency and electrical properties. This, added to the pursuit of low energy demanding and vacuum-free manufacturing, limits the vast number of available printing and coating techniques to a few that can be used in R2R processing of OPVs. Printing processes even have additional advantages in comparison to coating, as it can be patterned and have the potential of minimal waste of material.

2.1.1.1. Flexo printing (FL)

Well-known and available procedures in the commercial printing industry can be optimized and adapted for the inks used to manufacture of OPVs. An example is the flexography or flexo printing which is a very fast method, with speeds up to hundreds of meters per minute. Figure 2.2 presents the illustration showing the printing method steps on the left and a picture of the printing happening in the R2R machine from Figure 2.1. The flexo printing unit is comprised of four rolls, named fountain roller, anilox roller, printing plate cylinder, and impression cylinder respectively. The fountain roller is partially immersed in the ink bath and has the function of transferring the ink to the anilox roller. Its surface should be soft and could be made with different materials with diverse hardness, depending on the ink used. The second roll is called the anilox roller and is made of ceramics and filled with ink coming from the fountain roller. It has an engraved surface with cavities that carry specific volumes of ink to the next roller, with wet layer thickness

controlled by a doctor blade. The next roll is the printing plate cylinder, which has the pattern that will be printed on the substrate on the impression cylinder. The amount of ink received by the printing plate is very well defined, keeping the printing quality over the substrate. Parameters like the anilox volume, ink surface tension, printing speed and nip pressure can be adjusted for obtaining the desired result. More detailed information of flexography applied for OPV, printed and/or organic electronics and printing in general can be found in the literature [1,3–7].

Flexography is a very important technique to replace the ITO front electrodes with Ag-grids [8–11]. An example of this replacement in large scale is the first of the freely available OPV modules [12] which had flexo printing applied for the Ag-grid front electrode finger pattern and the Ag modules contacts, where the ink used is based on silver nanoparticles (AgNP). In the modelling for three different metal based front electrodes that will be presented in Chapter 3, this printing technique is also considered for copper and aluminium based inks. Flexo coating, using a similar principle, is used for the application of UV-cured adhesive presented in the encapsulation Section (2.1.2). The inks used for the further layers of the OPV device present very different viscosities, therefore other printing or coating techniques are used as shown further on.

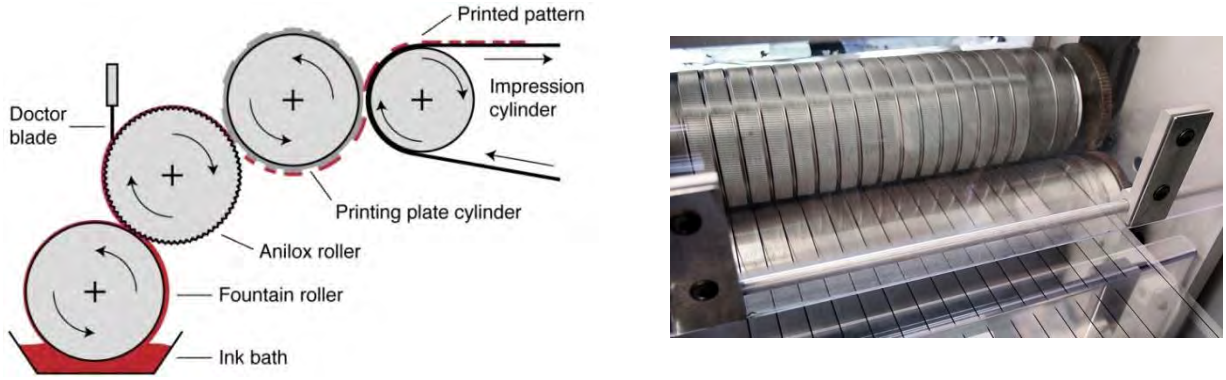

Figure 2.2 - Left: Simplified scheme of flexo printing used in the manufacture organic solar cells. Right: Picture of the flexo printing of silver nanoparticle OPV front electrode. Adapted with permission from [13].

2.1.1.2. Screen printing (SP)

This technique has a very low cost and is a very common printing technique, used in several different fields such as graphics art industry, manufacturing of printed circuit boards, and metallization of silicon solar cells. In Figure 2.3 the principle of the flat bed screen printing is shown on the left. The setup is comprised of a screen and a squeegee. The screen can be made of polyester, nylon or stainless steel covered with an emulsion layer. For the printing procedure, the screen is placed few millimetres above the substrate and the ink placed on the screen is spread and pressed by the squeegee through the screen pattern, contacting and depositing the ink on the substrate. Further and very detailed studies can be found in the related literature [6,14,15].

Figure 2.3 also shows the principle of rotary screen printing, which is basically the same as the flatbed screen printing, but with the squeegee fixed inside a cylindrical screen that rotates relative to the squeegee with the same speed as the substrate. Both flatbed and rotary SP techniques are R2R compactible, although flatbed requires the substrate to move in steps or have a moving screen, while rotary SP is fully R2R compactible with speeds of 180 m min^{-1} easily reached.

Some ink proprieties such as volatility and viscosity are required for this technique resulting in a good OPV device. In this context, some commercially available inks of PEDOT:PSS and silver, for instance, may

need adjustments. In OPV manufacture, SP techniques are more often applied in the printing of PEDOT:PSS and back silver contacts layers. In this chapter, the rotary SP is additionally applied in the printing of ZnO, active layer and back carbon contacts, making fully printed OPV devices.

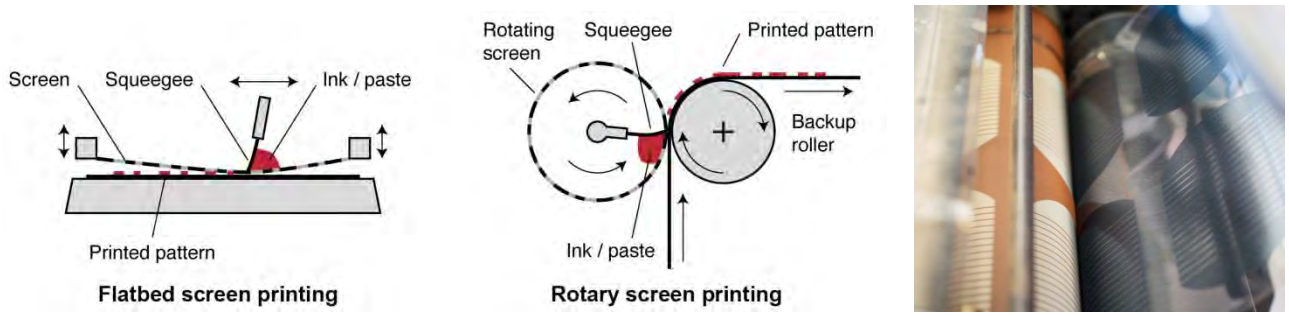

Figure 2.3 - Left and centre: Flatbed and rotary screen printing principles. Right: Picture of the rotary screen printing of PEDOT:PSS OPV front electrode. Adapted with permission from [13].

2.1.1.3. Slot-die coating (SD)

The solution processed OPV devices can be R2R manufactured using a number of coating techniques, for instance blade, spray or slot-die coating [1]. However, in this work, the modules use only one (if any) coating technique: slot-die coating. Figure 2.4 shows the coating principle comprising a coating head supplied by ink with a meniscus that guides the ink to the moving substrate, letting minimal ink contact with air prior the deposition. This technique allows the deposition of homogeneous wet films with high uniformity and thickness control. The parameters which control the wet thickness are the ink flow rate and the coating speed and width. Hence, the dry thickness d (cm) can be defined by the relation:

$$d = \frac{f}{v.w}.\frac{c}{\rho}$$

where f is the flow rate in (cm^3 min^{-1}), v is the coating speed (cm min^{-1}), w is the coating width (cm), c is the solid concentration in the ink (g cm^{-3}), and ρ the density of the material in the dry film (g cm^{-3}). The coating speeds typical for OPV layers are in the range 0.5 to 2 m min^{-1}. Further details of this technique can be found in several works [16–19].

As shown in the picture of Figure 2.4, the SD technique deposits continuous stripes, having some areas that will not be active in the full device, especially in the fabrication of small modules. However, the stripes-like coating is very convenient for the fabrication of OPV devices allowing easy stacking of further layers in a device with serially connected cells. In this chapter, SD was used for the ZnO and active layers (more often than SP), although it can also be used for the deposition of other layers [20–22].

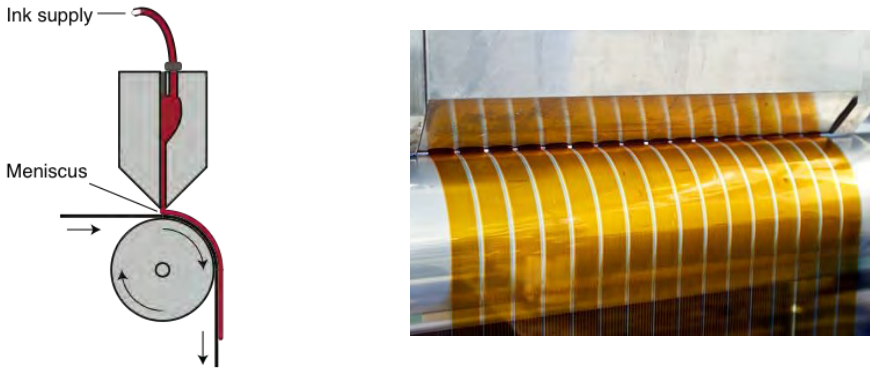

Figure 2.4 - Left: Slot-die coating principle. Right: Picture of the slot-die coating of 16 stripes of P3HT:PCBM active layer in a R2R machine. Adapted with permission from [13].

2.1.2. Encapsulation

Final encapsulation of the devices is highly important for the OPV operation. First due to the layers sensitivity to oxygen and to water [23,24]; second for avoiding leaching of materials to the environment during outdoor installation [25,26]. In practice, the quality of the encapsulation has a direct relation to the lifetime of the OPV devices. For the flexible devices fabricated for this work, the encapsulation foil is a multilayer PET-based SiO_x coated barrier foil, also used as substrate. The barrier foil purchased from Amcor (Ceramis® Matt PET without UV protection) has a thickness of 42 µm, with water vapour transmission rate (WVTR) of 0.04 g m^{-2} day^{-1} and oxygen transmission rate (OTR) of 0.01 cm^3 m^{-2} day^{-1}.

The encapsulation foil is applied as illustrated in Figure 2.5, using high-viscous and solvent-free UV-curable epoxy resin (DELO LP655). The adhesive is directly applied onto the corona-treated barrier foil with a flexo coating with an anilox volume of 30 ml m^{-2}, and continues to the encapsulation nip unit to be attached to the substrate foil containing the printed OPV [1,7]. The UV-laminator speed was 2 m min^{-1} in order to accomplish the required exposure time. The UV lamps power are 2 kW (power rating) and 350 W (optical output) light-emitting diode (LED). After curing, the final thickness of the adhesive layer was about 20 µm.

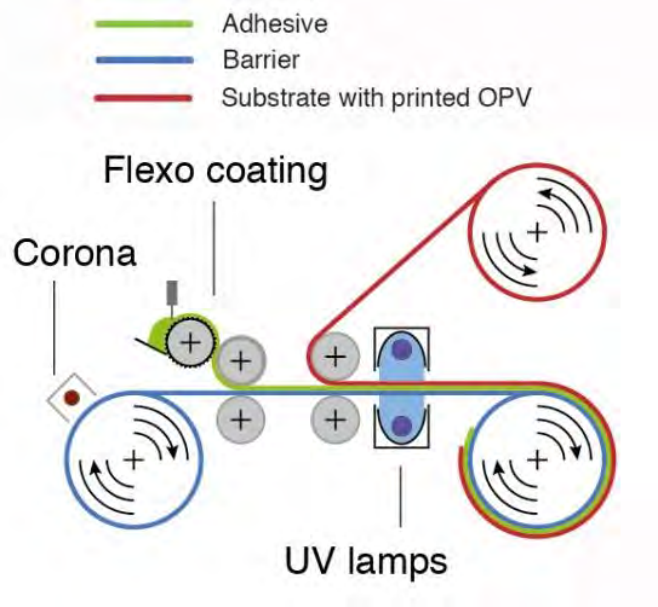

Figure 2.5 - Application of encapsulation using UV-curing adhesive. Adapted with permission from [1].

2.2.Reproducibility of large scale produced carbon based OPV

The final R2R produced OPV module comprises several interconnected single cells which sum up the open circuit voltages (V_{OC}), as shown in the zoom-in on Figure 2.6 for a postcard sized carbon-based OPV module (C-OPV). The correspondent photogenerated current of each cell, in a series connection, will be equal through the whole circuit, therefore the cell with the lowest short-circuit current (I_{SC}) will drive the total current and thus the module performance. The coating and printing techniques described in the previous subchapter is able to deposit homogeneous layers with high quality in a continuous web with precision for effective series connected modules. The conductivity and sheet resistance of the electrode materials limit the width of the single cell [27] and in the case of C-OPV this is what defines its design with 4 mm wide cells, making the whole module comprised of 16 cells. The smaller cells width plus the shift needed for the series connection consequentially leads to a reduced active area per module.

The first generation of freely available OPV (freeOPV) was silver-based OPV (Ag-OPV) which employed state-of-the-art printed grid electrode structures with a ±5° slant to minimize comb line cross-overs that often lead to shunts [12,29]. The silver grid associated with a thin PEDOT:PSS layer enables a low sheet resistivity electrode and allow cell dimensions of 9 to 15 mm. The current densities in this case range from 6 to 12 mA cm^{-2} [12]. For a front electrode based on PEDOT:PSS alone, previous devices with cell dimensions of 1–2 mm were possible to be made without loss, where carbon was also reported as a printed electrode [30–32]. Operational stability in these devices proved to be challenging due to the short edges around and towards the connection of the modules.

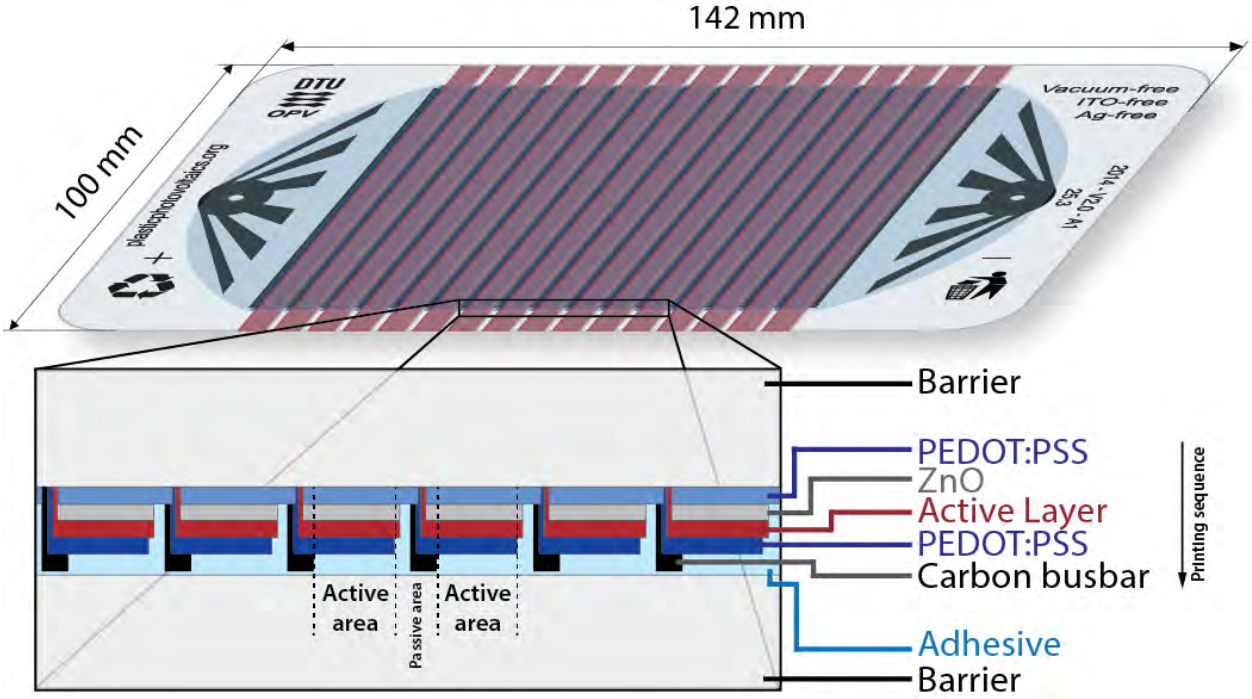

Figure 2.6 - C-OPV module standard structure with zoom-in showing serial connected cells in an inverted structure, its correspondent active and passive areas and layers. Adapted with permission from [28].

Ag-OPV freeOPV was developed with a thin (<250 nm) flexo-printed Ag contacts that enables a good edge seal, contacting the module externally with pressed buttons. As shown in the design in the Figure 2.6 above and in Figure 2.7 below (indicated with blue arrows), C-OPV modules (also a freeOPV) were built with a thin PEDOT:PSS layer employed with the same edge sealing purpose, since carbon does not enable a

good sealing as it is a diffusion path of oxygen into the device. The carbon extraction lines do not extend until the device area with highly reproducible performance as shown in the following subchapters. Comparing the modules current-voltage curve (IV-curve), the efficiency per active area (or power conversion efficiency, PCE) was very similar to Ag-OPV, but the poorer geometric fill factor, a consequence of the larger number of cells (16 versus 8), makes the module power around 50 mW while in the Ag-OPV it's normally 100 mW.

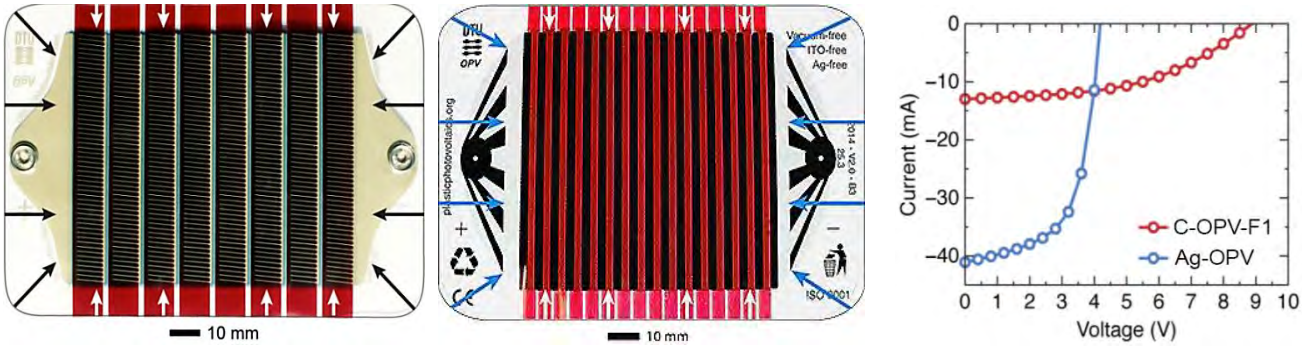

Figure 2.7 - Comparison of the diffusion path into the postcard sized Ag-OPV (left) and C-OPV (centre) postcard sized devices. IV-curve of the C-OPV-F1 in comparison to the Ag-OPV module (right). Adapted with permission from [33].

2.2.1. Carbon based OPV encapsulated with bubble prone foil (C-OPV-F1)

The first large scale C-OPV produced with the new design, presented in Figure 2.6 and 2.7, used the barrier foil from Amcor as the substrate and encapsulation foil (described in Section 2.1.2). This first batch, however, showed to be prone to bubble formation during the later lifetime tests shown in Chapter 4. As the second batch, used for the subsequent C-OPV with different active layer or printing techniques, didn't present this issue, this first collection was named C-OPV with foil #1: C-OPV-F1.

C-OPV-F1 had an inverted structure, with PEDOT:PSS (front electrode) rotary screen printed with a nominal wet thickness of 20 µm, a web speed of 10 m min^{-1}, and infrared (IR) drying and a hot air oven temperature of 140 °C. ZnO (electron transporting layer, ETL) was slot-die coated at 10 m min^{-1} a nominal wet thickness of 7 µm, and dried using both ovens (90 °C and 140 °C). The P3HT:PCBM (active layer) was slot-die coated at 2 m min^{-1} to ensure thermal annealing of P3HT:PCBM, with a nominal wet thickness of 12 µm having both ovens at 140 °C. The rotary screen printing of PEDOT:PSS (hole transporting layer, HTL) was made at a speed of 4 m min^{-1} with a nominal wet thickness of 20 µm, infrared drying and hot air oven set to 140 °C. The carbon (back electrode) was rotary screen printed in two steps. Firstly the text pattern and the extraction lines were printed with a nominal wet thickness of 10 µm at 10 m min^{-1}, IR drying and the hot air oven set to 140 °C. In a secondary printing step the interconnections between the cells were rotary screen printed with a nominal wet thickness of 40 µm at a web speed of 4 m min^{-1} using the same drying conditions. The devices were R2R tested before lamination that was carried out using adhesive and encapsulation barrier foil as described in the Section 2.1.2. The fully laminated rolled OPV were laser-cut into modules using a laser cutter and the devices were lastly contacted using snap-button contacts.

Front PEDOT:PSS ink was purchased from Heraeus (PH1000) and diluted in isopropanol (10:3 w/w); ZnO used was an in house formulation composed of nanoparticles with concentration of 56 mg mL^{-1} in acetone; P3HT is from BASF (Sepiolid P-200) and PCBM from Merck, both at a concentration of 30 mg mL^{-1} in chlorobenzene; HTL PEDOT:PSS was from Agfa (EL-P-5010) and diluted in isopropanol (10:2 w/w); and carbon ink was purchased from Acheson (Electro- dag PF-407), that contains graphite and carbon black. As

the web width of 305 mm is used, the rotary screen printing cylinder had a 304.8 x 304.8 mm motif shown in Figure 2.8. Each motif includes 6 postcard modules where two modules were processed simultaneously, here referred to as the A-side and the B-side. In the first printing step (PEDOT:PSS), a barcode was inkjet printed on each motif for identification. This "barcode side" is defined as the B-side and the barcode number is kept in the measurement registration of the module.

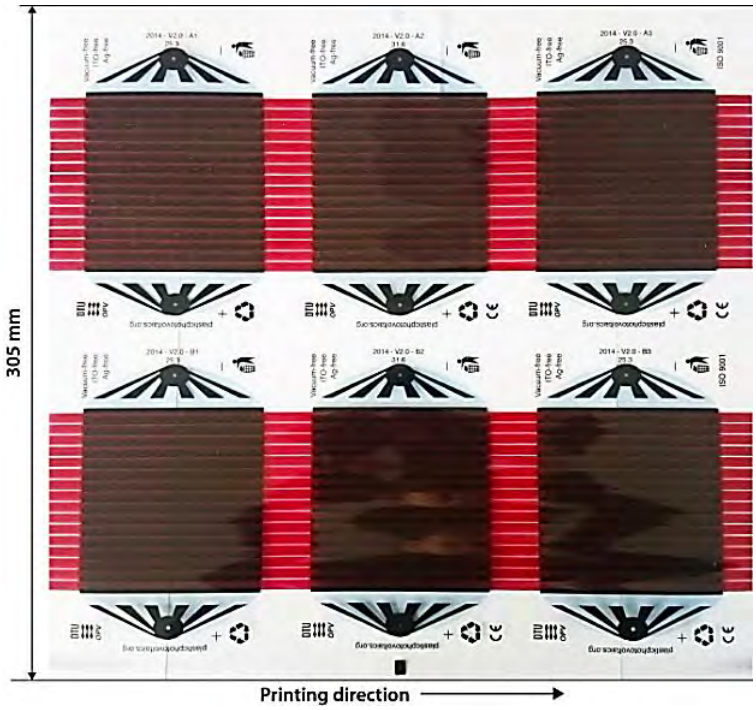

Figure 2.8 - Motif with 6 C-OPV modules. The 3 above are the A-side and the 3 below the B-side.

Figure 2.9 shows the parameters from the IV-curve of 500 C-OPV modules corresponding to 83 printed motifs. The parameters are namely power conversion efficiency (PCE), open-circuit voltage (V_{OC}), short-circuit current (I_{SC}), fill factor (FF), and maximum power (P_{max}).

Between the two sides there are differences and some experimental variation due to processes with slightly different gap widths. The evidence is even more clear as the pattern is repeated every three modules of each side. Table 2.1 shows the average, maximum and standard deviation of the parameters from Figure 2.9. The standard deviations attest the high reproducibility of the large scale C-OPV-F1 production.

The IV-curves were measured both from the front and back side on the modules. Figure 2.10 shows the photovoltaics parameters histograms comparing the front and back illumination measurements; and Table 2.2 shows their correspondent average, maximum and standard deviation. The same wet thickness was employed for both front and back PEDOT:PSS indicating that the optical path from the front and back would be similar enabling bi-facial operation. However the back PEDOT:PSS ink has a slightly higher solid content reducing the transparency of the back side, leading to a slightly lower current and automatically higher fill factor, and lower PCE and P_{max}.

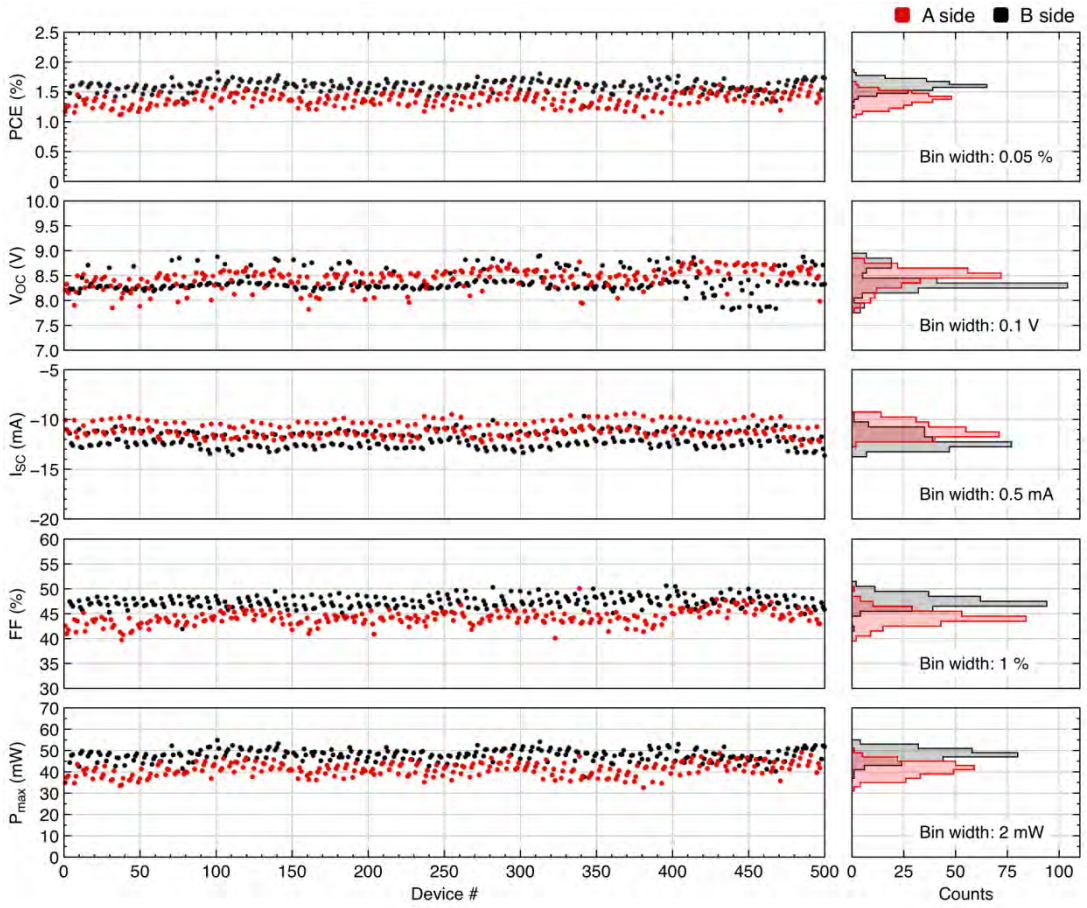

Figure 2.9 - Reproducibility of 500 C-OPV-F1 modules (250 A-side, 250 B-side) is shown in relation to the photovoltaic parameters. The histograms on the right highlight the differences between the two sides of the web and the relatively narrow distribution of performance. Reprinted with permission from [33].

Table 2.1 - The photovoltaic parameters for 500 C-OPV-F1 modules from the two different sides of the web. Adapted with permission from [33].

	***PCE* [%] A side**	***PCE* [%] B side**	***V_{OC}* [V] A side**	***V_{OC}* [V] B side**	***I_{SC}* [mA] A side**	***I_{SC}* [mA] B side**	***FF* [%] A side**	***FF* [%] B side**	***P_{max}* [mW] A side**	***P_{max}* [mW] B side**
Average	1.37	1.60	8.45	8.37	11.02	12.11	44.22	47.51	41.20	48.14
Standard deviation	0.11	0.09	0.20	0.22	0.71	0.76	1.47	1.15	3.22	2.64
Maximum	1.64	1.83	8.78	8.91	12.55	13.60	50.13	50.67	49.15	54.96

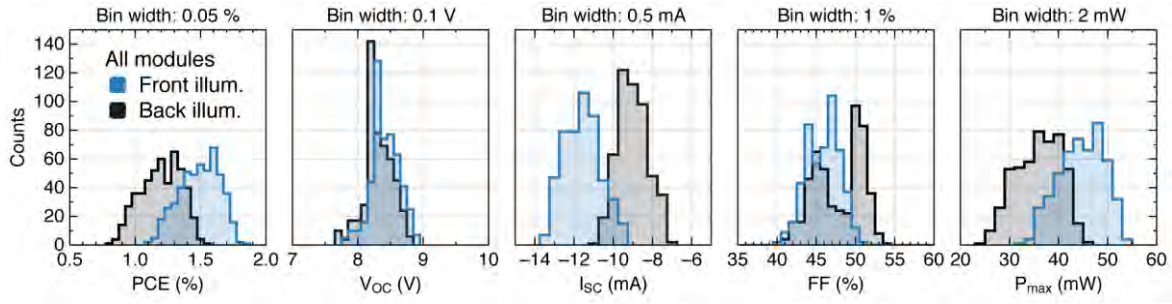

Figure 2.10 - Front-versus-back illumination of 500 modules shown as histograms with the bin width quoted on top of each graph. Adapted with permission from [33].

Table 2.2 - The photovoltaic parameters for 500 C-OPV-F1 modules from front and back illumination. Adapted with permission from [33].

	PCE [%] Front	*PCE* [%] Back	V_{OC} [V] Front	V_{OC} [V] Back	I_{SC} [mA] Front	I_{SC} [mA] Back	*FF* [%] Front	*FF* [%] Back	P_{max} [mW] Front	P_{max} [mW] Back
Average	1.49	1.20	8.41	8.31	11.57	9.01	45.86	47.85	44.67	35.90
Standard deviation	0.15	0.15	0.21	0.22	0.92	0.78	2.11	3.11	4.55	4.55
Maximum	1.83	1.54	8.91	8.80	13.60	10.81	50.67	53.74	54.96	46.19

2.2.2. Carbon based OPV encapsulated with bubble free foil (C-OPV-F2)

In this second C-OPV batch, a bubble free foil was used purchased from the same provider (see Section 2.1.2). This second collection was named C-OPV with foil #2: C-OPV-F2.

C-OPV-F2 had also an inverted structure, same design and precisely the same technical features as C-OPV-F1 as with printing and coating techniques, speeds and inks, with one exception: the active layer is P3HT:ICBA, where P3HT is from BASF (Sepiolid P-200) and ICBA from Plextronics. Figure 2.12 and Table 2.3 show the parameters from the IV-curves of 100 C-OPV-F2 modules corresponding to 17 printed motifs. It was measured one motif (6 modules) in intervals of 20 motifs. The differences of the A-side and the B-side are noticed once again. The reproducibility is high and the standard deviations quite correspondent to C-OPV-F1, just FF had slightly more spread values.

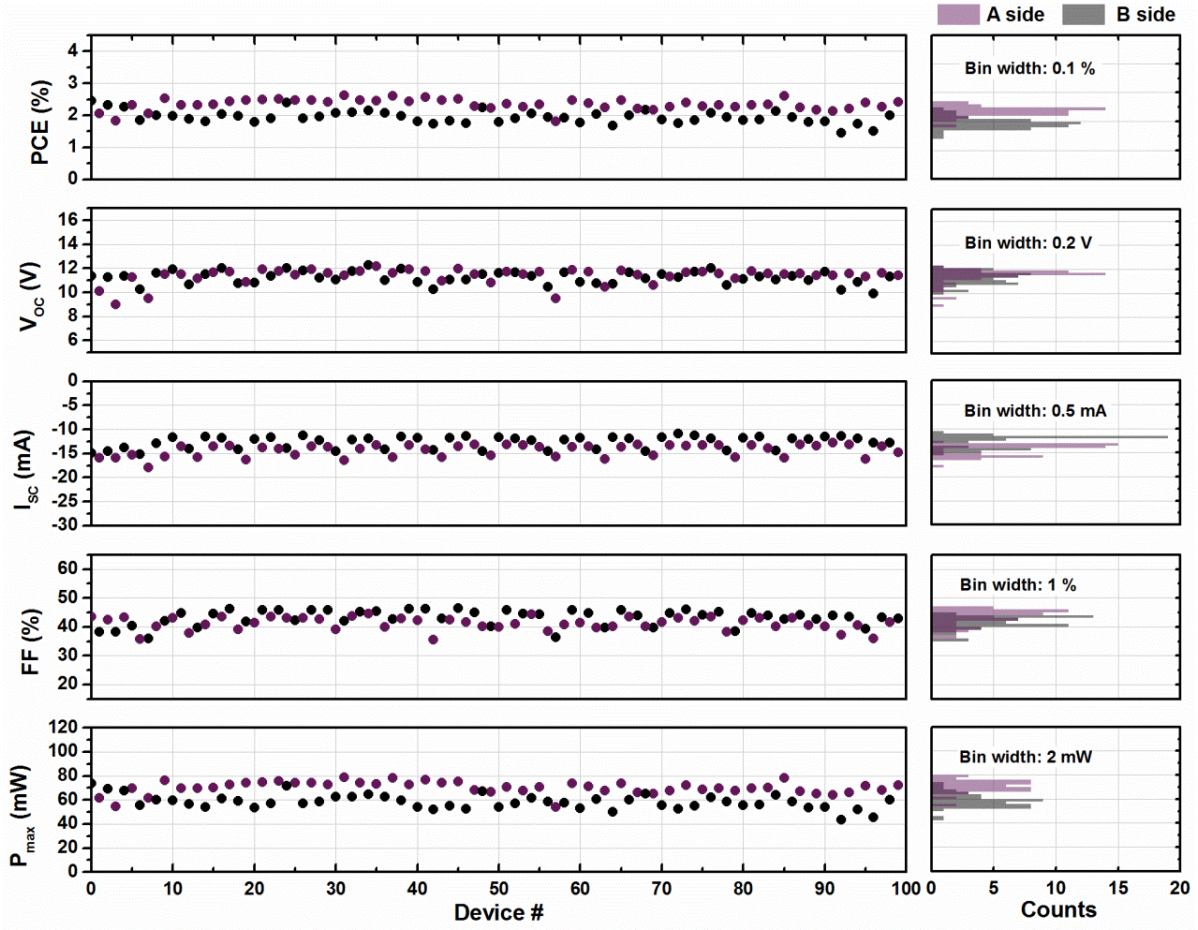

Figure 2.11 - Reproducibility of 100 C-OPV-F2 modules (50 A-side, 50 B-side) is shown in relation to the photovoltaic parameters. The histograms on the right highlight the differences between the two sides of the web and the relatively narrow distribution of performance.

Table 2.3 - The photovoltaic parameters for 100 C-OPV-F2 modules, from the two different sides of the web.

	PCE [%] A side	*PCE* [%] B side	V_{OC} [V] A side	V_{OC} [V] B side	I_{SC} [mA] A side	I_{SC} [mA] B side	*FF* [%] A side	*FF* [%] B side	P_{max} [mW] A side	P_{max} [mW] B side
Average	2.34	1.94	11.36	11.24	14.37	12.63	43.21	41.16	70.21	58.27
Standard deviation	0.17	0.20	0.65	0.53	1.26	1.28	2.74	2.24	5.20	5.95
Maximum	2.62	2.46	12.15	12.26	12.82	10.89	46.40	44.62	78.73	73.68

2.2.3. Carbon based OPV fully screen printed (C-OPV-SP)

One more printed collection of C-OPV modules had all the layers manufactured with the rotary screen printed technique. This batch was then named C-OPV screen printed: C-OPV-SP.

C-OPV-SP had the same structure, design and technical features as C-OPV-F1, the same bubble free foil as C-OPV-F2, but the two slot-die coated layers (ZnO and the active layer), were screen printed instead. ZnO was printed at 10 m min^{-1} with nominal wet thickness of 10 µm and dried using both ovens (90 °C and 140 °C). The P3HT:PCBM active layer was printed at 6-25 m min^{-1} to ensure thermal annealing of P3HT:PCBM, with a nominal wet thickness of 6-14 µm having both ovens at 140 °C. The inks concentrations were the same as for C-OPV-F1.

Figure 2.13 shows the C-OPV-SP module picture with the diffusion paths indicated by the blue arrows, and the IV-curve compared with C-OPV-F1. Using only printing techniques, the amount of ink used for the production of OPV is even more optimal and the avoidance of having ink passing through the edges of the module avoids paths for the oxygen and water. However, since the SP was not fully optimized, the active layer was not smooth and homogeneous; consequently the efficiency was lower than for the modules with the slot-die coated active layers. Figure 2.13 and Table 2.4 shows the parameters from the IV-curves of 100 C-OPV-SP modules corresponding to 17 printed motifs. It was measured one motif (6 modules) in intervals of 5 motifs. The differences of the A-side and the B-side can be observed, but less pronounced and possibly unnoticed for FF and V_{OC}. The reproducibility is very high and the standard deviations equal or rather lower than C-OPV-F1.

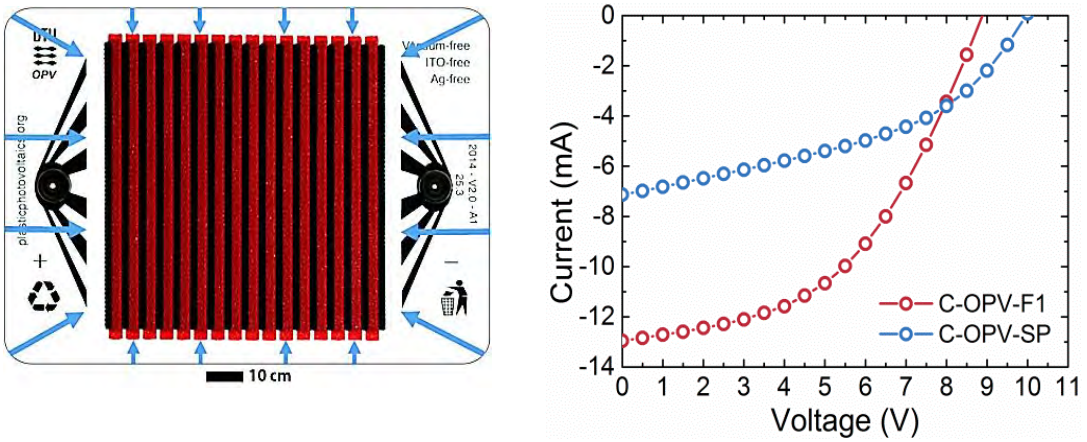

Figure 2.12 - Comparison of the diffusion path into the postcard sized C-OPV-F1 and C-OPV-SP (left). IV-curve of the C-OPV-F1 in comparison to the C-OPV-SP module (right).

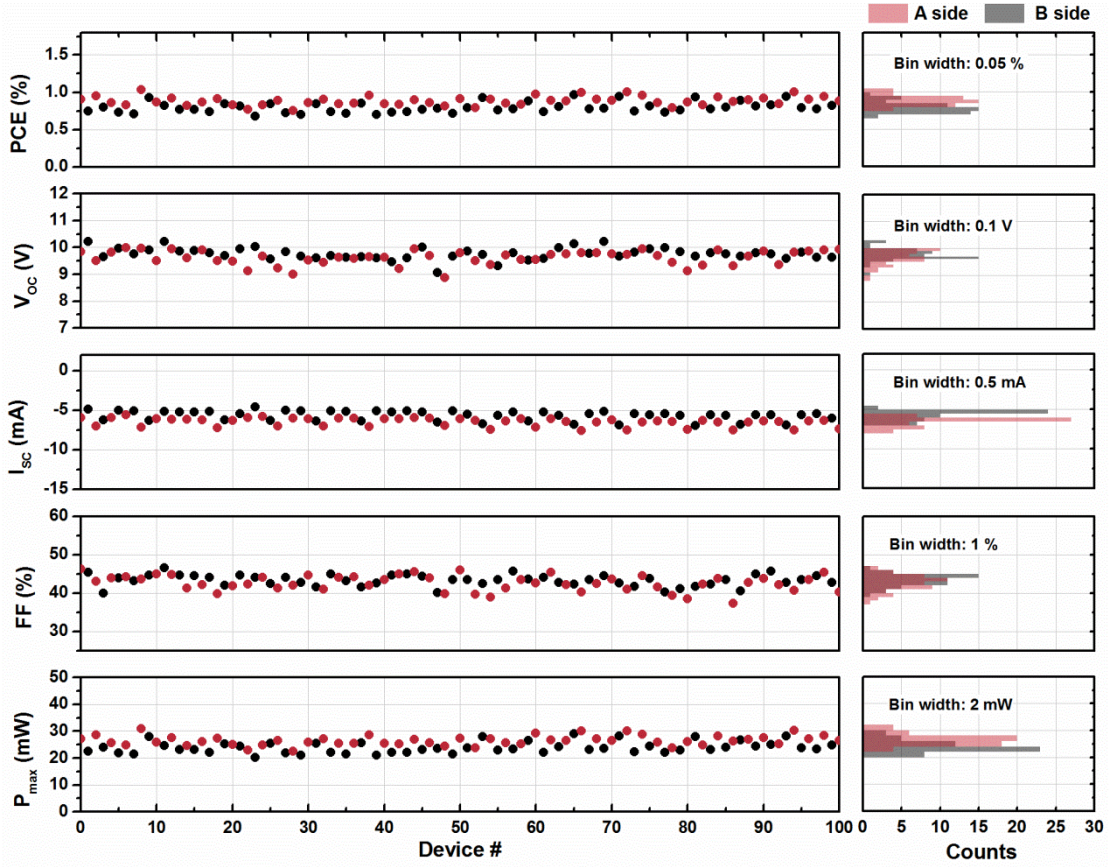

Figure 2.13 - The reproducibility of 100 C-OPV-SP modules (50 A side, 50 B side) is shown with respect to the photovoltaic parameters and is also presented in a histogram (right) to highlight the distinct differences between the two sides of the web but also the relatively narrow distribution of performance.

Table 2.4 - The photovoltaic parameters for 100 C-OPV-SP modules, from the two different sides of the web.

	PCE [%] A side	*PCE* [%] B side	V_{OC} [V] A side	V_{OC} [V] B side	I_{SC} [mA] A side	I_{SC} [mA] B side	*FF* [%] A side	*FF* [%] B side	P_{max} [mW] A side	P_{max} [mW] B side
Average	0.88	0.80	9.62	9.77	6.51	5.67	42.58	43.32	26.52	23.91
Standard deviation	0.06	0.07	0.27	0.22	0.55	0.62	2.07	1.52	1.82	2.15
Maximum	1.03	0.97	9.98	10.23	5.62	4.59	46.27	46.61	30.99	29.01

2.2.4. Carbon based OPV with low band gap active material (C-OPV-LB)

These C-OPV modules were manufactured with a low band gap polymer, PBDTTTz-4, as the donor material which molecular structure is shown in Figure 2.14. These modules are called C-OPV with low band gap active polymers: C-OPV-LB.

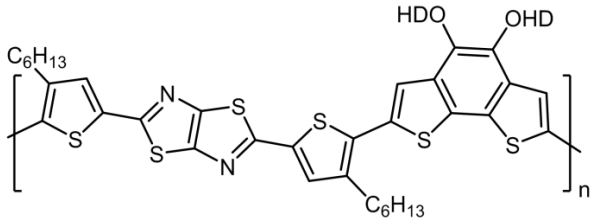

Figure 2.14 - PBDTTTz-4 chemical structure

C-OPV-LB had the same structure, design and technical features as C-OPV-F1 as with printing and coating techniques, speeds and inks, the same a bubble free foil as C-OPV-F2, but the active layer was

PBDTTTz-4:PCBM, with PBDTTTz-4 synthetized in house and PCBM purchased from Merck Chemicals Ltd. The ink had 1:1.5 ratio by weight, dissolved in CB:ODCB (4:1, by volume) with a concentration of 30–40 mg mL^{-1}. The active layer was slot-die coated at a speed of 1–5 m min^{-1} with a wet thickness ranging from 11 to 20 µm and dried at 90 °C, resulting in a dry thickness in the range of 240–600 nm. Figure 2.15 and Table 2.5 shows the parameters from the IV-curve of 100 C-OPV-LB modules corresponding to 33 printed motifs. The differences of the A-side and the B-side are noticed, but in the histograms the differences are pronounced only for V_{OC}. The reproducibility is high and the standard deviations slightly higher than C-OPV-F1.

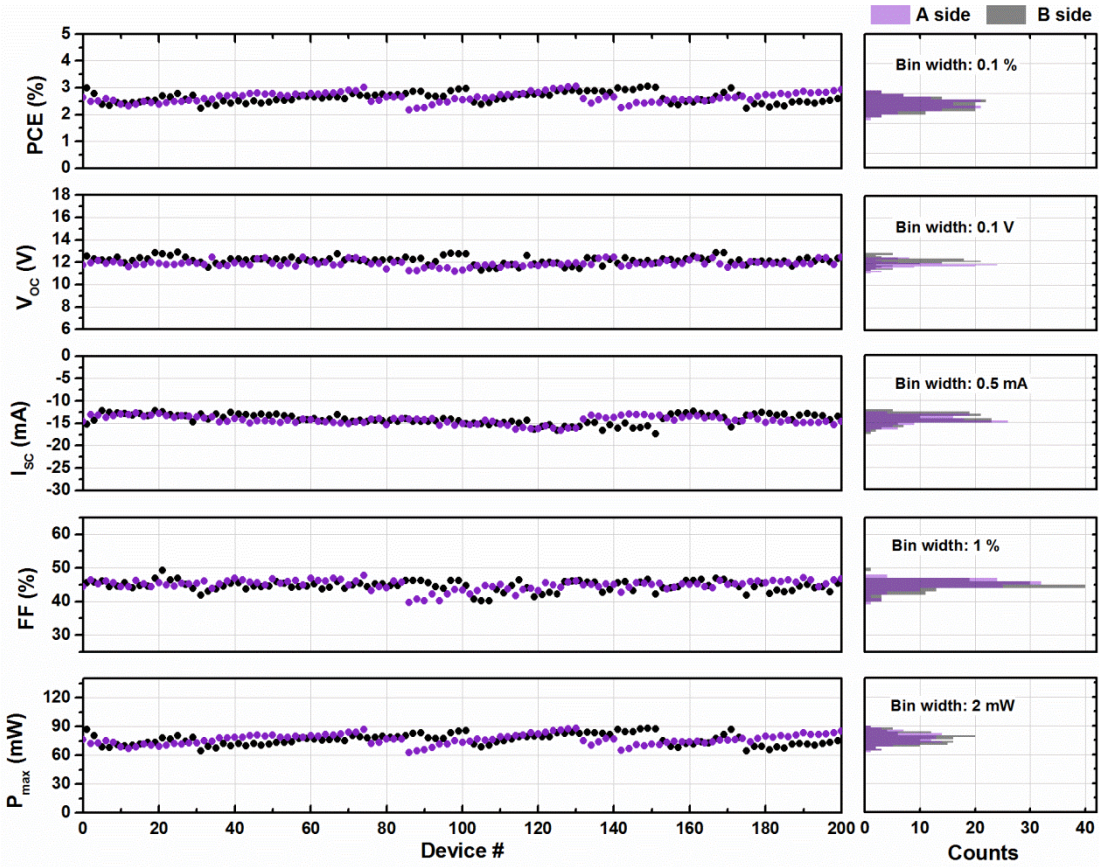

Figure 2.15 - Reproducibility of 200 C-OPV-LB modules (100 A-side, 100 B-side) is shown in relation to the photovoltaic parameters. The histograms on the right highlight the differences between the two sides of the web and the relatively narrow distribution of performance.

Table 2.5 - The photovoltaic parameters for 200 C-OPV-LB modules, from the two different sides of the web.

	PCE [%] A side	*PCE* [%] B side	V_{OC} [V] A side	V_{OC} [V] B side	I_{SC} [mA] A side	I_{SC} [mA] B side	*FF* [%] A side	*FF* [%] B side	P_{max} [mW] A side	P_{max} [mW] B side
Average	2.63	2.63	11.87	12.17	14.34	14.06	44.90	44.61	76.39	76.24
Standard deviation	0.19	0.20	0.28	0.34	0.89	1.15	1.50	1.56	5.38	5.84
Maximum	3.04	3.05	12.46	12.87	12.66	12.23	47.76	49.19	88.26	88.30

2.3.Freely available OPV distribution

The freeOPV platform was conceived to enable OPV module development of processing, testing of new materials, and also importantly the free distribution of OPVs to anybody with an interest [12,34]. A total of 8020 samples have been sent to 1883 individuals from 136 countries. The freeOPV had been distributed to school children in a very successful beginning, and used as part of the course material for

teaching purposes in the context of the massive open online courses (MOOCs) [35]. By the end of the distribution with the exhaustion of the modules, the majority of the shipments (~31%) were made to MOOC students.

The demography of freeOPV is of special importance as it shows how a future OPV product is likely to be distributed in the world. Figure 2.16 shows the distribution of the shipped Ag-OPV and C-OPV freeOPV throughout to all continents, bringing up that the management of the OPV end-of-life is challenging in many of the locations, demanding proper eco-design of the product in this concern. C-OPV was then successfully created in order to be disposed of as regular plastic waste and at the same time maintaining the performance and functionality as a teaching tool.

Figure 2.16 - Map showing the demography of 8020 freeOPV modules shipped around the world. Ag-OPVs are shown in red dots and C-OPVs as blue dots.

2.4.Conclusions

In this chapter we present details of the printing and coating techniques for manufacturing fully solution processed OPV using R2R machinery, which can be done without vacuum or clean room. It was accomplished by the reproducible production of vacuum-, ITO-, and silver-free solar cells in a fully packaged form using only R2R processing. The C-OPV is about one third cheaper than the previous freeOPV generation that contained Ag. It keeps the flexibility and the active area efficiency, and it makes the OPV modules environmentally safe. The replacement of Ag with carbon allows the same fast printing and coating not affecting the R2R production. The C-OPV production opens the door to new possible applications where Ag recycling is not manageable. The C-OPV modules lead the philosophy of truly green energy production and can even be disposed in a normal household waste for incineration or recycling. Compared with metals, C-OPV is likely the most sustainable choice for the electrode, which will be attested in the following chapter. The stability of the C-OPV modules is studied in Chapter 4.

2.5.References

1. Hösel, M.; Krebs, F. C. Large-scale Roll-to-Roll Fabrication of Organic Solar Cells for Energy Production, Technical University of Denmark, **2013**.

2. Hösel, M.; Angmo, D.; Krebs, F. C. Organic solar cells (OSCs). In *Handbook of organic materials for optical and (opto)electronic devices: Properties and applications*; Ostroverkhova, O., Woodhead Publishing, **2013**;

473.

3. Hösel, M.; Krebs, F. C. Large-scale roll-to-roll photonic sintering of flexo printed silver nanoparticle electrodes. *J. Mater. Chem.* **2012**, *22*, 15683.

4. Huebler, A. C.; Doetz, F.; Kempa, H.; Katz, H. E.; Bartzsch, M.; Brandt, N.; Hennig, I.; Fuegmann, U.; Vaidyanathan, S.; Granstrom, J.; Liu, S.; Sydorenko, A.; Zillger, T.; Schmidt, G.; Preissler, K.; Reichmanis, E.; Eckerle, P.; Richter, F.; Fischer, T.; Hahn, U. Ring oscillator fabricated completely by means of mass-printing technologies. *Org. Electron. physics, Mater. Appl.* **2007**, *8*, 480.

5. Huebner, C. F.; Carroll, J. B.; Evanoff, D. D.; Ying, Y.; Stevenson, B. J.; Lawrence, J. R.; Houchins, J. M.; Foguth, A. L.; Sperry, J.; Foulger, S. H. Electroluminescent colloidal inks for flexographic roll-to-roll printing. *J. Mater. Chem.* **2008**, *18*, 4942.

6. Kipphan, H. Handbook of Print Media. *Handb. Print Media* **2001**, 1173.

7. Roth, B.; Søndergaard, R. R.; Krebs, F. C. *Roll-to-roll printing and coating techniques for manufacturing large-area flexible organic electronics*; Elsevier Ltd, **2014**.

8. Yeo, J.-S.; Yun, J.-M.; Kim, S.-S.; Kim, D.-Y.; Kim, J.; Na, S.-I. Variations of cell performance in ITO-free organic solar cells with increasing cell areas. *Semicond. Sci. Technol.* **2011**, *26*, 34010.

9. Kim, T. S.; Na, S. I.; Oh, S. H.; Kang, R.; Yu, B. K.; Yeo, J. S.; Lee, J.; Kim, D. Y. All-solution-processed ITO-free polymer solar cells fabricated on copper sheets. *Sol. Energy Mater. Sol. Cells* **2012**, *98*, 168.

10. Andersen, T. R.; Dam, H. F.; Andreasen, B.; Hösel, M.; Madsen, M. V.; Gevorgyan, S. A.; Søndergaard, R. R.; Jørgensen, M.; Krebs, F. C. A rational method for developing and testing stable flexible indium- and vacuum-free multilayer tandem polymer solar cells comprising up to twelve roll processed layers. *Sol. Energy Mater. Sol. Cells* **2014**, *120*, 735.

11. Espinosa, N.; García-Valverde, R.; Urbina, A.; Krebs, F. C. A life cycle analysis of polymer solar cell modules prepared using roll-to-roll methods under ambient conditions. *Sol. Energy Mater. Sol. Cells* **2011**, *95*, 1293.

12. Krebs, F. C.; Hösel, M.; Corazza, M.; Roth, B.; Madsen, M. V.; Gevorgyan, S. A.; Søndergaard, R. R.; Karg, D.; Jørgensen, M. Freely available OPV-The fast way to progress. *Energy Technol.* **2013**, *1*, 378.

13. Søndergaard, R. R.; Hösel, M.; Krebs, F. C. Roll-to-Roll fabrication of large area functional organic materials. *J. Polym. Sci. Part B Polym. Phys.* **2013**, *51*, 16.

14. Krebs, F. C. Fabrication and processing of polymer solar cells: A review of printing and coating techniques. *Sol. Energy Mater. Sol. Cells* **2009**, *93*, 394.

15. Riemer, D. E. The Theoretical Fundamentals of the Screen Printing Process. *Microelectron. Int.* **1989**, *6*, 8.

16. Stephan F. Kistler; Peter M. Schweizer *Liquid Film Coating*; Springer Science+Business Media Dordrech, **1997**.

17. Chi-Feng Lin; Bo-Kai Wang; Carlos Tiu; Ta-Jo Liu On the Pinning of Downstream Meniscus for Slot Die Coating. *Adv. Polym. Technol.* **2013**, *32*, E249.

18. Nam, J.; Carvalho, M. S. Two-layer tensioned-web-over-slot die coating: Effect of operating conditions on coating window. *Chem. Eng. Sci.* **2010**, *65*, 4065.

19. Nam, J.; Carvalho, M. S. Flow in tensioned-web-over-slot die coating: Effect of die lip design. *Chem. Eng. Sci.* **2010**, *65*, 3957.

20. Krebs, F. C. All solution roll-to-roll processed polymer solar cells free from indium-tin-oxide and vacuum

coating steps. *Org. Electron.* **2009**, *10*, 761.

21. Krebs, F. C. Polymer solar cell modules prepared using roll-to-roll methods: Knife-over-edge coating, slot-die coating and screen printing. *Sol. Energy Mater. Sol. Cells* **2009**, *93*, 465.

22. Angmo, D.; Hösel, M.; Krebs, F. C. All solution processing of ITO-free organic solar cell modules directly on barrier foil. *Sol. Energy Mater. Sol. Cells* **2012**, *107*, 329.

23. Andreasen, B.; Tanenbaum, D. M.; Hermenau, M.; Voroshazi, E.; Lloyd, M. T.; Galagan, Y.; Zimmernann, B.; Kudret, S.; Maes, W.; Lutsen, L.; Vanderzande, D.; Würfel, U.; Andriessen, R.; Rösch, R.; Hoppe, H.; Teran-Escobar, G.; Lira-Cantu, M.; Rivaton, A.; Uzunoğlu, G. Y.; Germack, D. S.; Hösel, M.; Dam, H. F.; Jørgensen, M.; Gevorgyan, S. a; Madsen, M. V; Bundgaard, E.; Krebs, F. C.; Norrman, K. TOF-SIMS investigation of degradation pathways occurring in a variety of organic photovoltaic devices--the ISOS-3 inter-laboratory collaboration. *Phys. Chem. Chem. Phys.* **2012**, *14*, 11780.

24. Gevorgyan, S. A.; Madsen, M. V.; Dam, H. F.; Jørgensen, M.; Fell, C. J.; Anderson, K. F.; Duck, B. C.; Mescheloff, A.; Katz, E. A.; Elschner, A.; Roesch, R.; Hoppe, H.; Hermenau, M.; Riede, M.; Krebs, F. C. Interlaboratory outdoor stability studies of flexible roll-to-roll coated organic photovoltaic modules: Stability over 10,000h. *Sol. Energy Mater. Sol. Cells* **2013**, *116*, 187.

25. Zimmermann, Y.-S.; Schäffer, A.; Corvini, P. F.-X.; Lenz, M. Thin-film photovoltaic cells: long-term metal(loid) leaching at their end-of-life. *Environ. Sci. Technol.* **2013**, *47*, 13151.

26. Espinosa, N.; Zimmermann, Y.-S.; dos Reis Benatto, G. A.; Lenz, M.; Krebs, F. C. Outdoor fate and environmental impact of polymer solar cells through leaching and emission to rainwater and soil. *Energy Environ. Sci.* **2016**, *9*, 1674.

27. Hoppe, H.; Seeland, M.; Muhsin, B. Optimal geometric design of monolithic thin-film solar modules: Architecture of polymer solar cells. *Sol. Energy Mater. Sol. Cells* **2012**, *97*, 119.

28. dos Reis Benatto, G. A.; Corazza, M.; Roth, B.; Schütte, F.; Rengenstein, M.; Gevorgyan, S. A.; Krebs, F. C. Inside or Outside? Linking Outdoor and Indoor Lifetime Tests of ITO-Free Organic Photovoltaic Devices for Greenhouse Applications. *Energy Technol.* **2016**, doi: 10.1002/ente.201600335.

29. Krebs, F. C.; Espinosa, N.; Hösel, M.; Søndergaard, R. R.; Jørgensen, M. 25th Anniversary Article: Rise to Power - OPV-Based Solar Parks. *Adv. Mater.* **2014**, *26*, 29.

30. Espinosa, N.; Lenzmann, F. O.; Ryley, S.; Angmo, D.; Hösel, M.; Søndergaard, R. R.; Huss, D.; Dafinger, S.; Gritsch, S.; Kroon, J. M.; Jørgensen, M.; Krebs, F. C. OPV for mobile applications: an evaluation of roll-to-roll processed indium and silver free polymer solar cells through analysis of life cycle, cost and layer quality using inline optical and functional inspection tools. *J. Mater. Chem. A* **2013**, *1*, 7037.

31. Krebs, F. C.; Fyenbo, J.; Tanenbaum, D. M.; Gevorgyan, S. A.; Andriessen, R.; van Remoortere, B.; Galagan, Y.; Jørgensen, M. The OE-A OPV demonstrator anno domini 2011. *Energy Environ. Sci.* **2011**, *4*, 4116.

32. Larsen-Olsen, T. T.; Søndergaard, R. R.; Norrman, K.; Jørgensen, M.; Krebs, F. C. All printed transparent electrodes through an electrical switching mechanism: A convincing alternative to indium-tin-oxide, silver and vacuum. *Energy Environ. Sci.* **2012**, *5*, 9467.

33. dos Reis Benatto, G. A.; Roth, B.; Madsen, M. V.; Hösel, M.; Søndergaard, R. R.; Jørgensen, M.; Krebs, F. C. Carbon: The Ultimate Electrode Choice for Widely Distributed Polymer Solar Cells. *Adv. Energy Mater.* **2014**, *4*, 1400732.

34. Andersen, T. R.; Dam, H. F.; Hösel, M.; Helgesen, M.; Carle, J. E.; Larsen-Olsen, T. T.; Gevorgyan, S. a; Andreasen, J. W.; Adams, J.; Li, N.; Machui, F.; Spyropoulos, G. D.; Ameri, T.; Lemaitre, N.; Legros, M.; Scheel, A.; Gaiser, D.; Kreul, K.; Berny, S.; Lozman, O. R.; Nordman, S.; Valimaki, M.; Vilkman, M.;

Sondergaard, R. R.; Jorgensen, M.; Brabec, C. J.; Krebs, F. C. Scalable, ambient atmosphere roll-to-roll manufacture of encapsulated large area, flexible organic tandem solar cell modules. *Energy Environ. Sci.* **2014**, *7*, 2925.

35. Bundgaard, E.; Krebs, F.; Jorgensen, M.; Madsen, M. Organic Solar Cells - Theory and Practice - Technical University of Denmark (DTU) | Coursera https://www.coursera.org/learn/solar-cell (accessed Nov 25, **2016**).

Chapter 3

The best electrode choice for more environmentally friendly OPV

This chapter presents the life-cycle assessment methodology for attesting the environmental friendliness of carbon based OPV (C-OPV) compared with OPV based on metal electrodes, such as silver (Ag), copper (Cu) and aluminium (Al). Life cycle assessment (LCA) methodology is used for it and a complete "cradle-to-grave" life cycle is performed, considering three disposal scenarios.

3.1.Profile of four electrode materials

For any new technology aiming at large scale production, the challenge is to find the most environmentally sustainable solution, with low environmental impacts from its manufacturing through its operation up to its final disposal. With the intention of quantifying the impact on the environment, life-cycle assessment (LCA) ecodesign can work as a guide for building environmentally friendly OPV [1].

Printed metal grids in R2R manufacturing of flexible OPV modules having silver grids as both front and back electrode is one of the most promising attempts to replace ITO [2,3]. Silver (Ag) can be printed in a thin pattern allowing the transmission of light, and with a transparent layer of PEDOT:PSS, still maintain good conductibility as front electrode. For the back electrode the same configuration can be used, with PEDOT:PSS having the role of a hole transporting layer. This architecture leads to more efficient and environmentally friendly devices than those using ITO [4,5]. Yet, Ag is a scarce and expensive material bringing limitations to the large-scale production of OPV. Although the replacement of ITO using Ag makes the materials impact in OPV much more balanced [6], a recent study indicated that nearly all environmental impacts of an entire solar park installation using OPV modules with Ag electrodes were dominated by the contribution from the silver electrodes [1]. Therefore, in this section, the substitution of silver with three other materials: carbon (C), aluminium (Al) and copper (Cu) is explored.

In the Table 3.1, the current reserves, prices, and properties like recyclability, deposition, and conductivity of the four compared electrode materials are presented.

Table 3.1 - Reserves, prices and recyclability of silver, carbon (graphite), aluminium and copper

	Silver [7–12]	**Carbon** [13,14]	**Aluminium** [15–17]	**Copper** [18,19]
Reserves (million tons)	0.57	130-800	28000	720
Price (US$/Kg)	525.99	1.0	1.85	5.7
Recyclability	High	Low. Usually recycled with other similar PET based products or safely disposed in normal	High. Around 18 million tonnes/yr. Ca. 75% of the aluminium ever mined is still in use	Very high (1/3) remelted and used directly without losing any property
Deposition/ Printability	• Vacuum-free processing • Screen, flexo printing and several other printing techniques • No need for curing process	• Screen-printing in air • No need of special treatments	• Evaporated/Printed in vacuum chambers -to prevent the oxidation	• Deposited in controlled atmosphere • Cured under very high energy light or temperature
Conductivity (S/m)	6.30×10^7	2.00×10^5 to 3.00×10^5	3.50×10^7	5.69×10^7

All considered materials can technically be printed using grid-patterns in R2R processes and have exceptional properties to be applied in OPV devices, but also some disadvantages. Ag has unique properties of ductility, reflectivity and is the most conductive of all metals, although its high cost and scarcity impose a high recycling rate. It can be easily recycled from the OPV device through shredding, dissolution, and precipitation of AgCl [20]. Using Ag over ITO means an energy payback time (EPBT) four times lower for the same performance (2% PCE) corresponding to 0.5 years [6]. Replacing Ag with C the EPBT goes even 20% lower, is 3 times cheaper and may indicate very low environmental impacts. For this reason carbon based OPV (C-OPV) have been proved being the “ultimate electrode” due to its advantages concerning material availability, cost and easy deposition [21]. C inks for electronics usually contain graphite and carbon black, and can be printed using rotary screen printing. Al is the most abundant metal in earth crust; it is light, cheap and has good mechanical properties for flexible devices. The mining and extraction of aluminium from bauxite is a highly energy demanding process, which requires recycling practices, just as the case of silver. Cu, due its good conductivity, abundance, corrosion resistance and relatively low cost, is a widely used metal for wiring and is also a suitable candidate for electrodes in OPV modules. Al and Cu, to be conductive in a thin printed layer, need to be cured under high temperatures, which can limit the use of flexible substrates if not compatible with the option of high energy curing light.

3.2.Methodology and experimental procedure

Complete or cradle-to-grave life cycle assessment (LCA) has been applied to a solar park installation of OPV modules using the four different electrodes. The functional unit (FU) is defined as the supply of 1 kWh of electricity. FU is a quantitative description of the systems that guarantees functionality equivalence for comparisons. Large scale ITO-free modules have already been tested under ISOS protocols and under harsh weather conditions in Denmark with operational lifetime outdoors over 2 years with a simple low-cost barrier [22]. Therefore, the same lifetime performance is expected for aluminium and copper OPV devices. The balance of the system (BOS), i.e. inverter, structure, cabling and all components needed for the full deployment of the OPV modules can be disregarded, since they are the same for all electrode options per FU.

The boundaries of the system are described in Figure 3.1, where the main processes (in orange) are the manufacturing (in Denmark), including the raw materials, energy (in green) and transport (in blue), followed by the usage and the disposal stages. The two main disposal alternatives explored are recycling and incineration, while landfill has a very low percentage in a Danish average waste management scenario (see Table 3.3). Using system expansion in the LCA model, the materials and energy recovered at the recycling and incineration, respectively, replaced certain amount of virgin materials production and energy (electricity and thermal) production.

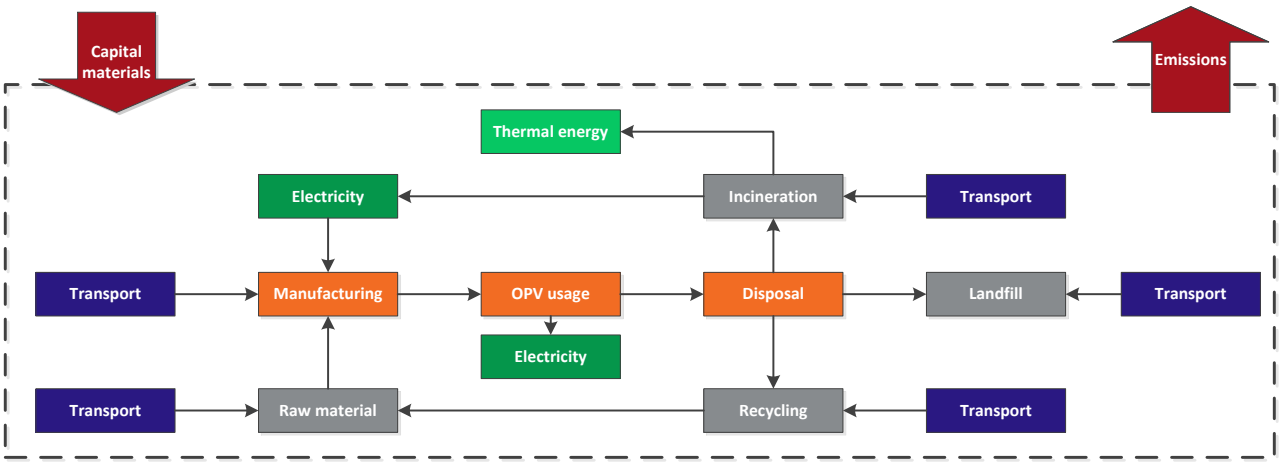

Figure 3.1 - System boundaries of the OPV modules LCA.

The production of the OPV modules is based on a R2R processing scenario (Figure 3.1) under ambient conditions. The processes included flexography printing, slot die coating, and rotary screen printing with speeds up to 20 m min^{-1}. The electrode materials were a silver nanoparticle ink (Novacentrix PChem PFI-722) for the front electrode and silver flake paste (Dupont 5025) for the back electrode. Carbon ink was purchased from Acheson (Electrodag PF-407), that contains graphite and carbon black. Aluminium ink was a recipe from a project partner (VTT Technical Research Centre of Finland), where a ball mill is used to convert the aluminium into flakes for the ink. Copper oxide based ink was obtained from Novacentrix (ICI-021). The remaining materials of the OPV stack are the same as the C-OPV-F1 described in the Subchapter 2.2.1. The modules were printed on a 305 mm wide PET-based barrier foil purchased from Amcor and were encapsulated using the process and the materials described in Section 2.1.2. In Table 3.2, a summary of the technical characteristics of the modules with different electrodes is shown. Figure 3.2 displays the layer stack, the printing sequence, and the correspondent printing/coating technique applied for the four electrodes modules. The layout of the modules can be seen in Figure 3.3.

Table 3.2 - Characteristics of the four electrodes OPV systems [23].

	Silver	Carbon	Aluminium	Copper
Cell efficiency	2%	2%	2%	2%
Geometric fill factor*	50%	36.8%	50%	50%
Module efficiency	1%	0.7%	1%	1%
Electrode	Front/Back	Back	Front	Front
Solid content in the ink	60% Ag	29% C	40% Al	50% Cu

*Based on the current design of fabricated modules at DTU. Not yet fully optimized

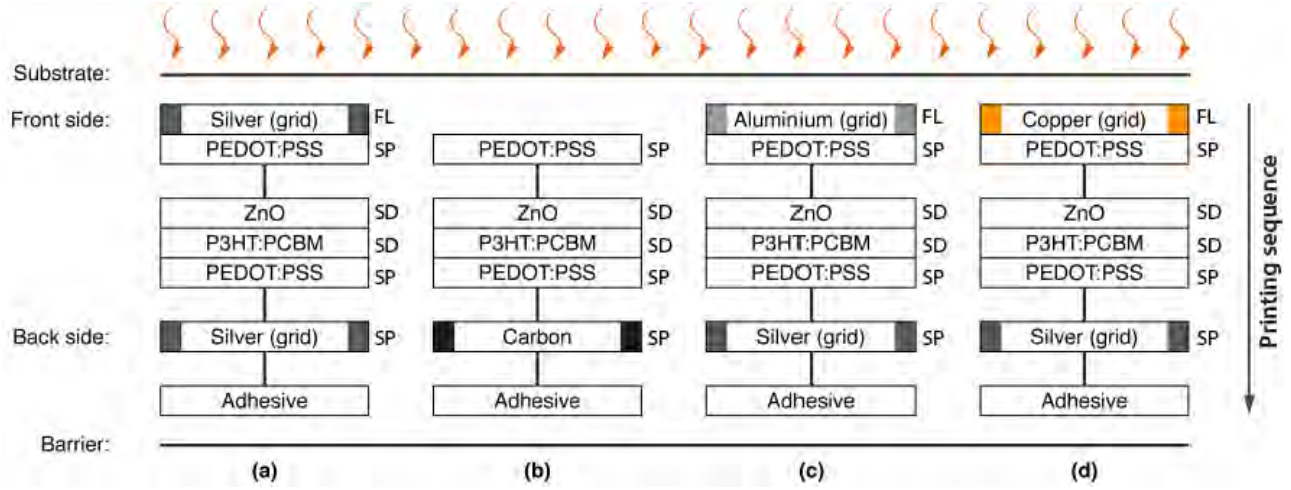

Figure 3.2 - Layers stack of the four electrodes modules. FL: flexo printing; SD: Slot-die coating; SP: Rotary screen printing. Reprinted with permission from [23].

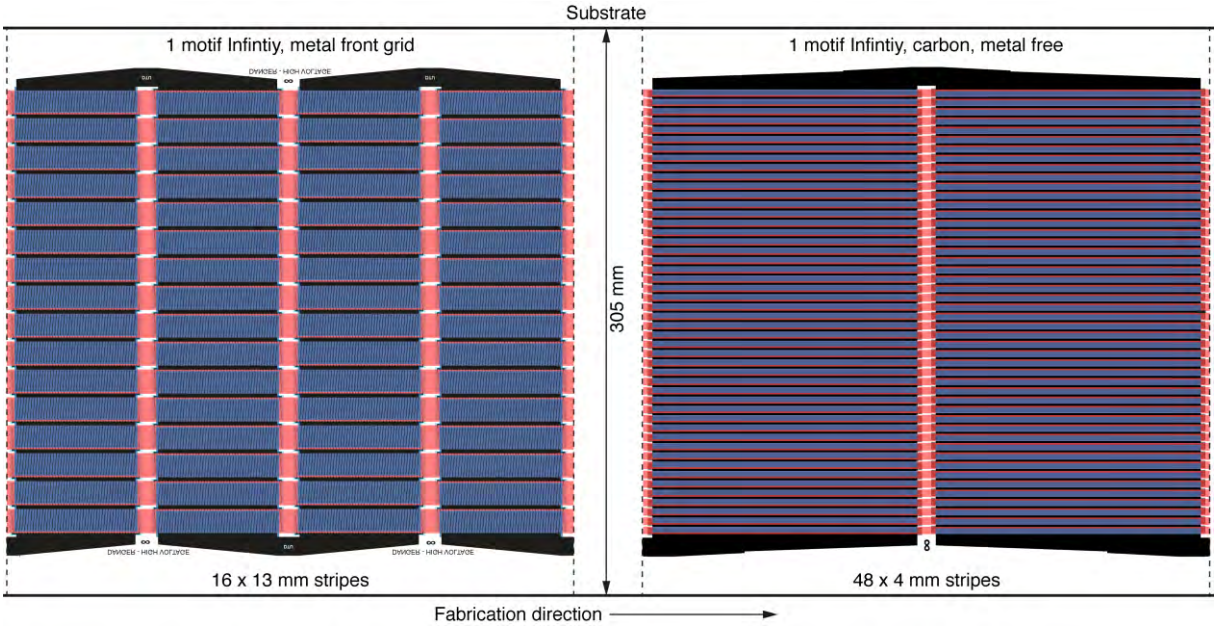

Figure 3.3 - Layout of the fabricated modules used for the calculations in this study, on the left the pattern for the metal grids (Ag, Al, Cu). Reprinted with permission from [23].

There were challenges with the processing of aluminium and copper inks. The CuO electrode had to have high thickness in order for the copper oxide to be reduced and be conductive. The Al electrode needed to be processed under inert atmosphere. Consequentially, these two metal grids have a pure theoretical evaluation for a vacuum free production. Moreover, CuO ink reduction by photonic sintering would destroy the highly light absorbing pre-printed layers and could not be used as back electrode.

For raw materials and background data, life cycle inventories from the ecoinvent 3.1 database [24] were used combined with the primary data of materials and energy needed for the manufacture of the OPV modules. The modelling used is based on the detailed model for silver based OPV (Ag-OPV) [1] adapted for the new electrodes materials and processes. The C-OPV is based on the postcard principle from Chapter 2 upscaled to the layout presented in Figure 3.3.

The disposal of the OPV modules was considered in three scenarios detailed in Table 3.3, which was applied before in the LCA of Ag-OPV [1]. They are defined as i) Recycling route (DK-1); ii) Incineration route (DK-2); and iii) Average route (DK-3), with the municipal solid waste management landscape for Denmark.

Table 3.3 - Modelling of disposal scenarios [1,23]

Scenario	Description	Modelling and assumptions
DK-1 Recycling	Solar cells are assumed to be collected by a specialized company, which will extract valuable materials (PET + metals). Representing a scenario in case of handling of solar cells as industrial or hazardous waste.	Recycling pathways with PET recovered from delamination (sent to recycling) and silver recovered from acid treatment. Incineration of the mixed plastics and remains with energy recovery.
DK-2 Incineration	Due to the high caloric value from plastic content, solar cells are assumed to be collected and directly sent to municipal incineration. Representing controlled deployment.	Incineration modelled as PET municipal incineration (energy recovery); no differentiation due to composition of solar cells.
DK-3 Average mix	29% Recycling; 69% Incineration; 2% Landfill. Representing a large and diffuse deployment of solar cells in Denmark.	Recycling path follows scenario DK-1. Incineration path follows scenario DK-2. Landfill is modelled as landfill of PET with amount of metals corrected to match content in the OPV module.

3.3.Environmental impact assessment

Emissions and resource consumptions from the OPV life cycle are translated into potential impact indicator scores using life cycle impact assessment (LCIA) methods as the International Reference Life Cycle Data System (ILCD) methodology (ILCD 2011 v1.04 [25], in SimaPro 8.0.4.26 software [26]). This method was chosen as it is recommended for the best practice of LCIA [27]. Human health, natural resources, and ecosystems quality are the agreed areas of protection in LCA community, which in ILCD method is expressed in the midpoint impact score categories presented in Figure 3.4. They are climate change; ozone depletion; human toxicity separated in carcinogenic and non-carcinogenic effects (meaning the toxicity of chemicals to human health); respiratory inorganics (impacts caused by inorganics via formation of particulate matters); ionizing radiation impacting human health; photochemical ozone formation; acidification potential; terrestrial, freshwater and marine eutrophication; freshwater ecotoxicity (toxicity of chemicals on freshwater ecosystems); land use; water and non-renewable resources depletion. The impact scores of the four systems are expressed in the three disposal scenarios and only manufacturing.

At first sight, the results can be well distinguished between the metal-based modules (Ag, Al and Cu based) and the C-OPV modules, where the metal-based present the highest environmental impact scores. In climate change, ozone depletion and water resource depletion, metal-based OPV modules are 2 to 5 times higher, while all other impact indicator scores are generally one order of magnitude higher than the C-OPV modules. The difference between metal-based and carbon reach up to two orders of magnitude for non-renewable resource depletion and human toxicity. The contribution of Ag to the total impact stands out due to its relatively high scarcity, high toxicity when emitted to the environment, and its mining and production processes which have important energy requirements. The production of metal-based modules itself has significantly higher impact scores than the carbon, with the highest contribution coming from the back electrode, which consists of Ag in all of them. The substitution of the back metal electrode with a low-impact material can have very significant environmental improvement to an energy production system and should be prioritized by OPV eco-designers.

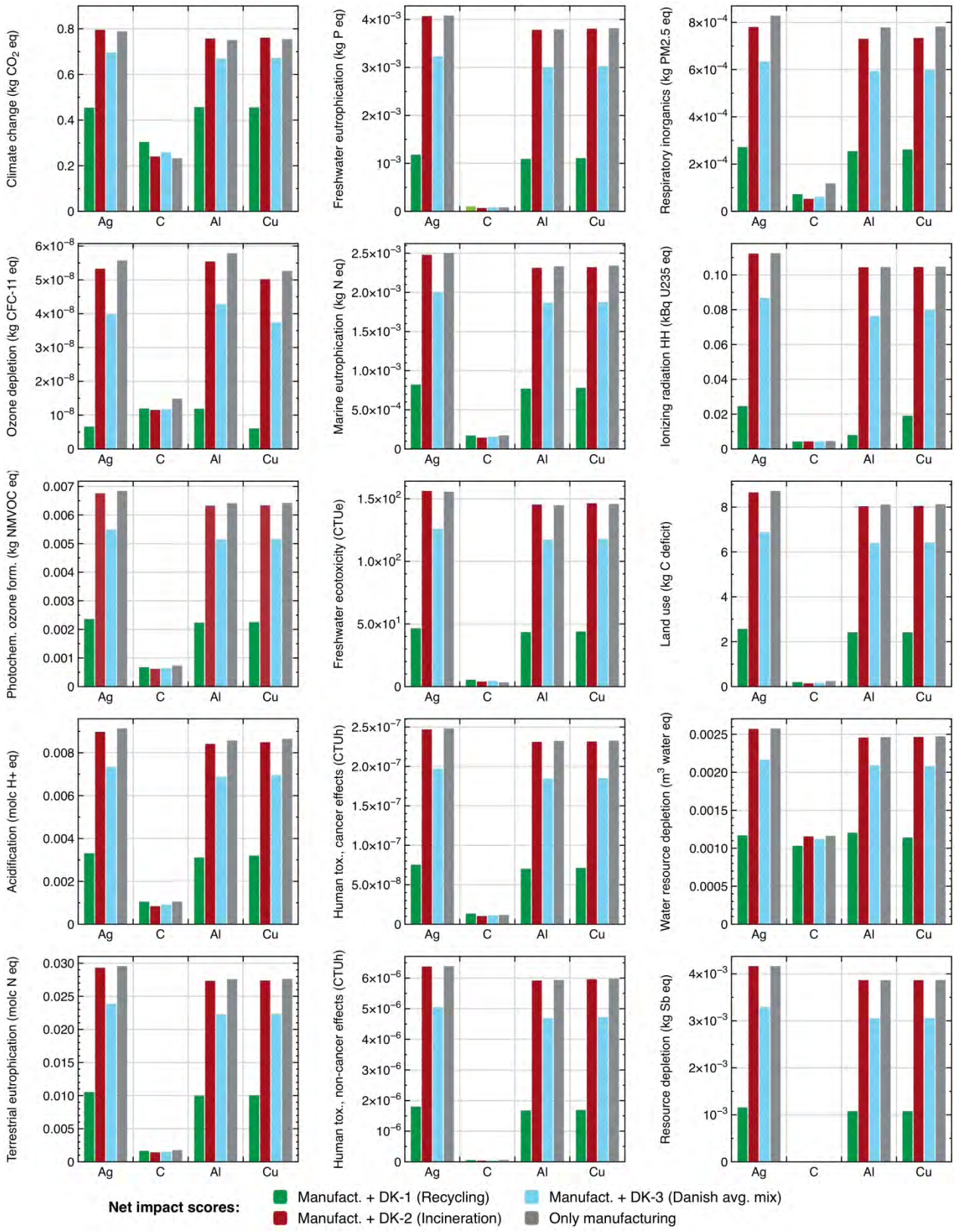

Figure 3.4 - Impact scores comparison for 1 kWh OPV modules with the four different electrodes: Ag, C, Al and Cu. Reprinted with permission from [23].

The disposal options recycling and incineration can greatly affect the final environmental profile; the recovery of materials and energy can compensate the main impacts from the manufacture. For metal-based modules, recycling is the most beneficial option as it saves impacts from the production of virgin metals. Also because the recovery of metals is relatively efficient (around 72% [1]). Recycling C-OPV modules, on the contrary, have nuanced effects on the impact scores when recycled. OPV printed layers are very thin, 80 to 90% of the OPV weight is correspondent to PET. For the four electrodes in general, the recycling of polymers, avoiding the production of new ones, is advantageous over incineration with energy recovery if the recycling rates are close to 100% [28]. Although, many impact categories scored higher when carbon modules are recycled than when they are incinerated with energy recovery. The high efficiency of Danish incinerators may also contribute to these results [29]. For the average scenario (29% recycling, 69% incineration and 2% landfilling) the scores stay in between the scores for recycling and incineration for the four electrodes options, as it was expected.

3.4.Conclusions and remarks

The results indicate that if high-value materials such as metals are involved, recycling should be prioritized, saving not only the extraction of scarce resources and economical value, but also leading to a desirable decrease of environmental burden. This was exactly the case for OPV with metal-based electrodes. Take-back systems could be established for this propose, bringing the recycling responsibility to the manufacturer.

After comparatively exploring the four electrode choices for OPV, the metal electrodes, i.e. Ag, Al and Cu, perform considerably worse than C-OPV modules in all environmental impact indicators. Metals (Ag, Al and Cu) stand for being major contributors to the environmental burden of the OPV modules. Therefore, their substitution for abundant and low impact materials, if still matching low sheet resistivity and vacuum free R2R printing, such as carbon, should be highly recommended to be further investigated by designers and researchers in the field. Additional strategies can include the reduction of the amount of material used in the electrodes, maintaining its technical proprieties.

⇦ Silver	Carbon ⇨
Low usage	Moderate usage
High conductivity	Low conductivity
Higher performance	Low performance
High active area cells	Low active area cells [a]
Toxicity problem	Non toxic
Scarce	Abundant
High cost	Low cost
High recyclability [b]	Highly recyclable

[a] Narrower stripes are required; [b] Limited to high degree of collection

Figure 3.5 - List with the advantages and disadvantages of silver and carbon based postcard modules. Adapted with permission from [23].

In Figure 3.5 a list of advantages and disadvantages of Ag and C-OPV modules are presented. C-OPV modules are designed taking into consideration the lower conductivity of carbon and the proper performance of the PEDOT:PSS alone as front electrode. These factors impose that the C-OPV active area has to be smaller. The external contacts and series connection in C-OPV modules are directly reliant on the highly hydrophilic PEDOT:PSS, consequently the edge sealing become even more important. Module efficiency per active area in C-OPV is correspondent to Ag-OPV modules, however the area per module is smaller for C-OPV modules since the area usage is not optimal. From the results in the previous subchapter, C-OPV modules are good candidates to be incinerated and energy can be recovered. In comparison with the metal electrode based modules, the harm is also lower the case they would end up their lives disposed in landfills or in an uncontrolled environment.

Table 3.4 shows the comparison of the impact scores for C-OPV modules produced at the pilot-scale presented in this chapter, with 1% efficiency, and traditional silicon photovoltaics (c-Si PV) manufactured in optimised production and large volumes. Comparing the production of 1 kWh from both PV panels, C-OPV modules with much lower efficiency (consequently, much more material/area was needed to produce 1 kWh), have almost all impact categories lower than those for c-Si PV panels. Only climate change impact category shows higher results, which most probably would be different if C-OPV production grows into optimised large volume as c-Si PV is produced. The impact scores from c-Si PV panels surpass largely the C-OPV in a range of 1.6-8.5 times higher for the remaining environmental impact categories. The high impact score for resource depletion of c-Si PV panels comes from the various metals required in their production.

Table 3.4 - Results of the impact assessment for 1 kWh produced from a single-Si wafer photovoltaic panel (5.41E-4 m^2) and C-OPV [23]..

Impact categories	c-Si PV	C-OPV	% Increase over C-OPV production
Climate change (kg-CO_2eq/pers)	1.79E-01	2.32E-01	77%
Ozone depletion (kg CFC-11 eq)	2.51E-08	1.48E-08	169%
Photochemical ozone formation (kg NMVOC eq)	7.52E-04	7.30E-04	169%
Acidification (mol H+ eq)	1.50E-03	1.05E-03	255%
Terrestrial eutrophication (mol N eq)	2.23E-03	1.76E-03	170%
Freshwater eutrophication (kg-Peq/pers)	1.37E-04	7.98E-05	472%
Marine eutrophication (kg-Neq/pers)	2.27E-04	1.71E-04	103%
Freshwater ecotoxicity (CTUe/pers)	3.74E+00	3.30E+00	143%
Human toxicity. cancer effects (CTUh/pers)	1.97E-08	1.17E-08	127%
Human toxicity. non-cancer effects (CTUh/pers)	1.50E-07	5.88E-08	172%
Respiratory inorganics (kg-PM2.5eq/pers)	2.00E-04	1.18E-04	132%
Ionizing radiation (kBq-U235eq/pers)	2.12E-02	4.50E-03	113%
Land use (kg C deficit)	2.84E-01	2.38E-01	119%
Water resource depletion (m^3 water)	2.12E-03	1.16E-03	182%
Resource depletion (kg-Sbeq/pers)	6.29E-02	7.35E-06	856%

Compared with metals, carbon based OPV is by far the most environmentally sustainable choice for the electrode. Although its geometry restricts their power per module, the installation of larger areas should produce the satisfactory amounts of energy. Ag-OPV could be an environmentally sustainable option with a posterior recycling.

The research efforts presented in this chapter highly recommend the production for OPV with metal free-electrodes or significantly lowering the amounts of metal when feasible keeping the technical and PV proprieties as conductivity, flexibility, and efficiency. Recent efforts have been also presented in this second strategy with the use of Ag nanowires (AgNW) [30]. In this context, the eco-design of electrodes should go

together with improvements in printing for a better area coverage and more efficient energy production, which will automatically lower the environmental footprint per kWh of the OPV technology.

3.5.References

1. Espinosa, N.; Laurent, A.; Krebs, F. C. Ecodesign of organic photovoltaic modules from Danish and Chinese perspectives. *Energy Environ. Sci.* **2015**, *8*, 2537.

2. Hösel, M.; Søndergaard, R. R.; Jørgensen, M.; Krebs, F. C. Fast Inline Roll-to-Roll Printing for Indium-Tin-Oxide-Free Polymer Solar Cells Using Automatic Registration. *Energy Technol.* **2013**, *1*, 102.

3. Sommer-Larsen, P.; Jørgensen, M.; Søndergaard, R. R.; Hösel, M.; Krebs, F. C. It is all in the Pattern-High-Efficiency Power Extraction from Polymer Solar Cells through High-Voltage Serial Connection. *Energy Technol.* **2013**, *1*, 15.

4. Espinosa, N.; García-Valverde, R.; Urbina, A.; Lenzmann, F.; Manceau, M.; Angmo, D.; Krebs, F. C. Life cycle assessment of ITO-free flexible polymer solar cells prepared by roll-to-roll coating and printing. *Sol. Energy Mater. Sol. Cells* **2012**, *97*, 3.

5. Emmott, C. J. M.; Urbina, A.; Nelson, J. Environmental and economic assessment of ITO-free electrodes for organic solar cells. *Sol. Energy Mater. Sol. Cells* **2012**, *97*, 14.

6. Espinosa, N.; Hösel, M.; Angmo, D.; Krebs, F. C. Solar cells with one-day energy payback for the factories of the future. *Energy Environ. Sci.* **2012**, *5*, 5117.

7. Grandell, L.; Thorenz, A. Silver supply risk analysis for the solar sector. *Renew. Energy* **2014**, *69*, 157–165.

8. Helgesen, M.; Carlé, J. E.; Andreasen, B.; Hösel, M.; Norrman, K.; Søndergaard, R.; Krebs, F. C. Rapid flash annealing of thermally reactive copolymers in a roll-to-roll process for polymer solar cells. *Polym. Chem.* **2012**, *3*, 2649.

9. Yu, J.-S.; Kim, I.; Kim, J.-S.; Jo, J.; Larsen-Olsen, T. T.; Søndergaard, R. R.; Hösel, M.; Angmo, D.; Jørgensen, M.; Krebs, F. C. Silver front electrode grids for ITO-free all printed polymer solar cells with embedded and raised topographies, prepared by thermal imprint, flexographic and inkjet roll-to-roll processes. *Nanoscale* **2012**, *4*, 6032.

10. Krebs, F. C. Fabrication and processing of polymer solar cells: A review of printing and coating techniques. *Sol. Energy Mater. Sol. Cells* **2009**, *93*, 394.

11. George, M. W. Silver, Mineral Commodity Summaries http://minerals.usgs.gov/minerals/pubs/commodity/silver/mcs-2016-silve.pdf (accessed Dec 15, **2016**).

12. COMEX - CME Group Index Mundi - Silver Monthly Price - US Dollars per Metric Ton http://www.indexmundi.com/commodities/?commodity=fish-meal&months=60 (accessed Dec 15, **2016**).

13. USGS Graphite Natural statistics, mineral commodity summaries http://minerals.usgs.gov/minerals/pubs/commodity/graphite/mcs-2014-graph.pdf (accessed Dec 15, **2016**).

14. Media, N. G. Graphite Pricing http://northerngraphite.com/graphite-pricing/ (accessed Dec 15, **2016**).

15. Norgate, T. E.; Jahanshahi, S.; Rankin, W. J. Assessing the environmental impact of metal production processes. *J. Clean. Prod.* **2007**, *15*, 838.

16. COMEX - CME Group Index Mundi - Aluminum Monthly Price - US Dollars per Metric Ton http://www.indexmundi.com/commodities/?commodity=aluminum (accessed Dec 15, **2016**).

17. E. Lee Bray Bauxite and alumina https://minerals.usgs.gov/minerals/pubs/commodity/bauxite/mcs-

2016-bauxi.pdf (accessed Dec 15, **2016**).

18. Mark Brininstool Copper http://minerals.usgs.gov/minerals/pubs/commodity/copper/mcs-2016-coppe.pdf (accessed Dec 15, **2016**).

19. COMEX - CME Group Index Mundi - Copper Monthly Price - US Dollars per Metric Ton http://www.indexmundi.com/commodities/?commodity=fish-meal&months=60 (accessed Dec 15, **2016**).

20. Søndergaard, R. R.; Espinosa, N.; Jørgensen, M.; Krebs, F. C. Efficient decommissioning and recycling of polymer solar cells: justification for use of silver. *Energy Environ. Sci.* **2014**, *7*, 1006.

21. dos Reis Benatto, G. A.; Roth, B.; Madsen, M. V.; Hösel, M.; Søndergaard, R. R.; Jørgensen, M.; Krebs, F. C. Carbon: The Ultimate Electrode Choice for Widely Distributed Polymer Solar Cells. *Adv. Energy Mater.* **2014**, *4*, 1400732.

22. Angmo, D.; Krebs, F. C. Over 2 Years of Outdoor Operational and Storage Stability of ITO-Free, Fully Roll-to-Roll Fabricated Polymer Solar Cell Modules. *Energy Technol.* **2015**, *3*, 774.

23. Espinosa, N.; Laurent, A.; dos Reis Benatto, G. A.; Hösel, M.; Krebs, F. C. Which Electrode Materials to Select for More Environmentally Friendly Organic Photovoltaics? *Adv. Eng. Mater.* **2016**, *18*, 490.

24. Swiss Centre for Life Cycle Inventories The Ecoinvent Database v3.1 **2014**.

25. European Commission - Joint Research Centre - Institute for Environment and Sustainability *International Reference Life Cycle Data System (ILCD) Handbook -- General guide for Life Cycle Assessment -- Detailed guidance*; First edit.; Publications Office of the European Union: Luxembourg, **2010**.

26. PRé Consultants SimaPro 8.0.4.26 **2014**.

27. Hauschild, M. Z.; Goedkoop, M.; Guinée, J.; Heijungs, R.; Huijbregts, M.; Jolliet, O.; Margni, M.; De Schryver, A.; Humbert, S.; Laurent, A.; Sala, S.; Pant, R. Identifying best existing practice for characterization modeling in life cycle impact assessment. *Int. J. Life Cycle Assess.* **2013**, *18*, 683.

28. Michaud, J.-C.; Farrant, L.; Jan, O.; Kjær, B.; Bakas, I. *Environmental benefits of recycling - 2010 update*; **2010**.

29. Energinet.dk *Personal Communication (February **2015**)*.

30. Espinosa, N.; Søndergaard, R. R.; Jørgensen, M.; Krebs, F. C. Flow Synthesis of Silver Nanowires for Semitransparent Solar Cell Electrodes: A Life Cycle Perspective. *ChemSusChem* **2016**, *9*, 893.

Chapter 4

Operational lifetime of environmentally friendly OPV

For commercialisation, it is essential that the OPV modules are durable and resistant to outdoor conditions. In this chapter, the stability performance under ISOS conditions of the C-OPV modules described in Chapter 2 is presented, together with silver nanowire based OPV which represents a new strategy to environmental friendly OPV, without losing power per area. In addition to ISOS conditions, a special stability test is performed in greenhouses and compared with outdoor data. All the samples operational lifetime is then compared using the o-diagram in Subchapter 4.5.

4.1. ISOS conditions

As OPV devices reached good efficiencies for commercialization, developed into large scale devices and started to be submitted to stability tests, it came up the need for specific stability tests, since their behaviour lacked some constancy in power output over time which was typical for mature PV technologies. The degradation mechanisms in OPV, due to the many interfaces between different materials with different properties, are highly complex [1,2]. The protocols were established in 2011 at the International Summit on Organic and Hybrid Solar Cells Stability (ISOS) and are a powerful tool, providing guidelines for OPV lifetime tests in both indoor and outdoor conditions, making possible the comparison of data within different laboratories reported in the literature [3,4]. Furthermore, these protocols leaded to highly significant developments in the field, such as the establishment of reference baselines for stability performance and a database to be used as pass-fail standards and for the development of prediction tools [5–7].

A degradation curve example is shown in Figure 4.1, representing the behaviour of a photovoltaic parameter E (PCE, V_{OC}, I_{SC}, FF or P_{max}) over time. For the report of the operational lifetime, the guidelines take into account the universally used metric called "T_{80}", which corresponds to the time a module takes to reach 80% of its initial performance. Nevertheless, the T_{80} alone does not express the

degradation process and reporting the degradation curve is always recommended, since several competing aging mechanisms often take place at the same time in OPV devices, resulting in several variations in aging behaviour. For the description of the stability curves, the four data pairs listed below are of highly importance. In Figure 4.1 they represented by the red spots.

$[E_0;T_0]$ - E_0 is the initial testing measurement of an OPV device immediately after final fabrication of the device, at time=0, T_0. In the case of stability curves with an initial increase followed by a reduction, this point can be defined as the maximum at its corresponding time;

$[E_{80};T_{80}]$ - E_{80} is the testing measurement of an OPV device after the device has decayed 20% from the initial testing measurement, E_0. T_{80} is the time it took to decay to E_{80};

$[E_S;T_S]$ - E_S is the performance at the start of a more stabilised phase of an OPV device, where the degradation is less strong, defined arbitrarily by the user as some time, T_S, after the fabrication of a device;

$[E_{S80};T_{S80}]$ - E_{S80} is the testing measurement of an OPV device after the device has decayed 20% from the second testing measurement, E_S. T_{S80} is the time it took to decay to E_{S80}.

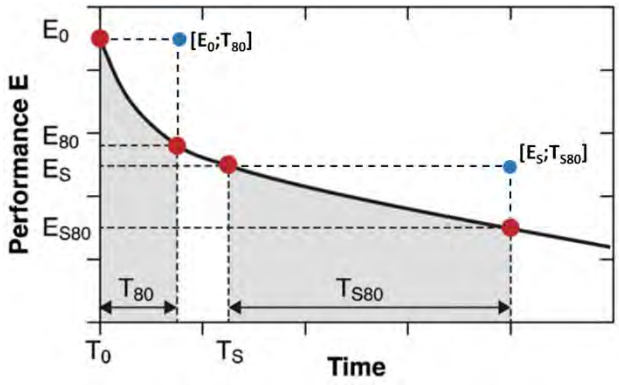

Figure 4.1 - Typical degradation curve of an OPV device, marking the four data pairs $[E_0;T_0]$, $[E_{80};T_{80}]$, $[E_S;T_S]$ and $[E_{S80};T_{S80}]$ in red, and the lifetime markers $[E_0;T_{80}]$ and $[E_S;T_{S80}]$ in blue. Adapted from [6].

The consideration of a more stabilised phase avoids the negligence of a good and stable module that presents an initial burn-in phase. Although, if E_S is less than half of E_0, the sample is considered to have degraded before stabilization and therefore this phase should not be considered for practical operational lifetime.

In order to compare several OPV technologies, the recent publications in the current OPV stability status [6,7] define generic lifetime markers, in blue on Figure 4.1. They are not only a time parameter (as T_{80} and T_{S80}), but the combination $[E_0;T_{80}]$ and $[E_S;T_{S80}]$, while a comparison of only the lifetime between a fresh and a degraded sample (that normally degrades slower) can be misleading. The choice of one or another marker is defined by the following:

$[E_0;T_{80}]$ - Used if the area corresponding to $E_0 \times T_{80}$, is larger than $E_S \times T_{S80}$;

$[E_S;T_{S80}]$ - Used if the area corresponding to $E_S \times T_{S80}$, is larger than $E_0 \times T_{80}$.

In the case of the measurements stopped before reaching the 20% degradation, the last measurement is used instead of T_{80} or T_{S80}, named "T_{final}", representing the minimum possible lifetime. The complete steps for the determination of the lifetime markers are described in the works from Gevorgyan et al. [6,7]. For the conclusion of this chapter, the markers are used in order to compare the operational lifetime of all OPV with eight different layer configurations, with stability curves presented in the next sections.

In Table 4.1, the ISOS condition parameters used in this chapter are shortly detailed. The conditions are named with "D" standing for dark storage tests, "L" for laboratory weathering or light simulation tests and "O" for outdoors. The numbers represent the test levels, concerning the number of parameters that need to be monitored, named basic (Level 1), intermediate (Level 2) and advanced (Level 3). All the ISOS tests presented in this chapter, including accurate IV-testing under calibrated light sources and outdoor measurement, were performed in the Characterization Laboratory for Organic Photovoltaics (CLOP) at the Department of Energy Conversion and Storage, DTU, Roskilde, Denmark (latitude 55°41' N, longitude 12°06' E). Most of the tests involved the samples being periodically removed from the ageing setup and tested under a calibrated solar simulator with AM1.5G spectrum and 1000 W m^{-2} of illumination (Metal Halide Lamp Solar Constant 1200). The recorded IV-curves were used to construct the degradation curves as recommended in the ISOS protocols [3]. A Microsoft Excel based macro was used for raw data processing and analysis [8].

Table 4.1 - List of the main parameters used in the different ISOS protocols [3].

Conditions	ISOS-D-1	ISOS-D-2	ISOS-D-3	ISOS-L-2	ISOS-L-3	ISOS-O-1	ISOS-O-2
Aging light source	None	None	None	Simulator AM1.5G	Simulator AM1.5G	The sun, outdoor	The sun, outdoor
Temperature (°C)	Ambient	65 (oven)	65	65	85	Ambient outdoor	Ambient outdoor
Relative humidity (%)	Ambient	Ambient	85	Ambient	50 (Controlled)	Ambient outdoor	Ambient outdoor
Characterization light source	Solar Simulator	Solar Simulator	Solar Simulator	Solar Simulator	Solar Simulator	Solar Simulator	Sunlight

4.1.1. Dark storage tests

The three levels of darks storage tests were performed in this chapter. For ISOS-D-1 (shelf) no control is required besides that the samples should be left in the dark under ambient conditions. According to ISO291 (2008), ambient conditions are defined as 23 °C and 50% relative humidity (RH) in general; and 27 °C and 65% RH is accepted for tropical countries. For ISOS-D-2 (high temperature storage) the samples were stored in an oven (Figure 4.2 on the left) with constant temperature of 65 °C. In ISOS-D-3 (damp heat) the samples were placed in an environmental chamber (from Thermotron - Figure 4.2 on the right) set at 85% relative humidity (RH) and 65 °C air temperature. In these tests the samples were left with no load.

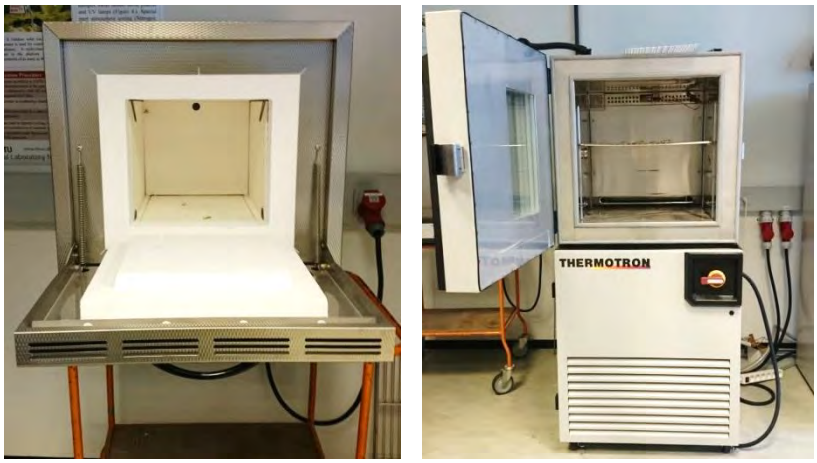

Figure 4.2 - ISOS-D-2 (left) and ISOS-D-3 (right) setups.

4.1.2. Laboratory weathering tests

The light sources' details for these tests are crucial, since OPV are very sensitive to different spectra and a lamp with spectrum as close as possible to the sun is desirable for accurate comparison of laboratory testing and real life. The lamps used for these tests are the recommended in the protocols. The light heat test (ISOS-L-2) and light heat with controlled humidity test (ISOS-L-3) were performed in thesis. For ISOS-L-2 (Figure 4.3 on the left), the experiment was carried out in the ambient at 65 °C under 1 Sun illumination of a calibrated light source from metal halide lamps with daylight filter. The temperature was monitored and controlled with the use of ventilators, as the lamps heated the samples to temperatures up to 75 °C. The IV-curve tracing of the samples was performed using an automated acquisition setup with a Keithley 2400 source measure unit (SMU). For ISOS-L-3, a weathering chamber (from Q-Lab - Figure 4.2 on the right) with a xenon arc with daylight filter, set to 65 °C air temperature, 85 °C device temperature (black panel), 50% RH and illumination of around 0.7 Sun.

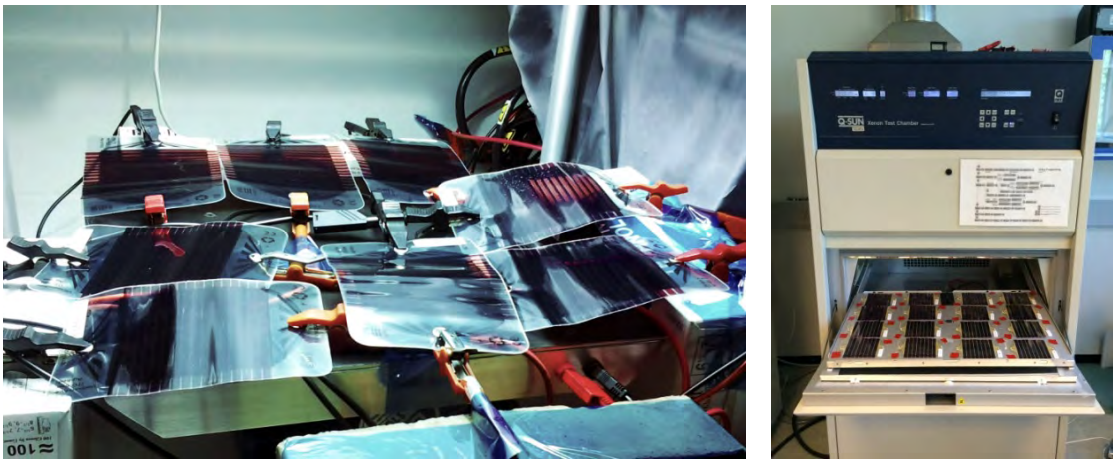

Figure 4.3 - ISOS-L-2 and ISOS-L-3 setups.

4.1.3. Outdoor tests

Apparently the most straight forward way of testing the stability of OPV actually can come with a large range of issues as the effects of temperature variations, coverture of clouds and many others, such as wind, snow, rain, leaves and all kinds of covering from birds or bio-accumulation. In this chapter, most of the samples are tested under ISOS-O-1 condition, where the modules are kept outside and taken periodically to be measured under the solar simulator. The samples were placed either on a fixed platform facing south (Figure 4.4 on the left) or in a platform equipped with a solar tracker (Figure 4.4 on the right). ISOS-O-1 was performed either on a fixed platform facing south (Figure 4.4 on the left) or in a platform equipped with a solar tracker (Figure 4.4 on the right). For a more accurate track of the ageing behaviour, ISOS-O-2 tests were also performed where devices are kept outside and measured outside under daylight. For this test, the samples were placed on the solar tracker and the IV-curve tracing of the samples was performed *in situ* using an automated acquisition setup with a Keithley 2400 SMU. The IV-curves in this case were normalised to 1 Sun in order to be comparable to ISOS-O-1 results. The outdoor experiments presented here were carried out at the same time only if they manufacture were performed separately, what is the case for C-OPV modules. The detailed starting dates are informed further on each sample lifetime description.

Figure 4.4 - Fixed (left) and tracked (right) platform for outdoor tests. Some of the samples used in this work are marked with blue (ISOS-O-1) and green (ISOS-O-2) squares.

4.2.Carbon based OPV stability performance

Carbon-based OPV (C-OPV) were full, R2R produced comprising the layers shown in Figure 4.5. The details of their production are shown in Chapter 2. The names and dissimilar characteristics of the four types of C-OPV presented in this Subchapter are:

C-OPV-F1: Active layer consisting of P3HT:PCBM and substrate/encapsulation barrier foil prone to develop bubbles during aging;

C-OPV-F2: Active layer consisting of P3HT:ICBA;

C-OPV-SP: Active layer screen printed instead of slot-die coated;

C-OPV-LB: Active layer consisting of low band gap polymer donor PBDTTTz-4 and PCBM.

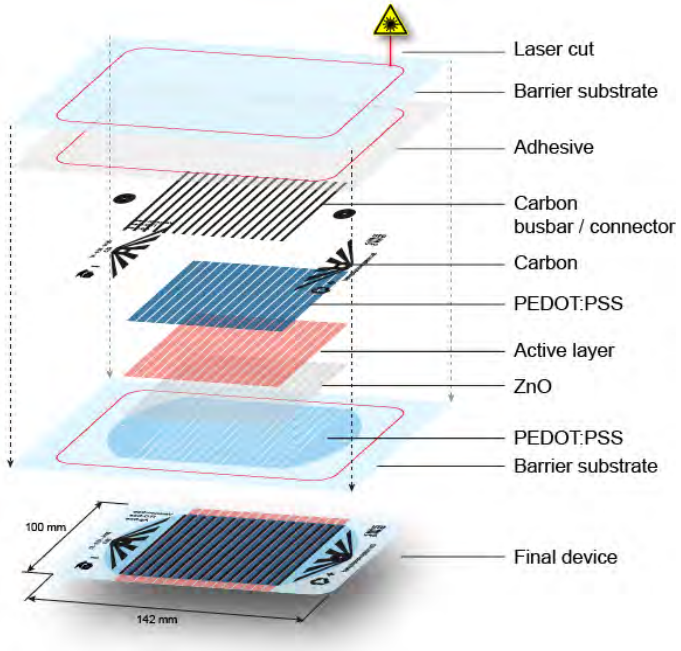

Figure 4.5 - C-OPV modules structure. Adapted from [9].

The stability tests for different sorts of C-OPV are presented in the next sections with the PCE photovoltaic parameter in order to represent mainly how the devices efficiency behave during energy production. The initial PCE is informed in Section 4.5 in the o-diagram.

4.2.1. C-OPV-F1

C-OPV-F1 are C-OPV modules with slot-die coated P3HT:PCBM active layer and manufactured with substrate and encapsulation barrier foil prone to develop bubbles during aging. The tests for this type of C-OPV had eight modules per condition, chosen carefully with very close photovoltaic parameters, bringing very good statistics for the lifetime determination. Figure 4.6 presents the average stability curves with the shade following the curves corresponding to their standard deviation. The curves are expressed in normalised by the maximum PCE.

The shelf test (ISOS-D-1) was performed for a period of time for 878 days. In the first 200 days the samples remained over 90% of the initial efficiency, followed by a smooth decay with all samples reaching T_{80} in 400 days. The period from 500 to 750 days, the samples performance remained stable at around 70%, followed by a new decline. By the end of the test, the samples were around 60% from the maximum (in this case also initial) PCE. The dark test under high temperature (ISOS-D-2) was carried out for 762 days. The samples started to suffer a more accentuated decline in efficiency only after 170 days reaching T_{80} around 210 days of test. The decay continues until approximately the day 420 with circa 40% of the initial PCE, when a more stabilised phase starts. By the end of the test, the samples present only 21% of the initial PCE in average. The damp heat test (ISOS-D-3) is a very harsh test for OPV in general. The PCE was stable for the first 3 days and then had a very fast decay; the samples reach T_{80} in maximum 5 days and suffered failure in 15 days of test.

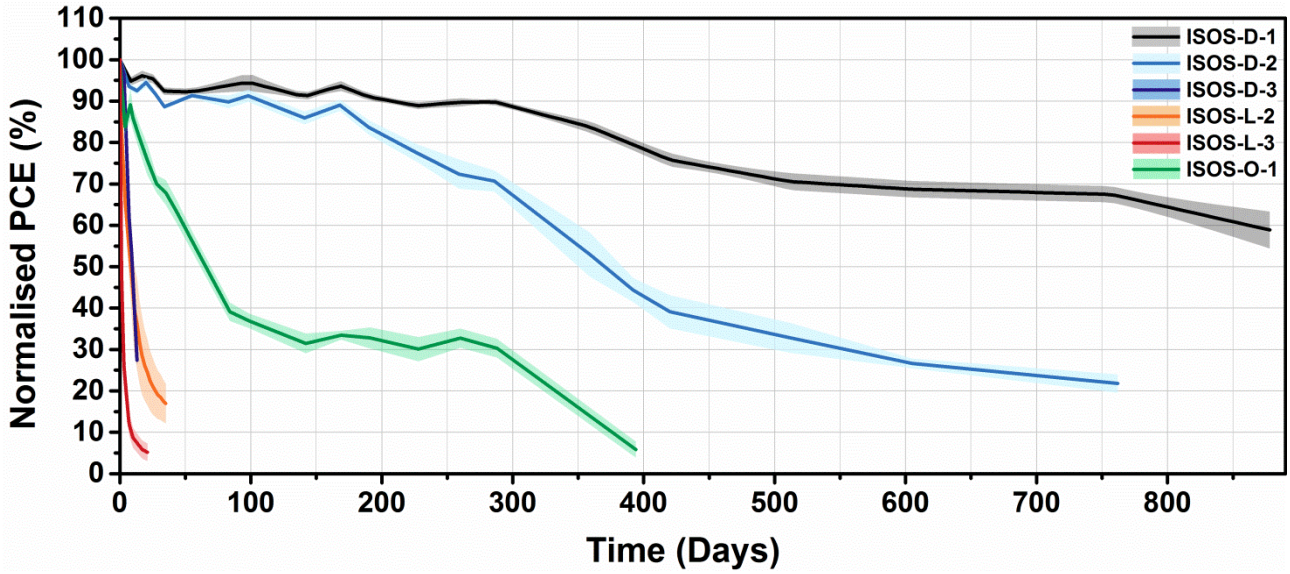

Figure 4.6 - Average stability curves of the C-OPV-F1 modules under six ISOS conditions.

The light heat test (ISOS-L-2) lasted for 35 days. The samples suffer a very harsh burn in and only start to have more stable phase below 40% of the initial PCE. T_{80} was at 1.5 day in average. In this test the disposition of the barrier foil to develop bubbles or blisters was detected. The effect started to be visible after 4 days under illumination and Figure 4.7 shows how the samples looked like before and after 28 days

of test. Scanning electron microscopy (SEM) images showed the formation of a bubble between SiOx barrier layers [9]. Although at first the samples continue working without specific inactive areas observed in LBIC (not shown), this had severe implications in the performance of the modules in a long term, since the barrier defects allowed water and oxygen ingress, leading to failure of the areas underneath the bubbles. To avoid this issue, it was developed an efficient R2R based method to detect microbubbles prior to use of the barrier foil and an enormous range of bubbles were found in foils from some suppliers and even in different batches from the same supplier [9].

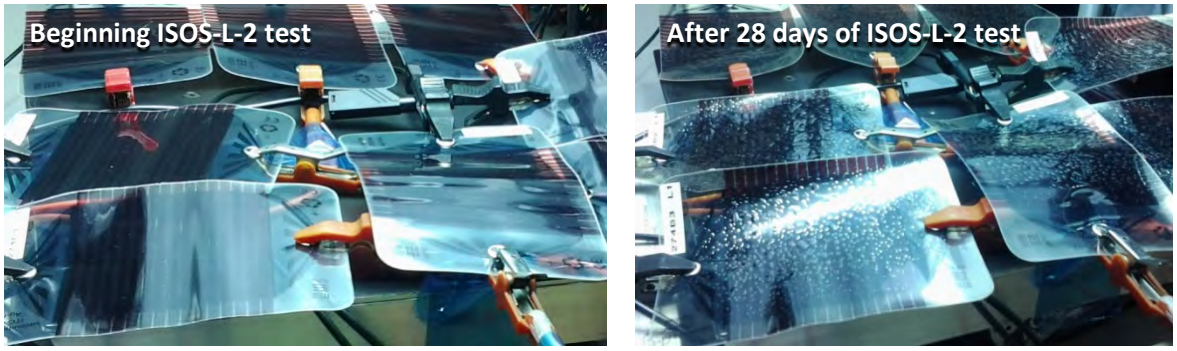

Figure 4.7 - C-OPV-F1 modules before (left) and after (right) the appearance of bubbles due to light and heat.

The test that submits the modules to light, heat and controlled humidity (ISOS-L-3) lasted 21 days and had an even harsher effect over the C-OPV-F1 modules than ISOS-D-3 and ISOS-L-2. T_{80} was reached after less the half a day and the stabilised phase started after 6 days with about 15% only of the initial PCE. The outdoor test with periodic removal of the samples to be tested under a solar simulator (ISOS-O-1) started in June 2nd 2014. The samples were placed in a fixed platform from Figure 4.4 on the left due to the lack of space in the tracked platform. The PCE had an initial drop in the first 4 days of test, had a recover a new decay reaching T_{80} after around 15 days of test. E_S was correspondent to less the 40% of E_0 and in this phase the PCE of the modules remained stable until 290 days of test, when the very damaged barrier foil (due to the bubbles mentioned in the light heat test) most likely provoked the failure of the devices.

In collaboration with the Bangor University (Wales, UK) and Ben-Gurion University of the Negev (Israel), nine C-OPV-F1 samples were tested outdoor using two distinct UV-filters, i) A commercial coated on an adhesive PET foil which is clued on top of the OPV; and ii) A luminescent down-shifting (LDS) based material Eu(hfac)(phen):PMMA (Eu:PMMA) that is directly screen printed on the OPV module. The commercial UV filter though showed substantial decrease in photocurrent of -17.5% while Eu:PMMA LDS does not compromised the performance of the device itself. The samples were additionally protected with glass (on the backside) and cover with the organosilicon polydimethylsiloxane (PDMS) to avoid any effect from the oxygen and water ingression. The test were performed under ISOS-O-2 conditions in Sede Boqer, the Negev desert, Israel; where the sun spectrum measured at 2–3 h around noon time of a cloudless day matches almost identically to the AM1.5G spectrum. T_{80} was improved in average from 41 days for reference samples without filter, to 59 days with Eu:PMMA LDS and 67 days for the commercial UV filter. The details of the experiments and results can be seen in the work from Kettle et al. [10].

4.2.2. C-OPV-F2

C-OPV-F2 are C-OPV modules with slot-died P3HT:ICBA active layer fabricated with bubble-free barrier foil. The tests for this type of C-OPV had four modules per condition, chosen with close photovoltaic parameters. Figure 4.8 presents the average stability curves with the shade following the curves representing the standard deviation. The curves are plotted in PCE normalised by the maximum.

The ISOS-D-2 test or dark test under high temperature was carried out for 586 days and is still ongoing. After a rather stable phase in the first 10 days, the samples had more accentuated efficiency decline reaching T_{80} in around 140 days of test. A more stabilised phase started at 180 days of test, with E_S varying from 70 to 75% of the maximum PCE. By the latest measurement, three of the four samples had still not reached T_{S80}. The ISOS-D-3 or damp heat test had a very similar behaviour for C-OPV-F2 as for C-OPV-F1 modules. The PCE stayed stable for the first 3 days approximately and had a very fast decline, failing in 15 days and reaching T_{80} in maximum in about 5 days of test.

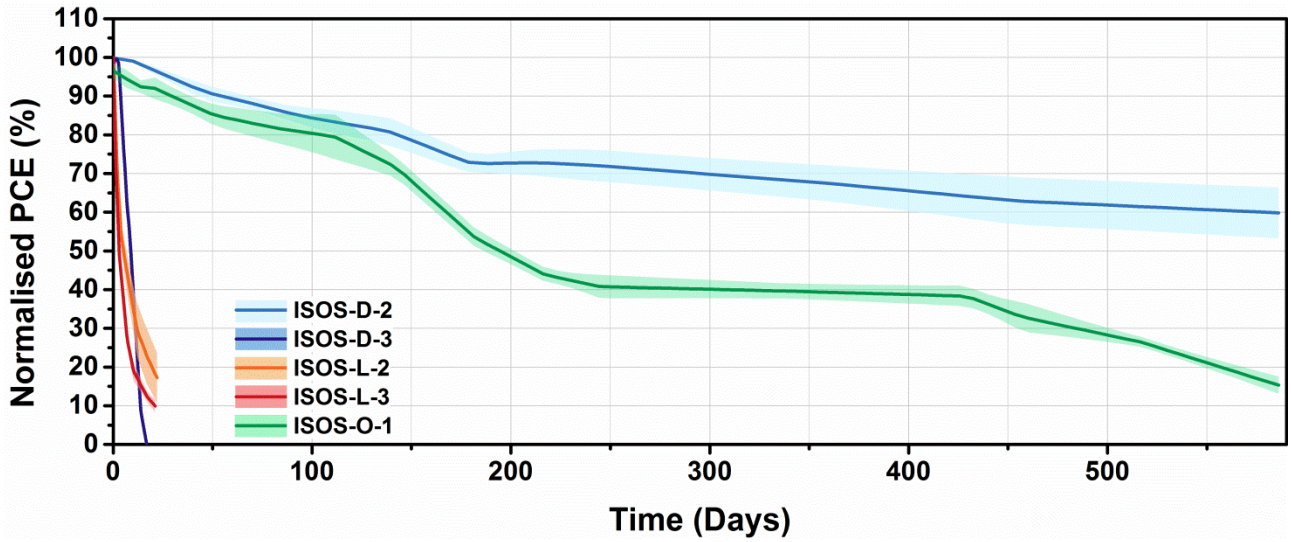

Figure 4.8 - Average stability curves of the C-OPV-F2 modules under five ISOS conditions.

The ISOS-L-2 or light heat test was carried on for 22 days. The samples had again a very similar behaviour as the C-OPV-F1, with a very harsh burn in, stable phase starting below 40% of the maximum PCE, and T_{80} was at 1.3 day in average. Even though the PET foil looked bended and yellowed, its integrity was intact and no bubble effect was observed by the end of the test. The ISOS-L-3 test or test under light, heat conditions with controlled humidity lasted for 21 days. The stability curve had a similar shape as ISOS-L-2 but with a faster PCE decay. T_{80} was reached after little less the one day (about 21 hours) and the stabilised phase started after 10 days of test with about 20% only of the initial/maximum PCE.

The ISOS-O-1 outdoor test lasted 584 days and started in November 26th 2014 (autumn in Denmark) few days after the modules manufacture. The samples were placed in the tracked platform shown in Figure 4.4 on the right. The PCE had an initial drop in the first 6 days of test and a slight more stable phase after it. The aging curve presented a large standard deviation in the range of 50 to 150 days of test, with T_{80} then ranging from 70 to 127 days. The period from 245 to 427 days of aging was a very stable phase with E_S around 40% of E_0. After this period the samples started to degrade even more, finishing the test with around 15% of its maximum efficiency. Comparatively, C-OPV-F2 performs better in stability than C-OPV-F1 outdoors and in the dark heat test, and similarly in the harsher tests, i.e. ISOS-L-2 ISOS-L-3 and ISOS-D-3.

4.2.3. C-OPV-SP

C-OPV-SP are C-OPV modules fully rotary screen printed devices with P3HT:PCBM active layer. Four C-OPV-SP modules were chosen per ISOS condition, with very close initial photovoltaic parameters. Figure 4.9 presents the average stability curves with the shade following the curves representing the standard deviation.

The ISOS-D-2 test was carried out for 610 days. The first 50 days of test presented a very stable phase followed by an efficiency decline. A second very stable phase started after 125 days of test with E_S at (or just before) 80% of the maximum PCE. Until 484 days of test the PCE had even a slight increase and started to degrade once more. The modules at the end of the test presented 66-52% and were below 80% of the maximum PCE only after 490-507 days of test. The ISOS-D-3 did not show a 3 days stable period, with T_{80} of around 2 days and the modules failing after 8 days of test.

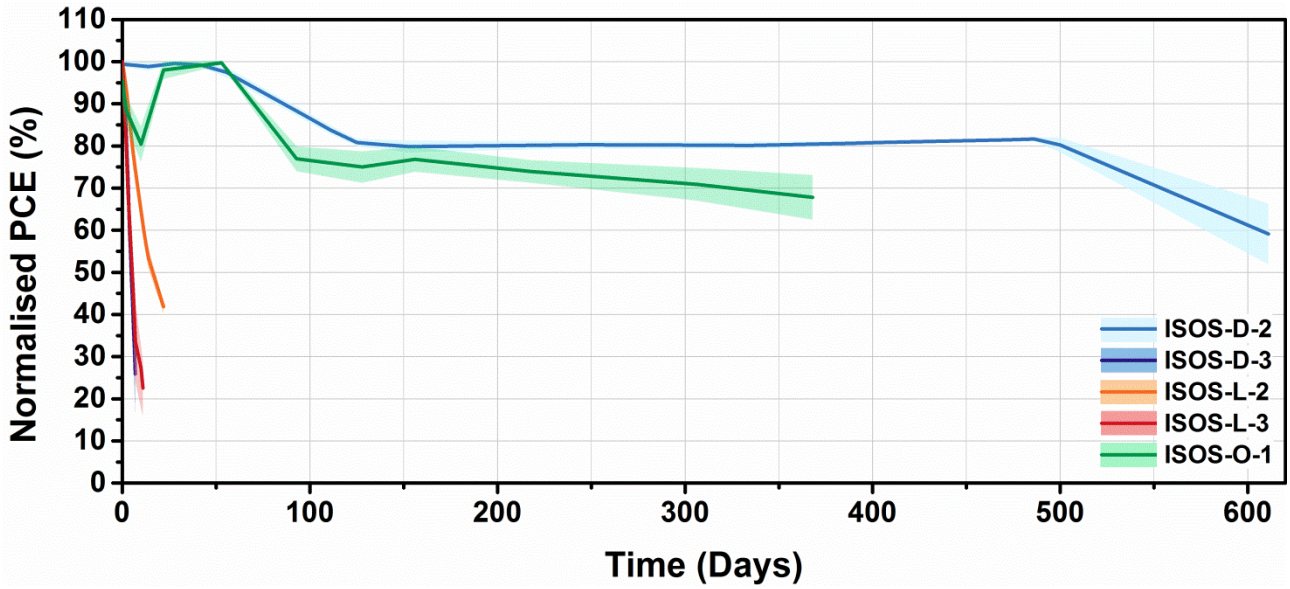

Figure 4.9 - Average stability curves of the C-OPV-SP modules under five ISOS conditions.

The ISOS-L-2 was carried on for 22 days. The initial burn in typical of this test is less harsh for C-OPV-SP modules with T_{80} reached after 5.4 days of test in average. A more stable phase is observed by the day 14 at 53%, but still with a considerable fast degradation, finishing the test with the average of 41% of the maximum PCE. The ISOS-L-3 test lasted for 11 days. The stability curve almost overlaps ISOS-D-3, but with a more stable phase PCE decay. T_{80} was reached after little less the one day (about 21 hours) and the stabilised phase started after 10 days of test with about 20% only of the initial/maximum PCE.

The ISOS-O-1 test was carried on for 368 days and started in February 23rd 2015 (winter in Denmark) few days after the modules manufacture. The samples were placed in the tracked platform shown in Figure 4.4 on the right. The PCE had a much accentuated initial drop in the first 10 days, with some samples reaching T_{80} but recovering in the sequence. As PCE is normalised by the maximum, in this test the initial PCE was around 95% of the maximum, since after 50 days of test all the four sample reached their maximum efficiency. This recover period matches with increase of illumination in that season in Denmark. After this peak, the PCE decay until the 93 days of test when a more stable phase started. T_{80} for all samples were approximately 88 days. E_S was around 77% of the maximum PCE and by the end of the test none of the samples had reached T_{S80}.

In general the ISOS tests for C-OPV-SP modules were stopped earlier due to their low efficiency, which were already initially low. Those values are presented and discussed with the o-diagram plot in the Section 4.5. In comparison to C-OPV-F1 and C-OPV-F2, C-OPV-SP is much better stable outdoors in the dark heat test, comparable to C-OPV-F1 performance in the shelf test.

4.2.4. C-OPV-LB

C-OPV-LB are C-OPV modules with slot-die coated PBDTTTz-4:PCBM active layer, where PBDTTTz-4 is a low band gap polymer. Four C-OPV-LB modules were used per ISOS condition, with close initial photovoltaic parameters. The average stability curves with the shade following the curves representing the standard deviation are shown in Figure 4.10.

The ISOS-D-2 test continued for 579 days and is still ongoing. In average, the PCE had an almost linear decay during the first 100 days of test with T_{80} of 74-96 days. The period from 100 to 134 days the samples were more stable, subsequently PCE decayed again and after 177 days of test, a longer stable phase started and remained until the end of the test. Average E_S was 66% and the modules last measurement had 64-58% of the initial/maximum PCE. In comparison to the other C-OPV, C-OPV-LB had a remarkable stability under the dark heat test. The ISOS-D-3 did not show a clear 3 days stable period and it took at least 3 days for the sample reach T_{80}, also failing after 14 days of test.

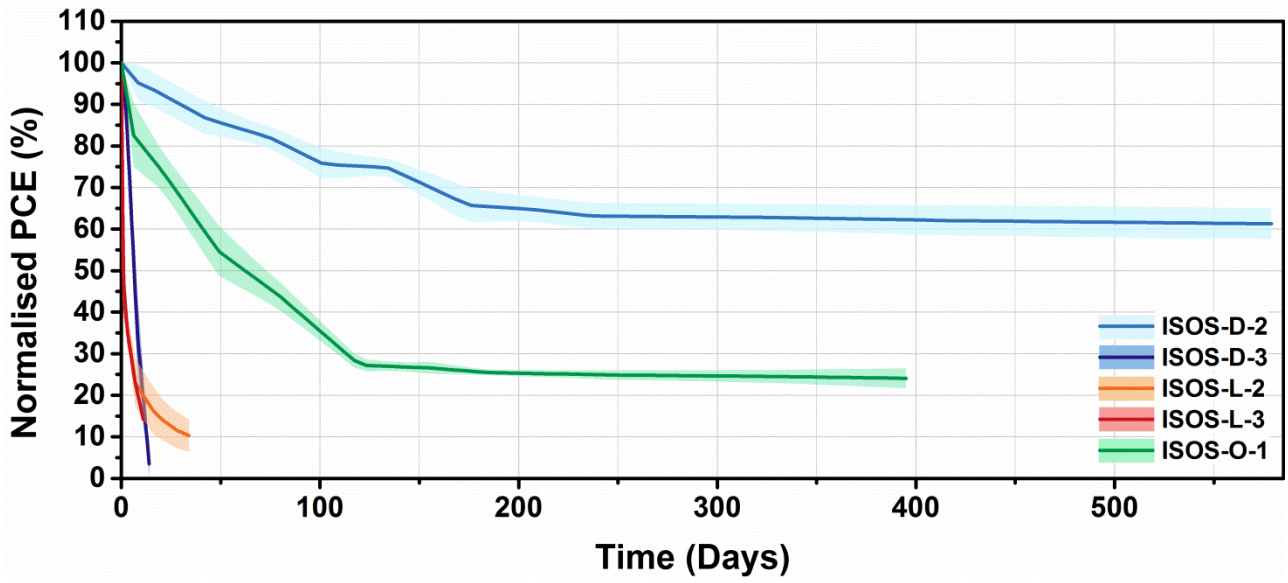

Figure 4.10 - Average stability curves of the C-OPV-LB modules under five ISOS conditions.

The ISOS-L-2 was carried out for 34 days. The initial burn in for C-OPV-LB is the severest of the four C-OPV structures. T_{80} is reached in about 8 hours of test and in 1 day, all the samples were already below 50% of the initial/maximum efficiency. The more stable phase started in 7 days with around 23%, finishing the test with the average of 10% of the maximum PCE. The ISOS-L-3 test was performed for 11 days. The stability curve overlaps ISOS-L-2 until day 7, but did not show a more stable phase. T_{80} was reached in around 9 hours and ended the test with about 14% of the initial/maximum PCE.

The ISOS-O-1 test was performed for 395 days and started in January 27th 2015 (winter in Denmark) few days after the modules manufacture and preparation. The samples were placed in the tracked platform shown in Figure 4.4 on the right. The PCE had a pronounced initial drop in the first 6 days. The average

degradation rate was slightly lower after that, however the standard deviation was large in this period with T_{80} varying between 4.3 and 18.2 days. A more stable phase started after around 117 days of test with E_S around 28% of the maximum in average. The samples efficiency remained very stable and ended the test with 26-22% of the maximum PCE.

4.3.AgNW based OPV stability performance

Economic simulations and life-cycle assessments had demonstrated that the replacement of the ITO front electrode with PEDOT:PSS and silver nanoparticles (AgNP) significantly reduce both the cost and the environmental impact of the OPV panels [11–15]. The most promising front electrodes from an environmental point of view are the ones based on high-conductive PEDOT:PSS (as used for C-OPV) and silver nanowires (AgNW) [14,15]. The environmental impact of AgNW based OPV devices (AgNW-OPV) is several orders of magnitude lower than devices using ITO or Ag-grid comprised of AgNP. In addition, AgNW-OPV have the potential for intrinsically longer lifetimes [6,16]. A recently publish report presents AgNW without encapsulation very stable when exposed to high levels of humidity and even increases conductivity when exposed to light [17]. Furthermore, as Ag-OPV, AgNW-OPV can achieve higher power per area than C-OPVs, therefore requiring less area to produce the same amount of electricity (see Chapter 2).

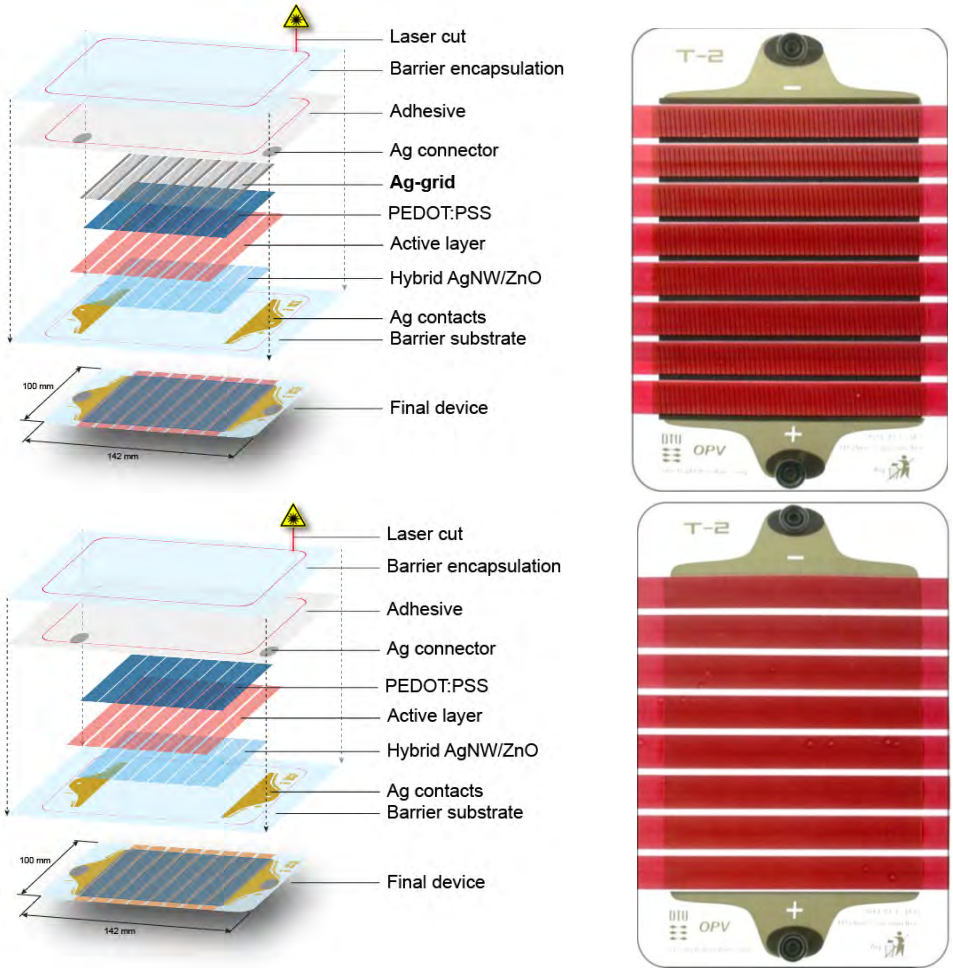

Figure 4.11 - AgNW-OPV modules structure and photographs. Top: AgNW-OPV structure with Ag-grid back electrode (left) and picture of the corresponding module (right). Bottom: AgNW-OPV structure with PEDOT:PSS back electrode (left) and picture of the corresponding module (right). Adapted from [16].

Figure 4.11 on the left shows the structures of the AgNW-OPV modules which lifetime is presented in the following sections. Mainly the two structures are the same, differentiating only by the back electrode. The structure in top of Figure 4.11 shows a module with a Ag-grid back electrode with PEDOT:PSS ensuring the role of HTL. The structure in the bottom of Figure 4.11 shows a module without a Ag in the back electrode with PEDOT:PSS have both the role of HTL and back electrode. Notice in the modules pictures on the top and bottom right that the Ag-grid and Ag contacts are the only opaque layers in the AgNW-OPV modules.

The AgNW-OPV modules were fully R2R manufactured using slot-die coating, flexo and rotary screen printing techniques described in the Subchapter 2.1. The web speeds, inks and other processing details are the same used for the first freeOPV generation (Ag-OPV) [18]. The difference is that the Ag-OPV freeOPV front layers which were AgNP-grid/PEDOT:PSS/ZnO printed in three steps was here replaced by a rotary screen printed hybrid AgNW/ZnO electrode that was printed in a single printing step, saving a considerable amount of material, time, and energy. The printing order is from the bottom to the top of the structures depicted in the Figure 4.11 on the left. The front Ag contacts were processed by flexo-printing on flexible PET barrier foil (see Subchapter 2.1.2) with a cut-off towards shorter wavelengths <350 nm. The active layer was slot-die coated and two different active layers are used for AgNW-OPV: P3HT:PCBM and PBDTTTz-4:PCBM. Each active layer was manufactured with the different electrodes commented in the previous paragraph, giving a total of four types of AgNW-OPV modules tested in this subchapter. The devices had identical PEDOT:PSS thickness and were processed in the same manufacturing run where half of the modules were subjected to a final printing step with Ag-grid printed using rotary screen printing.

In summary, the names and divergent characteristics of the four types of AgNW-OPV presented in this subchapter are:

AgNW-OPV-PT-Ag: Active layer consisting of polythiophene based donor material P3HT:PCBM and Ag-grid back electrode;

AgNW-OPV-PT-PEDOT: Active layer consisting of polythiophene based donor material P3HT:PCBM and PEDOT:PSS back electrode;

AgNW-OPV-LB-Ag: Active layer consisting of low band gap donor material PBDTTTz-4:PCBM and Ag-grid back electrode;

AgNW-OPV-LB-PEDOT: Active layer consisting of low band gap donor material PBDTTTz-4:PCBM and PEDOT:PSS back electrode.

The stability tests for AgNW-OPV are presented based on PCE photovoltaic parameter in order to represent mainly how the devices efficiency behaves during energy production. The initial PCE is informed in Section 4.5 in the o-diagram were these and C-OPV operational performance is compared. As all the four different types of devices were manufactured at the same time, the ISOS conditions could be performed with all modules at the same time, minimizing any equipment or environmental factor that could compromise the comparability between them. ISOS-L-2 was an exception, due to restrict space under solar simulators, forcing PT and LB samples to be tested separately. All outdoor tests of AgNW-OPV modules started in July 11th 2014 (mid-summer in Denmark) few days after the modules manufacture and preparation. For the outdoor stability tests, the samples were placed in the tracked platform shown in Figure 4.4 on the right. As the samples were exposed to the same conditions, four samples were prepared with 2 of them connected to the automated acquisition setup for a more complete track of the aging behaviour (ISOS-O-2) while other two samples were removed periodically (ISOS-O-1), as no more channels

were available in the automatic SMU. The PCE from ISOS-O-2 was first normalized to 1000 W m^{-2} (1 Sun) since the devices were measured under sunlight.

4.3.1. AgNW-OPV-PT-Ag

AgNW-OPV-PT-Ag are AgNW-OPV modules with P3HT:PCBM active layer and Ag-grid back electrode. PT stands for P3HT which is a polythiophene based donor material. The stability tests for this AgNW-OPV kind of modules had four devices test for most of the conditions (unless stated otherwise), chosen with photovoltaic parameters as close as possible. The outdoor tests ISOS-O-1 and ISOS-O-2 had four samples tested in total. Figure 4.12 shows the average stability curves with their standard deviation represented by the shade surrounding them. The curves are presented normalised by the maximum PCE.

The dark test under high temperature (ISOS-D-2) was carried out for 672 days. For the first 82 days of test, the samples suffered variations in the PCE between 90 and 100% of the maximum. Some samples had the maximum at the beginning of the test and others had the maximum efficiency after around 70 days of test. From day 82 until day 124 the average PCE of the samples had a decline and then started a more stable phase with E_S around 84% of the maximum PCE. T_{80} had a range of 75 to 95 days between the samples. Three of the samples continued their decline rate finishing the test with around 45%, while one sample kept more stable and finished the test with 63% of the maximum PCE. The damp heat test (ISOS-D-3) was a very harsh AgNW-OPV-PT-Ag in the beginning with T_{80} reached in average after 12 hours. After 3 days of test though, a more stable phase started with E_S at around 25% of the initial PCE. One of the samples failed after 15 days and the other three failed after 24 days of test.

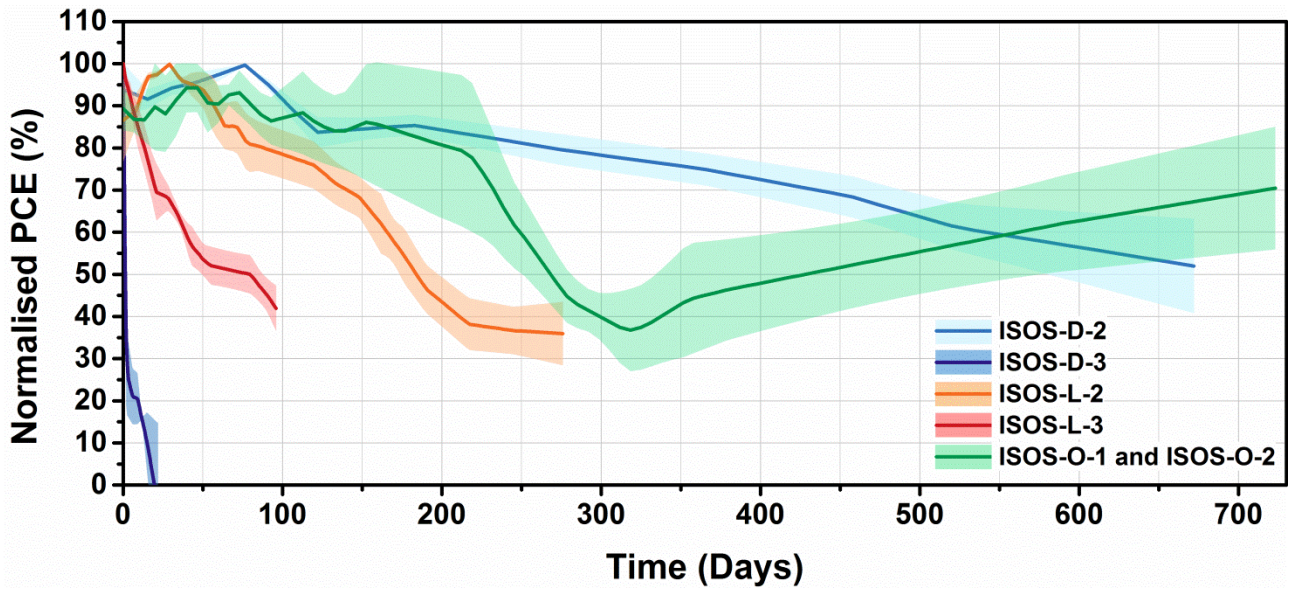

Figure 4.12 - Average stability curves of the AgNW-OPV-PT-Ag modules under six ISOS conditions. Outdoor tests are plotted together with ISOS-O-2 PCE normalised to 1 Sun.

The light heat test (ISOS-L-2) was carried out for 276 days with 5 samples. In average, the PCE of the samples started below 90% of the maximum PCE which is reached after 29 days of test. Therefore, AgNW-OPV-PT-Ag samples presented no burn in phase. After the maximum, a degradation phase started and T_{80} was reached in 88 days in average with large variation. A more stable phase started after 218 days of test and by the end the samples had efficiency close to E_S of 35±7% of the maximum PCE. The test that submits

the modules to light, heat and controlled humidity (ISOS-L-3) was performed for 96 days. The PCE had a continuous drop from the beginning until approximately the 43th day of test with T_{80} of 13±3 days and E_S of 57% from the initial PCE. By the end of the test the efficiency was around 42% of the initial/maximum PCE.

After 120 days of ISOS-L-2 test and 15 days of ISOS-L-3 test, a bubble effect was observed for these samples. Differently of the bubbles from the barrier foil detected in C-OPV-F1, this new effect was directly associated to the failure areas on the modules. Figure 4.13 shows the picture of one of the samples under ISOS-L-2 and the correspondent LBIC image measured after 240 days of test, with inactive areas precisely corresponding to the bubbles position. As the bubbles emanate from the back Ag-busbar and the back Ag-grid is highly porous with the Ag solid content corresponding to just 60% of the grid volume [19] solvents and/or gas trapped in the porosity of the back electrode could feasibly be the cause of the bubble formation due to expansion of gases in response to variation in temperature [20,21].

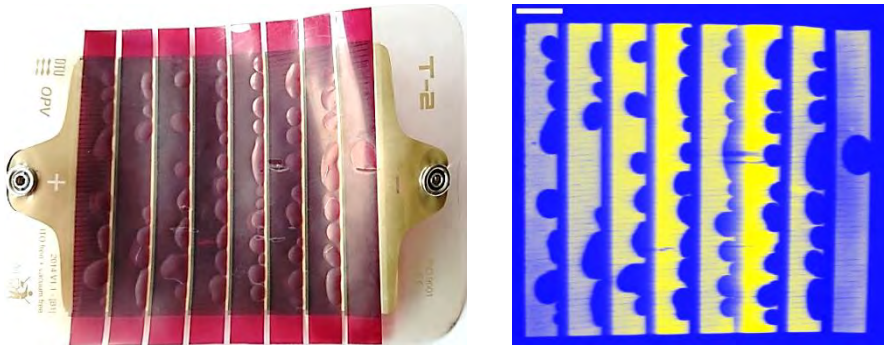

Figure 4.13 - AgNW-OPV-PT-Ag sample under ISOS-L-2 for 240 days (left) and its corresponding LBIC image (right). Adapted from [16].

The outdoor tests lasted for 724 days and are still ongoing. In the first 154 days of test, the PCE presented variations around 80 and 100% of the maximum PCE that was reached several times independently by samples during this period. In the following, all samples decayed, with one sample T_{80} at 101 days, another at 161 days and two at 243 days. The samples continued degrading until the restart of warmer and more illuminated season. By the latter measurement, two samples recovered to about 60% and the others to around 85% of the maximum PCE (one from ISOS-O-1 and another from ISOS-O-2). This recovering behaviour had already been observed for OPVs as reported by Gevorgyan et al. and Angmo et al. [22,23].

In collaboration with the Bangor University (Wales, UK), AgNW-OPV-PT-Ag samples were applied as BIPVs using corrugated roof cladding what is only possible for such flexible PV modules as the ones described in this thesis. In general, the approach performed could yield the OPV as they have profound advantages over existing BIPV products or conventional Si-PV technologies, in particular for countries at higher angles of latitudes. Different curvature angles and orientations were tested and three advantages rose from the modules being deployed in 3-dimensional shape cladding:

- The coverage area or the modules “footprint” is reduced, leading to improved power output or efficiency per unit area of roofing. This was demonstrated with indoor measurements conducted under AM1.5G illumination and it was shown that the effective PCE could be enhanced by ~10%.
- Improvement in performance under diffuse lighting conditions. This makes the three-dimension configuration geographically well-suited to countries with high latitude, due to the enhanced diffuse light

levels. The measured maximum enhancement in performance during the peak demand hours was as much as 60%.

• Enhanced performance under oblique angle irradiation, leading to substantial increased output during early morning and evening illumination. Under indoors characterisation, an enhancement of 9 times in efficiency was found and outdoors 4.5 times enhancement was measured, both compared with flat reference modules. For the best of the author's knowledge, this was the first time this enhancement has been reported using an existing building substrate, which can be directly integrated into new buildings.

The details of the experiments and analysis can be seen in the work from Kettle et al. [24].

4.3.2. AgNW-OPV-PT-PEDOT

AgNW-OPV-PT-PEDOT are AgNW-OPV modules with P3HT:PCBM active layer and PEDOT:PSS having the role of HTL and back electrode. PT stands for P3HT which is a polythiophene based donor material. The stability tests for this AgNW-OPV kind of modules had four devices per condition, with devices chosen with photovoltaic parameters as close as possible. Figure 4.14 shows the average stability curves with their standard deviation represented by the shade surrounding them. The curves are presented normalised by the maximum PCE.

The ISOS-D-2 was carried out for 640 days. The PCE had an initial decline followed by variations between 80 and 100% of the maximum PCE. 83 days of tests, a new decline happened and after 121 days of test, a stable phase started with the sample at 80±5% of maximum PCE. T_{80} ranged from 100 to 114 days with one of the samples not reaching it until 566 days of test. This specific sample had a very stable behaviour in the period from 121 to until 526 days, while the other samples had a decay trend reaching T_{S80} at 232 days in average. At the end of the test, the four samples average PCE was 50% of the initial/maximum. ISOS-D-3 test was in the beginning also severe for AgNW-OPV-PT-PEDOT as it was for AgNW-OPV-PT-Ag samples, with T_{80} of about 17 hours. After 3 days of test a more stable phase started even with a recover of the performance from 25 to 30% PCE from the maximum PCE. The samples continued stable until 29 days and failed after 36 days of test.

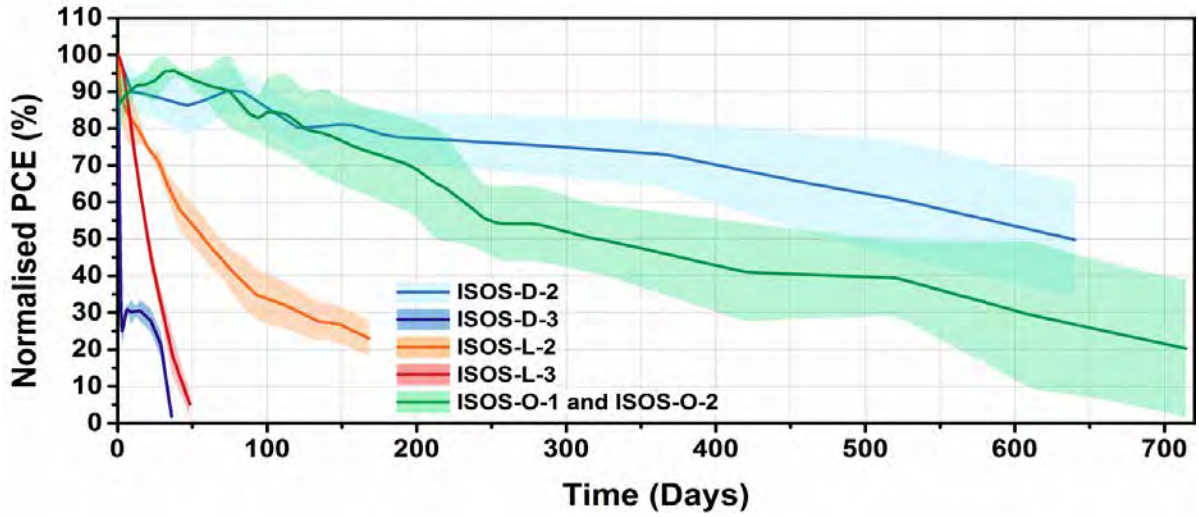

Figure 4.14 - Average stability curves of the AgNW-OPV-PT-PEDOT modules under six ISOS conditions. Outdoor tests are plotted together with ISOS-O-2 PCE normalised to 1 Sun.

The light and heat test lasted for 168 days. Under ISOS-L-2 conditions, the samples had a short burn in until 2 days of test and then decayed continuously with T_{80} of 13 days in average. A slight more stable phase occurred at 93 days of test at 35% of the initial PCE, and by the end the samples had 53% in average of the initial/maximum PCE. The test with light, heat and controlled humidity lasted 48 days. The samples under ISOS-L-3 test had a fast decay after the first 3 days of test with T_{80} of about 9 days. Differently of the modules with back Ag-grid, these modules failed after 48 days. It was also noticed that the samples with PEDOT:PSS back electrode, i.e. with the final Ag-grid, did not show intrinsic bubble formation under ISOS-L-2 and ISOS-L-3 conditions (shown in the previous Section 4.3.1). Figure 4.15 show the different appearance of those samples by the end of ISOS-L-3 test.

Figure 4.15 - AgNW-OPV-PT-PEDOT samples (left) and AgNW-OPV-PT-Ag (right) under ISOS-L-3. The four samples with PEDOT:PSS back electrode had no bubbles formed and the four samples with Ag-grid back electrode had extensive bubble formation. Adapted from [16].

The outdoor tests of AgNW-OPV-PT-PEDOT samples were carried on for 714 days. The samples varied between 85 and 100% of maximum PCE in the first 74 days of test with an overall increase of efficiency when compared with the initial PCE. A decay of performance after this period happened for some of the samples and was followed later by the others. T_{80} was reached in 74, 89, 168 and 220 days. Around 252 days of test the samples had a rather more stable phase. By the end, two samples had around 38% of the maximum PCE, one sample 20% and the other sample failed completely.

4.3.3. AgNW-OPV-LB-Ag

AgNW-OPV-LB-Ag are AgNW-OPV modules with PBDTTTz-4:PCBM active layer where PBDTTTz-4 is a low band gap (LB) donor material. Additionally its structure comprises Ag-grid as the back electrode. The stability tests for this AgNW-OPV kind of modules had four devices per condition, with devices chosen with photovoltaic parameters as close as possible. Figure 4.16 shows the average stability curves with their standard deviation represented by the shade surrounding them. The curves are presented normalised by the maximum PCE.

The dark heat test was carried out for 670 days and is still ongoing. The PCE varied around 100% and 80% of the maximum during the first 180 days of test and continued very stable after this period. After 364 days they seemed to have some decay but they recover after 522 days of test. The very last measurement is actually the maximum PCE for two samples. This structure showed real outstanding stability performance under ISOS-D-2. Similarly to C-OPV-LB, but without and initial decrease, AgNW-OPV-LB-Ag

modules have an outstanding stability under ISOS-D-2 conditions. Under damp heat test though the usual severe effect if observed, with T_{80} of about 10 hours and failure of the modules after 20 days of test.

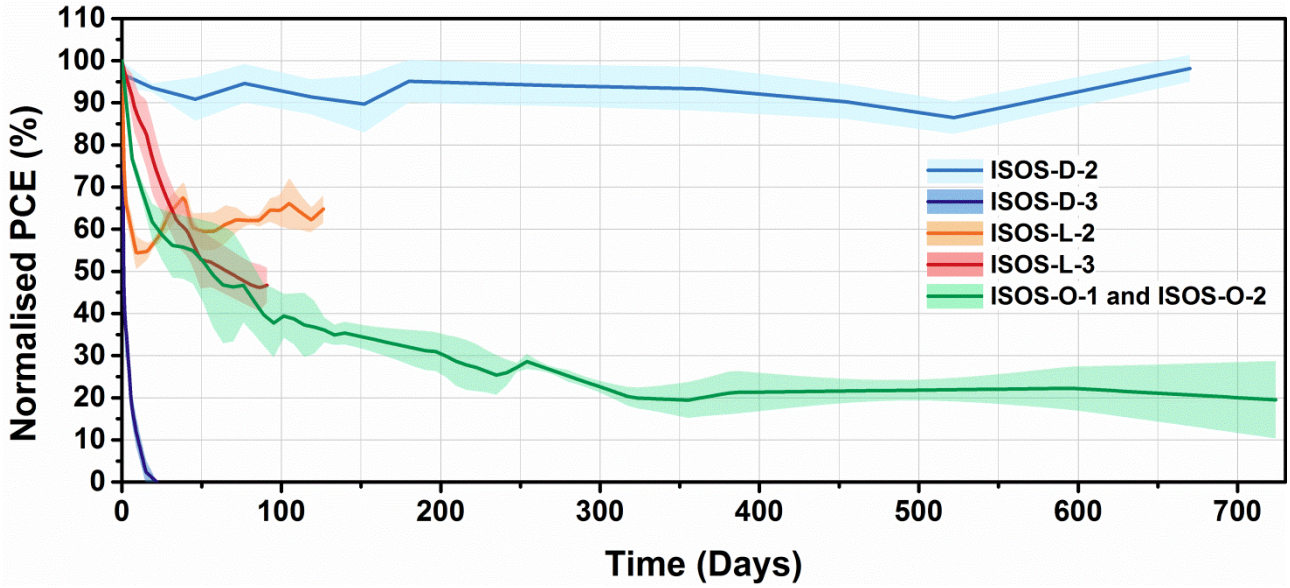

Figure 4.16 - Average stability curves of the AgNW-OPV-LB-Ag modules under six ISOS conditions. Outdoor tests are plotted together with ISOS-O-2 PCE normalised to 1 Sun.

The ISOS-L-2 was carried out for 126 days. The beginning of the test is marked by a burn in with the modules reaching T_{80} in 1 day in average. After 9 days of test, the performance stabilised shortly, with 55% of the maximum PCE and started to recover. The samples then reached a peak at day 38 with about 67% of maximum PCE, and from that point suffered variations of PCE between 55% and 72% of the maximum. The test was stopped when the samples were with 65% of the maximum PCE in average. ISOS-L-3 was performed for 91 days. Similarly to AgNW-OPV-PT-Ag sample, AgNW-OPV-LB-Ag showed a remarkable resistance the light and heat conditions with controlled humidity, especially when compared with the structures without the back Ag-grid, which normally failed after max. 20 days of test for C-OPV and 50 for AgNW-OPV with PEDOT:PSS back electrode. The PCE had a continuous drop from the beginning until the 49th day of test, with T_{80} of 17±5 days and E_S of 53% from the initial PCE. At the end of the test the average efficiency was 45% of the initial/maximum PCE. As for AgNW-OPV-PT samples, AgNW-OPV-LB samples with back Ag-grid had also the intrinsic formation of bubbles in light tests (see Figure 4.15).

The outdoor tests carried on for 724 days. The PCE had a pronounced drop with identically for the four samples in the first 15 days of test, with T_{80} of around 5 days. After this point, the samples presented variation between them, but still presenting a decay trend. Roughly, after 133 of test, a more stable phase started with E_S of 35% of the max. PCE. The final PCE was 20±9% from the maximum.

4.3.4. AgNW-OPV-LB-PEDOT

AgNW-OPV-LB-PEDOT are AgNW-OPV modules with PBDTTTz-4:PCBM active layer and PEDOT:PSS as the back electrode. LB stands for low band gap which is a characteristic of PBDTTTz-4 donor material. Figure 4.17 shows the average stability curves with their standard deviation represented by the shade surrounding them. The curves are presented normalised by the maximum PCE. The stability tests had four devices per condition, with devices chosen with photovoltaic parameters as close as possible.

The ISOS-D-2 test was carried on for 670 days and is still ongoing. The PCE varied around 100% and 80% of the maximum, very similarly as AgNW-OPV-LB-Ag, having a slight decay and recovering as well after 524 days of test. The last measurement was also back to 100% of maximum PCE for one of the samples. Likewise AgNW-OPV-LB-Ag modules, AgNW-OPV-LB-PEDOT have as exceptional stability under dark heat conditions. Under ISOS-D-3, AgNW-OPV-LB-PEDOT had a typical fast decay, with T_{80} of about 11 hours. A more stable phase started after 3 days and the modules failed in 21 days of test.

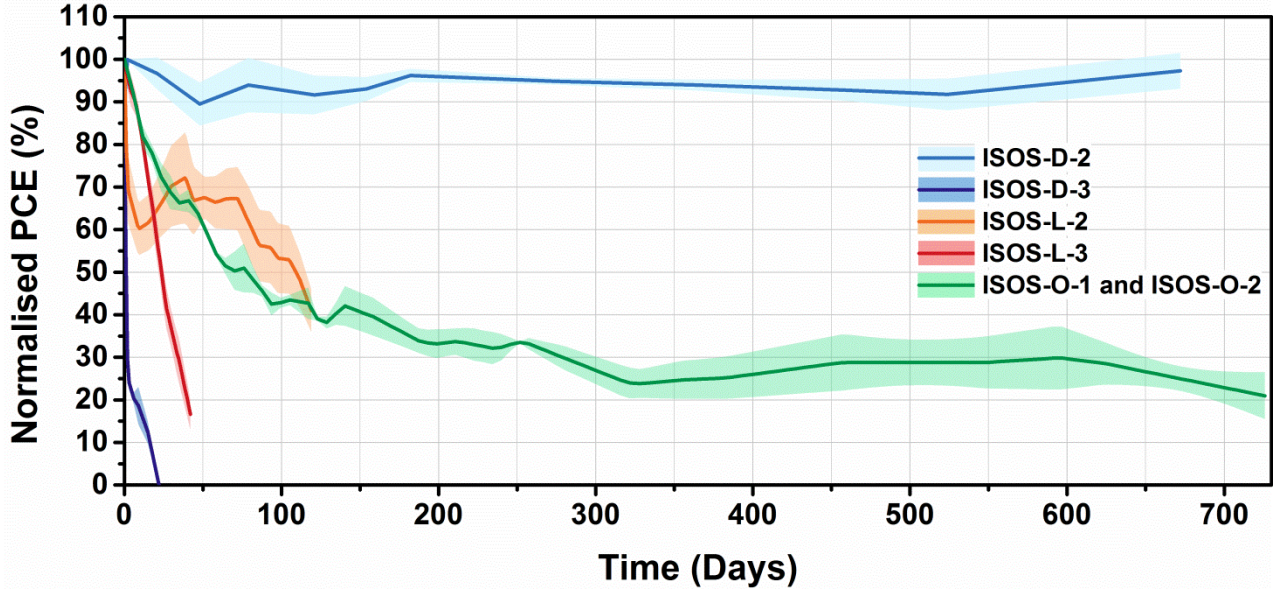

Figure 4.17 - Average stability curves of the AgNW-OPV-LB-PEDOT modules under six ISOS conditions. Outdoor tests are plotted together with ISOS-O-2 PCE normalised to 1 Sun.

The ISOS-L-2 carried on for 119 days. The samples had a burn in phase with T_{80} of about 30 hours. After 9 days of test the samples started to recover, reaching a peak at 38 days very similarly as AgNW-OPV-LB-Ag, but with larger variations between the samples. A more accentuated decay started after 72 days of test and by the end the samples had about 42% of the maximum PCE. ISOS-L-3 was performed for 42 days. The PCE had a decline a slight more stable part at the 27th day. T80 was about 12 days in the end of the test the sample were around 17% of the initial/maximum PCE, and about the fail. Identically as for AgNW-OPV-PT samples, AgNW-OPV-LB samples without back Ag-grid had not intrinsically formed bubbles in light tests (see Figure 4.15).

The outdoor tests lasted for 724 days. The PCE of the four samples declined until about 130 days of test when an apparent more stable stage started. T_{80} was around 14 days, E_S about 38% of the maximum PCE and final PCE was 21±5% from the maximum.

4.4.Greenhouse test

OPV requires larger light-harvesting areas, due to lower efficiencies in comparison to their inorganic counterparts. This may be challenging when land mass is scarce. From this perspective, the use of OPVs in areas already in use as greenhouses is a favourable solution. Currently the large-scale efficiency to make OPV economically viable has already been achieved [25,26]. Furthermore, numerous strategies for the integration OPV with textiles [27,28] and them may possibly act as a replacement or complement for textile

screens and shading systems which are already used for light management in greenhouses [29]. OPV panels based on flexible plastic are well-suited and similar to materials already used for building greenhouses. Additionally, the semitransparency of OPVs is also an advantage over opaque silicon and thin-film solar cells. The opaque area of the large-scale printing pattern of OPVs (as shown in Chapter 3) can be less than 25% for AgNW-OPV, with active area transmission of 40% [11]. Moreover, OPV have the unique option of tuning the absorption range of the active polymer to match the spectrum with the right portion of sunlight needed for a particular crop [26].

Considering that some greenhouse structures have very short lifetimes for specific seasonal crops, OPV panels could be easily replaced with the updated technology every season, following improvements in the field, as it was already shown to be a distinct advantage of low-cost OPVs [25,30]. Stable OPVs in greenhouse conditions can lead to standalone greenhouses where the electricity needed for automated shading, climate control and nocturnal illumination systems is fully generated using solar power. In this subchapter C-OPV and AgNW-OPV lifetimes modules were studied inside greenhouses and compared with outdoors tests data in order to determinate which would be the more stable condition for each OPV technology.

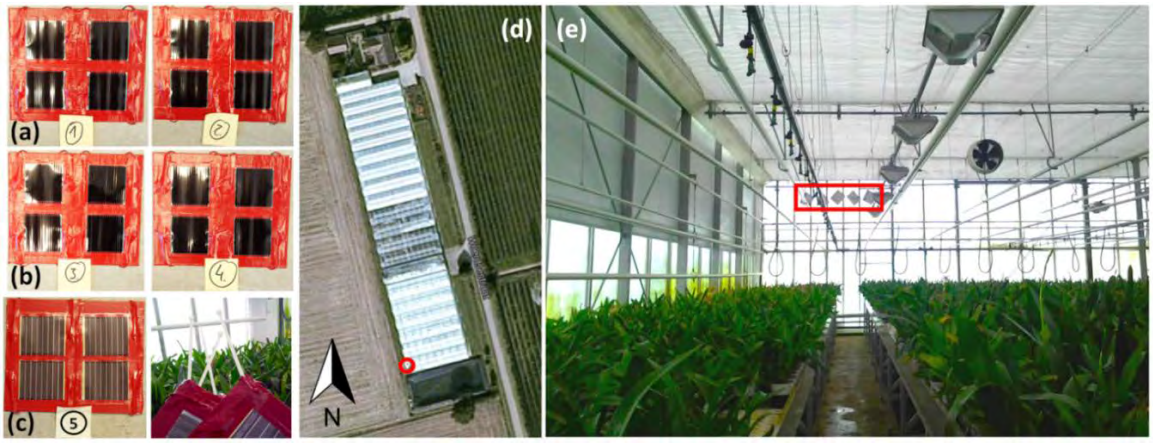

Figure 4.18 - (a) Plates 1 and 2 with C-OPV-F1 modules; (b) plates 3 and 4 with C-OPV-F2 modules; (c) plate 5 with AgNW-OPV-PT-Ag modules and attached plastic strips used for plate installation; (d) Google Maps satellite view of the climate-controlled greenhouse with red circle marking the position where the OPV samples were installed; and (e) plates installed inside the greenhouse highlighted by the red square. Reprinted with permission from [31].

For the lifetime study under greenhouse conditions, eight C-OPV-F1, eight C-OPV-F2 and four Ag-OPV-PT-Ag were used. The modules were installed inside an orchid's greenhouse in Nijmegen, Netherlands, with the modules turned to the most transparent wall towards the sun that remained unshaded, as the roof and other walls had all sorts of shades and light regulators. The position is indicated in Figure 4.18d and greenhouse installation shown in Figure 4.18e. Figure 4.18a-c shows the modules placed on plates for easy installation and safe transportation.

To access lifetime of the OPV samples, it was necessary to place the modules in different greenhouses, because they were seasonally adapted to the cultivated crop. Table 4.2 shows the detailed greenhouse conditions that the samples studied were submitted. The greenhouse wall, where the modules were place in front of, was made of plastic that attenuated around 70% of the sunlight. The environment in the greenhouse had controlled RH (approximately 90%) and temperature (average 25 ^{o}C, limiting the variation to maximum 10 ^{o}C between night and day). These greenhouse conditions were called

"greenhouse 1". After three months of test, the orchid's greenhouse stopped operating. The samples were kept there, with the greenhouse without plants and without the environmental control. This new condition was named "greenhouse 2". After 217 days of test, the modules plates were transferred to a tomato-crop glasshouse in Paderborn, Germany. They were placed towards the sun and the environment had no control of temperature or humidity. This last greenhouse condition was then called "greenhouse 3". Based on simulations from Fitz-Rodríguez et al. for similar greenhouse structures and climate [32], the temperature in the uncontrolled greenhouses was estimated to be 10±5 °C higher than the outdoors during the day and maximum 5 °C higher during the night. RH was considered around 23% lower than outdoors humidity for greenhouse without plants and 20% for a greenhouse with tomato crops. The modules plates were periodically removed from the aging condition and shipped to Denmark to be tested under a solar simulator. The total process, from the moment the samples were taken out of the greenhouse until they were fixed back, took six days. The installation, transportation and measurements dates, as well as outdoor conditions (temperature, illumination and RH), are show in the graphs of Figure 4.19.

Table 4.2 - Description of greenhouse conditions. Adapted from [31].

Conditions	Greenhouse 1	Greenhouse 2	Greenhouse 3
Light source	The sun, indoor with plastic wall Transmission ~70%	The sun, indoor with plastic wall Transmission ~70%	The sun, indoor with glass roof/wall Transmission ~90%
Temperature	Avg. 25 °C with a variation of maximum 10 °C between day and night (controlled)	Day: 10 °C ± 5 °C above the outdoors Night: max. 5 °C above the outdoors (uncontrolled) [32]	Day: 10 °C ± 5 °C above the outdoors Night: max. 5 °C above the outdoors (uncontrolled) [32]
Relative humidity	~90% (controlled)	~23% below the outdoors - no plants (uncontrolled)	~20% below the outdoors (uncontrolled)
Characterization light source	Solar simulator	Solar simulator	Solar simulator

Figure 4.19 shows the average stability curves for the greenhouse (a) and outdoor tests (b), combined with the outdoor data (c). The shade following the stability curves represents the corresponding standard deviation. The outdoor tests curves are the same shown in Sections 4.2.1, 4.2.2 and 4.3.1, replotted here for comparison with the greenhouse results. The Roskilde region in Denmark, where the outdoor tests were performed, as well as the areas in the Netherlands and Germany, where the greenhouse tests were performed, are in the same climate area as in the Köppen-Geiger climate classification system [33]; therefore, these areas have similar average temperature, seasonality and precipitation. Figure 4.19c shows the irradiation (dark yellow line), RH (black line) and temperature (purple line) data in the outdoor test location (Denmark), which was compared to the conditions in the greenhouse locations and they had very good correspondence [34].

The greenhouse tests were carried out for 285 days when disregarding transportation days. It started on the 1st of December 2014, whereas the outdoor tests started on the 2nd of June (C-OPV-F1), 11th July (AgNW-OPV-PT-Ag) and 26th November 2014 (C-OPV-F2). The starts of the outdoor tests vary due to the different production date of the samples, as reported in the previous sections. C-OPV-F1 modules had an initial average performance of 1.4% whereas C-OPV-F2 had an average of 2.2% and AgNW-OPV-PT-Ag 2.1%. 34 days after test under greenhouse 1 conditions, the module efficiencies decayed similarly for all C-OPV devices. As only ~70% of sunlight reached the samples through the plastic wall, this degradation is ascribed to the effects of the high humidity. AgNW-OPV modules suffer less with such conditions, remaining rather stable. After 144 days of test (disregarding transportation days) which corresponded to 83 days under greenhouse 1 and 61 days in greenhouse 2 conditions, the C-OPV-F1 modules degraded to 68% of the initial

efficiency, C-OPV-F2 recovered back to 100%, and AgNW-OPV-PT-Ag devices remained stable. RH was around 70% in the greenhouse 2 conditions in the period of these 61 days. By the end of the test, the performance of C-OPV-F1 and C-OPV-F2 were 20% and 42% of their initial efficiencies respectively. AgNW-OPV-PT-Ag modules decayed to 79% of their initial PCE in average after this last period which corresponded to 60 days under greenhouse 2 and 81 days under greenhouse 3 conditions.

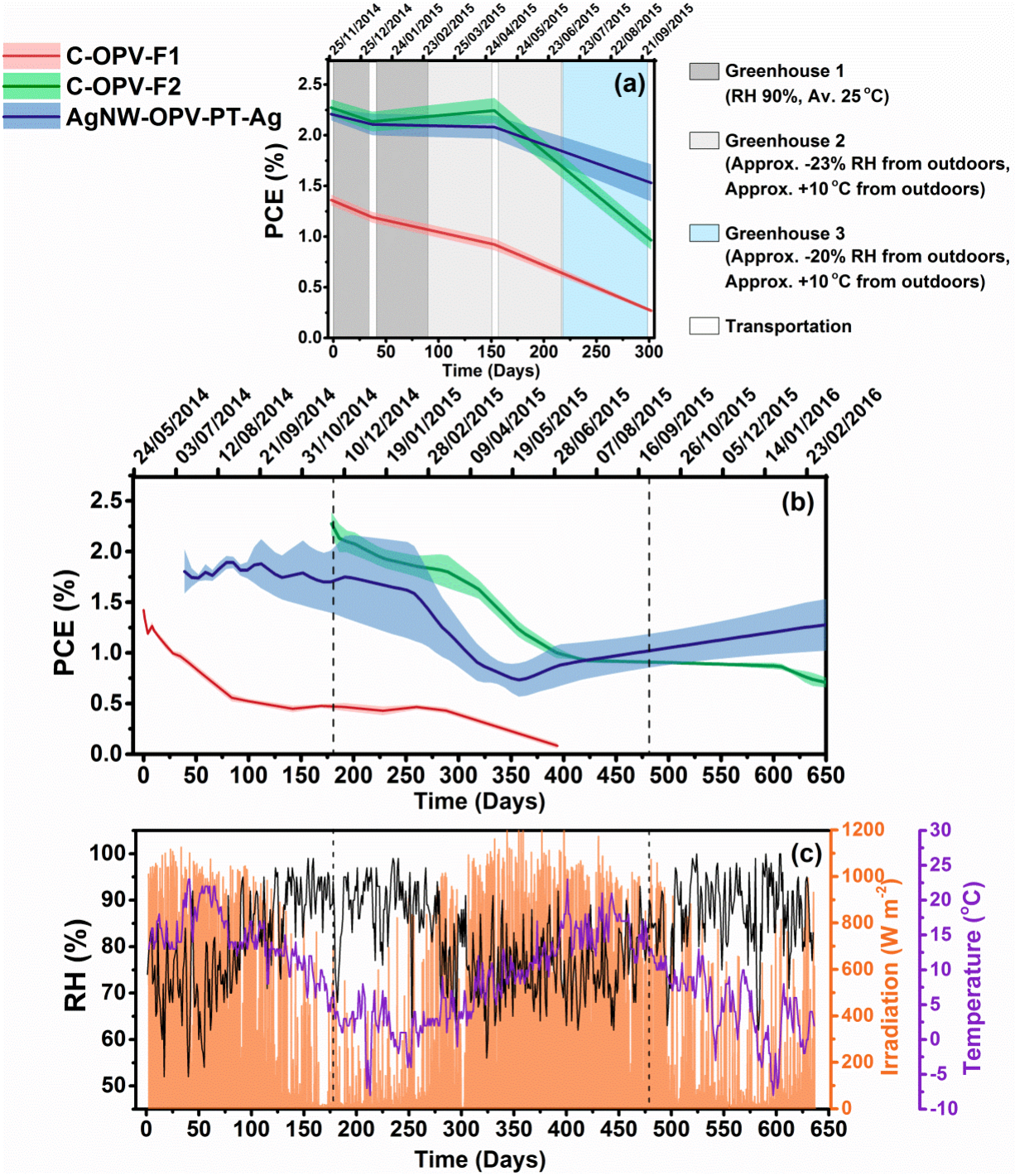

Figure 4.19 - Average stability curves for the (a) greenhouse and (b) outdoor tests of C-OPV-F1, C-OPV-F2 and AgNW-OPV; and (c) outdoors data for RH (black line), irradiation (dark yellow line) and temperature (purple line). The dashed vertical lines in (b) and (c) mark the corresponding first and last days of greenhouse test (a). Reprinted with permission from [31].

The average stability curves of the outdoor tests in Figure 4.19b are represented in real PCE value instead of normalised as shown in the previous Sections 4.2.1, 4.2.2 and 4.3.1, where the stability behaviour were detailed. Comparing the greenhouse and outdoor tests, it is remarkable that overall the OPV samples inside the greenhouses had slower degradation rates. In the first 34 days of the greenhouse test, the effect of the high humidity is less damaging for the C-OPV than the high illumination period under outdoor conditions. For AgNW-OPV, this first period in the greenhouse seemed to be the similar or slightly harsher (although it is hard to tell with the large variations) than outdoors, but the modules remained stable during the following period. The greenhouse test from day 40 until 150 was only harsh for C-OPV-F1, probably due to the issues with the bubble barrier (commented in Section 4.2.1). During the same period outdoor, C-OPV-F2 and AgNW-OPV-PT-Ag severely affected by the weather conditions while the greenhouses acted as a protective shelter. From day 157 until the end of the greenhouse test, the greenhouse conditions did not minimise the effect of the weather and high illumination over the C-OPVs. The AgNW-OPV-PT-Ag modules degraded less in the greenhouses than outdoors, and if the test would be continued, it was expected that the modules would recover similarly as in the outdoor conditions.

4.5.Operational lifetime

To express the operational lifetime of the OPV devices of every condition tested in this work, the lifetime markers [E_0;T_{80}] and [E_S;T_{S80}] (presented in Section 4.1 of this table) and the o-diagram are used. The o-diagram, where “o” stands for OPV, is a scatter plot which has the purpose to categorize the performance of the samples by means of simple time units. The time scale in the X-axis is Log_4 (days) making possible the straightforward comparison in common time units shown in the upper part of the diagram, and also allows establishing the relations between the different tests. The Y-axis represents the initial PCE and [E_0;T_{80}] and [E_S;T_{S80}] are shown in solid and open symbols, respectively, as represented in the diagram legend. When T_f is taken instead of T_{80} or T_{S80}, the marker is followed with an arrow in the sample corresponding colour.

Some important remarks for the o-diagram plot in Figure 4.20 included:

- Several of the curves presented in Subchapter 4.2 and 4.3 had an initial increase followed by a reduction. For defining the lifetime markers in the o-diagram, the maximum was considered as the new E_0 at corresponding T_0. The initial section of the curve was then disregarded as stablished in the baselines [7]. The only exception was for AgNW-OPV-PT-Ag outdoor tests, where for 100 days the PCE increased and reduced several times making unclear if this rule was applicable.
- Even though the markers should be one or another, when the proper lifetime marker is [E_S;T_{S80}], both markers are shown, in order to present the initial efficiencies of the correspondent sample.
- There are red and green shaded blocks in the diagram of ISOS conditions. Those areas correspond respectively to the median and maximum lifetime values for encapsulated OPV devices after the scanning of more than 600 papers [6,7]. Those baselines can serve as reference, for instance, if device stability outperforms the median, then the sample has an improved lifetime; and if the stability performance of a device is in the maximum region or beyond, then the sample has an outstanding or record lifetime. However, the baselines report all dark tests in one group, making no distinction between ISOS-D-2 and ISOS-D-3; as well as for light tests, not differentiating between ISOS-L-2 and ISOS-L-3.

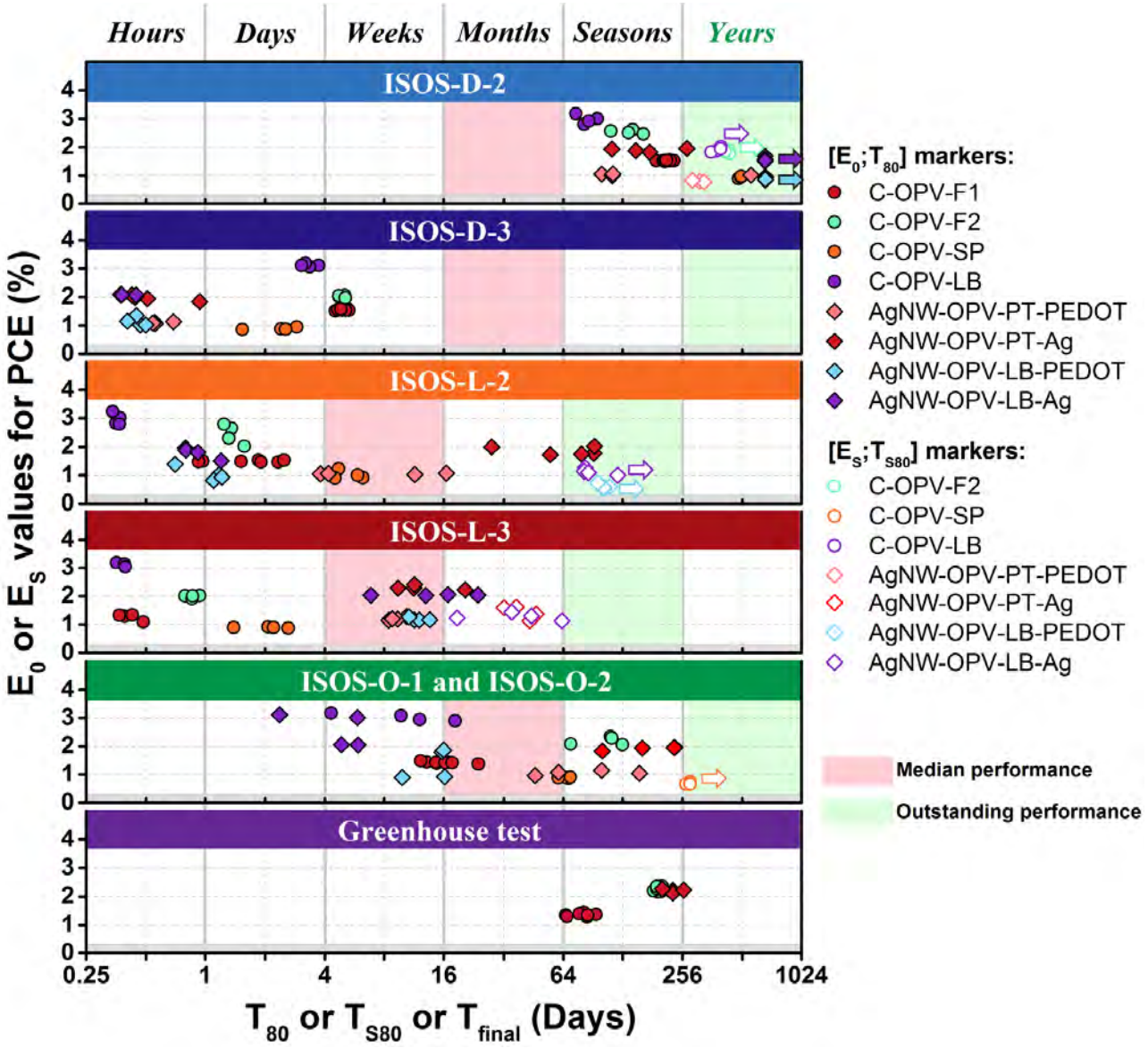

Figure 4.20 - The o-diagram presenting $[E_0;T_{80}]$ and $[E_S;T_{S80}]$ values for all tested samples under indoor (ISOS-D-2, ISOS-D-3, ISOS-L-2, ISOS-L-3), outdoor (ISOS-O-1 and ISOS-O-2), and greenhouse (1, 2 and 3) conditions detailed in tables 4.1 and 4.2. The arrows show the data where T_{final} was used instead of T_{80} or T_{S80}.

In ISOS-D-2, all devices tested had improved lifetime when compared with the baselines. C-OPV-F1 had lifetime in the range of seasons for ISOS-D-2 and in the range of years for ISOS-D-1 with similar E_0 (not shown in the o-diagram since it was the only sample to be under shelf test). C-OPV-F2 and C-OPV-LB had $[E_0;T_{80}]$ also in seasons although the proper operational lifetime marker based on E_S did not reached T_{S80} and T_f was already in the range of years revealing outstanding stability performances of those modules structures and even possibility of records, with PCE still around 2%. C-OPV-SP had initially lower efficiencies than the other C-OPV due to the thicker printed active layer (see Subchapter 2.2.3) and had operational lifetime also in the range of years. AgNW-OPV-PT modules (both Ag-grid back and PEDOT back electrode) had most of the samples with $[E_0;T_{80}]$ in seasons, with the exception of one sample each. AgNW-OPV-PT-PEDOT though had $[E_S;T_{S80}]$ as the proper lifetime marker, then in the range of years. Both AgNW-OPV-LB modules had a remarkable performance in the dark heat test, which are plotted in terms of T_f and have strong potential to be a record of lifetime as the test is still ongoing. In ISOS-D-3, as it is a very harsh

dark test for OPV, all samples below the baseline for dark tests in general. Overall, the C-OPV samples had a longer lifetime for damp heat conditions, especially C-OPV-F1 and F2. AgNW-OPV-PT modules seemed to have slight better resistance to damp and heat than AgNW-OPV-LB modules. In this plot was easy to discern and compare the initial PCE value of each structure.

In ISOS-L-2, the lifetime time of OPV devices was very different from sample to sample, even for devices of the same type that behaved very similarly in the dark conditions. This is an indication that for light tests, more samples should be tested in order to obtain good statistics. C-OPV-F1, C-OPV-F2 and C-OPV-LB underperformed the median lifetime performance for OPV, and C-OPV-SP had the best lifetime performance under ISOS-L-2 of C-OPV technologies, but yet showing improvements in OPV in general for this condition. AgNW-OPV modules in the other hand presented several improved lifetime results (baselines). AgNW-OPV-PT-Ag had two samples in the "improved lifetime" region and three in the "outstanding lifetime" region. AgNW-OPV-PT-PEDOT samples were around the median lifetime; AgNW-OPV-LB had both Ag-grid and PEDOT back electrode structures with $[E_0;T_{80}]$ markers of weeks/hours, but $[E_S;T_f]$ marker in seasons (outstanding region) although with lower PCE than the initial values.

ISOS-L-3 was generally a harsher test than ISOS-L-2 for the OPV devices, due to the controlled humidity. In this test C-OPV-SP had once more the longer lifetime of the C-OPV devices. For AgNW-OPV the performance observed for the modules with and without the back Ag-grid were similar disregarding the different active layer. Only the modules with Ag-grid had $[E_S;T_{S80}]$ marker and improved operational lifetimes in the range of months in such severe test. In comparison to AgNW-OPV with PEDOT as the back electrode, the Ag-grid seemed to have a great deal in holding the conductivity of the device even with the intrinsic bubble formation (see Figure 4.15). The better stability performance of AgNW-OPV over C-OPV under light both tests was possibly due to the AgNW good resistance and even increased conductivity under illumination [35]; plus the foil with UV cut-off used in the manufacture of those modules.

For the outdoor tests, the lifetimes had also a big spread from sample to sample as for ISOS-L-2. As mentioned before, the fabrication dates of C-OPV were different while AgNW-OPV samples were made at the same time. For this reason, while AgNW-OPV outdoor tests started together, C-OPV-F1 tests started 39 days before, C-OPV-F2 started 138 days after, C-OPV-SP started 227 days after and C-OPV-LB started 2000 days after the AgNW-OPV outdoor tests. This can make the comparison of outdoor tests not completely comparable between the OPV types, although in real installed conditions the OPV should be stable under any outdoor weather. At first, the samples with active layer using low band gap polymer donor material had the shorter lifetimes, overlapped later by C-OPV-F1 modules. Leaving the median and entering the improved lifetime period of seasons are C-OPV-F2, AgNW-OPV-PT-PEDOT and AgNW-OPV-PT-Ag. The only sample to have $[E_S;T_{S80}]$ marker was C-OPV-SP actually not even reaching T_{S80} and represented by $[E_S;T_f]$ already in the range of years, though with PCE lower than 1%. Anyway, such longer lifetime could be because those are the only samples which are fully printed, not having paths for the ingression of water and oxygen through coated layers that touch the module edges.

Comparing the outdoor lifetime of the samples also tested under greenhouse conditions (see Section 4.4), C-OPV-F1 and C-OPV-F2 modules under greenhouse conditions had a considerably longer operational lifetime than under outdoor conditions. For C-OPV-F1 specially, if used to generate electricity from inside the greenhouse, their lifetime changes from weeks/months to seasons. AgNW-OPV-PT-Ag modules inside the greenhouses and outdoors had very similar lifetime performances; therefore the protection provided by the greenhouse structure did not bring much improvement in the lifetime of AgNW-OPV modules compared to the encapsulation itself.

An important remark is that for ISOS-D-3, ISOS-L-3 and ISOS-O-1 the main reason ascribed for degradation was the diffusion of humidity through the rather short edges of the modules and the channels created at the device external contacts (metal snaps), which had been demonstrated earlier for similar modules [22].

4.6.Conclusions

In this chapter the stability behaviour of 8 different OPV structures were described. In total seven ISOS conditions were performed and a vast number of samples were observed to have outstanding lifetimes and some even with the potential to reach records in the future. Table 4.3 summarise the operational lifetime of the OPV types in intuitive time units. Taking into account the OPV baselines presented by Gevorgyan et al. [7], the shades marked in green indicate outstanding lifetime, in blue improved lifetime, red median lifetime and grey inferior to median lifetime.

Table 4.3 - Summary of the best lifetime of OPV modules in common time units. Based on the OPV baselines [7], green shading indicate outstanding lifetime, blue improved lifetime, red median lifetime and grey inferior to median lifetime.

Device	Dark	Light AM1.5G	Outdoor
C-OPV-F1	Seasons	Days	Months
C-OPV-F2	Years*	Days	Seasons
C-OPV-SP	Years	Weeks	Years*
C-OPV-LB	Years*	Hours	Weeks/Months
AgNW-OPV-PT-Ag	Seasons	Seasons	Seasons
AgNW-OPV-PT-PEDOT	Years	Weeks	Seasons
AgNW-OPV-LB-Ag	Years*	Seasons*	Weeks
AgNW-OPV-LB-PEDOT	Years*	Seasons*	Weeks/Months

* Lifetime expressed in T_f as the modules did not reach T_{80} or T_{S80} by the competition of this work. Especially for dark conditions, those devices have the potential to have record lifetimes in the future.

Some specialised greenhouses have temporary structures, reinstalled every season, where both C-OPV and AgNW-OPV achieved the needed operation lifetime to be compatible with the timespan of such structures. The C-OPV modules that represent the most environmentally friendly OPV technology can be safely disposed even in normal municipal waste. C-OPV application in developing countries could be made on a very large scale and they have the potential for running stand-alone greenhouses and surrounding communities with harmless environmental impacts. AgNW-OPV modules have the better operational performance and the potential for higher efficiencies and higher power per area.

In large-scale outdoor OPV installations, several engineering strategies, such as OPV fabricated with larger edges, UV-filters (exemplified in Section 4.2.1) and roof cladding (shown in Section 4.3.1) are applicable in order to prolong the operational lifetime and increase energy production, where for the postcard modules tested in this chapter, a somewhat faster degradation approach was taken with the use of limited edges, simple encapsulation and not highly protected contacts.

4.7.References

1. Grossiord, N.; Kroon, J. M.; Andriessen, R.; Blom, P. W. M. Degradation mechanisms in organic photovoltaic devices. *Org. Electron.* **2012**, *13*, 432.

2. Cheng, P.; Zhan, X. Stability of organic solar cells: challenges and strategies. *Chem. Soc. Rev.* **2016**, *45*, 2544.

3. Reese, M. O.; Gevorgyan, S. A.; Jørgensen, M.; Bundgaard, E.; Kurtz, S. R.; Ginley, D. S.; Olson, D. C.; Lloyd, M. T.; Morvillo, P.; Katz, E. a.; Elschner, A.; Haillant, O.; Currier, T. R.; Shrotriya, V.; Hermenau, M.; Riede, M.; R. Kirov, K.; Trimmel, G.; Rath, T.; Inganäs, O.; Zhang, F.; Andersson, M.; Tvingstedt, K.; Lira-Cantu, M.; Laird, D.; McGuiness, C.; Gowrisanker, S. (Jimmy); Pannone, M.; Xiao, M.; Hauch, J.; Steim, R.; DeLongchamp, D. M.; Rösch, R.; Hoppe, H.; Espinosa, N.; Urbina, A.; Yaman-Uzunoglu, G.; Bonekamp, J.-B.; van Breemen, A. J. J. M.; Girotto, C.; Voroshazi, E.; Krebs, F. C. Consensus stability testing protocols for organic photovoltaic materials and devices. *Sol. Energy Mater. Sol. Cells* **2011**, *95*, 1253.

4. Gevorgyan, S. a.; Corazza, M.; Madsen, M. V.; Bardizza, G.; Pozza, A.; Müllejans, H.; Blakesley, J. C.; Dibb, G. F. a.; Castro, F. a.; Trigo, J. F.; Guillén, C. M.; Herrero, J. R.; Morvillo, P.; Maglione, M. G.; Minarini, C.; Roca, F.; Cros, S.; Seraine, C.; Law, C. H.; Tuladhar, P. S.; Durrant, J. R.; Krebs, F. C. Interlaboratory indoor ageing of roll-to-roll and spin coated organic photovoltaic devices: Testing the ISOS tests. *Polym. Degrad. Stab.* **2014**, *109*, 162.

5. Corazza, M.; Krebs, F. C.; Gevorgyan, S. A. Lifetime of organic photovoltaics: Linking outdoor and indoor tests. *Sol. Energy Mater. Sol. Cells* **2015**, *143*, 467.

6. Gevorgyan, S. A.; Madsen, M. V.; Roth, B.; Corazza, M.; Hösel, M.; Søndergaard, R. R.; Jørgensen, M.; Krebs, F. C. Lifetime of Organic Photovoltaics: Status and Predictions. *Adv. Energy Mater.* **2015**, *6*, 1501208.

7. Gevorgyan, S. A.; Espinosa, N.; Ciammaruchi, L.; Roth, B.; Livi, F.; Tsopanidis, S.; Züfle, S.; Queirós, S.; Gregori, A.; Benatto, G. A. dos R.; Corazza, M.; Madsen, M. V.; Hösel, M.; Beliatis, M. J.; Larsen-Olsen, T. T.; Pastorelli, F.; Castro, A.; Mingorance, A.; Lenzi, V.; Fluhr, D.; Roesch, R.; Maria Duarte Ramos, M.; Savva, A.; Hoppe, H.; Marques, L. S. A.; Burgués, I.; Georgiou, E.; Serrano-Luján, L.; Krebs, F. C. Baselines for Lifetime of Organic Solar Cells. *Adv. Energy Mater.* **2016**, 1600910.

8. Corazza, M.; Krebs, F. C.; Gevorgyan, S. A. Predicting, categorizing and intercomparing the lifetime of OPVs for different ageing tests. *Sol. Energy Mater. Sol. Cells* **2014**, *130*, 99.

9. Roth, B.; Dos Reis Benatto, G. A.; Corazza, M.; Søndergaard, R. R.; Gevorgyan, S. A.; Jørgensen, M.; Krebs, F. C. The Critical Choice of PEDOT:PSS Additives for Long Term Stability of Roll-to-Roll Processed OPVs. *Adv. Energy Mater.* **2015**, *5*, 1401912.

10. Kettle, J.; Bristow, N.; Gethin, D. T.; Tehrani, Z.; Moudam, O.; Li, B.; Katz, E. A.; dos Reis Benatto, G. A.; Krebs, F. C. Printable luminescent down shifter for enhancing efficiency and stability of organic photovoltaics. *Sol. Energy Mater. Sol. Cells* **2016**, *144*, 481.

11. Espinosa, N.; Laurent, A.; Dos Reis Benatto, G. A.; Hösel, M.; Krebs, F. C. Which Electrode Materials to Select for More Environmentally Friendly Organic Photovoltaics? *Adv. Eng. Mater.* **2016**, *18*, 490.

12. Dos Reis Benatto, G. A.; Roth, B.; Madsen, M. V. M. V.; Hösel, M.; Søndergaard, R. R. R. R.; Jørgensen, M.; Krebs, F. C. F. C. Carbon: The Ultimate Electrode Choice for Widely Distributed Polymer Solar Cells. *Adv. Energy Mater.* **2014**, *4*, 1400732.

13. Hösel, M.; Angmo, D.; Søndergaard, R. R.; dos Reis Benatto, G. A.; Carlé, J. E.; Jørgensen, M.; Krebs, F. C. High-Volume Processed, ITO-Free Superstrates and Substrates for Roll-to-Roll Development of Organic Electronics. *Adv. Sci.* **2014**, 1400002.

14. Espinosa, N.; Søndergaard, R. R.; Jørgensen, M.; Krebs, F. C. Flow Synthesis of Silver Nanowires for

Semitransparent Solar Cell Electrodes: A Life Cycle Perspective. *ChemSusChem* **2016**, *9*, 893.

15. Emmott, C. J. M.; Urbina, A.; Nelson, J. Environmental and economic assessment of ITO-free electrodes for organic solar cells. *Sol. Energy Mater. Sol. Cells* **2012**, *97*, 14.

16. dos Reis Benatto, G. A.; Roth, B.; Corazza, M.; Søndergaard, R. R.; Gevorgyan, S. A.; Jørgensen, M.; Krebs, F. C. Roll-to-roll printed silver nanowires for increased stability of flexible ITO-free organic solar cell modules. *Nanoscale* **2016**, *8*, 318.

17. Mayousse, C.; Celle, C.; Fraczkiewicz, A.; Simonato, J. Stability of silver nanowire based electrodes under environmental and electrical stresses. *Nanoscale* **2015**, 2107.

18. Krebs, F. C.; Hösel, M.; Corazza, M.; Roth, B.; Madsen, M. V.; Gevorgyan, S. a.; Søndergaard, R. R.; Karg, D.; Jørgensen, M. Freely available OPV-The fast way to progress. *Energy Technol.* **2013**, *1*, 378.

19. Dam, H. F.; Andersen, T. R.; Pedersen, E. B. L.; Thydén, K. T. S.; Helgesen, M.; Carlé, J. E.; Jørgensen, P. S.; Reinhardt, J.; Søndergaard, R. R.; Jørgensen, M.; Bundgaard, E.; Krebs, F. C.; Andreasen, J. W. Enabling Flexible Polymer Tandem Solar Cells by 3D Ptychographic Imaging. *Adv. Energy Mater.* **2014**, 3.

20. Roth, B. B.; Dos Reis Benatto, G. A.; Corazza, M.; Carlé, J. E. J. E.; Helgesen, M.; Gevorgyan, S. A. S. A.; Jørgensen, M.; Søndergaard, R. R. R. R.; Krebs, F. C. F. C. Improving the Operational Stability of PBDTTTz-4 Polymer Solar Cells Modules by Electrode Modification. *Adv. Eng. Mater.* **2016**, *18*, 511.

21. Dos Reis Benatto, G. A.; Roth, B.; Corazza, M.; Søndergaard, R. R.; Gevorgyan, S. A.; Jørgensen, M.; Krebs, F. C. Roll-to-roll printed silver nanowires for increased stability of flexible ITO-free organic solar cell modules. *Nanoscale* **2015**, *8*, 318.

22. Gevorgyan, S. A.; Madsen, M. V.; Dam, H. F.; Jørgensen, M.; Fell, C. J.; Anderson, K. F.; Duck, B. C.; Mescheloff, A.; Katz, E. A.; Elschner, A.; Roesch, R.; Hoppe, H.; Hermenau, M.; Riede, M.; Krebs, F. C. Interlaboratory outdoor stability studies of flexible roll-to-roll coated organic photovoltaic modules: Stability over 10,000 h. *Sol. Energy Mater. Sol. Cells* **2013**, *116*, 187.

23. Angmo, D.; Krebs, F. C. Over 2 Years of Outdoor Operational and Storage Stability of ITO-Free, Fully Roll-to-Roll Fabricated Polymer Solar Cell Modules. *Energy Technol.* **2015**, *3*, 774.

24. Kettle, J.; Bristow, N.; Sweet, T. K. N.; Jenkins, N.; Dos Reis Benatto, G. A.; Jørgensen, M.; Krebs, F. C. Three dimensional corrugated organic photovoltaics for building integration; Improving the efficiency, oblique angle and diffuse performance of solar cells. *Energy Environ. Sci.* **2015**, *8*.

25. Azzopardi, B.; Emmott, C. J. M.; Urbina, A.; Krebs, F. C.; Mutale, J.; Nelson, J. Economic assessment of solar electricity production from organic-based photovoltaic modules in a domestic environment. *Energy Environ. Sci.* **2011**, *4*, 3741.

26. Emmott, C. J. M.; Röhr, J. A.; Campoy-Quiles, M.; Kirchartz, T.; Urbina, A.; Ekins-Daukes, N. J.; Nelson, J. Organic photovoltaic greenhouses: a unique application for semi-transparent PV? *Energy Environ. Sci.* **2015**, *8*, 1317.

27. Krebs, F. C.; Biancardo, M.; Winther-Jensen, B.; Spanggard, H.; Alstrup, J. Strategies for incorporation of polymer photovoltaics into garments and textiles. *Sol. Energy Mater. Sol. Cells* **2006**, *90*, 1058.

28. Krebs, F. C.; Hösel, M. The Solar Textile Challenge: How It Will Not Work and Where It Might. *ChemSusChem* **2015**, *8*, 966.

29. Systems, E. pro-solar OMBRA-DLS® http://www.elasol.eu/en/what-is-ombra-dls.html (accessed Dec 28, **2016**).

30. Espinosa, N.; Hösel, M.; Angmo, D.; Krebs, F. C. Solar cells with one-day energy payback for the factories of the future. *Energy Environ. Sci.* **2012**, *5*, 5117.

31. dos Reis Benatto, G. A.; Corazza, M.; Roth, B.; Schütte, F.; Rengenstein, M.; Gevorgyan, S. A.; Krebs, F. C. Inside or Outside? Linking Outdoor and Indoor Lifetime Tests of ITO-Free Organic Photovoltaic Devices for Greenhouse Applications. *Energy Technol.* **2016**, doi: 10.1002/aenm.201600910.

32. Fitz-Rodríguez, E.; Kubota, C.; Giacomelli, G. A.; Tignor, M. E.; Wilson, S. B.; McMahon, M. Dynamic modeling and simulation of greenhouse environments under several scenarios: A web-based application. *Comput. Electron. Agric.* **2010**, *70*, 105.

33. M. Kottek, J. Grieser, C. Beck, B. Rudolf, F. R. World Map of the Köppen-Geiger climate classification updated. *Meteorol. Zeitschrift* **2006**, *15*, 259.

34. Historical Weather https://www.wunderground.com/history/ (accessed Feb 1, **2016**).

35. Mayousse, C.; Celle, C.; Moreau, E.; Mainguet, J.-F.; Carella, A.; Simonato, J.-P. Improvements in purification of silver nanowires by decantation and fabrication of flexible transparent electrodes. Application to capacitive touch sensors. *Nanotechnology* **2013**, *24*, 215501.

Chapter 5

Environmental impact of OPV during the use phase and end-of-life

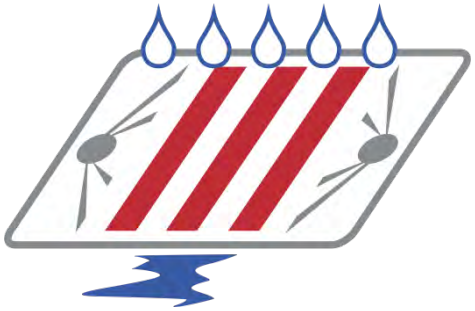

With the mass-production and projected deployment of OPV technologies, challenges associated with their end-of-life management and during operation must be addressed. In this chapter the emission of Ag and Zn to the environment from OPV in both situations was quantified in simulated use phase and landfilling scenario experiments. The quantitative data is also assessed environmentally and can serve to adjust the inputs for LCA models, allowing for realistic assessments of the sustainability of OPV.

5.1. Use phase

OPV panels for energy production are well packaged with a thin plastic barrier designed to protect it from liquid water ingress. During operation, while producing electricity, no leaching or emission should take place, as the contacts would be properly protected. A number of stresses constantly challenge the integrity of the OPV, such as UV radiation, thermal expansion, rain, snow, as reoccurring stresses; and also singular ones as heavy winds and hail. Damage to encapsulation as crack formation or delamination can eventually happen allowing the ingress of air and water, and/or the emission of OPV compounds to the environment. Such effects could also come out from unintended induction from improper installation or manufacture. The detrimental effects from OPV components emitted into environmental sections such as air, soil, water and biota have as yet not been quantified [1]. At the same time, only the systematic and quantitative field data would be able to verify the potential environmental impact associated with OPV components in such case.

It is possible to quantify the emission of metals to the environment with OPV devices subjected to simulated and controlled failure. The metal release data can serve to adjust the inputs for LCA models, allowing for realistic assessments of the sustainability of OPV. For measuring the release of metallic

components from an OPV outdoor installation, a new a rain runoff setup has been design, simulating use-phase.

Besides metals, it would be of particularly important to look at the environmental factors of the organic molecules contained in OPV. But, these organic molecules do not yet exist in databases [2], and the main challenge of using toxicology indicators in LCA is still the lack of data in life cycle inventories [3].

5.1.1. Experimental details

5.1.1.1. Samples description

The Ag-OPV samples are the same presented in Chapter 3, with layer stack and printed layout shown in Figure 3.2 and 3.3 respectively. The architecture of the devices was comprised of barrier/Ag-grid/ PEDOT:PSS/ZnO/P3HT:PCBM/PEDOT:PSS/Ag-grid/adhesive/barrier. Concerning the metal content, 4.9 g of Ag and 0.07 g of Zn were contained in 1 m^2 of Ag-OPV. The here called C-OPV samples for shorten are C-OPV-F1 samples shown in Subchapter 2.2 and detailed in Section 2.2.1 from Chapter 2. They were ITO-, vacuum- and Ag-free OPV modules. Their architecture was comprised of barrier/PEDOT:PSS/ ZnO/P3HT:PCBM/PEDOT:PSS/carbon/adhesive/barrier. Concerning the metal content, only 52.3 mg of Zn was contained in 1 m^2 of C-OPV.

5.1.1.2. Rain runoff experiment setup

The rain runoff installation was set up in at DTU Risø campus, Roskilde, Denmark. In Figure 5.1 the installation can be seen in the OPV solar park structure. The following OPV samples were installed for rain runoff setup with total area of 0.46 m^2, which correspond to the area needed to produce 1kWh with Ag-OPV panels:

- Ag-OPV samples damaged by regular knife cutting a worst case with severe mechanical stress, such as prolonged exposure to hail, wind, thermal stress, etc. (insight of Figure 5.1).
- Ag-OPV intact samples.
- Sets of 32 postcard sized intact C-OPV (0.1 x 0.14 m; total area 0.46 m^2).
- Blank areas as references.

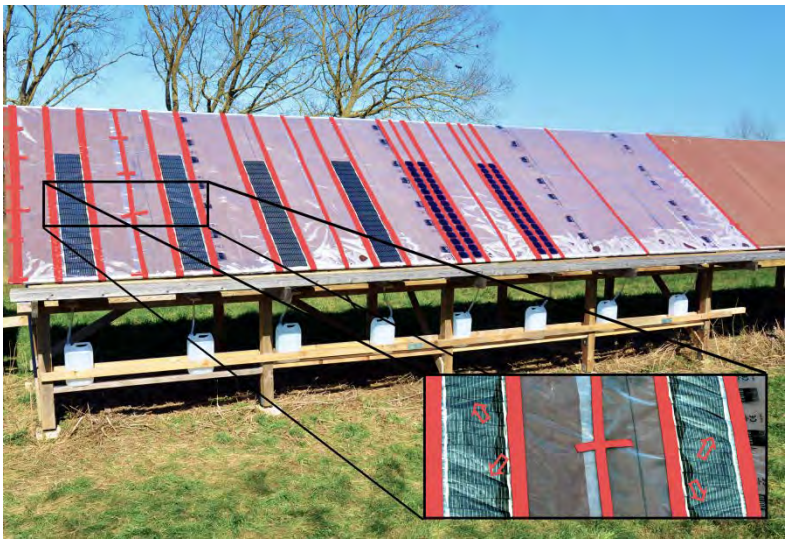

Figure 5.1 - Rain run-off experiment setup at DTU, Risø campus (Denmark), used to study the emission of elements to the environment from OPV during operation and failure. The inset shows the damage provoked in the first two Ag-OPV samples, simulating a worst case scenario. Reprinted with permission from [4].

The experiment was carried out in duplicate, with the focus on the correlation of visible damage (therefore, performance) with the release of metals, and evaluation of environmental concerns in case of failure during the use phase. A plastic foil was placed on the total collection area, underneath the samples, in order to protect and avoid metal contamination from nails and screws of the wooden platform structure. The rain water and water from condensation (dew and fog) was collected with plastic gutters (0.4 m long) installed with funnels connected through plastic tubes into plastic canisters of 10 L. Although the OPV area per sample was 0.46 m^2, the total area of collection per sample was 0.84 m^2. Water samples were taken when the canisters were full depending on the precipitation. Water samples of 250 mL were collected from 10 L homogenised water (though shaking of the full canister's content) and stored for analysis. Online information for precipitation was acquired from the local weather station at the DTU wind research facility also in Risø campus [5]. The experiment started on April 10th 2015 and finished on October 15th 2015. The total precipitation during six months period was 446.8 L m^2.

5.1.1.3. Metal detection

The metal content in the water samples was determined by digestion and inductively coupled plasma mass spectrometry (ICP-MS) analysis. Every water sample was acidified to a final concentration of 1% HNO_3 prior to analysis. Semiconductor grade acids were used for ICP-MS sample preparation. Ag and Zn were quantified using matrix matched calibration (1% HNO_3) with multi-element standards (Sigma-Aldrich). The isotopes ^{7}Li, ^{23}Na, ^{24}Mg, ^{27}Al, ^{39}K, ^{44}Ca, ^{47}Ti, ^{52}Cr, ^{55}Mn, ^{57}Fe, ^{59}Co, ^{60}Ni, ^{65}Cu, ^{66}Zn, ^{69}Ga, ^{75}As, ^{78}Se, ^{85}Rb (as internal standard), ^{98}Mo, ^{106}Cd, ^{107}Ag, ^{115}In, ^{118}Sn, ^{121}Sb, and ^{208}Pb were analysed on an Agilent 7500cx ICP-MS (Agilent Technologies AG, Basel, Switzerland) using a dwell time of 0.3 seconds per isotope. The argon plasma was operated at 1550 W, 15 mL min^{-1} plasma gas, 0.79 mL min^{-1} carrier gas and 0.35 mL min^{-1} makeup gas. The octopole was pressurized with 5.0 mL min^{-1} helium, except for ^{78}Se, where 3.6 mL min^{-1} hydrogen was used. The amounts of leached metals were then corrected to be represented by means of 1 m^2.

5.1.2. Emission of Ag and Zn during use phase

Figure 5.2 shows the OPV samples appearance after the six months of experiment. Some modules were damaged, while only Ag-OPV intact no. 2 did not show delamination with visible water ingress. Figure 5.3 shows the cumulative metal leaching (Ag and Zn) during the rain runoff experiment. The amounts are expressed in mg per m^2 of OPV (right axis) and the corresponding share of leached material (left axis). For the reference samples, the amounts were calculated as if the cells were installed, therefore the corresponding share did not apply. A virtually linear release of Ag to the environment from the damaged Ag-OPV modules was observed, reaching 7.9 and 14.3 mg of Ag from 1 m^2 OPV over the whole six months. This corresponded to 0.16-0.29% of the total contained Ag. The duplicated samples differed by a factor of almost two by the end of the experiment, since between days 129 and 182, a clog in the rain gutter of sample Ag-OPV damaged no2 in the Figure 5.2 was unnoticed and rain water was lost. If the linear trend is extrapolated between day 35 and day 129, it is suggested that the module would have emitted a similar amount of Ag compared to the duplicate Ag-OPV damaged sample.

For Zn, the similar linear leaching trend was observed, reaching 65.7 and 79.0 mg of Zn from 1 m^2 OPV, corresponding to the complete release of the Zn contained originally in the sample (94-113% of the theoretical total value). The relatively small scale of the field set up may be the cause for the variation between the duplicates. Until day 90, the Ag-OPV intact samples did not release any of its contained metals (Ag, Zn). After that, sample Ag-OPV intact (1) started to delaminate (marked with an asterisk in the graphs

from Figure 5.3). Subsequently, Ag leaching reached 0.29% of the total contained Ag, which was very similar to Ag-OPV damaged, but within a shorter time period (~165 vs. ~95 days). Zn started to leach after delamination as well, reaching 54% of the overall contained Zn by the end of the experiment.

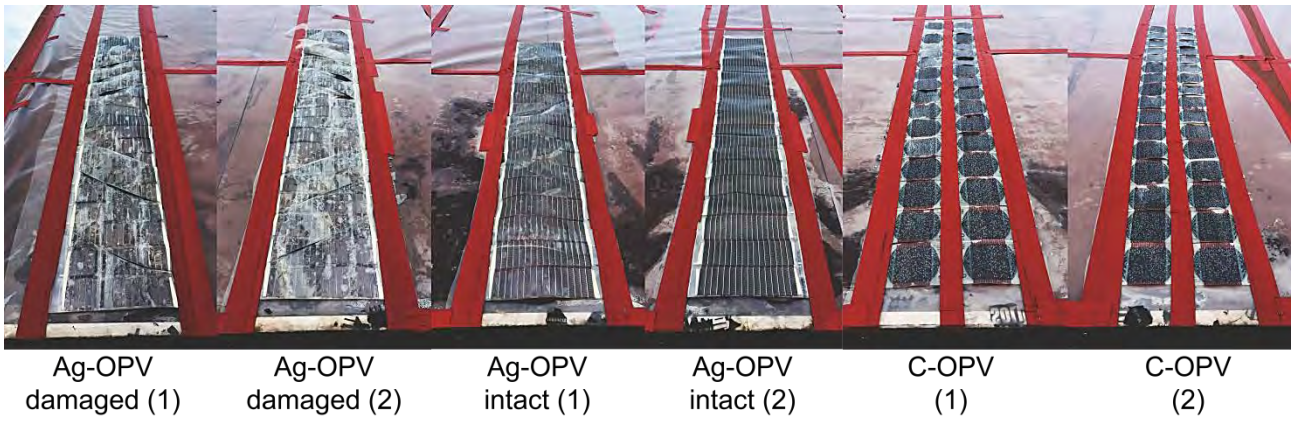

Figure 5.2 - Photography of the rain run-off samples at the end of the experiment. Note that only the sample Ag-OPV intact (2) did not show delamination with visible water ingress. Reprinted with permission from [4].

For the Ag-OPV intact (2), the Ag and Zn emissions were in the range of the blank references, from unadulterated rain, atmosphere and dust in the outside. Similar levels of Zn were also observed in the reference samples and in Ag-OPV intact (2). There was no sign of Ag in the references, C-OPV or Ag-OPV intact (2) samples, and only when failure took place (either induced or spontaneous) that emission levels arose. C-OPV only started to emit Zn after four months of outdoor exposure, as they were not specifically sealed on the edges, thus providing a path to water ingress. C-OPV released Zn in the range of 25-31% of the contained Zn, with a similar rate to Ag-OPV damaged and delaminated.

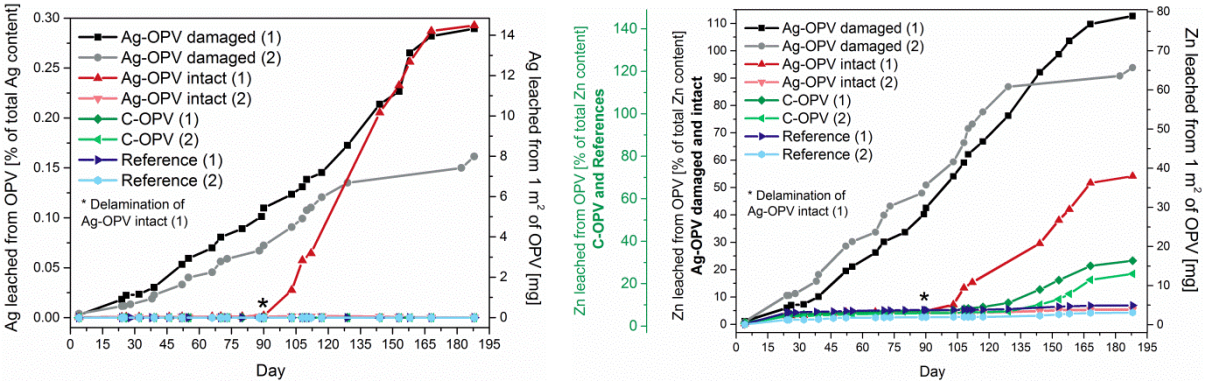

Figure 5.3 - Cumulative Ag (left) and Zn (right) leaching from the samples in the rain run-off experiment conducted in duplicate. See text for detailed description. Reprinted with permission from [4].

5.2.End-of-life - Landfill

The end-of-life (EOL) of a product disposal can include recycling, incineration and/or landfilling/open dumping. The experiment presented here is a part of a project which had already performed simulations for recycling and incineration of Ag-OPV samples. The recycling experiments with de-installed OPV showed that up to 95% of the originally Ag used in the OPV fabrication could be recovered [6]. In incineration, recovery of Ag from the ashes could also be accomplished, but with significant reduction of materials and

treatment time (in comparison with the recycling treatment) and in addition had the potential for heat recovery during incineration [7]. Both simulations showed the Ag is completely justifiable to be used in OPV as an electrode for mass production when the decommissioning includes such processes.

Nevertheless, not always recycling and incineration are available. In this context, a soil sequestration experiment with OPV buried in soil was built, simulating uncontrolled waste disposal. Such experiment has the goal of quantifying Ag and Zn emission to the environment and the soil proprieties concerning metal sequestration, using shredded OPV as the worst case, and intact rolled modules as the best case.

5.2.1. Experimental details

For the soil sequestration experiment, it was used identical samples as described in Section 5.1.1.1, i.e. Ag-OPV and C-OPV.

5.2.1.1. Soil sequestration experiment setup

For this experiment, OPV samples were either shredded or left entire (rolled up), and buried in soil columns exposed to outdoor conditions. Figure 5.4 shows photographs of the setup with bottles at the bottom of the columns to collect the leachate as a result of natural rain fall; as well as the plant growth during the spring and snowfall during the winter. The experiment ran for over a year, including all seasons and their distinct weather conditions.

Four OPV samples were buried:

- Ag-OPV with 0.25 m^2 rolled-up.
- Ag-OPV with 0.158 m^2 shredded in fragments measuring 4 x 20 mm.
- C-OPV postcard sized samples with 0.25 m^2 rolled-up.
- C-OPV postcard sized samples with 0.158 m^2 shredded in fragments measuring 4 x 20 mm.

Figure 5.4 - Soil sequestration setup at DTU, Risø campus (Denmark) (left). Plant growth (top right) and snowfall (bottom right). Adapted with permission from [4].

Glass columns, with cross-sectional area of 122.72 cm^2 were the compartments where the samples buried in soil were placed. The column were mounted on a trolley and placed outdoors at DTU, Risø Campus, Denmark. The rolled-up samples were buried in a total of 4.5 kg of soil, placed in the centre, leaving soil up and down in the column. The shredded samples were homogenously distributed in 2 kg of soil. 10 cm of soil was added on top as a cover layer in all columns. The leachates were collected in glass flasks connected to the columns with glass funnels. A layer of sand and 120 mesh polyester filters were placed between the soil and funnel, to avoid soil loss to the collection flasks. The structure was exposed to outdoor conditions (Figure 5.5) from November 5th 2014 to October 29th 2015. The leachates were collected when the glass flasks were full. By the end of the experiment, the column contents were divided into five soil layers, with three soil samples taken from every depth layer, and also from the sand layer.

5.2.1.1. Metal detection

The same procedure for the water samples in the rain runoff experiment (Section 5.1.1.3) were applied to the leachates of the soil sequestration experiment. The soil and sand samples were digested as follows: 501 ± 4mg of material was digested with 2 mL of aqua regia (65% HNO_3 and 32% HCl, 1:3 v/v) at room temperature overnight and diluted to a final concentration of 5% aqua regia prior to analysis. Ag and Zn were quantified using matrix matched calibration (1% HNO3 or 5% aqua regia) with multi-element standards, as already describe in Section 5.1.1.3 as well.

5.2.2. Emission of Ag and Zn during landfilling

Figure 5.5 shows the soil profile and the water for Ag content from 1 m^2 of OPV in the four soil columns after one year of experiment. The added up amount of leached Ag from shredded Ag-OPV (771.7 mg) corresponds to 15.7% of the total Ag contained originally in the module. The amount from rolled up Ag-OPV (25.6 mg) corresponds to 0.5% of its total Ag content.

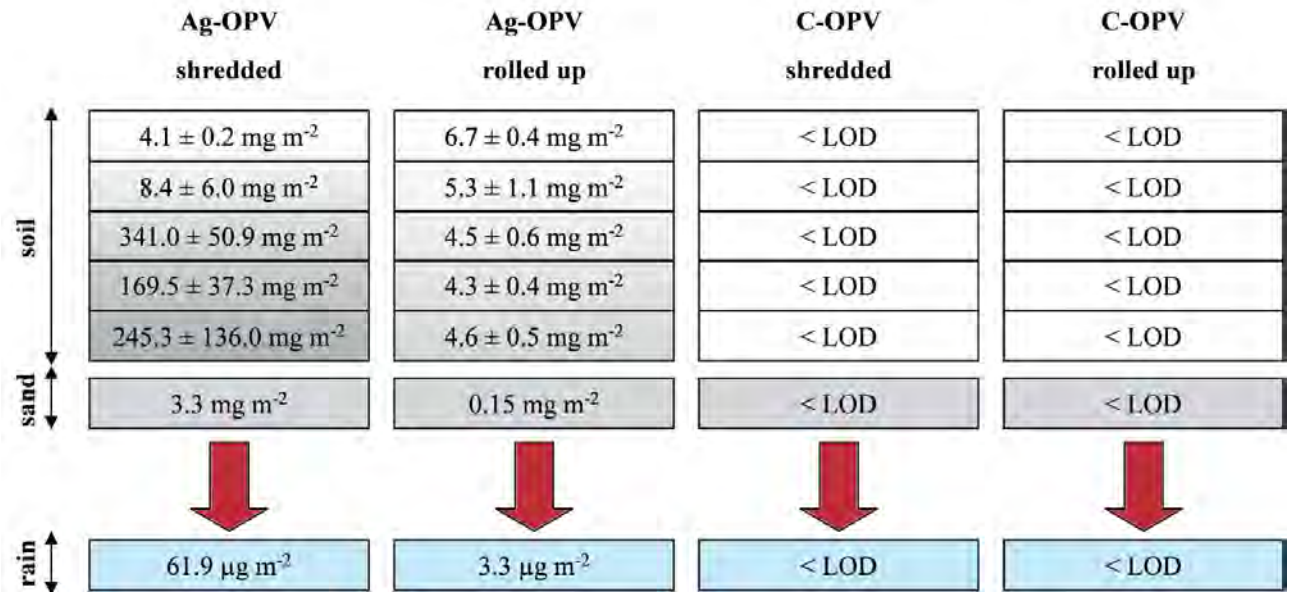

Figure 5.5 - Profile of Ag content in the four soil columns and rain water from 1 m^2 of OPV expressed in mg or µg of Ag, respectively. Adapted with permission from [4].

On the timescale explored, a higher overall amount of Ag reached the soil matrix and leachates and the deeper column layers showed an enrichment of Ag, both in the case of shredded Ag-OPV. For the rolled

up Ag-OPV soil column, Ag had a more homogeneous distribution and the absence of Ag in the leachate columns indicated that the soil had sufficient intrinsic capacity of sequestering Ag, whereas the mechanism may be complex and dependent on the dominant redox conditions in the soil layers [8]. However, the migration of Ag to the bottom of the column with Ag-OPV shredded strongly points towards the fact that the natural sequestration capacity after a year of experiment was exceeded, though break-through was not yet reached.

Comparing with the maximal release during the use phase in the rain runoff scenario (0.29% of total Ag), contact with the soil considerably enhanced the release of Ag (maximum of 15.7% of total Ag), and represented a strong increase to laboratory leaching studies using (other) shredded OPV [9]. A number of soil related properties, such as redox-chemistry, microbial communities and their exudates, and/or perturbation by micro-/macrofauna, may favour the Ag release. This certainly warrants further detailed studies, due to the inherent risks associated with Ag.

Concerning the Zn emission, besides the very low natural Zn content in Danish soil (~ lowest 15% of European top soils [10]), the release of all Zn contained in the Ag-OPV modules would only increase the soil Zn concentration (57-73 mg kg^{-1}) by a factor of ~ 3 to 4. As European top soils contain in average 52 mg kg^{-1}, the impact of OPV-born Zn can be considered minor. Correspondingly, Zn addition from C-OPV modules to soil can be considered minor, since they contained even less Zn than Ag-OPV (see Section 5.1.1.1). These results provide important indications towards EOL managements that include landfilling.

In a modern landfill, the physic-chemical conditions, matrix and hydrology are substantially different from the soil columns. Nevertheless, the observation of the release of Ag upon failure of the embedding material integrity was fast (upon delamination in the rain runoff experiment) and extensive (in soil column experiment). And it appears to be a common phenomenon and potentially not limited to OPV, but also other TFPV technologies. It is also important to point out that mechanical damage during landfilling is very likely, resulting in rapid release of large amounts of Ag. This may represent a challenge for landfill management regarding leachate treatment, especially if part of the treatment relies on biological processes, considering the antibiotic properties of Ag [11].

5.3.Ecotoxicological implications

The World Health Organization (WHO) enforces the edge value for Ag in drinking water at 100 µg L^{-1}. The measured rain runoff Ag concentrations exceeded this limit twice: 127 µg Ag L^{-1} for the Ag-OPV damaged (1) by the day 158 and 181 µg Ag L^{-1} for Ag-OPV intact (1) which delaminated over time, by the day 144. The Ag concentrations in the rain water during all the other days remained below the WHO limit. As the drinking water limits are set most conservatively, seems improbable that any acute or chronic effect by exposure to such a peak concentrations may occur. Though, higher concentrations may occur depending on the covered area and the precipitation.

The WHO drinking water limit for Zn is 3000 µg Zn L^{-1}, while the highest measured Zn environmental concentration was 665 µg Zn L^{-1} for the Ag-OPV damaged (2) by the day 88, therefore not exceeding the established limits. Such results are in good agreement with a previous laboratory study, where the environmental emissions from OPV (other) did not exceed WHO values as well [9]. The peak concentrations observations and direct effects of delamination is an important fact that stressed that field studies are a must for the verification of laboratory derived models.

The release of Ag from buried shredded cells resulted in a maximum of 852.5 mg Ag per kg of soil in the central layer of the 5 depth layers, which was a considerably increased concentration that even exceeded the soil Ag sequestration capacity. Such concentrations certainly depend on the actual amount of OPV that is dumped per volume of soil, where a scenario using ~1/20 m^2 of OPV modules per kg soil does not seem to be an unrealistic approach.

The damaging effect of Ag will surely depend on the complex interaction of chemical/biological redox-reactions influencing Ag speciation in soils. Nevertheless, the overall Ag content resulting from Ag-OPV release raises a considerable eco-toxicological concern, specially towards the fact that for a number of soil enzymatic activities, the ‘‘median effective concentration’’ causing 50% inhibition was found in the sub mg kg^{-1} range of the total soil Ag in a work from in Peyrot et al. [12].

5.4.Life-cycle assessment

While LCA databases are generally very complete for accounting for impacts from raw materials to their disposal, compounds without particular concern for ecotoxicity or unknown fate [1] usually are not represented in standard databases [4]. Nanoparticles in general, for example, can raise nano-toxicity concerns [13,14], though this has been questioned [15]. Released Ag and Zn from OPV might indeed be in nanoparticulate form.

LCA methodology was applied to the rain runoff results in order to evaluate the potential environmental impact on groundwater from metal leaching. The International Reference Life Cycle Data System (ILCD) methodology was used [16], as it was the recommended methodology for the evaluation of the impact potential [17]. The LCA model of the process was a simple one, accounting for the long term effects that the metal emissions in the rain runoff setup to groundwater would cause. The results of the model of emissions to water compared to the corresponding OPV production impacts are shown in Table 5.1.

Table 5.1 - Results of the impact assessment for 1 m^2 OPV production and leaching metals in the rain runoff experiment. ILCD 2011 Midpoint+ V1.05 / EU27 2010 [4].

Impact categories	Ag-OPV Damaged	Ag-OPV Intact	C-OPV	Ag-OPV production	C-OPV production
Climate change (kg-CO_2eq/pers)	0	0	0	7.90E-01	2.32E-01
Ozone depletion (kg CFC-11 eq)	0	0	0	5.57E-08	1.48E-08
Human toxicity. cancer effects (CTUh/pers)	0	0	0	2.48E-07	1.17E-08
Human toxicity. non-cancer effects (CTUh/pers)	9.52E-07	6.97E-08	1.26E-07	6.39E-06	5.88E-08
Particulate matter (kg-PM2.5eq/pers)	0	0	0	8.27E-04	1.18E-04
Ionizing radiation HH (kBq-U235eq/pers)	0	0	0	1.10E-01	4.50E-03
Ionizing radiation E (CTUe)	0	0	0	2.85E-07	1.57E-08
Photochemical ozone formation (kg NMVOC eq)	0	0	0	6.84E-03	7.30E-04
Acidification (mol H+ eq)	0	0	0	9.12E-03	1.05E-03
Terrestrial eutrophication (mol N eq)	0	0	0	2.95E-02	1.76E-03
Freshwater eutrophication (kg-Peq/pers)	0	0	0	4.08E-03	7.98E-05
Marine eutrophication (kg-Neq/pers)	0	0	0	2.49E-03	1.71E-04
Freshwater ecotoxicity (CTUe/pers)	47.2	2.24	3.85	155.65	3.3
Land use (kg C deficit)	0	0	0	8.72E+00	2.38E-01
Water resource depletion (m^3 water)	0	0	0	2.57E-03	1.16E-03
Resource depletion (kg-Sbeq/pers)	0	0	0	4.16E-03	7.35E-06

From all ILCD categories evaluated, only 2 of them showed an impact and the rest of the scores were equal to zero. The two scored categories were human toxicity non-cancer effects and freshwater

ecotoxicity. The share of the Ag leaching from the Ag-OPV damaged modules is 15% and 30% for human toxicity non-cancer and freshwater ecotoxicity, respectively, from the total impact during manufacture of the OPV, (i.e. 100%). From Ag-OPV intact, this share is only 1% for both categories, since much less Ag emissions were measured. As can be seen from the results presented in the previous section, the eco-toxicological implications are aligned with LCA the results. Ag concentrations were mostly below even drinking water limits in the rain runoff, meaning no direct adversative impact on either freshwater environments or humans, just as demonstrate the small fraction of 1% of the impact of Ag-OPV production. For the C-OPV the Zn leaching implied 214% and 117% higher impacts for human toxicity non-cancer and freshwater ecotoxicity, respectively, when compared to manufacture impacts. Although it seems high, this is relative to an original very low impact of an Ag-free and low energy demanding production (see Section 1.4, and Chapter 3). The relative potential impact of the leached Zn is therefore several times higher in comparison to the manufacturing, but still has not high ecotoxicological concerns as expressed in the previous section.

The environmental processes leading to the rapid and increased release of materials are not always known, anticipated or expected, and thus LCA results may be too conservative. Furthermore, environmental factors which may change the speciation of a pollutant, presenting different levels of toxicity are hard to include in LCA.

5.5.Conclusions

The leaching of metals from the rain runoff experiment was observed only in modules visibly damaged and in delaminated OPV modules. Apart from a few exceptions, the leached metal concentrations did not exceed the WHO limit for drinking water. This indicates that quality of the encapsulation and the edge sealing during an outdoor use phase of OPV are essential for both lifetime performance and environmental concerns. Likewise, the appropriate replacement of failed modules is not only needed from the electricity production point of view, but also to prevent peak concentrations of metals leaching upon delamination.

Overall, the three major eco-toxicological implications come out from the rain runoff and soil sequestration experiments results:

- Little Ag was leached during the use phase, yet peak concentrations occurred only a few days upon delamination. Consequently, this strain the need of fast action upon failure in order to restrain the Ag release to the environment.
- During release, Zn concentrations did not exceed even the most stringent drinking water limits at any time, and Zn is concluded to be of less concern.
- Shredded Ag-OPV had a more complete release of Ag when buried in soil (15.7% of the total contained Ag), leading to a critically elevated Ag content in the soil. This result thus highlight that landfilling is not a viable option and Ag must be recovered from waste.

The actual amount of Ag and Zn released from OPV were account for in LCA studies, where only two environmental categories showed impact scores. In terms of the OPV production, the contribution of the Ag leaching from Ag-OPV damaged modules was 15% and 30% for human toxicity non-cancer and freshwater ecotoxicity, respectively, and only 1% for both categories when the Ag leaching is from the Ag-OPV intact modules. There are still several challenges of using toxicology indicators in LCA, mainly due to the lack of data in life-cycle inventories and characterization models. With such results, this study purposes

a wide road opening for further investigations on the environmental behaviour of, not only OPV, but other TFPV as well. In the next chapter (as well as in Chapter 3), the LCA performed in OPV accounted for the quantified data from the three waste management options: recycling [6], incineration [7] and landfill (this study).

5.6.References

1. Zimmermann, Y.-S.; Schäffer, A.; Hugi, C.; Fent, K.; Corvini, P. F.-X.; Lenz, M. Organic photovoltaics: potential fate and effects in the environment. *Environ. Int.* **2012**, *49*, 128.

2. Rosenbaum, R. K.; Bachmann, T. M.; Gold, L. S.; Huijbregts, M. a J.; Jolliet, O.; Juraske, R.; Koehler, A.; Larsen, H. F.; MacLeod, M.; Margni, M.; McKone, T. E.; Payet, J.; Schuhmacher, M.; Van De Meent, D.; Hauschild, M. Z. USEtox - The UNEP-SETAC toxicity model: Recommended characterisation factors for human toxicity and freshwater ecotoxicity in life cycle impact assessment. *Int. J. Life Cycle Assess.* **2008**, *13*, 532.

3. European Commission - Joint Research Centre - Institute for Environment and Sustainability *International Reference Life Cycle Data System (ILCD) Handbook -- General guide for Life Cycle Assessment -- Detailed guidance*; First edit.; Publications Office of the European Union: Luxembourg, **2010**.

4. Espinosa, N.; Zimmermann, Y.-S.; dos Reis Benatto, G. A.; Lenz, M.; Krebs, F. C. Outdoor fate and environmental impact of polymer solar cells through leaching and emission to rainwater and soil. *Energy Environ. Sci.* **2016**, *9*, 1674.

5. Risø project overview http://rodeo.dtu.dk/rodeo/ProjectOverview.aspx?&Project=5&ProjectListFormat=map&Rnd=30223 (accessed Jan 4, **2016**).

6. Søndergaard, R. R.; Espinosa, N.; Jørgensen, M.; Krebs, F. C. Efficient decommissioning and recycling of polymer solar cells: justification for use of silver. *Energy Environ. Sci.* **2014**, *7*, 1006.

7. Søndergaard, R. R.; Zimmermann, Y.-S.; Espinosa, N.; Lenz, M.; Krebs, F. C. Incineration of organic solar cells: Efficient end of life management by quantitative silver recovery. *Energy Environ. Sci.* **2016**, *9*, 857.

8. Hashimoto, Y.; Takeuchi, S.; Mitsunobu, S.; Ok, Y. S. Chemical speciation of silver (Ag) in soils under aerobic and anaerobic conditions: Ag nanoparticles vs. ionic Ag. *J. Hazard. Mater.* **2017**, *322*, 318.

9. Zimmermann, Y.-S.; Schäffer, A.; Corvini, P. F.-X.; Lenz, M. Thin-film photovoltaic cells: long-term metal(loid) leaching at their end-of-life. *Environ. Sci. Technol.* **2013**, *47*, 13151.

10. Lado, L. R.; Hengl, T.; Reuter, H. I. Heavy metals in European soils: A geostatistical analysis of the FOREGS Geochemical database. *Geoderma* **2008**, *148*, 189.

11. Kurniawan, T. A.; Lo, W.; Chan, G.; Sillanpää, M. E. T. Biological processes for treatment of landfill leachate. *J. Environ. Monit.* **2010**, *12*, 2032.

12. Peyrot, C.; Wilkinson, K. J.; Desrosiers, M.; Sauvé, S. Effects of silver nanoparticles on soil enzyme activities with and without added organic matter. *Environ. Toxicol. Chem.* **2014**, *33*, 115.

13. Navarro, E.; Piccapietra, F.; Wagner, B.; Marconi, F.; Kaegi, R.; Odzak, N.; Sigg, L.; Behra, R. Toxicity of Silver Nanoparticles to Chlamydomonas reinhardtii. *Environ. Sci. Technol.* **2008**, *42*, 8959.

14. Lopes, S.; Ribeiro, F.; Wojnarowicz, J.; Łojkowski, W.; Jurkschat, K.; Crossley, A.; Soares, A. M. V. M.; Loureiro, S. Zinc oxide nanoparticles toxicity to Daphnia magna: size-dependent effects and dissolution. *Environ. Toxicol. Chem.* **2014**, *33*, 190.

15. Brun, N. R.; Lenz, M.; Wehrli, B.; Fent, K. Comparative effects of zinc oxide nanoparticles and dissolved

zinc on zebrafish embryos and eleuthero-embryos: Importance of zinc ions. *Sci. Total Environ.* **2014**, *476–477*, 657.

16. Jrc ILCD Handbook: Framework and requirements for LCIA models and indicators First edition. *Cycle* **2010**, 102.

17. Owsianiak, M.; Laurent, A.; Bjørn, A.; Hauschild, M. Z. IMPACT 2002+, ReCiPe 2008 and ILCD's recommended practice for characterization modelling in life cycle impact assessment: a case study-based comparison. *Int. J. Life Cycle Assess.* **2014**, *19*, 1007.

Chapter 6

Power bank case study

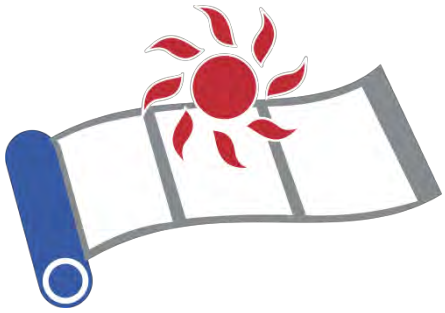

The OPV was applied in a commercial product with the release of HeLi-on from infinity PV ApS, probably for the very first time. Regular power banks harvest energy from the grid only. HeLi-on is however a power bank what includes a portable OPV panel, enabling the possibility to be charged from the sun and not only from the grid. In parallel, the company Bushnell, traditional in the production of equipment for outdoor sports launched a series of outdoor products that include amorphous silicon solar panels (a-Si PV). In this chapter, the environmental burden of three power banks products is quantified with the aim of indicate ecodesign improvements and point out how better performs a portable solar panel used in Denmark and in China.

6.1.Goal

The application of OPV has been extensively discussed around the scientific community. The application in niche technologies as portable electronics for the use in isolated places and camping sites has been an option for the application of TFPV in general. Power or battery banks have been traditionally used in remote locations, relying in the use phase on charges from the grid. The fact that the electricity can be acquired from a solar panel attached to the device, has two positive effects: the electricity will have no emissions during the battery charge and there might be in addition economic advantage for the user. The LCA is an important tool to compare quantitatively the potential environmental advantage of a product over another.

This case study has the purpose of comparing environmental performances of three power bank products, which collect electricity and store it in a battery. The electricity can come from an OPV panel; from an a-Si PV panel; or from the grid only. The assessing takes into consideration the Product Environmental Footprint (PEF) and eco-design rules of electronic devices [1]. The assessment was carried out following the technical details of the International Reference Life Cycle Data System (ILCD) handbook [2]. The results of this study can lead to decisions for the HeLi-on production, currently under improvement

stage (eco-design study). Therefore, according to ILCD handbook, this assessment can be identified as situation A. Target audience is the scientific community, stakeholders, companies' shareholders and possibly general public.

6.1.1. Products description

When compared, the products "SolarWrap Mini" from Bushnell and HeLi-on from infinityPV have very similar proprieties, such as battery capacity, width and power. Both a-Si and OPV panel present flexibility, light weight. Both products manufacturers state that the solar panel works even in partial shade and that the time for charging the battery is approx. 10 hours under full sun. The a-Si PV area is about three times smaller for the same power output whereas OPV weight is roughly three times lighter, which makes that both panels are very much alike in terms of total weight (around 30g). The three power banks contain a lithium ion battery, a circuit board with USB ports, cabling, and are finally protected by a plastic case.

6.1.1.1. HeLi-on

The manufacture of OPV modules is very similar to the described in the Chapter 2. The modules are Ag-based and have an especial design in order to maximise the geometric factor. The modules are normally rolled when stored in a protective case of the HeLi-on. The contacts of the OPV modules to the electronic circuit and battery in the HeLi-on are made with contacting tapes and soldering; and the attachments are made with protective commercially available tapes. The battery capacity is 2600 mAh. The plastic case has an out and inner shell to separate the rolled module from the electronics when stored. The final product weights circa 150g. HeLi-on is still a new product in pilot form, and several improvements are about to come in a very short future.

6.1.1.2. SolarWrap mini

The SolarWrap mini in the market since 2013 is a well-established product. The manufacture of the a-Si used in the SolarWrap mini is performed by PowerFilm Solar Inc. and reported to be produced using internally developed true roll-to-roll processes. The general process steps are vacuum deposition (back metal, amorphous silicon, and transparent top contact), printing and laser scribing, bus bar/lead attachment, encapsulation, and die cutting. The patterned modules have 30.5 cm (13 inches) wide web where the length of the roll up to 731.5 m (2400 feet) long [3]. As a proxy for the model, the ecoinvent data base v.3.1 process for Photovoltaic laminate, a-Si is considered, since the available manufacture details match closely [4]. The materials used for substrate and encapsulation have been replaced by the correspondent materials as published by PowerFilm, namely polyimide foil and polyester respectively. The module is lined with textile and finished up with a longer piece to be wrapped around the module for its protection when stored. The case has two lids joined with elastics to protect the USB ports from dust. The battery capacity is 2200 mAh and the final product weights 88g.

6.1.1.3. Regular power bank

A regular power bank has a very simple construction which comprises a battery with capacity of 2600 mAh, circuit board, USB ports and a plastic case. With small variations, these components are common between the three products to be accounted in this study.

6.2.Scope

6.2.1. System boundaries

The complete or “cradle-to-grave” LCA of the products is performed, comprising the supply of the raw materials for the production, the manufacturing and assembly, transportation, the energy necessary during the use phase (no maintenance required), and their end-of-life. The system boundaries are shown in Figure 6.1. The HeLi-on and SolarWrap mini contribute to the generation of electricity during the use phase and the three power bank products contribute to avoided materials if recycled and avoided electricity when incinerated. As the focus of the study is to describe the relevant environmental burden of the products, consequential modelling is applied.

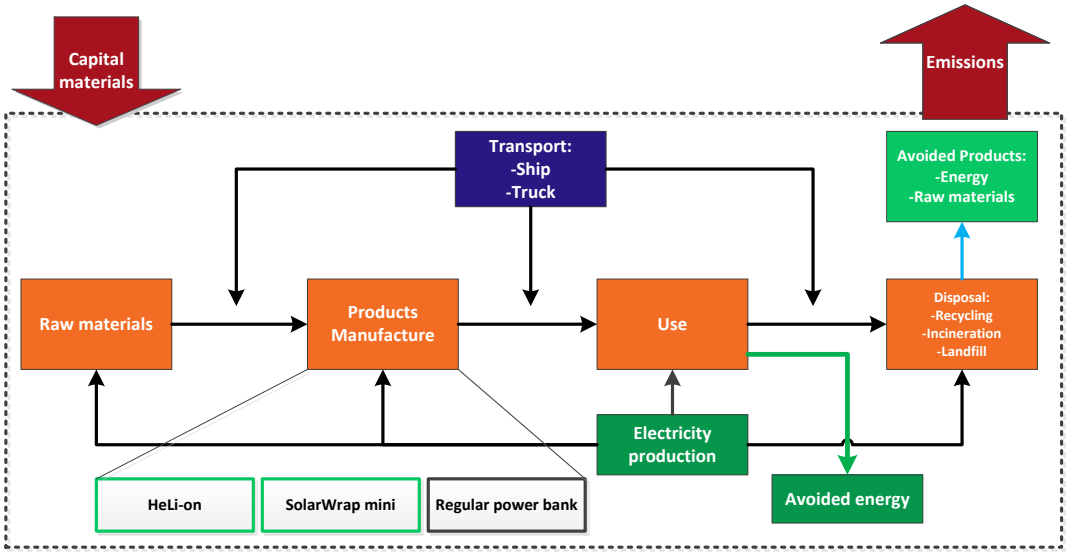

Figure 6.1 - System boundaries. Note that only HeLi-on and SolarWrap mini contribute to avoided energy during the use phase.

6.2.2. Functional unit and reference flow

The functional unit (FU) quantifies the primary function of the products, allowing comparative assessments. Detailed FU and reference flow are presented in Table 6.1. The comparable main function of the products is to collect electricity (from the grid or from a solar panel), store it and release it to charge, e.g. electronic devices. The amount of charges is considered as 300 times for a period of 2 years. This assumption for the use phase is made considering the following: i) Power banks are used preferentially in weekends or in a trip; ii) Electronic devices can have relatively shortened lifetime, due to the fast replacement for updated technologies. The reference flow is 1 power bank charged 300 times from the grid; where for HeLi-on and SolarWrap mini, 150 charges are made through the solar panel and 150 from the grid; and for the regular power bank 300 charges are made.

6.2.3. Geographical scope

HeLi-on is manufactured in Denmark, SolarWrap mini in United States and a regular power bank is considered to be manufactured in China. The data collection is mainly based in ecoinvent processes (see details in Section 6.3), where the raw materials extraction and processing are considered globally. The use and disposal of the products are considered for two scenarios: Denmark and China. Use phase considers the energy mix of the correspondent country. In this approach, the solar illumination of both countries is

not considered since the functional unit has been chosen independently, assuming that the users charge the power bank battery fully using the solar panels, apart from the particular conditions of sun exposition. For the disposal the average mix representative of municipal solid waste was defined in the work from Espinosa et al. detailed in Section 6.3 [5].

Table 6.1 - Functional unit and reference flow definition

Product	Functional unit	Reference flow	Key parameters
HeLi-on 	Collection, storage and release of electricity from the sun or grid for 300 charges 2 years.	1 power bank with OPV solar panel. Charged 150 charges from the sun and 150 from the grid.	No maintenance required No emissions during the use phase Charges from the grid with Danish and Chinese electricity mixes.
SolarWrap mini 		1 power bank with a-Si solar panel. Charged 150 charges from the sun and 150 from the grid.	
Regular power bank 		1 power bank. 300 charges from the grid.	

6.3.Inventory analysis

The production of OPV modules involved in the HeLi-on is made on a pilot-scale at the Technical University of Denmark what leads to highly representative data for the building up of the inventory. The details can be found in a set of published papers [5–9]. Data from the other components of the power banks and background inventories are based in inventory from consequential ecoinvent database 3.1 [10], where the processes were combined with the known materials and energy requirements from primary data and manufacturers description. Ecoinvent 3.1 is established as the most comprehensive database for life cycle inventories [5,11]. The model was built in the LCA software SimaPro v.8.05.13 [12]. For the a-Si PV modules in SolarWrap mini, the process found in ecoinvent of a-Si PV manufactured by Uni-Solar is taken into account [4]. As far as informed by both manufacturers, their manufacture process is similar in materials and scale. The substrate and encapsulation are adapted to the correspondent materials informed by PowerFilm (polyimide and polyester respectively), and the mass balance is based on the informed final weight of the modules. The further components of the power banks are conventional products (rechargeable Li-ion battery, printed wiring board, cables, polyethylene high density injection moulded, and tapes, textile, among others if applicable) and the life cycle inventory used is from ecoinvent 3.1 database. The correspondent amounts are related in Table 6.2.

Table 6.2 - Components of the power banks

	HeLi-on	SolarWrap mini*	Regular power bank*
Solar cell	0.1001 m^2	0.0243 m^2	-
Circuit board	0.0010 m^2	0.0010 m^2	0.0005 m^2
Battery	0.0445 kg	0.0280 kg	0.0445 kg
Cables	0.0015 kg	0.0015 kg	0.0015 kg
Plastic case	0.0495 kg	0.0247 kg	0.0247 kg
Other components	0.0060 kg	0.0034 kg	-

*Assumed from the products details available from manufacturers.

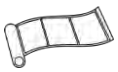

Two scenarios for the use and disposal of the devices were considered:

- Use and disposal in Denmark.
- Use and disposal in China.

Both countries differ largely in terms of energy and disposal mixes. For the disposal in each country, the average mix of the waste management is taken into account, as a "real life" scenario for the EOL of the power bank devices, following the municipal solid waste management landscape presented by Espinosa et al. [5]. In Denmark, the average mix representative of municipal solid waste corresponds to 29% recycling, 69% incineration, and 2% landfill; and in China 17% recycling, 22% incineration, 21% landfill and 40% open dump. Such percentages are given in mass for the whole devices, expressing in real terms, the percentage of devices submitted to the different waste treatments. An overview of each product distribution for the two scenarios is shown in Table 6.3. In the recycling, the OPV module from HeLi-on is presumed to have its valuable materials extracted (PET and silver) and reused (material recovery). As a-Si PV has no defined waste treatment, is it assumed for it a similar treatment with copper extraction and plastic recovery (mixed plastics treatment). The remaining power bank components are considered to be manually disassembled and recovered using correspondent waste treatments in ecoinvent 3.1 database with correspondent materials recovery. The recycling in China is adapted to Chinese conditions, wherever possible, using energy mixes for China for example. For incineration, the entire devices are sent to incineration with energy recovery corresponding to plastics and solid waste. For OPV, the PET incineration process is considered with adjusted silver emissions and updated incinerator efficiencies (the last valid only for Denmark). For landfill, the entire product is sent to sanitary landfill, where for OPV the PET landfilling was assumed, with adjustments for Ag emissions based on soil sequestration experiment presented in Chapter 5. Open dump in China is a landfill without leachate treatment.

Table 6.3 - Description of the two scenarios per product

Product	**HeLi-on**							**SolarWrap mini**							**Regular power bank**						
Production	Denmark							United States							China						
Scenario	**Scenario 1**			**Scenario 2**				**Scenario 1**			**Scenario 2**				**Scenario 1**			**Scenario 2**			
Transport	Transport DK-DK			Transport DK-CN				Transport US-DK			Transport US-CN				Transport CN-DK			Transport CN-CN			
Use	Electricity from Danish production mix			Electricity from Chinese production mix				Electricity from Danish production mix			Electricity from Chinese production mix				Electricity from Danish production mix			Electricity from Chinese production mix			
Disposal	Re 29 %	Inc 69 %	Lf 2%	Re 17 %	Inc 22 %	Lf 21 %	Od 40 %	Re 29 %	Inc 69 %	Lf 2%	Re 17 %	Inc 22 %	Lf 21 %	Od 40 %	Re 29 %	Inc 69 %	Lf 2%	Re 17 %	Inc 22 %	Lf 21 %	Od 40 %

Re stands for recycling; Inc for incineration; Lf for landfilling; and Od for open dump.

6.4.Impact assessment

As recommended for best practice in LCIA [13], the International Reference Life Cycle Data System (ILCD) methodology. The precise version used was ILCD 2011 Midpoint+ V1.05, equal weighting, in SimaPro 8.0.5.13 [12]. Human health, natural resources, and ecosystems quality are the agreed areas of protection in LCA community, which in ILCD method is expressed in the midpoint impact categories. They are climate change, ozone depletion, human toxicity separated in carcinogenic and non-carcinogenic effects (meaning

the toxicity of chemicals to human health), particulate matter (formed by release of inorganics leading to respiratory impacts), ionizing radiation impacting human health (HH), photochemical ozone formation, acidification potential, terrestrial, freshwater and marine eutrophication, freshwater ecotoxicity (meaning toxicity of chemicals on freshwater ecosystems), land use, water and non-renewable resources depletion. Further details and description of these environmental impact indicators can found in the publications from Laurent et al. [11,14]. The impact scores of the three products are represented in production only (grey), production + use in DK (light green) and CN (light red) including the distribution transportation, and the scores of the entire life cycle (production + use + disposal) in DK (green) and CN (red).

Figure 6.2 illustrates the impact scores of the three systems with differentiation between the stages of the life cycle and the considered disposal scenarios in Denmark and China. Looking at the impact scores for the production individually, the regular power bank had the lowest impact across all impact categories. The reason lies in the fact that it is a simpler device that only includes a battery and not a solar panel. Overall the highest impact when comparing production stages was found in HeLi-on, with the exceptions of ozone depletion and ionizing radiation categories. Here, the scores of SolarWrap mini are higher, even being the latter produced in much larger industrial scale and having a more optimised production than HeLi-on.

For the two power bank products that include solar panel, the difference between the production only and the production plus the use phase is minimal and it corresponds to the transport in the distribution of the product. Production and use phase for the regular power bank showed increased scores than for the production only due to the electricity needed for the 300 charges specified in the FU. Especially for certain categories such as climate change, particulate matter and acidification potential, the impact scores of the sum of production, use and disposal of the regular power bank in China largely surpasses the scores for the production only of HeLi-on and SolarWrap mini. Water resource depletion from the regular power bank also presented very intense scores after use and disposal in China.

The disposal in China was in general worse than in Denmark, with the most marked differences in freshwater ecotoxicity in the case of silver based OPV and, of course, the regular power bank due to the use phase as mentioned. The negative contributions in water resource depletion (regular power bank) and resources depletion (SolarWrap mini and regular power bank) are attributed to the Li-ion battery, which is produced from recycled batteries in the process from ecoinvent database.

The main contribution to the total impact scores of HeLi-on were stemming to a large extent from the use of Ag in the printed contacts of the OPV module (see Chapter 3). Such high scores are due to the relative high scarcity of Ag, high toxicity when released into the environment (as in the landfill and open dumps), and energy demands during mining. The Ag recycling rate is 90%, which would mean a total of 26.1% of Ag recovered in Denmark, corresponding to the average 29% considered for recycling; and 15.3% Ag recovered in China, corresponding to the average 17% of recycling. The higher the recycling rate the lower the impact scores. These results point out the importance of Ag recycling for OPV and the urgency of increasing recycling rates, possibly with take-back policies.

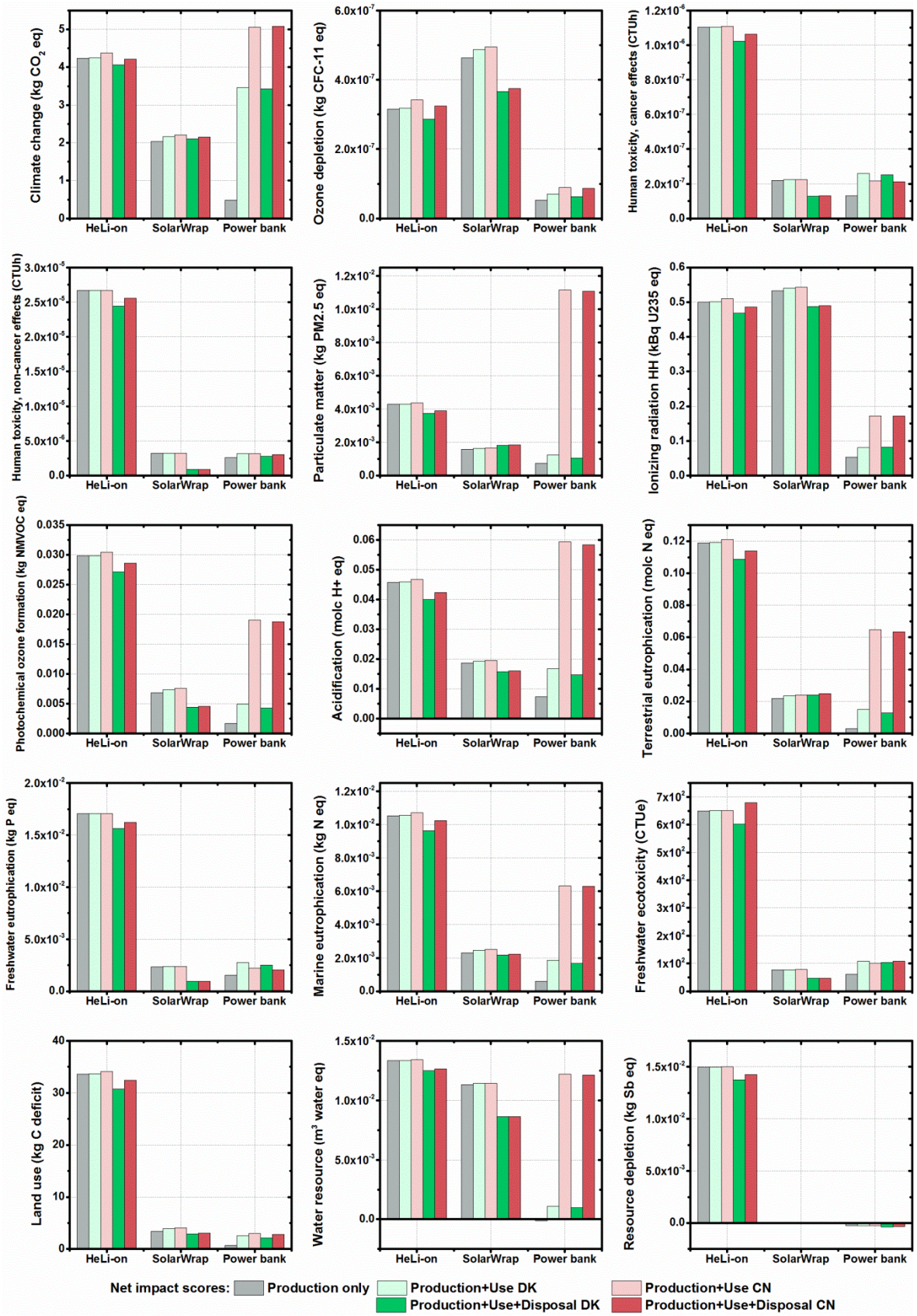

Figure 6.2 - Net ILCD 2011 v1.04 characterized impact scores for the three power bank products: HeLi-on, SolarWrap mini and a regular power bank. The scores for production alone, production + use and the whole life-cycle (production + use + disposal) under the Danish (DK) and the Chinese (CN) scenarios for used electricity and average waste management are shown for comparison.

Countless places in the world have similar or even worse energy mixes than China environmentally speaking (India for instance). The comparison of products that include option that can produce electricity from clean and free sources as the sun brings up the importance of saving energy from the grid, especially concerning climate change, particulate matter and acidification potential. The FU considers the same amount charges from the grid and from the sun during a period of two years. In real life, if this balance is broken by charging the device's battery using solar energy more times than using the location energy mix, the environmental impact of the product lifetime will get proportionally (to the energy mix, times of charge) lower and lower.

6.5.Cumulative Energy Demand

Figures 6.3, 6.4 and 6.5 show the Cumulative Energy Demand (CED) calculated with the method CED v1.09 integrated in the Simapro 8.0.5.13 software [12] from the processes of the three analysed products. The CED was expressed in terms of FU, not including the final product transportation to the customer. The dominant energy demanding share was from the "energy related component" used for charging the battery; i.e. the PV panels (79% for HeLi-on, 65% for SolarWrap) and the energy used for the FU by the regular power bank (79% for DK energy mix and 83% for CN energy mix).

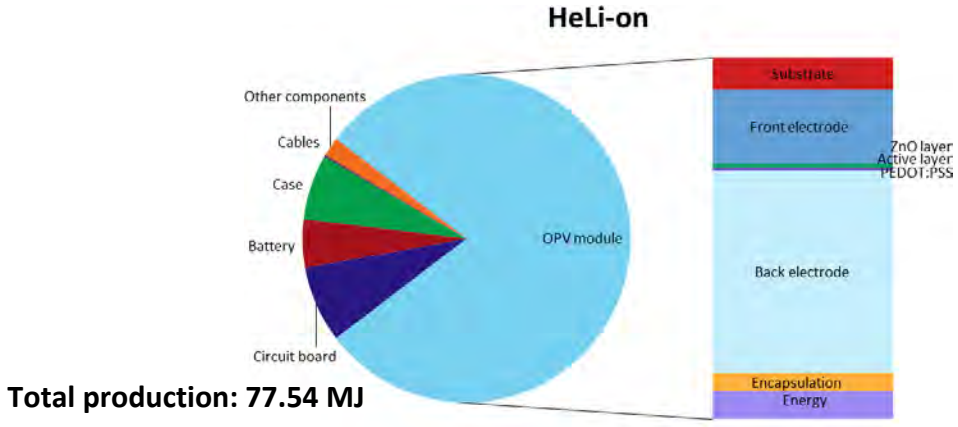

Figure 6.3 - Embodied energy per process from HeLi-on manufacture, showing CED of the energy used for the OPV module production. The electricity for the FU is balanced by the electricity produced by the solar panel.

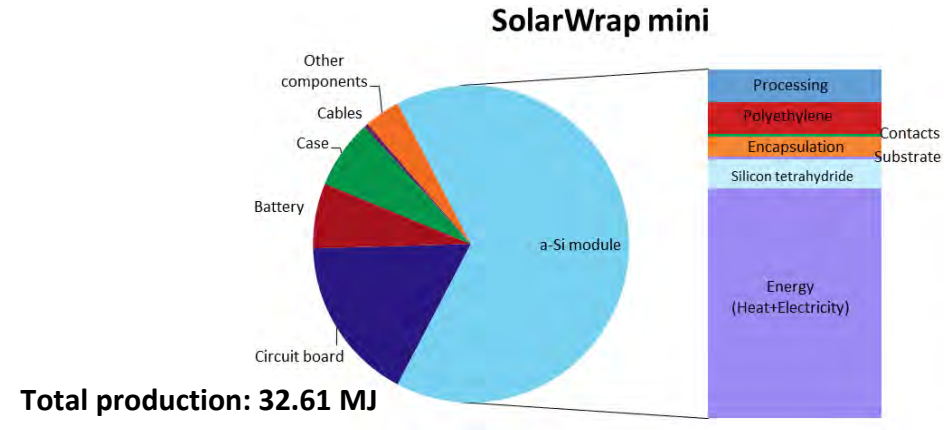

Figure 6.4 - CED per process for SolarWrap mini manufacture, showing CED of the energy used for the a-Si PV module production. The electricity for the FU is balanced by the electricity produced by the solar panel.

Comparing the production of the PV panels only, the 8% of the CED for the OPV manufacture is related to electricity, while for a-Si PV represents a 66%. This fact is typically observed in new technologies where the materials are relatively more costly (in this case in energy terms) than the requirements of energy. Improvements in the environmental burden of SolarWrap mini should be focused in the minimisation of energy demanding processes. Recalling that OPV production is still in a pilot scale, it has a larger potential to be industrially optimised and, in a short future, HeLi-on can have much lower CED both for energy and materials consumption. The main contribution in the OPV CED comes from the Ag in the back electrode. It corresponds to 56% alone and together, front and back electrodes, contribute the 76% of the energy demand of OPV. Overall, Ag contributes to 61% of the total HeLi-on CED. As discussed in Chapter 3, the substitution of the metal electrodes in OPV with a low-impact material would bring a real significant environmental improvement. In this case, the replacement of Ag or a significant reduction of it should be prioritized by the OPV producer during the product optimisation, being beneficial as well from an economic point of view (see metals profile in Section 3.1). The fast development of OPV efficiency would lead to the need of a smaller panel to generate the same power. In this case, less amount of material, and therefore less Ag, would be needed for the HeLi-on OPV panel.

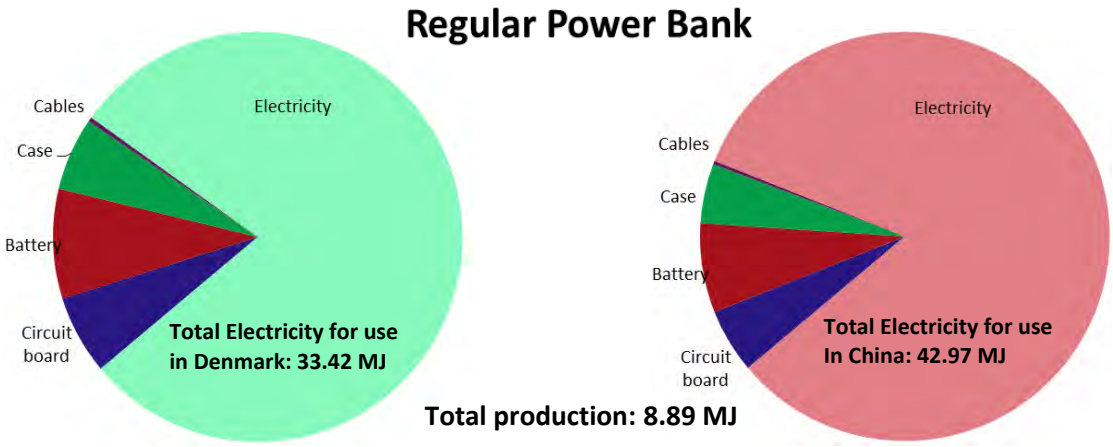

Figure 6.5 - CED per process for Regular Power Bank manufacture and the electricity for the FU.

Comparing the CED for the FU of the regular power bank and the CED of the power banks with solar panels, the regular power bank energy used in Denmark has the same share of the OPV production, and the energy used in China has the highest “energy related component” of all three systems. The disposal in China is worse than in Denmark, although the use of HeLi-on and SolarWrap mini in China is more advantageous, since they save energy from a worse energy mix when charged by the sun.

Taking into consideration the design for disassembly/dismantling (DfD), which would facilitate reuse and recycling operations; HeLi-on is designed allowing for very easy processes of assembly/disassembly. The OPV manufacturer has an important focus in “do it yourself” (DIY) costumers. For recycling operations, automatic disassembly is highly applicable. The reuse is also an option for the upgrade of new OPV panel, which are in constant progress to higher energy conversion efficiencies [15], and the electronics of the circuit board was specially designed to support 40% higher power than the current OPV panel. Furthermore, the OPV is a strong candidate for a take-back policy, which could raise the recycling rates of HeLi-on, to the point of lowering considerably its impact due to the Ag electrodes (see Ag recycling results in Figure 3.4). On the other hand, SolarWrap mini comes from two different manufacturers, one focused in

the a-Si PV and electronics and the other that improved the external design and finishing. The specific assembly of the product is unknown, but it is expected that electronics and PV connections to be similar to HeLi-on, while disassembly of the textile protection could be by some means challenging.

6.6.Conclusions

This study performed the comparison of the environmental performances of three power bank products, where two comprised solar panels in order store electricity generated by sunlight and/or from the grid, and one regular power bank which battery could be charged only from the grid. The comparison of their environmental scores revealed that charging the battery from the sun had a very important relevance on the effects on climate change. Two disposal scenarios are considering here the use of the devices in China and Denmark, in a realistic approach considering the current average municipal solid waste management in each country [5]. In the scenario that considers the use of the power banks in China, the environmental impacts increase drastically in contrast with their use in Denmark; not only in terms of climate change scores, but also in categories such as acidification, particulate matter, water depletion, marine, and terrestrial eutrophication. Despite the facts that the OPV based product is very new in the market and it has a much more detailed inventory with primary data collection, its scores are lower than the a-Si based power bank in ionizing radiation and ozone depletion.

Improvements regarding SolarWrap mini environmental burden should be focused in reducing the energy demanding processes in the solar panel manufacture. HeLi-on has room for a number of improvements and a larger potential to be industrially optimised, as it has relatively more costly materials (in energy terms) than the energy requirements, typical in new technologies. The replacement of Ag or the use of lower amounts would lead to significant reduction of environmental burden and it should be prioritized by the OPV producer during the product optimisation.

Recalling that, compared to other commercial TFPV as CdTe and CIGS, OPV performs better in several LCA studies [9,16–18] and present much less concerning the release of pollutants to the environment [19,20]; HeLi-on was a product conceived with high environmental concern and with high inclination to DfD, DIY, take-back programs, while efficient production are in the way to be addressed. This way OPV is few steps away to enter definitely in the PV market, with environmental concerns quantified and highly addressed.

Products like HeLi-on and SolarWrap mini have both the advantage of giving the power of lowering the environmental impact in the hands of the user. For this modelling, every time the user chooses to charge the power bank with solar energy balances the impacts generated from the product manufacture.

6.7.References

1. Talens Peiró, L.; Ardente, F. *Environmental Footprint and Material Efficiency Support for product policy - Analysis of material efficiency requirements of enterprise servers*; **2015**.

2. European Commission - Joint Research Centre - Institute for Environment and Sustainability *International Reference Life Cycle Data System (ILCD) Handbook -- General guide for Life Cycle Assessment -- Detailed guidance*; First edit.; Publications Office of the European Union: Luxembourg, **2010**.

3. FAQ - PowerFilm Solar http://www.powerfilmsolar.com/faq/ (accessed Nov 7, **2016**).

4. Pacca, S.; Sivaraman, D.; Keoleian, G. a Life Cycle Assessment of the 33 kW Photovoltaic System on the

Dana Building at the University of Michigan : Thin Film Laminates, Multi-crystalline Modules, and Balance of System Components. *Rep. No. CSS05-09* **2006**.

5. Espinosa, N.; Laurent, A.; Krebs, F. C. Ecodesign of organic photovoltaic modules from Danish and Chinese perspectives. *Energy Environ. Sci.* **2015**, *8*, 2537.

6. Espinosa, N.; Laurent, A.; Dos Reis Benatto, G. A.; Hösel, M.; Krebs, F. C. Which Electrode Materials to Select for More Environmentally Friendly Organic Photovoltaics? *Adv. Eng. Mater.* **2016**, *18*, 490.

7. García-Valverde, R.; Cherni, J. A.; Urbina, A. Life cycle analysis of organic photovoltaic technologies. *Prog. Photovoltaics Res. Appl.* **2010**, *18*, 535.

8. Espinosa, N.; García-Valverde, R.; Krebs, F. C. Life-cycle analysis of product integrated polymer solar cells. *Energy Environ. Sci.* **2011**, *4*, 1547.

9. Espinosa, N.; Hösel, M.; Angmo, D.; Krebs, F. C. Solar cells with one-day energy payback for the factories of the future. *Energy Environ. Sci.* **2012**, *5*, 5117.

10. Swiss Centre for Life Cycle Inventories The Ecoinvent Database v3.1 **2014**.

11. Laurent, A.; Espinosa, N. Environmental impacts of electricity generation at global, regional and national scales in 1980–2011: what can we learn for future energy planning? *Energy Environ. Sci.* **2015**, *8*, 689.

12. PRé Consultants SimaPro 8.0.5.13 **2015**.

13. Hauschild, M. Z.; Goedkoop, M.; Guinée, J.; Heijungs, R.; Huijbregts, M.; Jolliet, O.; Margni, M.; De Schryver, A.; Humbert, S.; Laurent, A.; Sala, S.; Pant, R. Identifying best existing practice for characterization modeling in life cycle impact assessment. *Int. J. Life Cycle Assess.* **2013**, *18*, 683.

14. Laurent, A.; Olsen, S. I.; Hauschild, M. Z. Limitations of carbon footprint as indicator of environmental sustainability. *Environ. Sci. Technol.* **2012**, *46*, 4100.

15. Azzopardi, B.; Emmott, C. J. M.; Urbina, A.; Krebs, F. C.; Mutale, J.; Nelson, J. Economic assessment of solar electricity production from organic-based photovoltaic modules in a domestic environment. *Energy Environ. Sci.* **2011**, *4*, 3741.

16. Espinosa, N.; García-Valverde, R.; Urbina, A.; Krebs, F. C. A life cycle analysis of polymer solar cell modules prepared using roll-to-roll methods under ambient conditions. *Sol. Energy Mater. Sol. Cells* **2011**, *95*, 1293–1302.

17. Hengevoss, D., Zimmermann, Y.S., Brun, N., Hugi, C., Lenz, M., Corvini, P.F.X., Fent, K. Environmental aspects of printable and organic electronics (POE). In *Organic and Printed Electronics: Fundamentals and Applications.*; Ganz, S., Lupo, D., Nisato, G., Ed.; Pan Stanford Publishing Pte. Ltd.: Singapore, **2015**.

18. Espinosa, N.; Lenzmann, F. O.; Ryley, S.; Angmo, D.; Hösel, M.; Søndergaard, R. R.; Huss, D.; Dafinger, S.; Gritsch, S.; Kroon, J. M.; Jørgensen, M.; Krebs, F. C. OPV for mobile applications: an evaluation of roll-to-roll processed indium and silver free polymer solar cells through analysis of life cycle, cost and layer quality using inline optical and functional inspection tools. *J. Mater. Chem. A* **2013**, *1*, 7037.

19. Brun, N. R.; Wehrli, B.; Fent, K. Ecotoxicological assessment of solar cell leachates: Copper indium gallium selenide (CIGS) cells show higher activity than organic photovoltaic (OPV) cells. *Sci. Total Environ.* **2016**, *543*, 703.

20. Zimmermann, Y.-S.; Schäffer, A.; Corvini, P. F.-X.; Lenz, M. Thin-film photovoltaic cells: long-term metal(loid) leaching at their end-of-life. *Environ. Sci. Technol.* **2013**, *47*, 13151.

Chapter 7

Conclusions and Outlook

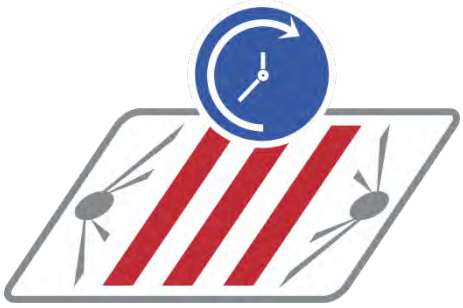

This PhD thesis had the overall focus of evaluating large scale produced OPV, in terms of its operational lifetime and environmental friendliness. The reproducibility of large scale produced vacuum-, ITO-, and Ag-free OPV modules using only R2R processing was reported and verified. The replacement of Ag for carbon electrodes permitted fast processing, conservation of the OPV flexibility, and the active area efficiency. After comparatively exploring four electrode choices for OPV using LCA methodology, the metal electrodes, i.e. Ag, Al and Cu, performed considerably worse than carbon based (C-OPV) modules in all environmental impact indicators. Metals (Ag, Al and Cu) were the major contributors to the environmental burden of the OPV modules. Designers and researchers in the field are highly encouraged to further investigate metal substitution for abundant and low impact materials for OPV electrodes application. C-OPV geometry however restricts the power per module, but the installation of larger areas should produce the satisfactory amounts of energy. Ag-OPV becomes an environmentally sustainable option if recycling is performed upon disposal. Take-back systems could be established for this purpose, bringing the recycling responsibility to the manufacturer.

Taking the recently established OPV baselines into account, the ISOS conditions performed over eight different OPV structures revealed several outstanding operational lifetimes in dark tests, some (AgNW-OPV) in light tests and one of them (C-OPV-SP) outdoors. Both C-OPV and AgNW-OPV technologies tested achieved the needed operation lifetime to be compatible with the timespan of seasonal greenhouse structures. In developing countries, C-OPV installation could be made in very large scale, in addition to be harmless to the environment. AgNW-OPV modules have the potential of achieving higher efficiencies and higher power per area; and in this stability analysis, had the overall higher operational lifetime. Such technologies are very close to comply with all the requirements for commercialisation. The use of UV-filters and roof cladding strategies could improve its functionality even further, while most of the degradation mechanisms could be attributed to water ingress through edges and contacts. Concerning such observations, investigation on large scale encapsulation and engineering strategies are highly encouraged toward the OPV community.

The rain runoff experiment simulating the use phase of an OPV installation showed that leaching of metals was only observed in visibly damaged or delaminated OPV modules. Apart from a few exceptions, the leached metal concentrations did not exceed the most stringent WHO drinking water limits. The major eco-toxicological implication from this experiment was the peak concentrations occurred few days upon delamination, which stress the need of acting fast upon failure in order to restrain the Ag release to the environment. Either from rain runoff and soil sequestration experiments, the resulting Zn concentrations did not exceed either drinking water limits at any time; therefore Zn is concluded to be of less concern. In the landfilling disposal simulation, shredded Ag-OPV had a more complete release of Ag when buried, leading to a critically elevated Ag content in the soil. This result thus highlight that landfilling is not a viable option and that Ag must be recovered from waste. Due to the inherent risks associated with Ag, this certainly warrants further detailed studies. The performed LCA on OPV accounted for the quantified data from the landfill waste management based on this study.

The full power bank product that included an OPV portable panel had its environmental impact analysed. The case study compared the environmental performances of three power bank products, two of them with a coupled solar panel (OPV or a-Si PV) and a regular power bank to be changed from the grid only. The interpretation of the results revealed that charging the battery from the sun had a very important relevance on the effects on climate change. Two realistic approaches were considered for use phase and disposal scenarios in China and Denmark. In the Chinese use phase scenario of a regular power bank, the environmental impacts increased drastically in several impact categories, in contrast with their use in Denmark. Improvements regarding SolarWrap mini environmental burden should be focused in reducing the energy demanding processes in the solar panel manufacture. HeLi-on has room for a number of improvements and a larger potential to be industrially optimised. Furthermore, the replacement of Ag or a significant reduction of it should be prioritized by the OPV producer during the product optimisation.

Unlike any other TFPV such as CdTe and CIGS, OPV was conceived with high environmental concern, and should guide to a solid tendency to take-back systems, when needed, in the future. With a full product release, OPV is few steps away to enter definitely in the PV market, with environmental concerns addressed and quantified.

Appendix

The list of contributions to the scientific community and attached papers related to the work presented in this thesis are presented in this appendix.

List of publications and participation in conferences and events

Publications

The following list shows the papers reproduced by this appendix.

1. S. A. Gevorgyan, N. Espinosa, L. Ciammaruchi, B. Roth, F. Livi, S. Tsopanidis, S. Züfle, S. Queirós, S., A. Gregori, G. A. dos Reis Benatto, M. Corazza, M. V. Madsen, M. Hösel, M. J. Beliatis, T. T. Larsen-Olsen, F. Pastorelli, A. Castro, A. Mingorance, V. Lenzi, V., D. Fluhr, R. Roesch, R., M. M. Duarte Ramos, A. Savva, H. Hoppe, H., L. S. A. Marques, I. Burgués, E. Georgiou, L. Serrano-Luján, F. C. Krebs.

   Title: **Baselines for Lifetime of Organic Solar Cells.**

   Published in: Adv. Energy Mater., p. 1600910, 2016.

   DOI: 10.1002/aenm.201600910

2. G. A. dos Reis Benatto, M. Corazza, B. Roth, F. Schütte, M. Rengenstein, S. A. Gevorgyan, F. C. Krebs.

   Title: **Inside or Outside? Linking Outdoor and Indoor Lifetime Tests of ITO-Free Organic Photovoltaic Devices for Greenhouse Applications.**

   Published in: Energy Technol., vol. 4, 2016.

   DOI: 10.1002/ente.201600335

3. N. Espinosa, Y.-S. Zimmermann, G. A. dos Reis Benatto, M. Lenz, and F. C. Krebs.

Title: **Outdoor fate and environmental impact of polymer solar cells through leaching and emission to rainwater and soil.**

Published in: Energy Environ. Sci., vol. 9, p. 1674, 2016.

DOI: 10.1039/C6EE00578K

4. N. Espinosa, A. Laurent, G. A. dos Reis Benatto, M. Hösel, and F. C. Krebs.

Title: **Which Electrode Materials to Select for More Environmentally Friendly Organic Photovoltaics?**

Published in: Adv. Eng. Mater., vol. 18, no. 14, p. 490, 2016.

DOI: 10.1002/adem.201500509

5. J. Kettle, N. Bristow, D. T. Gethin, Z. Tehrani, O. Moudam, B. Li, E. A. Katz, G. A. dos Reis Benatto, and F. C. Krebs.

Title: **Printable luminescent down shifter for enhancing efficiency and stability of organic photovoltaics.**

Published in: Sol. Energy Mater. Sol. Cells, vol. 144, p. 481, 2016.

DOI: 10.1016/j.solmat.2015.09.037

6. G. A. dos Reis Benatto, B. Roth, M. Corazza, R. R. Søndergaard, S. A. Gevorgyan, M. Jørgensen, and F. C. Krebs.

Title: **Roll-to-roll printed silver nanowires for increased stability of flexible ITO-free organic solar cell modules.**

Published in: Nanoscale, vol. 8, p. 318, 2016.

DOI: 10.1039/C5NR07426F

7. M. Helgesen, J. E. Carlé, G. A. dos Reis Benatto, R. R. Søndergaard, M. Jørgensen, E. Bundgaard, and F. C. Krebs.

Title: **Making Ends Meet: Flow Synthesis as the Answer to Reproducible High-Performance Conjugated Polymers on the Scale that Roll-to-Roll Processing Demands.**

Published in: Adv. Energy Mater., vol. 5, p. 1401996, 2015.

DOI: 10.1002/aenm.201401996

8. B. Roth, G. A. dos Reis Benatto, M. Corazza, J. E. Carlé, M. Helgesen, S. A. Gevorgyan, M. Jørgensen, R. R. Søndergaard, and F. C. Krebs.

Title: **Improving the Operational Stability of PBDTTTz-4 Polymer Solar Cells Modules by Electrode Modification.**

Published in: Adv. Eng. Mater., vol. 18, no. 4, p. 551, 2015.

DOI: 10.1002/adem.201500361

9. B. Roth, G. A. dos Reis Benatto, M. Corazza, R. R. Søndergaard, S. A. Gevorgyan, M. Jørgensen, and F. C. Krebs.

   Title: **The Critical Choice of PEDOT:PSS Additives for Long Term Stability of Roll-to-Roll Processed OPVs.**

   Published in: Adv. Energy Mater., vol. 5, p. 1401912, 2015.

   DOI: 10.1002/aenm.201401912

10. J, Kettle, N. Bristow, T. K. N. Sweet, N. Jenkins, G. A. dos Reis Benatto, M. Jørgensen, and F. C. Krebs.

    Title: **Three dimensional corrugated organic photovoltaics for building integration ; improving the efficiency , oblique angle and diffuse performance of solar cells.**

    Published in: Environ. Sci. Technol., no. 8, p. 3266, 2015.

    DOI: 10.1039/C5EE02162F

11. M. Hösel, D. Angmo, R. R. Søndergaard, G. A. dos Reis Benatto, J. E. Carlé, M. Jørgensen, and F. C. Krebs.

    Title: **High-Volume Processed, ITO-Free Superstrates and Substrates for Roll-to-Roll Development of Organic Electronics.**

    Published in: Adv. Sci., vol. 1, p. 1400732, 2014.

    DOI: 10.1002/advs.201400002

12. G. A. dos Reis Benatto, B. Roth, M. V. Madsen, M. Hösel, R. R. Søndergaard, M. Jørgensen, and F. C. Krebs.

    Title: **Carbon: The Ultimate Electrode Choice for Widely Distributed Polymer Solar Cells.**

    Published in: Adv. Energy Mater., vol. 4, no. 15, p. 1400732, 2014.

    DOI: 10.1002/aenm.201400732

Papers submitted or to be submitted

As the following papers are not yet published, the titles might have minor changes.

1. Suren A. Gevorgyan, Ilona Maria Heckler, Eva Bundgaard, Michael Corazza, Markus Hösel, Roar R. Søndergaard, Gisele A. dos Reis Benatto, Mikkel Jørgensen and Frederik C. Krebs.

   Title: **Improving, characterizing and predicting the lifetime of organic photovoltaics.**

2. Gisele A. dos Reis Benatto, Yannick-Serge Zimmermann, Benedikt Lassalle, Eric D. van Hullebusch, Frederik C. Krebs, and Markus Lenz.

Title: **Sulphur K-edge XANES spectroscopy as a tool to assess failure mechanisms and biodegradation in thin-film photovoltaics.**

3. Yannick-Serge Zimmermann, Gisele A. dos Reis Benatto, Pavel Schilinsky, Frederik C. Krebs, Philippe F.-X. Corvini, Andreas Schäfferb, and Markus Lenz.
   Title: **Insights into the release of metals from commercial thin film photovoltaic modules during their use-phase.**

4. Hande Unay, Gisele A. dos Reis Benatto, Suren A. Gevorgyan, Pelin Kavak, Sema Memiş, Ali Cirpan, Levent Toppare, Elif Alturk Parlak, Frederik C. Krebs.
   Title: **High Stability of Benzotriazole and Benzodithiophene Containing Medium Band-Gap Polymer Solar Cell.**

5. Roar R. Søndergaard, Gisele A. dos Reis Benatto, and Frederik C. Krebs.
   Title: **Fully rotary screen printed cabon-based organic photovoltaics.**

6. Gisele A. dos Reis Benatto, Nieves Espinosa and Frederik C. Krebs.
   Title: **Life-cycle assessment of solar charger with integrated organic photovoltaics.**

7. Dechan Angmo, Gisele A. dos Reis Benatto, and Frederik C. Krebs.
   Title: **Four years outdoor and storage stability of ITO-free,fully roll-to-roll fabricated polymer solar cell modules.**

Participation in Conferences and Events

1. Oral Presentation in the DTU Energy's annual PhD symposium, 2016. Lyngby, Denmark. (Congress).
   Title: **Environmental Impact of Organic Photovoltaics (OPV).**

2. Oral Presentation in the 9th International Summit on Organic and Hybrid Solar Cells Stability (ISOS-9), 2016. Freiburg, Germany. (Congress).
   Title: **Environmental Impact of Organic Photovoltaics Installed and Disposed Outdoors - Emissions to Rainwater and Soil.**

3. Oral Presentation in the Global Organic Photovoltaic e-Conference (eGOPV), 2016. Roskilde, Denmark. (e-Conference).
   Title: **Operational lifetime of large-scale fast manufactured vacuum- and ITO-free devices with different electrodes.**

4. Stand in the Roskilde Festival, 2016. Roskilde, Denmark. (Music Festival).
   Title: **Organic Solar Cells.**

5. Oral Presentation in the XIV Brazil MRS meeting at the section 8th International Summit on Organic and Hybrid Solar Cells Stability (ISOS-8), 2015. Rio de Janeiro, Brazil. (Congress).
   Title: **ISOS stability tests of large-scale environmental friendly OPV devices with different electrodes.**

6. Flash Talk and Poster Presentation in the 7th International Summit on Organic and Hybrid Solar Cells Stability (ISOS-7), 2014. Barcelona, Spain. (Congress).
   Title: **How to do reliable stability tests under different ISOS conditions.**

7. Poster Presentation in the DTU Energy Conversion's second yearly PhD symposium with industry participation, 2014. Lyngby, Denmark. (Congress).
   Title: **Reproducible R2R processed ITO-, vacuum- and silver-free organic solar cells.**

8. Poster Presentation in the International Summer School on Organic Photovoltaics, 2014. Strasbourg, France. (Summer school).
   Title: **Roll-to-roll fast processed ITO-, vacuum- and silver-free organic solar cells.**

Published papers

The following papers are reprinted with permission of the publishers and authors.

Baselines for Lifetime of Organic Solar Cells

Suren A. Gevorgyan, Nieves Espinosa, Laura Ciammaruchi, Bérenger Roth, Francesco Livi, Stylianos Tsopanidis, Simon Züfle, Sara Queirós, Alberto Gregori, Gisele Alves dos Reis Benatto, Michael Corazza, Morten V. Madsen, Markus Hösel, Michail J. Beliatis, Thue Trofod Larsen-Olsen, Francesco Pastorelli, António Castro, Alba Mingorance, Veniero Lenzi, Daniel Fluhr, Roland Roesch, Marta Maria Duarte Ramos, Achilleas Savva, Harald Hoppe, Luís Silvino Alves Marques, Ignasi Burgués, Efthymios Georgiou, Lucia Serrano-Luján, and Frederik C. Krebs*

The process of accurately gauging lifetime improvements in organic photovoltaics (OPVs) or other similar emerging technologies, such as perovskites solar cells is still a major challenge. The presented work is part of a larger effort of developing a worldwide database of lifetimes that can help establishing reference baselines of stability performance for OPVs and other emerging PV technologies, which can then be utilized for pass-fail testing standards and predicting tools. The study constitutes scanning of literature articles related to stability data of OPVs, reported until mid-2015 and collecting the reported data into a database. A generic lifetime marker is utilized for rating the stability of various reported devices. The collected data is combined with an earlier developed and reported database, which was based on articles reported until mid-2013. The extended database is utilized for establishing the baselines of lifetime for OPVs tested under different conditions. The work also provides the recent progress in stability of unencapsulated OPVs with different architectures, as well as presents the updated diagram of the reported record lifetimes of OPVs. The presented work is another step forward towards the development of pass-fail testing standards and lifetime prediction tools for emerging PV technologies.

Dr. S. A. Gevorgyan, Dr. N. Espinosa, B. Roth, F. Livi, G. A. dos R. Benatto, M. Corazza, Dr. M. V. Madsen, Dr. M. Hösel, M. J. Beliatis, T. T. Larsen-Olsen, F. Pastorelli, F. C. Krebs
Department of Energy Conversion and Storage
Technical University of Denmark
Frederiksborgvej 399, 4000 Roskilde, Denmark
E-mail: surg@dtu.dk

L. Ciammaruchi
ICFO, The Institute of Photonic Sciences
Av. Carl Friedrich Gauss 3, 08860 Castelldefels, Barcelona, Spain

S. Tsopanidis, S. Queirós, A. Castro, V. Lenzi, M. M. D. Ramos, L. S. A. Marques
Center of Physics, Department of Physics
University of Minho
Campus de Gualtar, 4710-057 Braga, Portugal

S. Züfle
Institute of Computational Physics, Zurich University of Applied Sciences
Wildbachstrasse 21, 8401 Winterthur, Switzerland

S. Züfle
Fluxim AG, Technoparkstr. 2, 8406 Winterthur, Switzerland

A. Gregori
Université de Pau et des Pays de l'Adour
Institut des Sciences Analytiques et de Physico-Chimie pour l'Environnement et les Materiaux (IPREM)
CNRS, UMR 5254
Equipe de Physico-Chimie des Polymeres, 64053 Pau Cedex 9, France

A. Mingorance
Catalan Institute of Nanoscience and Nanotechnology (ICN2)
Campus UAB
Bellaterra 08193, Barcelona, Spain

DOI: 10.1002/aenm.201600910

A. Mingorance
Barcelona Institute of Science and Technology (BIST)
Campus UAB
Bellaterra 08193, Barcelona, Spain

D. Fluhr
Institut für Physik
Technische Universität Ilmenau
Weimarer Str. 32, 98684 Ilmenau, Germany

D. Fluhr
Laboratory of Organic and Macromolecular Chemistry (IOMC)
Friedrich Schiller University Jena
07743 Jena, Germany

R. Roesch,[+] H. Hoppe[+]
Institut für Physik, Technische Universität Ilmenau
Weimarer Str. 32, 98684 Ilmenau, Germany

A. Savva, I. Burgués, E. Georgiou
Molecular Electronics and Photonics Laboratory
Department of Mechanical Engineering and Materials Science and Engineering
Cyprus University of Technology
Limassol 3603, Cyprus

L. Serrano-Luján
Department of Materials, Imperial College London
Exhibition Road, South Kensington, London SW7 2AZ, United Kingdom

[+]Current address: Center for Energy and Environmental Chemistry Jena (CEEC Jena), Friedrich-Schiller-University Jena, Philosophenweg 7a, 07743 Jena, Germany

1. Introduction

There exists a set of international test standards with pass-fail criteria (typically published by IEC and ASTM standards organizations) in the photovoltaic (PV) world and if the new manufactured (Si based) PV pass these tests, then there is a high probability that the product will survive 20–30 years in the end use environment.[1] Such a confidence however is mostly originating from the many years of experience in the field and the large set of tested Si based modules and therefore is very much customized for these types of technologies. Meanwhile, rapidly developing emerging PV technologies, such as organic photovoltaics (OPV), dye sensitized solar cells (DSSC), perovskite solar cells (PVSK) and others alike, due to their relatively young age still lack the field experience and generated reproducible data for building test procedures, which if passed, would allow to state with confidence the necessary reliability of these products in the end use environment. The lessons learned from the inorganic technologies cannot be utilized either, since the emerging PV technologies considerably differ in architecture from their inorganic counterparts[2] and due to their increased sensitivity towards the testing environments,[3–6] the common testing standards are not suitable for these technologies.[7]

These challenges however have received significant attention in the recent years especially in the field of OPVs. In particular, at the sequence of International Summits on Organic solar cell Stability (ISOS) the issue of reliable testing of OPVs was thoroughly addressed, and in 2011 recommendations were published based on the consensus of a large number of renowned research groups in the field, that outlined guidelines for reliable stability testing of organic solar cells.[8] The guidelines set certain criteria on the test conditions and therefore allowed reproducibly recording the aging of the samples under specific controllable conditions, in both indoor and outdoor testing environments. While this very much helped in reducing the spread in the testing procedures among the different groups, as well as improving the reproducibility of the reported device lifetimes,[9] the question still remained: how to develop a methodology that would allow either conducting pass-fail tests and building confidence around the product durability or predicting its lifetime in end use environment, based on accelerated testing. Significant efforts are put today towards resolving this. In particular, the group in Technical University of Denmark has recently demonstrated an approach based on statistical analyses, where a large variety of OPV samples were tested under different ISOS tests and the average lifetime of the samples under each test condition was determined.[10,11] The values were then used to calculate the ratio between the accelerated and real outdoor tests, which could potentially be utilized for predicting device performance. However, despite the relatively large datasets the studies were limited to only a few architectural variations and while they well demonstrated the concept, the established values could not be regarded as sufficiently generic for application beyond the reported studies.

The works however continued and recently a manuscript was published by the same group, where the same statistical approach was utilized for analyzing the entire literature related to stability of OPVs.[12] In that study, the authors collected and analyzed all the articles reported until March 2013 covering stability studies of OPVs (total of 2500 articles). A generic lifetime marker was developed that allowed gauging and intercomparing the stability of the different OPV devices reported in these articles. The lifetime of the samples was categorized depending on the device type and architecture, as well as test conditions, which helped to better understand and elucidate the typical bottlenecks for the device stability. The study additionally helped to establish averages for the lifetimes of OPVs,

Suren A. Gevorgyan is a senior scientist at the Technical University of Denmark. He was born in Armenia in 1982 and received his PhD from the Technical University of Denmark in 2010. From the early years of his career Suren has been working in the field of organic photovoltaics and specializing in characterization and stability improvements of the devices. His main research interests include standard testing, electro-optical characterization and device engineering of organic and perovskite solar cells.

Nieves Espinosa holds a position as researcher at Universidad Politécnica de Cartagena. The focus of her research has been on the eco-design of selected energy technologies, such as organic photovoltaics, products and processes investigating the life cycle impacts associated. Special attention is given to their implementation and integration in buildings or smart grids. Currently she is group leader in an EU COST Action StableNextSol devoted to unraveling the degradation mechanisms of organic solar cells.

Laura Ciammaruchi received her PhD degree from the University of Rome "Tor Vergata" in 2014, with a thesis titled "Studies on Stability and Degradation of Hybrid and Organic Solar Cells". Half of her doctoral activity was carried out at the University of Rochester, NY (USA) in Prof. Ching W. Tang's lab. Her expertise includes fabrication and characterization of various OPV technologies, with a specific focus on stability and degradation analyses.

tested under different test conditions. However, due to the limited amount of data for certain test conditions (especially for outdoor data) some averages lacked statistical significance and thus, could not be regarded as reliable baselines for device lifetime. The initiative therefore continued with the purpose of further enriching the lifetime database with both data reported in literature and experimental data and converting the database into a generic hub of baselines for the lifetime of OPVs and other emerging PV technologies alike, and utilizing the data for establishing test standards and prediction tools.

This work is a complementary to the aforementioned earlier reported study and is presenting the results of the follow-up literature analyses for an additional period from March-2013 until March-2015. The data analysis provides more solidified distributions of the lifetimes and allows drawing conclusions on the baselines for the OPV lifetimes tested under specific conditions. An updated version of the lifetime progress diagram is presented as well.

2. Methodology

2.1. Literature Data

The data collection procedure is explained in detail elsewhere.[12] Briefly, the articles were identified using the search engine ScienceDirect and exploring expressions based on different combinations of words such as polymer, plastic, organic, solar cells, photovoltaics, stability, aging and lifetime. For the clarity, the articles, analyzed in the earlier study, mentioned in the introduction, will be referred to as "2013 dataset" (since it was limited to reports until year 2013). The new dataset, which is mostly based on articles published between March-2013 and March 2015 and a few papers published in conference proceedings dating before 2013, will be referred to as "2015 dataset". The new dataset was inserted into an online database for further analyses. The total number of articles in 2015 dataset was 2286, out of which 303 contained actual lifetime data, while the rest only discussed the theory behind the stability issue. The 303 articles presented aging curves for a total of 983 devices, which are called data points. For the comparison, for 2013 dataset a total of 2500 articles were scanned, which also revealed precisely 303 articles with reported experimental lifetime data. This shows the increasing interest towards the OPV stability in the recent years.

2.2. Lifetime Determination

The online database with the new articles (hosted at http://plasticphotovoltaics.org/) was shared among and analyzed by different groups from consortia of the COST Action project StableNextSol (http://www.stablenextsol.eu). The analysis involved scanning each article individually, identifying whether the article contains experimental lifetime data, registering the reported data by filling the database with the reported sample structures, encapsulation, testing conditions and determining the lifetime from the reported aging curves. The lifetime T_{80} is defined as the time when the device is degraded by 20% from the initial value. Since the OPV devices however in most cases show rapid initial decay followed by slower degradation, in the ISOS guidelines it was proposed to identify two starting points, E_0 and E_S where the second point is defined at a stage when the aging is changed to a slower pace. Accordingly, the two values T_{80} and T_{S80} calculated from the two starting points define the lifetime of the device at the initial and at the stabilized stages. **Figure 1**a demonstrates a number of commonly observed aging curves for OPVs and the reason for such diversity in shapes is the multitude of aging mechanisms and competing annealing processes that take place at the same time in the device when the latter is exposed to different aging conditions. Figure 1a and **Table 1** explain how for different shapes the two lifetime parameters are identified. The approach was applied for identifying the lifetime for all the reported aging curves in the literature. In case the T_{80} value was not reached within the duration of the experiment, the time of the last measurement T_{final} was chosen to represent the lifetime (the minimum possible lifetime). Figure 1b together with Table 1 explain how after identification of the two lifetime values T_{80} and T_{S80} the best one is identified to represent the device by simply choosing the one where the most amount of energy is produced. Graphically this will correspond to the highlighted surface areas on the plot in Figure 1b, denoted as I and II. A more detailed explanation is provided in the previous study.[12]

The established database is publicly available at http://plasticphotovoltaics.org/lifetime-predictor.html, where an online interface can be found that allows analyzing and reproducing the collected data and utilizing special filters for specific sorting of the data. An instruction video is additionally provided in the website for navigating though the tool and the database.

3. Status of OPV Lifetime

The data collected from 2015 dataset was compared with the older dataset. The comparison revealed no significant difference in the data distribution between the two, but rather one complemented the other. The two datasets were therefore combined, which improved the intercomparison and baselining of the lifetime distributions under different test conditions.

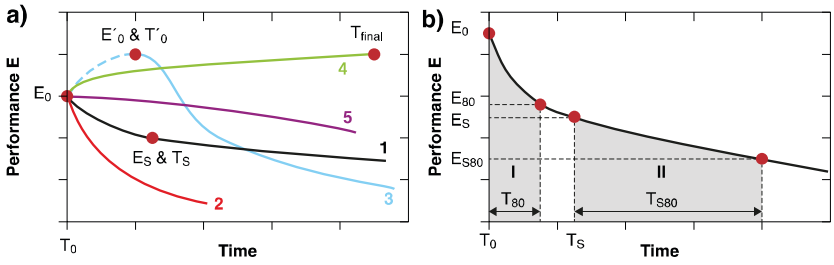

Figure 1. a) Examples of commonly observed shapes of aging curves in OPVs taken from real data. The figure shows how the different lifetime parameters are identified for the different curves. b) Example of identifying the best section of the curve defining the stability of the sample. The best section is mathematically defined by the largest surface area among the two gray regions denoted with I and II. Reproduced with permission.[12] Copyright 2015, John Wiley and Sons.

Table 1. The list of steps for determining the lifetime marker. Reproduced with permission.[12] Copyright 2015, John Wiley and Sons.

Parameters	Method
***Determination of starting point E_0 & T_0** E_0 – initial performance T_0 – initial time	T_0 & E_0 pair is either chosen at the first measurement point or if the curve has an initial increase followed by a reduction (such as the curve 3 in Figure 1a) then T_0 & E_0 is set at the maximum point.
Determination of stabilized section E_S & T_S E_S – performance at the start of stabilized section T_S – starting time of stabilized section	If after a certain point the aging curve enters into a more stable phase (commonly observed during solar cell aging), then a second pair of starting values T_S & E_S is identified, typically chosen at a point from where the aging rate almost doesn't change anymore, as shown on curve 1 in Figure 1a).
Determination of T_{80} and T_{S80} T_{80} – time when performance reaches 80% of E_0 T_{S80} – time when performance reaches 80% of E_S	T_{80} (or if applicable T_{S80}) is determined by subtracting T_0 (or T_S) from the time when 80% of E_0 (or E_S) is reached. Figure 1b highlights the areas determined by T_{80} and T_{S80}
Lifetime marker [E_0;T_{80}] or [E_S;T_{S80}]	The largest area among I and II in Figure 1b (part of the curve where the sample produces the largest amount of energy) will then determine the pair that will describe the lifetime. The simple geometrical calculations reveal that the ratio of the areas of the trapezoids I and II are proportional to the ratio of the areas of the rectangles defined by the products of $E_0 \times T_{80}$ and $E_S \times T_{S80}$. Thus the lifetime marker can be mathematically identified according to these rules: if $\frac{[E_0 * T_{80}]}{[E_S * T_{S80}]} \geq 1$ then the marker is [E_0;T_{80}] if $\frac{[E_0 * T_{80}]}{[E_S * T_{S80}]} < 1$ then the marker is [E_S;T_{S80}]
Exceptions	Exceptions are made in the following cases: • If E_S is less than half of E_0, in which case the sample is considered to have degraded before stabilization (see curve 2 in Figure 1a), then [E_0;T_{80}] is chosen by default to represent the lifetime. • If the measurements has been stopped prior to reaching the 80% threshold then "$T_{final} - T_0$" or "$T_{final} - T_S$", where T_{final} is the point of last measurement (see curve 4 in Figure 1a) is chosen instead to represent the minimum possible lifetime.

Figure 2 shows the reported lifetime values plotted against each year, where the triangles show the data tested under light and the circles represent the dark tests. The solid line is showing the total number of reports for each year (corresponding to the right axes). The plot clearly demonstrates the significant increase in the device stability and quantity of the reported lifetime data in the recent years with the total number of data points reaching beyond 300 for the past few years, which corresponds to more than 100 articles per year (given that one article contains approximately 3 data points). This is a clear indication of the significantly growing importance of the issue of lifetime in the recent years.

3.1. Baseline for Lifetime

The combination of the two datasets significantly increased the total amount of data points and therefore improved the statistical significance of the lifetime distributions for the samples tested under different test conditions. This enabled the possibility for establishing baselines based on such distributions. In order to do so, the data were categorized according to four groups, similar to the earlier reported study[12]: Group 1 and Group 2 represented the unencapsulated samples (samples that did not contain extra packaging layers) tested under light and in dark, respectively, and Group 3 and Group 4 hosted the encapsulated samples (samples that were packaged with barrier materials) correspondingly tested under light and in dark. The tests under light were further distinguished by:

- indoor soaking under light source with spectrum close to AM 1.5 and intensity close to 1 sun
- indoor exposure to low UV or low intensity light
- outdoor testing under real sun

Figure 3 shows the lifetime data distribution of the devices with and without encapsulation for each test condition. The time axes use the logarithmic scale with base 4 and divide the plot into blocks, such that each block can be associated with the common time units shown on the top of the plots, which enables a more intuitive data interpretation. (as was reported earlier for o-diagram[10]). The figure shows the distribution of the number of devices with the lifetime falling under each time block. Figures 3a,e and f represent the data from Groups 4, 2 and 1, respectively, while Figures 3b–d represent the data from Group 3. The data for outdoor and low UV for unencapsulated samples is not shown due to insufficient amount of reported

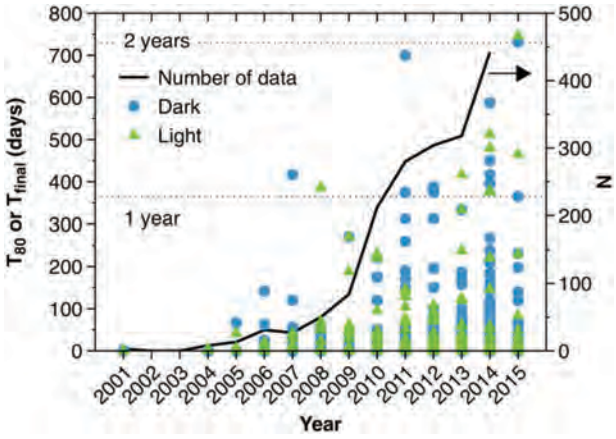

Figure 2. The scatter plot shows the T_{80} lifetime (or T_{final} in case the measurement was stopped before reaching T_{80}) values versus the reporting year for the samples tested under light (green triangles) and in dark (blue circles). The black line shows the number of reported data-points per year until 2014 (2015 is not shown since data is available only until March).

data points. Each test category is also associated with, but not limited to the ISOS testing procedures shown in the legends. For each data distribution peak, "median" defines the region with the most commonly reported lifetimes and "maximum" defines the region with the highest lifetime values, which are highlighted by red and green bands, respectively. The corresponding time-ranges for the median and maximum are also listed in the table on the right lower corner of Figure 3.

The established baselines can serve as references for the performance under given test conditions for any newly produced sample:

- If the sample outperforms the median, then the sample has an improved stability.
- If the performance is in the maximum region or beyond, then the sample has an outstanding or record lifetime, respectively.

Group 2 of unencapsulated samples tested in dark (Figure 3 (e)) contains two medians associated with normal and inverted device layouts, which are discussed in the next section. From the right plots in Figure 3 it becomes obvious that while the unencapsulated samples tested in dark may show impressive stability reaching beyond a few months, the large majority of the devices fail within minutes when tested under light. Therefore, it is highly advisable to use both condition or as a minimum, the light tests in order to truly assess the potential of the manufactured device in terms of stability. For the encapsulated samples when looking at the outdoor tests, the most commonly reported lifetimes are within a few months and only a few are

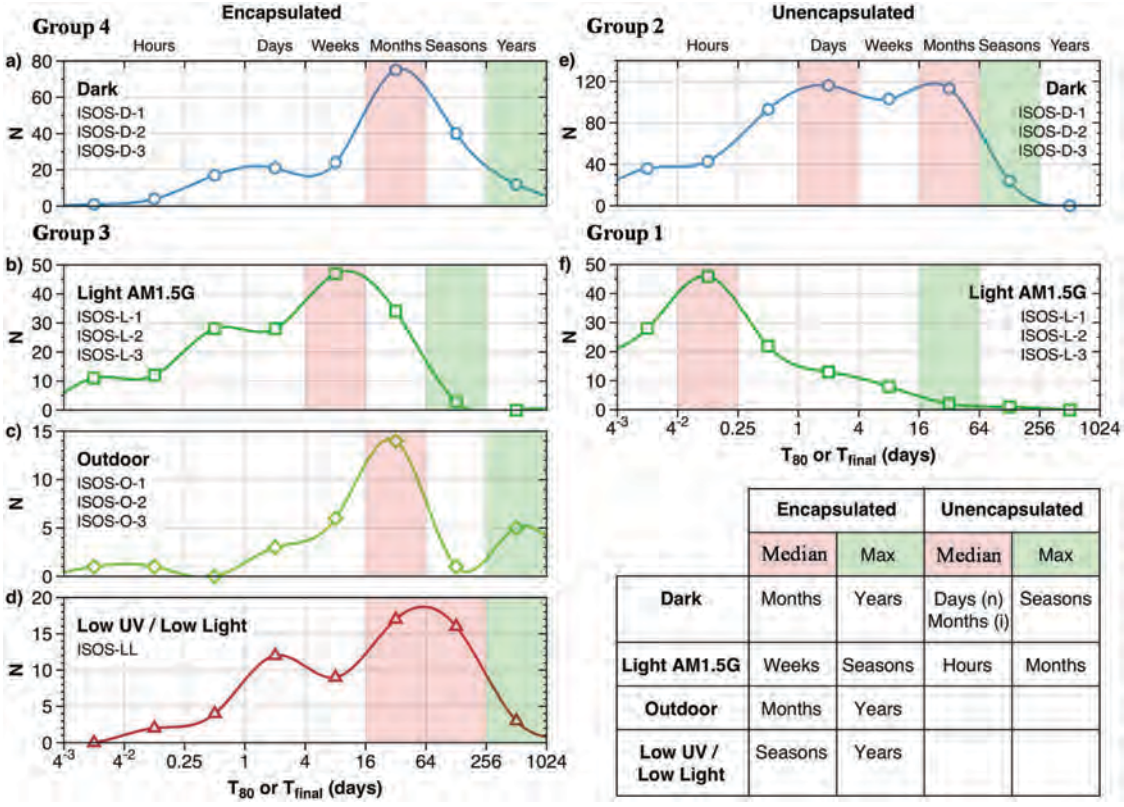

	Encapsulated		Unencapsulated	
	Median	Max	Median	Max
Dark	Months	Years	Days (n) Months (i)	Seasons
Light AM1.5G	Weeks	Seasons	Hours	Months
Outdoor	Months	Years		
Low UV / Low Light	Seasons	Years		

Figure 3. Baselines of the lifetime of OPVs tested under different aging conditions for encapsulated (left plots) and unencapsulated (right plots) samples. The plots represent the number of data points against the time in days represented in logarithmic scale with base 4. The scale is divided into blocks and associated with the common time units shown on the top x-axis of each plot. The median and maximum lifetime values for each peak distribution are highlighted with red and green bands and are listed in the table on the right lower corner. For unencapsulated samples tested in the dark two distinct peaks were found, i.e., two median values corresponding to days and months, which are associated with the normal and inverted structures (see Section 3.2). The test conditions are associated with, but not limited to the ISOS test conditions.

reported to reach a few years. Instead, in the case of indoor light soaking a few weeks appear to be the most common duration of the lifetime and only in a few cases samples lasting longer than a couple of seasons were reported. As a word of precaution, an attempt to predict the lifetime of the sample in outdoor test conditions, based on the ratios of the indoor light soaking and outdoor tests may lead to erroneous results, since one is not the acceleration of the other. For simulation of the outdoor tests a more complicated set of accelerated tests are required, such as a combination of a number of ISOS test procedures. Unfortunately, at this stage the database presented here does not contain sufficient data for each individual ISOS test procedure for in depth analyses. However, with the gradual increase of the database with time the intercomparison of the data for ISOS will also become possible, enabling the development of such a prediction tool.

Consequently, the presented baselines should mainly be regarded as generic reference points for lifetime of organic photovoltaics under given test conditions according to the aforementioned grouping.

3.2. Normal vs Inverted Structures

In Figure 3e the unencapsulated samples tested in the dark show two distinct peaks. These correspond to devices with normal (also known as conventional) and inverted architectures. The former typically employs aluminum back electrodes, while the latter has silver or gold based electrodes. **Figure 4** similarly to Figure 3 utilizes the time blocks of the logarithmic scale with base 4 to break down the data distribution for conventional and inverted devices tested in dark. The upper plot corresponds to the samples with normal configuration and the plot in the bottom represents the inverted devices. The squares and circles correspond to unencapsulated and encapsulated devices, respectively. From the figure it

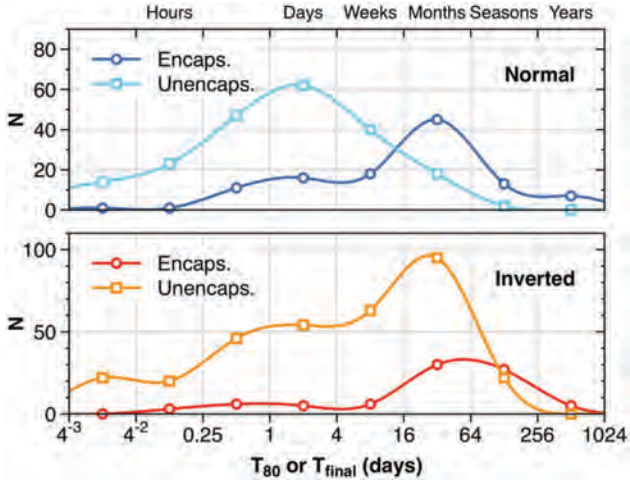

Figure 4. For the samples tested in the dark the distribution of the number of lifetime data points versus the time blocks defined by the logarithmic scale with base 4 is shown. The upper and lower plots correspond to the conventional and inverted device structures. The circle and square labels correspond to the samples with and without encapsulation respectively.

is apparent that there is a significant difference in the stability between the two layouts for unencapsulated samples, which is less pronounced in the case of encapsulated samples. It has been established earlier that the normal structures are significantly less resistant towards moisture due to the high sensitivity of the aluminum,[13–16] therefore they show inferior stability when tested in the dark. When encapsulated, the sample becomes well protected from the humid environment and therefore the reaction of the electrode with moisture is significantly reduced. As a result, the encapsulation of the normal structure devices has a major impact on the stability for normal devices, while in the case of inverted structures, since the samples are already significantly stable in the dark without extra protection, the role of encapsulation does not seem to be significant, as can be seen in Figure 4. The plot demonstrates how the device geometry may significantly alter the stability and therefore precautions are necessary when comparing the lifetime of devices with different structures and while reporting stability it is always useful to report the full structure and composition of the devices. In the case of indoor light tests (not shown here), there is no obvious difference in the stability of the two structures for samples both with and without encapsulation, which is possibly because the heat produced by the light source creates a rather dry environment around the sample diminishing the effect of humidity.

3.3. Winning Structures

A section in the earlier publication of 2013 dataset analyses[12] listed a number of device architectures with reported best stabilities without utilization of external packaging. It is important to clarify here that this category of samples may still contain certain protective layers, such as a substrate from one side and a solid metal electrode from the other and this is actually the case for the most stable samples reported for this category in the previous study. Nevertheless, the difference from the other categories is that no external packaging is utilized. In addition, for the same reason the term "intrinsic stability" used for describing the stability of such unencapsulated samples in the previous study will not be used here in order not to mislead the reader. Similar to the previous study, in this work a number of reports with unencapsulated samples of outstanding stability were registered, which are listed in **Table 2**. The table highlights the structures of the reported samples tested under light or in dark and their corresponding lifetime and efficiency values. The most impressive report corresponds to the sample tested under light showing an impressive lifetime of 96 days.[17] Unfortunately, the details of the top electrode configuration were not reported, but it was stated that it contained a combination of different metals. It is also worth mentioning that one of the samples tested in dark and showing an outstanding stability of 120 days, was produced in a roll-to-roll compatible process utilizing coating and printing techniques.[10] Nevertheless, despite a number of reports of impressive stability, producing encapsulation free samples in a roll-to-roll compatible process with sufficient stability under light test presents a serious challenge that still needs to be addressed.[18]

Table 2. Structure and performance parameters of unencapsulated devices tested in dark and under light. The active layer of all the materials is identical and consists of P3HT:PC[60]BM.

	Dark		Light		
Back Electrode	Ag/Ag+Al/Ag	Ag grid	Al	Multilayer metal electrode	Ag
Transport Layer 2	*MoOx/PEDOT:PSS/None	PEDOT:PSS	Cs2CO3	PEDOT:PSS	MoOx
Active Layer	P3HT:PCBM	P3HT:PCBM	P3HT:PCBM	P3HT:PCBM	P3HT:PCBM
Transport Layer 1	TiOx/ZnOx/ZnOx	PEDOT:PSS + ZnOx	**Other	ZnOx	ZnOx
Front Electrode	ITO	Ag grid	ITO	ITO	ITO
Substrate	Glass	PET	Glass	Glass	Glass
Structure	Inverted	Inverted	Normal	Inverted	Inverted
PCE (%)	3.7/3.5/2.5	0.93	3.6	1.9	2.85
Lifetime (days)	198/187/146	120	100	96	17.5
Reference	[19–21]	[10]	[22]	[17]	[23]

*MoOx modified with Nafion; **Phenothiazine, 4-phenothiazin-10-yl-anisole (APS).

3.4. Plot of the Record Lifetimes

In the previous report of 2013 dataset,[12] a so-called "lifetime progress diagram" was presented, which highlighted the best reported lifetimes of organic solar cells tested under different conditions. This diagram has been updated by additions from the new dataset and is now presented in **Figure 5**. The references to the reports are provided in the table below the diagram. The data is differentiated according to four test conditions: dark, indoor light soaking with AM1.5G spectrum light, light soaking with low UV light source and outdoor exposure. The conditions are differentiated by the colors in the plot. The arrows show the data points, which were defined by the last measurement of the experiment (T_{final}), since the device did not reach the T_{80} lifetime during the experiment. The data points are connected with dashed lines in order to highlight

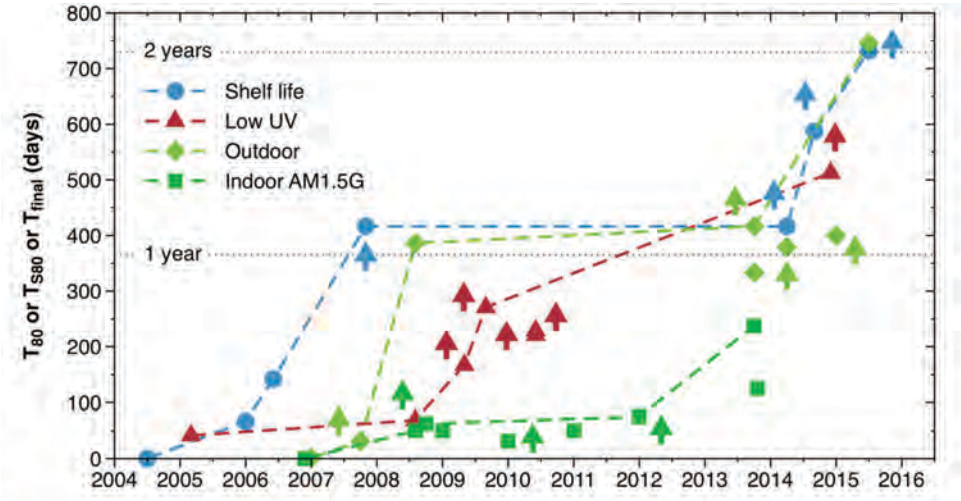

Indoor AM1.5G			Shelf life			Outdoor			Low UV		
PCE (%)	Lifetime (days)	Ref.	PCE (%)	Lifetime (days)	Ref.	PCE (%)	Lifetime (days)	Ref.	PCE (%)	Lifetime (days)	Ref.
1.08	0.083	[24]	0.8	0.042	[25]	0.0024	2	[26]	2.5	42	[27]
NA	50	[29]	0.035	67	[30]	4.2	31	[31]	4.1	69	[32]
NA	63	[28]	0.16	142	[34]	NA	386	[20]	2.32	167	[35]
1.09	50	[37]	2.8	417	[38]	1.43	417	[39]	5.9	271	[40]
3.54	31	[41]	1.27	417	[42]	1.43	333	[39]	2.7	229	[43]
NA	50	[44]	6.05	587.5	[45]	NA	379	[42]	6.07	221	[46]
2.1	75	[47]	1.06	732	[48]	1.42	400	[49]	2.7	513	[50]
3.42	125	[51]				1.11	746	[48]			
2.59	238	[52]									

Figure 5. Best lifetime values for different test conditions reported for each year. The table below shows the corresponding initial efficiencies and references. The arrows mark the lifetimes that have been defined by the last measurement T_{final} of the experiment, since the 20% aging threshold was not reached during the test. The dashed lines connect the data points to highlight the evolvement of record values. The horizontal dotted lines mark the 1 and 2 year values.

Table 3. The list of outstanding lifetime values of samples tested in high humidity conditions reported in literature.

High humidity measurements				
PCE [%]	Lifetime [days]	Temperature [°C]	Relative humidity [%]	Ref.
NA	52	65	85	[28]
4.4	70	25	85	[33]
3	333	65	85	[36]
2.7	75	85	85	[50]

the evolution of the reported record values. The additional data points that fall below the dashed lines show the data that are only slightly inferior to the record values. The low UV component light exposure is differentiated, since the UV plays a major role in the aging during the light exposure and therefore, the low UV category can be considered as a more moderate test compared to the full spectrum exposure. The figure demonstrates the rapid increase of the best reported lifetime values especially in the past few years, and such a progress is a good indicative of the fact that OPVs are rapidly approaching to the reliability level necessary for various industrial applications and especially for bulk energy production. In addition to the record lifetime diagram, **Table 3** presents the outstanding lifetime reports of the samples tested in high humidity conditions. The table lists device PCE and lifetime together with the temperature and relative humidity of test conditions. It is worth stressing that the sample showing 75 days in 85 °C and 85% relative humidity conditions[50] passed the standard damp heat test criteria of 1000 hours stated in IEC 61646.

4. Conclusions

This article has presented the results of the analysis of published literature related to the stability of organic solar cells reported in the recent years. The progress in the number of reports per year dealing with the lifetime of OPVs has been shown, which asserts the ever increasing interest towards resolving the stability issue of this technology. From the extended dataset, the distribution of the reported lifetime data on time axes was established for OPVs tested under five test conditions, such as shelf life, high humidity test, outdoor exposure, indoor light soaking with full spectrum and low UV spectrum. The peaks of the distributions were utilized for establishing baselines for OPV lifetime under different aging conditions, which can serve as a reference for determining whether a newly reported data has an improved or record lifetime compared to commonly reported values. It was revealed that the most commonly reported lifetime values of OPVs are laying in the vicinity of months in outdoor tests and only weeks for indoor light soaking. A few reports however demonstrated lifetimes of years under outdoor conditions. It was also observed that the unencapsulated samples tested in dark revealed two distinct peaks for lifetime distribution, which was shown to be caused by the difference between the conventional and inverted devices structures. This highlighted the importance of considering the device structure when comparing and reporting device stability. In addition, a list of devices without external packaging with outstanding stability has been listed together with the detailed analysis of their structures. The most stable unencapsulated sample was shown to last up to 96 days under light exposure with multilayer back electrode protection. The updated version of the diagram of the record stabilities has been presented as well showing the significant improvements in the lifetime of OPVs in recent years and highlighting the fact that OPVs are rapidly approaching the durability level necessary for the commercialization of the technology. This work constitutes a step forward towards the development of pass-fail testing standards and prediction tools for reliable assessment of the sample durability. The major challenge is still the significant lack of experimental data for each individual ISOS testing condition and in particular for the outdoor tests. Therefore, this work is another call to the community of emerging PV technologies for joining the forces and further developing the database into an international data hub with extended datasets.

Acknowledgements

This work has been supported by the European Commission's StableNextSol COST Action MP1307. The research leading to these results has received funding from the European Union Seventh Framework Programme (FP7/2007-2013) under grant agreement n° 609788 (CHEETAH) and n° 290022 (ESTABLIS). ICN2 acknowledges the support of the Spanish MINECO through the Severo Ochoa Centers of Excellence Program under Grant Nos. SEV-2013-0295 and ENE2013-48816-C5-4-R. Thanks goes to Agencia de Gestio d'Ajuts Universitaris i de Recerca for the support through the Xarxa de Referencia en Materials Avançats per a l'Energia (XaRMAE) and consolidated research group No. 2014SGR-1212. This work has been carried out under the Materials Science Ph.D. Degree for A.M. of the Universitat Autònoma de Barcelona. R.R. and H.H. are grateful for financial support from BMBF (grant number 03EK3502) and ESF. F.P. received support from the European Union's Horizon 2020 research and innovation programme under the Marie Skłodowska-Curie grant agreement no. 659747. L.S. and M.R. received supported from the Portuguese Foundation for Science and Technology in the framework of the Strategic Program UID/FIS/04650/2013.

Received: May 2, 2016
Revised: June 24, 2016
Published online:

[1] R. Roesch, T. Faber, E. von Hauff, T. M. Brown, M. Lira-Cantu, H. Hoppe, *Adv. Energy Mater.* **2015**, *5*, 1501407.
[2] J. Jean, P. R. Brown, R. L. Jaffe, T. Buonassisi, V. Bulović, *Energy Environ. Sci.* **2015**, *8*, 1200.
[3] M. Jørgensen, K. Norrman, F. C. Krebs, *Sol. Energy Mater. Sol. Cells* **2008**, *92*, 686.
[4] N. Grossiord, J. M. Kroon, R. Andriessen, P. W. M. Blom, *Org. Electron.* **2012**, *13*, 432.
[5] M. Jørgensen, K. Norrman, S. A. Gevorgyan, T. Tromholt, B. Andreasen, F. C. Krebs, *Adv. Mater.* **2012**, *24*, 580.
[6] M. Giannouli, V. M. Drakonakis, A. Savva, P. Eleftheriou, G. Florides, S. A. Choulis, *ChemPhysChem* **2015**, *16*, 1134.
[7] O. Haillant, *Sol. Energy Mater. Sol. Cells* **2011**, *95*, 1284.
[8] M. O. Reese, S. A. Gevorgyan, M. Jørgensen, E. Bundgaard, S. R. Kurtz, D. S. Ginley, D. C. Olson, M. T. Lloyd, P. Morvillo, E. a. Katz, A. Elschner, O. Haillant, T. R. Currier, V. Shrotriya, M. Hermenau, M. Riede, K. R. Kirov, G. Trimmel, T. Rath,

O. Inganäs, F. Zhang, M. Andersson, K. Tvingstedt, M. Lira-Cantu, D. Laird, C. McGuiness, S. Gowrisanker, M. Pannone, M. Xiao, J. Hauch, R. Steim, D. M. Delongchamp, R. Rösch, H. Hoppe, N. Espinosa, A. Urbina, G. Yaman-Uzunoglu, J. B. Bonekamp, A. J. J. M. Van Breemen, C. Girotto, E. Voroshazi, F. C. Krebs, *Sol. Energy Mater. Sol. Cells* **2011**, *95*, 1253.

[9] S. A. Gevorgyan, M. Corazza, M. V. Madsen, G. Bardizza, A. Pozza, H. Müllejans, J. C. Blakesley, G. F. a. Dibb, F. a. Castro, J. F. Trigo, C. M. Guillén, J. R. Herrero, P. Morvillo, M. G. Maglione, C. Minarini, F. Roca, S. Cros, C. Seraine, C. H. Law, P. S. Tuladhar, J. R. Durrant, F. C. Krebs, *Polym. Degrad. Stab.* **2014**, *109*, 162.

[10] M. Corazza, F. C. Krebs, S. A. Gevorgyan, *Sol. Energy Mater. Sol. Cells* **2014**, *130*, 99.

[11] M. Corazza, F. C. Krebs, S. A. Gevorgyan, *Sol. Energy Mater. Sol. Cells* **2015**, *143*, 467.

[12] S. A. Gevorgyan, M. V. Madsen, B. Roth, M. Corazza, M. Hösel, R. R. Søndergaard, M. Jørgensen, F. C. Krebs, *Adv. Energy Mater.* **2016**, *6*, 1.

[13] M. T. Lloyd, D. C. Olson, P. Lu, E. Fang, D. L. Moore, M. S. White, M. O. Reese, D. S. Ginley, J. W. P. Hsu, *J. Mater. Chem.* **2009**, *19*, 7638.

[14] M. Wang, F. Xie, J. Du, Q. Tang, S. Zheng, Q. Miao, J. Chen, N. Zhao, J. B. Xu, *Sol. Energy Mater. Sol. Cells* **2011**, *95*, 3303.

[15] V. M. Drakonakis, A. Savva, M. Kokonou, S. A. Choulis, *Sol. Energy Mater. Sol. Cells* **2014**, *130*, 544.

[16] S. Züfle, M. T. Neukom, S. Altazin, M. Zinggeler, M. Chrapa, T. Offermans, B. Ruhstaller, *Adv. Energy Mater.* **2015**, *5*, 1500835.

[17] M. T. Lloyd, D. C. Olson, J. J. Berry, N. Kopidakis, M. O. Reese, K. X. Steirer, D. S. Ginley, *2010 35th IEEE Photovoltaic Specialists Conference*, IEEE, **2010**, 001060.

[18] M. J. Beliatis, M. Helgesen, R. García-Valverde, M. Corazza, B. Roth, J. E. Carlé, M. Jørgensen, F. C. Krebs, S. A. Gevorgyan, *Adv. Engin. Mater.* **2016**, *18*, 1600119.

[19] W. Qiu, R. Müller, E. Voroshazi, B. Conings, R. Carleer, H.-G. Boyen, M. Turbiez, L. Froyen, P. Heremans, A. Hadipour, *ACS Appl. Mater. Interfaces* **2015**, *7*, 3581.

[20] E. Voroshazi, I. Cardinaletti, G. Uytterhoeven, A. Hadipour, B. P. Rand, T. Aernouts, *2013 IEEE 39th Photovoltaic Specialists Conference (PVSC)*, IEEE, **2013**, 3212.

[21] N. Chaturvedi, S. K. Swami, A. Kumar, V. Dutta, *Sol. Energy Mater. Sol. Cells* **2014**, *126*, 74.

[22] J.-H. Huang, K.-C. Lee, *ACS Appl. Mater. Interfaces* **2014**, *6*, 7680.

[23] N. K. Elumalai, C. Vijila, R. Jose, K. Zhi Ming, A. Saha, S. Ramakrishna, *Phys. Chem. Chem. Phys.* **2013**, *15*, 19057.

[24] K. Kawano, R. Pacios, D. Poplavskyy, J. Nelson, D. D. C. Bradley, J. R. Durrant, *Sol. Energy Mater. Sol. Cells* **2006**, *90*, 3520.

[25] S. Heutz, P. Sullivan, B. M. Sanderson, S. M. Schultes, T. S. Jones, *Sol. Energy Mater. Sol. Cells* **2004**, *83*, 229.

[26] E. A. Katz, S. Gevorgyan, M. S. Orynbayev, F. C. Krebs, *Eur. Phys. J. Appl. Phys.* **2006**, *36*, 307.

[27] X. Yang, J. Loos, S. C. Veenstra, W. J. H. Verhees, M. M. Wienk, J. M. Kroon, M. a. J. Michels, R. a. J. Janssen, *Nano Lett.* **2005**, *5*, 579.

[28] J. A. Hauch, P. Schilinsky, S. A. Choulis, S. Rajoelson, C. J. Brabec, *Appl. Phys. Lett.* **2008**, *93*, 103306.

[29] J. A. Hauch, P. Schilinsky, S. A. Choulis, R. Childers, M. Biele, C. J. Brabec, *Sol. Energy Mater. Sol. Cells* **2008**, *92*, 727.

[30] G. Dennler, C. Lungenschmied, H. Neugebauer, N. S. Sariciftci, A. Labouret, *J. Mater. Res.* **2005**, *20*, 3224.

[31] D. W. Laird, S. Vaidya, S. Li, M. Mathai, B. Woodworth, E. Sheina, S. Williams, T. Hammond, *SPIE 6656, Organic Photovoltaics VIII*, **2007**, 66560X–8.

[32] R. Franke, B. Maennig, A. Petrich, M. Pfeiffer, *Sol. Energy Mater. Sol. Cells* **2008**, *92*, 732.

[33] J. H. Tsai, Y. C. Lai, T. Higashihara, C. J. Lin, M. Ueda, W. C. Chen, *Macromolecules* **2010**, *43*, 6085.

[34] C. Lungenschmied, G. Dennler, G. Czeremuzskin, M. Latrèche, H. Neugebauer, N. S. Sariciftci, *SPIE 6197, Photonics for Solar Energy Systems*, **2006**, 619712–8.

[35] B. Zimmermann, U. Würfel, M. Niggemann, *Sol. Energy Mater. Sol. Cells* **2009**, *93*, 491.

[36] F. Yan, J. Noble, J. Peltola, S. Wicks, S. Balasubramanian, *Sol. Energy Mater. Sol. Cells* **2012**, *114*, 214.

[37] R. Tipnis, J. Bernkopf, S. Jia, J. Krieg, S. Li, M. Storch, D. Laird, *Sol. Energy Mater. Sol. Cells* **2009**, *93*, 442.

[38] W. J. Potscavage, S. Yoo, B. Domercq, J. Kim, J. Holt, B. Kippelen, *SPIE 6656, Organic Photovoltaics VIII*, **2007**, 66560R–10.

[39] S. A. Gevorgyan, M. V. Madsen, H. F. Dam, M. Jørgensen, C. J. Fell, K. F. Anderson, B. C. Duck, A. Mescheloff, E. A. Katz, A. Elschner, R. Roesch, H. Hoppe, M. Hermenau, M. Riede, F. C. Krebs, *Sol. Energy Mater. Sol. Cells* **2013**, *116*, 187.

[40] G. Schwartz, B. Maennig, C. Uhrich, W. Gnehr, S. Sonntag, O. Erfurth, E. Wollrab, K. Walzer, M. Pfeiffer, *SPIE 7416, Organic Photovoltaics X*, **2009**, 74160K–11.

[41] D. Gao, M. G. Helander, Z. Bin Wang, D. P. Puzzo, M. T. Greiner, Z. H. Lu, *Adv. Mater.* **2010**, *22*, 5404.

[42] D. Angmo, P. M. Sommeling, R. Gupta, M. Hösel, S. A. Gevorgyan, J. M. Kroon, G. U. Kulkarni, F. C. Krebs, *Adv. Eng. Mater.* **2014**, *16*, 976.

[43] M. Hermenau, K. Leo, M. Riede, *SPIE 7722, Organic Photonics IV*, **2010**, 77220K–10.

[44] S. Cros, R. De Bettignies, S. Berson, S. Bailly, P. Maisse, N. Lemaitre, S. Guillerez, *Sol. Energy Mater. Sol. Cells* **2011**, *95*, S65.

[45] J. Kong, S. Song, M. Yoo, G. Y. Lee, O. Kwon, J. K. Park, H. Back, G. Kim, S. H. Lee, H. Suh, K. Lee, *Nat. Commun.* **2014**, *5*, 5688.

[46] C. L. Uhrich, G. Schwartz, B. Maennig, W. M. Gnehr, S. Sonntag, O. Erfurth, E. Wollrab, K. Walzer, J. Foerster, A. Weiss, O. Tsaryova, K. Leo, M. K. Riede, M. Pfeiffer, *SPIE 7722, Organic Photonics IV*, **2010**, 77220G–8.

[47] D. M. Tanenbaum, M. Hermenau, E. Voroshazi, M. T. Lloyd, Y. Galagan, B. Zimmermann, M. Hösel, H. F. Dam, M. Jørgensen, S. A. Gevorgyan, S. Kudret, W. Maes, L. Lutsen, D. Vanderzande, U. Würfel, R. Andriessen, R. Rösch, H. Hoppe, G. Teran-Escobar, M. Lira-Cantu, A. Rivaton, G. Y. Uzunoğlu, D. Germack, B. Andreasen, M. V. Madsen, K. Norrman, F. C. Krebs, *RSC Adv.* **2012**, *2*, 882.

[48] D. Angmo, F. C. Krebs, *Energy Technol.* **2015**, *3*, 774.

[49] B. Roth, G. A. dos R. Benatto, M. Corazza, R. R. Søndergaard, S. A. Gevorgyan, M. Jørgensen, F. C. Krebs, *Adv. Energy Mater.* **2015**, *5*, 1401912.

[50] S. B. Sapkota, A. Spies, B. Zimmermann, I. Dürr, U. Würfel, *Sol. Energy Mater. Sol. Cells* **2014**, *130*, 144.

[51] R. Roesch, K. R. Eberhardt, S. Engmann, G. Gobsch, H. Hoppe, *Sol. Energy Mater. Sol. Cells* **2013**, *117*, 59.

[52] A. Karpinski, S. Berson, H. Terrisse, M. Mancini-Le Granvalet, S. Guillerez, L. Brohan, M. Richard-Plouet, *Sol. Energy Mater. Sol. Cells* **2013**, *116*, 27.

Inside or Outside? Linking Outdoor and Indoor Lifetime Tests of ITO-Free Organic Photovoltaic Devices for Greenhouse Applications

Gisele A. dos Reis Benatto,[a] Michael Corazza,[a] Bérenger Roth,[a] Franz Schütte,[b] Markus Rengenstein,[b] Suren A. Gevorgyan,[a] and Frederik C. Krebs*[a]

We present results from an installation of fully roll-to-roll printed and coated polymer solar cell modules in a greenhouse environment over the course of roughly 2 years (650 days). We explored two different device architectures based on either fully carbon-based electrodes or silver nanowire (AgNW)-based electrodes and two different barrier materials. We followed the ISOS protocols while studying the devices in three different greenhouse conditions in the Netherlands and compared to reference devices mounted outdoors in Denmark tested according to ISOS-O-1 and ISOS-O-2. We studied each condition and type in multiples to obtain acceptable statistics and found that the AgNW-based devices performed best in terms of stability.

Introduction

The global energy consumption is constantly increasing and it is essential for preserving the environment to fulfil the energy demand using renewable energy production. Organic photovoltaics (OPV) is an emerging technology ready for large-scale production[1,2] and one of the most promising potentially green energy sources due to its low cost of production and low environmental impact.[3–5] Properties such as flexibility, fast and low cost processing, fast installation and large potential for eco-design, low cost deployment and safe decommissioning make this PV technology unique.[6,7]

Due to lower efficiencies (in comparison to inorganic counterparts), OPV requires larger light-harvesting areas, which may be challenging in certain areas where land mass is scarce. From this perspective the use of OPVs in greenhouses is a favourable solution. They may possibly act as a replacement or complement for textile screens and shading systems, which are already used for certain crops that have their best growth with partial shade such as orchids, basil, parsley and many others. The integration of OPVs with textiles can be realized using numerous strategies as has been successfully tested before,[8,9] and the efficiency in large scale to make OPV economically viable has already been achieved.[10,11]

The replacement of the indium tin oxide (ITO) front electrode with poly(3,4-ethylenedioxythiophene) polystyrene sulfonate (PEDOT:PSS) or silver nanowires (AgNWs) was demonstrated to significantly reduce both the cost and the environmental impact of the organic solar panels. This was determined considering economic simulations performed for applications of OPVs in greenhouses and life-cycle assessments of production and use phase of OPV modules.[7,12–14] As the electrodes are the most expensive and energy-costing parts of the OPV, the devices using PEDOT:PSS and carbon electrodes have the cost and the cumulative energy demand (CED) of less than half of a OPV using silver electrodes.[13,14] The environmental impact of AgNW-based OPVs (AgNW-OPVs) is several orders of magnitude lower than devices using ITO or silver-grid electrodes and has the potential for intrinsically longer lifetimes.[15–17] Moreover, AgNW-OPVs can achieve higher efficiencies than carbon-based OPVs (C-OPVs), therefore requiring less area to produce the same amount of electricity.[14]

Flexibility makes the handling of plastic OPV panels similar and compatible to materials already used in large crop greenhouses. The semitransparency of OPVs is also an additional advantage for utilising more light than the opaque silicon and other thin-film solar cells can allow. The opaque area of the large-scale printing pattern of OPVs is less than 25%, with an active area transmission of 40%, where the absorption range of the active polymer can be optimised to not match the absorption spectrum needed for the photosynthesis.[7,11,18] OPV devices have also the unique freedom of using different active materials, making possible the modelling of specific solar cells for good use of sunlight in a particular crop. Bringing into consideration the short duration of some greenhouse structures for specific seasonal crops, the installed OPVs can be easily replaced with updated OPV technology following improvements in the field. Life-cycle-cost assessments performed previously proved that this strategy represents a distinct advantage of low-cost OPVs.[10,19]

[a] G. A. d. . Reis Benatto, Dr. M. Corazza, Dr. B. Roth, Dr. S. A. Gevorgyan, Prof. F. C. Krebs
Department of Energy Conversion and Storage
Technical University of Denmark
Frederiksborgvej 399, 4000 Roskilde (Denmark)
E-mail: frkr@dtu.dk

[b] F. Schütte, M. Rengenstein
Penn Textile Solutions GmbH
An der Talle 20, 33102 Paderborn (Germany)

The degradation mechanisms in OPV, due to the many interfaces between different materials with different properties, are highly complex.[20–23] The ISOS protocols established in 2011 have been a powerful tool, providing guidelines for lifetime tests both indoor and outdoor whereas a greenhouse environment can represent a combination of several conditions.[24] Recent developments in lifetime data bases and predictions have been accomplished by Corazza et al. and Gevorgyan et al.[17,25] Following these guidelines, we verify the stability performance and the operational lifetime of two different ITO-free environmentally friendly OPV technologies (carbon and AgNW based) inside greenhouses, that is, in a real application environment. We also compare these results with outdoor studies. Stable OPVs can lead to standalone greenhouses where the electricity needed for automated shading, climate control and nocturnal illumination systems is fully generated using solar power, that is, smart, efficient and environmentally friendly greenhouses.

Sample description

Postcard-sized OPV modules used for the lifetime tests were fabricated using fast and fully additive roll-to-roll processing.[12] Three types of modules were tested. The carbon-based OPV modules had two different types of modules. The first type was manufactured with a barrier used both as substrate and encapsulation foil, which later was found to be prone to formation of bubbles during operation (exposure to heat/light), leading to faster degradation of the modules. These modules were named C-OPV-L. The other type of C-OPV modules, called C-OPV-N, was manufactured using a better quality barrier foil. This newer barrier foil was also used for substrate and encapsulation of AgNW-OPV modules. Both C-OPV module fabrications were identical, and the details were reported earlier.[13] For the AgNW-OPV modules first-generation freeOPV[26] design was used and their fabrication was also described in literature.[16,27] C-OPV and AgNW-OPV samples were fully roll-to-roll processed using printing and coating techniques, encapsulated identically and by the end cut to a postcard size using a laser cutter.[13,26,28] None of the modules tested in this work utilised UV filters (the barrier foil has a cut-off towards shorter wavelengths <350 nm). In Table 1, the device architecture is described together with the amount of modules tested both in greenhouses and under outdoors conditions. The design, size and architecture of the modules are also shown in Figure 1. In the photograph of the modules facing the sun in Figure 1c it is possible to see the semi-transparency of the devices, which allows plants to receive some light through the OPV. The module active areas were 29 cm^2 for C-OPV and 57 cm^2 for AgNW-OPV.

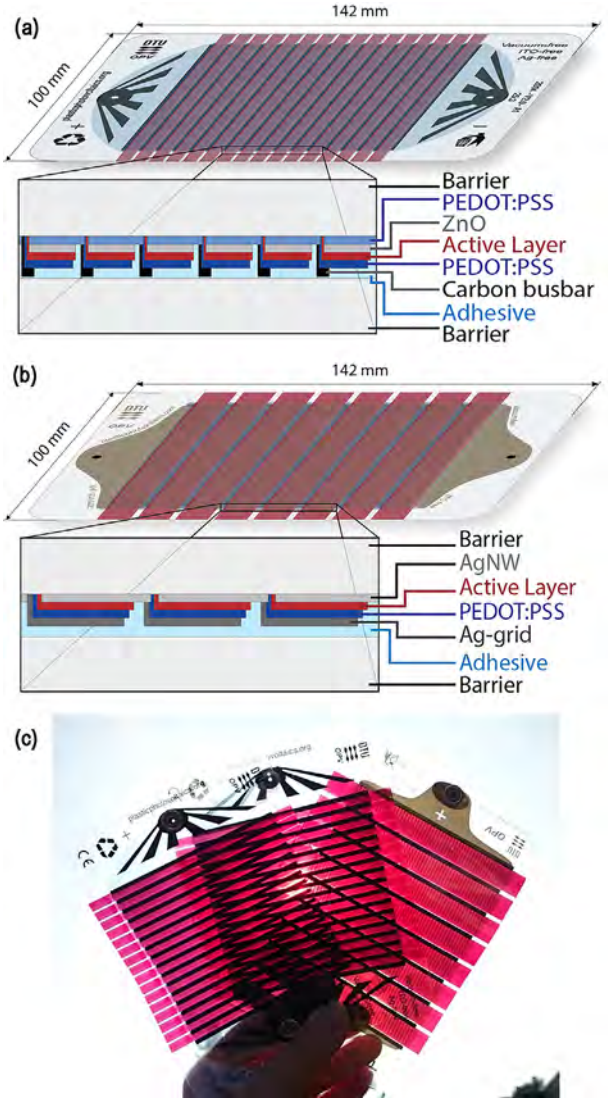

Figure 1. Module architectures of C-OPV (a) and AgNW-OPV (b) devices. (c) Photograph showing the transparency of the modules C-OPV-L, C-OPV-N and AgNW-OPV from left to right.

Greenhouse test description

Greenhouses are seasonally adapted to the cultivated crop. Thus, to access lifetime of these OPV samples, it was necessary to place the modules in different greenhouses. The mod-

Table 1. Description of the samples tested under greenhouse and outdoor conditions.

Samples	Structure	Number of samples tested	
		greenhouse	outdoor
carbon-based OPV with low-quality barrier [C-OPV-L]	PEDOT:PSS/ZnO/P3HT:PCBM/PEDOT:PSS/Carbon	8	8
carbon-based OPV with new barrier [C-OPV-N]	PEDOT:PSS/ZnO/P3HT:ICBA/PEDOT:PSS/Carbon	8	4
silver nanowire-based OPV with new barrier [AgNW-OPV]	AgNW:ZnO/P3HT:PCBM/PEDOT:PSS/Ag-grid	4	4

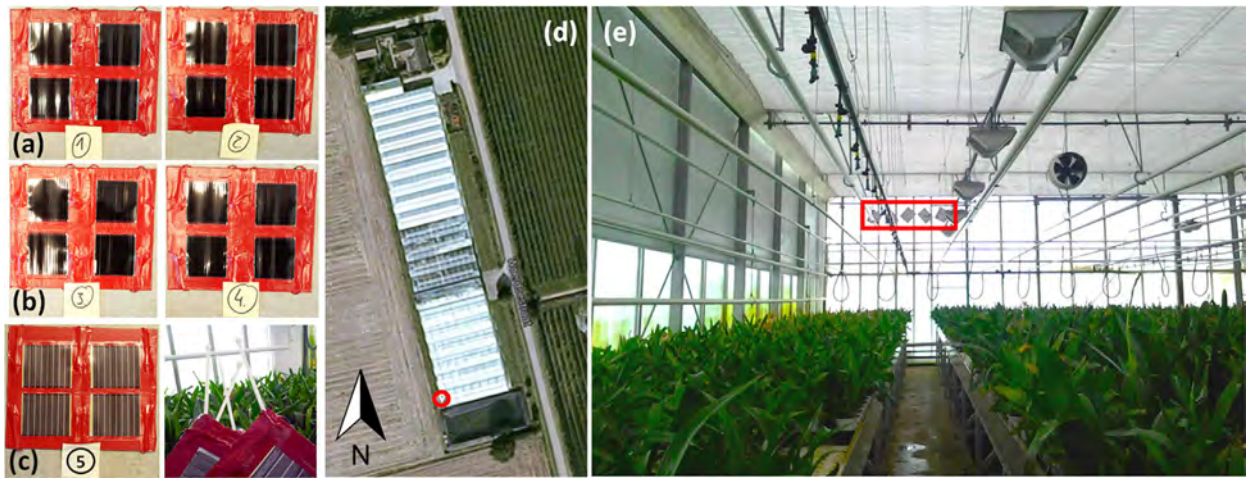

Figure 2. (a) Plates 1 and 2 with C-OPV-L modules; (b) plates 3 and 4 with C-OPV-N modules; (c) plate 5 with AgNW-OPV modules and attached plastic strips used for plate installation; (d) Google Maps satellite view of the climate-controlled greenhouse with red circle marking the position where the OPV samples were installed; and (e) plates installed inside the greenhouse highlighted by the red square.

ules were placed on plates for easy installation and safe transportation (Figure 2a–c). The installation was made inside a greenhouse growing orchids in Nijmegen, Netherlands, with the modules turned to the most transparent wall towards the sun that remained unshaded (Figure 2d and e). The walls of this greenhouse were made of plastic, which attenuated around 70% of the sunlight. This greenhouse had controlled relative humidity (RH; approximately 90%) and temperature (average 25 °C, limiting the variation to maximum 10 °C between night and day). These greenhouse conditions were named "greenhouse 1". The modules were periodically removed and shipped to Denmark to be tested under a solar simulator. The total process for the measurements took six days (from the moment the samples left the greenhouse until they were mounted back). Three months after first installation, this greenhouse stopped operating. The samples were kept in the greenhouse without plants and without any temperature or humidity control. This new condition was then called "greenhouse 2". Finally, the sample plates were placed towards the sun in a tomato-crop glasshouse in Paderborn, Germany, which also had no temperature or humidity control, protected only by the window glass of the greenhouse. This last greenhouse condition was called "greenhouse 3". The temperature in the uncontrolled greenhouses was estimated to be 10 °C ± 5 °C higher than the outdoors during the day and maximally 5 °C higher during the night. RH was approx. 23% lower than the outside humidity for a greenhouse without plants and 20% for a greenhouse with tomato crops. These approximations were made based on simulations from Fitz-Rodrígues et al. for a similar structure and climate.[29] The descriptions of the greenhouse conditions are summarised in Table 2. The precise dates of transport and measurements are indicated in the graph of Figure 3a.

Outdoor test description

C-OPV samples were tested using ISOS-O-1 protocols, and AgNW-OPV samples were tested using ISOS-O-1 and ISOS-O-2, measuring two samples for each condition. C-OPV-L samples were left outside on a fixed platform towards the south whereas C-OPV-N and AgNW-OPV samples were placed on a solar tracker. The tests were performed in the Characterization Laboratory for Organic Photovoltaics (CLOP) at the Department of Energy Conversion and Storage (DTU), Roskilde, Denmark. The conditions for the

Table 2. Description of greenhouse and outdoor conditions.

Conditions	Greenhouse 1	Greenhouse 2	Greenhouse 3	ISOS-O-1	ISOS-O-2
light source	sun, indoor with plastic wall transmission ≈ 70%	sun, indoor with plastic wall transmission ≈ 70%	sun, indoor with glass roof/wall transmission ≈ 90%	sun, outdoor	sun, outdoor
temperature	avg. 25 °C with a variation of maximum 10 °C between day and night (controlled)	day: 10 °C ± 5 °C above outdoors night: max. 5 °C above outdoors (uncontrolled), Ref. [22]	day: 10 °C ± 5 °C above outdoors night: max. 5 °C above outdoors (uncontrolled), Ref. [22]	ambient outdoor	ambient outdoor
relative humidity	≈ 90% (controlled)	≈ 23% below outdoors—no plants (uncontrolled)	≈ 20% below outdoors (uncontrolled)	ambient outdoor	ambient outdoor
characterization light source	solar simulator	solar simulator	solar simulator	solar simulator	sunlight

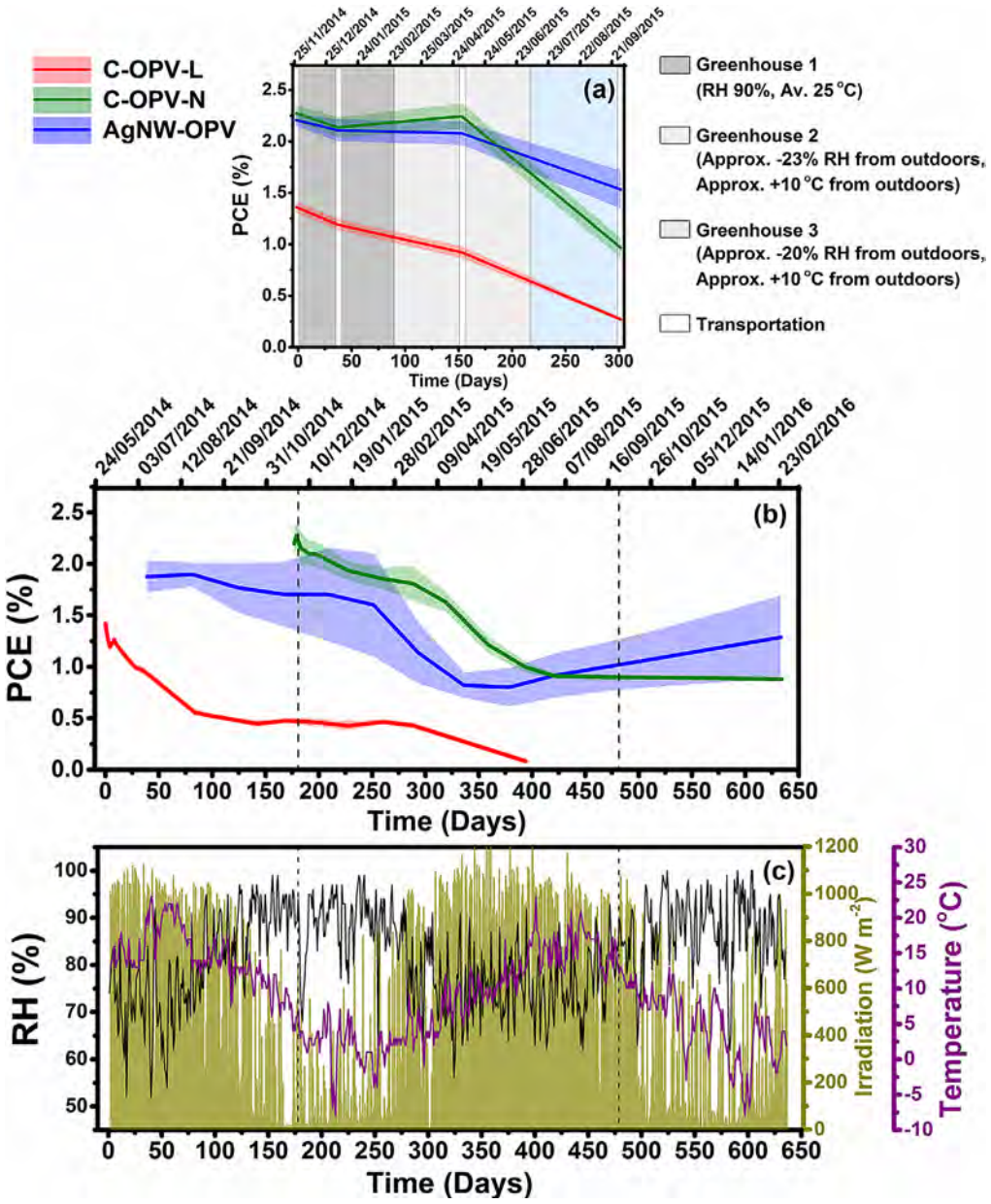

Figure 3. Average stability curves for the (a) greenhouse and (b) outdoor tests of C-OPV-L, C-OPV-N and AgNW-OPV; and (c) outdoors data for RH (black line), irradiation (dark yellow line) and temperature (purple line). Greenhouse conditions are detailed in Table 2. PCE = power conversion efficiency.

tests as well as the greenhouse conditions are described in Table 2. The dates of the outdoor tests for the observation of the stability as function of seasons are indicated together with the results in Figure 3b. The samples tested with ISOS-O-1 were periodically removed from the ageing setup and tested under a calibrated solar simulator, and for the samples tested with ISOS-O-2, the current–voltage (*I–V*) curve measurements were performed in situ under natural sunlight.

Results and Discussion

The average stability curves for the greenhouse and outdoor test are combined in Figure 3, with the shade following the curves representing the corresponding standard deviation. For the outdoor tests, the start and time span of the tests differ due to the different time of production of the samples. The Roskilde region in Denmark, where the outdoor tests were performed, as well as the areas in the Netherlands and Germany, where the greenhouse tests were performed, are in the same climate area as in the Köppen–Geiger climate classification system;[30] therefore, these areas have similar average temperature, seasonality and precipitation. Figure 3c shows the irradiation (dark yellow line), RH (black line) and temperature (purple line) data in the outdoor test location. The weather history data were checked and they had good correspondence to the conditions of the greenhouse locations.[31]

The greenhouse tests started on the 1st of December 2014 while the outdoor tests started on the 2nd of June (C-OPV-L), 15th July (AgNW-OPV) and 26th November 2014 (C-OPV-N). C-OPV-L modules had an initial average performance of 1.4% whereas C-OPV-N had an average of 2.2% and AgNW-OPV 2.1%. After 34 days under greenhouse 1 conditions, the module performances decayed for both C-OPV-L and C-OPV-N devices even with only ≈70% of sun light transmitted through the plastic windows. This degradation is ascribed mainly to the effects of the high humidity. After further 49 days in greenhouse 1 and 60 days in greenhouse 2, the C-OPV-L modules degraded to 68% of the initial efficiency whereas C-OPV-N modules recovered back to 100%. The humidity in these last 60 days was around 70% in the greenhouse without plants and climate control. After an additional 60 days in greenhouse 2 and 81 days in greenhouse 3, the performance of C-OPV-L decayed to 20% of its initial value and that of C-OPV-N decayed to 42%. AgNW-OPV modules started the test with similar PCEs as C-OPV-N on average. In the first period, the performances decayed similarly to both C-OPV-L and C-OPV-N modules under the conditions of greenhouse 1. In the second period, in between greenhouse conditions 1 and 2, PCE of AgNW-OPV remained stable and at the end of the test, after having been under greenhouse 2 and 3 conditions the PCE was 69% of the initial value. For the greenhouse test, the AgNW-OPV showed the best stability performance.

Figure 3b shows the average stability curves for outdoor tests. C-OPV module results are for ISOS-O-1 only, whereas AgNW-OPV results are for ISOS-O-1 and ISOS-O-2, which leads to a larger standard deviation envelope as they were measured using different light sources (solar simulator and sunlight, respectively), although their operational lifetimes are similar (see Figure 4). The C-OPV-L test started first in late spring and suffered a burn-in phase of 84 days. Coinciding with a period of less sunny days in Denmark, after 84 days the samples remained stable with about 33% of its initial PCE until the barrier was substantially damaged causing failure of most modules. Outside testing for AgNW-OPV modules started midsummer in Denmark, at which time C-OPV-L had already been tested for 50 days. The average degradation curve for AgNW-OPV modules showed a slight decrease of performance after 200 days of testing; the ISOS-O-2 provides lower performances since they were measured with sunlight (albeit normalized with respect to insulation). The performance dropped considerably after this period, which matches the late winter season and the start of increased illumination, temperature and decreased RH (due to spring). Then, performance stabilised at around 43% of the initial PCE for around 40 days and had a recovering effect from late spring and onwards. This behaviour has already been observed for OPVs as reported by Gevorgyan et al.[32] and Angmo et al.[33] The best sample recovered to 90% of the initial PCE. This effect is attributed to the combination of higher illumination and temperature as the recovery of AgNW-OPV starts when both increase. The same effect is not observed in C-OPV samples, indicating that it can be also associated with the presence of Ag electrodes preserving better the conductivity of the device.[16,34] The C-OPV-N outdoor test started shortly before the greenhouse test and the modules degraded slightly in the first 100 days of test in the season of low sun illumination. Thereafter from day 100 to 200 the degradation rate increased considerably, coinciding with the highly illuminated season, somewhat corresponding with the burn-in phase observed in C-OPV-L (both in late spring and midsummer). There is less correlation between performance and variation in temperature/RH compared to variation in illumination. These samples then became stable until the end of the test with about 41% of the initial PCE. In general, illumination affects more directly the degradation of the devices than RH and temperature; therefore, the addition of UV filters to the modules during manufacture should increase greatly the stability of OPV devices.

The dashed lines in Figure 3b and c mark the corresponding day zero and day 300 from the greenhouse test in Figure 3a. Comparing the two tests, it is remarkable that overall the OPV samples inside the greenhouses have a slower degradation rate. In the first period of the greenhouse test, the effect of the high humidity greenhouse is less damaging for the C-OPV than the high illumination period under outdoor conditions. For AgNW-OPV this period is slightly more damaging although the modules remain stable during the second period and the comparison of stability for both tests is the same on average. The second period of the greenhouse test is only harsh for C-OPV-L due to the barrier. During the same period, C-OPV-N and AgNW-OPV were affected by the weather conditions outdoors while the greenhouses acted as a protective shelter. During the third period of the greenhouse test, even without controlled humidity, the greenhouse conditions did not minimise the effect of the weather and of the high illumination over C-OPV. The AgNW-OPV modules tested in the greenhouse degraded less than outdoors, and after the end of the test it was expected that the modules would recover in a fashion similar to outdoor conditions.

Figure 4 shows the o-diagram, which is a method for categorizing OPV lifetime. The diagram division in logarithm (to the base 4) time blocks allows establishing the relations between the different tests. The plot represents lifetime markers $[E_0;T_{80}]$ and $[E_S;T_{S80}]$ when applicable to compare real operational conditions.[17,25] The operational lifetime is defined by the initial PCE (E_0) as a function of time that the initial PCE reaches 80% (T_{80}) or the PCE of the stabilised section (E_S) as a function of time that E_S reaches 80% (T_{S80}).[17] The greenhouse test showed no initial burn-in, so the markers shown are only $[E_0;T_{80}]$. For the outdoor test, AgNW-OPV also did not present an initial burn-in or clearly identifiable stable phase whereas C-OPV samples had a long and marked stable phase, being represented with both markers $[E_0;T_{80}]$ (solid markers) and $[E_S;T_{S80}]$ (open markers) in the o-diagram. The second case accordingly has a lower operational PCE.

In the greenhouse test, AgNW-OPVs have the best stability performance with PCE, taking seasons to reach T_{80}, fol-

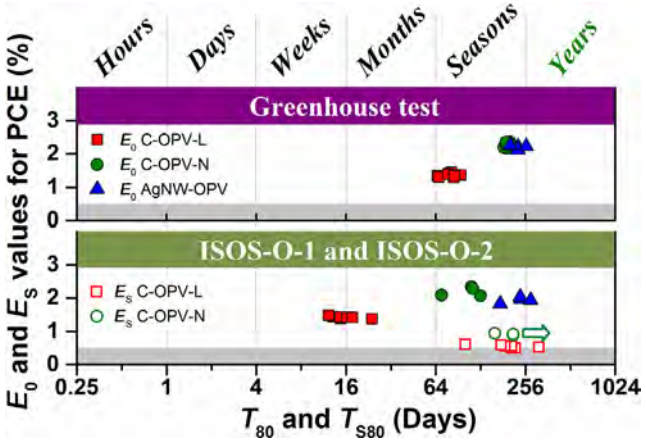

Figure 4. The o-diagram presenting $[E_0;T_{80}]$ and $[E_S;T_{S80}]$ values for all tested samples under greenhouse (1, 2 and 3) and outdoor (ISOS-O-1 and ISOS-O-2) conditions detailed in Table 2. Red squares represent C-OPV-L, green circles C-OPV-N and blue triangles AgNW-OPV. The arrow shows the data where T_{final} was used instead of T_{S80}. The greenhouse test has only $[E_0;T_{80}]$ markers (see text for further details).

lowed very closely by C-OPV-N modules, also in the range of seasons. C-OPV-L modules are clearly inferior, with operational lifetimes in the range of a few seasons; nevertheless, the stability performance would be expected to be similar to C-OPV-N in the case a good-quality barrier is used. For the long-term outdoor tests, the operational stability of C-OPV-L with $[E_0;T_{80}]$ is in the range of weeks to months whereas the $[E_S;T_{S80}]$ is in the range of weeks to seasons. For C-OPV-N, both lifetime markers are in the range of seasons although the second marker $[E_S;T_{S80}]$ shows 3 of 4 samples with the time limited by the duration of the conducted experiment (T_{final}) because 3 modules did not reach T_{S80}; thus, it is expected that this time will be in the range of years as these samples have no potential for catastrophic failure. However, the operational PCE of the C-OPVs are on average 0.44 % (C-OPV-L) and 0.73 % (C-OPV-N), which will require at least three times more OPV area coverage to produce the same kWh produced with the initial PCE. For AgNW-OPVs the operational lifetime is in the range of seasons to years under outdoor conditions.

Comparing tests, the C-OPV modules under greenhouse conditions had a considerably longer operational lifetime than under outdoor condition for $[E_0;T_{80}]$ markers. In contrast, both C-OPV samples had very similar operational lifetime outdoors during the stabilised phase when compared to the lifetime performance of C-OPV-N under greenhouse conditions. The utilization of barriers with UV filters could result in a significant increase of the stability for C-OPV modules as their burn-in/degradation is considerably affected by the intense illumination. AgNW-OPV modules inside the greenhouses and outdoors had very similar lifetime performances. UV filters in this case would possibly, under any of the conditions, improve the operational lifetime. At the phase at which the production of electricity would be the highest this would guarantee that any degradation produced by UV light would be minimised. The protection provided by the greenhouses however did not bring much improvement in the lifetime of AgNW-OPV modules compared to the encapsulation itself. The overall comparison of operational lifetime for each sample of the same kind points to the reliability of the lifetime tests based on the statistics of at least four samples per condition.

Conclusions

The stability performance and real operational conditions of carbon-and silver-nanowire-based photovoltaic (C-OPV and AgNW-OPV) modules under greenhouse and outdoor conditions have been investigated in this work. Comparison between greenhouse and outdoor conditions demonstrated that the protection of the greenhouse structure slowed the degradation of the modules and generally enhanced their stability. Some exceptions are applicable to C-OPV-L where the barrier had lower quality. The operational lifetime is better for C-OPVs under greenhouse conditions than outdoors; however, it is virtually the same for AgNW-OPV samples in both conditions, showing that they are equally affected by humidity and irradiance. The C-OPV samples inside the greenhouses are operational for seasons and C-OPV-N, with a higher quality barrier than C-OPV-L, lasts outdoors also in a range of seasons. AgNW-OPV modules under greenhouse or outdoor conditions have similar operational performance, remaining above 80 % of its initial power conversion efficiency (PCE) for several seasons. For temporary greenhouse structures reinstalled every season, both OPV technologies presented (C-OPV and AgNW-OPV) achieved the needed operation lifetime. The C-OPV modules that represent the most environmentally friendly OPV technology can be safely discarded even in a normal bin. C-OPV application in developing countries could be made on a very large scale and they have the potential for running stand-alone greenhouses and surrounding communities with harmless environmental impacts. For low-cost greenhouse installations, this technology has the efficiency and stability for practical applications. AgNW-OPV modules have the best stability, operational performance and the potential for higher efficiencies. Additions of UV filters and other improvements can further this technology not only for low-cost applications but possibly also for fully sustainable building-integrated OPVs.

Experimental Section

Sample preparation

C-OPV-L modules were manufactured using a flexible 42 μm thick PET-based barrier purchased from Amcor (Ceramis® Matt PET without UV protection) with water vapor transmission rate (WVTR) of 0.04 $g\,m^{-2}\,day^{-1}$ and oxygen transmission rate (OTR) of 0.01 $cm^3\,m^{-2}\,day^{-1}$. C-OPV-N modules were manufactured using a better quality barrier foil from the same company and brand, which had the same specifications, but from a different batch. This newer barrier foil was also used for the silver nanowire-based modules (AgNW-OPV). The back carbon electrode was printed using carbon ink from Electrodag PF-407C (from

Acheson) and dried with IR and hot air in an oven set to 140 °C. Further details can be found in the publication by dos Reis Benatto et al.[13] The AgNW-OPV modules were prepared using the first-generation freeOPV[26] design and its fabrication was also described in the literature.[16,27] C-OPV and AgNW-OPV samples were fully roll-to-roll processed using printing and coating techniques and roll-to-roll encapsulated identically using the UV-curable adhesive DELO-Katiobond LP655.[27,28]

Measurements procedure

ISOS-O-1 and ISOS-O-2 protocols were performed in the Characterization Laboratory for Organic Photovoltaics (CLOP) at the Department of Energy Conversion and Storage (DTU), Roskilde, Denmark. The samples under ISOS-O-1 condition were periodically removed and tested under a calibrated solar simulator with AM 1.5G spectrum and 1000 $W m^{-2}$ illumination; the samples under ISOS-O-2 had the IV-curve tracing performed using an automated acquisition setup with a Keithley 2400 SMU. For the greenhouse tests the modules were periodically removed, shipped to Denmark and tested under the same solar simulator as used for ISOS-O-1. The recorded IV curves were used to construct the degradation curves as recommended in the ISOS protocols.[24] A Microsoft excel-based macro was used for raw data processing and analysis.[35]

Acknowledgements

This work was supported by Energinet.dk (project no. 12144), the Eurotech Universities Alliance project "Interface science for photovoltaics (ISPV)" the Danish Ministry of Science, Innovation and Higher Education under a Sapere Aude Top Scientist grant (no. DFF-1335-00037A).

Keywords: greenhouse · ISOS tests · lifetimes · organic photovoltaics · stability tests

[1] F. C. Krebs, T. D. Nielsen, J. Fyenbo, M. Wadstrøm, M. S. Pedersen, *Energy Environ. Sci.* **2010**, *3*, 512.
[2] N. Espinosa, M. Hösel, M. Jørgensen, F. C. Krebs, *Energy Environ. Sci.* **2014**, *7*, 855.
[3] M. Said, M. EL-Shimy, M. A. Abdelraheem, *Sustain. Energy Technol. Assessments* **2015**, *9*, 37–48.
[4] C. J. Mulligan, C. Bilen, X. Zhou, W. J. Belcher, P. C. Dastoor, *Solar Energy Mater. Solar Cells* **2015**, *133*, 26–31.
[5] S. Lizin, S. Van Passel, E. De Schepper, W. Maes, L. Lutsen, J. Manca, D. Vanderzande, *Energy Environ. Sci.* **2013**, *6*, 3136.
[6] N. Espinosa, A. Laurent, F. C. Krebs, *Energy Environ. Sci.* **2015**, *8*, 2537–2550.
[7] N. Espinosa, A. Laurent, G. A. dos Reis Benatto, M. Hösel, F. C. Krebs, *Adv. Eng. Mater.* **2016**, *18*, 490–495.
[8] F. C. Krebs, M. Biancardo, B. Winther-Jensen, H. Spanggard, J. Alstrup, *Solar Energy Mater. Solar Cells* **2006**, *90*, 1058–1067.
[9] F. C. Krebs, M. Hösel, *ChemSusChem* **2015**, *8*, 966–969.
[10] B. Azzopardi, C. J. M. Emmott, A. Urbina, F. C. Krebs, J. Mutale, J. Nelson, *Energy Environ. Sci.* **2011**, *4*, 3741.
[11] C. J. M. Emmott, J. A. Röhr, M. Campoy-Quiles, T. Kirchartz, A. Urbina, N. J. Ekins-Daukes, J. Nelson, *Energy Environ. Sci.* **2015**, *8*, 1317–1328.
[12] M. Hösel, D. Angmo, R. R. Søndergaard, G. A. dos Reis Benatto, J. E. Carlé, M. Jørgensen, F. C. Krebs, *Adv. Sci.* **2014**, *1*, 140002.
[13] G. A. dos Reis Benatto, B. Roth, M. V. Madsen, M. Hösel, R. R. Søndergaard, M. Jørgensen, F. C. Krebs, *Adv. Energy Mater.* **2014**, *4*, 1400732.
[14] N. Espinosa, R. R. Søndergaard, M. Jørgensen, F. C. Krebs, *ChemSusChem* **2016**, *9*, 893–899.
[15] C. Mayousse, C. Celle, A. Fraczkiewicz, J. Simonato, *Nanoscale* **2015**, *7*, 2107–2115.
[16] G. A. dos Reis Benatto, B. Roth, M. Corazza, R. R. Søndergaard, S. A. Gevorgyan, M. Jørgensen, F. C. Krebs, *Nanoscale* **2016**, *8*, 318–326.
[17] S. A. Gevorgyan, M. V. Madsen, B. Roth, M. Corazza, M. Hösel, R. R. Søndergaard, M. Jørgensen, F. C. Krebs, *Adv. Energy Mater.* **2016**, *6*, 1501208.
[18] F. Livi, N. K. Zawacka, D. Angmo, M. Jørgensen, F. C. Krebs, E. Bundgaard, *Macromolecules* **2015**, *48*, 3481–3492.
[19] N. Espinosa, M. Hösel, D. Angmo, F. C. Krebs, *Energy Environ. Sci.* **2012**, *5*, 5117.
[20] N. Grossiord, J. M. Kroon, R. Andriessen, P. W. M. Blom, *Org. Electron.* **2012**, *13*, 432–456.
[21] P. Cheng, X. Zhan, *Chem. Soc. Rev.* **2016**, *45*, 2544–2582.
[22] P. Cheng, C. Yan, T.-K. Lau, J. Mai, X. Lu, X. Zhan, *Adv. Mater.* **2016**, *28*, 5822–5829..
[23] P. Cheng, H. Bai, N. K. Zawacka, T. R. Andersen, W. Liu, E. Bundgaard, M. Jørgensen, H. Chen, F. C. Krebs, X. Zhan, *Adv. Sci.* **2015**, *2*, 1500096.
[24] M. O. Reese, S. A. Gevorgyan, M. Jørgensen, E. Bundgaard, S. R. Kurtz, D. S. Ginley, D. C. Olson, M. T. Lloyd, P. Morvillo, E. A. Katz, A. Elschner, O. Haillant, T. R. Currier, V. Shrotriya, M. Hermenau, M. Riede, K. R. Kirov, G. Trimmel, T. Rath, O. Inganäs, F. Zhang, M. Andersson, K. Tvingstedt, M. Lira-Cantu, D. Laird, C. McGuiness, S. Gowrisanker, M. Pannone, M. Xiao, J. Hauch, R. Steim, D. M. DeLongchamp, R. Rösch, H. Hoppe, N. Espinosa, A. Urbina, G. Yaman-Uzunoglu, J.-B. Bonekamp, A. J. J. M. van Breemen, C. Girotto, E. Voroshazi, F. C. Krebs, *Solar Energy Mater. Solar Cells* **2011**, *95*, 1253–1267.
[25] M. Corazza, F. C. Krebs, S. A. Gevorgyan, *Solar Energy Mater. Solar Cells* **2015**, *143*, 467–472.
[26] F. C. Krebs, M. Hösel, M. Corazza, B. Roth, M. V. Madsen, S. A. Gevorgyan, R. R. Søndergaard, D. Karg, M. Jørgensen, *Energy Technol.* **2013**, *1*, 378–381.
[27] M. Hösel, R. R. Søndergaard, M. Jørgensen, F. C. Krebs, *Energy Technol.* **2013**, *1*, 102–107.
[28] R. R. Søndergaard, M. Hösel, F. C. Krebs, *J. Polym. Sci. Part B* **2013**, *51*, 16–34.
[29] E. Fitz-Rodríguez, C. Kubota, G. A. Giacomelli, M. E. Tignor, S. B. Wilson, M. McMahon, *Comput. Electron. Agric.* **2010**, *70*, 105–116.
[30] M. Kottek, J. Grieser, C. Beck, B. Rudolf, F. Rubel, *Meteorol. Z.* **2006**, *15*, 259–263.
[31] "Historical Weather", *Weather Underground*, https://www.wunderground.com/history, accessed 1 February **2016**.
[32] S. A. Gevorgyan, M. V. Madsen, H. F. Dam, M. Jørgensen, C. J. Fell, K. F. Anderson, B. C. Duck, A. Mescheloff, E. A. Katz, A. Elschner, R. Roesch, H. Hoppe, M. Hermenau, M. Riede, F. C. Krebs, *Solar Energy Mater. Solar Cells* **2013**, *116*, 187–196.
[33] D. Angmo, F. C. Krebs, *Energy Technol.* **2015**, *3*, 774–783.
[34] B. Roth, G. A. dos Reis Benatto, M. Corazza, J. E. Carlé, M. Helgesen, S. A. Gevorgyan, M. Jørgensen, R. R. Søndergaard, F. C. Krebs, *Adv. Eng. Mater.* **2016**, *18*, 511–517.
[35] M. Corazza, F. C. Krebs, S. A. Gevorgyan, *Solar Energy Mater. Solar Cells* **2014**, *130*, 99–106.

Received: May 27, 2016
Revised: July 8, 2016
Published online on ■■ ■■, 0000

Energy & Environmental Science

COMMUNICATION

View Article Online
View Journal | View Issue

Cite this: *Energy Environ. Sci.*, 2016, **9**, 1674

Received 24th February 2016,
Accepted 11th April 2016

DOI: 10.1039/c6ee00578k

www.rsc.org/ees

Outdoor fate and environmental impact of polymer solar cells through leaching and emission to rainwater and soil†

Nieves Espinosa,‡[a] Yannick-Serge Zimmermann,‡[bc] Gisele A. dos Reis Benatto,[a] Markus Lenz[bd] and Frederik C. Krebs*[a]

The emission of silver and zinc to the aqueous environment (rain, fog, dew) from polymer solar cells installed outdoors is presented. Studies included pristine solar cells and solar cells subjected to mechanical damage under natural weather conditions in Denmark. We find the emission of silver and zinc to the environment through precipitated water for damaged solar cells, and also observed failure and emission from an initially undamaged device in an experiment that endured for 6 months. In the case of the damaged cells, we found that the drinking water limits for Ag were only exceeded on a few single days. We also progressed our studies to include end-of-life management. To assess the implications of improper practices (uncontrolled disposal, landfilling) at the end-of-life, we buried different OPV types in intact and damaged forms in soil columns. In the case of high Ag emission (shredded cells), the potential for migration was confirmed, even though the soil was found to exhibit sequestration of silver. We conclude that recycling of Ag at the end-of-life is mandatory from an environmental point of view.

Broader context

The projected and large scale use of novel photovoltaic technologies will present a challenge to the environment either in the case of failure during operation or during the end-of-life management. In this study we established the emission of the constituents (Ag and Zn) to the environment from organic photovoltaic modules prepared entirely using printing methods on thin flexible foil. The foil samples were deployed outdoors in a rain runoff setup where all precipitated water was collected and analyzed. Both intact and deliberately damaged devices were studied. In a separate experiment, we buried solar cells in soil columns to simulate the effect of a land filling scenario and collected natural rain water filtered through the soil columns. In the simulated use phase experiment we found significant emission of both Ag and Zn for the damaged devices, whereas normally operating devices exhibited no emission, showing that emission-free operation is possible in a properly monitored system and emission can be avoided or significantly minimized if rapid action is taken upon failure. In the land filling scenario, emission of both Ag and Zn was observed, showing that recycling or recovery is mandatory and land filling is not recommended.

1. Introduction

The environmental emission of pollutants through novel energy technology has important implications for their environmental sustainability, and we must ask the questions and find answers to: how "green" are new energy technologies? Most often, the manufacturing stages are studied in great detail, with respect to both energy and material use (referred to as "cradle-to-gate"). Still, the use phase and the end-of-life management often impacts the overall sustainability significantly (referred to as "gate-to-grave"). Organic photovoltaics (OPV) have in the past few years progressed from the minimal manual laboratory scale preparation to serial production in a larger and marketable scale. They have been subject to a number of detailed life cycle assessment (LCA) studies focussed on the manufacturing stages. They have been heralded as the only energy technology that potentially presents energy payback times as short as one day and an ultra-low environmental impact (in a cradle-to-gate scenario).[1–4] Since they have now progressed to operational trials, it is crucial to provide proof of their validity as a future large scale energy technology that is truly green (*i.e.* from cradle-to-grave). The first kilowatt-scale deployment was successfully installed in 2013.[5] Significant efforts within the OPV scientific community are currently directed towards studying their Achilles heel: degradation/stability.

[a] *Department of Energy Conversion and Storage, Technical University of Denmark, Frederiksborgvej 399, 4000 Roskilde, Denmark. E-mail: frkr@dtu.dk; Fax: +45 46 77 47 91; Tel: +45 46 77 47 99*
[b] *Institute for Ecopreneurship, School of Life Sciences, University of Applied Sciences and Arts Northwestern Switzerland, Gründenstrasse 40, 4132 Muttenz, Switzerland*
[c] *Institute for Environmental Research (Biology V), RWTH Aachen University, 52074 Aachen, Germany*
[d] *Department of Environmental Technology, Wageningen University, 6708 WG Wageningen, The Netherlands*

† Electronic supplementary information (ESI) available: Detailed description of soil characterisation and further information about LCA. See DOI: 10.1039/c6ee00578k

‡ Both authors made an equal contribution to this publication.

Despite having a shorter operational lifetime compared to other thin-film PV technologies (aSi, CIGS, CdTe), they present the advantage of avoiding highly toxic/bioaccumulative elements such as cadmium (Cd), selenium (Se) or tellurium (Te) through the use of organic polymers as light-absorbing layers.[6] Numerous (benchtop) studies[3,4,7,8] have shown that OPV perform considerably better in life cycle assessments (LCA) when compared to other thin-film photovoltaic technologies, and based on this, have been regarded as a truly green energy technology. First (direct) experimental evidence points to OPV releasing minor amounts of metals to the environment in comparison to other thin film technologies in laboratory studies.[9] However, direct evidence of such release in actual outdoor installations is completely lacking today. In particular, impaired physical integrity may result in the increased release of cell materials. Thus, the potential environmental impact associated with OPV cell components being released to the environment can only be established in a systematic and quantitative manner by field data.

OPV are well packaged in a thin plastic barrier that is designed to be impervious to liquid water. When in operation (*i.e.* when producing electricity), no leaching or emission to the environment should thus take place, even when the solar cells are deployed outdoors. A complex interplay of reoccurring stress factors (UV radiation, thermal expansion, freeze–thaw, rain, snow, sea spray, *etc.*) or singular events (heavy winds, hail) constantly challenge the integrity of the operating solar cell. Eventually this may cause damage to the encapsulation, *e.g.* crack formation or delamination. Cracking or delamination at the edge are opening paths for air and water to enter. In this event, OPV cell compounds will be emitted to the environment, either to surface waters or soils. It should be noted that such degradation mechanisms include unintended induction of damage during manufacture or improper installation leaving the embedding layers scratched.

Next to the emissions during use, the emission of compounds at the end-of-life will, in particular, negatively impact the overall environmental burden. Whereas the recycling of metals is a proactive means of counteracting the latter, it is likely that some solar cell material is not recycled or decommissioned in the recommended manner.[10]

Though generally LCA can account for impacts associated from the mining of raw materials to their disposal, compounds with an unknown fate and/or particular concern for ecotoxicity[11] are not represented in standard databases. For instance, released silver (Ag) and zinc (Zn) might be in nanoparticulate form, raising nano-toxicity concerns[12,13] (though this has been questioned).[14] However, harmful effects from OPV components emitted into environmental compartments such as air, soil, water and biota have as yet not been quantified.[11] Besides metals, it would be of particular interest to look at the environmental factors of the organic molecules contained in OPV. These organic molecules are highly degradable by light, oxygen and water (*e.g.* P3HT, PEDOT:PSS and PCBM), and do not yet exist in databases.[15] The main challenge of using toxicology indicators in LCA is the lack of data in life cycle inventories.[16] Although we cannot provide molecular data on the myriad of organic degradation components that form during the degradation of OPV, we can quantify the emission of metals to the environment when OPV devices are subject to simulated and controlled failure as a result of normal (intended) operation, and operation subject to deliberate damage. These data can serve to adjust the inputs for LCA models, allowing for realistic assessments of the sustainability of OPV.

For the purpose of measuring the enhanced release of OPV-borne metallic components into the environment in real outdoor OPV installations, two novel set-ups were designed:

(1) a rain runoff scenario with OPV installed outdoors, simulating use-phase

(2) a soil sequestration scenario with OPV buried in soil, simulating uncontrolled waste disposal

The rain runoff experiment was set up in Denmark at the DTU OPV solar park at Risø campus in a 1 kWp grid-connected solar park with OPV modules. Duplicate samples of all OPV types were mounted on the tilted structure, placing a gutter at the end of each sample to collect the rain water and water from condensation (dew and fog). The water was collected by a tube where it was stored in a canister, from where periodical sampling over half a year was performed (Fig. 1). Since the focus of our work was to correlate visible damage (and performance) with the release of metals during the use phase, and evaluate environmental concerns in case of failure and for the end-of-life of the devices, we chose to carry out the experiment in duplicate. For the soil sequestration experiment, different OPV samples (shredded and non-shredded, containing silver and silver-free) were buried in soil columns exposed to outdoor conditions (Fig. 2). The experiment ran for over a year, including all seasons and their distinct weather conditions. For both scenarios, samples were analysed by inductively coupled plasma mass spectrometry (ICP-MS) for their metal content. Eventually, we included this quantitative data and assessed the environmental impact in a refined life cycle impact assessment.

Fig. 1 Rain run-off leaching setup at DTU, Risø campus (Denmark), used to study the emission of elements to the environment from organic solar cells during operation and failure. At the end of each row, a gutter collects the rain (and fog/dew), and a plastic tube guides this to a storage canister. The inset shows the damage caused deliberately in some Ag-OPV samples (see text for further details).

Fig. 2 Mobile soil sequestration/leaching setup at DTU, Risø campus (Denmark) (left). The bottles at the bottom of the columns collect the leachate as a result of natural rain fall. Plant growth (top right) and snowfall (bottom right).

2. Material and methods

2.1. OPV samples, chemicals and soil characterization

The "Ag-OPV" samples were manufactured as described previously[5] employing ITO- and vacuum-free processing. The architecture of the devices was comprised of barrier/Ag-grid/PEDOT:PSS/ZnO/P3HT:PCBM/PEDOT:PSS/Ag-grid/adhesive/barrier. Concerning the metal content, 4.9 g of Ag and 0.07 g of Zn were contained in 1 m^2 of Ag-OPV. The "C-OPV" samples were ITO-, vacuum- and Ag-free, the manufacturing of which was described earlier.[17] Their architecture was comprised of barrier/PEDOT:PSS/ZnO/P3HT:PCBM/PEDOT:PSS/carbon/adhesive/barrier. Concerning the metal content, only 52.3 mg of Zn was contained in 1 m^2 of C-OPV. All chemicals were purchased from Sigma-Aldrich Chemie GmbH (Buchs, Switzerland). The soil used in this study was taken from DTU, Risø campus, Roskilde, Denmark and homogenized prior to usage. Analyses of moisture content (method DS 204, gravimetric), pH ($CaCl_2$, PD. FAJ. III 8), organic carbon content [ISO 10694 Dumas (TCD)],[18] $CaCO_3$ content (Ca content based on SM 3120, ICP-OES), electric conductivity (PD. FAJ. VI 1) and C/N ratio[19] was performed by Eurofins Miljø A/S, Vejen, Denmark (Table S1, ESI†). Metal content was determined by digestion and ICP-MS analysis, as described below.

2.2. Scenarios description

2.2.1. Rain-runoff scenario. The rain runoff installation was set up in the solar park structure at DTU Risø campus, Roskilde, Denmark (Fig. 1). The following three OPV samples (each in duplicate; total area of 0.46 m^2) were installed for rain runoff leaching collection:

(i) Ag-OPV damaged by regular cutting (scissors) simulating severe mechanical stress (prolonged exposure to hail, wind, thermal stress *etc.*; see Fig. 1 for detail)

(ii) pristine Ag-OPV without any damage

(iii) set of 32 laser cut postcard sized (0.1 × 0.14 m; total area 0.46 m^2) pristine C-OPV without any damage.

Two areas on the installation were left blank as a negative control. The area of sample collection was protected with a plastic foil in order to limit metal contamination from external sources (nails, screws from the wooden platform structure, dust). For the rain collection, plastic rain gutters (0.4 m long) were installed with funnels connected through plastic tubes to 10 L plastic canisters. The total area of collection per sample was 0.84 m^2. Water samples were taken when the canisters were full depending on the precipitation. The content of the canisters was homogenised (shaking) and samples of 250 mL were stored for analysis. The DTU wind research facility, at the same campus, provided an online information source for precipitation from the local weather station.[20] The set-up was completed and the experiments started on April 10th 2015 and finished on October 15th 2015. The total precipitation during that half a year period was 446.8 L m^{-2}.

2.2.2. Soil sequestration scenario. At DTU, Risø campus, Roskilde, Denmark, a novel setup to study the outdoor soil sequestration behaviour of OPV components was installed (Fig. 2). The following four OPV samples were selected to be buried:

(i) 0.25 m^2 pristine Ag-OPV foil rolled-up.

(ii) 0.158 m^2 Ag-OPV shredded to fragments measuring 4 × 20 mm.

(iii) 0.25 m^2 pristine C-OPV rolled-up.

(iv) 0.158 m^2 C-OPV shredded to fragments measuring 4 × 20 mm.

The samples buried in soil were filled in glass columns (cross-sectional area of 122.72 cm^2), mounted on a trolley and placed outdoors at DTU, Risø Campus, Denmark. Rolled-up OPV modules were buried in the centre of the column, in a total of 4.5 kg of soil, leaving soil up and down in the column, whereas shredded OPV modules were buried homogenously distributed in all columns in 2 kg of soil. In all columns, 10 cm of soil was added on top as a cover layer. Leachates were collected below the columns in glass flasks connected with glass funnels. Between the soil and funnel, a layer of sand and 120 mesh polyester filters was applied to avoid soil loss to the collection flasks. This trolley was exposed to outdoor conditions (Fig. 2) for almost one year, starting on November 5th 2014 and ending on October 29th 2015. Leachates were taken when the glass flasks were full. At the end of the experiment, all column contents were divided into five soil depth layers and three soil samples were taken from every depth layer, as well as from the sand layer.

2.3. Sampling and elemental analysis

Rain runoff was taken after every rain event and acidified to a final concentration of 1% HNO_3 prior to analysis. Semiconductor grade acids were used for ICP-MS sample preparation. The same was applied to the leachates of the soil column experiment. The soil and sand samples were digested as follows: 501 ± 4 mg of material was digested with 2 mL of aqua regia (65% HNO_3 and 32% HCl, 1 : 3 v/v) at room temperature overnight and diluted to a final concentration of 5% aqua regia prior to analysis. Ag and Zn were quantified using matrix matched calibration (1% HNO_3 or 5% aqua regia) with multi-element standards (Sigma-Aldrich). The isotopes ^{7}Li, ^{23}Na, ^{24}Mg, ^{27}Al, ^{39}K, ^{44}Ca, ^{47}Ti, ^{52}Cr, ^{55}Mn, ^{57}Fe, ^{59}Co, ^{60}Ni, ^{65}Cu, ^{66}Zn, ^{69}Ga, ^{75}As, ^{78}Se, ^{85}Rb (as internal standard),

^{98}Mo, ^{106}Cd, ^{107}Ag, ^{115}In, ^{118}Sn, ^{121}Sb, and ^{208}Pb were analysed on an Agilent 7500cx ICP-MS (Agilent Technologies AG, Basel, Switzerland) using a dwell time of 0.3 s per isotope. The argon plasma was operated at 1550 W, 15 mL min^{-1} plasma gas, 0.79 mL min^{-1} carrier gas and 0.35 mL min^{-1} makeup gas. The octopole was pressurized with 5.0 mL min^{-1} helium, except for ^{78}Se, where 3.6 mL min^{-1} hydrogen was used.

2.4. Life cycle assessment methods

LCA methodology was applied to evaluate the potential environmental impact on groundwater from metal leaching in the rain-runoff setting. ILCD, the recommended methodology for the evaluation of the impact potential, was used.[21] The model of the process was a simple one, accounting for the long term effects that the emissions to groundwater would cause. More details can be found in the ESI.†

3. Results and discussion

3.1. The need for monitoring: preventing constituents from reaching the environment

As outlined above, a thorough environmental assessment should consider the emission of pollutants of particular concern during the use-phase (which should include unintended use) of the life cycle. The outdoor-installed OPV modules were therefore studied in the context of their potential emission of inorganic pollutants to the environment during both their normal (intended) use phase operation and when inadequately disposed at the end of their life. In addition, the experiments assessed the kinetics of pollutant release. This allowed conclusions on the requirements for the immediacy of reaction: how critical it is to react fast in the case of a catastrophic failure that opens up the device, to minimize the emissions to the environment?

3.2. Emission of silver and zinc into rain runoff during use

The rain runoff setting concluded after a 6 month period with some modules damaged (Fig. 3), whereas only pristine Ag-OPV No. 2 did not show delamination with visible water ingress. The cumulative element leaching (Fig. 4) showed a virtually linear release of Ag to the environment from the damaged Ag-OPV modules, reaching 7.9 and 14.3 mg of Ag from 1 m^2 OPV over the six months (Fig. 4). This corresponded to about 0.16–0.29% of the total contained Ag. The two samples differed by a factor of almost two at the end of six months, since between days 129 and 182, a clog in the rain gutter of sample No. 2 was unnoticed and rain water was lost. Extrapolating the linear trend between day 35 and day 129 suggested that the module had emitted a similar amount of Ag compared to the duplicate module.

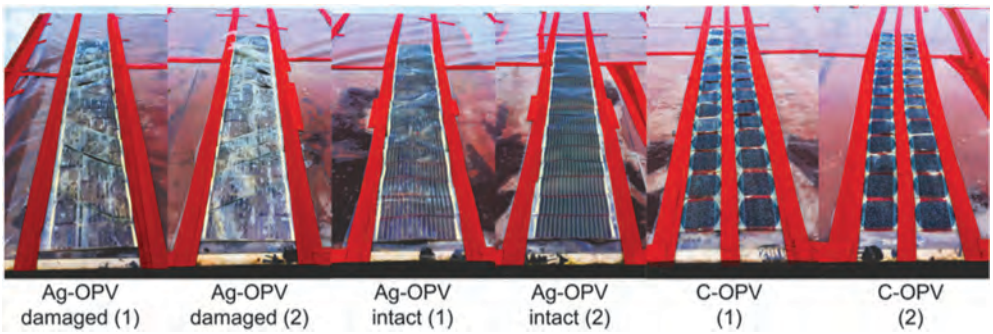

Fig. 3 Photography of the rain run-off samples at the end of the experiment. Note that only the sample Ag-OPV intact (2) did not show delamination with visible water ingress.

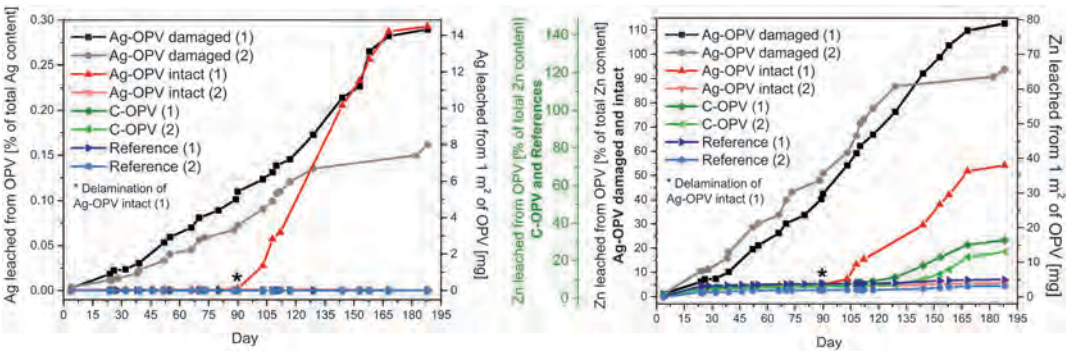

Fig. 4 Cumulative Ag (left) and Zn (right) leaching from the samples in the rain run-off experiment conducted in duplicate. The amounts are expressed in mg per m^2 of OPV (right axis) and the corresponding share of leached material (left axis). For the reference samples (blank rain), the amounts were calculated as if the cells were installed, and the corresponding share did not apply. The asterisk "*" is the point in time where the Ag-OPV intact (1) sample started to delaminate.

Concerning Zn, the same linear leaching behaviour was observed, reaching 65.7 and 79.0 mg of Zn from 1 m^2 OPV, corresponding to the complete release of the Zn contained (94–113% of the theoretical value). Again, some of the variation between the duplicates may be due to the relatively small scale of the field set up. The pristine Ag-OPV did not release any of its contained metals (Ag, Zn) until day 90. Then, one of the duplicates started to delaminate (Fig. 3, and marked with an asterisk in Fig. 4). Thereafter, Ag leaching reached 0.29% of the total contained Ag, which was very similar to the case for the deliberately damaged Ag-OPV, yet within a shorter time period (~165 *vs.* ~95 days). Simultaneously, Zn started to leach after the onset of delamination, reaching 54% of the overall contained Zn by the end of the experiment. The Ag and Zn emissions for the Ag-OPV intact (2) are in the range of the reference devices coming from rain, atmosphere and dust in the outside setup. As shown in Fig. 4, we observed similar levels of Zn in the reference samples and in Ag-OPV intact (2), while there was no sign of Ag in any of the references, C-OPV or Ag-OPV intact (2) samples. Only when failure took place (either induced or spontaneous) did the emission levels rise.

Obviously, the Ag-free devices (C-OPV) did not release any Ag, however, in contrast to the reference, C-OPV released Zn in the range of 25–31% of the overall contained Zn, with a similar rate to Ag-OPV (damaged and delaminated). It should be stressed that C-OPV only started to emit Zn after 4 months of outdoor exposure. C-OPV devices were not specifically sealed on the edges after being cut into their final shape, thus providing a path to water ingress.

3.3. Silver and zinc sequestration in soil at the end of life

The second scenario tested whether metals could be sequestrated by soil throughout a whole year after unintended disposal (using shredded materials as the worst case, and intact rolls as the best case). We made two clear observations:

(1) A higher overall amount of Ag reached the soil matrix and leachates in the case of the shredded Ag-OPV on the timescale we explored.

(2) The deeper column layers showed an enrichment of Ag in the case of shredded Ag-OPV.

The homogeneous distribution of Ag and the absence of Ag in the leachate of the intact Ag-OPV soil columns (Fig. 5) indicated that the soil had a sufficient, inherent capacity of sequestering Ag (whereas the actual mechanism may be complex and depend on the prevailing redox conditions in the soil layers).[22] The migration of Ag towards the bottom of the column in the worst case scenario, however, strongly points towards the fact that the natural sequestration capacity was exceeded, though break-through was not yet reached, even after a year of experiment. In comparison to the rain runoff scenario (maximal release of 0.29% of total Ag), the release of Ag was considerably enhanced by contact with the soil (maximal release of 15.7% of total Ag), which represents a strong increase in contrast to laboratory leaching studies using (other) shredded OPV.[9] This suggests that soil related properties, such as redox-chemistry, microbial communities and their exudates, and/or perturbation by micro-/macrofauna, may favour Ag release. Due to the inherent risks associated with Ag, this certainly warrants further detailed studies.

In the case of Zn, we found a low natural content in the soil (~lowest 15% of European top soils).[23] Despite this very low content, the release of all Zn contained in the Ag-OPV modules would only increase soil Zn concentration by a factor of ~3 to 4, to a concentration between 57–73 mg kg^{-1}, depending on the scenario. Since EU top soils contain as much as 52 mg kg^{-1} (median), the impact of OPV derived Zn can be considered minor. Similarly, the impact of C-OPV modules regarding Zn addition to soils can be considered minor, since they contained even less Zn than Ag-OPV.

The results also give important indications towards an end-of-life management scheme that would involve land-filling.

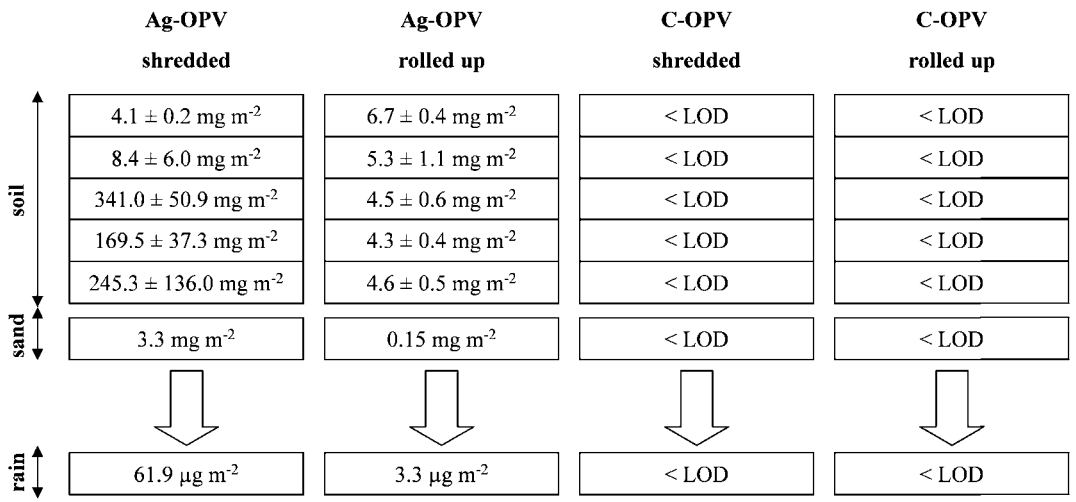

Fig. 5 Profile of silver content in the four soil columns. Results are expressed in mg or µg of silver, respectively, leached from 1 m^2 of OPV. The added up amount of leached silver from shredded Ag-OPV (771.7 mg) corresponds to 15.7% of the total silver contained, and the amount from rolled up Ag-OPV (25.6 mg) corresponds to 0.5% of the total.

Certainly, the physico-chemical conditions, matrix and hydrology of a modern landfill are substantially different in comparison to the soil columns. However, the fast (*e.g.* upon delamination in the rain runoff experiment) and extensive (soil column experiments) release of Ag upon failure of the embedding material integrity appears to be a common phenomenon (and potentially not limited to OPV, but also other thin film PV technologies). Mechanical damage during landfilling itself is very likely. The resulting rapid release of large amounts of Ag may thus represent a challenge for landfill management with regards to leachate treatment (peak loads). This holds particularly true if part of the treatment relies on biological processes, considering the antibiotic properties of Ag.[24]

3.4. Ecotoxicological implications

From the present study, we derive three major eco-toxicological implications:

(1) Though little Ag was leached during the use phase, peak concentrations occurred after only a few days upon delamination, thus stressing the need to act fast upon failure to limit the release to the environment.

(2) Zn concentrations did not exceed even the most stringent drinking water limits at any time, and Zn is concluded to be of less concern.

(3) A more complete release of Ag occurred when shredded Ag-OPV were incubated in soil (15.7% of the total contained Ag), resulting in critically elevated soil Ag contents, thus highlighting that landfilling is not a viable option and Ag must be recovered from waste.

The threshold value for Ag in drinking water enforced by the World Health Organization (WHO) is at 100 μg L^{-1}. In this study, the measured rain runoff Ag concentrations exceeded this limit twice: 127 μg Ag L^{-1} for the damaged Ag-OPV No. 1 (day 158) and 181 μg Ag L^{-1} for pristine Ag-OPV No. 1 delaminating over time (day 144). All the other Ag concentrations in the rain water remained below the WHO limit. Since the drinking water limits are set most conservatively, any acute/chronic effect by exposure to such a peak concentrations seems improbable. Still, depending on the covered area of an actual installation and the precipitation collected, higher concentrations certainly may occur. Similarly, the highest measured Zn environmental concentration was at 665 μg Zn L^{-1} for the damaged Ag-OPV No. 2 (day 88), not exceeding the WHO limit of 3000 μg Zn L^{-1}. Overall, the results are in good agreement with our previous laboratory study, where we predicted the environmental emissions not to exceed WHO values.[9] The fact that here we observe peak concentrations and direct effects of delamination, however, stresses that such field studies are a must for the verification of laboratory derived models.

When shredded cells were buried in the soil, we found that the release of Ag resulted in considerably increased concentrations (15.7% of the total contained Ag released; Fig. 5), *i.e.* a maximum of 852.5 mg Ag per kg of soil in the central layer of the 5 depth layers (exceeding the soil Ag sequestration capacity). Whereas the resulting concentrations certainly depend on the actual amount of OPV that is dumped per volume of soil, a scenario using $\sim$1/20 m^2 of OPV modules per kg soil does not seem to be an unrealistic loading. The detrimental effect of Ag will certainly depend on the complex interplay of chemical/biological redox-reactions influencing Ag speciation in soils. However, the fact that for a number of soil enzymatic activities, the "median effective concentration" causing 50% inhibition was found in the sub mg kg^{-1} range of the total soil Ag (*e.g.* in Peyrot *et al.*),[25] the overall Ag content resulting from Ag-OPV release raises a considerable eco-toxicological concern.

3.5. Life cycle impact assessment

Life cycle impact assessment was performed on the metal emissions in the rain runoff setup. The model of emissions to water and the table with the scores for the impact categories are shown in Table S2 and Fig. S1 (ESI†). All ILCD categories were evaluated, but only 2 of them showed an impact (the rest of the scores were equal to zero): *i.e.* human toxicity (non-cancer effects) and freshwater ecotoxicity. By taking the total impact during manufacture of the solar cells as a baseline (*i.e.* 100%), the share of the Ag leaching from the damaged modules is (in comparison) 15% and 30% for human toxicity non-cancer and freshwater ecotoxicity, respectively. It is only 1% for both categories when the Ag leaching is from the intact modules, since much less emissions were observed. As can be seen from the above, the actual eco-toxicological implications are aligned with LCA results. Ag concentrations in the rain runoff were mostly below even drinking water limits, suggesting no direct adverse impact on either freshwater environments or humans as the small fraction of 1% with respect the total impact of the modules shows. However, environmental processes leading to the rapid and increased release of materials are not always known, anticipated or expected (as in the soil experiments), and thus LCA results (based on the best knowledge) may be too conservative. Further, environmental factors changing the speciation of a pollutant to show increased or decreased toxicity are hard to include in LCA.

4. Conclusions

We conducted field experiments collecting direct, quantitative data on elements released by OPV. The only elements found in elevated quantities in leachates were Zn and Ag (no Al, Sb or any other element were found in contrast to the controls; data not shown). In a rain runoff scenario, the leaching of metals from the OPV modules were observed in modules with a visibly damaged barrier and in OPV that delaminated. Still, apart from a few exceptions, the metal concentrations did not exceed the WHO limit for drinking water. It is important to point out that the quality of the encapsulation and the edge sealing during an outdoor use phase of OPV are essential both for lifetime performance and environmental concerns. The timely replacement of failed modules is thus not only needed from the electricity production point of view, but also to prevent peak concentrations of metals leaching upon delamination. LCA studies could account for the actual amount of Ag and Zn released from OPV.

Only two environmental categories showed impact scores: human toxicity (non-cancer effects) and freshwater ecotoxicity. The contribution of the Ag leaching from damaged modules to these categories are 15% and 30% respectively in terms of the production of the solar cells, and only 1% for both categories when the Ag leaching is from the intact modules, since much less emissions were observed. There are still several challenges of using toxicology indicators in LCA, such as the lack of data in Life Cycle Inventories and model characterisation. With this work, we aim to open the wide road for further investigations on the environmental behaviour of organic photovoltaics.

Acknowledgements

We thank Markus Hösel, Marios D. Chatzisideris and Rafael García-Valverde for assisting in daily monitoring and collection of rainwater and rain water processing. We thank Torben Kjær and Kristian Larsen for constructing the leaching setup and rain runoff. The School of Life Sciences (HLS) of the University of Applied Sciences and Arts Northwestern Switzerland (FHNW) is gratefully acknowledged for internal funding. This work has been also supported by the Danish Ministry of Science, Innovation and Higher Education under a Sapere Aude Top Scientist grant (no. DFF – 1335-00037A). The COST Action MP1307 is thanked for their funding of a short term scientific mission.

References

1 A. L. Roes, E. A. Alsema, K. Blok and M. K. Patel, *Prog. Photovoltaics*, 2009, **17**, 372–393.
2 R. García-Valverde, J. A. Cherni and A. Urbina, *Prog. Photovoltaics*, 2010, **18**, 535–558.
3 N. Espinosa, R. García-Valverde, A. Urbina and F. C. Krebs, *Sol. Energy Mater. Sol. Cells*, 2011, **95**, 1293–1302.
4 N. Espinosa, M. Hösel, D. Angmo and F. C. Krebs, *Energy Environ. Sci.*, 2012, **5**, 5117.
5 F. C. Krebs, N. Espinosa, M. Hösel, R. R. Søndergaard and M. Jørgensen, *Adv. Mater.*, 2014, **26**, 29–39.
6 N. R. Brun, B. Wehrli and K. Fent, *Sci. Total Environ.*, 2016, **543**, 703–714.
7 N. Espinosa, F. O. Lenzmann, S. Ryley, D. Angmo, M. Hösel, R. R. Søndergaard, D. Huss, S. Dafinger, S. Gritsch, J. M. Kroon, M. Jørgensen and F. C. Krebs, *J. Mater. Chem. A*, 2013, **1**, 7037.
8 D. Hengevoss, Y.-S. Zimmermann, N. Brun, C. Hugi, M. Lenz, P. F.-X. Corvini and K. Fent, in *Organic and Printed Electronics: Fundamentals and Applications*, ed. G. Nisato, D. Lupo and S. Ganz, Pan Stanford Publishing Pte. Ltd., Singapore, 2015, ch. 12, pp. 429–472.
9 Y.-S. Zimmermann, A. Schäffer, P. F.-X. Corvini and M. Lenz, *Environ. Sci. Technol.*, 2013, **47**, 13151–13159.
10 R. R. Søndergaard, Y.-S. Zimmermann, N. Espinosa, M. Lenz and F. C. Krebs, *Energy Environ. Sci.*, 2016, **9**, 857–861.
11 Y.-S. Zimmermann, A. Schäffer, C. Hugi, K. Fent, P. F.-X. Corvini and M. Lenz, *Environ. Int.*, 2012, **49**, 128–140.
12 E. Navarro, F. Piccapietra, B. Wagner, F. Marconi, R. Kaegi, N. Odzak, L. Sigg and R. Behra, *Environ. Sci. Technol.*, 2008, **42**, 8959–8964.
13 S. Lopes, F. Ribeiro, J. Wojnarowicz, W. Łojkowski, K. Jurkschat, A. Crossley, A. M. V. M. Soares and S. Loureiro, *Environ. Toxicol. Chem.*, 2014, **33**, 190–198.
14 N. R. Brun, M. Lenz, B. Wehrli and K. Fent, *Sci. Total Environ.*, 2014, **476–477**, 657–666.
15 R. K. Rosenbaum, T. M. Bachmann, L. S. Gold, M. a. J. Huijbregts, O. Jolliet, R. Juraske, A. Koehler, H. F. Larsen, M. MacLeod, M. Margni, T. E. McKone, J. Payet, M. Schuhmacher, D. Van De Meent and M. Z. Hauschild, *Int. J. Life Cycle Assess.*, 2008, **13**, 532–546.
16 *ILCD Handbook: Framework and requirements for LCIA models and indicators*, JRC, European Commission, 2010.
17 G. A. dos Reis Benatto, B. Roth, M. V. Madsen, M. Hösel, R. R. Søndergaard, M. Jørgensen and F. C. Krebs, *Adv. Energy Mater.*, 2014, **4**, 1400732.
18 *ISO 10694: Soil quality – Determination of organic and total carbon after dry combustion (elementary analysis)*, International Organisation for Standardisation (ISO), Geneve, Switzerland, 1995.
19 *ISO 13878: Soil quality – Determination of total nitrogen content by dry combustion ('elemental analysis')*, International Organisation for Standardisation (ISO), Geneve, Switzerland, 1998.
20 Technical University of Denmark, 2016 (Risø project overview, http://rodeo.dtu.dk/rodeo/ProjectOverview.aspx?&Project=5&ProjectListFormat=map&Rnd=30223, accessed January 2016).
21 M. Owsianiak, A. Laurent, A. Bjørn and M. Z. Hauschild, *Int. J. Life Cycle Assess.*, 2014, **19**, 1007–1021.
22 Y. Hashimoto, S. Takeuchi, S. Mitsunobu and Y.-S. Ok, *J. Hazard. Mater.*, 2015, 1–7.
23 L. R. Lado, T. Hengl and H. I. Reuter, *Geoderma*, 2008, **148**, 189–199.
24 T. A. Kurniawan, W. Lo, G. Chan and M. E. T. Sillanpää, *J. Environ. Monit.*, 2010, **12**, 2032–2047.
25 C. Peyrot, K. J. Wilkinson, M. Desrosiers and S. Sauvé, *Environ. Toxicol. Chem.*, 2014, **33**, 115–125.

ADVANCED ENGINEERING MATERIALS

COMMUNICATION

DOI: 10.1002/adem.201500509

Which Electrode Materials to Select for More Environmentally Friendly Organic Photovoltaics?**

By *Nieves Espinosa, Alexis Laurent, Gisele A. dos Reis Benatto, Markus Hösel* and *Frederik C. Krebs**

The transformative power of photovoltaics depends on both the cost of the system and on the cost and availability of electricity in the area of installation. For any new technology targeting large scale energy production, another challenge lies in the need for finding a solution that is as environmentally sustainable as possible, with low environmental impacts over the entire life cycle of the system, i.e., from its manufacturing through its deployment and operation up to its final disposal.

Despite having lower power conversion efficiency in its present form, the polymer solar cell technology already offers significant advantages over traditional solar cells through i) the minimizing of material losses during the manufacturing thanks to fast and low-temperature printing techniques[1] for the deposition of the layers, ii) the possibility for using non-critical resources (e.g., rare earth metals),[2] and iii) rapid deployment of organic photovoltaics. The relatively low performance does in spite of the advantages warrant further reduction of the environmental impacts of the system while increasing its energy output. Through the use of life cycle assessment (LCA), which allows for quantifying environmental impacts over the entire life cycle of a technology or system, ecodesign can help move toward more environmentally friendly organic photovoltaics.[2]

The contact electrodes in solar cells often involve the use of scarce, toxic, and/or expensive materials, such as silver (for the contacts) and indium (for a transparent oxide that increases conductivity).[3] In particular for organic photovoltaics (OPV), indium tin oxide (ITO) is currently the most commonly used front electrode for OPV research at the laboratory scale.[4] This oxide was identified in past LCA studies as a bottleneck for the technology due to its energy intensive manufacturing processes and its insufficient abundance when considering a large-scale OPV deployment. Given a technology-dependent material intensity, installed PV capacity will translate directly to material requirements.[3,5] The choice of printable materials for each layer is therefore essential to grant the low energetic, financial and environmental cost of this new technology.

There are two approaches to lessen these concerns: i) to reduce the amounts of materials used and ii) to replace the critical materials. The second option with focus on replacement of those materials in use that have been demonstrated to embody environmental problems (e.g., toxicity, scarcity of the resources, large energy requirements), quickly leads to improvements in the environmental profile of the modules. However, until now, little work has been done in replacing materials used in traditional photovoltaics. In the search of replacing ITO a number of reports have been published proposing a wide range of candidates.[4,6–9] However, none of these reports have assessed the environmental impacts associated with these solutions in a life cycle perspective, which thus compromises their relevance and may lead to suboptimization, since it does not address the feasibility of the solution at a real scale. One of the most promising attempts to replace ITO with a printed metal grid was the manufacturing of flexible solar modules processed by roll-to-roll (R2R) methods having silver grids as both front and back electrode.[10,11] Silver is a good candidate because it can be printed in a thin pattern that permits the transmission of light, only blocking a few percent of light harvesting area. The association of silver with a hole transport layer as PEDOT:PSS as a composite electrode, has been demonstrated to lead to more efficient and environmentally friendly devices than those using ITO.[12,13]

The bulk solar cell waste material in such a case contains elements in concentrations that are higher than the primary geological ores and from this point of view decommissioned PV technologies can be used as a secondary source. A few recent studies have started to shed light on the benefits of materials recycling and how this positively influences the environmental footprint of the PV modules.[2,14] Silver, despite having abundance similar to indium does have the

[*] *Prof. F. C. Krebs, Dr. N. Espinosa, G. A. dos Reis Benatto, Dr. M. Hösel*
Department of Energy Conversion and Storage, Technical University of Denmark, Frederiksborgvej 399, 4000, Roskilde, Denmark
E-mail: frkr@dtu.dk
Dr. A. Laurent
Division for Quantitative Sustainability Assessment, Department of Management Engineering, Technical University of Denmark, 2800, Kgs. Lyngby, Denmark

[**] *N. Espinosa, G. A. dos Reis Benatto, and F. C. Krebs acknowledge funding from a Sapere Aude Top Scientist grant (no. DFF – 1335-00037A). (Supporting Information is available online from the Wiley Online Library or from the author).*

advantage that it can be easily recycled from the polymer solar cell through shredding, dissolution, and precipitation of AgCl.[14] The advantage of using silver over indium meant an improvement in the energy payback time (EPBT) by a factor of four for the same performance (2% PCE) giving an EPBT of 0.5 years.[15]

However, silver remains a scarce metal and its large-scale use in the upscaling of the polymer solar cell technology poses a significant risk. In a recent study it was demonstrated that nearly all environmental impacts of a solar park using OPV modules with silver electrodes were dominated by the contribution from the silver electrodes.[2] Here, we therefore explore its substitution with three other materials: carbon, copper and aluminum. The replacement of silver with carbon can bring down the energy pack back time to low levels (down to 5 months with the reported PCE values) and may imply large environmental impact savings. Aluminum and copper are both excellent conductors and present a much higher abundance than silver (or indium). Technically, all these four materials for electrodes (i.e., silver, aluminum, copper, and carbon) can be roll-to-roll processed in grid-patterns. The printing sequence and the layout of the fabricated modules can be seen in Figure 1; see technical characteristics of the modules with different electrodes in Table 1. Detailed information is provided in Supplementary Information, Tables S-1 and S-2.

Life cycle assessment, allowing for the selection of the more environmentally sustainable solution, has been applied to the four systems, covering their entire life cycles. The functional unit for comparing the four systems, i.e., the quantitative description of the main function of the systems that guarantees functionality equivalence, and thus fairness in the comparisons, is defined as the supply of an average 1 kWh of electricity. ITO-free modules have been tested under harsh weather conditions in Denmark and under stability protocols showing operational lifetimes over 2 years outdoors. The modules maintained the maximum power point (MPP) above T_{80} (the duration over which a solar cell retains above 80% of its initial MPP) over two years using a simple low-cost packaging barrier.[16] Based on these results aluminum and copper module lifetimes are expected to have equal lifetimes. Therefore, the components of the utility, i.e., inverter, structure, cabling (the so called balance of system (BOS)) contribute equally per functional unit for all electrode options and can, therefore, be disregarded. The considered system boundaries are outlined in Figure 2. The life cycle stages include i) the raw materials extraction to produce the different components of the OPV modules, ii) the manufacturing of

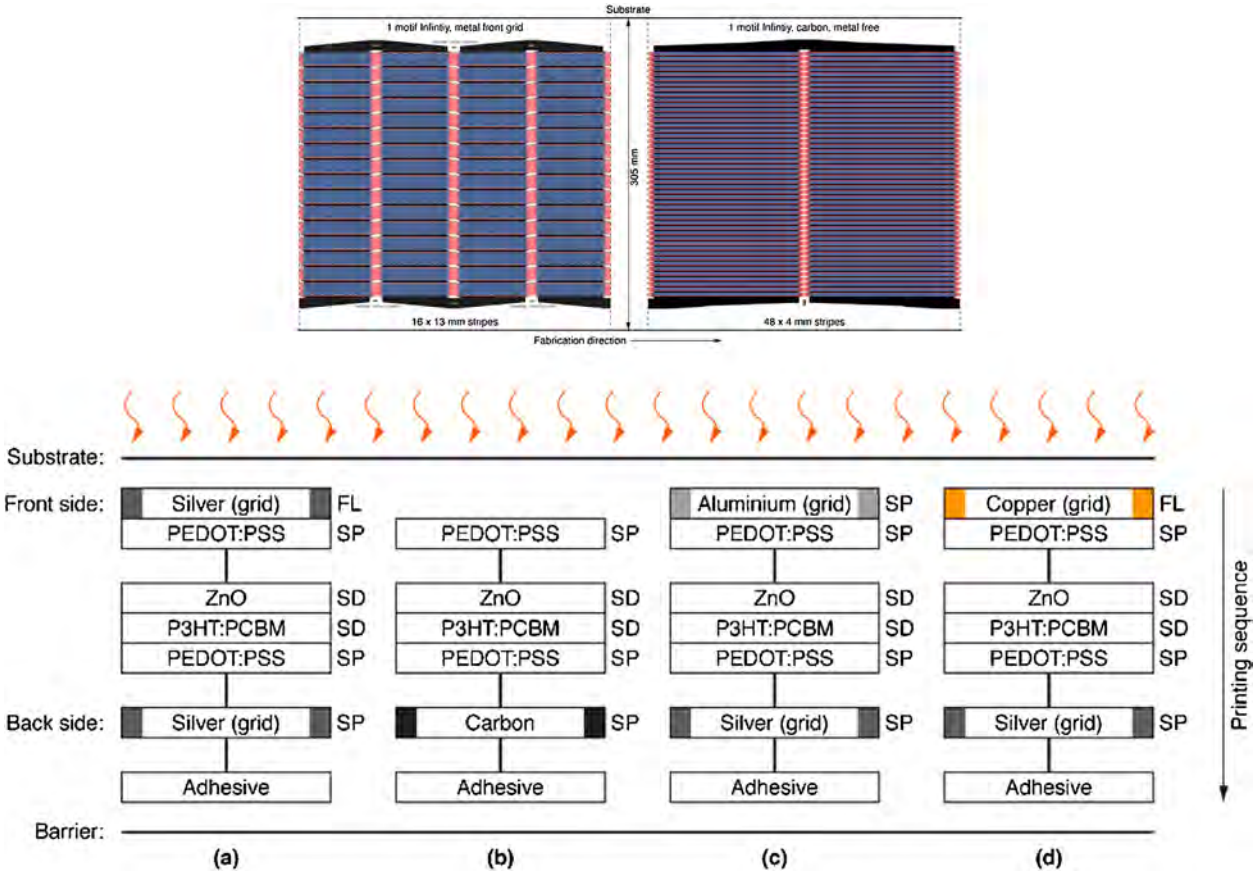

Fig. 1. Top. Layout of the fabricated modules used for the calculations in this study, on the left the pattern for the metal grids (Ag, Al, Cu) and on the right the pattern for carbon based solar cells. The carbon based design was evaluated based on the previously manufactured freeOPV solar cells. The exploitation of the different layers that form them is shown below.

Table 1. Characteristics of the four electrodes analyzed. More details in Tables S1 and S2 in Supplementary Information.

	Silver	Aluminum	Copper	Carbon
Cell Efficiency	2%	2%	2%	2%
Geometric fill factor[a)]	50%	50%	50%	36.80%
Module efficiency	1%	1%	1%	0.7%
Electrode	Front/Back	Front	Front	Back
Solid content in ink	60% Ag	40% Al	50% Cu	29% C

[a)] Based on the current design of fabricated modules at DTU. Not yet fully optimized

OPV modules as currently taking place in Denmark, iii) the operational phase, where maintenance is neglected, and iv) the disposal of the modules, which are modeled as either being recycled or incinerated (with energy recovery). Crediting of the thus-recovered materials and energy, which substitute the production of virgin materials or the generation of energy by conventional means, was performed using system expansion in the modeling.

For the production stage (since OPV modules are fabricated on a pilot-scale at the Technical University of Denmark that leads to highly representative data) background life cycle inventories from the ecoinvent 3.1 database[17] were combined with the known materials and energy requirements for the manufacture of the OPV modules. Aggregated life cycle inventories of the materials extraction, the production and the disposal of the four electrodes were built based on the requirements. The electrode ink composition and the rest of the components are available in Table S1 and S3, in the Supplementary Information. The complete model of solar cells based on silver electrodes, has been detailed in the literature[2] and the same model is used here with the adaptation of electrode materials and associated processes. The carbon-based metal-free version is based on the principle structure presented earlier.[18] Three scenarios for the disposal of the OPV modules were considered following the model established already.[2] These include a recycling route (DK-1), where the modules are recycled to recover the electrode materials and some of the plastic insulator prior to being sent to incineration (with energy recovery); an incineration route (DK-2), where the modules are directly sent to incineration with energy recovery; and an average route (DK-3), which presents the municipal solid waste management landscape for Denmark, i.e., 29% recycling, 69% incineration, and 2% landfill. Further details about the modeled scenarios can be found in the literature[2] and in the Supplementary Information.

Total pollutant emissions and resource consumptions derived from the production, installation, and decommission of the solar cells, are translated into potential impact indicator scores by use of life cycle impact assessment (LCIA) methods. The International Reference Life Cycle Data System (ILCD) methodology (ILCD 2011 v1.04, in SimaPro 8.0.4.26 software[19]) was used as it is recommended best practice in LCIA.[20] The LCA community agrees that the key areas of protection are human health, natural resources, and ecosystems quality. The assessed impact categories, therefore, include climate change, toxicity of chemicals to human health (termed 'human toxicity'), differentiated between carcinogenic effects and non-carcinogenic effects, acidification potential, photochemical ozone formation, toxicity of chemicals impacting freshwater ecosystems (termed "freshwater ecotoxicity"), eutrophication in freshwater and marine environments, respiratory impacts caused by inorganics via formation of particulate matters (termed "respiratory inorganics"), ionizing radiation impacting human health, land use, and depletion of water and non-renewable resources. Detailed descriptions and sources of the different LCIA methods for each of these impact categories have been published elsewhere.[21,22] Figure 3 illustrates the impact scores of the four systems with differentiation between the three considered disposal scenarios.

The obtained results can be distinguished between the metal-based modules and the carbon-based modules. The metal-based electrode modules are those presenting the largest environmental impacts. With the exception of climate change, stratospheric ozone depletion and water resource depletion, which are a factor of ca. 2–5 higher, all impact

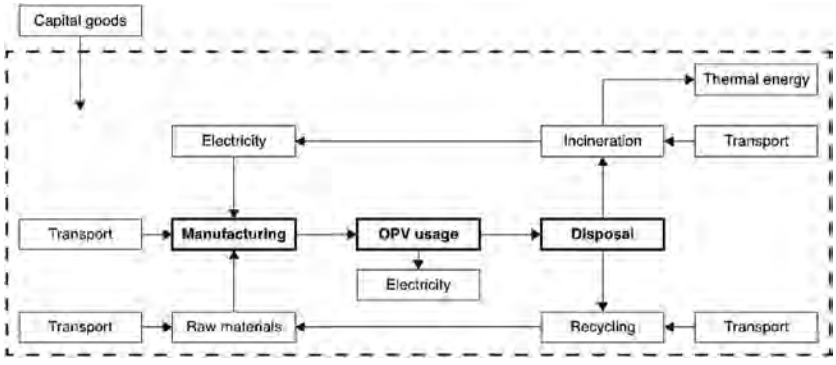

Fig. 2. Life-cycle stages of the OPV modules. From left to right the main processes are the manufacturing, involving the use of raw materials, energy and transport, followed by the usage and the disposal stage, where the two alternatives explored have been shown; recycling and incineration.

ADVANCED ENGINEERING MATERIALS

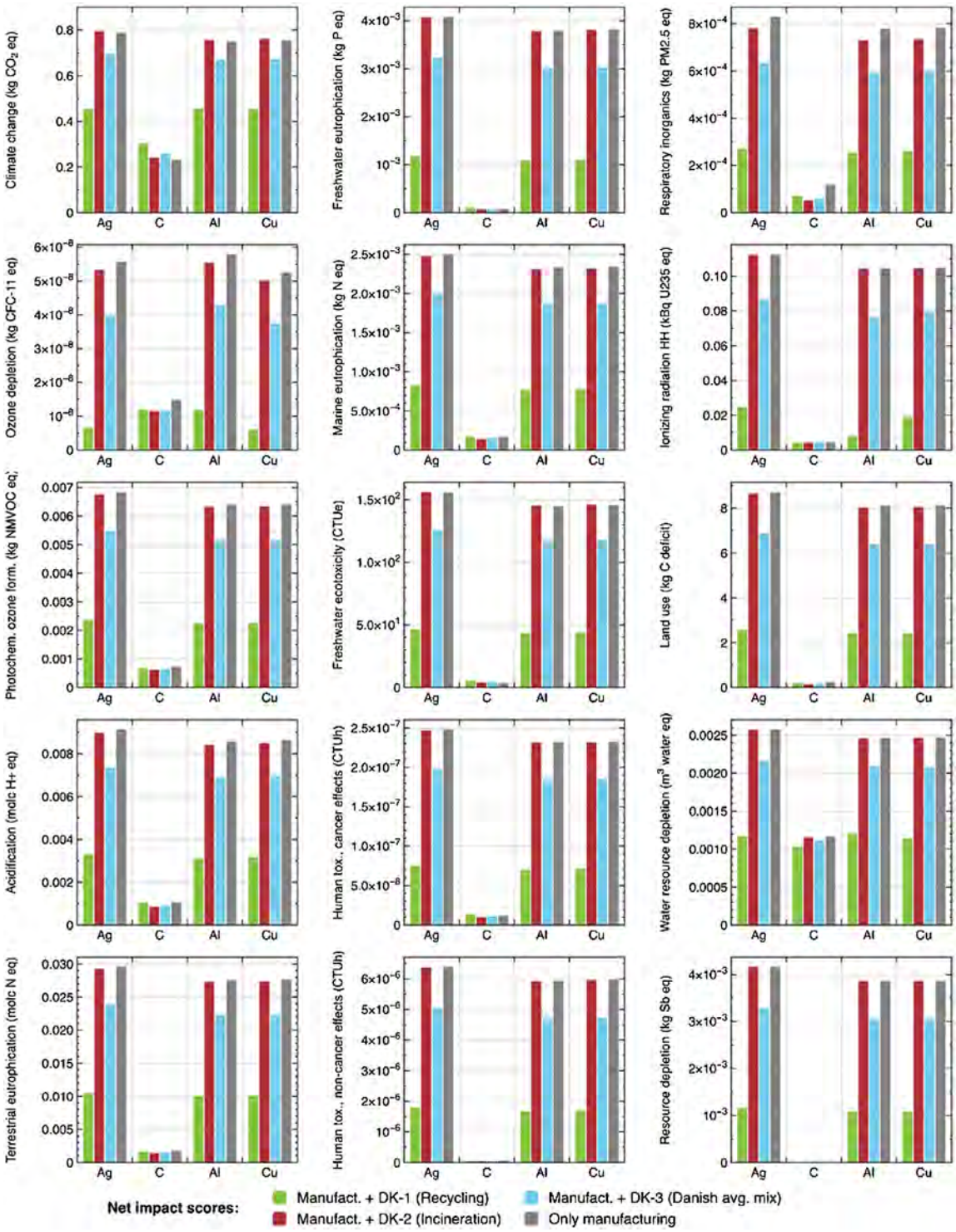

Fig. 3. Net ILCD 2011 v1.04 characterized impact scores for 1 kWh OPV modules with the different electrodes. The considered disposal under the three scenarios for waste management is shown versus the manufacturing to compare. Normalized impact scores are given in Tables S-7–S-10 and shown in Figure S-1, in Supplementary Information.

indicator scores for metal-based OPV modules generally are one order of magnitude higher than the carbon-based modules (see Table S-7–S-10). For impacts such as non-renewable resource depletion (metals, fossils) and chemical pollution impacting human health (termed human toxicity), the differences reach up to two orders of magnitude. Among the metal-based alternatives, silver use leads to the largest impacts because of its high toxicity when emitted to the environment, its relatively high scarcity, and its important energy requirements for mining and production processes.

The manufacturing of metal-based modules has considerably higher impact scores than the carbon. The highest

contribution for the emissions in the production of the metal-based electrode modules is the back electrode, which consists of silver in all of them. As reflected in the carbon-based system, the substitution of the back metal electrode with lower-impact materials (still meeting technical specifications of low sheet resistivity, roll-to-roll printing compatibility) can bring significant environmental benefits to the systems. The material substitution for that electrode should thus be prioritized by OPV designers.

The largest impacts in the manufacturing are offset by the benefits in the disposal for all systems because of recovered materials and energy. Recycling of modules represents the most beneficial option for metal-based modules because the relatively efficient recovery of metals, i.e., ca. 72%,[2] saves impacts associated with the production of virgin metals.

In contrast, the type of waste management for the carbon-based modules leads to more nuanced results. Solar cells are made of 80–90% by weight of PET. When the production of virgin polymers is avoided because of recycled polymers at rates close to 100%, the recycling scenario is more advantageous than that of incineration with energy recovery.[23] However, for some impact categories, such as freshwater ecotoxicity or human toxicity, the energy required for the recycling of carbon electrodes contributes to give the recycling scenario a higher impact score than if they are incinerated with energy recovery. The large efficiencies of the Danish incinerators also contribute to such results.[24] For the average scenario, where 69% of components are incinerated, 29% is recycled, and 2% is landfilled, the impact scores for the four systems across impact categories logically lies in between the scores for recycling and the scores for incineration. These findings, therefore, suggest that in the presence of high-value materials such as metals in OPV modules, recycling should be prioritized by stakeholders because it not only saves the extraction of scarce resources but also leads to overall decrease of the environmental burden. For such purposes, take-back systems, as generally advocated,[2] could be implemented to put responsibility on the manufacturer or operator of the solar park. From this explorative study, metal-electrode-based OPV seem to perform significantly poorer than carbon-based-electrode OPV modules with respect to all analyzed environmental indicators. Metal-electrodes, such as silver, have been demonstrated to be large contributors to the environmental impacts of the OPV modules, and their substitution by other types of materials, such as carbon, should therefore be further investigated by system designers and researchers in the PV field. Figure 4 provides an overview of "pros and cons" in the use of silver and carbon in OPV modules. From the results above, carbon modules are good candidates to be incinerated and energy can be recovered. In comparison with the metal electrode based modules, the harm is lower as well in the case they end up their lives disposed in landfills or in an uncontrolled environment. However, carbon-based module architecture is derived from the low conductivity of carbon. As it has been described by dos Reis Benatto et al.,[18] this fact imposes that the modules have to be smaller.

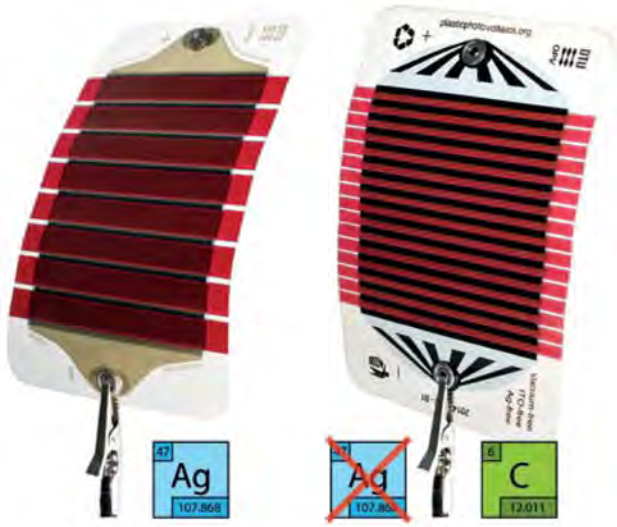

Silver	Carbon
Low usage	Moderate usage
High conductivity	Low conductivity
Higher performance	Low performance
High active area cells	Low active area[a]
Toxicity problems	Non toxic
Scarce	Abundant
High cost	Low cost
High recyclability[b]	Highly recyclable

[a] Narrower stripes are required consequently
[b] limited to a high degree of collection

Fig. 4. Comparison of silver and carbon. Image of organic solar cells printed in freeOPV pattern,[18] either with silver or carbon, where are shown the requirements of edge sealing, bus-bars, and connectors. Balance or list with the advantages, disadvantages, and the precautions of using one or another.

The edges require extra sealing. The cells built with carbon electrodes have the same efficiency per active area than the metal based cells. However, the power conversion efficiency of the modules (formed connecting cells in series) is smaller for carbon based modules since the area usage is not optimal. Carbon-based OPV modules produced at the pilot–scale, with 1% efficiency, have been compared to traditional inorganic modules (i.e., silicon solar cells), manufactured in large production volumes. The comparison of the production of 1 kWh reveals that despite carbon modules have lower efficiency, nearly all impact categories are lower than those for Si panels. Only one impact category, namely climate change, show higher results. For the remaining categories, silicon PV panels largely exceed the organic modules scores—ranging from 1.6 to 8.5 times higher. Significantly high is the impact for resource depletion stemming from the numerous metals required in the production of Si panels (Table S11 in Supplementary Information shows all the scores). The recommended research efforts of moving to metal free-electrodes should be conducted hand-in-hand with improving the coverage of the modules when printing in order to enhance their efficiencies, which consequently decreases the

environmental footprint of the OPV technology per unit of energy output.

1. Experimental Section

1.1. Materials

The electrode materials employed in this study are a silver nanoparticle ink (Novacentrix PChem PFI-722) for the front electrode and silver flake paste (Dupont 5025) for the back electrode. Aluminum ink followed an in house recipe. For the manufacturing, a ball mill is used to convert the aluminum into the precise flakes that are required for the ink to be usable. Copper oxide based ink has been purchased from Novacentrix (ICI-021). Carbon ink was purchased from Acheson (Electrodag PF-407), that contains graphite and carbon black. For the rest of the materials employed in the solar stack, data can be found elsewhere.[18,25]

1.2. Device Preparation

The solar cells were produced entirely using roll-to-roll equipment entirely under ambient conditions. The manufacturing was carried out using flexographic printing, slot-die coating, and rotary screen printing at speeds up to 20 m min^{-1}. The details are described elsewhere.[15,18,25] The necessary photonic sintering process to reduce CuO to a conductive Cu layer could not be carried out satisfactorily. Two different commercial flash systems (Novacentrix and Xenon Sinteron) have been carefully tested but the flexo printed CuO layer was to thin and porous in the microscopic range. Compact, but too thick, screen printed layers could be easily flashed to achieve conductivity. Insufficient post-treatment of CuO ink and the challenging processing of Al ink under inert atmosphere resulted in a pure theoretical evaluation of these two metal grids. Furthermore, CuO ink cannot be used as back electrode, since photonic sintering destroys the preprinted layers due to their high absorbance of light.

Article first published online: October 26, 2015
Manuscript Received: October 8, 2015

[1] F. C. Krebs, *Org. Electron.* **2009**, *10*, 761.
[2] N. Espinosa, A. Laurent, F. C. Krebs, *Energy Environ. Sci.* **2015**, *8*, 2537.
[3] J. Jean, P. R. Brown, R. L. Jaffe, T. Buonassisi, V. Bulović, *Energy Environ. Sci.* **2015**, *8*, 1200.
[4] D. Angmo, N. Espinosa, F. Krebs, in *Low-Cost Nanomater* (Eds: Z. Lin, J. Wang), Springer London, London **2014**, 189.
[5] R. L. Moss, E. Tzimas, H. Kara, P. Willis, J. Kooroshy, *Critical Metals in Strategic Energy Technologies – SETIS*, European Commission, Joint Research Centre, Luxembourg **2011**.
[6] M. W. Rowell, M. A. Topinka, M. D. McGehee, H.-J. Prall, G. Dennler, N. S. Sariciftci, L. Hu, G. Gruner, *Appl. Phys. Lett.* **2006**, *88*, 233506.
[7] Y. H. Kim, C. Sachse, M. L. Machala, C. May, L. Müller-Meskamp, K. Leo, *Adv. Funct. Mater.* **2011**, *21*, 1076.
[8] D. Angmo, F. C. Krebs, *J. Appl. Polym. Sci.* **2013**, *129*, 1.
[9] Y. Galagan, B. Zimmermann, E. W. C. Coenen, M. Jørgensen, D. M. Tanenbaum, F. C. Krebs, H. Gorter, S. Sabik, L. H. Slooff, S. C. Veenstra, J. M. Kroon, R. Andriessen, *Adv. Energy Mater.* **2012**, *2*, 103.
[10] M. Hösel, R. R. Søndergaard, M. Jørgensen, F. C. Krebs, *Energy Technol.* **2013**, *1*, 102.
[11] P. Sommer-Larsen, M. Jørgensen, R. R. Søndergaard, M. Hösel, F. C. Krebs, *Energy Technol.* **2013**, *1*, 15.
[12] N. Espinosa, R. García-Valverde, A. Urbina, F. Lenzmann, M. Manceau, D. Angmo, F. C. Krebs, *Sol. Energy Mater. Sol. Cells* **2012**, *97*, 3.
[13] C. J. M. Emmott, A. Urbina, J. Nelson, *Sol. Energy Mater. Sol. Cells* **2012**, *97*, 14.
[14] R. R. Søndergaard, N. Espinosa, M. Jørgensen, F. C. Krebs, *Energy Environ. Sci.* **2014**, *7*, 1006.
[15] F. C. Krebs, N. Espinosa, M. Hösel, R. R. Søndergaard, M. Jørgensen, *Adv. Mater.* **2014**, *26*, 29.
[16] D. Angmo, F. C. Krebs, *Energy Technol.* **2015**, *3*, 774.
[17] *The Ecoinvent Database v3.1. Swiss Centre for Life Cycle Inventories*, Ecoinvent Centre **2014**.
[18] G. A. dos Reis Benatto, B. Roth, M. V. Madsen, M. Hösel, R. R. Søndergaard, M. Jørgensen, F. C. Krebs, *Adv. Energy Mater.* **2014**, *4*, 1614.
[19] *SimaPro 8.0.4.26*, PRé Consultants, Amersfoort, NL **2015**.
[20] M. Z. Hauschild, M. Goedkoop, J. Guinée, R. Heijungs, M. Huijbregts, O. Jolliet, M. Margni, A. De Schryver, S. Humbert, A. Laurent, S. Sala, R. Pant, *Int. J. Life Cycle Assess.* **2013**, *18*, 683.
[21] A. Laurent, S. I. Olsen, M. Z. Hauschild, *Environ. Sci. Technol.* **2012**, *46*, 4100.
[22] A. Laurent, N. Espinosa, *Energy Environ. Sci.* **2015**, *8*, 689.
[23] J. C. Michaud, L. Farrant, O. Jan, B. Kjaer, I. Bakas, *Waste Resour. Action Programme Banbury* **2010**.
[24] *Energinet (2015)* Personal Communication (February 2015).
[25] F. C. Krebs, M. Hösel, M. Corazza, B. Roth, M. V. Madsen, S. A. Gevorgyan, R. R. Søndergaard, D. Karg, M. Jørgensen, *Energy Technol.* **2013**, *1*, 378.

Solar Energy Materials & Solar Cells 144 (2016) 481–487

Contents lists available at ScienceDirect

Solar Energy Materials & Solar Cells

journal homepage: www.elsevier.com/locate/solmat

Printable luminescent down shifter for enhancing efficiency and stability of organic photovoltaics

J. Kettle [a,*], N. Bristow [a], D.T. Gethin [b], Z. Tehrani [b], O. Moudam [a], B. Li [c], E.A. Katz [c,d], G.A. dos Reis Benatto [e], F.C. Krebs [e]

[a] School of Electronic Engineering, Bangor University, Dean St, Gwynedd, Bangor LL57 1UT, Wales, UK
[b] Welsh Coating and Printing Centre (WCPC), Swansea University, Singleton Park, Swansea SA2 8PP Wales, UK
[c] Department of Solar Energy and Environmental Physics, Swiss Institute for Dryland Environmental and Energy Research, J. Blaustein Institutes for Desert Research, Ben-Gurion University of the Negev, Sede Boker Campus, 84990, Israel
[d] Ilse Katz Inst. of Nano-Science and Technology, Ben-Gurion University of the Negev, Be'er Sheva 84105, Israel
[e] National Laboratory for Sustainable Energy, Technical University of Denmark, Frederiksborgvej 399, DK-4000 Roskilde, Denmark

ARTICLE INFO

Article history:
Received 24 June 2015
Accepted 24 September 2015
Available online 23 October 2015

Keywords:
Organic photovoltaics
Degradation
Outdoor performance
UV filter
Luminescent material

ABSTRACT

The proof of concept of using luminescent down shifting (LDS) layers as alternative UV filters for P3HT:PCBM OPVs is demonstrated using a lanthanide-based metal complex. The results are verified using a combination of indoor light soaking, with single cell devices, and outdoor performance monitoring, using a 16-cell monolithically connected OPV module. By applying the LDS layer, a ~5% relative enhancement in photocurrent is observed for both sets of devices. More significantly, indoor light soaking tests on single cell devices without encapsulation showed an 850% enhancement in the measured half-life ($T_{50\%}$). The OPV modules were encapsulated and tested for outdoor stability over a 70 day period in the Negev desert, Israel. The modules made with the LDS filter are shown to match the stability of those made with a commercial UV filter and outperform the modules with no filter applied, with a 51% enhancement in the measured stability ($T_{75\%}$). Significantly, the work provides clear experimental evidence that the LDS layer can act as a UV filter in OPVs without compromising the efficiency of the solar cell, thus providing an added benefit over commercial UV filters.

1. Introduction

Organic photovoltaics (OPVs) based on solution processable polymers and fullerenes have attracted remarkable interest during the last decade because of their potential for low cost, printability and flexibility. Recent research in this area has led to the report of a power conversion efficiency (PCE) of over 10% [1]. However, there are still challenges that the technologists developing OPVs need to overcome before it can become a mainstream solar technology, in particular combining high efficiency and long term operational stability in outdoor environments [2]. The causes of instability are numerous and complex and are induced or accelerated by a range of environmental effects such as temperature, water and ultraviolet (UV) light exposure [3], with the latter leading to photo-oxidation of active layer components or polymer chain scission [4,5]. As a result, the technology is unsuitable for outdoor applications unless a UV filter is applied. One major disadvantage of incorporating a UV filter into the module is that the application is normally accompanied by a reduction in efficiency, due to increased optical losses [6].

In recent years, luminescent down-shifting (LDS) materials have been widely studied and applied to photovoltaics to improve the PCE [7,8]. These materials absorb photons at wavelengths (λ) where the PV responds poorly ($\lambda < 400$ nm) and re-emit photons in the visible spectrum, where the spectral response of the PV is much greater. For this reason, the application of an LDS onto an OPV could actually serve two purposes: (1) to filter the incident UV light and to suppress OPV degradation and (2) to improve the response of the OPV at short-wavelength.

Whilst the potential for efficiency and stability enhancements via LDS layers have been reported in a wide range of PV technologies, including Dye Sensitised Solar Cells (DSSCs) [9], there are only a limited number of studies that have been carried out on OPV materials [10] and devices [11–13]. In particular, Sloff et al. and Engmann et al. have reported promising results that show a photocurrent improvement by applying LDS layers in OPVs, but the stability issue was not addressed. This paper reports the proof

* Corresponding author. Tel.: +44 1248 382471.
E-mail address: j.kettle@bangor.ac.uk (J. Kettle).

http://dx.doi.org/10.1016/j.solmat.2015.09.037
0927-0248/

of concept of improvement of both the lifetime and efficiency of OPV cells by applying LDS layers. The LDS layer can replace conventional UV filters, which are known to reduce the solar cell performance after application. The results are verified using a combination of indoor light soaking and outdoor performance monitoring, which was conducted over a 70 day period in the Negev desert in Israel.

2. Experimental

2.1. Single cell fabrication and indoor stability measurements

OPV cells were initially prepared in a clean room environment using indium tin oxide (ITO) coated glass substrates ($R_s = 16\ \Omega^{-2}$) that were cleaned using solvents, then treated in a UV–ozone reactor with oxygen plasma for 10 min. A layer of zinc oxide (ZnO) film was deposited on ITO/glass substrate in a sputtering system at ambient temperature. Poly(3,4-ethylenedioxythiophene)–poly (styrenesulfonate) (PEDOT:PSS) was spin coated on at 5000 rpm for 30 s and baked on a hotplate at 120 °C, before moving the samples into a nitrogen glovebox. Active layer blends using P3HT and [6,6]-phenyl-C_{61}-butyric acid methyl ester (C_{61}-PCBM), supplied by Nano-C Inc. USA, with weight ratios 1:0.8 were prepared and mixed with chlorobenzene solvent with a concentration of 30 mg/mL. Prior to coating, the blend was allowed to dissolve for 24 h on a hot plate stirrer and filtered using a 0.45 μm PTFE filter. Samples were transferred into a nitrogen atmosphere glovebox ($[O_2]$, $[H_2O] < 1$ ppm), where the active layer was applied by spin-casting from a 60 °C solution (1500 rpm for 60 s). The active layer was annealed at 140 °C for 1 h. Finally, thermal evaporation of the anode was performed through a shadow mask to define device area and consisted of 10 nm of molybdenum trioxide (MoO_3) and 100 nm of silver (Ag).

The LDS layer was dissolved in PMMA (20 mg/mL). The films were formed by doctor blading, with a final thickness measured at ~1 μm. The doctor bladed layers were dried at room temperature for one hour. The LDS used for these tests was Tris(hexafluoroacetylacetonate) mono(1,10-phenanthroline)europium(III) [sym.: Eu(hfac)(phen)], which was purchased from Lumtec, Taiwan and used as received. Overall, a schematic of the cell is shown in Fig. 1(a) and an image of the LDS under UV excitation is shown in Fig. 1(b). Absorption and transmission were measured with UV–vis–NIR (UV-3600 SHIMADZU). Photoluminescence was measured with a Fluoromax-4 spectrophotometer.

OPVs were checked for initial performance prior to lifetime testing using a Newport solar simulator with 100 mW cm^{-2} AM1.5G output (calibrated using a silicon reference cell from RERA in the Netherlands) and a Source Measurement Unit (SMU) for taking current density–voltage (*J–V*) measurements. For stability measurements, the cells were tested in accordance with ISOS-L-2 standards [14]. The cells were placed under the solar simulator for light soaking and were kept at open circuit in between measurements, with *J–V* measurements were made every 30 min for 550 h. Whilst the temperature of the cells was not controlled, it was measured and stayed relatively constant during the testing at 40 ± 5 °C.

2.2. Large area LDS printing for outdoor testing

In order to apply the LDS coatings over larger areas for outdoor performance monitoring, a DEK 248 screen printer was used for printing the Eu(hfac)(phen):PMMA (abbreviated to 'Eu:PMMA') inks. For screen printable inks, the LDS layer was dissolved in PMMA (10 mg/mL) with 4 wt% polyethylene glycol 400 (PEG 400) to act as a binder. The LDS coatings were printed onto a

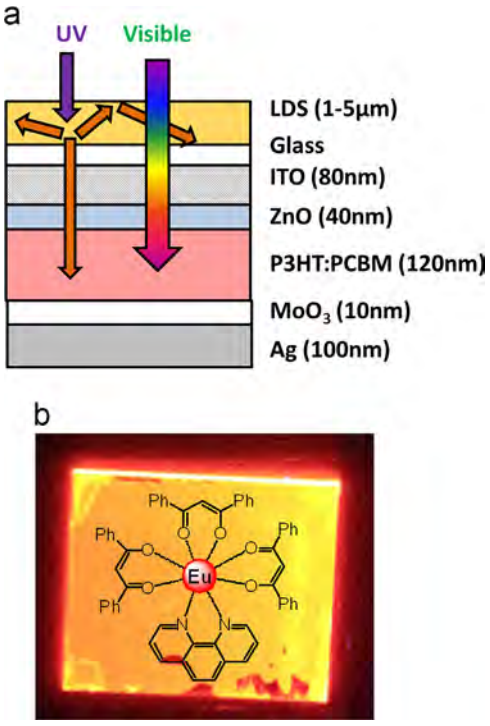

Fig. 1. (a) Schematic of the device used for single cell and 16-cell OPVs, with the LDS applied to the top surface and (b) the Europium complex and photoluminescent response from above using UV excitation.

polyethylene terephthalate (PET) carrier substrate of thickness = 125 μm, supplied by DuPont Teijin Films, UK. Trials were performed to optimise the ink transfer onto the substrate by studying the level of the snap-off gap and squeegee load that produced acceptable prints for the Eu:PMMA inks. After optimisation, it was discovered that optimal flood and print speed was 70 mm/min and Squeegee load was 10 kg. The PMMA inks were dried at 90 °C for 3–5 min on a belt dryer. The LDS layers were printed into rectangular patterns with dimensions of 8.5 × 10 cm^2. As the film thickness of the screen-printed LDS layer was 5 μm, wave-guiding losses to the edge of the substrate were minimised and are estimated to contribute also to < 0.5% of optical losses. As the printed LDS was slightly thicker than the layers described in Section 2.1, the concentration of LDS material was reduced to compensate. Measurements of the surface roughness of the printed LDS layer show the formed layer is very smooth ($R_A = 3$ nm). Fig. 2(a) shows a photograph of the PET substrate before and after Fig. 2(b) coating of the LDS layer, with no obvious change in visible appearance. The photoluminescence from UV excitation of the uncoated and coated LDS samples are shown in Fig. 7(c) and (d), respectively, confirming the uniformity of the LDS material dispersed in PMMA after screen printing.

2.3. Module (16-cell) fabrication and outdoor stability measurements

Roll-to-roll (R2R) coated OPV modules were produced without UV-filter and used for the outdoor performance tests. The fabrication of these modules followed the literature reports with the exception that the barrier material employed did not include a UV-filter, as part of the 'free OPV programme' at www.plasticphotovoltaics.org [15,16]. The devices had an ITO free structure of Carbon/PEDOT:PSS/ZnO/P3HT:PCBM/PEDOT:PSS/Carbon/PET-substrate (Fig. S1 in Supporting information). Outdoor performance monitoring of these type of R2R coated OPVs which possess only a PET barrier layer is known to lead to rapid degradation in less than

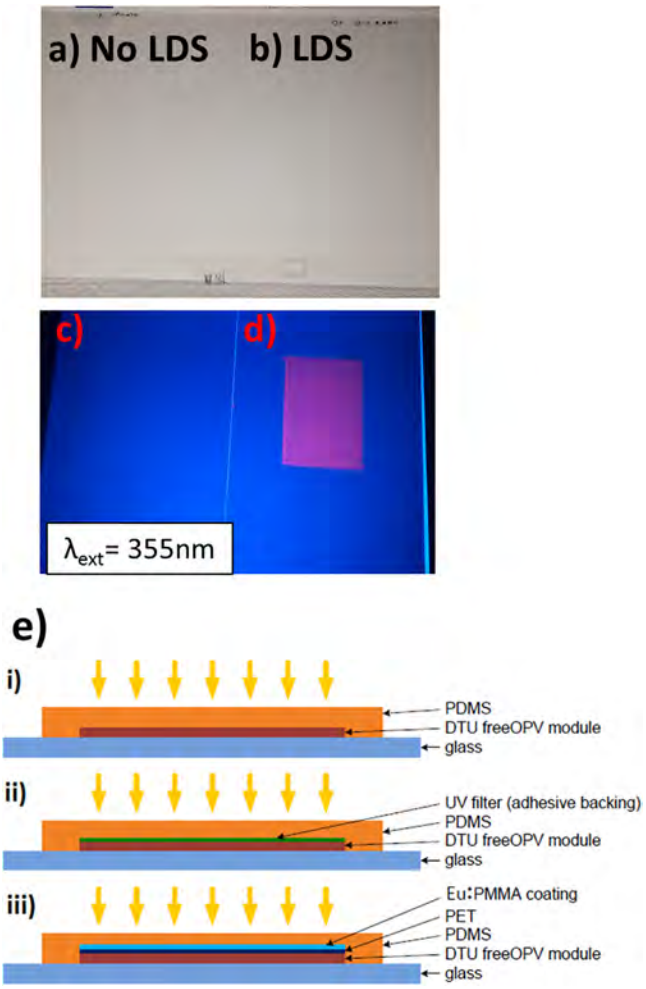

Fig. 2. Roll-to-roll (R2R) coated OPV modules. Photograph of the PET substrate (a) without and (b) with the Eu:PMMA LDS printed, with photolum inescense response from UV excitation shown also for substrates (c) without and (d) with the Eu:PMMA LDS layers. The rectangular LDS coated area was cut and attached the OPV module using an optical adhesive layer (e) and encapsulated in PDMS. All modules were mounted onto a rigid glass substrate before outdoor testing.

3 months of outdoor operation [17]. Therefore to ensure long term stability, the modules were encapsulated in PDMS prior to testing. PDMS has been used in polycrystalline silicon PVs as an alternative to EVA and it only weakly affects UV light transmission from 400 nm to 280 nm [18] Therefore, the encapsulant does not significantly filter the UV components of incident sunlight, enabling the effectiveness of the LDS layer to be evaluated, whilst preventing oxygen and water ingress. A comparison of three configurations was undertaken, as shown in Fig. 2(e): (i) a control module without a UV filter, (ii) a module with a commercially available UV blocking layer from Solaronix SA (Part number 49132) and (iii) a module with the Eu:PMMA LDS layer (printed on PET as described above). The Eu:PMMA LDS layer was attached to the top of the active area using a thin layer of PMDS to act as an adhesive (Fig. 2(e)).

Outdoor current–voltage (*I–V*) measurements of roll-to-roll (R2R) coated OPV modules were performed for a period of 70 days during daylight hours (from 10 a.m. to 3 p.m. 6 times a day) starting from 28.12.2014 in Sede Boker (the Negev desert, Israel). This was conducted in accordance with ISOS-O-2 standards [14]. Global intensity of incident sunlight was measured with a calibrated thermopile pyranometer (Eppley PSP). During the measurements the modules had ambient temperatures measured by thermocouples. The stand was placed outdoor during the entire measurement period. It should be noted that the spectrum measured at noon time $\pm$2–3 h of a cloudless day at Sede Boker (Lat. 30.8°N, Lon. 34.8°E, Alt. 475 m) matches almost identically to the AM1.5G spectrum [19], providing a vigorous test for the ability of the Eu:PMMA layer to filter UV light.

3. Results and discussion

3.1. Photophysical characterisation

In this work, LDS coatings were prepared by using Eu(hfac)(phen) dissolved in a PMMA host layer (abbreviated to 'Eu:PMMA'). The Eu:PMMA films were prepared and their photoconversion properties were studied by measuring excitation and emission spectra and luminescent efficiency (Fig. 3). Samples were prepared with 2% weight LDS in PMMA and applied to a glass sample using doctor blading, leading to a coated thickness of around 1 μm. Light from the LDS layer is emitted isotropically; therefore losses can occur away from the cell and through wave guiding perpendicular to the active layer. Wave guiding losses are minimised by ensuring the LDS layer is as thin as possible and it is estimated that these amount to less than 1% of losses occur as a result, when considering the samples sizes used for these tests.

The reasoning for using Eu(hfac)(phen) is shown well in Fig. 3: its large Stokes shift prevents reabsorption of emitted light and good spectral breadth in the UV region limits UV light transmission into the active layer. For the Eu:PMMA sample, UV absorption occurred from 300 nm up to around 415 nm with the peak absorption occurring at $\lambda_{peak,abs} \approx 360$ nm. A narrow luminescence is observed with a peak emission at 610 nm, which is consistent with other europium phosphor complexes [20]. Overlaid on the data is the External Quantum Efficiency (EQE) of a P3HT:PCBM OPV and it is apparent that the LDS material has an the overlap in the emission spectrum with the EQE of P3HT:PCBM.

3.2. Single cell performance and indoor stability results, conducted in accordance ISOS-L-2

Single cell devices were fabricated and tested using the Eu:PMMA, LDS with a schematic of device architecture shown in Fig. 4 (a). The *J–V* characteristics of the representative P3HT:PCBM cells both with and without the Eu:PMMA LDS are shown in Fig. 4(a). OPVs were prepared with 2%, 5% and 8% weight LDS in PMMA, with the thickness kept approximately constant. The LDS layers were applied to a glass surface using doctor blading as the sample

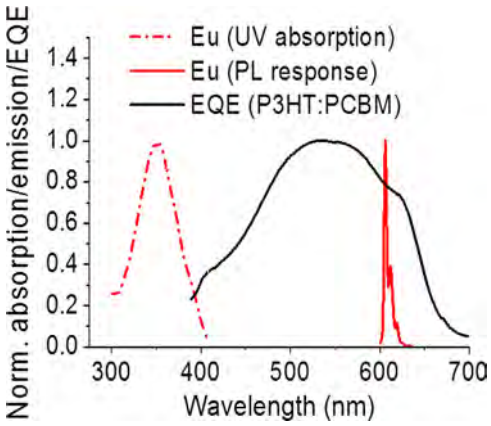

Fig. 3. Relative absorption and photoluminescence (PL) emission (λ_{exc}=355 nm) of the Eu:PMMA layer. The PL response shows good overlap with the External Quantum Efficiency (EQE) of P3HT:PCBM solar cell (also shown).

sizes were relatively small (4 cm^2). The key performance parameters including open-circuit voltage (V_{oc}), short-circuit current density (J_{sc}), fill factor (FF) and power conversion efficiency (PCE) are summarised in Table 1.

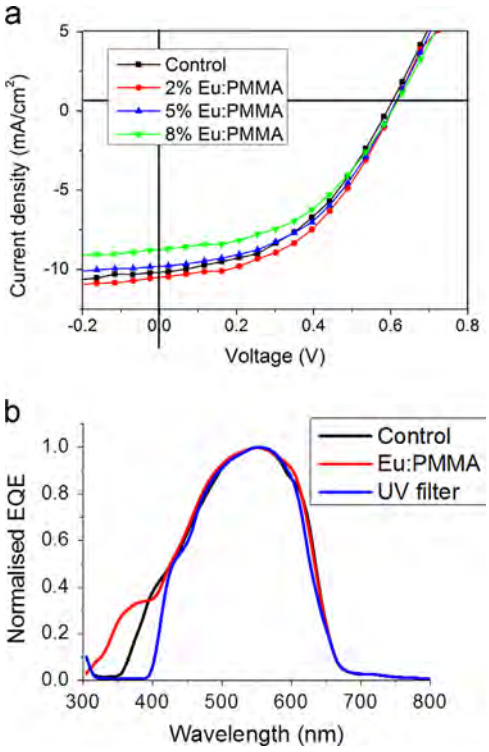

Fig. 4. (a) The measured current–voltage characteristics under AM1.5G of the representative P3HT:PCBM cells without LDS and with EU:PMMA (2%, 5% and 8%) and (b) the External Quantum Efficiency (EQE) of the cells without LDS and with EU:PMMA (2%) and also the performance with a commercially available UV filter from Solaronix SA (Part no. 49132).

For the control devices, fabricated without an LDS, the average short-circuit current density (J_{sc}) was measured at 10.01 mA/cm^2 and PCE at 2.79%. For devices fabricated with the Eu:PMMA LDS, the optimum concentration was found at 2 wt%, with the average (J_{sc}) measured at 10.54 mA/cm^2 and a PCE of 3.04%. It can be seen from Fig. 4(b), the EQE of the OPVs with Eu:PMMA layer has been moderately improved over non-coated samples. In particular, at wavelengths between 310 and 400 nm, the EQE has been enhanced by application of the layer. Therefore, the relative increase in J_{sc} can be attributed to the UV down-conversion, leading to an increase in visible light into the OPV active region. The level of PCE increase is small and the primary reason for this is

Table 1
Performance of the OPV devices, measured under AM1.5G illumination. The single cells were used to optimise the Eu:PMMA concentration and an optimum of 2 wt% in solution was found. The 16-cell (module) performance was measured and benchmarked against a control sample (no UV filter) and a module fitted with a commercial UV filter.

Sample	PCE (%)	V_{oc} (V)	I_{sc} (mA)	FF (%)	Relative I_{sc} change	Relative PCE change
Single cell (For indoor testing using ISOS-L-2)						
Control	2.79	0.598	10.01	46.6		
2% Eu: PMMA	3.04	0.604	10.54	47.5	+5.1	+8.4
5% Eu: PMMA	2.82	0.607	9.84	47.2	−1.7	+1.1
8% Eu: PMMA	2.31	0.604	8.24	46.4	−16.7	−16.8
***16-cell module* (*For outdoor testing using ISOS-O-2*)**						
Control	2.39	12.13	13.68	43.37		
UV filter	1.97	11.94	10.59	46.77	−17.5	−22.8%
Eu:PMMA	2.44	11.70	14.62	42.97	+6.5	+2.1%

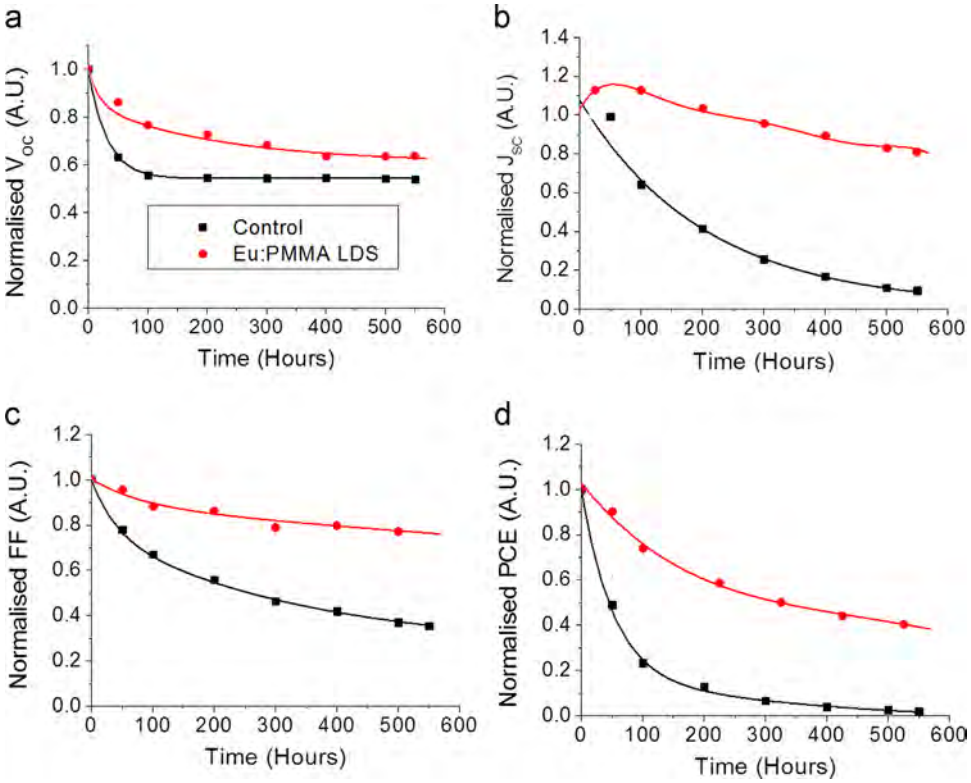

Fig. 5. Evolution of the principle photovoltaic parameters [(a) V_{oc}, (b) I_{sc}, (c) FF and (d) PCE)] of the representative P3HT: PCBM cells with and without LDS under long term illumination at AM1.5G condition (100 mW/cm^2).

due to low proportion of UV light in the AM1.5G. Based on the Standard Reference Spectra (ASTM G-173-03), UV energy accounts for only 9.16% of light irradiation from the sun (AM1.5G). In addition, light is emitted isotopically from the LDS complex and light that possesses an angle of up to 38° perpendicular to the OPV surface is likely emitted out of the PMMA host layer. Based on this emission escape cone calculation and the low waveguide losses due to the thinness of the LDS layer, there is only likely to be a maximum of ~6.9% relative increase in performance by application of an LDS layer onto an OPV cell, which indicates that the Eu:PMMA layer used in these devices is operating at around 57% of the maximum attainable enhancement, which could be improved by using materials with higher photoluminescent quantum yields. However, one of the principle advantages of the LDS layer is that it eliminates the need for a conventional UV filter. Fig. 4(b) shows the EQE of the device with a commercial UV filter applied (Solaronix SA, part number 49132). It is evident that any light with a $\lambda < 400$ nm does not generate photocurrent, which leads to an overall drop in the solar cell performance.

The effectiveness of the LDS for protecting OPVs against photodegradation was tested by indoor light soaking using the AM1.5G spectrum in accordance with ISOS-L-2 standards. Lifetime stability tests were carried out for 550 h for non-encapsulated devices with and without the Eu:PMMA LDS layer. Fig. 5 shows how the key performance parameters of V_{oc}, J_{sc}, FF and PCE for the P3HT:PCBM solar cells changed relative to their initial values during light soaking. As expected, the overall performance of devices without encapsulation decreased rapidly with trend matching closely an exponential decay, emphasising the need for encapsulation if devices are to be put to practical use [21,22].

It is also evident that for devices fabricated with an LDS layer, the stability was much improved. For the control device, the time taken to reach 50% of the original PCE ($T_{50\%}$) is 38 h. This compares with $T_{50\%}$=322 h for the device with Eu:PMMA, leading to an overall improvement in half-life by 850%. When considering the relative changes of each parameter for the devices, the main causes of the rapid decrease in $t_{1/2}$ are due to reductions in V_{oc}, FF and J_{sc} (with this order of precedence). The drop in V_{oc} can be equated to a modification of the HOMO of P3HT, due to polymer doping [23]. It is known that upon exposure to oxygen and UV-light, a shift of the occupied states of about 0.3 eV is observed, which correlates well to the measured drop in V_{oc} ($\Delta V_{oc} \approx 0.27$ V) in the control experiment. For the control device, no UV filtering is present, so this modification occurs rapidly after the commencement of the experiment ($t \sim 100$ h). The fall in FF and J_{sc} follows the expected trend with other papers [21], showing a negative exponential drop from $t=0$ h, due to the chemical and physical degradation mechanisms of the photoactive PCBM:P3HT layer and electrode interfaces. *T* is worth noting, the V_{oc} and FF of OPV with such a device architecture may also degrade under UV-light due to generation of shunts in the ZnO hole blocking layer [15].

3.3. Module (16-cell) performance and outdoor stability results, conducted in accordance ISOS-O-2

Roll-to-roll (R2R) coated OPV modules prepared without UV-filter were used for evaluating the performance of the LDS layers in outdoor environments. Previous tests on these modules showed rapid degradation as the barrier layer possesses a relatively high Water Vapour Transmission Rate (WVTR) [24]. Therefore, the OPV module was entirely encapsulated in PDMS to limit the water and oxygen penetration into the active layer. PDMS was selected due to its high UV transparency, as shown in Fig. 6(a), which shows the absorption cut-off of PDMS at around $\lambda \approx 298$ nm, which is beyond the spectral range of AM1.5G. To compare the effectiveness of the LDS layer, three samples of each configuration were prepared;

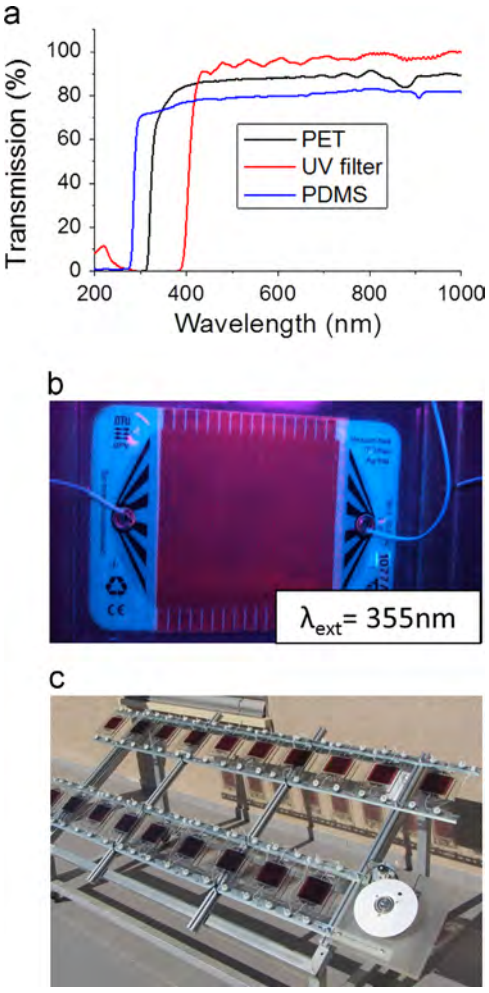

Fig. 6. (a) Transmission of light through the PET, PDMS encapsulation layers and through the commercial UV filter, (b) image of the OPV module with LDS filter under UV excitation and (c) image of experimental setup at the Jacob Blaustein Institutes for Desert Research, which is part of the Ben-Gurion University, Negev desert, Israel.

three control samples with no UV filter, three modules with a laminated commercial UV filter (the transmission profile shown in Fig. 6(a)) and three modules with the screen-printed Eu:PMMA filter attached (an image of the module illuminated with UV light is shown in Fig. 6(b)). All of the studied modules and the pyranometer were mounted on a fixed angle (30° to horizontal) stand (FAS) (Fig. 6(c)).

Table 1 shows the averaged solar cell performance the OPV modules under AM1.5G irradiation, prior to outdoor stability testing. The best performing module is fabricated with the Eu:PMMA LDS layer, which shows the highest J_{sc} and PCE, despite a lower V_{oc} and FF. In Table SI-1, the initial performance data (before application of the UV filters or PDMS encapsulation) for all modules are shown. These data indicate that the modules initially matched closely in performance. The EQE of the modules with and without LDS layers and with the commercial UV filter is shown in Fig. SI-2. One of the main advantages of the OPV modules with the Eu:PMMA LDS layer becomes evident when comparing their performance to that for the modules with the commercial UV filter in Table 1. By applying the UV filter, a substantial decrease in J_{sc} and PCE is observed, indicating that a compromise in efficiency is normally needed to obtain the improved stability when using such a filter. The principle reason for this decrease is the high refractive index of the commercial UV filter; typically these are based on metal oxide films (with $n \sim 2.5$). Such as high refractive index leads

to increased reflection of incident light and haze. In contrast, the variations in refractive indices of the layers used in the LDS-coated module are small, leading to limited normal incidence reflection. Therefore, by using an LDS layer as the UV filter, the performance drop is removed, whilst retaining the characteristic to filter out UV light.

The PCE of OPV modules operating outdoor has a complicated dependence on time during the day due to diurnal variation of the intensity and spectrum of sunlight and ambient temperature. This dependence is beyond the scope of the present paper and will be reported elsewhere. Here, for analysis of the OPV outdoor stability, we selected only one value of the module parameters (PCE, FF, V_{oc} and I_{sc}) for every day of testing, which corresponded to the moment of maximum PCE (during a day). These values were normalised in the following manner; firstly, J_{sc} values were adjusted to the standard irradiance value of 1000 W/m^2, by assuming a linear increase of J_{sc} with light intensity [25]. V_{oc} values were then adjusted to the standard temperature of 25° assuming decrease of the OPV V_{oc} with temperature [26]. Then all values of PCE, FF, V_{oc} and I_{sc} were normalised to their initial values (results of the first out-door measurements in Sede Boker on 28.12.2014). Fig. 7(a)–(d) illustrates evolution of such normalised parameters for a representative module over a 70 day testing period in Sede Boker. Based on this data, it can be concluded that:

1. PDMS modules (without any UV-filter or LDS layer) exhibited the fastest degradation of the PCE (Fig. 5(a)). The worst performing module after degradation was found to have 57% of the initial PCE value by the end measurement period. Meanwhile modules with UV filter and Eu:PMMA LDS layer showed considerably slower degradation during the long term test (their PCE decreased to only ~75% of the initial values). The results show the Eu:PMMA improves the time for the modules to drop 75% ($T_{75\%}$) of the original value by 51%.
2. During first 50 days of the experiment outdoor PCE degradation occurred mostly due to the degradation of FF (Fig. 5(c)) while V_{oc} and J_{sc} exhibited relatively stable behaviour (Fig. 5(a) and (b)). However, during the final exposure period (days 50–70) reduction of V_{oc} and J_{sc} was found to contribute to the PCE degradation as well.

There is a marked difference in the kinetics of the photovoltaic performance degradation of non-encapsulated samples (Figs. 5 and 8(a)) and encapsulated modules (Figs. 7 and 8(b)). The encapsulated modules are observed to possess an initial "stable period", before degrading at a much quicker rate thereafter (see Fig. 8(b)), which is a trend observed in other OPV modules [19]. We can speculate that this trend originates from the gas permeation through the encapsulation layer and the initial stability is due to the "transition phase" in which steady state gas diffusion has not been reached, resulting in very small or no observable permeation and limited OPV performance fall-off. This is followed by a steady-state regime where diffusion has reached equilibrium, giving a constant flux of gas species permeating through the barrier films during this period oxygen or moisture can penetrate into the encapsulated sample or/and degradation of the encapsulation layer occurs.

4. Conclusions

The proof of concept of using LDS layers as UV filters for P3HT:PCBM OPVs has been demonstrated. Non-encapsulated single cell devices were fabricated and tested indoors. By applying the LDS layer, a 5% relative enhancement in photocurrent and an 850%

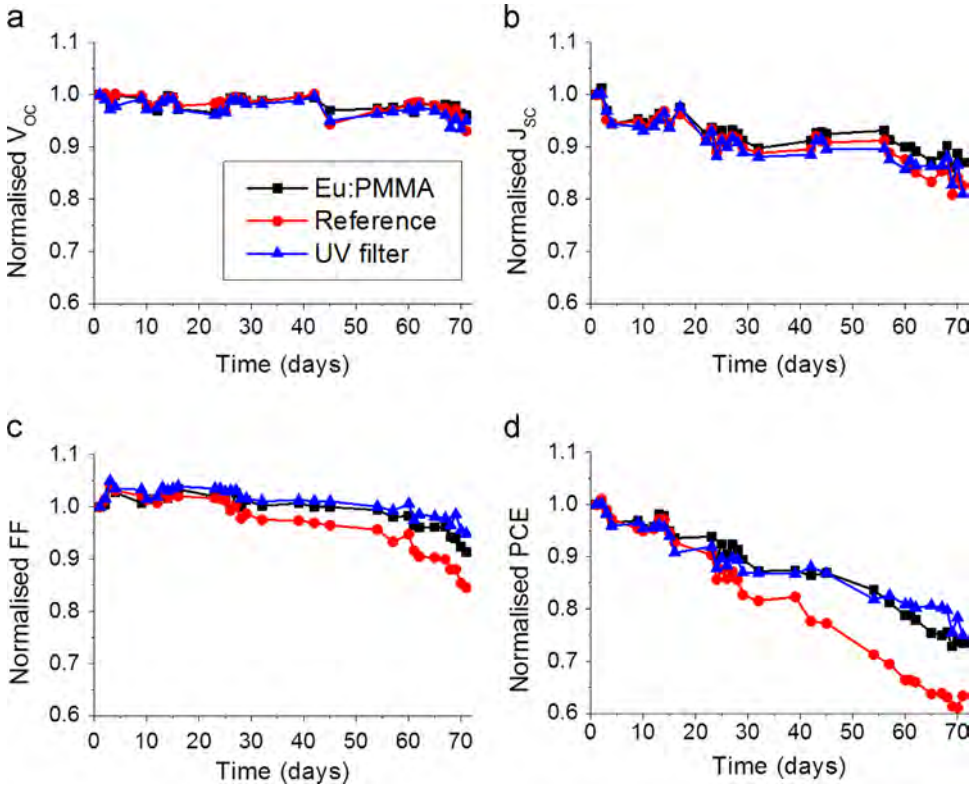

Fig. 7. Evolution of principle photovoltaic parameters ((a) V_{oc}, (b) I_{sc}, (c) FF and (d) PCE) of the representative module over a 70 day period of outdoor solar exposure in the Negev desert for the i) control modules and ii) those with a commercial UV filter and iii) the Eu:PMMA LDS filter. Performance parameters were averaged across data from three modules.

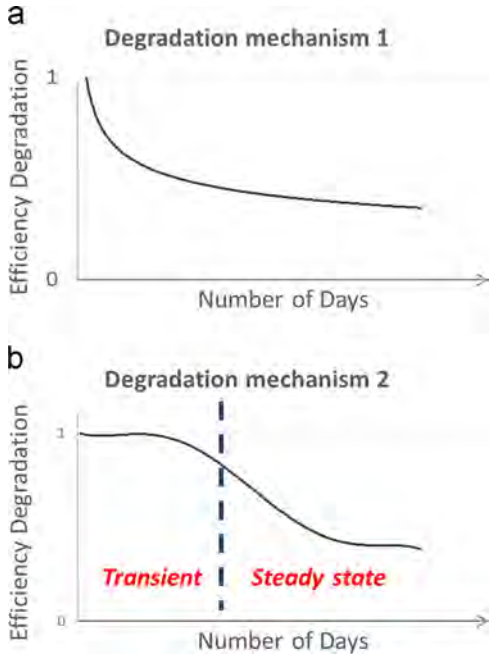

Fig. 8. Degradation kinetics for non-encapsulated (a) and encapsulated OPV modules (b).

enhancement in the half-life ($T_{50\%}$) were observed using indoor light testing protocols, indicating improvement in both performance and lifetime. Encapsulated modules based on 16-cell R2R-coated OPVs with the LDS layer were also tested under indoor test conditions and showed a 6.5% relative enhancement in photocurrent, when compared to a control device. More significantly, modules prepared with a commercial UV filters showed a substantial decrease in photocurrent (-17.5%), indicating that LDS layers could be used as alternative UV filters without compromise to device efficiency. The OPV modules were tested for outdoor stability over a 70 day period in the Negev desert, Israel and the modules made with the LDS filter are shown to match the performance of those using the commercial UV filter and outperform the modules with no filter applied. The work indicates that the LDS layer can act as a UV filter for substantial improvement of the OPV operational stability, without a loss in photocurrent as witnessed with the commercial filter.

Acknowledgements

JK and EK would like to acknowledge the support of the European Commission's StableNextSol COST Action MP1307. JK would like to thank Sêr Cymru national research network in Advanced Engineering and Materials. In addition, JK and DG would like to thank the Wales Ireland Network for Innovative Photovoltaic Technologies (WIN-IPT) project, funded through Interreg IVA. Dr Ziqian Ding is thanked for the device fabrication and experimental testing.

Appendix A. Supplementary material

Supplementary data associated with this article can be found in the online version at http://dx.doi.org/10.1016/j.solmat.2015.09.037.

References

[1] C.C. Chen, W.-H. Chang, K. Yoshimura, K. Ohya, J. You, J. Gao, Z. Hong, Y. Yang, Adv. Mater. 26 (32) (2014) 5670–5677.
[2] H. Cao, W. He, Y. Mao, X. Lin, K. Ishikawa, J.H. Dickerson, W.P. Hess, J. Power Sources 264 (2014) 168–183.
[3] N. Grossiord, J.M. Kroon, R. Andriessen, P.W.M. Blom, Org. Electron. 13 (3) (2012) 432–456.
[4] J. Abad, N. Espinosa, R. García-Valverde, J. Colchero, A. Urbina, Sol. Energy Mater. Sol. Cells 95 (5) (2011) 1326–1332.
[5] M.O. Reese, A.M. Nardes, B.L. Rupert, R.E. Larsen, D.C. Olson, M.T. Lloyd, S. E. Shaheen, D.S. Ginley, G. Rumbles, N. Kopidakis, Adv. Func. Mater. 20 (20) (2010) 3476–3483.
[6] M.S. Ryu, H. Cha, J. Jang, Sol. Energy Mater. Sol. Cells 94 (2) (2010) 152–156.
[7] D. Alonso-Alvarez, E. Klampaftis, D. Ross, B.S. Richards, IEEE J. Photovolt. 4 (6) (2014) 1532–1537.
[8] S.D. Hodgson, S. Jones, P.J. Holliman, S.L. Rugen-Hankey, V. Barrioz, S.J. C. Irvinem, Mater. Lett. 130 (2014) 120–122.
[9] M. Zahedifar, Z. Chamanzadeh, S.M. Hosseinpoor Mashkani, J. Lumin. 135 (2013) 66–73.
[10] W. Xu, H. Song, D. Yan, H. Zhu, Y. Wang, S. Xu, X. Bai, B. Dong, Y. Liu, J. Mater. Chem. 21 (33) (2011) 12331–12336.
[11] M. Prosa, A. Sagnella, T. Posati, M. Tessarolo, M. Bolognesi, S. Cavallini, S. Toffanin, et al., RSC Adv. 84 (2014) 44815–44822.
[12] L.H. Slooff, R. Kinderman, A.R. Burgers, N.J. Bakker, J.A.M. Van Roosmalen, A. Büchtemann, R. Danz, M. Schleusener, J. Sol. Energy Eng. 129 (3) (2007) 272–276.
[13] S. Engmann, M. Machalett, V. Turkovic, R. Rösch, E. Rädlein, G. Gobsch, H. Hoppe, J. Appl. Phys. 112 (3) (2012) 034517.
[14] M.O. Reese, S.A. Gevorgyan, et al., Sol. Energy Mater. Sol. Cells 95 (2011) 1253.
[15] F.C. Krebs, M. Hösel, M. Corazza, B. Roth, M.V. Madsen, S.A. Gevorgyan, R. R. Søndergaard, D. Karg, M. Jørgensen, Energy Technol. 1 (7) (2013) 378–381.
[16] G.A. dos Reis Benatto, B. Roth, M.V. Madsen, M. Hösel, R.R. Søndergaard, M. Jørgensen, F.C. Krebs, Adv. Energy Mater. 4 (15) (2014) 1400732.
[17] A. Manor, E.A. Katz, T. Tromholt, F.C. Krebs, Adv. Energy Mater. 1 (5) (2011) 836–843.
[18] O. Hasan, A.F.M. Arif, Sol. Energy Mater. Sol. Cells 122 (2014) 75–87.
[19] E.A. Katz, S. Gevorgyan, M.S. Orynbayev, F.C. Krebs, Eur. Phys. J. Appl. Phys. 36 (03) (2006) 307–311.
[20] A. O'Riordan, E. O'Connor, S. Moynihan, X. Llinares, R. Van Deun, P. Fias, P. Nockemann, K. Binnemans, G. Redmond, Thin Solid Films 491 (1) (2005) 264–269.
[21] C.H. Peters, T. Sachs-Quintana, J.P. Kastrop, S. Beaupré, M. Leclerc, M. D. McGehee, Adv. Energy Mater. 1 (4) (2011) 491–494.
[22] H. Waters, N. Bristow, O. Moudam, S. Chang, C. Su, W. Wu, U. Jeng, M. Horie, J. Kettle, Org. Electron. 15 (10) (2014) 2433–2438.
[23] H. Hintz, H.-J. Egelhaaf, H. Peisert, T. Chassé, Polym. Degrad. Stab. 95 (5) (2010) 818–825.
[24] N. Bristow, J. Kettle, J. Renew. Sustain. Energy 7 (1) (2015) 013111.
[25] T. Tromholt, E.A. Katz, B. Hirsch, A. Vossier, F.C. Krebs, Appl. Phys. Lett. 96 (2010) 073501.
[26] E.A. Katz, D. Faiman, S.M. Tuladhar, J.M. Kroon, M.M. Wienk, T Fromherz, F Padinger, C.J. Brabec, N.S. Sariciftci, Temperature dependence for the photovoltaic device parameters of polymer-fullerene solar cells under operating conditions, J. Appl. Phys. 90 (2001) 5343–5350.

Nanoscale

PAPER

View Article Online
View Journal | View Issue

Cite this: *Nanoscale*, 2016, **8**, 318

Roll-to-roll printed silver nanowires for increased stability of flexible ITO-free organic solar cell modules

Gisele A. dos Reis Benatto, Bérenger Roth, Michael Corazza, Roar R. Søndergaard, Suren A. Gevorgyan, Mikkel Jørgensen and Frederik C. Krebs*

We report the use of roll-to-roll printed silver nanowire networks as front electrodes for fully roll-to-roll processed flexible indium-tin-oxide (ITO) free OPV modules. We prepared devices with two types of back electrodes, a simple PEDOT:PSS back electrode and a PEDOT:PSS back electrode with a printed silver grid in order to simultaneously explore the influence of the back electrode structure on the operational stability of the modules that did not include any UV-protection. We subjected the devices to stability testing under a number of protocols recommended by the international summit on OPV stability (ISOS). We explored accelerated ISOS-D-2, ISOS-D-3, ISOS-L-2, ISOS-L-3, ISOS-O-1 and ISOS-O-2 testing protocols and compared the performance to previous reports employing the same testing protocols on devices with PEDOT:PSS instead of the silver nanowires in the front electrode. We find significantly increased operational stability across all ISOS testing protocols over the course of the study and conclude that replacement of PEDOT:PSS in the front electrode with silver nanowires increase operational stability by up to 1000%. The duration of the tests were in the range of 140–360 days. The comparison of front and back electrode stability in this study shows that the modules with silver nanowire front electrodes together with a composite back electrode comprising PEDOT:PSS and a silver grid present the best operational stability.

Received 25th October 2015,
Accepted 19th November 2015

DOI: 10.1039/c5nr07426f

www.rsc.org/nanoscale

Introduction

Organic solar cells have been subject to intense studies with the general purpose of increasing the power output and stability in order to push the technology towards commercialization. Most of the research however has been focusing on laboratory scale devices that do not truly reflect the vision of a low cost solution processable technology with high throughput. To develop an economically viable OPV technology it is necessary to tackle a number of issues, such as eliminating the use of indium-tin-oxide (ITO) and developing fast roll-to-roll (R2R) processing methods with little or no loss of material. These issues have received more focus in recent years and several reports of ITO-free organic solar cells have been published with alternative transparent electrodes. Graphene,[1–3] highly conducting PEDOT:PSS,[4–6] highly conducting PEDOT:PSS in combination with silver grids[7–10] and silver nanowires (AgNWs)[11–13] have for example been used as transparent electrode substitutes for ITO demonstrating similar or even better performance in comparison. Comparison of transparent electrodes includes a relationship between the conductivity of the electrode and the transmittance of light in the region of interest for the absorber of the solar cell. AgNW electrodes have in this context demonstrated extremely good conductivity/transmittance relationships which makes them a very interesting candidate for future use. The processability of AgNW by R2R has already been shown[14] and the fact that only very little silver is used in the process could justify the use of silver in the form of nanowires in spite of the relatively low abundance of silver in nature. This would require that the electrode is proven stable – something that could be questioned because of the very large surface-to-volume ratio of the nanowires which could result in faster failure than bulk silver based electrodes due to promotion of degradation mechanisms at the surface. An excellent report published recently by Mayousse *et al.* studied the stability of pristine AgNW without encapsulation over a period of more than 2 years upon stress by elevated temperatures and high humidity, exposure to light, exposure to elevated concentrations of hydrogen sulphide and under electrical stress.[15] The AgNWs were found to be very stable over time when left in ambient atmosphere in the dark and when exposed to high levels of humidity but showed decreasing conductivity over time when exposed to elevated temperatures due to breaking of some of the nanowires. The same

Department of Energy Conversion and Storage, Technical University of Denmark, Frederiksborgvej 399, DK-4000 Roskilde, Denmark. E-mail: frkr@dtu.dk

effect was observed if the nanowires were covered with a thin layer of PEDOT:PSS and stored in the dark in which case some of the nanowires seemed to slowly be etched away by the acidic components of PEDOT:PSS. When exposed to light the electrodes experience an increase in conductivity due to sintering of the nanowire network. The overall conclusion was that although the AgNW electrode in itself is generally very stable, further studies aimed directly at the intended use of the AgNW electrodes are necessary – something that to our knowledge has not yet been performed for organic solar cell modules. Additionally, from the environmental point of view, a printed front electrode comprising a hybrid AgNW/ZnO layer saves 2 printing steps and a substantial amount of energy in the flexible OPV manufacturing.

In this paper we describe a detailed stability study of fully R2R produced ITO-free organic solar cell modules using R2R printed AgNWs as front electrode, considering two different back electrodes (PEDOT:PSS with and without a printed Ag-grid) and investigating the influence on device stability. The modules were tested under ISOS-D-2, ISOS-D-3, ISOS-L-2, ISOS-L-3, ISOS-O-1, and ISOS-O-2 conditions and the results were compared with previously reported stability data for similarly sized modules that did not employ AgNWs. Our results demonstrate an increase in operational stability from a few days up to seasons under accelerated testing for polymer solar cell modules employing AgNWs.

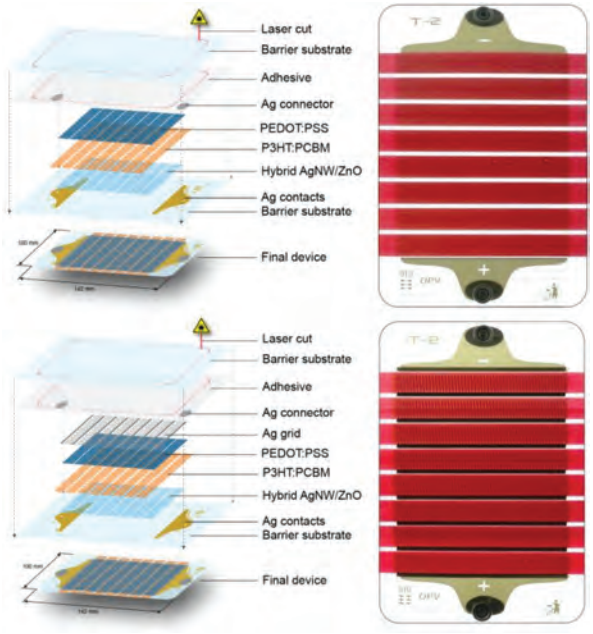

Fig. 1 Top: Architecture of the device with AgNW front electrode and PEDOT:PSS back electrode (left) and picture of the corresponding module (right). Bottom: Architecture of the device with AgNW front electrode and Ag-grid back electrode (left) and picture of the corresponding module (right). The dimensions of the modules are 14 × 10 cm.

Experimental procedures

Module processing

The modules were manufactured using previously described procedures.[9] The front silver contacts were processed by flexo-printing on flexible barrier foil (water vapour transmission rate 4×10^{-2} g m^{-2} day^{-1}, oxygen transmission rate 1×10^{-2} cm^3(STP) m^{-2} day^{-1}) without UV-filter. The previously reported 3 printing steps for the front electrode using a silver nanoparticle based Ag-grid in combination with highly conductive PEDOT:PSS and a nanoparticle ZnO layer was replaced by a rotary screen printed hybrid AgNW/ZnO electrode that was printed in a single printing step. The active layer of P3HT:PCBM was slot-die coated. Two types of modules were tested which differed only in the nature of the back electrode (Fig. 1). The modules with PEDOT:PSS/Ag-grid back electrode had the PEDOT:PSS as hole extraction layer and the Ag-grid as the back electrode, while the PEDOT:PSS back electrode modules do not have the printed Ag-grid. This means that one printing step and silver is saved in the latter case. The two device types had identical PEDOT:PSS thickness and were processed in the same manufacturing run where half of the modules were subjected to a final printing step where the silver grid/busbars were printed using rotary screen printing.

Measurements

2 to 5 modules of each of the two geometries were used per ISOS test. The exact number for each test was mainly dependent on the space availability in the test setups for each test described in Table 1 and the number of available test channels. All the tests, including accurate *IV*-testing under calibrated light sources and outdoor measurement, were performed in the Characterization Laboratory for Organic Photovoltaics (CLOP) at the Department of Energy Conversion and Storage, DTU, Roskilde, Denmark. The outdoor experiments started on July 11th 2014 which is mid-summer in Denmark. For ISOS-D-2 the samples were kept in an oven at 65 °C; for ISOS-D-3 the samples were placed in a damp heat chamber (from Thermotron) set at 85% relative humidity (RH) and 65 °C air temperature. For ISOS-L-3 a xenon lamp based weathering chamber (from Q-Lab) was set to 65 °C air temperature, 85 °C device temperature (black panel), 50% RH and illumination of around 0.7 Sun. In ISOS-L-2 the experiment was carried out in the ambient at 65 °C under a solar simulator while in ISOS-O-1 and ISOS-O-2 the samples were left outside on a solar tracker. For both ISOS-L-2 and ISOS-O-2 the *IV*-curve tracing of the samples was performed using an automated acquisition setup with a Keithley 2400 SMU. In the other tests the samples were periodically removed from the ageing setup and tested under a calibrated solar simulator with AM1.5G spectrum and 1000 W m^{-2} of illumination. The recorded *IV*-curves were used to construct the degradation curves as recommended in the ISOS protocols.[16] A Microsoft excel based macro was used for raw data processing and analysis.[17] Images of the samples were taken using non-destructive light beam induced current (LBIC)[18] mapping on a desktop system (from infinityPV ApS) and an optical microscope.

Table 1 List of the main parameters used in the different ISOS protocols

	ISOS-D-2	ISOS-D-3	ISOS-L-2	ISOS-L-3	ISOS-O-1	ISOS-O-2
Light source	None	None	Simulator AM1.5G	Simulator AM1.5G	The sun, outdoor	The sun, outdoor
Temperature	65 °C (oven)	65 °C	65 °C	85 °C	Ambient outdoor	Ambient outdoor
Relative humidity	Ambient (low)	85% (environ. chamber)	Ambient (low)	Controlled (50%)	Ambient outdoor	Ambient outdoor
Characterization light source	Solar simulator	Solar simulator	Solar simulator	Solar simulator	Solar simulator	Sunlight

Results and discussion

Two different types of fully R2R processed solar cell modules with AgNW front electrode were tested in this study with the difference being in the nature of the back electrode. Fig. 1 shows the device architecture as well as a photograph of the devices. P3HT:PCBM was used as the active material and either a PEDOT:PSS layer or a PEDOT:PSS layer combined with a silver grid were used for the back electrode. The active area of the modules was determined by LBIC and was found to be approximately 57 cm^2 for all the tested modules. The modules were all tested according to ISOS-D-2, ISOS-D-3, ISOS-L-2, ISOS-L-3, ISOS-O-1, and ISOS-O-2 protocols. The main parameters of the different protocols are listed in Table 1. Not all the indoor tests were carried out for the same amount of time. Space issues, retrospective acknowledgement of the necessity of additional testing and device performances descending below the threshold where meaningful data could be extracted were the reasons for the differences in time span. Generally, experiments were discontinued once the devices had descended below T_{50} (the time it takes to reach 50% of the initial efficiency) while still presenting rapid decline in performance. Fig. 2, 4 and 9 illustrate the normalized power conversion efficiencies (PCE), open circuit voltage (V_{OC}), short circuit current (I_{SC}), and fill factor (FF) over time for the different tests and Fig. 3, 5 and 10 show the *IV*-curves of the modules before, at the beginning, halfway and close to the end of the tests.

Dark tests

Fig. 2 it is obvious that in dry heat conditions (ISOS-D-2) the samples with Ag-grid back electrode show an increase in the current during the first 80 days of the test, while the samples with PEDOT:PSS exhibit rather stable performance. Nevertheless, when the humidity level is increased (ISOS-D-3), it results in a rapid degradation of all the samples after only a few days.

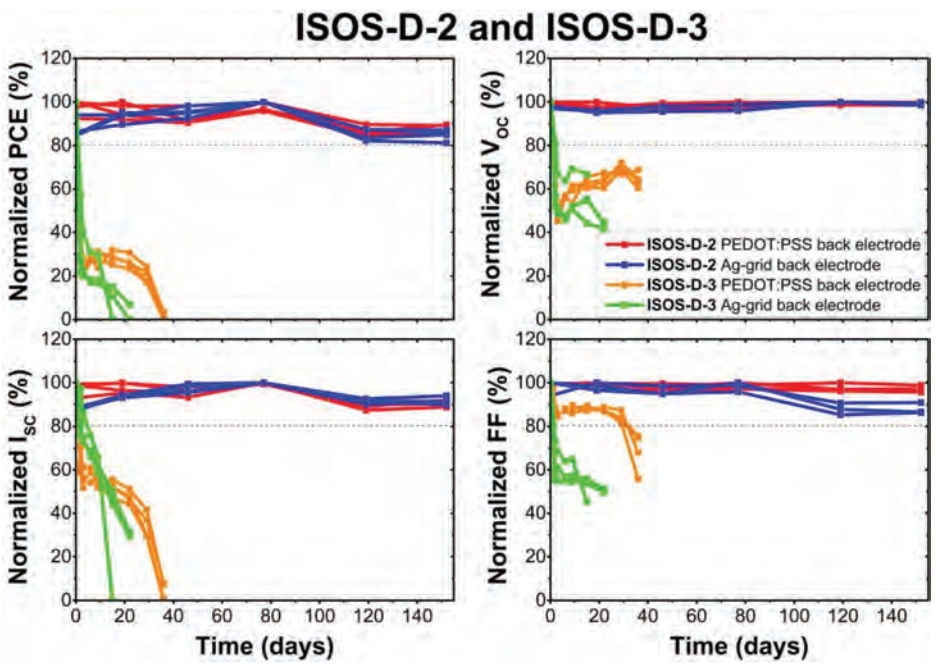

Fig. 2 Dry heat test (ISOS-D-2) and damp heat test (ISOS-D-3) on AgNW front electrode modules. Normalized stability curves of PCE, V_{OC}, I_{SC} and FF of samples with PEDOT:PSS back electrode and samples with Ag-grid back electrode.

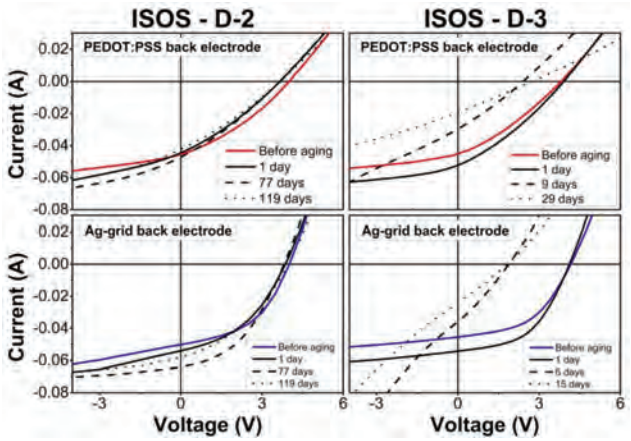

Fig. 3 *IV*-curves of ISOS-D-2 (left) and ISOS-D-3 (right) tests of beginning, halfway and close do the end of the test for AgNW front electrode modules. Sample with PEDOT:PSS back electrode (top) and sample with Ag-grid back electrode (bottom).

The reason is ascribed to the diffusion of humidity through the edges of the module and the channels created at the device terminals (metal snaps), which has been demonstrated earlier for similar modules.[19] In damp heat both kinds of samples experience rapid decay across all the photovoltaic parameters. The *IV*-curve evolution of the samples during these ageing tests is demonstrated in Fig. 3, where for the samples under ISOS-D-2 the PEDOT:PSS back electrode devices present a slight variation of current and decrease in both FF and V_{OC}. The Ag-grid back electrode modules present an increase in performance until the 77th day and later a small decrease of current and fill factor. For the *IV*-curves of the ISOS-D-3 testing all samples exhibit a drastic decrease in the photovoltaic parameters. The PEDOT:PSS back electrode modules present a very slight S-shape after 9 days and for the Ag-grid back electrode it is evident indicating either de-doping of ZnO, water absorption by the PEDOT:PSS and/or further oxidation of the PEDOT:PSS/Ag interface.[19]

Indoor light tests

The tests under illumination further confirm the deteriorating effect of the humidity when comparing the results of the ISOS-L-2 dry test and ISOS-L-3 high humidity test (Fig. 4). In the test with only light and heat (ISOS-L-2) the Ag-grid back electrode samples show an increase in performance during the first 40 days and then start to degrade. This increase also matches the results of improved conductivity of the AgNW layer under light exposure as reported by Mayousse *et al.*[15] that demonstrated sintering of the silver nanowires at the crossing points leading to improved conductivity. Overall, the samples with Ag-grid back electrode show better stability under illumination compared to the PEDOT:PSS based samples. In the light, heat and humidity test (ISOS-L-3), the PEDOT:PSS back electrode samples show a linear decay while the Ag-grid back electrode samples stabilize at significantly lower efficiency after 40 days. The result is somewhat surprising, since such encapsulation was previously shown to result in similar rapid ageing of the samples under both ISOS-L-3 and ISOS-D-3 test conditions or even faster decay for the former.[17,20] This is a possible indication that PEDOT:PSS indeed loses the conduct-

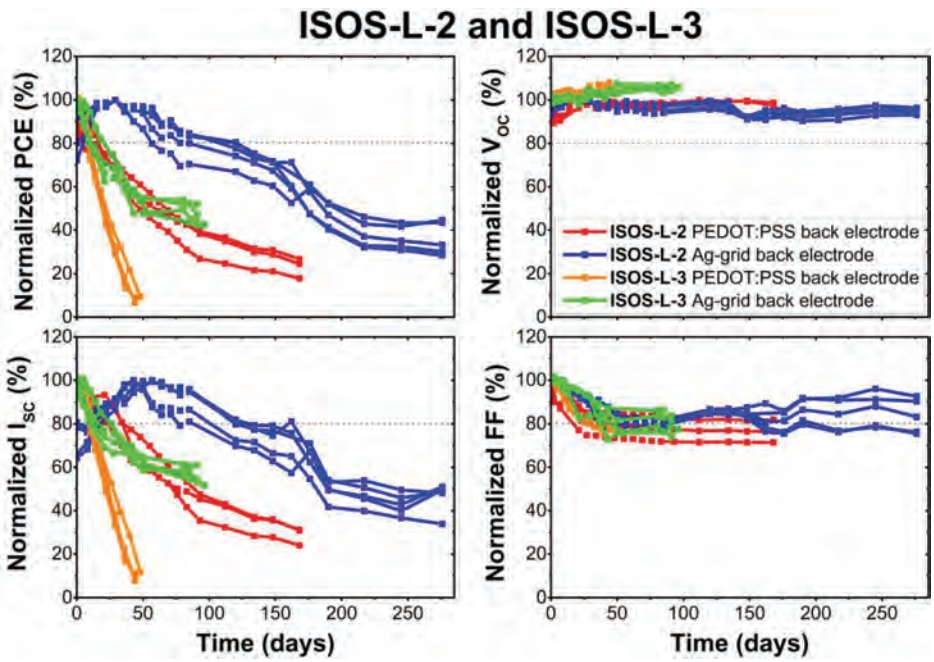

Fig. 4 Light dry heat test (ISOS-L-2) and light damp heat test (ISOS-L-3) on AgNW front electrode modules. Normalized stability curves of PCE, V_{OC}, I_{SC} and FF of samples with PEDOT:PSS back electrode and samples with Ag-grid back electrode.

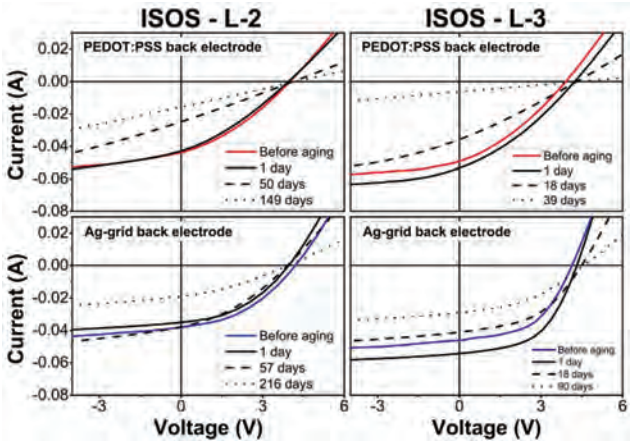

Fig. 5 *IV*-curves of ISOS-L-2 (left) and ISOS-L-3 (right) tests of beginning, halfway and close do the end of the test on AgNW front electrode modules. Sample with PEDOT:PSS back electrode (top) and sample with Ag-grid back electrode (bottom).

ing properties when exposed to high levels of humidity and application of the Ag-grid is believed to compensate for this failure mechanism. The almost linear decrease in the current along with the drop in the fill factor further confirms the reduction of the conductivity of the PEDOT:PSS, which has also been reported in the literature.[21]

In relation to the *IV*-curves (Fig. 5), in the ISOS-L-2 tests we observe a clear decrease in I_{SC} and FF for both types of devices. The rectifying properties of the PEDOT:PSS back electrode samples are fully lost, however they are still present in the Ag-grid back electrode samples. In the ISOS-L-3 test it is also possible to observe an increase in the first day and then the strong decrease of the fill factor and current of the samples with PEDOT:PSS back electrode. The samples with a Ag-grid back electrode also present an increase followed shortly thereafter by a decrease in I_{SC} and FF, but they clearly retain their rectifying properties.

Bubble effect

During the ageing of the samples under illumination large bubble-like defects were gradually formed in the modules with Ag-grid back electrode. In the ISOS-L-2 test, nevertheless these defects were not observed in the first 120 days of testing. The area around the bubbles became inactive resulting in partial decrease of the photocurrent as it was possible to verify with LBIC imaging (see Fig. 6). Formation of bubble-like defects was also observed during the ISOS-L-3 test, again only in the samples with Ag-grid back electrodes (Fig. 7). The effect was in this case observed after only 15 days of testing. In Fig. 8 the microscope images of the areas with and without bubbles are compared and we can observe formation of cracks in the active layer and in the AgNW/ZnO layer in the vicinity of the areas where the bubbles formed. The cracks seem to emanate from the printed Ag-busbar. The back Ag-grid is the thickest printed layer in the OPV stack and it is highly porous with the Ag solid

Fig. 6 Samples with AgNW front electrode and Ag-grid back electrode under ISOS-L-2 for 240 days (left). One of these samples (centre) and its corresponding LBIC image (right).

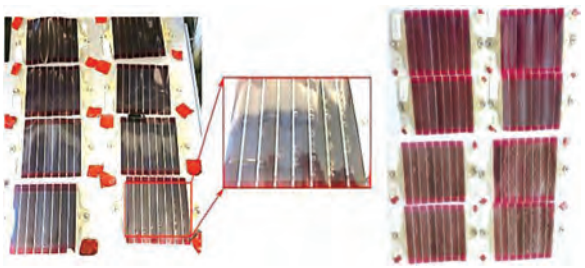

Fig. 7 Samples under ISOS-L-3 test with AgNW front electrode. Left: Samples after 2 weeks. Centre: Detail of the sample at the right bottom corner of the picture in the left. Right: Samples after finishing the test. Four samples on top are with PEDOT:PSS back electrode (no bubbles formed) and the four samples in the bottom with Ag-grid back electrode (extensive bubble formation).

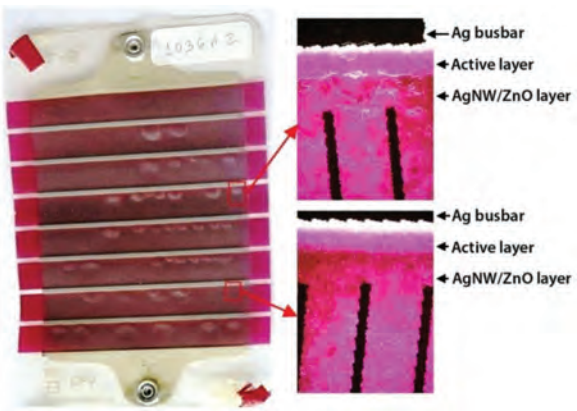

Fig. 8 Microscope images of a sample with AgNW front electrode and Ag-grid back electrode under ISOS-L-3 of a region with (right top) and without (right bottom) a bubble defect.

content corresponding to just 60% of the grid volume.[22] Solvents and/or gas trapped in the porosity of the printed Ag-grid could feasibly be the root cause of the bubble formation due to expansion/contraction of gasses in response to cyclic vari-

ation in temperature. However, further investigation is necessary to confirm the true nature of the effect. Even with such defects, the Ag-grid back electrode samples must be categorized as exhibiting stable behaviour until the end of the light tests although a catastrophic failure may be expected. Also, in the event that the bubble formation and subsequent delamination could be avoided, the performance over time would be much better as the decrease in short circuit current is mostly a result of active area loss due to delamination.

Outdoor tests

Fig. 9 shows the outdoor tests which were carried out for the entire duration of this study starting on July 11th 2014. The samples for ISOS-O-1 and ISOS-O-2 tests were placed on the same solar tracking platform. While the ISOS-O-1 samples were regularly dismounted from the platform to be measured indoors under a solar simulator and then remounted, the ISOS-O-2 samples stayed fixed on the platform connected to an automated acquisition setup. Results from these two tests are in good agreement with each other when taking all the factors that can affect the device performances into account (temperature, humidity, weather conditions, external contacts oxidation, *etc.*). For the ISOS-O-2 experiment the PCE and I_{SC} data were first normalized to 1000 W m^{-2} since the solar cells are measured under sunlight.

Most of the samples subjected to the outdoor tests start to show degradation after around 150 days of testing. For the Ag-grid back electrode samples under ISOS-O-1 the degradation seems to be evident even later after around 220 days. However these samples degrade severely after that, with a drop in both I_{SC} and V_{OC}, and in the end of the test they seem to stabilise at a level underperforming the PEDOT:PSS back electrode samples and the samples under the ISOS-O-2 test.

For the PEDOT:PSS back electrode modules a slight decrease in I_{SC}, V_{OC} and FF is observed with none of the parameters being especially dominant for ISOS-O-1 but evidently being the main cause of decrease in current for the ISOS-O-2 tests.

Fig. 10 show the PEDOT:PSS back electrode modules losing their rectifying properties, while the Ag-grid back electrode modules still preserve them as observed in the ISOS-L-3 test.

Although the fluctuating curves do not allow making clear comparison, one obvious difference among the samples stands out in the ageing curves: the fill factor ageing is surprisingly faster for the Ag-grid back electrode devices. However, when looking at the *IV*-curves, it is obvious that the fill factor of the PEDOT:PSS based devices is already lower from the very start and thus the comparison is somewhat biased.

The complete ISOS-O-2 measurement can be seen in Fig. 11. The four samples show an increase in PCE during the first 20 days and a decrease during the autumn and winter time, which is due to the ageing, but also gradually decreasing irradiance and temperature.

When the frequency of sunny days and irradiance intensities increase at the beginning of the spring, there is a tendency for a further increase in PCE with illumination and temperature. However PCE decreases again after a short period of low irradiance (around day 260) with the final values at around 0.4% PCE for PEDOT:PSS back electrode and 0.5% PCE for Ag-grid back electrode devices.

Taking into consideration that many degradation mechanisms are linked to humidity, the AgNW modules demonstrate

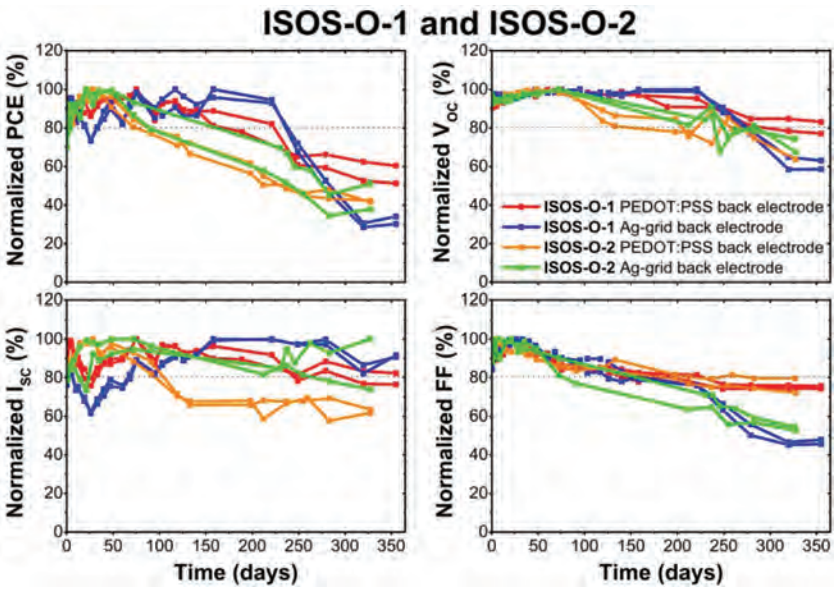

Fig. 9 Outdoor test (ISOS-O-1) and outdoor measured under sunlight test (ISOS-O-2) on AgNW front electrode modules. Normalized stability curves of PCE, V_{OC}, I_{SC} and FF of samples with PEDOT:PSS back electrode and samples with Ag-grid back electrode. Stability data measured under sunlight had PCE and I_{SC} normalized to 1 Sun (1000 W m^{-2}).

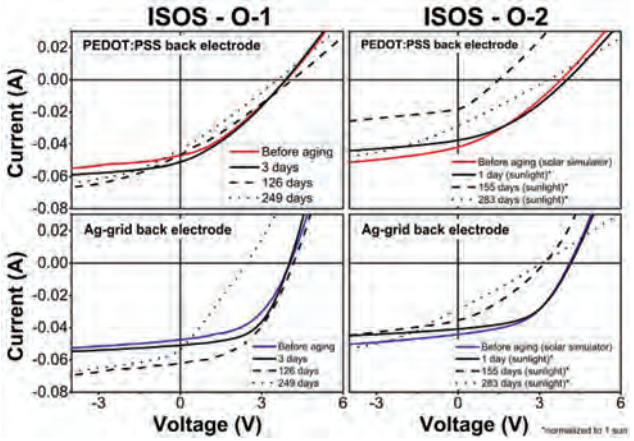

Fig. 10 *IV*-curves of ISOS-O-1 (left) and ISOS-O-2 (right) tests of beginning, halfway and close do the end of the test on AgNW front electrode modules. Sample with PEDOT:PSS back electrode (top) and sample with Ag-grid back electrode (bottom). *IV*-curves measured under sunlight had PCE and I_{SC} normalized to 1 Sun (1000 W m^{-2}).

considerable stability during one year of outdoor exposure. Since it is attributed to water diffusion through edges and electrodes with metal snaps, larger edges and new options for the contacts in these samples would make the devices last considerably longer.[19,23]

Comparison of devices with different front and back electrodes

The following paragraph compares the samples presented in this work with the previously reported stability of freeOPV modules.[17] These modules have the layer stack Ag-grid/PEDOT:PSS/ZnO/P3HT:PCBM/PEDOT:PSS/Ag-grid, therefore differing from the Ag-grid back electrode devices presented here only by the front electrode (no AgNW). The time that the device reaches 80% of its initial efficiency (T_{80}) gives very practical information for future application and highlights where developments are needed. Typical OPV devices often experience initial rapid ageing (burn in) followed by a more stabilized phase, however in the tests performed in this work many of the stability curves show no clear stabilization phase. We therefore considered the time it takes for the device to reach 50% of its initial efficiency (T_{50}) for better comparison. For the comparative presentation a diagram with logarithmic scale called the "o-diagram" with "o" referring to OPV is used (Fig. 12).[24] The time scale is chosen to be Log_4 (days) for the *X*-axis in order to associate the *X*-axis with the common time units shown in the upper part of the diagram. E_0 and E_{50} values are represented by the *Y*-axis. Combined in the o-diagram are the T_{80} (filled markers) and T_{50} (open markers) values *versus* the initial PCE (E_0) and 50% of initial PCE (E_{50}) respectively for the devices measured in this work and for the previously reported free OPV modules (no AgNW).

Under ISOS-D-2 test conditions, all samples are very stable and tend to last for years. For ISOS-D-3, similarly low T_{80} and T_{50} are obtained for all the devices, since the modules have identical packaging and thus experience the same edge diffusion failure mechanisms. ISOS-L-2 presents a remarkable increase in T_{80} for the AgNW devices, from one day (Ag-grid front and back electrode sample) to weeks for the PEDOT:PSS back electrode devices and to months for the Ag-grid back electrode devices with the best performing devices taking seasons to reach T_{80}. T_{50} also takes proportionally longer to be reached. For ISOS-L-3 a very important stability increase for the AgNW devices is also registered and even with the sensitivity of the whole device to humidity, the Ag-grid back electrode devices remain stable until the end of the test, although a catastrophic failure was expected due to the formation of bubbles previously mentioned. ISOS-O-1 show a much longer T_{80} from weeks for the front and back Ag-grid modules to seasons for the AgNW based devices. The modules with a PEDOT:PSS back electrode are generally less stable than the devices with Ag-grid, except in ISOS-O-1 although the variations between

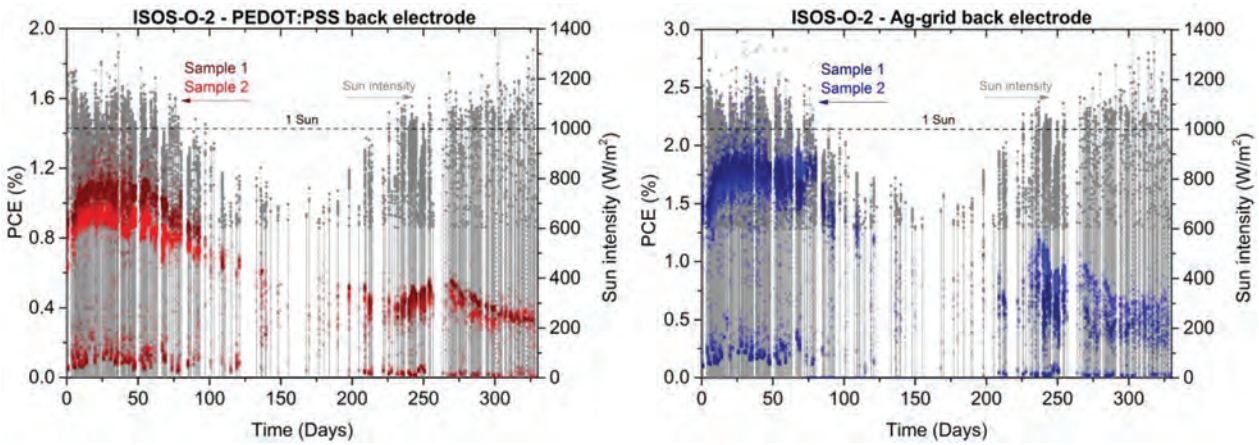

Fig. 11 ISOS-O-2 complete stability curves of two samples with PEDOT:PSS back electrode (left) and Ag-grid back electrode (right), all with AgNW front electrode. Sun intensity lower than 600 W m^{-2} were disregarded in order to consider the day light measurements only.

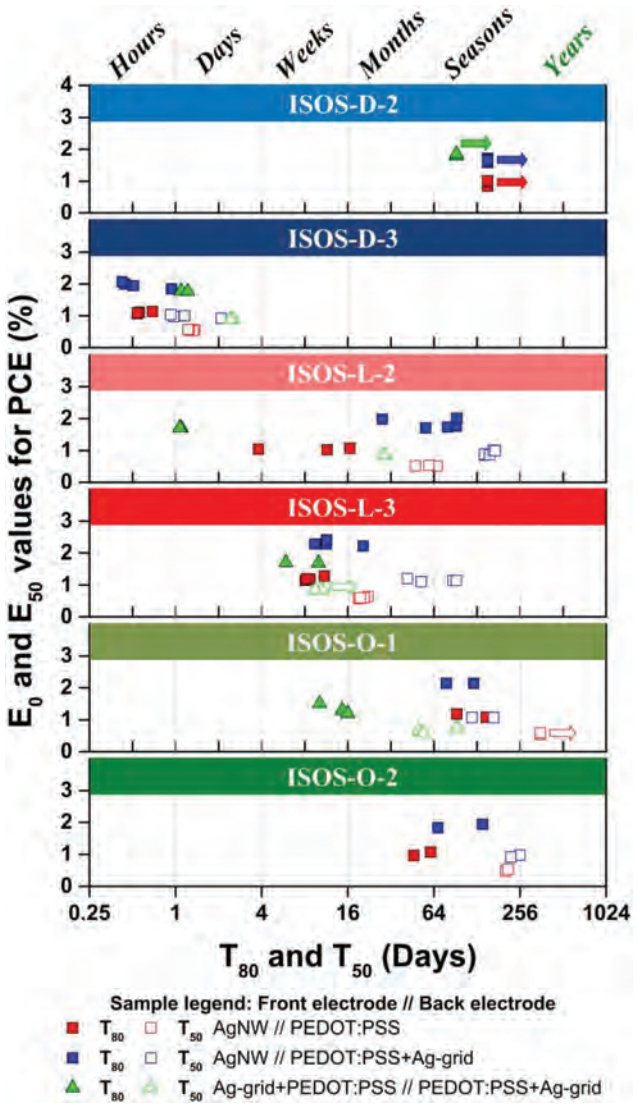

Fig. 12 The o-diagram presents the T_{80} (filled markers) and T_{50} (open markers) values of OPV modules with (square markers) and without (triangle markers) AgNW as the front electrode under different ISOS test conditions referred in Table 1.

ISOS-O-1 and ISOS-O-2 indicate that the T_{80} and T_{50} of both AgNW based modules are in the range of variation of outdoor tests.

As mentioned before, the degradation mechanisms leading to the loss of the rectifying properties of the OPV is linked to both oxygen and water that affects the conductivity of the ZnO and PEDOT:PSS layers leading to further oxidation of the Ag-grid. The characteristic S-shape of the *IV*-curve indicating these mechanisms is only observed in the ISOS-D-3 test during the stability study of the AgNW based devices, possibly representing the minimization of these mechanisms with the use of the AgNW/ZnO hybrid layer as front electrode instead of a ZnO layer as well as the use of PEDOT:PSS only in the back electrode. Even though the AgNW based devices are still sensitive to humidity due to the contacts and short edge seal, the increase in T_{80} and T_{50} in the light and outdoor tests in comparison to modules with Ag-grid front and back electrodes present a substantial development in stability for large scale R2R produced OPV using AgNWs as the front electrode.

Conclusions

In the course of the stability tests and considering the overview provided by the o-diagram, we observed the following points:

(a) The stability curves and T_{80} and T_{50} parameters of ISOS-L-2 test for the samples with AgNW front electrode and Ag-grid back electrode indicate that the AgNW have a positive influence on the performance and stability of devices due to the sintering of the nanowire network under light exposure which corroborates the work of Mayousse *et al.*;

(b) Bubble formation in the samples with Ag-grid back electrode was observed and its cause associated to solvents and/or gas trapped in the porous volume of the printed Ag-grid that expands with exposure to light and high temperature cycling.

(c) The better performance and stability of the Ag-grid back electrode samples points to the importance of the Ag-grid in conjunction with PEDOT:PSS to maintain a high back electrode conductivity in the devices;

(d) Modules with AgNWs as the front electrode demonstrate an improved stability under ISOS-L-2, ISOS-L-3 and ISOS-O-1 conditions possibly due to the use of hygroscopic PEDOT:PSS in only one of the OPV electrodes and the printing of the ZnO in a hybrid layer together with the AgNW.

The use of AgNW as the front electrode in OPV saves 2 printing steps making the manufacture of the devices faster and more environmentally friendly and such improvements in the stability of the OPV devices bring them closer to commercialization. Further improvements are expected to be achievable by increasing the edge sealing and also by employing a UV-protective filter on the front face of the modules. Finally, development of new and less porous back electrode structures that avoid the bubble formation may provide OPV devices with longer lifetimes.

Acknowledgements

The authors would like to acknowledge Dechan Angmo for help during writing of this paper. This work has been supported by the Danish Ministry of Science, Innovation and Higher Education under a Sapere Aude Top Scientist grant (no. DFF – 1335-00037A).

References

1 W. S. Koh, C. H. Gan, W. K. Phua, Y. A. Akimov and P. Bai, *J. Sel. Top. Quantum Electron.*, 2014, **20**, 1.
2 Z. C. Gomez, L. De Arco, Y. Zhang, C. W. Schlenker, K. Ryu and M. E. Thompson, *ACS Nano*, 2010, **4**, 2865.

3 K. Kim, S. H. Bae, C. T. Toh, H. Kim, J. H. Cho, D. Whang, T. W. Lee, B. Özyilmaz and J. H. Ahn, *ACS Appl. Mater. Interfaces*, 2014, **6**, 3299.
4 Y. Zhou, F. Zhang, K. Tvingstedt, S. Barrau, F. Li, W. Tian and O. Inganäs, *Appl. Phys. Lett.*, 2008, **92**, 1.
5 S. I. Na, S. S. Kim, J. Jo and D. Y. Kim, *Adv. Mater.*, 2008, **20**, 4061.
6 M. Kaltenbrunner, M. S. White, E. D. Głowacki, T. Sekitani, T. Someya, N. S. Sariciftci and S. Bauer, *Nat. Commun.*, 2012, **3**, 770.
7 D. Angmo, T. T. Larsen-Olsen, M. Jørgensen, R. R. Søndergaard and F. C. Krebs, *Adv. Energy Mater.*, 2013, **3**, 172.
8 F. C. Krebs, N. Espinosa, M. Hösel, R. R. Søndergaard and M. Jørgensen, *Adv. Mater.*, 2014, **26**, 29.
9 M. Hösel, R. R. Søndergaard, M. Jørgensen and F. C. Krebs, *Energy Technol.*, 2013, **1**, 102.
10 J.-S. Yu, I. Kim, J.-S. Kim, J. Jo, T. T. Larsen-Olsen, R. R. Søndergaard, M. Hösel, D. Angmo, M. Jørgensen and F. C. Krebs, *Nanoscale*, 2012, **4**, 6032.
11 S. Nam, M. Song, D.-H. Kim, B. Cho, H. M. Lee, J.-D. Kwon, S.-G. Park, K.-S. Nam, Y. Jeong, S.-H. Kwon, Y. C. Park, S.-H. Jin, J.-W. Kang, S. Jo and C. S. Kim, *Sci. Rep.*, 2014, **4**, 4788.
12 W. Gaynor, S. Hofmann, M. G. Christoforo, C. Sachse, S. Mehra, A. Salleo, M. D. McGehee, M. C. Gather, B. Lüssem, L. Müller-Meskamp, P. Peumans and K. Leo, *Adv. Mater.*, 2013, **25**, 4006.
13 J. H. Yim, S. Y. Joe, C. Pang, K. M. Lee, H. Jeong, J. Y. Park, Y. H. Ahn, J. C. De Mello and S. Lee, *ACS Nano*, 2014, **8**, 2857.
14 M. Hösel, D. Angmo, R. R. Søndergaard, G. A. dos Reis Benatto, J. E. Carlé, M. Jørgensen and F. C. Krebs, *Adv. Sci.*, 2014, 1.
15 C. Mayousse, C. Celle, A. Fraczkiewicz and J. Simonato, *Nanoscale*, 2015, 2107.
16 M. O. Reese, S. A. Gevorgyan, M. Jørgensen, E. Bundgaard, S. R. Kurtz, D. S. Ginley, D. C. Olson, M. T. Lloyd, P. Morvillo, E. a. Katz, A. Elschner, O. Haillant, T. R. Currier, V. Shrotriya, M. Hermenau, M. Riede, K. R. Kirov, G. Trimmel, T. Rath, O. Inganäs, F. Zhang, M. Andersson, K. Tvingstedt, M. Lira-Cantu, D. Laird, C. McGuiness, S. Gowrisanker, M. Pannone, M. Xiao, J. Hauch, R. Steim, D. M. DeLongchamp, R. Rösch, H. Hoppe, N. Espinosa, A. Urbina, G. Yaman-Uzunoglu, J.-B. Bonekamp, A. J. J. M. van Breemen, C. Girotto, E. Voroshazi and F. C. Krebs, *Sol. Energy Mater. Sol. Cells*, 2011, **95**, 1253.
17 M. Corazza, F. C. Krebs and S. A. Gevorgyan, *Sol. Energy Mater. Sol. Cells*, 2014, **130**, 99.
18 F. C. Krebs and M. Jørgensen, *Adv. Opt. Mater.*, 2014, **2**, 465.
19 S. A. Gevorgyan, M. V. Madsen, H. F. Dam, M. Jørgensen, C. J. Fell, K. F. Anderson, B. C. Duck, A. Mescheloff, E. a. Katz, A. Elschner, R. Roesch, H. Hoppe, M. Hermenau, M. Riede and F. C. Krebs, *Sol. Energy Mater. Sol. Cells*, 2013, **116**, 187.
20 F. Yan, J. Noble, J. Peltola, S. Wicks and S. Balasubramanian, *Sol. Energy Mater. Sol. Cells*, 2012, **114**, 214.
21 J. Liu, M. Agarwal, K. Varahramyan, E. S. Berney IV and W. D. Hodo, *Sensors Actuators, B*, 2008, **129**, 599.
22 H. F. Dam, T. R. Andersen, E. B. L. Pedersen, K. T. S. Thydén, M. Helgesen, J. E. Carlé, P. S. Jørgensen, J. Reinhardt, R. R. Søndergaard, M. Jørgensen, E. Bundgaard, F. C. Krebs and J. W. Andreasen, *Adv. Energy Mater.*, 2015, **5**, 1400736.
23 D. Angmo and F. C. Krebs, *Energy Technol.*, 2015, **3**, 774.
24 S. A. Gevorgyan, M. Corazza, M. V. Madsen, G. Bardizza, A. Pozza, H. Müllejans, J. C. Blakesley, G. F. a. Dibb, F. a. Castro, J. F. Trigo, C. M. Guillén, J. R. Herrero, P. Morvillo, M. G. Maglione, C. Minarini, F. Roca, S. Cros, C. Seraine, C. H. Law, P. S. Tuladhar, J. R. Durrant and F. C. Krebs, *Polym. Degrad. Stab.*, 2014, **109**, 162.

Making Ends Meet: Flow Synthesis as the Answer to Reproducible High-Performance Conjugated Polymers on the Scale that Roll-to-Roll Processing Demands

*Martin Helgesen, Jon E. Carlé, Gisele A. dos Reis Benatto, Roar R. Søndergaard, Mikkel Jørgensen, Eva Bundgaard, and Frederik C. Krebs**

Continuous flow methods are employed for the controlled polymerization of the roll-to-roll (R2R) compatible polymer PBDTTTz-4 including optimization and upscaling experiments. The polymerization rate and materials' quality can be increased significantly with the continuous flow method where reaction times down to 10 min afforded PBDTTTz-4 with high molecular weight and a constant quality. The flow method enables full control of the molecular weight via tuning of the flow speed, catalyst loading, and temperature and avoids variation in materials' quality associated with conventional batch synthesis. Upscaling from 300 mg batch synthesis to 10 g flow synthesis affords PBDTTTz-4 with a production rate of up to 120 g day^{-1} for a very simple in-house build flow reactor. An average power conversion efficiency (PCE) of 3.5% is achieved on a small scale (1 cm^2) and an average PCE of 3.3% is achieved on a large scale (29 cm^2). This shows that small device efficiencies can be scaled when using full R2R processing of flexible and encapsulated carbon-based modules without the use of vacuum, indium-tin-oxide, or silver, with the best achieving a PCE of 3.8% PCE.

1. Introduction

Organic photovoltaics (OPVs) are envisioned as a potential low cost and flexible alternative to the inorganic photovoltaics that today are mainly based on Silicon. In order for OPVs to fulfill this vision, large area and high throughput fabrication needs to be realized in order to keep the production cost to a minimum. This can be achieved by applying roll-to-roll (R2R) processing of solution based materials on flexible carriers such as polyethylene terephthalate (PET) or a barrier foil that possess the ability to protect the devices from exposure to oxygen, water and UV-light. But so far only a few examples of large scale fully R2R processed OPVs have been published.[1] The performance of these devices is in the range of 1%–2.5% which is somewhat far from the more than 10% reported for small scale laboratory devices.[2] One of the reasons behind this discrepancy is that the large scale fabrications, reported so far, almost only rely on poly(3-hexylthiophene) (P3HT) and [6,6]-phenyl-C_{61}-butyric acid methyl ester (PCBM) as the active layer. Both, P3HT and PCBM, are commercially available in kilogram quantities needed for R2R manufacture, and it is generally accepted that this system gives efficiencies of 4%–5% under optimized conditions which is somewhat closer to the PCE obtained when applied in large scale.[3] In contrast, the highly efficient small laboratory devices rely on extremely engineered, complex and costly materials, which are not normally available in the quantities needed in order to perform large scale processing experiments.[4] Active layer materials are needed on 1–10 g scale in order to allow for the fabrication of an entire set of large scale modules by R2R processing and on the 10–100 g scale initially when optimizing the processing conditions. Therefore, to increase the general performance of large scale R2R processed OPVs it is necessary to develop polymers and polymerization methods that allows for large scale production of high efficiency materials at a relatively low cost.

While it is possible to produce large quantities of materials using traditional batch synthesis, problems such as variability from synthesis to synthesis leads to batch-to-batch variations in the molecular weight distribution which is a very influential parameter for most polymer systems in terms of delivering uniform high efficiency OPVs. Batch-to-batch variations are especially a challenge when scaling up polymerizations, as a result of mass and heat-transfer issues, which most often makes it difficult to reproduce the degree of polymerization just by copying reaction conditions from a small scale (subgram level) polymerization reaction to a large scale (multigram level) polymerization reaction.[5,6] This can lead to deterioration in materials' quality leading to differences in the physical and chemical characteristics and thus the film forming quality.

As an alternative to traditional batch chemistry, continuous flow methods are often applied in the industry, where large quantities of materials has to be produced, because the technique offers several advantages, i.e., safe handling of reactive

Dr. M. Helgesen, Dr. J. E. Carlé, G. A. dos Reis Benatto, Dr. R. R. Søndergaard, Dr. M. Jørgensen, Dr. E. Bundgaard, Prof. F. C. Krebs
Department of Energy Conversion and Storage
Technical University of Denmark
Frederiksborgvej 399, 4000 Roskilde, Denmark
E-mail: frkr@dtu.dk

DOI: 10.1002/aenm.201401996

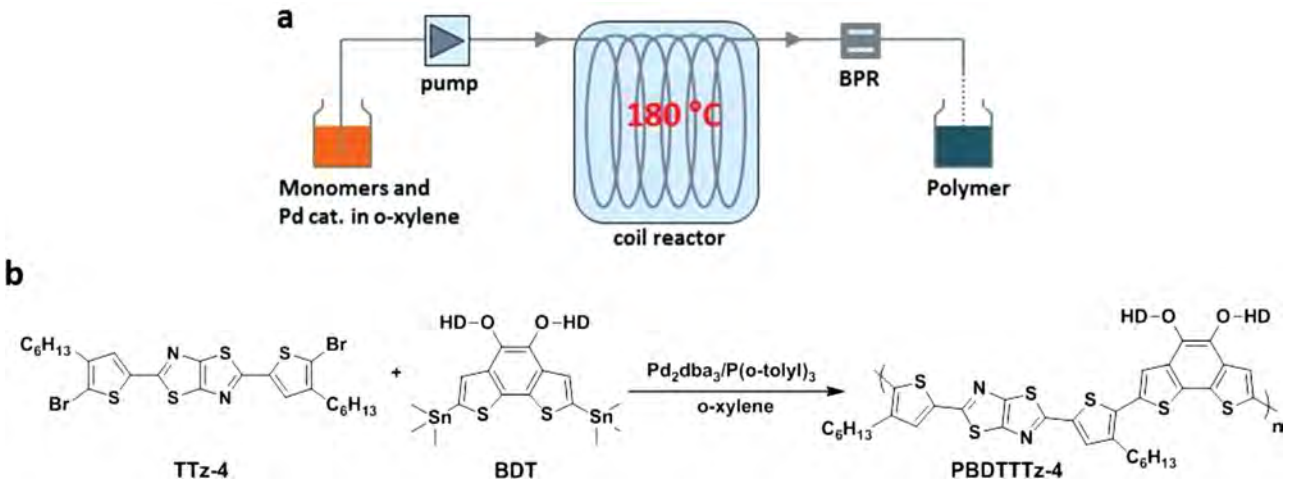

Figure 1. a) Schematic presentation of the flow synthesis setup. BPR: Back pressure regulator. b) Synthesis of the polymer PBDTTTz-4. HD: Hexyldecyl.

intermediates, high reaction reproducibility through accurate parameter control, easy boosting of reaction rates with superior high temperature heating and reagent mixing, fast reaction optimization, and straightforward upscaling of reactions.[5,7] There has been a recent interest in polymer synthesis using continuous flow methods and reports from the literature has illustrated the adaptability and scope of the flow process using among others a commercially available benchtop flow reactor.[8,9] Seyler et al. translated various polymerization reactions (i.e., Stille coupling, Suzuki coupling, and Kumada coupling) to the flow process where equivalent polymer molecular mass distributions were attained in flow reactions compared to batch reactions though with a significant reduction in reaction times. A slightly different approach was applied by Bannock et al. who utilized a droplet-based microfluidic reactor for the flow synthesis of P3HT in large quantities (≈15 g) and with high regioregularity (98%) by Grignard metathesis.[10]

In this work we report the continuous flow synthesis of the conjugated polymer PBDTTTz-4 (see **Figure 1**) including optimization and upscaling experiments in order to investigate the reproducibility of the polymer molecular mass distribution, when going from small to large scale. We started at a scale of 300 mg and went up to 5 g polymer on a commercially available flow chemistry system, whereas further upscaling to 10 g polymer and above was performed on a simple in-house built flow reactor, designed for larger scale polymer synthesis, with the aim of enhancing the synthesis scale tolerance and simplicity of the flow system. Following on from this we validated the upscaling experiments through the preparation of bulk heterojunction (BHJ) OPVs using flow-synthesized PBDTTTz-4 batches in different scales and demonstrated the consistency. Finally the flow synthesized PBDTTTz-4 was applied in a full R2R process of large area, indium-tin-oxide (ITO) and silver free modules demonstrating the potential of flow synthesis as an advantageous approach for upscaling reproducible and high quality polymer material for OPVs. The purpose of our work was to validate flow synthesis in the context of preparing materials for mass production of OPVs and demonstrate a synthetic factory with a materials output (per time) comparable to the consumption of materials on our large scale R2R machine and also demonstrate that the required materials consistency could be achieved.

2. Results and Discussion

In our previous work,[11] PBDTTTz-4 was applied in the preparation of small scale mini roll coated OPV modules and efficiencies of more than 3% were achieved which is comparable to single cell devices prepared in the same roll process. This designates PBDTTTz-4 as a convincing candidate for high-throughput full R2R production of OPV. As mentioned in the Introduction, large quantities of materials are required in order to perform large scale R2R processing experiments. However, to date we have not yet succeeded in upscaling the polymerization of PBDTTTz-4 using conventional batch synthesis (**Figure 2**c). Attempts to scale up from the subgram level to larger quantities polymer using conventional batch synthesis generally resulted in poorly soluble polymer products. The products could be partially dissolved in hot o-dichlorobenzene (ODCB) but precipitated (gelled) upon cooling, also at low concentration, which complicates solution processing and thus its application in a roll process for OPV. On the contrary, the small scale (300 mg) batch synthesized polymer is soluble in chlorinated and other aromatic solvents at room temperature and the number average molecular weight was estimated, with size exclusion chromatography (SEC), to be 38 kDa (M_n). It still formed a gel in concentrated solution but it was possible to coat rapidly after preparation of the solution using a mini roll coating process for OPV without too many complications (Table 2, entry 6). Clearly it is essential to be able to control and reproduce the molecular weight of PBDTTTz-4 in order to realize solution processing without complications in terms of precipitation and viscosity extremes. Continuous flow synthesis is ideal for fast optimization of polymerizations through boosting of reaction rates with a high reaction temperature, fast heating, and efficient mixing of reactants. Conventional batch polymerizations typically run for days to ensure polymers with high molecular weight. On the contrary, the polymerization rate can be increased significantly with continuous flow syn-

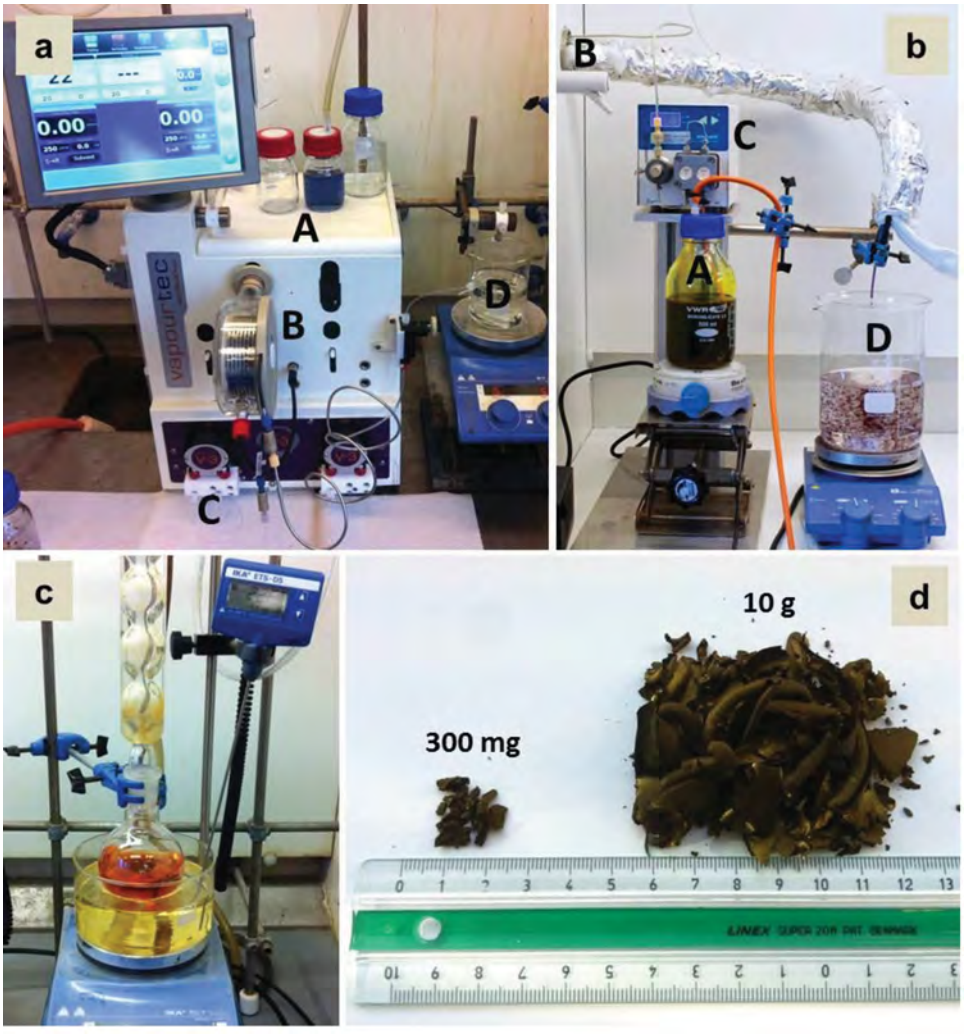

Figure 2. a) Vapourtec flow chemistry system. A: Reactant solution. B: Coil tube reactor. C: Pump (maximum output pressure of 10 bars). D: Collection of product. b) In-house build flow chemistry system. A: Reactant solution. B: Outlet/inlet to oven. C: Pump (maximum output pressure of 400 bars). D: Collection of product. c) Traditional batch reaction in a round-bottom flask. d) Picture of PBDTTTz-4 (small and large scale) as it appears to the eye. The ruler for scale is in cm.

thesis which we experienced during our first attempts to optimize the reaction conditions for the flow synthesis of PBDTTTz-4. The continuous flow reactions were performed on a commercially available coil tube flow reactor with a 20 mL tube volume (see Figure 2a). The temperature limit of the reactor is 180 °C which is the temperature that we chose to run our reactions at in order to increase the polymerization rate as much as possible. In a typical flow experiment, the monomer units, BDT and TTz-4 (see Figure 1), together with the catalyst system Pd_2dba_3/P(*o*-tolyl)$_3$ was dissolved in *o*-xylene and pumped into the reactor with a flow speed ranging from 0.44 to 1.33 mL min^{-1}, keeping the pressure at 4–6 bars. In order to speed up the polymerization rate we first increased the concentration of the monomers from 0.025 to 0.035 M, but this resulted in an overpressure and shutdown of the pump due to increased viscosity of the polymer solution inside the flow reactor. All polymerizations were therefore performed with a monomer concentration of 0.025 M. We then tried to change the amount of catalyst in the polymerization from 1 to 5 mol% (**Table 1** and **Figure 3**a, entries 1–3), while keeping the reaction time constant at 30 min, in order to study the effect on the polymer molecular weight. A clear enhancement of the molecular weight, from 8 to 17 kDa, is detected when the catalyst loading is increased from 1 to 3 mol% whereas an additional increase of the catalyst loading to 5 mol% does not further increase the molecular weight. Subsequently, we tried to alter the reaction time (Table 1 and Figure 3a, entries 4 and 5), while keeping the catalyst loading at 3 mol%, which showed that we could reduce the reaction time to only 15 min and still get an acceptable molecular weight of 17 kDa. When the reaction time was increased to 45 min we did not detect an increase of the molecular weight, compared to a reaction time of 15–30 min (Table 1 and Figure 3a, entry 2), whereas the viscosity of the collected polymer solution out of the reactor was, from a qualitative observation, increasing along with longer reaction time (>45 min). Thus, in order to avoid the chance of reactor fouling

Table 1. SEC data (molecular weight, M_n, and polydispersity index, PDI) and average photovoltaic performance of BHJ OPVs (ten single junction devices with an active area of 1 cm^2) based on flow synthesized PBDTTTz-4 under different reaction conditions ([monomer] = 0.025 M in 12 mL *o*-xylene, temperature 180 °C).

Entry	Reaction time [h]	Catalyst [mol%]	M_n [kDa]/PDI	J_{sc} [mA cm^{-2}]	V_{oc} [V]	FF [%]	PCE [%]
1	0.5	1	8/1.9	6.44 ± 0.67	0.78 ± 0.00	49 ± 1	2.46 ± 0.26
2	0.5	3	17/2.3	8.52 ± 0.17	0.78 ± 0.01	54 ± 2	3.56 ± 0.11
3	0.5	5	15/2.3	8.32 ± 0.29	0.79 ± 0.01	52 ± 1	3.41 ± 0.10
4	0.25	3	17/2.2	8.29 ± 0.25	0.78 ± 0.01	54 ± 1	3.47 ± 0.13
5	0.75	3	16/2.3	8.57 ± 0.24	0.78 ± 0.00	54 ± 1	3.57 ± 0.11

we did not try to enhance the reaction time further. Also, when the aim is upscaling we want to be able to produce the polymer as rapidly as possible and therefore an acceptable polymer molecular weight prepared with a reaction time of 15–30 min is warranted over a higher polymer molecular weight prepared with a longer reaction time. Of course, this is only viable if the flow synthesized PBDTTTz-4 can give a consistent high performance in BHJ solar cells and we therefore prepared individual BHJ polymer:PCBM solar cells for each polymer batch, on an earlier reported mini roll-coater employing fully printed, flexible and ITO-free substrates that are identical similar to the substrate used for large scale R2R processing.[12] Under optimized conditions, the active layer blend was slot-die coated from ODCB + 3% 1-chloronaphtalene (CN) (v/v) having a wet thickness of 17 µm and a dry thickness of ≈400 nm. The average photovoltaic performance of the small scale (1 cm^2) roll coated BHJ solar cells based on the different polymer batches are listed in Table 1 showing high PCEs around 3.5% for all batches except entry 1, where the PCE is lowered to 2.5%, which can be explained by a significantly lower molecular weight, compared to entries 2–5. According to Table 1, it can be argued that the PCE is very consistent around 3.5% when the number average molecular weight of PBDTTTz-4 is ≈15–17 kDa. Moreover, all polymer batches in this molecular weight regime were readily soluble and can be processed from solution without complications in terms of precipitation or gel formation. For our initial upscaling experiments we used the optimized reaction conditions with 3 mol% catalyst, a reactor temperature of 180 °C, and a reaction time of 30 min. A 1.5 g and up to 5 g polymer were synthesized on the commercially available flow chemistry system from Vapourtec. As can be seen in **Table 2**, entries 8 and 9, both upscaling experiments afforded polymer with a high molecular weight that is very comparable to the molecular weight afforded in the small scale (300 mg) flow experiment under equivalent reaction conditions (Table 1, entry 2). The molecular weight consistency demonstrates that the upscaling of PBDTTTz-4 is very straightforward with the use of continuous flow synthesis and we were encouraged to increase the synthesis scale further. However, the scale of our flow reactor from Vapourtec is limited with a 20 mL tube volume and a maximum temperature of 180 °C. Thus, the flow synthesis of 5 g PBDTTTz-4 takes ≈ 5.5 h, with a monomer concentration of 0.025 M and a reaction time of 30 min, and thus the flow synthesis on an even larger scale would be very tedious on this system. Therefore, upscaling to 10 g polymer was performed on a simple in-house built flow reactor with the aim of enhancing the synthesis scale tolerance and simplicity of the flow system. The in-house build flow chemistry system, designed for large scale polymer synthesis, consists of an oven with a temperature limit of 300 °C, a stainless steel coil tube with a ≈40 mL tube volume and a high performance liquid chromatography (HPLC) pump with pressure sensor from Knauer (Figure 2b). Thus, a higher tube volume and a higher temperature limit should aid in enhancing the synthesis scale tolerance. Two 10 g scale experiments (Figure 2d and Table 2, entries 10 and 11) were performed on the home made flow reactor to test its potential as a large scale synthesis system. The first experiment (Table 2 and Figure 3b, entry 10) was performed under the same reaction conditions as the lower scale experiments, though with a reaction time reduced from 30 to

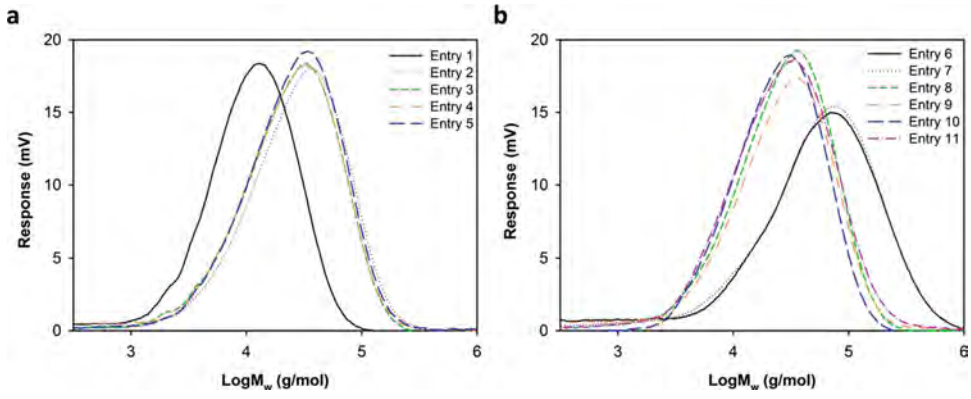

Figure 3. a) SEC traces of flow synthesized polymers under different polymerization conditions. b) SEC traces of batch polymers synthesized on different scales.

Table 2. SEC data and average photovoltaic performance of BHJ OPVs (ten single junction devices with an active area of 1 cm^2) based on flow and batch synthesized PBDTTTz-4 on different scales.

Entry[a)]	Scale [g]	Method	Reaction time [h]	M_n [kDa]/PDI	J_{sc} [mA cm^{-2}]	V_{oc} [V]	FF [%]	PCE [%]
6	0.3	Batch	24	38/2.6	7.0 ± 0.2	0.82 ± 0.01	52 ± 1	3.0 ± 0.1[11]
7	5	Batch	24	33/3.0	n/a	n/a	n/a	n/a
8	1.5	Flow	0.5	17/2.3	8.38 ± 0.30	0.79 ± 0.00	54 ± 1	3.56 ± 0.12
9	5	Flow	0.5	18/2.2	8.15 ± 0.20	0.79 ± 0.00	54 ± 1	3.46 ± 0.08
10	10	Flow	0.33	16/2.2	8.32 ± 0.16	0.77 ± 0.01	55 ± 1	3.52 ± 0.07
11	10	Flow	0.17	16/2.6	8.36 ± 0.16	0.80 ± 0.01	56 ± 2	3.72 ± 0.10

[a)]Reaction conditions (entries 6 and 7): [monomer] = 0.025 M in toluene, 3 mol% Pd_2dba_3, temperature = 110 °C. Reaction conditions (entries 8–10): [monomer] = 0.025 M in *o*-xylene, 3 mol% Pd_2dba_3, temperature = 180 °C. Reaction conditions (entry 11): [monomer] = 0.025 M in *o*-xylene, 3 mol% Pd_2dba_3, temperature = 200 °C.

20 min by increasing the flow rate. The molecular weight of the synthesized polymer was estimated to be 16 kDa which is within the desired molecular weight range, according to the SEC data in Table 1. In the second experiment (Table 2, entry 11) the reaction time was reduced further to 10 min while the reaction temperature was raised from 180 to 200 °C to compensate for the lower reaction time. The synthesized polymer had a satisfactory molecular weight, estimated to 16 kDa, which is equivalent to entry 10. Thus, 10 g PBDTTTz-4 with an acceptable high molecular weight could be flow synthesized on the home made flow reactor within 2 h which corresponds to ≈120 g day^{-1}. The effective production rate indicates the essential scalability of the continuous flow synthesis method where even higher production rates, required for industrial application, should be readily achievable by applying enhanced tube reactor volume, higher temperature and higher flow rates. The laboratory footprint of such a synthetic factory is very small compared to the size of the R2R coating machinery that it feeds materials to and it is envisaged that a synthetic factory could become an integral part of future R2R manufacturing plants for OPVs. Again, we prepared BHJ polymer:PCBM OPVs based on the flow synthesized PBDTTTz-4 on the different scales. The average photovoltaic performance of the small scale (1 cm^2) mini roll coated BHJ OPVs based on the different polymer batches are listed in Table 2 showing an anticipated PCE around 3.5% for all batches. Compared to solar cell data based on conventional batch synthesized PBDTTTz-4 (Table 2, entry 6) the efficiency of the solar cells based on flow synthesized PBDTTTz-4 in this work is about 17% higher which is ascribed to better quality processing of the flow synthesized PBDTTTz-4. All the flow synthesized polymer batches were readily soluble and can be processed from solution without complications. In contrast, the batch synthesized PBDTTTz-4 has a significantly higher molecular weight which can complicate solution processing due to precipitation or gel formation. Large scale R2R coating methods that rely on Newtonian ink behavior (i.e., requires that inks are stable over time in terms of viscosity and precipitation or gel formation) make use of such materials impossible. As a final point in this upscaling work, the flow synthesized PBDTTTz-4 was applied in a full R2R process of large area OPVs. Now when large quantities of reproducible high quality PBDTTTz-4 is readily achievable it is possible to optimize the large scale R2R processing thoroughly in terms of, e.g., printing/coating technique, web speed, ink flow, heating/drying, encapsulation, and contacting. Flexible, ITO- and silver-free modules with carbon as the electrode material were thus fabricated in a fully packaged form using only R2R coating and printing methods, as described by Benatto et al.,[3] see **Figure 4**c,d. Each module consists of 16 individual cells with a width of ≈2.2 mm and a length of ≈82 mm that are serially connected in the printing process giving a typical active area of 29 cm^2. Almost 800 modules were fabricated in the first run with 250 of these having an active layer dry thickness in the range of 240–275 nm, which is closest to the optimized thickness obtained for the mini roll coated single devices. These 250 modules were characterized and Figure 4a shows the distribution of the photovoltaic parameters represented as histograms. The best performing modules had a PCE of 3%, see Figure 4b, whereas the mean PCE, V_{oc}, I_{sc}, fill factor (FF), and maximum power values (P_{max}) values at the maximum power point (MPP) for all the 250 modules with the optimal thickness are 2.6%, V_{oc} = 12.0 V, I_{sc} = 14.2 mA, FF = 44.8%, and MPP = 76.5 mW, respectively. This is somewhat below the PCE of 3.5% achieved on the small scale roll coated devices so optimization of the R2R processing conditions, such as solvent choice, drying temperature/time, and active layer thickness, was warranted. It should be pointed out that each module consists of 16 individual cells with a narrow width which enhance the complexity of the processing significantly compared to mini roll coating of single devices (10 mm × 10 mm). Consequently, the first process trial included the solvent combination chlorobenzene/ODCB (4:1), instead of the optimal solvent ODCB + 3% CN, for the R2R coating of the active layer in order to enable good ink control and film quality of the coated stripes. However, after further R2R optimization in the second process trial we were able to R2R process from the optimal solvent, ODCB + 3% CN, which resulted in an enhancement of the average PCE to 3.3% with V_{oc} = 12.6 V, I_{sc} = 16.1 mA, FF = 47.5%, and MPP = 101.0 mW whereas the champion modules gave efficiencies up to 3.8%. Approximately 500 modules were fabricated in the second run and 125 of these had active layer optimal thickness of 500–600 nm. When compared to modules fabricated in the same manner but using P3HT:PCBM as the active layer an increase by more than a factor 2 in average PCE has been achieved, going from an average PCE of 1.5% (P3HT:PCBM) to 3.3% (PBDTTTz-4:PCBM).[3]

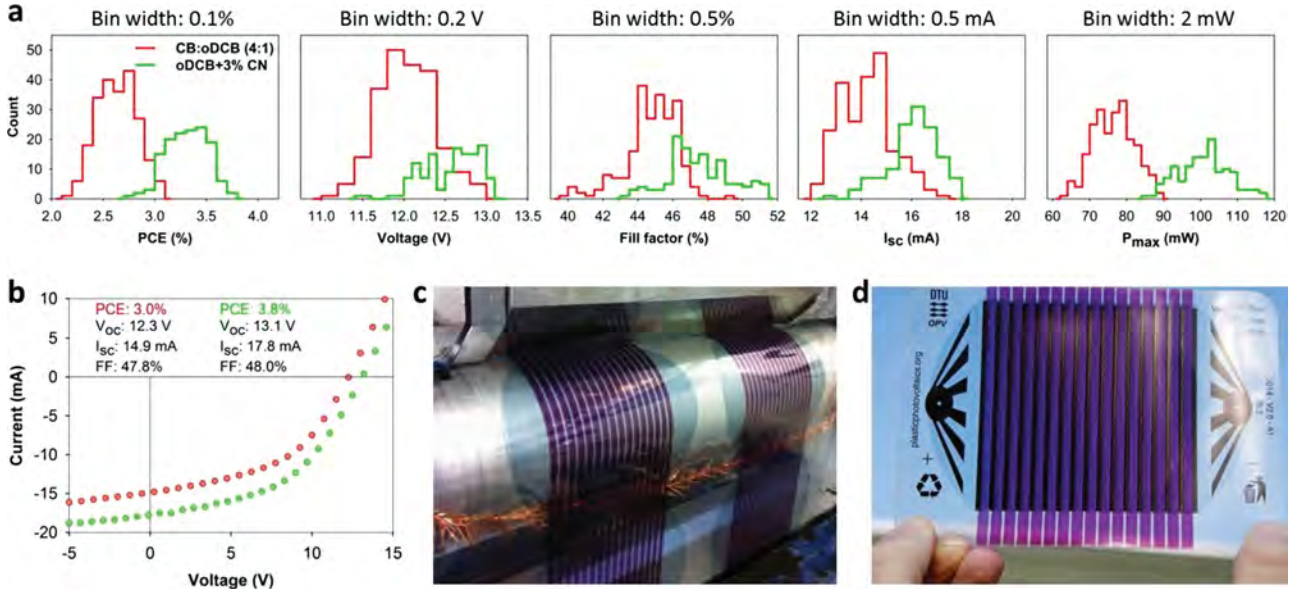

Figure 4. a) The distribution of the photovoltaic parameters (PCE, V_{oc}, FF, I_{sc}, and P_{max}) of 375 modules, processed with two different solvent combinations, represented as histograms. b) *IV*-curves of a champion module from each of the two solvent combinations. c) R2R slot-die coating of the active layer. d) Photograph of a finished module.

3. Conclusions

We have accomplished the upscaling of the polymer PBDTTT-4 from milligram to gram scale by applying continuous flow synthesis and demonstrated its further use in the intended fully sustainable large scale R2R process for OPVs. Initial optimization of the polymerization conditions were done on a commercially available flow chemistry system varying the monomer concentration, amount of catalyst and reaction time. The polymer molecular mass distribution when going from small (≈300 mg) to large scale (≈5 g) was highly reproducible and, when applied in roll coated ITO-free BHJ OPVs with PCBM, efficiencies were very consistent around 3.5% when the number average molecular weight of PBDTTTz-4 was around 15–18 kDa. Large scale production of PBDTTTz-4 (≈10 g) was performed on a simple in-house built flow reactor with the capability to accomplish an effective production rate of 120 g day^{-1}. The flow synthesized PBDTTTz-4 was further applied in a full R2R process of ITO- and silver-free large area OPV modules comprising 16 individual single junctions connected in series with total active area of 29 cm^2. A total of 1300 modules were fabricated in several different processes presenting different active layer thicknesses. The modules with the optimum thickness (375 in total) were carefully tested and characterized resulting in an average PCE of 3.3% using the optimized solvent combination and thickness with the best performing modules giving a PCE of 3.8% which is an increase by more than a factor 2 in average PCE compared to modules based on P3HT:PCBM.

4. Experimental Section

Materials: All chemicals and reagents were purchased from Sigma-Aldrich Chemical Co. Ltd, unless otherwise stated, and used as received. [C60]PCBM was purchased from Merck Chemicals Ltd. The monomers BDT and TTz-4 were synthesized according to the literature or with slight modifications.[13,14] Molecular weights of the polymers were analyzed against polystyrene standards with an Agilent PL-GPC 220 Integrated High Temperature SEC System equipped with refractive index, viscometer detectors and three columns in series (PL gel 10 µm MIXED-B LS). The eluent was 1,2,4-trichlorobenzene (TCB) and the analyzing temperature was set to 150 °C. The samples were dissolved in TCB for 1.5 h in 140 °C and filtered with a 0.5 µm metal filter before injection.

Small Scale Flow Synthesis Polymerization: A commercially available flow chemistry system (the E-Series) from Vapourtec with a Std Tube Reactor Assembly with 20 mL SS reactor was applied for the initial optimization and upscaling of the flow polymerization. In general a monomer solution 0.025 M in *o*-xylene was applied with a flow rate of 0.44–1.33 mL min^{-1} at 180 °C under 4–6 bars back-pressure.

Large Scale Flow Reactor: The home built flow reactor was constructed with a HPLC pump with pressure sensor (Smartline Pump 100) from Knauer. The acid resistant steel tube (steel 316, tube 1/8 inch outer diameter, length 16 m, volume of 37 mL) was connected to the pump via a check valve and in the output end via a 250 psi backpressure valve. The oven used for heating the reactions was a Memmert UF75, 74L with a hole on the side wall allowing for inlet and outlet of the tube. The outlet was heated using a heating band and thermally insulated all the way to the point of exit to avoid precipitation inside the tube when exiting the oven (Figure 2b). Generally a monomer concentration of 0.025 M in *o*-xylene was applied with a flow rate of 1.8–3.7 mL min^{-1} at 180–200 °C under a fixed pressure due to the 250 psi backpressure valve. For all flow syntheses the product was collected by discharging the reaction mixture into a stirring solution of methanol/$NH_4OH_{(aq)}$ 10:1 (v/v), followed by Soxhlet extraction with methanol, hexane, and finally chloroform. The chloroform fraction was precipitated in methanol, filtered and dried in vacuum to give the final product.

Mini Roll Coating: Single devices were prepared on a superstrate consisting of PET/Ag grid/hole transport layer/ZnO as reported in the literature,[15] using an earlier reported mini roll coater.[16] The active layer solution, consisting of PBDTTTz-4:PCBM (1:1.5, by weight) dissolved in ODCB + 3% CN (v/v) to a concentration of 30 mg mL^{-1}, was slot-die

coated at 90 °C with a flow rate of 0.14 mL min^{-1} and a web speed of 0.8 m min^{-1} giving a wet thickness of 17 µm corresponding to a dry thickness of ≈400 nm.

R2R Processing: The general R2R processing of large scale modules was performed as reported in the literature.[3] The active layer solution, consisting of PBDTTTz-4:PCBM (1:1.5, by weight) dissolved in chlorobenzene:ODCB (4:1, by volume) or ODCB + 3% CN (v/v) to a concentration of 30–40 mg mL^{-1}, was slot-die coated at 1–5 m min^{-1} with a wet thickness ranging from 11 to 20 µm, at 90 °C, corresponding to a dry thickness in the range of 240–600 nm.

Device Testing: IV-characteristics were measured with a Keithley 2400 source meter under 100 mW cm^{-2} white light source (AM1.5G) from a Steuernagel KHS1200 solar simulator. The active area was accurately measured for several modules using ultrafast light beam induced current (LBIC)[17] mapping giving an average active area of 29 cm^2. The numbers in the histograms are based on this nominal active area whereas the active area for the champion module was carefully determined by LBIC and the correction for the active area was 28.8 cm^2 as opposed to the nominal value of 29 cm^2.

Acknowledgements

This work was supported by Energinet.dk (Project No. 12144), the Villum Foundation's Young Investigator Programme (2nd round, project: *Materials for Energy Production*), the Danish Council for Independent Research, Technology and Production Sciences (Project No. 11-116864), the European Commission as part of the Framework 7 (Grant No. 288565), the Danish Ministry of Science, Innovation and Higher Education under a Sapere Aude Top Scientist Grant (No. DFF – 1335-00037A) and an Elite Scientist Grant (No. 11-116028).

Received: November 9, 2014
Revised: December 13, 2014
Published online: February 11, 2015

[1] R. R. Søndergaard, M. Hösel, F. C. Krebs, *J. Polym. Sci., Part B: Polym. Phys.* **2013**, *51*, 16.
[2] M. A. Green, K. Emery, Y. Hishikawa, W. Warta, E. D. Dunlop, *Prog. Photovoltaics Res. Appl.* **2014**, *22*, 1.
[3] G. A. dos Reis Benatto, B. Roth, M. V. Madsen, M. Hösel, R. R. Søndergaard, M. Jørgensen, F. C. Krebs, *Adv. Energy Mater.* **2014**, *4*, 1400732.
[4] G. Marzano, C. V Ciasca, F. Babudri, G. Bianchi, A. Pellegrino, R. Po, G. M. Farinola, *Eur. J. Org. Chem.* **2014**, *2014*, 6583.
[5] R. M. Myers, D. E. Fitzpatrick, R. M. Turner, S. V Ley, *Chemistry* **2014**, *20*, 12348.
[6] T. Meyer, *Org. Process Res. Dev.* **2003**, *7*, 297.
[7] C. Wiles, P. Watts, *Eur. J. Org. Chem.* **2008**, *2008*, 1655.
[8] H. Seyler, D. J. Jones, A. B. Holmes, W. W. H. Wong, *Chem. Commun.* **2012**, *48*, 1598.
[9] H. Seyler, J. Subbiah, D. J. Jones, A. B. Holmes, W. W. H. Wong, *Beilstein J. Org. Chem.* **2013**, *9*, 1492.
[10] J. H. Bannock, S. H. Krishnadasan, A. M. Nightingale, C. P. Yau, K. Khaw, D. Burkitt, J. J. M. Halls, M. Heeney, J. C. de Mello, *Adv. Funct. Mater.* **2013**, *23*, 2123.
[11] J. E. Carlé, M. Helgesen, M. V. Madsen, E. Bundgaard, F. C. Krebs, *J. Mater. Chem. C* **2014**, *2*, 1290.
[12] J. E. Carlé, M. Helgesen, N. K. Zawacka, M. V. Madsen, E. Bundgaard, F. C. Krebs, *J. Polym. Sci., Part B: Polym. Phys.* **2014**, *52*, 893.
[13] M. Zhang, Y. Sun, X. Guo, C. Cui, Y. He, Y. Li, *Macromolecules* **2011**, *44*, 7625.
[14] M. Helgesen, J. E. Carlé, F. C. Krebs, *Adv. Energy Mater.* **2013**, *3*, 1664.
[15] M. Hösel, R. R. Søndergaard, M. Jørgensen, F. C. Krebs, *Energy Technol.* **2013**, *1*, 102.
[16] J. E. Carlé, T. R. Andersen, M. Helgesen, E. Bundgaard, M. Jørgensen, F. C. Krebs, *Sol. Energy Mater. Sol. Cells* **2013**, *108*, 126.
[17] F. C. Krebs, M. Jørgensen, *Adv. Opt. Mater.* **2014**, *2*, 465.

ADVANCED ENGINEERING MATERIALS

DOI: 10.1002/adem.201500361

Improving the Operational Stability of PBDTTTz-4 Polymer Solar Cells Modules by Electrode Modification**

By *Bérenger Roth, Gisele A. dos Reis Benatto, Michael Corazza, Jon E. Carlé, Martin Helgesen, Suren A. Gevorgyan, Mikkel Jørgensen, Roar R. Søndergaard* and *Frederik C. Krebs**

PBDTTTz-4 is employed in the ambient manufacturing of fully Roll-to-Roll organic solar cell modules. Modules are manufactured using a novel silver nanowire electrode or a previously reported carbon electrode. The average PCE of carbon modules (3.07%) and AgNW modules (1.46%) shows that PBDTTTz-4 is a good candidate for upscaling. Stability measurements following the ISOS standards are used to compare the lifetime of the different modules. In all tests but one, the carbon modules are less stable. The higher stability of AgNW is attributed to the removal of the PEDOT:PSS in the front electrode. Finally during indoor light tests, a new degradation phenomenon is observed where bubbles are formed inside the modules contrary to previous reports of bubble formation by thermal expansion of trapped gas inside the barrier.

1. Introduction

Among the sustainable sources of energy, polymer solar cells (PSCs) have attracted a large interest, because they can be processed from solution which allows for high throughput R2R manufacturing.[1–4] Meaning that their manufacturing can be scaled up under ambient conditions at high speed. Consequently large-area organic photovoltaics (OPVs) would become an energy source with a high power to weight ratio and a short energy payback time.[5–9]

In order to compete with current photovoltaic technologies, however, low cost by itself is not enough and therefore the efficiency as well as the lifetime of PSCs need to be improved.[10,11] Through extensive research, the efficiency has steadily increased for both single and tandem devices and has now been reported to exceed a power conversion efficiency (PCE) of 10% for laboratory size cells ($\approx mm^2$).[12] Such PSCs are prepared with materials (glass, indium tin oxide…) and processing techniques (spin-coating, evaporation…), which are incompatible with the intended fast R2R processing and low cost manufacturing philosophy. Bridging the gap from lab-to-fab is technologically extremely challenging and real large-scale fully R2R processed PSCs have at best efficiencies in the range of 2–3%.[13–16]

Recently, high-performance polymers compatible with upscaling have been developed;[17–20] some of which show great potential. Particularly PBDTTTz-4 (Figure 1) has been reported by Carlé *et al*. to retain its efficiency,[17] when upscaled in ITO-free and fully R2R processed PSCs, at about 3% for both single cells (1 cm^2) and modules (8 and 29 cm^2). Initial efficiencies of PBDTTTz-4 cells are higher than typical large-area PSCs prepared with P3HT. However, their operational stability (another critical parameter) is much lower than the P3HT PSCs.[17] This probably relates to the fact that the current design of ITO-free, R2R processed PSCs has been optimized for P3HT and therefore needs to be modified to better fit PBDTTTz-4.

In this work, we present three different architectures of freeOPV modules with PBDTTTz-4:PCBM as the active layer (Figure 2) and various previously reported front and back electrodes.[21–23] The lifetimes of these modules are tested according to the standards defined by the International Summit on OPV stability (ISOS).

2. Results and Discussion

2.1. Modules Manufacturing and Characterization

In order to study PBDTTTz-4 as the absorber material in R2R processed large-area PSCs, the blend PBDTTTz-4:PCBM was integrated in three different freeOPV designs with similar stack architecture but with different front and back electrodes. A graphical representation of the architecture of these

[*] *B. Roth, G. A. dos Reis Benatto, M. Corazza, Dr. J. E. Carlé, Dr. M. Helgesen, Dr. S. A. Gevorgyan, Dr. M. Jørgensen, Dr. R. R. Søndergaard, Prof. F. C. Krebs*
Department of Energy Conversion and Storage, Technical University of Denmark, Frederiksborgvej 399 DK-4000, Roskilde, Denmark
E-mail: frkr@dtu.dk

[**] *This work has been supported the Eurotech Universities Alliance project "Interface science for photovoltaics (ISPV)".*

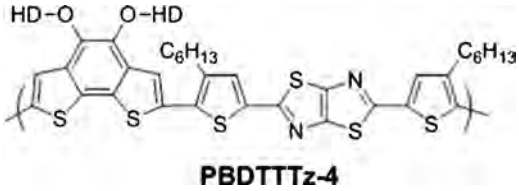

Fig. 1. Chemical structure of PBDTTTz-4.

modules is given in Figure 3 along with a "classical freeOPV" with P3HT:PCBM (Figure 3 left). The silver-free architecture (Figure 3 center) referred to as Carbon freeOPV has previously been extensively described and studied with P3HT:PCBM as the active layer.[22,24] The two final architectures, both included in the illustration to the right in Figure 2, represent the use of a novel front electrode made of silver nanowires (AgNW) and ZnO previously reported by Hösel *et al*.[23] and later integrated in R2R manufactured PSCs with P3HT:PCBM as active layer and subjected to stability studies as a function of PEDOT:PSS electrodes.[24] The two AgNW architectures differ in their back electrodes made with either a PEDOT:PSS layer in combination with a silver grid (similar to the first freeOPV generation) or only with a PEDOT:PSS layer. At the time of this study, the first generation of freeOPV[21] (Figure 2 left) was not manufactured anymore and therefore no modules with this architecture were made with PBDTTTz-4. However, when first reported, PBDTTTz-4 was extensively studied in PSC modules, prepared with a mini-roll coater,[17] having a stack architecture identical to the first-generation freeOPV with the exception of the active layer. The detailed compositions of each architecture are given in Table 1 along with their initial photovoltaic performance parameters: the power conversion efficiency (PCE), the open circuit voltage (V_{oc}), the short circuit current (I_{sc}), and the fill factor (FF).

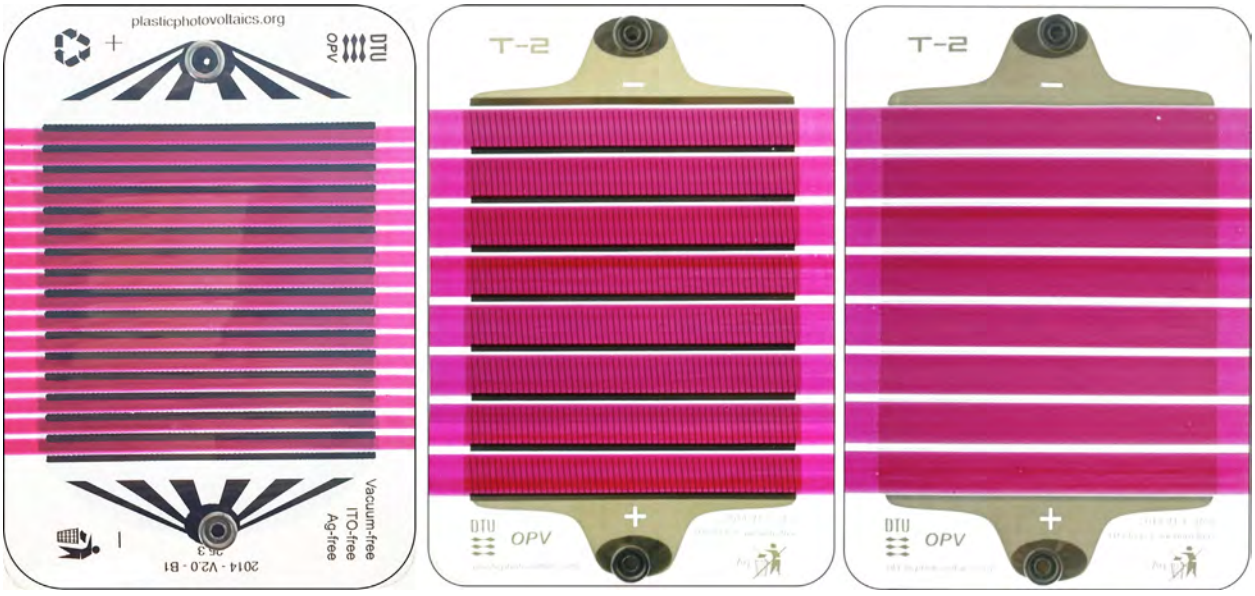

Fig. 2. Front photographs of the freeOPV PBDTTTz-4 devices manufactured respectively with a carbon back electrode (left), a silver back grid (center), and without a silver grid (right).

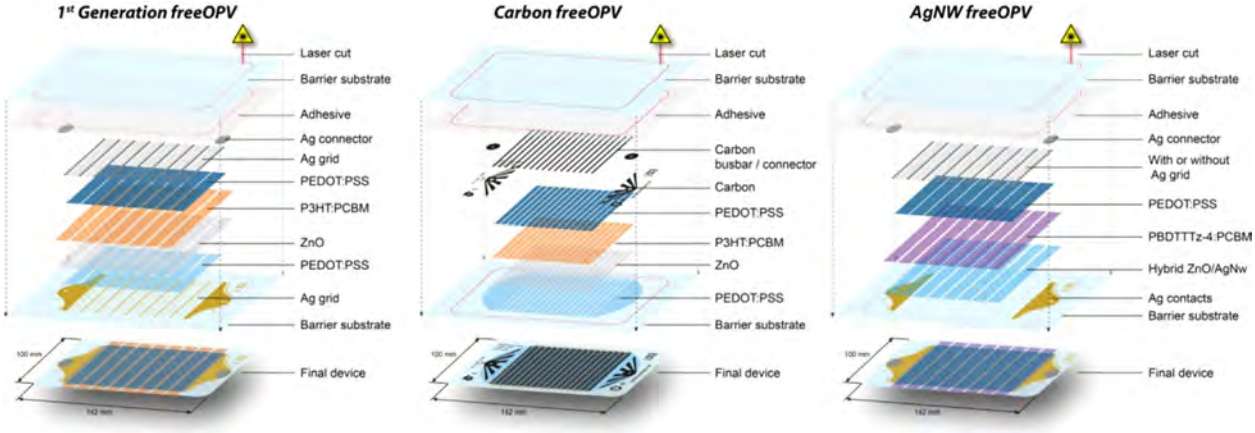

Fig. 3. The different freeOPV architectures: first generation (left), carbon (center), and AgNW (right).

Table 1. FreeOPV architectures and initial photovoltaic performances averaged over 19 modules for each architecture.

	1st Generation freeOPV[a]	Carbon freeOPV	AgNW–back PEDOT:PSS	AgNW–back Ag grid	Mini roll coated Ag grid[b]
Front electrode	Flextrode[34]	PEDOT:PSS/ZnO	AgNW/ZnO	AgNW/ZnO	Flextrode
Active layer	P3HT:PCBM	PBDTTTz-4:PCBM	PBDTTTz-4:PCBM	PBDTTTz-4:PCBM	PBDTTTz-4:PCBM
Back electrode	PEDOT:PSS/Ag grid	PEDOT:PSS/carbon	PEDOT:PSS	PEDOT:PSS/AG grid	PEDOT:PSS/Ag grid
Active area [cm^2]	57	30	57	57	8
Voc [V]	$4.1 \pm 0{,}3$	12.54 ± 0.08	4.89 ± 0.14	6.3 ± 0.3	3.22 ± 0.03
Isc [mA]	40 ± 2	16.4 ± 0.5	$37.\ 8 \pm 1.6$	41 ± 2.2	14.4 ± 0.8
FF [%]	60 ± 4	45 ± 1	31 ± 1.5	42 ± 3.2	50.4 ± 1.45
PCE [%]	1.75 ± 0.06	3.07 ± 0.06	1.01 ± 0.06	1.9 ± 0.2	2.9 ± 0.2

[a] Data extracted with permission from ref.[26]
[b] Data extracted with permission from ref.[17]

The upscaling from the smaller modules ($8\,cm^2$) to the freeOPV modules (30 or $57\,cm^2$) only results in a small drop in PCE for PBDTTTz-4 where most common polymers used in OPVs drastically lose performance when upscaled.[2] This illustrates that PBDTTTz-4 is a promising candidate for manufacture of large-scale R2R processed PSCs. However, the AgNW modules do have a lower starting efficiency which is attributed to a more challenging coating of the active layer on top of the AgNW/ZnO layer. Finally, the difference in performance between the two AgNW architectures is attributed to the lower conductivity of the back electrode when there is no Ag grid.

2.2. Polymer Solar Cell Stability Study

The different modules previously described underwent both indoor and outdoor stability tests which are described in the experimental part. The conditions of these tests followed the standards established by the "International Summit on OPV Stability" known as ISOS and are given in Table 2.[25] Following these guidelines, allows us to accurately compare the present results between the different architectures as well as with previous studies that used the same standards. A recent study by Corazza *et al*.[26] tackled the issue of comparing different PSCs architectures giving guidelines to compare PSCs uncoupled from processing methods and locations. From that study, it was observed that freeOPV modules are about twice as stable as the cells prepared with a mini roll-coater (for the same stack architecture). This allows comparison of results obtained from PSCs prepared by mini roll coating with the freeOPV modules used in this study.[17]

During this study, the PBDTTTz-4 modules underwent four indoor tests as well as two outdoor tests. For the indoor test, ISOS-D-2 and ISOS-D-3 are dark tests and the modules are only exposed to light when measured. During ISOS-L-2 and ISOS-L-3, the modules are continuously exposed to light from a solar simulator. While the ISOS-L-2 is carried out in the ambient atmosphere (resulting in a relatively low humidity because of the elevated temperature), the ISOS-L-3 is carried out in a humidity-controlled chamber. The three indoor tests ISOS-D-3, ISOS-L-2, and ISOS-L-3 are referred to as accelerated because of their harsh testing conditions, which result in faster degradation of the modules. For the two outdoor tests, the only difference is the light source used to characterize the modules. For the ISOS-O-1 test, the modules are dismounted from the sun tracking platform and measured under a sun simulator as described in the experimental section. In the case of ISOS-O-2, the photovoltaic performances are measured outdoor using natural sunlight which can yield day-to-day variation depending on the weather conditions. In order to get reliable statistics, four modules were used for each test except for ISOS-D-2 where only three modules were used, because of the general high stability of PSCs modules in this test (no light and low humidity) which rarely leads to extreme failure.[2] As for ISOS-O-2, only the two AgNW architectures were tested (two modules each). The reason here is purely technical; there were not enough free channels available to connect to

Table 2. ISOS tests conditions.

	ISOS-D-2	ISOS-D-3	ISOS-L-2	ISOS-L-3	ISOS-O-1	ISOS-O-2
Light source	None	None	Simulator AM1.5G	Simulator AM1.5G	The sun, outdoor	The sun, outdoor
Temperature	65 °C (oven)	65 °C	65 °C	85 °C	Ambient outdoor	Ambient outdoor
Relative humidity	Ambient	85% (Environment chamber)	Ambient	Controlled (50%)	Ambient outdoor	Ambient outdoor
Characterization light source	Solar simulator	Solar simulator	Solar simulator	Solar simulator	Solar simulator	Sunlight

the keithley 2400 SMU used to monitor the outdoor PSCs modules. Because of limited space availability for the different stability tests not all of these were started at the same time leading to variation in the testing times for ISOS-D-2, ISOS-L-2, and ISOS-O-1. All the stability data obtained from these tests have been grouped in Figure 4. For the three freeOPV module architectures, the evolution of the efficiency over time is plotted for all the ISOS tests. The main degradation parameters are also given: T_{80} (the time it takes for the module to reach the 80% of its initial performance), and T_{S80} the time it takes to degrade by 20% after stabilization.

2.3. Analysis

In the ISOS-D-2 test, the absence of two major factors that significantly accelerate the ageing mechanisms, the light, and the humidity (the latter is due to the elevated temperatures that create a dry environment around the sample) produce very moderate test condition for the samples.[27] Thus, as expected all the freeOPV modules tested under ISOS-D-2 in this study, regardless of their architecture, are stable and remained above 80% of their initial performances for the 3 months of testing. The carbon module efficiencies show an almost linear decrease during the whole study reaching 80% after approximately 3 months, whereas both types of AgNW modules still performed above 80% of their initial performances at the time this work was submitted. The tests of the modules are still ongoing and are expected to be stable for many more months.

The second dark test ISOS-D-3 introduces a high level of humidity. Water is a well-known degradation source for PSCs[4] and as expected all the freeOPV modules tested under the ISOS-D-3 conditions degraded extremely quickly. Both types of AgNW modules reached T80 in about a day and were fully degraded in about 2 weeks. Under ISOS-D-3, the carbon modules performed slightly better and only reached 80% of their initial efficiency after 3 days. However, the degradation

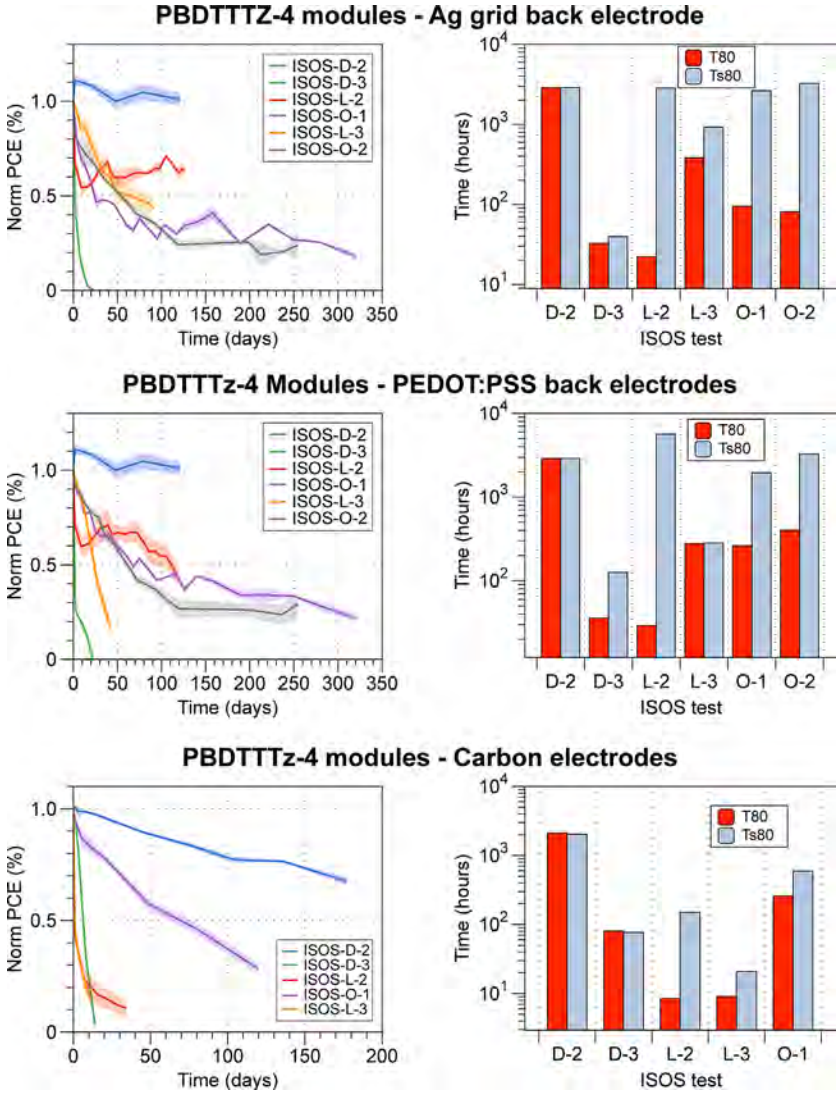

Fig. 4. Degradation curves and lifetime factors for PBDTTTz-4 freeOPV modules with silver grid back electrode (top), PEDOT:PSS back electrode (middle), and carbon electrodes (bottom). For ISOS-D-2, the final time (TF) is plotted instead of T_{80} and T_{S80} for both type of AgNW architectures as all modules retained more than 80% of their starting efficiency. For ISOS-L-2, in the case of the modules with AgNW front electrode (top and middle) T_F is plotted instead of T_{S80} as the modules are stable after the burn in phase.

never slowed down on the carbon modules that were completely degraded after 2 weeks.

The first indoor test with light (ISOS-L-2) has an intrinsically low humidity level because of the higher ambient temperature generated by the sun simulator. Under these conditions, the carbon modules proved to be the least stable and their performances dropped by 80% in a week. In contrast both types of AgNW modules stabilized at around half of their starting efficiency after a few days and remained stable for 3 months. However, the modules with only PEDOT:PSS in the back started slowly to degrade again toward the last weeks of the study while the modules with PEDOT:PSS/Ag grid as back electrode remained stable.

During the last indoor test (ISOS-L-3), which combines both light and humidity, the three different architectures showed drastic differences in degradation. The carbon modules reached T80 in a few hours and were fully degraded in 2 weeks. The modules with AgNW in the front and only PEDOT:PSS in the back degraded much slower than the carbon modules. These modules reached T80 in about a day and were fully degraded after 6 weeks. The last set of modules with AgNW as front electrode and PEDOT:PSS/Ag grid as back electrode degraded even slower with a T80 of 10 days. And after almost 2 months, their efficiency stabilized around 50% of their initial value.

Finally, for the outdoor tests, as mentioned earlier, no carbon modules underwent ISOS-O-2 due to lack of space. Only two AgNW modules of each architecture were tested. It is noticeable that as expected, the modules under ISOS-O-2 appear to degrade according to the same pattern as the modules under ISOS-O-1. The lower performance is due to the fact that the modules were measured outside in Denmark where the light intensity tends to be low especially during the winter. The study started on July 11th, 2014 so the dip in the degradation curve (Figure 4 top and middle) corresponds to the winter season.

Although the carbon modules do not degrade faster than the other two sets of modules with AgNW under ISOS-O-1 conditions, they do not stabilize and have lost 70% in efficiency after 4 months. The behavior of both types of AgNW modules is similar; they degraded to about 40–50% of their starting efficiency in a little over a month and after that their efficiency is stable for roughly 6 months before starting to slowly diminish again.

An overview of the results is given below in Table 3 with a ranking of the tested architectures in the different tests. All the ISOS tests except ISOS-D-3 show that the modules with AgNW as front electrode are more stable than the modules with carbon electrodes. This effect is attributed to the removal of PEDOT:PSS in the front electrode of the AgNW modules. In fact, PEDOT:PSS is known to impact OPV stability negatively because it is hygroscopic.[28–30] Increase of the water content in the PEDOT:PSS layer leads to a decrease in the conductivity of PEDOT:PSS[29,30] and corrosion of metal layers in contact with PEDOT:PSS can be observed[31] as well as an increase in the acidity of PSS.[32]

Between the two type of AgNW modules, the superiority of the ones with a silver grid on the back electrodes is also linked to PEDOT:PSS. As stated above, the absorption of water by PEDOT:PSS reduces its conductivity. The resulting higher sheet resistance has a less pronounced effect in the presence of Ag grid and the back electrode retains a good conductivity[23] compared to the modules with only PEDOT:PSS as the back electrode.

2.4. Elevated Temperature Degradation

During ISOS-L-2 and ISOS-L-3, a new type of degradation mechanism was observed. Bubbles appeared inside the module (Figure 5 left) contrary to a previously reported degradation mechanism where the bubbles formed inside the barrier laminate used for encapsulation.[24] In the case of ISOS-L-3, only the carbon modules and the AgNW modules with a silver grid exhibited this phenomena. However, during ISOS-L-2 all three types of freeOPV modules displayed bubbles. The initiations of the bubbles are probably due to trapped gas and/or solvents in the porous layers of the modules. Such trapped substances would be expected to expand under the high temperatures of both tests which could explain the bubbles. The porosity of the printed silver grid electrode has previously been identified by Dam *et al*.[33] to be above 60% of its volume and a similar porosity could be expected to be present in the carbon electrode. The phenomena is also observed during ISOS-L-2 for the modules with only PEDOT:PSS as back electrodes (without any porous layer). In that case, the hypothesis is that during encapsulation of the modules a small amount of gas is trapped. By light beam-induced current (LBIC), it is observed that the modules have delaminated at the locations of the bubbles (see Figure 5 right) and they are thus an additional source of degradation of the modules.

2.5. Conclusion

The study described in this work successfully identifies factors impacting the long-term stability of large-area R2R

Table 3. Ranking of the device architectures in the different lifetime studies.

Module type	ISOS-D-2	ISOS-D-3	ISOS-L-2	ISOS-L-3	ISOS-O-1
Carbon	−	+	−	−	−
AgNW/PEDOT:PSS	+	−	+	+	+
AgNW/PEDOT:PSS + Ag grid	+	−	++	++	++

Fig. 5. (Left) front picture of a degraded AgNW module with Ag grid in the back after ISOS-L-3. (Right) LBIC of the same module where the light yellow areas correspond to photovoltaic function and the blue areas to non-active or destroyed areas.

processed PSC modules prepared with the high-efficiency polymer PBDTTTz-4. Both indoor and outdoor stability measurements show that modules without a PEDOT:PSS layer in the front electrodes are more stable. One exception to that conclusion is the high humidity dark test (ISOS-D-3) were the carbon modules (with both a front and a back PEDOT:PSS layer) performed better. However, even with the improvement yielded by the use of AgNW front electrodes the lifetime of the best large-area PBDTTTz-4 modules still remains low compared to large-area P3HT modules with reported outdoor lifetimes above 1.5 years.[24] This clearly indicates the need to develop new electrode combinations tailored to PBDTTTz-4 and other high-performance polymers in order to improve their lifetimes. This study shows that PEDOT:PSS dramatically lowers the lifetimes and that the replacement of this component in both front and back electrodes should be a priority. Finally, for the fully R2R processed PSC modules a new type of degradation was identified during the high-temperature indoor tests. The thermal expansion of trapped gas/solvent leads to the formation of bubbles inside the solar cells which causes the cells to delaminate.

3. Experimental Section

3.1. Materials and Inks

The modules were manufactured on a polyethylene terephthalate (PET) flexible substrate (OTR = 0.01 $cm^3\ m^{-2}\ day^{-1}$ and WVTR = 0l04 $g\ m^{-2}\ day^{-1}$) without UV-filter obtained from Amcor. The substrate was also employed for the back encapsulation of the modules. The silver nanowire substrates were prepared as described previously.[23] The ZnO ink employed for manufacturing was prepared by dispersing nanoparticles in acetone with a concentration of 56 mg mL^{-1}. For the active layer, PBDTTTz-4 was synthesized as described previously.[17] Inks comprising PBDTTz-4 and[60] PCBM (from Nano-C) were prepared as described previously.[17] For the back electrodes of the AgNW modules, PEDOT:PSS purchased from Heraeus (Clevios PH1000) was used. For the carbon modules, both front and back PEDOT:PSS was obtained from Heraeus (Clevios PH1000). The carbon paste (Electrodag PF-407C from Acheson) was used as purchased. For the silver grid, back electrode Dupont 5025 was employed and used as received. Finally, the adhesive used for encapsulation (LP655) was purchased from DELO.

3.2. Polymer Solar Cells Preparation

The manufacturing of freeOPV modules was carried out as previously described.[21,22] The modules were prepared on a 305 mm wide substrate moving through an inline R2R manufacturing unit equipped with: an unwinder, an edge guide, a corona treater, a flexo printer, two slot-die coating units, two hot air ovens (2 m length), a rotary screen-printer, 3 IR drier (1.5 kW), an ink-jet printer, a barcode reader, and a rewinder. The modules were then laminated with a second R2R unit. Finally, the freeOPV modules were cut with a laser (90 W CO2) and contacted with snap buttons.

3.3. Device Characterization

All stability measurements were carried out following the ISOS standards[25] (shown in Table 2). Except for the ISOS-O-2 test, all the photovoltaic performances were acquired using a solar simulator with an AM1.5G spectrum of 1 000 W m^{-2} with a Keithley 2400 SMU. For the ISOS-O-2 studies, the performances were measured outdoor under natural sunlight illumination and ambient conditions using a Keithley 2400 SMU. A bolometer from Eppley Laboratories was employed to record the irradiance. For both outdoor tests (ISOS-O-1 and ISOS-O-2), the modules were placed on a solar tracking platform. A damp heat chamber (from Thermotron) was used for ISOS-D-3 and a xenon lamp-based weathering chamber (from Q-Lab) was used for ISOS-L-3. Finally, in the case of ISOS-L-2, the modules were placed under a solar simulator and IV-characteristics were continuously recorded with a Keithley 2400 SMU.

Article first published online: September 17, 2016
Manuscript Revised: August 13, 2015
Manuscript Received: July 15, 2015

[1] K. A. Mazzio, C. K. Luscombe, *Chem. Soc. Rev.* **2015**, *44*, 78.
[2] M. Jørgensen, J. E. Carlé, R. R. Søndergaard, M. Lauritzen, N. A. Dagnæs-Hansen, S. L. Byskov, T. R. Andersen, T. T. Larsen-Olsen, A. P. L. Böttiger, B. Andreasen, L. Fu, L. Zuo, Y. Liu, E. Bundgaard,

X. Zhan, H. Chen, F. C. Krebs, *Sol. Energy Mater. Sol. Cells* **2013**, *119*, 84.

[3] C. J. Brabec, J. A. Hauch, P. Schilinsky, C. Waldauf, *MRS Bull.* **2005**, *30*, 50.

[4] M. Giannouli, V. M. Drakonakis, A. Savva, P. Eleftheriou, G. Florides, S. A. Choulis, *Chem. Phys. Chem.* **2015**, *16*, 1134.

[5] N. Espinosa, M. Hösel, D. Angmo, F. C. Krebs, *Energy Environ. Sci.* **2012**, *5*, 5117.

[6] N. Espinosa, F. O. Lenzmann, S. Ryley, D. Angmo, M. Hösel, R. R. Søndergaard, D. Huss, S. Dafinger, S. Gritsch, J. M. Kroon, M. Jørgensen, F. C. Krebs, *J. Mater. Chem. A* **2013**, *1*, 7037.

[7] C. Powell, Y. Lawryshyn, T. Bender, *Sol. Energy Mater. Sol. Cells* **2012**, *107*, 236.

[8] C. J. Mulligan, M. Wilson, G. Bryant, B. Vaughan, X. Zhou, W. J. Belcher, P. C. Dastoor, *Sol. Energy Mater. Sol. Cells* **2014**, *120*, 9.

[9] C. J. Mulligan, C. Bilen, X. Zhou, W. J. Belcher, P. C. Dastoor, *Sol. Energy Mater. Sol. Cells* **2015**, *133*, 26.

[10] O. Haillant, *Sol. Energy Mater. Sol. Cells* **2011**, *95*, 1284.

[11] C. J. Brabec, *Sol. Energy Mater. Sol. Cells* **2004**, *83*, 273.

[12] M. A. Green, efficiency tables.

[13] F. C. Krebs, N. Espinosa, M. Hösel, R. R. Søndergaard, M. Jørgensen, *Adv. Mater.* **2014**, *26*, 29.

[14] P.-T. Tsai, K.-C. Yu, C.-Y. Chang, S.-F. Horng, H.-F. Meng, *Org. Electron.* **2015**, 1.

[15] F. Guo, P. Kubis, T. Przybilla, E. Spiecker, A. Hollmann, S. Langner, K. Forberich, C. J. Brabec, *Adv. Energy Mater.* **2015**, *5*, 1401779.

[16] M. Hösel, H. F. Dam, F. C. Krebs, *Energy Technol.* **2015**, *3*, 293.

[17] J. E. Carlé, M. Helgesen, M. V. Madsen, E. Bundgaard, F. C. Krebs, *J. Mater. Chem. C* **2014**, *2*, 1290.

[18] M. Helgesen, J. E. Carlé, G. A. dos Reis Benatto, R. R. Søndergaard, M. Jørgensen, E. Bundgaard, F. C. Krebs, *Adv. Energy Mater.* **2015**, *5*, 1401996.

[19] R. G. Brandt, W. Yue, T. R. Andersen, T. T. Larsen-Olsen, M. Hinge, E. Bundgaard, F. C. Krebs, D. Yu, *J. Mater. Chem. C* **2015**, *3*, 1633.

[20] W. Liu, S. Liu, N. K. Zawacka, T. R. Andersen, P. Cheng, L. Fu, M. Chen, W. Fu, E. Bundgaard, M. Jørgensen, X. Zhan, F. C. Krebs, H. Chen, *J. Mater. Chem. A* **2014**, *2*, 19809.

[21] F. C. Krebs, M. Hösel, M. Corazza, B. Roth, M. V. Madsen, S. A. Gevorgyan, R. R. Søndergaard, D. Karg, M. Jørgensen, *Energy Technol.* **2013**, *1*, 378.

[22] G. A. dos Reis Benatto, B. Roth, M. V. Madsen, M. Hösel, R. R. Søndergaard, M. Jørgensen, F. C. Krebs, *Adv. Energy Mater.* **2014**, *4*, 1400732.

[23] M. Hösel, D. Angmo, R. R. Søndergaard, G. A. dos Reis Benatto, J. E. Carlé, M. Jørgensen, F. C. Krebs, *Adv. Sci.* **2014**, *1*, 1400002.

[24] B. Roth, G. A. dos Reis Benatto, M. Corazza, R. R. Søndergaard, S. A. Gevorgyan, M. Jørgensen, F. C. Krebs, *Adv. Energy Mater.* **2015**, *5*, 1401912.

[25] M. O. Reese, S. A. Gevorgyan, M. Jørgensen, E. Bundgaard, S. R. Kurtz, D. S. Ginley, D. C. Olson, M. T. Lloyd, P. Morvillo, E. A. Katz, A. Elschner, O. Haillant, T. R. Currier, V. Shrotriya, M. Hermenau, M. Riede, K. R. Kirov, G. Trimmel, T. Rath, O. Inganäs, F. Zhang, M. Andersson, K. Tvingstedt, M. Lira-Cantu, D. Laird, C. McGuiness, S. (Jimmy) Gowrisanker, M. Pannone, M. Xiao, J. Hauch, R. Steim, D. M. DeLongchamp, R. Rösch, H. Hoppe, N. Espinosa, A. Urbina, G. Yaman-Uzunoglu, J.-B. Bonekamp, A. J. J. M. van Breemen, C. Girotto, E. Voroshazi, F. C. Krebs, *Sol. Energy Mater. Sol. Cells* **2011**, *95*, 1253.

[26] M. Corazza, F. C. Krebs, S. A. Gevorgyan, *Sol. Energy Mater. Sol. Cells* **2014**, *130*, 99.

[27] M. Jørgensen, K. Norrman, F. C. Krebs, *Sol. Energy Mater. Sol. Cells* **2008**, *92*, 686.

[28] H. Cao, W. He, Y. Mao, X. Lin, K. Ishikawa, J. H. Dickerson, W. P. Hess, *J. Power Sources* **2014**, *264*, 168.

[29] K. Kawano, R. Pacios, D. Poplavskyy, J. Nelson, D. D. C. Bradley, J. R. Durrant, *Sol. Energy Mater. Sol. Cells* **2006**, *90*, 3520.

[30] A. M. Nardes, M. Kemerink, M. M. de Kok, E. Vinken, K. Maturova, R. A. J. Janssen, *Org. Electron. Physics, Mater. Appl.* **2008**, *9*, 727.

[31] E. Voroshazi, B. Verreet, A. Buri, R. Müller, D. Di Nuzzo, P. Heremans, *Org. Electron.* **2011**, *12*, 736.

[32] L. Groenendaal, F. Jonas, D. Freitag, H. Pielartzik, J. R. Reynolds, *Adv. Mater.* **2000**, *12*, 481.

[33] H. F. Dam, T. R. Andersen, E. B. L. Pedersen, K. T. S. Thydén, M. Helgesen, J. E. Carlé, P. S. Jørgensen, J. Reinhardt, R. R. Søndergaard, M. Jørgensen, E. Bundgaard, F. C. Krebs, J. W. Andreasen, *Adv. Energy Mater.* **2015**, *5*, 1400736.

[34] M. Hösel, R. R. Søndergaard, M. Jørgensen, F. C. Krebs, *Energy Technol.* **2013**, *1*, 102.

The Critical Choice of PEDOT:PSS Additives for Long Term Stability of Roll-to-Roll Processed OPVs

*Bérenger Roth, Gisele A. dos Reis Benatto, Michael Corazza, Roar R. Søndergaard, Suren A. Gevorgyan, Mikkel Jørgensen, and Frederik C. Krebs**

The impact of additives mixed with poly(3,4-ethylenedioxythiophene):polystyrenesulfonate (PEDOT:PSS) on the stability of organic photovoltaic modules is investigated for fully ambient roll-to-roll (R2R) processed indium tin oxide free modules. Four different PEDOT:PSS inks from two different suppliers are used. The modules are manufactured directly on barrier foil without a UV filter to accelerate degradation and enable completion of the study in a reasonable time span. The modules are subjected to stability testing following well-established protocols developed by the international summit on organic photovoltaic stability (ISOS). For the harsh indoor test (ISOS-L-3) only a slight difference in stability is observed between the different modules. During both ISOS-L-3 and ISOS-D-3 one new failure mode is observed as a result of tiny air inclusions in the barrier foil and a R2R method is developed to detect and quantify these. During outdoor operation (ISOS-O-1) the use of ethylene glycol (EG) as an additive is found to drastically increase the operational stability of the modules as compared to dimethylsulfoxide (DMSO) and a new failure mode specific to modules with DMSO as the additive is identified. The data are extended in an ongoing experiment where DMSO is used as additive for long-term outdoor testing in a solar park.

1. Introduction

The promise of organic solar cells being a low cost alternative to current photovoltaic technologies has long been supported by the prospect of low cost and fast roll-to-roll (R2R) manufacturing. This forecast ensues from the organic photovoltaics (OPVs) having the ability to be coated and/or printed at high speed and low temperature on flexible substrates such as polyethyleneterephtalate. Recently, a study demonstrated the manufacture and deployment of a large solar park connected to the grid with an energy payback time lower than any other PV technology.[1] This shows that if given the possibility to cover very large areas at low cost the demand for very high efficiency becomes less crucial.

B. Roth, G. A. dos Reis Benatto, M. Corazza, Dr. R. R. Søndergaard, Dr. S. A. Gevorgyan, Dr. M. Jørgensen, Prof. F. C. Krebs
Department of Energy Conversion and Storage
Technical University of Denmark
Frederiksborgvej 399, DK-4000 Roskilde, Denmark
E-mail: frkr@dtu.dk

DOI: 10.1002/aenm.201401912

However, in addition to low cost OPV must also provide a high operational stability as this is also an essential requirement for commercial viability. In order to yield similar energy return factors, compared to first and second generation photovoltaics, a few years of operational stability are needed with the current materials and efficiencies.[2–6] Because of the complex multilayer structure, which contains not only several different materials but also a multitude of interfaces, OPVs can degrade through multiple pathways[2] and it can be very difficult to determine which materials combinations will provide the most stable cell. In addition to the materials, also the solvents used in the processing can have an influence on morphology and through that on the performance and operational stability of a device. Poly(3,4-ethylenedioxythiophene): polystyrenesulfonate (PEDOT:PSS) is an example of a material which is extensively used in OPVs as both hole-conductor and as a transparent conducting electrode. It comes in a multitude of formulations from different commercial suppliers (e.g., Agfa and Heraeus) with the properties (especially the conductivity) of PEDOT:PSS being tuned by doping or addition of high boiling solvents.[7–10] It is well known that PEDOT:PSS plays a major role in OPV stability[11–14] but the role of the high boiling additives on stability has not yet been examined. Because of their high boiling points, trace amounts of these additives are very likely to remain after coating/printing of the PEDOT:PSS and it is very plausible that such compounds could influence the long term operational lifetime of the OPV.

Here we present an extensive study on the stability of indium tin oxide-free OPV modules based on the previously reported freeOPV architecture (**Figure 1**) that is manufactured using full R2R processing for all steps under ambient conditions.[15,16] The initial prescreening was conducted on first generation freeOPV modules which has silver electrodes. The main study was then carried out with a second generation of freeOPV modules in which the silver electrodes have been replaced by printed carbon. The stability of these modules, where different types of PEDOT:PSS have been used at the front and the back of the cell, is studied in order to select the best PEDOT:PSS for long term stability of OPVs for large scale production.

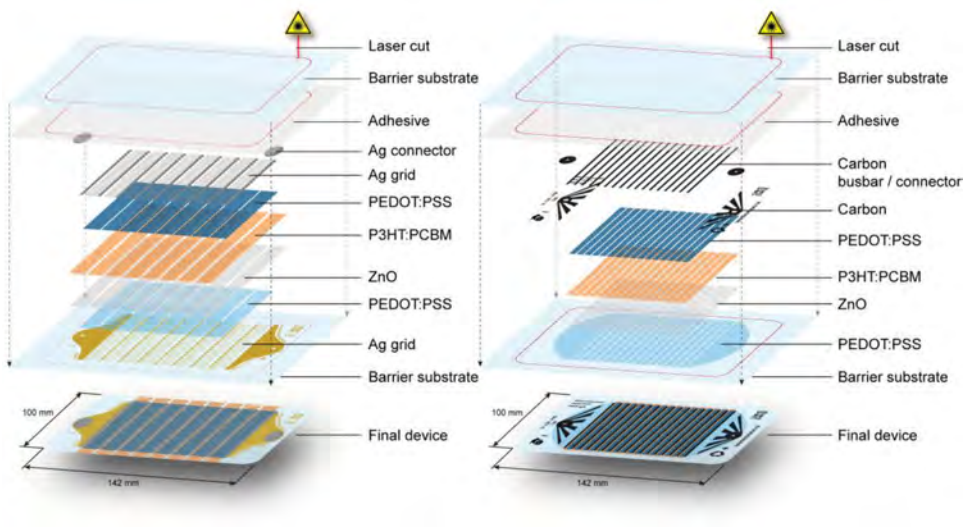

Figure 1. Illustration of the multilayer stack of the silver freeOPV (left) and of the carbon freeOPV (right). The left illustration is reproduced with permission.[15]

2. Results and Discussion

Four types of highly conductive PEDOT:PSS inks typically used in R2R manufacturing of OPVs were selected for this study. The preparation of these is described in the Experimental Section. The commercial name of the PEDOT:PSS and the high boiling additives associated with each of these are given in **Table 1**.

The architecture of the first generation of freeOPV (shown in Figure 1) comprises two PEDOT:PSS layers, one between the bottom silver grid and the zinc oxide (ZnO) layer and a second one on top of the active layers. These are in the following referred to as front PEDOT and back PEDOT, respectively.

The freeOPV process was developed using rotary screen printed PEDOT:PSS layers and this study therefore focuses only on the four PEDOT:PSS inks which we have found to be compatible with this type of screen printing process. Furthermore, the four inks are not all suitable for both the front and back PEDOT layer. The front PEDOT needs to be thin and highly conducting in order to let light through while maintaining good conductivity whereas the back PEDOT has no requirement for transparency but it should generally be thicker in order to comply with the silver or carbon printing. The state of the art stack at the beginning of this study used PEDOT:PSS with DMSO as high boiling additive (hereafter called PDMSO-1) as front PEDOT:PSS and P5010 as back PEDOT:PSS. Devices with this architecture have previously been shipped all around the world through the freeOPV initiative.[15] Five different combinations (C-1–C-5) of the four PEDOT types were selected for the prescreening as shown in **Table 2** together with their initial photovoltaic parameters: power conversion efficiency (PCE), open circuit voltage (V_{oc}), short circuit current (I_{sc}) and fill factor (FF). In addition to using DMSO as the high boiling solvent we also employed PEDOT:PSS mixed with ethylene glycol (hereafter called PEG). A sixth combination (C-6) which was later used in the main study is also shown in Table 2 which differs in that it employed carbon electrodes instead of silver and was chosen based on the outcome of the prescreening study.

Table 1. Composition of the commercially available PEDOT:PSS formulations.

	P5010	PDMSO-1[a)]	PEG-1	PDMSO-2[a)]
PEDOT:PSS	Agfa 5010	PH1000	PH1000	PH1000
High boiling additive	Unknown	DMSO	EG	DMSO
Solid content [% w/w]	3%	2.2	2.2	2.2
Additive content [% w/w]	Unknown	5	5	5

[a)]According to the manufacturer PDMSO-2 contains a surfactant and a cross-linking agent which do not enter in the composition of PDMSO-1.

The manufacture of modules using full R2R processing is time consuming and ensuing stability testing of a large number of those is necessary to obtain good statistics. The most rational approach is to make a shorter initial screening to get an indication of the spread and parameters followed by the main stability test. The ageing experiments were carried out for the most stable combinations under different conditions defined by the international summit on OPV stability (ISOS)[19] shown in **Table 3**. The initial test involved ten modules of each type for each condition.

2.1. Initial Screening

During this primary screening, modules of each combination underwent lifetime studies according to ISOS-L-2, ISOS-L-3, ISOS-D-3, and ISOS-D-2. As stated above, C-1 was the first one used in freeOPV and was therefore extensively studied at the time of its release.[17] The results from that study are compared with the four other combinations studied here. Comparing the results of both studies is only possible because both are following the ISOS standards and a sufficient number of modules were lifetime tested to ensure that data were representative and not dominated by singular defects from the manufacturing process.

Table 2. Initial performances of the PEDOT:PSS combinations on freeOPV modules comprising eight serially connected cells and silver grid electrodes. No UV-filter was employed in the barrier stack that accelerates degradation. The last column shows data for the C-6 PEDOT:PSS combination that was not a part of the initial screening study. C-6 was chosen as an additional PEDOT:PSS combination based on the outcome of the screening study (C-1–C-5).

Combination		C-1[a)]	C-2	C-3	C-4	C-5	C-6
Front PEDOT:PSS		PDMSO-1	PDMSO-1	PEG-1	PDMSO-1	PEG-1	PEG-1
Back PEDOT		P5010	PEG-1	PEG-1	PDMSO-2	PDMSO-2	P5010
Initial performances[b)]	PCE [%]	1.75 ± 0.06	1.1 ± 0.2	1.3 ± 0.1	1.14 ± 0.08	0.81 ± 0.07	1.57 ± 0.08
	V_{OC} [V]	4.1 ± 0.3	3.9 ± 0.2	3.9 ± 0.2	3.9 ± 0.1	3.1± 0.3	8.3 ± 0.2
	I_{SC} [mA]	40 ± 2	35 ± 4	39 ± 2	38 ± 2	40 ± 2	12.2 ± 0.8
	FF [%]	60 ± 4	47 ± 3	50 ± 2	44 ± 1	37 ± 2	47 ± 1

[a)]Data extracted from ref. [17,18]; [b)]Mean values of eight modules for C-1–C-5 and 35 modules for C-6.

Figure 2 shows the radar plot of the lifetime performance for the modules with different combinations expressed via T_{80} values (the time it takes for the module to reach the 80% of the initial performance). In the case where the efficiency had not decreased by 20% at the end of the study the final time (T_f) was used instead of T_{80}. In addition to T_{80} the other relevant degradation parameters are the performance value when the degradation pattern switches into a more stabilized mode (E_S) and the time it takes to reach 80% of the value calculated from that point (T_{S80}).

The results shown in Figure 2 show that C-4 underperforms in all the ISOS tests compared to the four other combinations. Therefore C-4 was discarded for the main study. All the other combinations perform relatively well in most tests especially C-2, C-3, and C-5. However modules manufactured with C-5 have a poor initial efficiency, and adding that the poor stability of C-4 seems to indicate that PDMSO-2 used as back PEDOT can lower the stability of the module, we chose to discard C-5 as well for the main study. Finally, the good stability of C-3 based modules indicates that PEG-1 is a promising candidate as front PEDOT. So in addition to the three that performed well in the prescreening we decided to add a new combination C-6 with PEG-1 as front PEDOT and P5010 as back PEDOT to the main study.

2.2. Main Stability Study

By the time the main stability study was started the design of the freeOPV had evolved[16] to a completely silver free architecture. The front electrode here consists solely of the high conducting front PEDOT:PSS and the back electrode of a combination of PEDOT:PSS and carbon layers. An illustration of the structure of such a module is shown in Figure 1. The modules with the combinations C-1, C-2, C-3, and C-6 used in the main stability study were manufactured using this architecture.

A total of 35 modules were tested for each combination: five modules for ISOS-L-3 and ten for the other tests. For a given combination all the modules had a similar initial efficiency. The grouping of the initial efficiencies is illustrated on the lower right in **Figure 3**. This illustrates the high reproducibility of the manufacturing process. The results of the collected stability studies are compiled in **Figures** 3 and **4**.

For ISOS-D-1, all the modules were kept in dark storage at room temperature. Under these conditions all the combinations were extremely stable and remained above 80% of their initial efficiency after 126 days as expected. At the end of the test C-1 and C-6 had degraded by roughly 10% while C-2 and C-3 retained efficiencies close to their initial values. The main conclusion from this study is that, when stored in the dark, PEG-1 gives a slightly better stability than P5010 as back PEDOT.

Under high humidity/high temperature conditions in the main stability test (ISOS-D-3 conditions) all the combinations degrade fast and almost no stabilization is seen for either combination (Figure 4). A small difference can be observed between those that have PDMSO-1 as front PEDOT (C-1 and C-2) and those that have PEG-1 (C-3 and C-6). After 14 days under the ISOS-D-3 conditions the C-1 modules have degraded by 56% and the C-2's by 70% whereas the degradation for C-3 and C-6 is 90% and 75%, respectively. The same trend is observed when looking at the degradation parameters (Figure 3). C-1 and C-2 have higher T_{80} and T_{S80} than C-3 and C-6. Therefore under ISOS-D-3 conditions modules with PDMSO-1 as front PEDOT perform more stable than modules with PEG-1. In addition under the hot and humid conditions P5010 seems to be slightly more stable as back PEDOT compared to PEG-1.

Table 3. ISOS conditions[19] employed in this study.

Test	ISOS-D-1	ISOS-D-2	ISOS-D-3	ISOS-L-2	ISOS-L-3	ISOS-O-1
Type	Dark	Dark	Dark	Light	Light	Outdoor
Temperature [°C]	Ambient	65	65	65	85	Ambient
Relative humidity [%]	Ambient	Ambient	85	Ambient	≈50%	Ambient

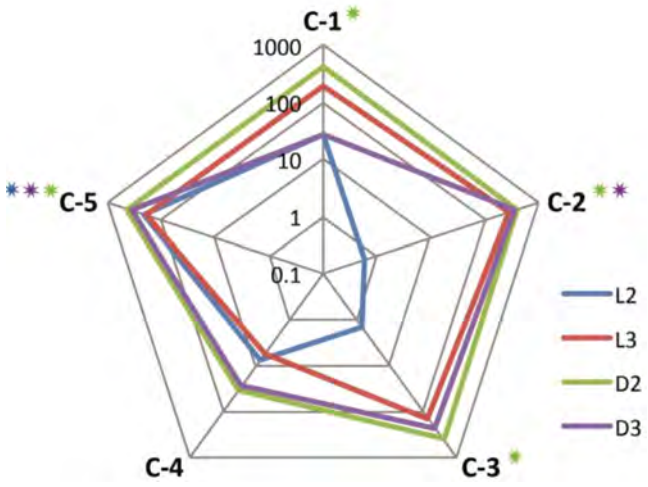

Figure 2. T_{80} in hours for each combination under different ISOS standards averaged over two samples for each structure. The colored star indicates when T_f was used.

Under ISOS-L-3 conditions, the last indoor test, all the combinations degraded by more than 80% during the first 7 days. This can be expected due to the absence of a UV-protective filter in the modules. The hard UV from the Q-sun rapidly degrades the performance in addition to the high humidity/temperature. The degradation curves in Figure 4 show that C-1, C-2, and C-3 behaved very similarly under these conditions with the C-6 modules degrading slightly faster. It is very difficult to draw any final conclusions from those results although the T_{80} values indicate that PEG-1 as back PEDOT (C-2 and C-3) yields slightly more stable modules than P5010.

The final test was conducted outdoor on a tracking platform which ensures that the plane of the modules is always perpendicular to the sun (maximum light exposure) when the sky is clear (see **Figure 5**). The study was performed in the period from May to September 2014. The degradation curves clearly show that C-3 and C-6 are much more stable outdoor than C-1 and C-2. C-3 and C-6 retained more than 50% of their starting efficiency after 50 days while C-1 and C-2 had degraded by more than 80% in 15 days. Similarly C-3 and C-6 had about ten times higher T_{80} and T_{S80}. These results show that outdoor modules with PEG-1 as front PEDOT are more stable.

The conditions of ISOS-L-3 and ISOS-D-3 are much harsher than the outdoor testing (ISOS-O-1). Therefore one would expect OPV modules to degrade much faster under these two tests than outdoor, which was the case for C-3 and C-6. However C-1 and C-2 modules degraded faster outdoor than during

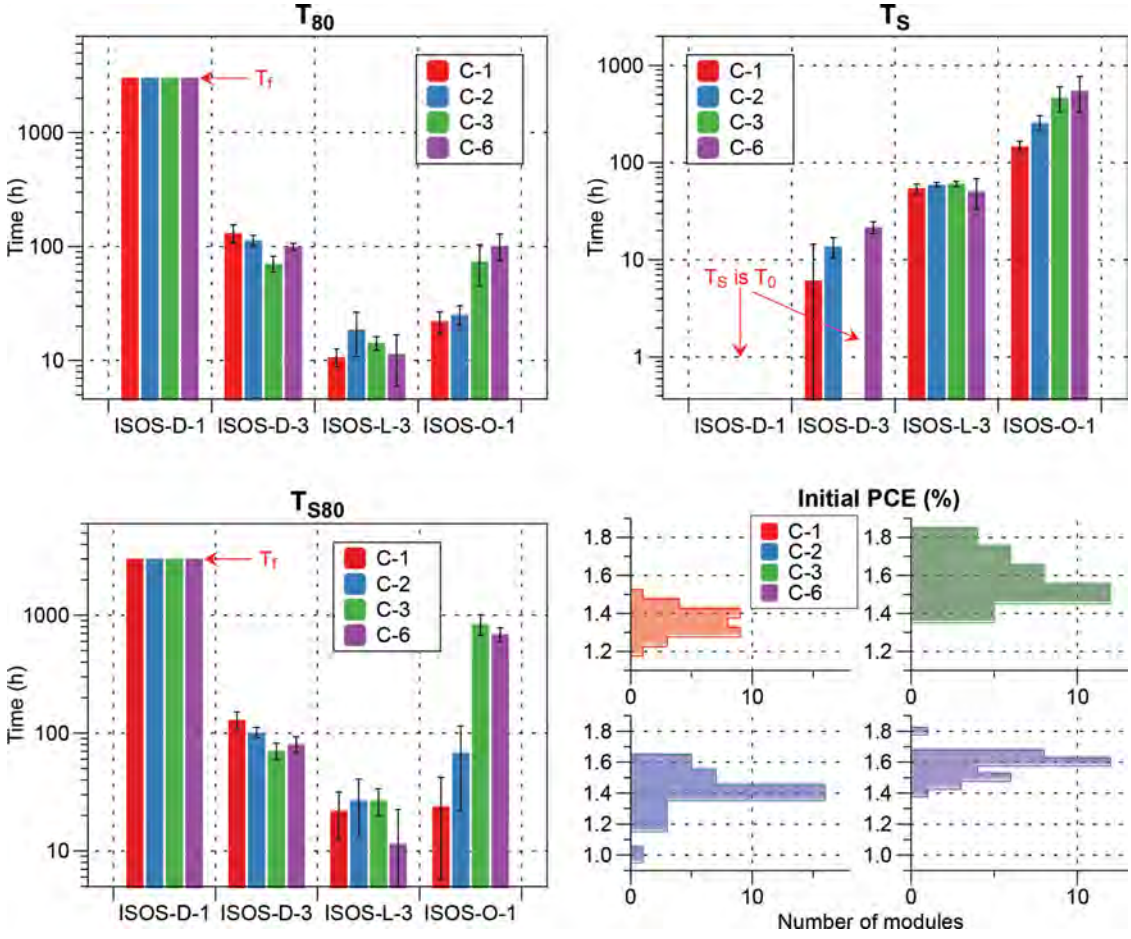

Figure 3. Degradation statistics T_{80} (top left), T_S (top right), T_{S80} (bottom left), and initial performances (bottom right) of the carbon freeOPV modules. The experiment was run for 3000 h.

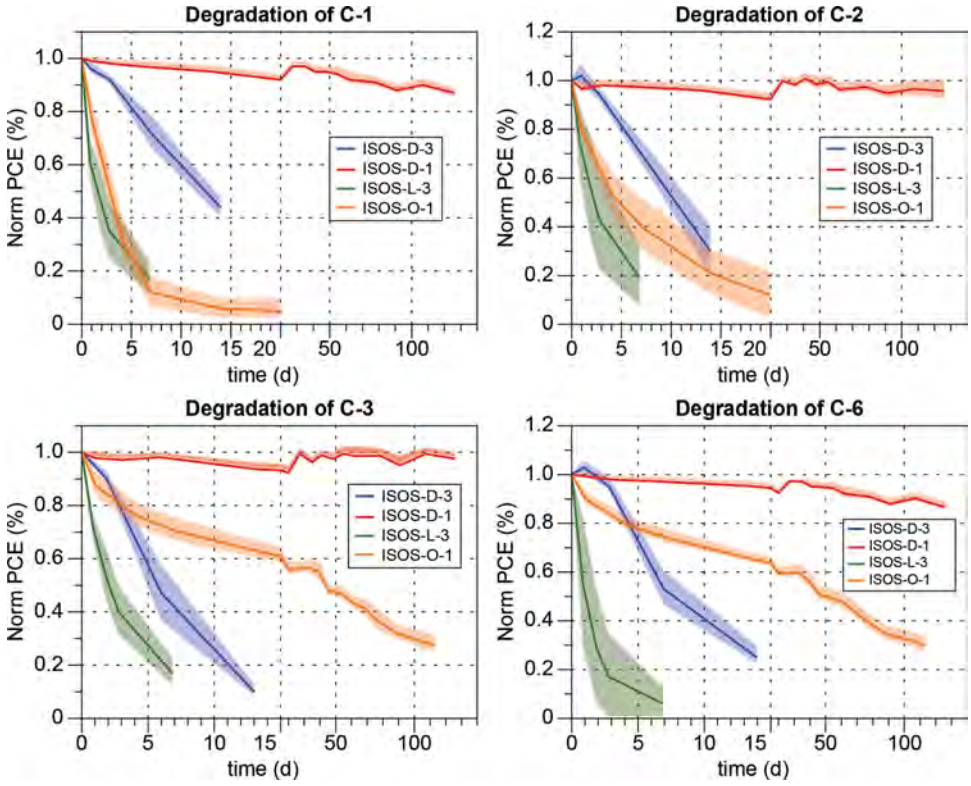

Figure 4. Degradation curves for each ISOS condition for the four chosen PEDOT:PSS combinations.

ISOS-D-3 testing and about as fast as the modules kept in the ISOS-L-3 chamber. The reason for this faster degradation should probably be ascribed to the fact that the modules were taped onto a plastic plate as shown in **Figure 6**. Such a setup allows for water to condensate between the module and the plastic plate when it rains or simply from the morning dew. The snap buttons used for contacting the module are punched through the barrier and are thus in direct contact with the PEDOT:PSS|carbon electrode. This creates a path for the water diffusion into the device where it is absorbed by PDMSO-1 which appears to be much more hydrophilic than its PEG-1 counterpart. This was confirmed by contact angle experiments with liquid water droplets on the surface of PEG-1, PDMSO-1, and PDMSO-2. This clearly shows that the printed PEDOT:PSS with DMSO as additive is much more hydrophilic than printed PEDOT:PSS with ethylene glycol (EG) as additive (Figure 6).

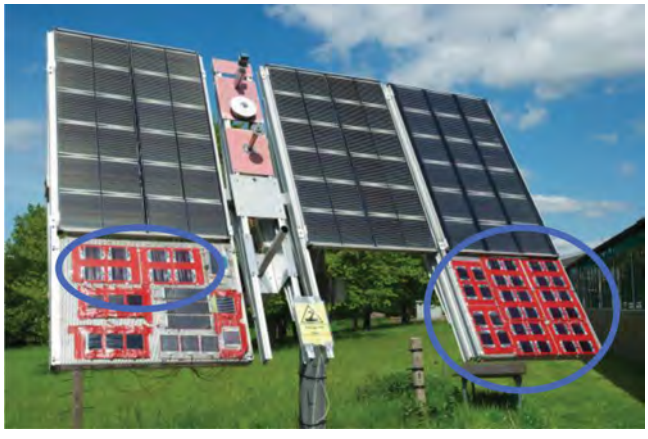

Figure 5. Carbon freeOPV modules mounted outside on a sun-tracking platform during ISOS-O-1 testing (the modules circled in blue are fixed in groups with red tape).

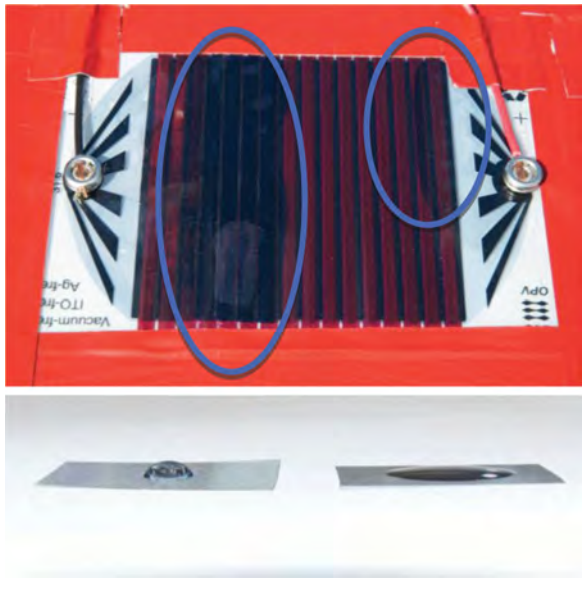

Figure 6. C-1 module carbon based freeOPV mounted outdoor. The water ingress is circled in blue (top). Below water droplets on surfaces of PEG-1 (left) and PDMSO-1 (right) show a much lower contact angle for PEDOT:PSS surfaces printed when using DMSO as high boiling additives.

While both types of surfaces are hydrophilic, printed surfaces of PEDOT:PSS with DMSO have a much lower contact angle (≈15°) compared to the surfaces of PEDOT:PSS printed with EG (75°). Little detail is available on commercial PEDOT:PSS formulations beyond the nature of the high boiling additives that we explore here. But we have tested the effect of the unknown additives indirectly through the PEG-1 and PDMSO-2 that are identical in formulation (except for the high boiling additive) and both contain the same cross linking agent and surfactant so we rule out that the effect is due to the presence/absence of those materials. In order to try and explain a mechanism that could account for this when considering the R2R based drying method which is fast (compared to, i.e., spin coating) we can view DMSO as being a highly polar ($\varepsilon_r = 48$) aprotic high boiling solvent and EG as a protic and less polar ($\varepsilon_r = 41$) high boiling solvent. During the drying process we propose that the liquid phase of the (initially) water based PEDOT:PSS dispersion to a large extent comprises only the high boiling solvent towards the end of the drying process. In the case of DMSO we believe that exposure of the ionic parts of the PEDOT:PSS gel particles are more favored thus yielding a more hydrophilic surface whereas in the case of EG the more apolar parts of the PEDOT:PSS gel particles are exposed. This is then reflected in the interaction between liquid water and the finally dried surface. The increased hydrophilicity of PEDOT:PSS films dried with DMSO as high boiling solvent is thus also a likely cause for the observed decrease in operational stability for these devices even in the absence of liquid water when used as a back electrode where electronic contact at the interface is critical for proper function. This is observed as rapid failure in C-4 devices and poor performance of C-5 devices. The use of DMSO as a high boiling additive for PEDOT:PSS back electrodes is thus not meaningful. When used as front electrode only the bulk electrical properties and optical transparency is needed and the critical interface with the active layer is buffered by ZnO thus rendering the device operation less reliant on the water content in PEDOT:PSS during operation and this makes the use of DMSO as high boiling additive for PEDOT:PSS front electrodes possible even though the operational stability is increased when using ethyleneglycol as high boiling additive.

The water ingress in the modules with PDMSO-1 was so significant that liquid water was accumulated inside the module in some cases (the black areas circled in blue in Figure 6). This failure mode of course resulted in significant acceleration of the ageing under outdoor conditions making the ageing rate of the modules comparable to the indoor harsh tests (ISOS-L-3 and ISOS-D-3). The failure mechanism is however not the same since liquid water was not observed under either ISOS-D-3 or ISOS-L-3. This underlines the fact that there is only so much, one can conclude from a degradation curve and comparison is only valid when the mode of degradation is confirmed to be the same. In the case of ISOS-O-1 the new failure mode with ingress of liquid water made the direct comparison with failure modes operating in ISOS-D-3 and ISOS-L-3 impossible (or at least very difficult). It is likely that the degradation of C-1 and C-2 devices would have exhibited similar degradation behavior to C-3 and C-6 devices in the case where liquid water was prevented from entering the device. It would of course be impractical to carry out extra sealing and the experiments simply show that the C-3 and C-6 devices are better technologies when operating under ISOS-O-1 conditions.

Table 4. Stability comparison of the different PEDOT:PSS combinations under different ISOS testing conditions.

		ISOS-D-1[a)]	ISOS-D-3	ISOS-L-3	ISOS-O-1
Front PEDOT:PSS	PDMSO-1	=	+	+	−
	PEG-1	=	−	−	+
Back PEDOT:PSS	P5010	−	=	−	=
	PEG-1	+	=	+	=

[a)] +, Under the given ISOS condition the PEDOT:PSS seems to relatively improve stability; −, seems to relatively lower stability; =, no apparent difference in stability.

The overall conclusions from the different stability tests are compiled in **Table 4**. For the back PEDOT experiments PEG-1 performs better than P5010 in ISOS-D-1 and ISOS-L-3. For the two other tests (ISOS-L-3 and ISOS-O-1) there are no significant differences. This shows that EG is better suited as high boiling additive for PEDOT:PSS printed on the anode side. For the front PEDOT there is no clear winner. PDMSO-1 performs better under the harsh indoor tests (ISOS-L-3 and ISOS-D-3) but PEG-1 is by far more stable when the modules are put outside. Assuming that outdoor operation is the ultimate goal for most photovoltaic technologies EG should in such cases also be favored as the conductivity inducing high boiling solvent in PEDOT:PSS for the cathode side of the device.

2.3. Upscaling Lifetime Testing

Recent developments of OPV manufacturing[1,20] have demonstrated the fast coating/printing of thousands of large area modules with a high yield (100% yield over 700 m of foil). The high reproducibility of such manufacturing allows for the preparation of a large number of similar OPV modules which when used for lifetime testing gives a high number of statistics. For example, for the study described in this work 180 modules were selected.

Ideally all the samples should be tested at the same time under the same conditions even though the implementation of ISOS standards does allow for comparing modules tested at different times. Obviously most research laboratories have a limited testing capacity (size of the climatic chambers or of the available "one sun" simulators) which will therefore limit the number of large area samples that can be tested (see **Figure 7**). For this reason there is a need to develop an optimal routine to allow obtaining good statistics with limited equipment.

Another concern is the homogeneity of the degradation conditions. For example during our tests we have encountered issues related to temperatures of the samples that were exposed to illuminated tests. Often the light exposure may not be 100% uniform, resulting in temperature differences among the samples, which may then create differences in the ageing rates (this can be the case even for the commercial weathering chambers). An example is shown in **Figure 8**. The foil used to encapsulate the carbon freeOPV is sensitive to temperature cycling and degrades by formation of bubbles or blisters when heated too much. Those lead to local delamination in the solar cell stack

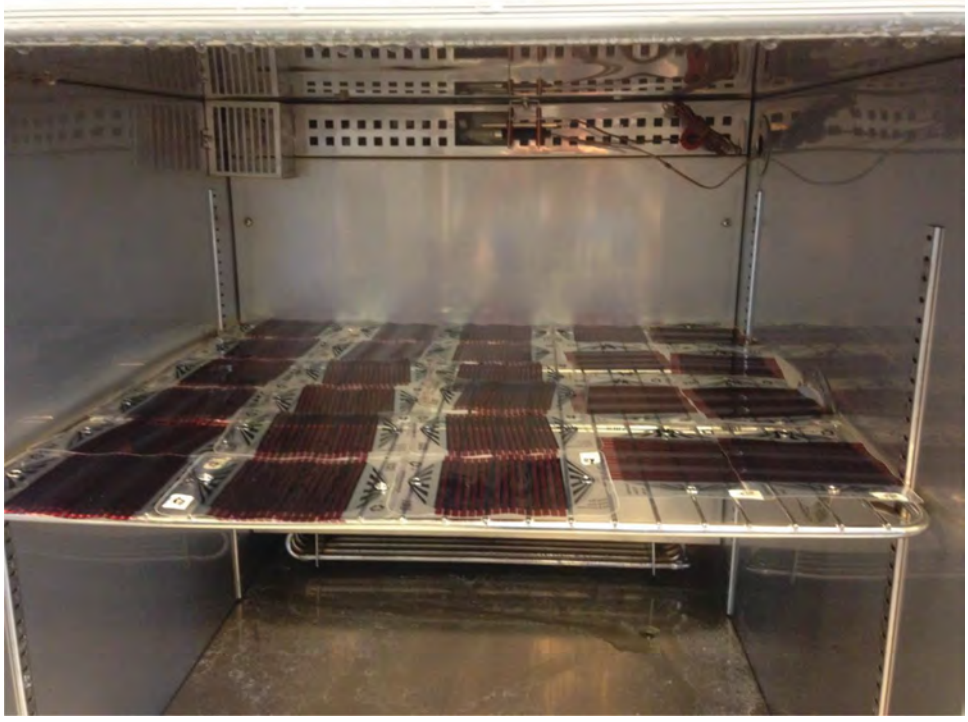

Figure 7. A photograph of the carbon-based freeOPV modules in the Thermotron chamber for ISOS-D-3 testing.

directly under the bubble defect. Through visual examination it was difficult to establish whether the bubbles derived from the solar cell stack itself or from the barrier and we subjected it to further analysis using electron microscopy (as shown in Figure 8). The scanning electron microscopy (SEM) image shows that the encapsulation foil is composed of barrier layers with a layer repeat of ≈10 µm. The image shows in particular the formation of a bubble between these barrier layers.

In addition we found that high temperature cycling leads to growth of these bubbles (both in number and size) depending on the source and batch of the barrier foil. As this has severe implications because of the delamination and eventually failure of the

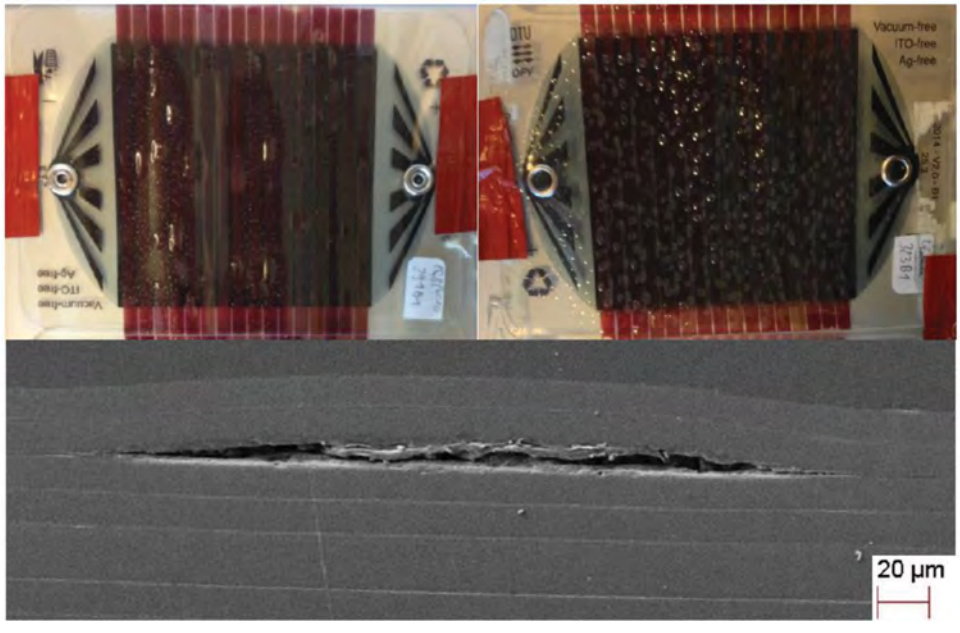

Figure 8. Photographs of carbon based freeOPV after 3 days in the ISOS-L-3 chamber exhibiting different degrees of bubbling due to slight differences in temperature (above). A SEM cross section of an area identified as a bubble was found between some of the layers in the barrier stack (below).

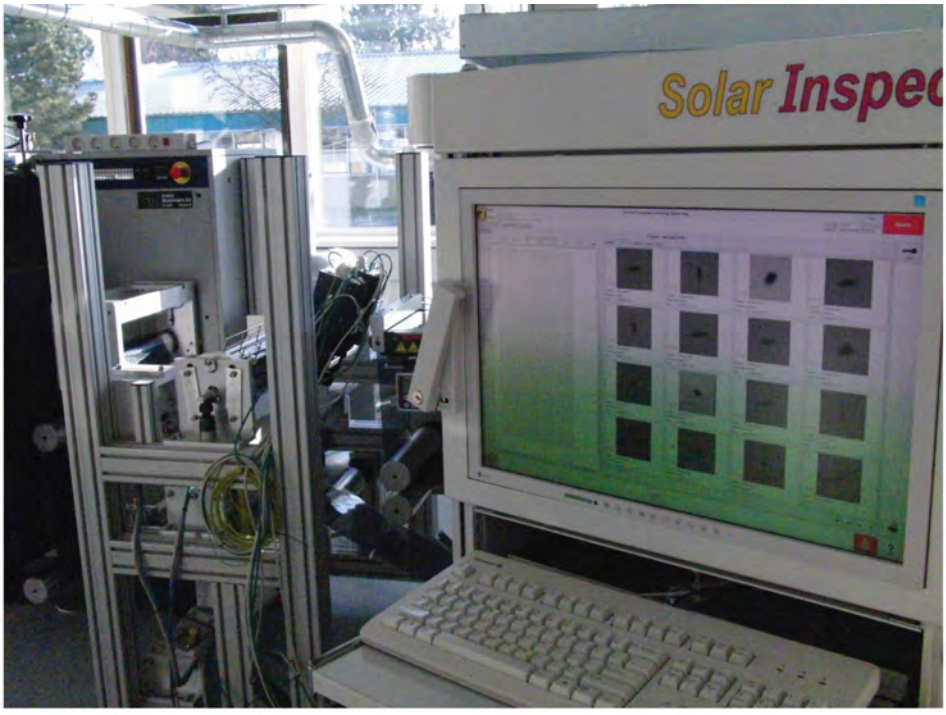

#Bubbles/m²	0	>190.000	>300.000
Image		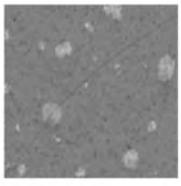	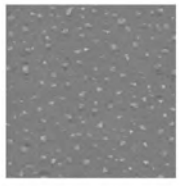

Figure 9. A photograph (above) of the Solar Inspect system with the R2R based line scanning cameras (in the red square). To the right of the photograph the operating system is shown where the defects are characterized. In the table (below) small images from the line scanning camera are shown highlighting the bubble count for different barrier foils.

device we had an interest in developing an efficient R2R based method to detect these microbubbles prior to use of the barrier foil and found an enormous range of bubbles present depending on the source and batch of the foil as shown in **Figure 9**.

The degradation of the foil also impacts the performances of the module by delamination and by allowing water and oxygen to penetrate faster. This was proven by comparing the degradation of two C-1 modules placed on each side of the weathering chamber for ISOS-L-3 test. The ageing curves of the two modules are compared in **Figure 10**. The module (#290B1) placed on the extreme right of the chamber degraded two times faster than the module (#291B1) placed on the other side of the chamber. To minimize effects stemming from such inhomogeneity, it is highly recommended both to check the temperature of all samples under test but also to periodically swap the sample positions to assure a more uniform ageing condition for all the samples. Ideally the sample stage should be rotating mechanically to ensure that all samples experience the same conditions during the test.

3. Future and Outlook

In terms of testing, the ISOS standards and methods have undoubtedly been established as a very important tool for developing stable OPV. However, one issue that arises is the dealing with the large amounts of samples and testing over long periods of time and the handling of the large amount of data generated by each study. For example during the full study presented here more than 1500 data points were taken (*IV* curves). And for each of them efficiency, V_{OC}, I_{SC}, and FF were extracted and analyzed. Ideally the data extraction and its analysis should be automated.[17] In this study the data were extracted and analyzed with a Microsoft Excel macro previously developed[17] but was then manually analyzed. Now, that fast R2R manufacturing of OPV has been demonstrated,[21] ISOS testing platforms and analysis tools having a throughput compatible with R2R manufacture need to be developed. A secondary aspect is of course how to project operational lifetime from the data, established using an approach as described here where a number of ISOS

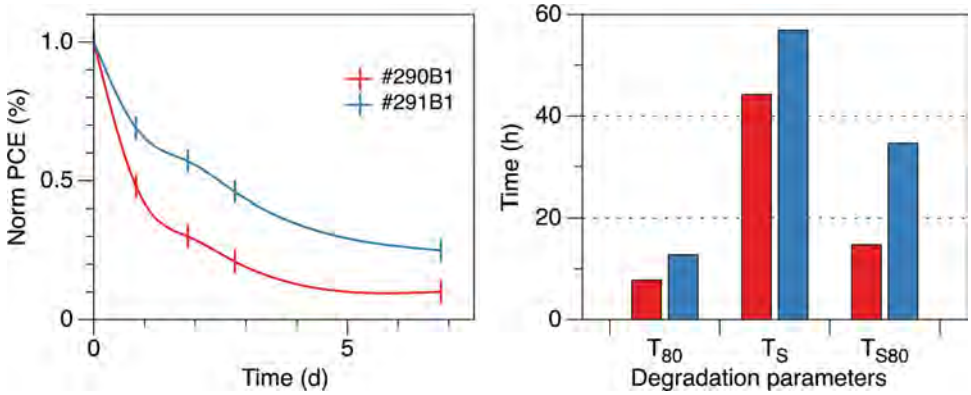

Figure 10. Evolution of the efficiency with time (left) and degradation parameters (right) for modules 290B1 and 291B1 that were adjacent in manufacture and near identical in performance at the start of the experiment.

test conditions are employed to chart the degradation behavior. In the case of OPV prepared using the C-1 PEDOT:PSS combinations an ongoing test on a large scale under ISOS-O-1 conditions have shown operational stabilities well in excess of 1 year (see **Figure 11**). The stability increase that is potentially offered by using PEDOT:PSS combinations of the C-2 or C-3 type is thus significant and a conservative estimate is that the increase is a factor of 3 but it could be significantly higher when considering the decay curves in Figure 4.

4. Conclusion

We have successfully demonstrated that the choice of the high boiling point additive used to prepare highly conductive PEDOT:PSS can significantly impact the stability of R2R processed OPV modules. The freeOPV modules prepared with a PEDOT:PSS mixed with EG are more stable outdoor than their counterpart manufactured with a PEDOT:PSS mixed with DMSO. However, it was found that for some indoor tests (ISOS-D-3 and ISOS-L-3) modules with PEDOT:PSS mixed with DMSO were slightly more stable. The undeniable impact of additives in PEDOT:PSS on the long term stability should always be kept in mind when optimizing an OPV device, since the PEDOT:PSS composition giving the best efficiency might include additives that reduce significantly the stability over extended periods of time. We observed a significant improvement in operational stability for devices where EG was used as a high boiling additive for PEDOT:PSS and ascribe this to a higher degree of hydrophilicity observed for PEDOT:PSS formulations where DMSO is used as a high boiling additive. This is most critical for the PEDOT:PSS used in the back where there is intimate contact with the active layer. While the use of DMSO in the PEDOT:PSS for the front electrode was found more tolerable since there is no direct contact between the PEDOT:PSS. A higher hydrophilicity for the PEDOT:PSS layers was found to be undesired. We finally also observed additional failure modes linked to the ISOS testing of the modules. The competing causes of death were linked both to the packaging method and to the packaging material and we developed a R2R method to quality check barrier foil before use.

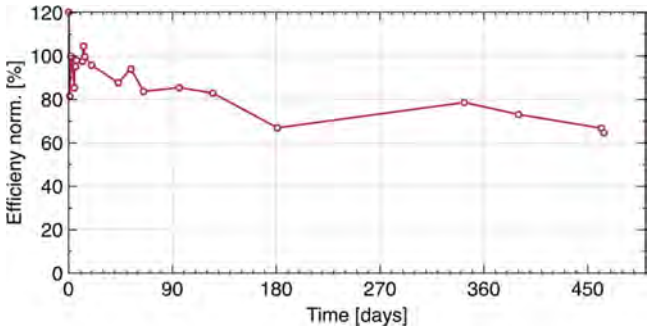

Figure 11. Operational stability over 1.5 years of large scale modules prepared using the C-1 PEDOT:PSS combination with UV-filtering. The module was prepared according to the Infinity concept[1] and had a nominal output of 215 W (100%). The efficiency has not been corrected for irradiance and the lower performance at 180 days and 570 days was lower due to the season (late autumn 2013 and 2014, respectively).

5. Experimental Section

Materials and Inks: PEDOT:PSS P5010 was purchased from Agfa (Orgacon EL-P-5010) and diluted with isopropanol 10:5 w/w and a had a viscosity of 270 mPa s. PEDOT:PSS PDMSO-1 had a solid content of 2.2% containing 5% w/w DMSO and a viscosity of 250 mPa s was purchased from Heraeus (Clevios FE T DK which is a PH1000 without cross linker and surfactant) and diluted with isopropanol 10:3 w/w. PDMSO-2 had a solid content of 2.2% containing 5% w/w DMSO and a viscosity of 230 mPa s was purchased from Heraeus (as PH1000) and diluted with isopropanol 10:3 w/w. PEG-1 having a solid content of 2.2% containing 5% w/w ethyleneglycol and a viscosity of 290 mPa s was purchased from Heraeus (Clevios F HC Solar 2) and diluted with isopropanol 10:3 w/w. All PEDOT:PSS from Heraeus are formulated using the same PH1000 base PEDOT:PSS material and only differ in the high boiling additive and in the case of PDMSO-1 also the absence of cross linker and surfactant. The barrier material employed was a 40 µm thick four-ply material from Amcor without UV-filter.

R2R Processing: The OPVs modules were manufactured as described in ref.[15] for the ones with silver electrodes and in ref.[16] for the ones with carbon electrodes. Briefly, the OPVs modules were manufactured with an inline coating/printing machine on a web of 305 mm width. This R2R is equipped in order with an unwinder, an edge guide, a corona unit, a flexo printing unit, a first slot-die coating unit, a hot air oven (2 m length), a rotary screen printer, a second slot-die unit, three 1.5 kW IR driers, a second hot air oven (2 m length), an ink jet printer (for barcodes),

barcode readers and finally, a rewinder. All the PEDOT:PSS formulations were rotary screen printed at a web speed of 8 m min^{-1} with a nominal wet thickness of 20 µm. The oven had a temperature of 140 °C and 3 × 1.5 kW infrared heaters were used. The lamination employed a R2R machine as described in the literature with DELO LP655 as adhesive.[22] Finally, the foil was cut into discrete OPV modules with a R2R laser-cutter (90 W CO_2) before snap buttons were added for contacts.

Testing: The modules were tested according to the ISOS standards described in the literature.[19] For outdoor testing, the modules were attached to the solar tracking platform. A damp heat chamber (from Thermotron) was used for ISOS-D-3 and a xenon lamp based weathering chamber (from Q-Lab) was used for ISOS-L-3. The IV characteristics were measured under a solar simulator with an AM1.5G spectrum of 1000 W m^{-2} in conjunction with a Keithley 2400 SMU. For ISOS-L-2 the modules were put under a sun simulator and IV characteristics were continuously monitored with a Keithley 2400 source measure unit.

SEM: A freeOPV module was cut and embedded in epoxy, in order to allow imaging of a cross section. The sample was then mechanically polished in order to achieve a flat specimen, followed by a thin carbon coating to limit charging effects. Details on the sample preparation can be found in the literature.[23] The image was finally acquired with a SEM model Zeiss Cross Beam XB1540 using a secondary electron detector.

Acknowledgements

This work was supported by the Eurotech Universities alliance project: "Interface Science for Photovoltaics" (ISPV). Partial financial support was also received from the European Commission as part of the Framework 7 project (Grant No. 288565). This work has been supported by Energinet.dk (Project No. 10728 and 12144). This work has been supported by the Danish Ministry of Science, Innovation and Higher Education under a Sapere Aude Top Scientist Grant (No. DFF – 1335-00037A) and an Elite Scientist Grant (No. 11-116028). The authors thank Dennis Huss and Arnulf Scheel for helpful discussions.

Received: October 29, 2014
Revised: January 16, 2015
Published online: February 16, 2015

[1] F. C. Krebs, N. Espinosa, M. Hösel, R. R. Søndergaard, M. Jørgensen, *Adv. Mater.* **2014**, *26*, 29.
[2] M. Jørgensen, K. Norrman, F. C. Krebs, *Sol. Energy Mater. Sol. Cells* **2008**, *92*, 686.
[3] C. J. Brabec, *Sol. Energy Mater. Sol. Cells* **2004**, *83*, 273.
[4] C. J. Brabec, J. A. Hauch, P. Schilinsky, C. Waldauf, *MRS Bull.* **2005**, *30*, 50.
[5] N. Espinosa, R. García-Valverde, A. Urbina, F. Lenzmann, M. Manceau, D. Angmo, F. C. Krebs, *Sol. Energy Mater. Sol. Cells* **2012**, *97*, 3.
[6] N. Espinosa, M. Hösel, M. Jørgensen, F. C. Krebs, *Energy Environ. Sci.* **2014**, *7*, 855.
[7] J.-S. Yeo, J.-M. Yun, D.-Y. Kim, S.-S. Kim, S.-I. Na, *Sol. Energy Mater. Sol. Cells* **2013**, *114*, 104.
[8] V. Singh, S. Arora, M. Arora, V. Sharma, R. P. Tandon, *Semicond. Sci. Technol.* **2014**, *29*, 045020.
[9] C. M. Palumbiny, C. Heller, C. J. Schaffer, V. Körstgens, G. Santoro, S. V Roth, P. Müller-Buschbaum, *J. Phys. Chem. C* **2014**, *118*, 13598.
[10] A. Keawprajak, W. Koetniyom, P. Piyakulawat, K. Jiramitmongkon, S. Pratontep, U. Asawapirom, *Org. Electron.* **2013**, *14*, 402.
[11] D. Angmo, P. M. Sommeling, R. Gupta, M. Hösel, S. A. Gevorgyan, J. M. Kroon, G. U. Kulkarni, F. C. Krebs, *Adv. Eng. Mater.* **2014**, *16*, 976.
[12] E. Voroshazi, B. Verreet, A. Buri, R. Müller, D. Di Nuzzo, P. Heremans, *Org. Electron.* **2011**, *12*, 736.
[13] C. Girotto, E. Voroshazi, D. Cheyns, P. Heremans, B. P. Rand, *ACS Appl. Mater. Interfaces* **2011**, *3*, 3244.
[14] V. M. Drakonakis, A. Savva, M. Kokonou, S. A. Choulis, *Sol. Energy Mater. Sol. Cells* **2014**, *130*, 544.
[15] F. C. Krebs, M. Hösel, M. Corazza, B. Roth, M. V. Madsen, S. A. Gevorgyan, R. R. Søndergaard, D. Karg, M. Jørgensen, *Energy Technol.* **2013**, *1*, 378.
[16] G. A. dos Reis Benatto, B. Roth, M. V. Madsen, M. Hösel, R. R. Søndergaard, M. Jørgensen, F. C. Krebs, *Adv. Energy Mater.* **2014**, *4*, 1400732.
[17] M. Corazza, F. C. Krebs, S. A. Gevorgyan, *Sol. Energy Mater. Sol. Cells* **2014**, *130*, 99.
[18] S. A. Gevorgyan, M. Corazza, M. V. Madsen, G. Bardizza, A. Pozza, H. Müllejans, J. C. Blakesley, G. F. A. Dibb, F. A. Castro, J. F. Trigo, C. M. Guillén, J. R. Herrero, P. Morvillo, M. G. Maglione, C. Minarini, F. Roca, S. Cros, C. Seraine, C. H. Law, P. S. Tuladhar, J. R. Durrant, F. C. Krebs, *Polym. Degrad. Stab.* **2014**, *109*, 162.
[19] M. O. Reese, S. A. Gevorgyan, M. Jørgensen, E. Bundgaard, S. R. Kurtz, D. S. Ginley, D. C. Olson, M. T. Lloyd, P. Morvillo, E. A. Katz, A. Elschner, O. Haillant, T. R. Currier, V. Shrotriya, M. Hermenau, M. Riede, K. R. Kirov, G. Trimmel, T. Rath, O. Inganäs, F. Zhang, M. Andersson, K. Tvingstedt, M. Lira-Cantu, D. Laird, C. McGuiness, S. (Jimmy) Gowrisanker, M. Pannone, M. Xiao, J. Hauch, R. Steim, D. M. DeLongchamp, R. Rösch, H. Hoppe, N. Espinosa, A. Urbina, G. Yaman-Uzunoglu, J.-B. Bonekamp, A. J. J. M. van Breemen, C. Girotto, E. Voroshazi, F. C. Krebs, *Sol. Energy Mater. Sol. Cells* **2011**, *95*, 1253.
[20] P. Sommer-Larsen, M. Jørgensen, R. R. Søndergaard, M. Hösel, F. C. Krebs, *Energy Technol.* **2013**, *1*, 15.
[21] M. Hösel, R. R. Søndergaard, M. Jørgensen, F. C. Krebs, *Energy Technol.* **2013**, *1*, 102.
[22] M. Hösel, R. R. Søndergaard, M. Jørgensen, F. C. Krebs, *Adv. Eng. Mater.* **2013**, *15*, 1068.
[23] K. Kjellsen, A. Monsøy, K. Isachsen, R. Detwiler, *Cem. Concr. Res.* **2003**, *33*, 611.

Energy & Environmental Science

PAPER

View Article Online
View Journal | View Issue

Cite this: *Energy Environ. Sci.*, 2015, **8**, 3266

Three dimensional corrugated organic photovoltaics for building integration; improving the efficiency, oblique angle and diffuse performance of solar cells†

Jeff Kettle,*[a] Noel Bristow,[a] Tracy K. N. Sweet,[b] Nick Jenkins,[b] Gisele A. dos Reis Benatto,[c] Mikkel Jørgensen[c] and Frederik C. Krebs[c]

Received 13th July 2015,
Accepted 9th September 2015

DOI: 10.1039/c5ee02162f

www.rsc.org/ees

The lamination of OPV modules to corrugated roof cladding has been undertaken. The 3-dimensional form of the cladding provides three advantages for outdoor OPV deployment; firstly the 'footprint' of the solar cell is reduced, which leads to ~10% improved power conversion (PCE) efficiency per unit area. Secondly, the oblique angle performance is enhanced, leading to increased output in the early morning and evening. Indoor characterisation showed a 9-fold enhancement in efficiency was obtainable, when compared to a flat module. Thirdly, an improvement in performance under diffuse lighting conditions was measured, when compared to a flat module. The average daily yield of the 3D module was 17–29% higher than a flat module, with higher relative enhancements observed on cloudier days. Geographically, the 3D module appears to be well-suited to countries with a high latitude, due to the enhanced diffuse light levels and the fact that tilting the module in both 'latitude' and 'longitude' directions away from normal, leads to the best achievable enhancement in solar cell performance. The approach set out in this paper could yield a product that has profound advantages over existing BIPV products and is potentially applicable to other flexible inorganic solar cell technologies.

Broader context

Building integrated PV's potential to seamlessly integrate into the building envelope holds aesthetic appeal for architects, builders, and property owners and is a market sector that is expected to grow dramatically over the next 5–10 years. Organic photovoltaics (OPVs) are among the most promising options for next-generation BIPVs due to their flexibility, which enables the possibility for lamination directly onto 3D structures. This work investigates the lamination of OPVs onto corrugated building products and we show the approach could yield a product that has profound advantages over existing BIPV products or conventional inorganic solar cell technologies, in particular for countries at higher angles of latitudes. The approach enables enhanced energy generating capabilities in early morning and late evening times and diffuse conditions, when traditional PV panels do not generate substantial output power.

1. Introduction

Organic photovoltaics (OPVs) based on solution processable polymers and fullerenes have attracted remarkable interest owing to their potential for low cost, printability, flexibility and rapid energy payback time.[1] Recent research in this area has led to reported power conversion efficiency (PCE) of over 11%.[2] There has been a growing recognition that OPV may not compete directly with mainstream PV technologies, but can compete where the technology has advantageous physical or economic properties. Examples include off-grid portable energy storage for re-charging, energy harvesting and Building Integrated Photovoltaic (BIPV) applications.[3,4] BIPV comprises a group of solar PV technologies that are built into (instead of installed onto) their host building and may actually replace some building materials (such as windows or roof tiles). BIPV's potential to seamlessly integrate into the building envelope holds aesthetic appeal for architects, builders, and property owners. They are increasingly being incorporated into the construction of new buildings, where their initial cost can be offset against the savings in traditional materials and labour. The market is estimated to be

[a] *School of Electronic Engineering, Bangor University, Dean St, Gwynedd, Bangor, LL57 1UT, Wales, UK. E-mail: j.kettle@bangor.ac.uk*
[b] *School of Engineering, Cardiff University, Queen's Buildings, The Parade, Cardiff, CF24 3AA, Wales, UK*
[c] *Department of Energy Conversion and Storage, Technical University of Denmark, Frederiksborgvej 399, DK-4000 Roskilde, Denmark*

† Electronic supplementary information (ESI) available. See DOI: 10.1039/c5ee02162f

worth £1.9 bn (€2.7 bn) in 2015, growing at a Compound Annual Growth Rate (CAGR) of 11.0 per cent in the period from 2012–2014.[5] The advantage of OPV in the context of BIPV is the free-form design that the printing approach automatically grants. This implies that the solar cells can be printed in any pattern. The additional thin outline and inherent flexibility of OPV adds several dimensions to possible installation scenarios.[6]

Given the large market size and the competitive nature of PV technologies, it is not surprising that a large number of different BIPV formats are available on the market. However, to date the market penetration for BIPVs, as opposed to retrofitted roof modules, has been very low.[7] There are two main reasons for this which are the performance and cost. For example, the cost per Watt peak of a solar roof tile is usually about 60% higher than that of an on roof solar panel PV system.[8] In addition whilst panels based on silicon technology generate over 150 Watts per square metre, BIPVs typically generate between 50 Watts and 120 Watts per square metre.[8,9] BIPVs based on 3rd generation technologies such as OPVs have been widely discussed and have the potential to significantly reduce the cost of manufacture and also possess a number of key advantages, including low weight, aesthetic value for architects and potentially lower cost.[3,4] This potentially represents an added value for consumers and architects/builders. One of the major advantages of the flexibility of OPVs could be the possibility for lamination onto 3D structures making relatively low cost BIPVs, without significant compromise in their efficiency.

In this work, OPV modules were assessed for their suitability for BIPV products based upon corrugated roof cladding. The benefit of using a corrugated geometry is threefold; firstly the PV could be positioned diagonally in such a way that the solar cell performance could be enhanced under oblique angle irradiation. Secondly, the overall 'footprint' of the solar cell is reduced, leading to greater efficiency, or power output per m^2 of roof area. Thirdly, the relative smoothness of the corrugation on roof cladding allows for OPVs to be laminated without significant stress at the point(s) of inflexion. For this work, PVC roof cladding was used, which is one of the most commonly used roofing materials on the market. This type of roofing is often used on sheds, garages, conservatories and commercial building. Typically, PVC cladding structures are guaranteed for 10 years for outdoor applications and retail at ~£6 m^{-2} (€9.3 m^{-2}).[8] This makes them well-suited as substrates for OPV devices as they are low cost and their lifetime is similar to the best reported outdoor OPV stability.[10] Potentially a combined OPV–PVC module could be replaced on 5–10 year cycles, when performance of the OPV module had dropped and/or the corrugated substrate had reached an unacceptable performance level.

2. Experimental

Roll-to-roll (R2R) coated OPV modules prepared in the format of the free OPV[11] were roll-to-roll manufactured using P3HT:PCBM as the active material and a silver nanowire front electrode.[12] The light was incident on the silver nanowires side of the module, which were selected as the transparent electrode due to their excellent properties for flexibility when subjected to repeat bending.[13] The 100 micron thick modules were laminated onto building substrates and used for the indoor and outdoor performance tests.

The substrates used for these tests were corrugated PVC roof cladding structures, supplied by Ariel plastics, Chesterfield, UK. These come in two standard corrugated sizes; with either 3″ or 1″ profiles. An image of the '3D OPVs' used for these tests are shown in Fig. 1. Modules A and B were laminated onto 3″ profiled substrates, with module A possessing a concave and module B a convex geometry, relative to the incident radiation. Modules C and D were laminated onto 1″ profiled substrates, with module C mounted in a manner whereby the monolithic cells were aligned parallel with the corrugations and module D perpendicular to the corrugations.

Indoor characterisation of the modules was conducted using AM1.5G performances to verify the performance before and after laminating. Laser Beam Induced Current (LBIC) mapping

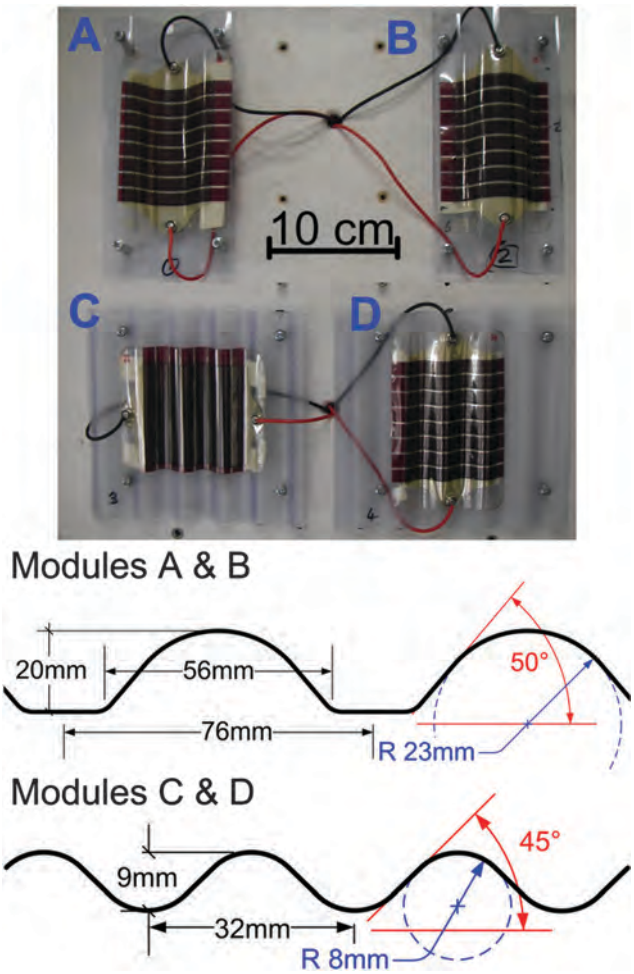

Fig. 1 Photographic images of modules A, B, C and D mounted onto corrugated roofing, with dimensions of the corrugated substrates shown below. Module A was laminated on the 'inside' of the corrugation, forming a concave structure, whereas module B was laminated to form a convex geometry.

was performed with a custom designed instrument as described previously.[14] In this setup a laser beam (405 nm, 65 mW, <100 μm spot size) is scanned over the surface of a solar cell while the current output is monitored. The data are then used to construct a map where a colour gradient (blue to yellow) represents low to high solar cell output (see Fig. 3). For both AM1.5G and LBIC, measurements were conducted with the sample tilted at 0°, 20° and 45° to gain insight into the performance at oblique angle. An average of 3 measurements were made.

The 3D architectures of the OPV modules were tested indoors at different solar altitude and azimuth angles using a Lucas Nuelle solar simulator equipped with a 500 W halogen bulb. The equipment provides solar simulation of the sun (pitch) angle in 15° increments with 120° total sweep angle. The elevation (yaw) angle was set in 10° increments with 180° range. The equipment enabled realistic PV performance data to be collected with respect to the dual axis variation of the sun's position throughout the day/year. For these measurements, solar cell efficiencies were lower than when illuminated by the standard spectrum AM1.5G due to the spectral mismatch between the Lucas Nuelle solar simulator and AM1.5G.

Outdoor current–voltage (*I–V*) measurements of the 3D OPV modules and a flat (reference) OPV module were performed for a period of 30 days during daylight hours in Bangor, Gwynedd, Wales, which has latitude and longitude of 53.2280 N, 4.1280 W and is located at low altitude (20 m above sea level) and 250 m from the Menai Straits (Irish Sea). This was conducted in accordance with ISOS-O-2 standards.[15,16] Global intensity of incident sunlight was measured with an IMT GmbH solar silicon reference cell. During the measurements the modules had ambient temperatures measured by thermocouples mounted to a locally positioned weather station. The stand was placed outdoors during the entire measurement period.

For PCE calculations, an 'effective PCE' was used. The effective PCE is calculated using the OPV footprint, rather than active area size. An advantage of the corrugated PV structure is that more PV can be installed on the same fixed roof size than Fas a flat module.

3. Results

3.1 Indoor testing using AM1.5G

Initially, the 3D OPVs were first tested under illumination using AM1.5G, with the modules positioned normal to the incident light. The overall performance is summarised in Table 1, where the four modules were compared before and after lamination. Prior to lamination, the modules showed very little variation with <6% relative difference in PCE observed (see Table 1).

After lamination, it can be seen that modules A and B experience an increase in PCE (with a relative enhancement of 3.7 and 10.9%, respectively), primarily due to enhancement in J_{SC}. The power conversion efficiency (PCE) of the 3D OPVs was calculated based on the area of the module footprint, rather than the active area of the cell (see Table 1). The effective PCE increases in modules A and B by 3.7% and 10.9%, respectively. However, the effective area of both modules reduces by ~20% when compared to a flat module. This indicates that the increase in effective PCE under normal incident irradiation does not scale directly with the reduction in footprint; (see ESI-2,† where the solar cell performance parameters as a function of corrugation angle are shown under direct irradiation). Overall, the effective PCE increases with corrugation angle, primarily due to the reduction in solar cell footprint. The V_{OC} appears to decrease with corrugation angle under direct irradiation, because of lower in-coupling of light. As V_{OC} increases are proportional with a logarithmic relationship to irradiance, as the corrugation increases, the V_{OC} drop becomes progressively worse. There appears to be not overall trend in variation of FF with corrugation angle.

Modules C and D experience a dramatic reduction in PCE, primarily due to a sharp fall in J_{SC}. These drastic changes in performance are unlikely to be due to changes in optical performance alone and are discussed further in Section 3.2.

Module performance was also evaluated at tilt angles of 20 and 45 degrees to evaluate the performance at oblique angles (see Table 2). Two different orientations were studied, as defined in Fig. 2, with data shown for A, B and the flat module only. It can be seen that the module B exhibits the best performance based on effective PCE, with a relative PCE enhancement of 5.6% (at 20°) and 19.4% (at 45°) compared to the flat module. Module B also performs much better at orientation 2 with a relative PCE enhancement of 14.2% (at 20°) and 10.6% (at 45°). The data indicates that module B should work well in either orientation and that it actually will work best when tilting the module away from normal, as this leads to the best achievable enhancement in solar cell performance. This is an interesting conclusion and shows that the corrugated module could have a particular use for power generation at morning or evening periods. Therefore electricity generation could be more evenly distributed throughout the day reducing expensive peak power demand from the grid.

Table 1 Performance of modules A–D before and after lamination onto corrugated PVC substrates under AM1.5G illumination

Before lamination (effective area 56.7 cm^2) (effective area: 56.7 cm^2)			After lamination				
	PCE (%)	J_{SC} (mA cm^{-2})	Effective area (cm^2)	Effective PCE (%)	J_{SC} (mA cm^{-2})	Effective PCE gain (%)	J_{SC} gain (%)
A	2.10	−0.92	47.37	2.18	−0.98	3.7	6.0
B	2.17	−0.96	46.65	2.41	−1.09	10.9	13.25
C	2.18	−0.96	49.99	1.29	−0.57	−40.7	−40.8
D	2.06	−0.91	51.68	1.78	−0.78	−13.7	−14.5

Table 2 Performance of module A, module B and flat reference module when measured at tilt angles of 20° and 45° under AM1.5G illumination, measured at orientation 1 and 2

	Module tilted at 20°			*Cf.* to flat module at 20°		Module tilted at 45°			*Cf.* to flat module at 45°	
	Effective area (cm^2)	PCE (%)	J_{SC} (mA cm^{-2})	PCE gain	J_{SC} gain	Effective area (cm^2)	PCE (%)	J_{SC} (mA cm^{-2})	PCE gain	J_{SC} gain
1 A	44.51	2.32	−1.04	2.28%	−4.5%	33.50	2.13	−0.98	−10.76%	−11.4%
1 B	43.84	2.39	−1.18	5.57%	8.1%	32.99	2.85	−1.33	19.39%	20.3%
1 Flat	53.28	2.27	−1.09		n/a	40.09	2.39	−1.11		
2 A	44.51	2.31	−1.02	1.24%	3.8%	33.50	2.59	−1.13	2.88%	−2.6%
2 B	43.84	2.60	−1.18	14.16%	10.4%	32.99	2.78	−1.18	10.62%	2.1%
2 Flat	53.28	2.28	−1.07		n/a	40.09	2.52	−1.16		

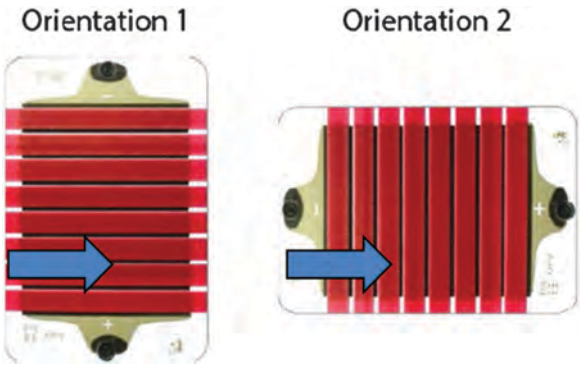

Fig. 2 Two orientations were measured when tiling the sample for IV measurements under AM1.5G illumination and LBIC measurements. The arrow indicates the side of the module which was tilted upwards.

Module A is the only other corrugated module to show an increase in efficiency, when the module is tilted; but only at orientation 2, with a relative effective PCE enhancement of 1.2% (at 20°) and 12.9% (at 45°). The relative enhancement seen at 20° is low, indicating that using this geometry works most effectively at oblique angles, in agreement with similar reports of 'V-shaped' OPVs.[17] Module A perform worst at orientation 1, as the module is likely to experience increased shading losses as it is tilted. At orientation 1, as the module is tilted, a slight increase of 2.3% in effective PCE is observed (at 20°). At 45° tilt, the raised topography of the corrugation shades the active area in shallow regions, leading to a 10.8% decrease in PCE compared to the flat profile module.

3.2 LBIC testing

Fig. 3 shows the LBIC images of modules A–D, which were undertaken in order to investigate the homogeneity of photocurrent generation across the four modules.

Module B indicates the most uniform current generation across the photoactive areas. This indicates that very little variation in reflection or photo-generation losses occur when the OPV is laminated onto this surface. The module performs optically and electrically very similar to the flat module, despite the curved nature of the substrate with very little spatial difference in photocurrent generation. Module A exhibits a slightly different trend, with the photocurrent at the edges and middle of the module slightly reduced. Interestingly, there appears to be two regions running perpendicular to the monolithic cells which show elevated photocurrent generation. These two regions correspond to the sharpest curvature of the solar cell (~50° to the normal). Whilst some of the laser beam will couple into the solar cell at this point, a large proportion is reflected off the module and guided to the bottom of the trench, where the light

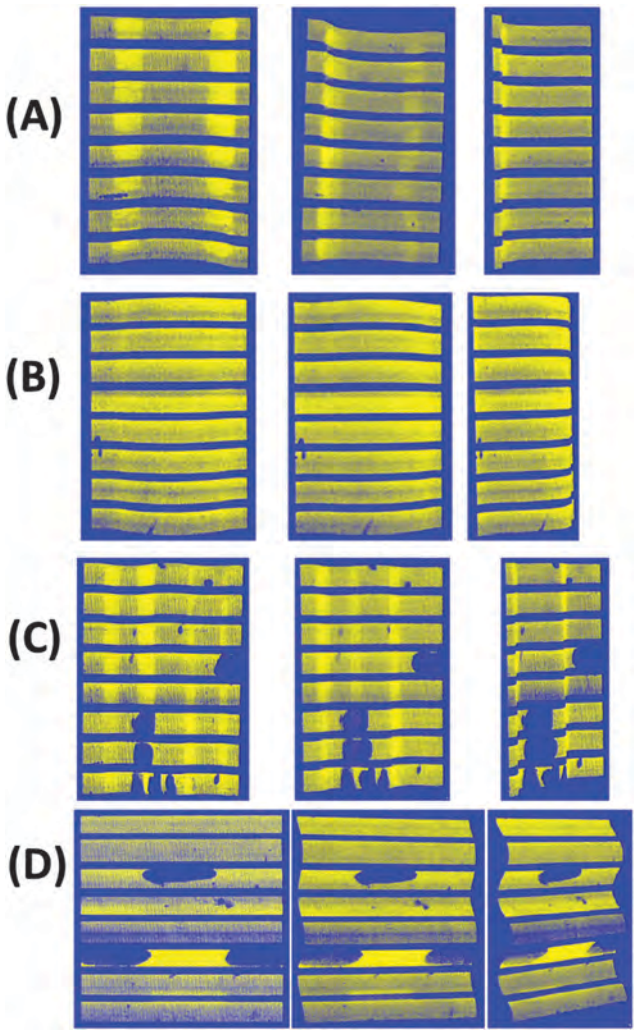

Fig. 3 Laser Beam Induced Current (LBIC) image of module A, B, C and D showing the photocurrent extraction across the module area. Bright yellow represents the area of greatest current extra, while blue represents the lowest current. The dark spots in modules C and D indicate delamination faults. The modules were measured with tilt occurring in the direction of orientation 1.

is then coupled into the module, however the enhancement in LBIC reading is measured at the point of reflection. This light trapping effect only appears to occur where the gradient of the module surface is at its steepest and reflection is maximal.

The LBIC images of module C and D show major defects on the sample surfaces and provide explanation for the lower efficiencies discussed in Section 3.1. The size and shape of these defects indicate severe delamination has occurred within these modules during the preparation where the solar cell is forced to comply with the corrugated surface. Modules C and D are mounted on substrates that possess smaller corrugated profiles and therefore experience much greater bend stressing, due to the smaller bend radius. This smaller bend radius appears to be the root cause of these faults as they are not observed on modules A and B, even after outdoor testing in Section 3.4. Whilst the modules used for these tests appear stable from cyclic bend tests, the stresses experienced by the modules in this work are physically different; the strain in this case is prolonged and the module is stressed in a fixed position. This is an interesting result for the OPV community and indicates that both cyclic and static bending testing should be considered when testing the flexibility of modules for their compliance with non-planar surfaces. The reproducibility of these delamination issues is confirmed from additional measurements which are available in ESI-3.†

3.3 Indoor angular testing

In order to better understand the PV module performance with angular changes, indoor PV cell testing was conducted on modules A and B. Modules C and D were excluded from these measurements due to the poor initial performance observed. Each module was measured across a range of pitch and yaw values in order to evaluate how the module would perform at different angles of incidence (see Fig. 4(a)). By varying the yaw of the light source, evaluation of the PV cell response to the diurnal passage of light was possible. Variation of the pitch allowed for simulation of the seasonal variation, latitude or tilt of the module.

Fig. 4(b) shows the effective PCE of a flat module as the pitch and yaw values are varied. As expected, the PCE is maximised when the irradiated at normal incidence. As the position of the light source is varied by altering the pitch and yaw, the PCE decreases as a function of angle. It is worth noting that the efficiency is lower due to the spectral mismatch between the halogen lamp source and the standard AM1.5G spectrum, leading to a lower effective PCE than measured in Section 3.2.

The effective PCE of module A and B as a function of pitch and yaw are shown in Fig. 5(a) and (b), respectively. The trend in PCE as pitch and yaw are varied is significantly different to the profile of the flat module, with greater PCE observed at both oblique angles of pitch and yaw. This is seen more clearly when viewing the relative enhancement of effective PCE in module A and B in comparison to the flat module, shown in Fig. 5(c) and (d), respectively. Each module as measured flat before being laminated and this showed that at angles of incidence close to normal (pitch = 0°, yaw = 90°), the relative enhancement in comparison to the flat module is small (module A = +15%, module B = +16%)

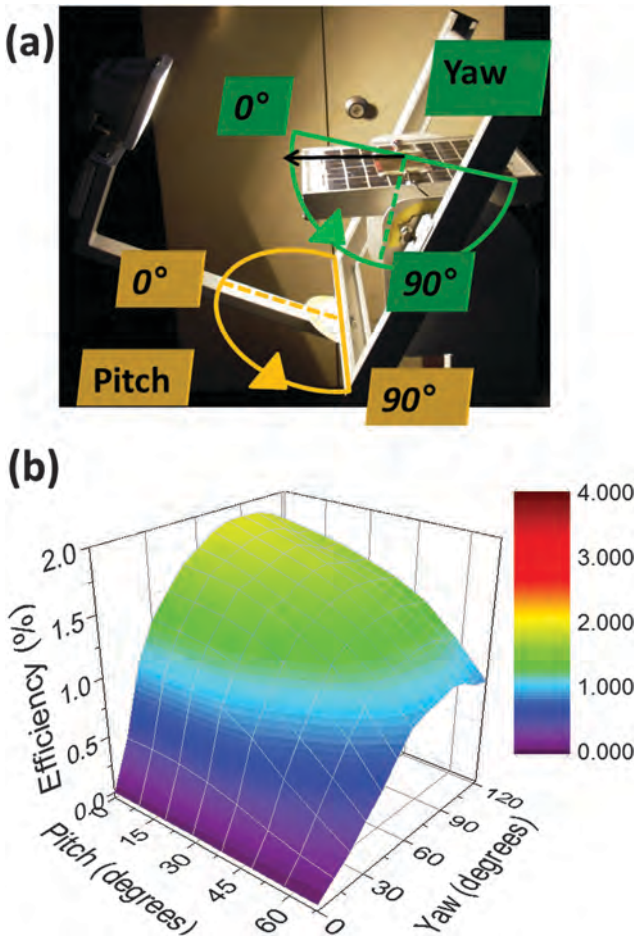

Fig. 4 (a) Experimental setup for measuring the OPV as a function of angle. By varying the yaw of the light source, evaluation of the solar cell response to the diurnal passage of light is possible. Variation of the pitch allows for simulation of the seasonal variation, latitude or tilt of the module. The performance of a flat/reference module is shown in (b), with the best efficiency seen at normal incidence.

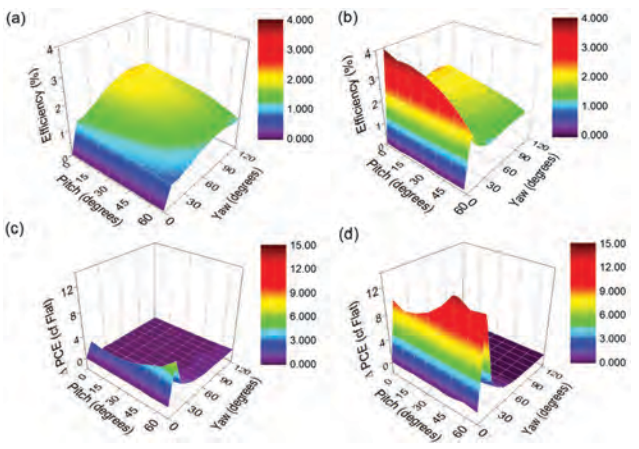

Fig. 5 Performance of (a) module A and (b) module B as a function of pitch and yaw, to evaluate power conversion efficiency at a variety of illumination angles. The relative enhancement when compared to a flat module is shown from modules A and B in (c) and (d), respectively.

and related to the reduction in module footprint. Considering first of all the variation in yaw; for modules A and B, the relative efficiency enhancement is relatively constant as the angle of yaw increases away from the normal, until a spike as the angle of incidence reaches at 70° away from normal (yaw = 20°). At this point, the efficiency of the OPV rapidly increases. For module B, this represents a 10-fold enhancement in PCE over the flat module, whereas module A sees nearly a 3-fold enhancement in PCE.

Interestingly, the greatest enhancement is seen when there is a combination of tilt in both directions. This is an interesting observation and shows that the corrugation could have major benefits when geographically positioning the modules at high angles of latitude such as in the UK or in Scandinavia. A similar report on macrostructured solar cells by Bernardi *et al.* supports the view that oblique angle irradiation in both angles leads to the most substantial relative enhancements.[18] At these latitudes, solar insolation is rarely at normal incidence, even at noon time. In the case of module A, this occurs when pitch = 60°, yaw = 20°, which leads to a relative enhancement of 6×. For module B, this occurs at yaw = 50°, pitch = 10°, which leads to a 15× relative enhancement. Further data confirming the reproducibility of these measurements is shown in ESI-4.†

The photocurrent generation characteristics under oblique angle are consistent with other reports.[19,20] Considering first of all the flat module in Fig. 4(a); at low incidents of angle, Fresnel reflection losses become significant as a result of the refractive index mismatch between PET and the air. This limits the in-coupling of radiation and subsequent photo-generation, which is confirmed from optical ray tracing in ESI-5.† Based upon this optical simulation, as the incident angle increases from 0° to 85°, the reflection losses increases from 12% to 85% (at wavelength, λ = 550 nm). When the light trapping characteristics of the corrugated modules are examined, it is clear that the Fresnel reflection losses are not as profound; due to a higher proportion of light that is close to normal with respect to the module. Ray tracing (shown in ESI-5†) indicates that a 9× enhancement in performance is possible using a corrugated module over a flat one at oblique angles, which is in close agreement with the experimental data.

3.4 Outdoor testing

Outdoor performance of modules A, B and the flat (reference) were monitored for four weeks during summer 2015 (start date: 13/05/2015). For this measurement campaign, all modules were inclined and mounted at the optimum angle (36°) for PV panels at the latitude of Bangor, North Wales (53° N).[21] Initially, two contrasting days were used to compare relative OPV performance of the 3D modules with that of a flat module. The 10th June (a sunny day with high Direct Normal Irradiance) and the 22nd May (an overcast day with largely diffuse sunlight) were selected and daily irradiance is shown in Fig. 6(a) and (b), which was measured using a calibrated reference cells mounted in-plane to the panels and horizontally. A direct comparison between the performances of the different geometries under diffuse and direct irradiation could be made. As the experiments were conducted reasonably close to one another, the effects of module degradation and changes to sun position are not considered to be significant.

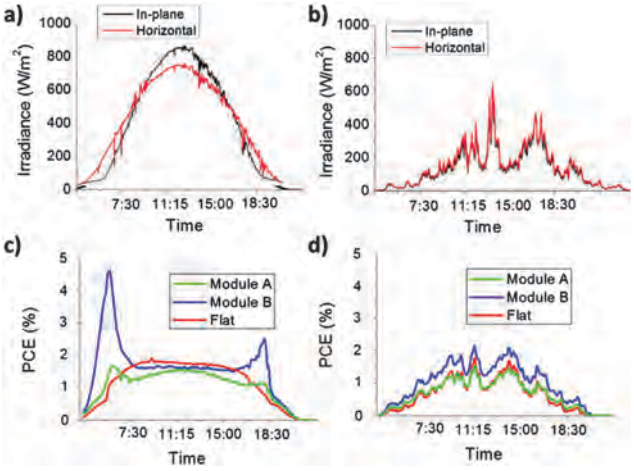

Fig. 6 Diurnal irradiance for the (a) 10th June 2015 ('sunny' day) and (b) 22nd May 2015 ('diffuse' day). The corresponding diurnal outdoor performance of module A, B and the flat cell during the sunny and diffuse day is shown in (c) and (d), respectively.

Considering the data for the 10th June [Fig. 6(a) and (c)], this represents a day of strong direct irradiation and where maximum horizontal daily irradiance reaches 950 W m^{-2} and total irradiance is measured at 8.1 kW h m^{-2}. The average and maximum ambient temperatures were measured at 14.3 °C and 17.2 °C. The flat module exhibits the diurnal performance that is typically observed from an OPV cell.[16] As the short circuit current (I_{SC}) of an OPV module is linearly dependent on irradiance, the effective PCE is determined primarily by variations in V_{OC} and FF. However, as V_{OC} and FF are relatively constant over the course of the day, the effective PCE is also approximately constant from 8 am to 5 pm.

In stark contrast, module B exhibits significantly improved PCE under oblique angles, which occur in the early morning and late evening, as seen in Fig. 6(c). Considering the time of the measurement and angle of the sun relative to the modules at these points of the day, these increases are consistent with the indoor data from Section 3.3. Module B exhibits a 4.2-fold enhancement in efficiency over the flat module, and PCE rises up to a maximum efficiency of 4.7%. The primary reason for this increase in effective PCE is due to increased I_{SC}, which is related to reduced reflection and thus improved light capture. Whilst this enhancement is substantial, it is lower than predicted from the data in Section 3.3. This could be due to a number of reasons including different spectral characteristics at early morning/late evening and shadowing due to nearby mountains close to the horizon. Nevertheless, this enhancement is substantial and represents a real benefit that 3D OPVs can have in ensuring that renewable PV electricity generation is more evenly spread over the course of the day. The enhancement witnessed in the evening period (4 pm–7 pm) is lower (~3-fold increase) due to slightly cloudier conditions during this time period, as observed in Fig. 6(a). This improved output in the evening is particularly significant as this time frame

corresponds to peak demand in the electricity grid when electricity tariff rates are at their highest. Module A exhibits a similar diurnal trend as module B, however, the relative enhancements seen in peak performance are not as great as module A, in agreement with the data from Section 3.3. Despite an average of 2 modules, the degradation in the modules used for A appears slightly greater, so overall daily performance is slightly lower than can be anticipated from AM1.5G measurements (Section 3.1).

Considering data from the 22nd May [Fig. 6(b) and (d)], where the irradiation levels are much lower, and mainly diffuse (2.4 kW h m^{-2}), as shown from the close overlap in the horizontal and in-plane irradiance data. Ambient temperatures are also slightly lower, with an average and maximum ambient temperatures of 13.4 °C and 15.0 °C. As OPVs possess a positive temperature coefficient, the effective PCE over the course of the day is reduced; for example the flat module exhibits an average effective PCE of 1.3% from 11 am–1 pm (22nd May), which compares to 1.8% over the same time period on the 10th June. During the 22nd May, the substantial enhancements at oblique angle incident light are not observed as the light during these time periods is not directly incident on the active area of the cell. However, it is apparent that the module B outperforms the flat module significantly over the entire day. In addition, module A appears to match more closely the performance of the flat module. The reproducibility of the diurnal outdoor data is confirmed by measurements across two additional measurement periods, with the data summarised in ESI-6.†

To provide a more conclusive understanding of the performance, the average daily PV yield was measured over the 4 week test period. The daily performance was categorised into diffuse, sunny or intermediate by considering the solar insolation levels relative to the nominal maximum daily irradiation for May–June in Bangor, Gwynedd, UK. Diffuse conditions were defined as days where daily insolation was $<40\%$, sunny days $\geq 80\%$ and intermediate days were classed as $\geq 40\%$ and $<80\%$ of the nominal maximum value. The data is summarised in Table 3 and it can be seen that module B outperforms the flat module within each type of irradiation category. On sunny days, module B outperforms the flat module due to the better oblique angle performance and lower footprint, leading to a relative enhancement of +17%. It also outperforms the flat module on diffuse days and interestingly, the relative enhancement module B increases under more diffuse conditions, rising to +29% relative enhancements. This result is particularly significant for northern latitude countries, where diffuse conditions are more predominant. One of the apparent benefits of the 3D OPVs appears to be the improved performance at morning/evening periods. This is particularly important in Western countries corresponding to sustained periods where electricity demand is significantly higher than average levels. Peak demand fluctuations may occur on daily and seasonal basis but in the UK this occurs from 1630–1930 and during this time retail electricity prices are elevated for many consumers.[22] Table 3 shows the average PV yield from a flat module and module A and B during this period. During this period, module B shows a 55–60% enhancement in yield over a flat module, from outdoor performance monitoring over a 4 week period (start date: 21/05/2015). This demonstrates another added benefit of the 3D module and could provide a means for significantly reducing the need for fossil fuel back-up on the grid and subsequent carbon dioxide (CO_2) emissions. Again, module A does not exhibit an increase in performance compared with the flat module, although the overall trends appear similar to module B.

Table 3 The average daily and peak-period yield from outdoor performance monitoring over a 4 week period (start date: 13/05/2015). The relative change in efficiency, compared to the flat module is shown in brackets

		Flat	Module A	Module B
Average daily yield (mW h cm^{-2})	Sunny	12.02	9.83 (−19%)	14.07 (+17%)
	Intermediate	6.34	5.37 (−15%)	7.67 (+21%)
	Diffuse	1.92	1.92 (0%)	2.48 (+29%)
Average yield at peak periods (1630–1930 pm) [mW h cm^{-2}]	Sunny	0.84	0.69 (−14%)	1.28 (+55%)
	Intermediate	0.73	0.62 (−11%)	1.15 (+57%)
	Diffuse	0.26	0.31 (−9%)	0.36 (+60%)

4. Conclusions

The application of OPV cells as BIPVs using corrugated roof cladding has been undertaken. The 3-dimensional form of the cladding provides three distinct advantages for OPV deployment. Firstly, the 'footprint' of the solar cell is reduced, which leads to improved power output or efficiency per unit area of roofing. This was demonstrated with indoor measurements conducted under AM1.5G illumination and it was shown that the effective PCE could be enhanced by $\sim$10% by using the convex design of module B. The second advantage is the substantially enhanced performance under oblique angle irradiation, leading to increased output in the early morning and evening. Indoor characterisation showed a 9-fold enhancement in efficiency was obtainable, when compared to a reference cell. Outdoor performance monitoring supported this enhancement, where a reduced, but still very significant, 4.5-fold enhancement in effective PCE was observed. A number of organisations have investigated the use of macro-structures to enhance oblique angle performance including 'V-shaped' OPVs[17] and cylindrical shaped PVs, such as those developed by Solyndra Inc. To our knowledge, this is the first time this enhancement has been reported by utilising an existing building substrate, which can be directly integrated into new buildings or retrofitted to existing ones.

The third advantage of the 3D architecture was the improvement in performance under diffuse lighting conditions, when compared to a flat module. Geographically, the 3D module appears to be well-suited to countries with a high latitude, due to the enhanced diffuse light levels and the fact that tilting the module in both 'latitude' and 'longitude' directions away from normal, leads to the best achievable enhancement in solar cell performance. The enhancement in performance of module B during the hours that correspond to peak demand is significant where a 60% enhancement is solar yield is measured.

Modules C and D showed significantly worse performance, which was equated to delamination faults due to the high mechanical stress experienced when laminating onto smaller corrugated structures.

Whilst this work focused on corrugated PVC roof structures that are currently available to purchase, optimised designs specifically for BIPVs could be developed that further improve the direct angle performance or enhancement under oblique irradiation. Potentially, better design of the corrugations might lead to a greater enhancement in the normal and oblique angle performance and manufacture of different 3D designs should be relatively easy to do as poly vinyl chloride (PVC) is a mouldable thermoplastic. Currently, there are few PV technologies that possess the flexibility of an OPV module. The approach set out in this paper could yield a product that has profound advantages over existing BIPV products or conventional inorganic solar cell technologies, in particular for countries at higher angles of latitudes.

Acknowledgements

JK would like to thank Sêr Cymru national research network in Advanced Engineering and Materials.

References

1 N. Espinosa, M. Hösel, D. Angmo and F. C. Krebs, Solar cells with one-day energy payback for the factories of the future, *Energy Environ. Sci.*, 2012, **5**(1), 5117–5132.
2 H. Zhou, Y. Zhang, C. Mai, S. Collins, G. Bazan, T. Nguyen and A. Heeger, *Adv. Mater.*, 2015, **27**, 1767.
3 S. Lizin, S. van Passel, E. de Schepper and L. Vranken, *Sol. Energy Mater. Sol. Cells*, 2012, **103**, 1.
4 B. van der Wiel, H. Egelhaaf, H. Issa, M. Roos and N. Henze, *MRS Online Proc. Libr.*, 2014, **1639**, 13.
5 G. Gunjan, ''Global Solar Power Market'', Frost & Sullivan, 26 Jun 2014.
6 S. Darling and F. You, *RSC Adv.*, 2013, **3**, 17633.
7 P. Heinstein, C. Ballif and L. Perret-Aebi, *Green*, 2013, **3**, 125.
8 Transparency market research, ''Building Integrated Photovoltaics (BIPV) Market: Global Industry Analysis, Size, Share, Growth, Trends and Forecast, 2013 – 2019'', published date: 2014-04-25.
9 P. Berdahl, H. Akbari, R. Levinson and W. Miller, *Construct. Build. Mater.*, 2008, **22**, 423.
10 S. Gevorgyan, M. Madsen, H. Dam, M. Jørgensen, C. Fell, K. Anderson and B. Duck, *et al.*, *Sol. Energy Mater. Sol. Cells*, 2013, **116**, 187.
11 F. Krebs, M. Hösel, M. Corazza, B. Roth, M. Madsen, S. Gevorgyan, R. Søndergaard, D. Karg and M. Jørgensen, *Energy Technol.*, 2013, **1**, 378.
12 M. Hösel, D. Angmo, R. Søndergaard, G. dos Reis Benatto, J. Carlé, M. Jørgensen and F. Krebs, *Adv. Sci.*, 2014, **1**, 1400002.
13 L. Andrés, M. Fe Menéndez, D. Gómez, A. Martínez, N. Bristow, J. Kettle, A. Menéndez and B. Ruiz, *Nanotechnology*, 2015, **26**, 265201.
14 F. Krebs and M. Jørgensen, *Adv. Opt. Mater.*, 2014, **2**, 465.
15 M. Reese, S. Gevorgyan, M. Jørgensen, E. Bundgaard, S. Kurtz, D. Ginley and D. Olson, *et al.*, *Sol. Energy Mater. Sol. Cells*, 2011, **95**, 1253.
16 N. Bristow and J. Kettle, *J. Renewable Sustainable Energy*, 2015, **7**(1), 013111.
17 S. Rim, S. Zhao, S. Scully, M. McGehee and P. Peumans, *Appl. Phys. Lett.*, 2007, **91**(24), 243501.
18 A. Bernardi, M. N. Ferralis, J. H. Wan, R. Villalon and J. C. Grossman, *Energy Environ. Sci.*, 2012, **5**, 6880–6884.
19 J. Kettle, A. Rees, E. B. Brousseau and M. Horie, *J. Phys. D: Appl. Phys.*, 2013, **46**(10), 105102.
20 S. Y. Chuang, C. C. Yu, H. L. Chen, W. F. Su and C. W. Chen, *Sol. Energy Mater. Sol. Cells*, 2011, **95**(8), 2141–2150.
21 Data sourced from PVGis – JRC on 20/6/15 (http://re.jrc.ec.europa.eu/pvgis/apps4/pvest.php).
22 A. Roscoe and G. Ault, *IET Renewable Power Generation*, 2010, **4**, 369.

High-Volume Processed, ITO-Free Superstrates and Substrates for Roll-to-Roll Development of Organic Electronics

*Markus Hösel, Dechan Angmo, Roar R. Søndergaard, Gisele A. dos Reis Benatto, Jon E. Carlé, Mikkel Jørgensen, and Frederik C. Krebs**

The fabrication of substrates and superstrates prepared by scalable roll-to-roll methods is reviewed. The substrates and superstrates that act as the flexible carrier for the processing of functional organic electronic devices are an essential component, and proposals are made about how the general availability of various forms of these materials is needed to accelerate the development of the field of organic electronics. The initial development of the replacement of indium-tin-oxide (ITO) for the flexible carrier materials is described and a description of how roll-to-roll processing development led to simplification from an initially complex make-up to higher performing materials through a more simple process is also presented. This process intensification through process simplification is viewed as a central strategy for upscaling, increasing throughput, performance, and cost reduction.

1. Introduction

The majority of current optoelectronic devices such as organic and polymer solar cells (OPVs) and organic light emitting diodes (OLEDs) are fabricated on glass carriers or small plastic sheets using a variety of fabrication processes for each of the functional layers including the electrodes, either semi-transparent or opaque. The most used transparent conductive electrode and carrier material is the combination of indium tin oxide (ITO) and glass with a share of over 95% throughout the scientific community.[1] Spin coating and subtractive patterning are commonly used for laboratory demonstrations and deliver impressive results for all the device-specific parameters but most of the processes lack the scalability for an industrially relevant fabrication procedure. On the other hand, it is often claimed that the future of (organic) optoelectronic devices will be made on plastic and in large-scale entirely through low-cost roll-to-roll (R2R) processes using multidimensional solution-based printing and coating processes. Only a limited number of reports exist where such an upscaled manufacturing procedure is presented for some of the functional layers.[2–6] OPV devices in which all layers including front and back electrodes are fully R2R solution processed are still the minority.[7–11] It should be mentioned that a lot of reports on organic (opto-) electronic devices have been published that employ and describe fabrication methods other than spin coating such as gravure, inkjet, spray coating, and doctor blading, but the proof of the ultimate upscaling potential is very limited.[12–14] So far, all reports on large-scale processed devices are also far removed from the record-breaking efficiencies, where the device sizes are most often significantly below 1 cm^2 with power outputs too low to be usable.[1] The most plausible reason is the lack of R2R equipment and the availability of active materials in high quantity, which is understandable, but also lack of suitable carrier materials with conductive electrodes (either transparent or opaque) in sufficient quantity, quality and layout to enable process development and fabrication of a reasonable amount of devices in large scale and area.

The development of R2R or sheet-based large-scale processes[15] for any given organic electronics product will by nature require availability of patterned and conductive carrier material in significant amounts. Ideally rolls of several hundreds of meters to kilometers will be needed initially and in the case where one wishes to explore subsequent processes with web speeds of 10 m min^{-1} or higher many kilometers will be needed. In addition to a high cost being a limiting factor the dependence upon a supplier of the base material is a clear limitation. From this point of view processes and techniques for in-house manufacture or outsourcing to local manufacturers of basic electrode structures are needed to ensure rapid development of processes and processing methods for printed electronics.

To date, almost all of the available publications on organic optoelectronics devices use the term "substrate" for the carrier on which the electrode and device is built. Although this is technically not wrong, the functional layers are deposited on

Dr. M. Hösel, Dr. D. Angmo, Dr. R. R. Søndergaard, G. A. dos Reis Benatto, Dr. J. E. Carlé, Dr. M. Jørgensen, Prof. F. C. Krebs
Department of Energy Conversion and Storage
Technical University of Denmark
Frederiksborgvej 399, DK-4000, Roskilde, Denmark
E-mail: frkr@dtu.dk

DOI: 10.1002/advs.201400002

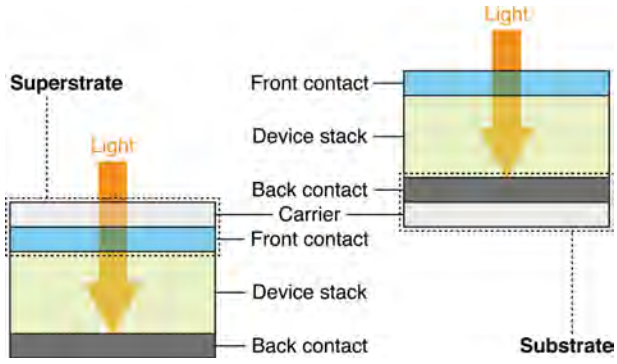

Figure 1. Simplified device stack of an OPV device to show the distinction between superstrate and substrate. Superstrates include a transparent conductive front contact, whereby substrates are the carriers with the back contact, either opaque or transparent.

the carrier below (Latin sub = behind, under), it is often not the correct terminology in the final device as it is operated. In this case, substrates are behind the functional layer stack where the light does not necessarily need to pass through the substrate. It can be opaque and its main function is electrical conductivity. The majority of semitransparent conductive electrode carrier structures in optoelectronic devices such as OPVs or OLEDs act as superstrate (Latin super = above, on), which are located between the sun (eye) and the functional layer stack. Therefore the superstrate is the carrier combined with the transparent conductive electrode layer where the light is supposed to pass the functional film (i.e., in case of a solar cell) or to reach the eye of the user if emitted from the functional film (i.e., in the case of a light emitting device). A schematic of the distinction between sub- and superstrates for optoelectronic devices (for an organic solar cell) is illustrated in **Figure 1**.

Here, we describe how kilometers of superstrates and substrates with semitransparent or opaque electrode structures can be prepared at high speed and we demonstrate how they can be used for manufacture of polymer solar cell devices and modules on a large scale. After a brief review of electrode structures in the literature, we describe the equipment needed, the ink quantities needed, and the time it actually takes to develop a new electrode structure suitable for large-scale processing. Once the initial challenge for finding a process and an ink system for a given machine has been surmounted, we describe how simple it is to alter patterns to suit further development needs. We further assess each of the presented superstrate and substrate strategies with respect to their technical parameters and simplicity in fabrication. The manufacturing of sample devices on each of the electrode structures concludes this report.

2. Electrode Materials – the Current Status

Conductive carrier structures for optoelectronic devices are the fundamental element of any organic optoelectronic device. The most common material for the subsequent electrode deposition is rigid glass but materials such as polyethylene terephthalate (PET) or polyethylene naphthalate (PEN) in the form of thin flexible foils are the only that can be easily used in R2R machinery.

Frederik C. Krebs is currently professor and Head of Section for Solar Energy at the Technical University of Denmark (DTU) with research focus on flexible organic electronics and foil based systems, their manufacture and processing (electrochromics, organic power transistors, thermoelectrics, PEMFCs, photocatalysts, light emitting devices, solar cells). In the context of transparent electrodes interests in addition to teaching include synthesis of new materials, stability, ink development, process development, advanced device structures, roll-to-roll processing, large scale manufacture, product integration, lifecycle analysis, recycling, installation, and operation.

ITO is the most used transparent conductive electrode for all of the organic optoelectronic devices and is used in 95% of all fabricated devices; it can be seen as the standard.[1] The OLED and touchscreen market also demands a majority of ITO. The scarcity and localized mining of indium have led to fluctuations and a general increase in cost over the recent years and have opened the quest for alternative electrodes.[16] Furthermore, the high embodied energy[17] due to vacuum sputtering processes and the poor mechanical properties and brittleness[18–20] has driven researchers to find new materials and processes with comparable or superior properties. In the case of a superstrate structure, the electrode should have a low sheet resistance combined with a high transparency to enable efficient current flow and large device areas. In case of flexible OPV devices with ITO-PET superstrates the typical sheet resistance is in the range of 50 to 60 Ω sq^{-1}, which limits the cell sizes.[21] ITO glass allows lower sheet resistances and is commonly used in laboratory-scale test devices with limited upscaling potential.

A huge variety of alternative electrode structures for OPV superstrates have emerged, based on conductive polymers such as poly(3,4-ethylene dioxythiophene):polystyrene (PEDOT:PSS), hybrid structures with metal grid and conductive polymers, metal nanowires (NW), ultrathin metals, carbon nanotubes, and graphene. An overview of optoelectronic devices with these superstrate electrodes is listed in **Table 1**; the table only shows a selection of publications. The entire spectrum of transparent electrode superstrate structures is covered elsewhere in more detailed review.[22–24] In case the device structure does not require a transparent conductive carrier the light has to pass the last deposited layer as previously shown in Figure 1. Hereby, the conductive substrate structure can be made from metal such as silver, or multilayer metal stacks from aluminum, titanium, and chromium on PET, glass, or paper. Steel has also been used as a conductive back contact layer that acts simultaneously as a carrier material in the form of steel foil. An overview with a selection of publications on organic optoelectronic devices with conductive opaque substrates is listed in **Table 2**.

Table 1. Overview of several organic optoelectronic devices with transparent conductive superstrate carrier structures.

Superstrate										
Carrier	Material	Device	R_s [Ω sq^{-1}]	T [%]	OPV eff. [%]	Methods, electrode	A active [cm^2]	R2R?	Notes	Ref.
PET	AgNP	EL	4	95		IJ	0.2		coffee rings	[25]
PET	AgNP grid	EL	9	>75		Evap. litho				[26]
PET	MWCNT	EL	16 300	66.3		IJ, RC				[27]
Glass	Au grid	OLED	15	63		SC, Litho, EV	0.08		Au hex grid	[28]
Glass	AgNW, PEDOT:PSS	OLED	5.8	84		Spray, SC			laser patterning	[29]
PET	AgNP grid, PEDOT:PSS	OPV i	<12 (Ag)		1.7	IJ, SP	15.4	X	R2R flash	[30]
Glass	Graphene	OPV i	30	>85	>3.5					[31]
Glass	AgNW	OPV i	13–18	>90	2.3	SC	0.24			[32]
Polymer	AgNW	OPV i	16	82.3	3.07	SC, peel off	0.38		embedded	[33]
PET	Ag	OPV i	5	30	1.6	SD or SC	1	X	0.25% for full R2R module	[34]
PET	AgNP grid, PEDOT:PSS	OPV i	10.4	68	1.6	FL, SP	66	X	module	[35]
PET	AgNP grid, PEDOT:PSS	OPV i	<20	>60	2	FL, SP	147000	X	module	[10]
PET	AgNP grid, PEDOT:PSS	OPV i	10	82	1.92	R2R imprint, SP	6	X		[36]
PET	PEDOT:PSS	OPV i	220	80	3	SC	0.03			[37]
Glass	Ag mesh	OPV i	10	86	2.14	EV	0.09		Crack template	[38]
PET	Graphene, PEDOT:PSS	OPV n+i, OLED	<80	>80	>4.6	CVD, SC	0.126 (4)		etching and transfer	[39]
Plastic	Ag grid, PEDOT:PSS	OPV n	0.5 (Ag)	n/a	1	Soft litho, SC	0.08			[40]
Glass	Ag grid, PEDOT:PSS	OPV n	8.5 (Ag grid)	> 87	2.8	IJ, DB	0.09			[41]
PET	PEDOT:PSS	OPV n	230	75	2.2	SC	0.06			[42]
PEN	AgNP grid, PEDOT:PSS	OPV n	1 (Ag grid)		1.93	SP, SC	4		embedded	[43]
Glass	AgNP, PEDOT:PSS	OPV n	<<20		1.4	IJ	4			[44]
Glass	Mo, Al, Mo	OPV n	<<27		1.47	EV, IJ	4			[44]
PET	PEDOT:PSS	OPV n		90	2.8	SC	0.04			[45]
PET	PEDOT:PSS	OPV n	100		4.2	SC	0.1		PET 1.4 μm stretchable	[46]
PEN	AgNP grid, PEDOT:PSS	OPV n	4.8 (Ag)		1.54	IJ	4			[47]
PEN	AgNP grid, PEDOT:PSS	OPV n	500 (PEDOT:PSS)		1.38	IJ	4.92		Flash	[48]
Glass	PEDOT:PSS, GMS	OPV n	98	80	7.06	SC	0.1			[49]
Glass	PEDOT:PSS, ITO	OPV n	36	84	3.21	Spray, Sputter				[50]
Glass	AgNP grid, PEDOT:PSS	OPV n			1.94	IJ	0.09			[51]
PET, PEN	AgNP grid, PEDOT:PSS	OPV n	0.21 (Ag)	77.5	2.15	SP, SC	4	(X)	embedded	[52]
Glass	AgNP grid, PEDOT:PSS	OPV n		>77	2.54	IJ, DB	0.25		embedded	[53]
PET	AgNP grid, graphene	OPV n	11.5	74.5	2.9	IJ, CVD	0.046			[54]
Glass	Au grid, PEDOT:PTS	OPV n	<17 (Au)	>70	>3	EV, litho, SC	0.06			[55]
Glass	Graphene	OPV n	100 k–500 k	85–95	0.4	SC	0.008			[56]
PET	Graphene	OPV n	230	72	1.18	CVD	0.0075			[57]
PET	Cu mesh, PEDOT:PSS	OPV n	22	>70	2.1	NIL, EV	0.0078		R2R demo	[58]
P(VDF-TrFE)	Graphene	OPV n	70	87	2.07	CVD, SC, etch, transfer				[59]
Glass	CuNiNW	OPV n	36	80	4.9	RC, Ni plating				[60]
Glass	Graphene	OPV t	521	70	8.02	SC, Litho	0.04		mesh	[61]

Table 1. *Continued*

Superstrate										
Carrier	Material	Device	R_s [Ω sq^{-1}]	T [%]	OPV eff. [%]	Methods, electrode	A active [cm^2]	R2R?	Notes	Ref.
PET, PUA	AgNW, GO	PLED	14	88		RC, soaking	800		stretchable	[62]
PET	AgNP grid	EC	<5	82		Evap. litho			EC with WO_3	[63]
PET	AgNP grid	EC				FL, SC	4	(X)		[64]

i = inverted, n = normal, t = tandem, GO = graphene oxide, NP = nanoparticle, NW = nanowire, MWCNT = multiwall cabon nanotube, EL = electroluminescent device, EC = electrochromic device, IJ = inkjet, RC = rod coating, EV = evaporation, SC = spin coating, GP = gravure printing, SD = slot-die coating, SP = screen printing, CVD = chemical vapor deposition, NIL = nano imprint lithography, DB = doctor blading, FL = flexo printing, P(VDF-TrFE) = poly(vinylidene fluoride-co-trifluoroethylene), PUA = polyurethane acrylate.

The majority of conductive electrodes requires sputtering, evaporation, or spin coating and requires patterning processes for proper device manufacturing. Masked evaporation or subtractive post-processes for full layer coatings lead to material waste and prevents efficient upscaling. Although some of the alternative electrodes show impressive parameters, the fabrication is very challenging or devices are processed only on very small areas in the range of several square millimeters. Most of the electrodes are made in limited quantities only for the scientific experiment and the upscaling potential is often questionable or pending several developments in other areas. ITO is not highlighted in the overview because it is the standard superstrate and is commercially available. It can be purchased on glass, PET, etc. and structuring can be carried out in the lab through etching or laser ablation processes or made on request by the supplier, e.g., using R2R etching, stripping, and cleaning. In all cases a subtractive process is used and material is wasted.

The most efficient way to fabricate a conductive carrier material is by using only additive steps through defined printing or coating processes. In this case the functional material is only deposited where it is necessary and material waste can be fully avoided or minimized to a very low fraction with respect to fabrication volume. The highest output is expected through fast R2R processes. Possible large-scale methods for conductive structures include flexo-printing,[35,77–79] gravure printing and coating,[80–82] rotary screen printing,[35,83] inkjet printing,[47,84,85] or a variety of coating processes including slot-die coating, all of which can be performed in a full R2R process[34,71,86–88] Embedding conductive structures inside the carrier material is an interesting method to smooth the layer but needs more complex equipment in a full R2R process.[52,89]

Table 2. Overview over several organic optoelectronic devices with opaque conductive substrate carrier structures.

Substrate									
Carrier	Material	Device	R_s [Ω sq^{-1}]	OPV eff. [%]	Methods, electrode	A active [cm^2]	R2R?	Notes	Ref.
Glass	Al, Ag	OLED			EV	0.06			[65]
Glass	Al, Ti	OPV i		3.4	EV	0.08			[66]
PET	Al, Ti	OPV i		1.8	EV	4		metal wrap through	[66]
Steel	Ag	OPV i		1.73	EV	0.01			[67]
Glass	Ag	OPV i		2.5	EV	0.02			[68]
PET	Cr, Al, Cr	OPV i		2.2	Sputter	13.2			[69]
Paper	Zn, ZnO	OPV i		1.3	GP, transfer	0.09	X		[8]
Paper	Zn, ZnO	OPV i		4.1	GP, transfer	0.1	(X)	Optim. polymer + structure	[70]
PET	Cr, Al, Cr	OPV i		2.9	Sputter	1.1		shadow mask	[3]
PEN	AgNP	OPV i	0.01	0.3	SD	120	X	module	[71]
PET	Ag	OPV i	<1	2.6	SD	1	X		[72]
Glass	Al	OPV n		3.17	EV	25		monolithic	[73]
PET	Al	OPV n		2.8	EV	25		monolithic	[74]
Steel	Steel	OPV n	0.5	1.3		50		1 cm^2 illum.	[75]
Paper	Au	PD			EV				[76]

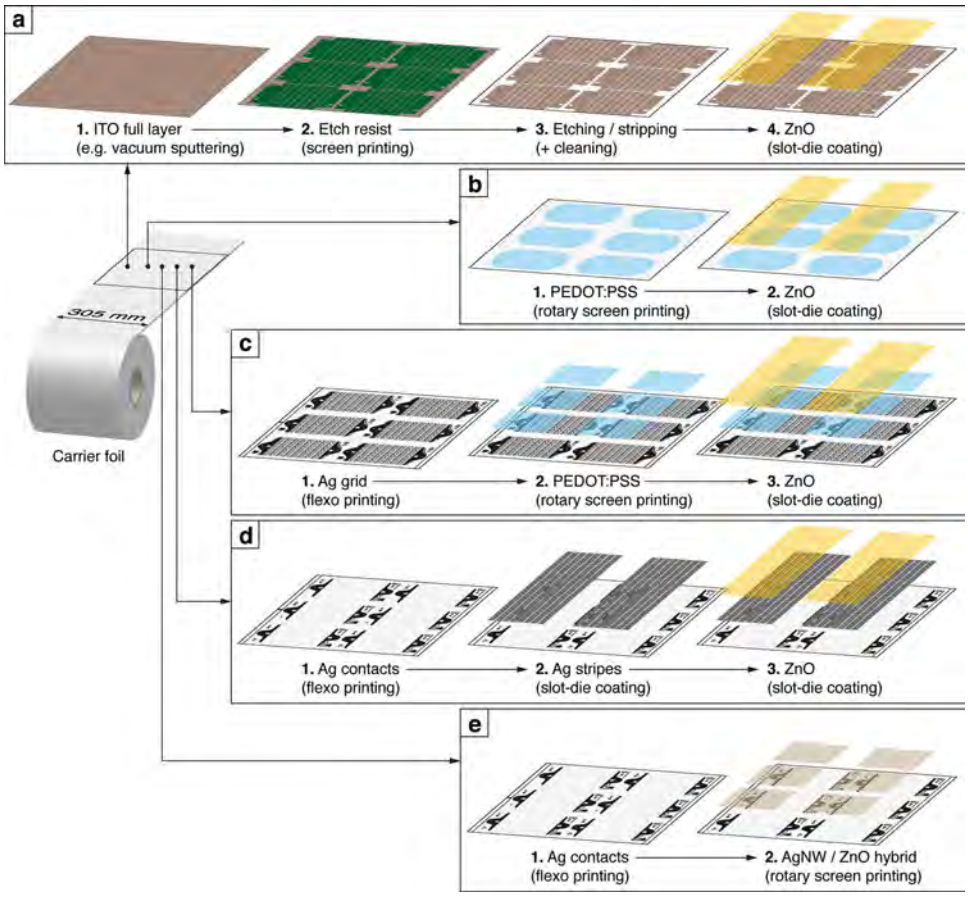

Figure 2. Fabrication workflow of patterned electron accepting superstrates with a) ITO/ZnO, b) PEDOT:PSS/ZnO, and c) silver grid/PEDOT:PSS/ZnO. d) An opaque full silver/ZnO substrate with additional printed silver contact electrodes. ZnO acts as electron transporting layer in all electrode configurations. The ultimate process simplification is reached with a hybrid AgNW/ZnO superstrate electrode that can be printed in a single printing step (e). Only outside contact are printed separately to improve device contacting.

3. Superstrates and Substrates for Everyone

This very brief review shows that there is much ongoing research in the field of conducting electrodes but most of the scientists still use ITO because no cheap alternatives are available in sufficent quantity that can be patterned entirely through additive processes. To show relevant results on large-scale processed devices the fundamental conductive substrate or superstrate is the first requirement, in addition to the availability of a highly efficient active layer material in large quantity. We believe that potential replacements for ITO and the methods of making them have to be made available to everyone in high volume; otherwise ITO will be replaced very slowly or perhaps never. Because the efficiencies of large-area and large-scale processed OPV devices are still low it requires very large areas to generate useful power output.[10] Even costly metals such as silver should be avoided or minimized, although it was shown that silver is highly recyclable.[90] Supporting metal grids can be justified for the optimization of current collection in larger single cells and for interconnection to modules,[10,91] but it might be unnecessary with a proper device design depending on the application.[92,93]

The fabrication steps and workflow of the proposed flexible superstrates and substrates with electron transport characteristics that we developed and process in our labs under ambient conditions are shown in **Figure 2**. Corresponding illustrations of a single module pattern with the size of a typical postcard are shown in **Figure 3**. The current designs are based on web widths of 305 mm and have six modules deposited per motif length of 12". The carrier material is a roll of pure PET or barrier foil when wishing to avoid further encapsulation of the corresponding device side. Fabrication of patterned ITO with fixed conductivity and transmittance, shown just for comparison, requires the most process steps and involves subtractive etching processes with high material loss. The entire process is typically outsourced to a specialized supplier who demands a desired pattern in digital form to fabricate screen printing masks for applying a positive mask before etching. The fabrication speed is rather slow and requires specialized machinery for handling the chemicals. Basic electrical and optical parameter change aside from the layout requires the etching of completely new rolls of ITO foil.

A superstrate with just two process steps is illustrated in Figure 2b, where highly conductive PEDOT:PSS is rotary screen

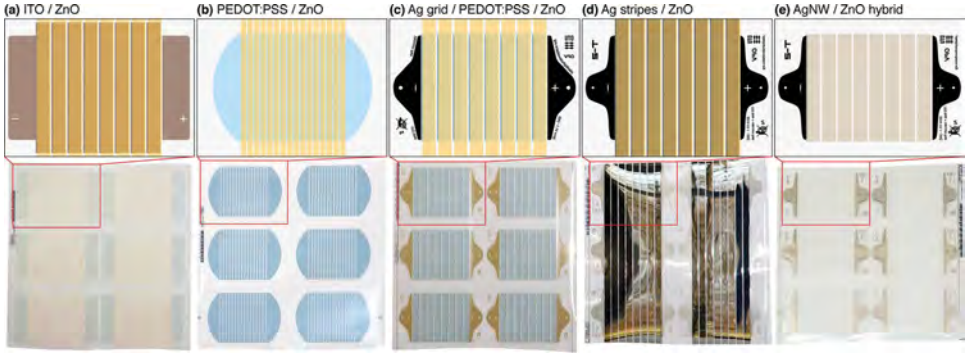

Figure 3. Postcard-sized module layout of the patterned superstrates with a) ITO, b) just PEDOT:PSS, and c) silver grid /PEDOT:PSS as conductive layer. An opaque substrate module layout with additional contact electrodes is shown in (d). The electron transporting ZnO layer is slot-die coated in panels (a–d). The hybrid AgNW/ZnO superstrate electrode (e) is fully printed without using slot-die processes. The top row shows a more detailed graphical illustration of the corresponding photographs of full 12" × 12" motifs in the bottom row.

printed and hole conducting ZnO is slot-die coated with a small lateral offset to enable contacting. Silver can be avoided due to 16 cells with a smaller width of just 4 mm, hereby the high fill factor (FF) is retained, instead of 8 cells with 10 mm width. The geometric fill factor also decreases. The active areas in a final module are in the range of 57 cm^2 for the 8-cell device or ca. 30 cm^2 for the 16-cell device. A supporting grid structure is not required for such small cell widths if sufficient highly conductive PEDOT:PSS is used. Outer electrodes for the final module connection are directly printed in the first step and coating of ZnO only needs lateral registration.[93]

The improved version for larger cell sizes employs an additional flexo-printed grid structure of silver nanoparticle (AgNP) ink prior to PEDOT:PSS and is shown in Figure 2c. Grid structures can range from hexagonal to diamond grid, or even parallel grid fingers, depending on the application and electrical layout. Our current version is based on 5° slanted grid fingers in the direction of the current flow and a grid pitch of 1.5 mm. Flexo-printing allows very fine structures below 100 µm. Outer electrodes are flexo-printed together with the grid electrode, while PEDOT:PSS is just printed in rectangular patterns over the individual cells. The PEDOT:PSS printing processes requires registration both in lateral and web directions. ZnO is slot-die coated in continuous stripes as usual with a slight lateral offset.[11]

OPV devices in a substrate structure do not require optical transmittance of the back contact. Full additive processing of slot-die coated reflecting silver stripes made from nanoparticle-free silver ink is shown in Figure 2d and Figure 3d. Studies also showed the possibility to R2R gravure print the full silver electrode stripes using commercial silver ink but the surface quality was poor compared to the slot-die coated electrode, mainly due to limitations in coating speed (2 m min^{-1}). External AgNP contacts and registration marks are flexo-printed prior to slot-die coating and allow for easy contacting in a final OPV module. Slot-die coated ZnO finalizes the electron conducting layer stack. Interestingly, the substrate can be easily transformed to a transparent superstrate stack by diluting the silver ink. Hereby the silver layer becomes semitransparent with some loss of conductivity.[34] The philosophy of pre-printed silver contacts and slot-die coated stripes of conducting ink is very practical for the fabrication of semi-patterned electrode structures for optoelectronic devices. Some inks, such as AgNW, CuNW, or special self-assembling ink mixtures, are still difficult to print directly into the necessary patterns (beyond stripes) and are often tailored for pure coating processes.

Nevertheless, we developed a process that allows printing AgNW and ZnO in a single run by using a hybrid ink mixture as illustrated Figure 2e and Figure 3e. This ultimate workflow simplification enables the fabrication of electron transporting superstrate electrodes in just one printing step while the outer contact silver electrodes are flexo-printed beforehand to allow proper device connection. They could of course be eliminated, thus enabling realization of a Flextrode in a single step (as opposed to three steps that are normally required for standard Flextrode).[35] Our ink formulations also allow separate printing of each component. Avoiding slot-die coating and using only printing processes results in the best material utilization for large-scale fabrication because the material is only deposited where it is necessary. The slot-die coating of ZnO in all other electrode workflow processes described before results in areas with unused material coverage. The hybrid process truly follows the "print only where needed" principle and allows free-form electrode layouts that are not limited to the well-known stripes from slot-die coating.

4. Experimental Workflow and Methods

Full layer ITO superstrate foil is produced through sputtering and used for further patterning that involves masking with etch resist, etching with aqueous copper chloride (or ferric chloride), stripping with sodium hydroxide, and washing with demineralized water. The exact process parameters such as fabrication speed are either confidential or not fully available. In the case of large scale manufacture of patterned ITO the overall process speed is significantly less than 1 m min^{-1}. Prior studies also revealed that ITO has a huge share of embodied energy with close to 87% in a final OPV device, which can be reduced significantly by using alternatives to ITO.[94]

The four replacements presented here are fabricated via all-additive processes with parameters listed in **Table 3**. The

Table 3. Process parameter for the R2R fabrication of ITO-free superstrates and substrates.

Material	Method	Speed [m min^{-1}]	Thickness [nm]	Drying
PEDOT:PSS/ZnO (superstrate, Figure 2b**)**				
PEDOT:PSS (Clevios PH1000 : IPA 10:3)	RSP	>10	≈400 (dry)	140 °C hot air + IR
ZnO in acetone	SD	10	≈100 (dry)	70/140 °C
AgNP grid/PEDOT:PSS/ZnO (superstrate, Figure 2c**)**				
AgNP (Nanopchem PFI-722)	FL	>20	≈200 (dry)	140 °C hot air + IR
PEDOT:PSS (Clevios PH1000 : IPA 10:3)	RSP	>10	≈200 (dry)	140 °C hot air + IR
ZnO in acetone	SD	10	≈100 (dry)	70/140 °C
AgNP contact/Ag full/ZnO (substrate, Figure 2d**)**				
AgNP (Nanopchem PFI-722)	FL	>20	≈200 (dry)	140 °C hot air + IR
Ag (Kunshan Hisense SC-100 : IPA 1:1)	SD	2	≈100 (dry)	140 °C hot air + IR
ZnO in acetone	SD	10	≈100 (dry)	70/140 °C
AgNP contact/AgNW/ZnO hybrid (superstrate, Figure 2e**)**				
AgNP (Nanopchem PFI-722)	FL	>20	≈200 (dry)	140 °C hot air + IR
AgNW/ZnO hybrid	RSP	15	≈100 (dry)	140 °C hot air + IR

fundamental carrier foils employed here were either PET (Melinex ST506, 125 µm) or Amcor barrier foil (50–70 µm). The three fabrication methods that are combined in different ways are flexo-printing (FL), rotary screen printing (RSP), and slot-die coating (SD), whereby the electrode fabrication workflow is illustrated in Figure 2. In brief, flexo-printing relies on a soft printing form where the raised parts define the image. Ink is transferred from a so-called anilox cylinder with a defined ink volume to the soft printing form and from there onto the foil using nip-induced surface interactions. Rotary screen printing employs a cylindrical mesh, in which the open parts define the printing pattern. An internal squeegee forces the ink or paste through the rotating mesh onto the foil. The wet layer thickness and printing definition are mainly defined by the mesh parameters. Slot-die coating employs a coating head with an internal ink distribution chamber, feed slot, and mask (shim) for coating stripes. The wet layer thickness of such a pre-metered process is based on ink flow rate, coating speed and coating width. All of the described printing and coating processes can go beyond 100 m min^{-1}, whereas the speeds in these studies are limited to around 10–20 m min^{-1} due to limited drying length (hot air and infrared (IR)) of the employed R2R equipment. Further details and photographs of the R2R machinery and individual process steps can be found elsewhere.[12,35,95]

OPV test cells and modules were fabricated using our standard procedures on a mini rollcoater[96–98] using slot-die coating of active layer and PEDOT:PSS electrode together with a flexo-printed Ag grid electrode, or in a full R2R process with slot-die coated active layer, rotary screen printed PEDOT:PSS, and rotary screen printed silver or carbon paste electrode.[11,93]

Transmittance and reflectance measurements were performed on a Shimadzu UV-3600 UV-VIS spectrometer. Reflectance and the transmittance for the AgNW/ZnO hybrid electrode were measured using an integrated sphere to collect all diffused and scattered light. Air was used as reference in all cases and transmittance values include the specific carrier substrate. The sheet resistances have been measured using a Jandel RM3 4-point station. Bending tests were carried out on a Mecmesin Multitest 2.5-i test bench and custom made data acquisition software to measure the resistance of electrode after each bend. The bending diameter for strain and compression tests was 10 mm. Solar cells were measured with a Keithley 2400 sourcemeter under a KHS 1200 solar simulator with an AM1.5G 1000 W m^{-2} intensity.

5. Results and Discussion

5.1. Optical Transmittance and Reflectance

All superstrates have in common that their transmittance in the visible range is high while the substrate described here has high specular reflectivity. The comparison of UV-vis spectrometer measurements for all electrodes is shown in **Figure 4**. The transmittance was measured for electrodes fabricated on a variety of carrier materials that have variable optical qualities. Normalization to the pure electrode was neglected because a real device cannot be made without a carrier that of course contributes to the final device performance. It also shows the variability of the electrode fabrication on different carriers. Furthermore, barrier foil was used with and without UV blocker, and therefore the region of interest for all transmittance values is from 400 nm and higher. The highest transmittance is presented by the AgNW/ZnO hybrid electrode with more than 88% transmission at 550 nm, which is better than ITO/ZnO along the entire visible spectrum. It presents a very optically neutral behavior with iridescence due to the AgNW. The plasmonic resonance of the AgNW also improves the transmittance and was

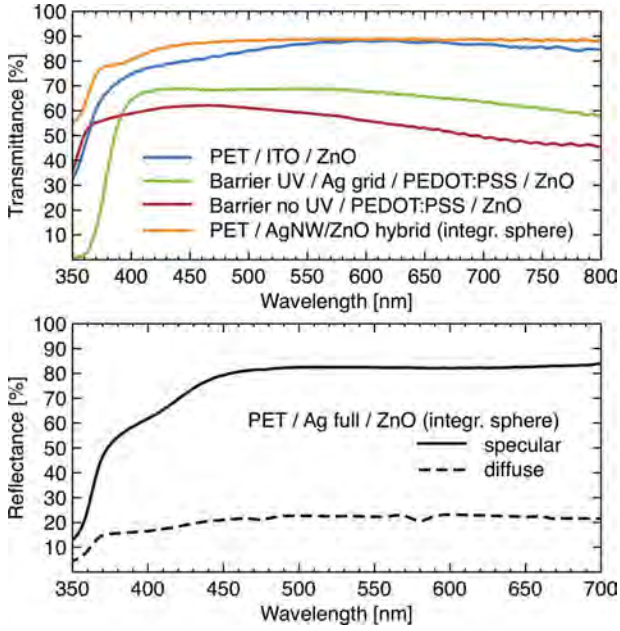

Figure 4. Transmittance (top) and reflectance (bottom) of five different electron conductive electrodes on a variety of carriers.

shown to be higher than the geometric aperture.[99] This electrode was measured using an integrating sphere to collect all scattered light. The other electrodes showed no substantial difference in the transmittance for measurements with or without integrating sphere.

The blue colored PEDOT:PSS based electrodes exhibit the typical drop in transmittance in the higher wavelengths and NIR range that makes them potentially less efficient for OPV devices with low bandgap polymer in the active layer. The electrode with supporting Ag grids has a transmittance close to 70% while the Ag grid-free electrode has a 10% lower transmittance. The main reason can be found in the thicker PEDOT:PSS layer to achieve a sheet resistance of 44 Ω sq^{-1} comparable to ITO. PEDOT:PSS electrodes with Ag grid support can tolerate less conductive and thinner films because the highly conductive Ag grid has the highest contribution to the conductivity in the electrode stack.

The opaque substrate studied here is a highly reflective electrode with a specular and diffuse reflectance >80% and >20% at 550 nm, respectively. This mirror-like behavior acts as backside reflector in an OPV and can largely contribute to an improved efficiency of the respective device.[72]

5.2. Flexibility

Flexible devices require highly flexible electrodes to tolerate mechanical stress not only during handling but also during the device fabrication using R2R machinery. ITO is known for its brittleness, which is also reflected here in the fast increase in sheet resistance after a couple of bending cycles as shown in **Figure 5**. The other electrodes are superior under bending stress and show no major performance loss even after 500 cycles.

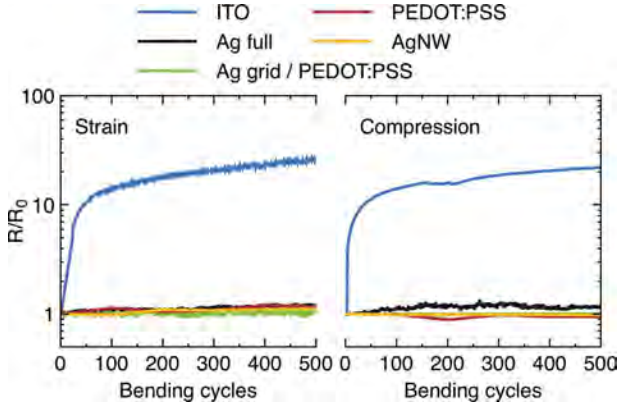

Figure 5. Bending test results for the electrodes shown for strain and compression over 500 bending cycles. The measured resistance R is normalized to the initial reference value R_0.

5.3. Process Workflow and Electrode Parameters

The best electrode with highest optical parameters and lowest sheet resistance is worthless if it is not processable on a large-scale for the desired application, such for OPV or OLED devices. The material usage and energy input during the fabrication has a high impact on the economy of the final device and should be considered from the beginning. Many incredible procedures for the fabrication of transparent electrodes can be found in the literature but most of them are only of academic value and are impossible (at least financially) to produce on a large scale. Despite the fact that patterning is often ignored, it would require subtractive processes that results in unnecessary material loss.

Our additive fabrication workflows shown in Figure 2 for ITO-free electrodes just require ordinary printing and coating equipment, which enables even local print shops to produce such printed electronics products without the need for making investments in highly specialized equipment. Research facilities investigating the processing of optoelectronic devices are also able to produce their own electrodes without dependence on an external supplier of etched ITO. Adjustments to the pattern or layout of the electrode can be made relatively fast to suit their own needs with a printing form supplier on hand. The density of such external services is much higher than finding an ITO etching service nearby. The key to the working electrode is the functional ink, of which the majority are already commercially available and optimized for the specific printing processes.

A comparison of the main characteristics of the five electron collecting electrode stacks in superstrate and substrate architecture is listed in **Table 4**. It is shown that all additive workflows require fewer process steps than the fabrication of patterned ITO with just two steps to the electron transport layer ZnO. The AgNW/ZnO hybrid electrode can be printed in just one step if the outer printed electrode is neglected. It also waives the use of slot-die coating and makes true free form devices possible.

Although all processes of the alternative electrodes are additive, they do involve material waste from the printing and coating processes. This can be substantially minimized when

Table 4. Comparison of the main characteristics of the five electron collecting electrode stacks in superstrate and substrate architecture.

	ITO/ZnO	Ag grid/PEDOT:PSS/ZnO	Ag full/ZnO	PEDOT:PSS/ZnO	AgNW/ZnO hybrid
Stack acronym		Flextrode	T2	SF	FLT
Type	Superstrate	Superstrate	Substrate	Superstrate	Superstrate
Additive	–	+	+	+	+
Printing required	+	+	+	+	+
Coating required	+	+	+	+	–
Vacuum required	+	–	–	–	–
Design freedom	– (stripe-like)	– (stripe-like)	– (stripe-like)	– (stripe-like)	+ (any shape)
# of steps to ETL (incl. outer contacts)	4	3	3	2	2
# of steps to ETL (excl. outer contacts)	4	3	2	2	1
Potential bifaciality	+	+	–	+	+
Transmittance including carrier (550 nm)	>86%	>68%	NA	>58%	>88%
NIR transmittance	+	–	NA	–	+
Iridescence	–	–	–	–	+
Sheet resistance	≈50 Ω/sq	<20 Ω/sq	≈575 mΩ/sq	≈44 Ω/sq	<20 Ω/sq
Flexibility	–	+	+	+	+

the continuous fabrication output is larger. The material waste due to unused ink and cleaning is the same if 10 m are printed or when or 10 km are printed, considering that all processes are optimized and controlled. The relative wastage is obviously much lower for large outputs than for small ones. Subtractive processes will have the same relative material waste independently of the output size and eventually require expensive recycling processes for all the material lost during patterning.

5.4. Device Examples

A selection of relevant *J–V* and *I–V* curves and parameters of sample OPV devices can be found in **Figure 6** and **Table 5**, respectively. The active layer polymers used were either standard P3HT or high performance low bandgap polymers in conjunction with PCBM as acceptor. The variety of devices, either R2R processed or laboratory-scale-sized on the mini-rollcoater, show their broad applicability in research and development and in industrialized methods.

The efficiency for ITO superstrate devices with P3HT:PCBM as active layer and full R2R processing following the ProcessOne routine are in the range of 1.7–2.3% depending on the device area and module configuration.[7] The device design was slightly different to the post-card sized module layout presented here but layer stack and fabrication conditions are similar.

First studies on R2R processed silver and ITO free devices based on rotary screen printed PEDOT:PSS layers were already performed earlier with the main purpose of life cycle assessment studies.[92] Efficiencies of 1.6% could be achieved on slightly smaller credit-card sized devices and an active area of 15.4 cm^2.[83] Single test devices manufactured on a mini-rollcoater and the current superstrate resulted in an efficiency of 1.61% for P3HT:PCBM and >2.8% for a low bandgap polymer without any further device optimizations. Fully R2R processed carbon-based modules completely without silver demonstrated

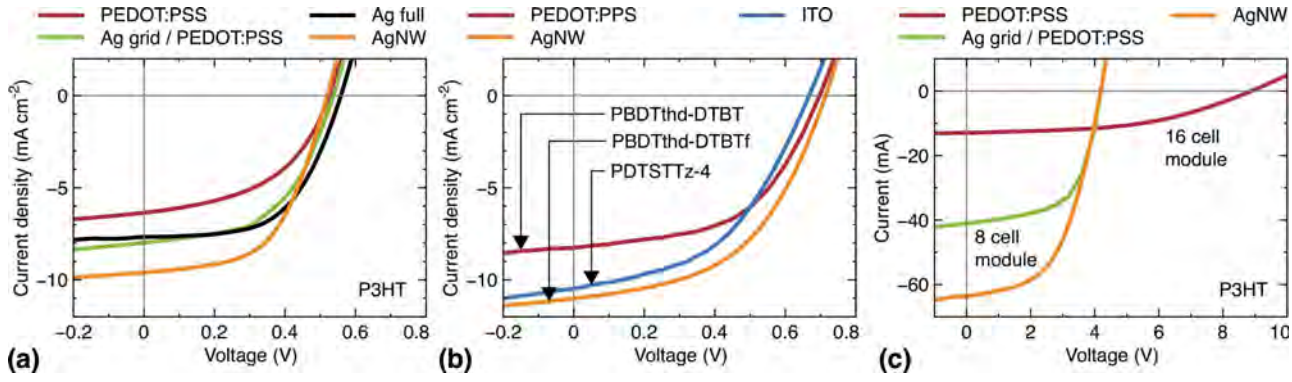

Figure 6. *J–V* curves of selected single cell devices with P3HT as a) donor polymer and b) low bandgap polymer fabricated on the mini-rollcoater. c) *I–V* curves of modules fabricated entirely through R2R processes.

Table 5. Solar cell characteristics of selected devices fabricated on superstrates and substrates presented here.

Single cells, on mini-rollcoater						
Conductive electrode	Polymer	V_{OC} [V]	J_{SC} [mA cm^{-2}]	FF [%]	PCE [%]	Area [cm^2]
PEDOT:PSS	P3HT	0.52	−6.35	48.4	1.61	0.2
PEDOT:PSS	PBDTthd-DTBT[100]	0.69	−7.64	52.9	2.82	0.4
Ag grid/PEDOT:PSS	P3HT	0.53	−7.98	52.3	2.24	0.7
Ag full	P3HT	0.55	−7.67	57.3	2.45	1.4
AgNW	P3HT	0.52	−9.6	55.1	2.75	0.71
AgNW	PBDTthd-DTBTf[100]	0.71	−11.01	49.7	3.9	0.7
ITO	PDTSTTz-4[101]	0.67	−10.46	47.1	3.29	0.8
Modules, R2R processed						
Conductive electrode			I_{SC} [mA]			
PEDOT:PSS	P3HT	8.88	−12.96	47.7	1.83	30 (16 cells)
Ag grid / PEDOT:PSS	P3HT	4.2	−41	60	1.82	57 (8 cells)
AgNW	P3HT	4.19	−63.65	52.7	2.46	57 (8 cells)

efficiencies up to 1.8% based on an active area of 30 cm^2. The statistical studies and further details on a dataset of 500 modules can be found elsewhere.[93]

The superstrate with Ag grid/PEDOT:PSS/ZnO, also known as Flextrode, achieved roughly 1.8% with P3HT:PCBM as active layer fabricated in a full R2R process. The modules known as freeOPV have (at the time of writing this account) been handed out to >9000 interested people.[11] Essentially all our recent publications are based on this superstrate type and a variety of different OPV devices have been fabricated including tandem devices,[102,103] modules with efficiencies up to 3.2%, and single cells of 3.8%,[98,100,101] The same superstrate stack but different module layout was used for the fabrication of very large and scalable modules with active areas beyond 14 m^2 and power outputs >250 W_{peak}.[10,104] Life cycle assessment calculations showed very promising energy paypack times <180 days for entire systems including mounting scaffolds.

The Flextrode superstrate itself is also available free of charge to all academics[35] and was already used by others to fabricate dye-sensitized solar cells (DSSC) with efficiencies beyond 6%.[105] In this case the electrode comprised only AgNP grid/PEDOT:PSS. Surface improvements due to ozone and plasma treatment have been found to be important for work function recovery of the ZnO layer after long storage time.[106]

The opaque substrate based on reflective silver has been successfully used to fabricate single P3HT:PCBM cells on the roll-coater with an efficiency of 2.45% (area 1.4 cm^2) and high fill factor >57%, where the silver layer simultaneously acts as back reflector and conductor. The best P3HT:PCBM cell achieved a PCE of 2.6% with slightly lower fill factor. The reflecting silver substrate is also suitable for fully solution-processed tandem solar cell devices with efficiencies beyond 2.35% on an area of 0.8 cm^2. More detailed studies on the silver layer and device fabrication have been published elsewhere.[72]

The hybrid AgNW/ZnO superstrate electrode has been used for the fabrication of functional OPV devices with efficiencies close to 4% on active areas of around 1 cm^2. Cells and modules were fabricated using small-scale roll coating equipment and large-scale R2R equipment, respectively. The device examples clearly show that all electrodes can be used either for full R2R production of OPV modules or for device preparation of small test cells using laboratory equipment. Hereby, pieces of electrodes are cut from the mother roll and used for further fabrication of devices to emulate large-scale processes. The achieved efficiencies of polymer solar cells fabricated under industrially relevant processes on the alternative electrodes without the use of vacuum are compatible or superior to ITO-based devices. The availability of kilometers of transparent electrodes on cheap carrier material is a necessity to prove R2R compatibility of new materials and device configurations.

6. Conclusion

We have introduced the distinction between superstrates and substrates based on the entire device stack of the optoelectronic device. If the carrier and electrode is viewed alone, without any application in mind, the substrate nomenclature is fully justified. We showed that the described superstrates and substrates are comparable or superior to ITO in electrode-specific parameters but also with respect to large-scale manufactured devices under ambient conditions. The results show that use of ITO is not necessary anymore, and all-additive fabrication routes are now state-of-the-art. The fabrication employs standard printing and coating processes that in principle can be fabricated by the local printing and coating industry or in-house if the required R2R equipment is available. Everybody is invited to test the available superstrates and substrates for their application and improve subsequent processes, and we believe that

general (and free) availability is key to both progress and finally replacing ITO.

Acknowledgements

This work has been supported by Energinet.dk (project no. 12144), the European Commission as part of the Framework 7 ICT 2009 collaborative project ROTROT (grant no. 288565), the Danish Ministry of Science, Innovation and Higher Education under a Sapere Aude Top Scientist grant (no. DFF – 1335–00037A) and an Elite Scientist grant (no. 11–116028). Samples of Flextrode materials for research can be acquired free of charge at www.plasticphotovoltaics.org.

Received: August 1, 2014
Revised: September 8, 2014
Published online: November 22, 2014

[1] M. Jørgensen, J. E. Carlé, R. R. Søndergaard, M. Lauritzen, N. A. Dagnæs-Hansen, S. L. Byskov, T. R. Andersen, T. T. Larsen-Olsen, A. P. L. Böttiger, B. Andreasen, L. Fu, L. Zuo, Y. Liu, E. Bundgaard, X. Zhan, H. Chen, F. C. Krebs, *Sol. Energy Mater. Sol. Cells* **2013**, *119*, 84.

[2] Y. Galagan, I. G. de Vries, A. P. Langen, R. Andriessen, W. J. H. Verhees, S. C. Veenstra, J. M. Kroon, *Chem. Eng. Processing* **2011**, *50*, 454.

[3] D. Kaduwal, H.-F. Schleiermacher, J. Schulz-Gericke, T. Kroyer, B. Zimmermann, U. Würfel, *Sol. Energy Mater. Sol. Cells* **2014**, *124*, 92.

[4] M. Schrödner, S. Sensfuss, H. Schache, K. Schultheis, T. Welzel, K. Heinemann, R. Milker, J. Marten, L. Blankenburg, *Sol. Energy Mater. Sol. Cells* **2012**, *107*, 283.

[5] C. Koidis, S. Logothetidis, A. Ioakeimidis, A. Laskarakis, C. Kapnopoulos, *Org. Electron.* **2013**, *14*, 1744.

[6] P. Apilo, J. Hiltunen, M. Välimäki, S. Heinilehto, R. Sliz, J. Hast, *Prog. Photovolt: Res. Appl.* **2014**, DOI: 10.1002/pip.2508.

[7] F. C. Krebs, S. A. Gevorgyan, J. Alstrup, *J. Mater. Chem.* **2009**, *19*, 5442.

[8] A. C. Hübler, B. Trnovec, T. Zillger, M. Ali, N. Wetzold, M. Mingebach, A. Wagenpfahl, C. Deibel, V. Dyakonov, *Adv. Energy Mater.* **2011**, *1*, 1018.

[9] F. Yan, J. Noble, J. Peltola, S. Wicks, S. Balasubramanian, *Sol. Energy Mater. Sol. Cells* **2013**, *114*, 214.

[10] F. C. Krebs, N. Espinosa, M. Hösel, R. R. Søndergaard, M. Jørgensen, *Adv. Mater.* **2014**, *26*, 29.

[11] F. C. Krebs, M. Hösel, M. Corazza, B. Roth, M. V. Madsen, S. A. Gevorgyan, R. R. Søndergaard, D. Karg, M. Jørgensen, *Energy Technol.* **2013**, *1*, 378.

[12] R. R. Søndergaard, M. Hösel, F. C. Krebs, *J. Polym. Sci. B Polym. Phys.* **2013**, *51*, 16.

[13] Y. Aleeva, B. Pignataro, *J. Mater. Chem. C* **2014**, *2*, 6436.

[14] E. Martínez-Ferrero, I. Burgués-Ceballos, M. Stella, P. Lacharmoise, *J. Mater. Chem. A* **2014**, *2* , 17711.

[15] J. Willmann, D. Stocker, E. Dörsam, *Org. Electron.* **2014**, *15*, 1631.

[16] M. Panayotova, V. Panyotov, *Ann. Univ. Mining Geol. St. Ivan Rilski* **2013**, *56*, 159.

[17] N. Espinosa, R. García-Valverde, A. Urbina, F. Lenzmann, M. Manceau, D. Angmo, F. C. Krebs, *Sol. Energy Mater. Sol. Cells* **2012**, *97*, 3.

[18] A. Iwan, I. Tazbir, M. Sibiński, B. Boharewicz, G. Pasciak, E. Schab-Balcerzak, *Mater. Sci. Semicond. Process.* **2014**, *24*, 110.

[19] K. Alzoubi, M. M. Hamasha, S. Lu, B. Sammakia, *J. Display Technol.* **2011**, *7*, 593.

[20] Y. Leterrier, L. Medico, F. Demarco, J. Månson, U. Betz, *Thin Solid Films* **2004**, *460*, 156.

[21] H. Hoppe, M. Seeland, B. Muhsin, *Sol. Energy Mater. Sol. Cells* **2012**, *97*, 119.

[22] D. Angmo, F. C. Krebs, *J. Appl. Polym. Sci.* **2013**, *129*, 1.

[23] C. Granqvist, *Sol. Energy Mater. Sol. Cells* **2007**, *91*, 1529.

[24] D. Angmo, I. Gonzalez-Valls, S. C. Veenstra, W. J. H. Verhees, S. Sapkota, S. Schiefer, B. Zimmermann, Y. Galagan, J. Sweelssen, M. Lira-Cantu, R. Andriessen, J. M. Kroon, F. C. Krebs, *J. Appl. Polym. Sci.* **2013**, *130*, 944.

[25] M. Layani, M. Gruchko, O. Milo, I. Balberg, D. Azulay, S. Magdassi, *ACS Nano* **2009**, *3*, 3537.

[26] M. Layani, S. Magdassi, *J. Mater. Chem.* **2011**, *21*, 15378.

[27] S. Azoubel, S. Shemesh, S. Magdassi, *Nanotechnology* **2012**, *23*, 344003.

[28] F. L. M. Sam, C. A. Mills, L. J. Rozanski, S. R. P. Silva, *Laser Photonics Rev.* **2013**, *8*, 172.

[29] W. Gaynor, S. Hofmann, M. G. Christoforo, C. Sachse, S. Mehra, A. Salleo, M. D. McGehee, M. C. Gather, B. Lüssem, L. Müller-Meskamp, P. Peumans, K. Leo, *Adv. Mater.* **2013**, *25*, 4006.

[30] D. Angmo, T. T. Larsen-Olsen, M. Jørgensen, R. R. Søndergaard, F. C. Krebs, *Adv. Energy Mater.* **2012**, *3*, 172.

[31] Wee Shing Koh, Choon How Gan, Wee Kee Phua, Y. A. Akimov, Ping Bai, *IEEE J. Sel. Topics Quantum Electron.* **2014**, *20*, 36.

[32] J. H. Yim, S.-Y. Joe, C. Pang, K. M. Lee, H. Jeong, J.-Y. Park, Y. H. Ahn, J. C. de Mello, S. Lee, *ACS Nano* **2014**, *8*, 2857.

[33] S. Nam, M. Song, D.-H. Kim, B. Cho, H. M. Lee, J.-D. Kwon, S.-G. Park, K.-S. Nam, Y. Jeong, S.-H. Kwon, Y. C. Park, S.-H. Jin, J.-W. Kang, S. Jo, C. S. Kim, *Sci. Rep.* **2014**, *4*, 4788.

[34] D. Angmo, M. Hösel, F. C. Krebs, *Sol. Energy Mater. Sol. Cells* **2012**, *107*, 329.

[35] M. Hösel, R. R. Søndergaard, M. Jørgensen, F. C. Krebs, *Energy Technol.* **2013**, *1*, 102.

[36] J.-S. Yu, I. Kim, J.-S. Kim, J. Jo, T. T. Larsen-Olsen, R. R. Søndergaard, M. Hösel, D. Angmo, M. Jørgensen, F. C. Krebs, *Nanoscale* **2012**, *4*, 6032.

[37] S. K. Hau, H.-L. Yip, J. Zou, A. K. Y. Jen, *Org. Electron.* **2009**, *10*, 1401.

[38] K. D. M. Rao, C. Hunger, R. Gupta, G. U. Kulkarni, M. Thelakkat, *Phys. Chem. Chem. Phys.* **2014**, *16*, 15107.

[39] B. H. Lee, J.-H. Lee, Y. H. Kahng, N. Kim, Y.-J. Kim, J. Lee, T. Lee, K. Lee, *Adv. Funct. Mater.* **2013**, *24*, 1847.

[40] K. Tvingstedt, O. Inganäs, *Adv. Mater.* **2007**, *19*, 2893.

[41] M. Neophytou, E. Georgiou, M. M. Fyrillas, S. A. Choulis, *Sol. Energy Mater. Sol. Cells* **2014**, *122*, 1.

[42] Y. Zhou, F. Zhang, K. Tvingstedt, S. Barrau, F. Li, W. Tian, O. Inganäs, *Appl. Phys. Lett.* **2008**, *92*, 233308.

[43] Y. Galagan, J.-E. J M Rubingh, R. Andriessen, C.-C. Fan, P. W. M. Blom, S. C Veenstra, J. M Kroon, *Sol. Energy Mater. Sol. Cells* **2011**, *95*, 1339.

[44] Y. Galagan, B. Zimmermann, E. Coenen, M. Jørgensen, F. C. Krebs, D. Tanenbaum, H. Gorter, S. Sabik, L. Slooff, S. C. Veenstra, J. Kroon, R. Andriessen, *Adv. Energy Mater.* **2012**, *2*, 103.

[45] S. Na, S. Kim, J. Jo, D. Kim, *Adv. Mater.* **2008**, *20*, 4061.

[46] M. Kaltenbrunner, M. S. White, E. D. Głowacki, T. Sekitani, T. Someya, N. S. Sariciftci, S. Bauer, *Nat. Commun.* **2012**, *3*, 770.

[47] Y. Galagan, E. W. C. Coenen, S. Sabik, H. H. Gorter, M. Barink, S. C. Veenstra, J. M. Kroon, R. Andriessen, P. W. M. Blom, *Sol. Energy Mater. Sol. Cells* **2012**, *104*, 32.

[48] Y. Galagan, E. W. C. Coenen, R. Abbel, T. J. van Lammeren, S. Sabik, M. Barink, E. R. Meinders, R. Andriessen, P. W. M. Blom, *Org. Electron.* **2013**, *14*, 38.

[49] W. Zhang, B. Zhao, Z. He, X. Zhao, H. Wang, S. Yang, H. Wu, Y. Cao, *Energy Environ. Sci.* **2013**, *6*, 1956.

[50] K. Lim, S. Jung, J.-K. Kim, J.-W. Kang, J. H. Kim, S.-H. Choa, D.-G. Kim, *Sol. Energy Mater. Sol. Cells* **2013**, *115*, 71.

[51] J. J. van Franeker, W. P. Voorthuijzen, H. Gorter, K. H. Hendriks, R. A. J. Janssen, A. Hadipour, R. Andriessen, Y. Galagan, *Sol. Energy Mater. Sol. Cells* **2013**, *117*, 267.
[52] H. J. van de Wiel, Y. Galagan, T. J. van Lammeren, J. F. J. de Riet, J. Gilot, M. G. M. Nagelkerke, R. H. C. A. T. Lelieveld, S. Shanmugam, A. Pagudala, D. Hui, W. A. Groen, *Nanotechnology* **2013**, *24*, 484014.
[53] I. Burgués-Ceballos, N. Kehagias, C. M. Sotomayor-Torres, M. Campoy-Quiles, P. D. Lacharmoise, *Sol. Energy Mater. Sol. Cells* **2014**, *127*, 50.
[54] Y. H. Kahng, M.-K. Kim, J.-H. Lee, Y.-J. Kim, N. Kim, D.-W. Park, K. Lee, *Sol. Energy Mater. Sol. Cells* **2014**, *124*, 86.
[55] K. Yang, M. A. Rahman, K. Jeong, H.-S. Nam, J. Kim, J. Lee, *Mater. Sci. Semicond. Process.* **2014**, *23*, 104.
[56] J. Wu, H. A. Becerril, Z. Bao, Z. Liu, Y. Chen, P. Peumans, *Appl. Phys. Lett.* **2008**, *92*, 263302.
[57] L. Gomez De Arco, Y. Zhang, C. W. Schlenker, K. Ryu, M. E. Thompson, C. Zhou, *ACS Nano* **2010**, *4*, 2865.
[58] M.-G. Kang, H. Joon Park, S. Hyun Ahn, L. Jay Guo, *Sol. Energy Mater. Sol. Cells* **2010**, *94*, 1179.
[59] K. Kim, S.-H. Bae, C. T. Toh, H. Kim, J. H. Cho, D. Whang, T.-W. Lee, B. Özyilmaz, J.-H. Ahn, *ACS Appl. Mater. Interfaces* **2014**, *6*, 3299.
[60] I. E. Stewart, A. R. Rathmell, L. Yan, S. Ye, P. F. Flowers, W. You, B. J. Wiley, *Nanoscale* **2014**, *6*, 5980.
[61] A. R. B. M. Yusoff, S. J. Lee, F. K. Shneider, W. J. da Silva, J. Jang, *Adv. Energy Mater.* **2014**, *4*, 1301989.
[62] J. Liang, L. Li, K. Tong, Z. Ren, W. Hu, X. Niu, Y. Chen, Q. Pei, *ACS Nano* **2014**, *8*, 1590.
[63] M. Layani, P. Darmawan, W. L. Foo, L. Liu, A. Kamyshny, D. Mandler, S. Magdassi, P. S. Lee, *Nanoscale* **2014**, *6*, 4572.
[64] J. Jensen, M. Hösel, I. Kim, J.-S. Yu, J. Jo, F. C. Krebs, *Adv. Funct. Mater.* **2014**, *24*, 1228.
[65] T. Schwab, S. Schubert, S. Hofmann, M. Fröbel, C. Fuchs, M. Thomschke, L. Müller-Meskamp, K. Leo, M. C. Gather, *Adv. Opt. Mater.* **2013**, *1*, 707.
[66] B. Zimmermann, M. Glatthaar, M. Niggemann, M. Riede, A. Hinsch, A. Gombert, *Sol. Energy Mater. Sol. Cells* **2007**, *91*, 374.
[67] W. Gaynor, J.-Y. Lee, P. Peumans, *Proc. SPIE* **2009**, *7416*, 741614.
[68] W. Gaynor, J. Lee, P. Peumans, *ACS Nano* **2009**, *4*, 30.
[69] B. Zimmermann, H. F. Schleiermacher, M. Niggemann, U. Würfel, *Sol. Energy Mater. Sol. Cells* **2011**, *95*, 1587.
[70] L. Leonat, M. S. White, E. D. Głowacki, M. C. Scharber, T. Zillger, J. Rühling, A. Hübler, N. S. Sariciftci, *J. Phys. Chem. C* **2014**, *118*, 16813.
[71] F. C. Krebs, *Org. Electron.* **2009**, *10*, 761.
[72] D. Angmo, H. F. Dam, T. R. Andersen, N. K. Zawacka, M. V. Madsen, J. Stubager, F. Livi, R. Gupta, M. Helgesen, J. E. Carlé, T. T. Larsen-Olsen, G. U. Kulkarni, E. Bundgaard, F. C. Krebs, *Energy Technol.* **2014**, *2*, 651 .
[73] H. Jin, C. Tao, M. Velusamy, M. Aljada, Y. Zhang, M. Hambsch, P. L. Burn, P. Meredith, *Adv. Mater.* **2012**, *24*, 2572.
[74] M. Hambsch, H. Jin, A. J. Clulow, A. Nelson, N. L. Yamada, M. Velusamy, Q. Yang, F. Zhu, P. L. Burn, I. R. Gentle, P. Meredith, *Sol. Energy Mater. Sol. Cells* **2014**, *130*, 182.
[75] Y. Galagan, D. J. D. Moet, D. C. Hermes, P. W. M. Blom, R. Andriessen, *Org. Electron.* **2012**, *13*, 3310.
[76] B. Lamprecht, R. Thünauer, M. Ostermann, G. Jakopic, G. Leising, *Phys. Status Solidi A* **2005**, *202*, R50.
[77] D. Deganello, J. A. Cherry, D. T. Gethin, T. C. Claypole, *Thin Solid Films* **2012**, *520*, 2233.
[78] D. Deganello, J. Cherry, D. Gethin, T. C. Claypole, *Thin Solid Films* **2010**, *518*, 6113.
[79] M. Hösel, F. C. Krebs, *J. Mater. Chem.* **2012**, *22*, 15683.
[80] P. Kopola, M. Tuomikoski, R. Suhonen, *Thin Solid Films* **2009**, *517*, 5757.
[81] D. Tobjork, H. Aarnio, T. Mäkelä, R. Österbacka, *MRS Proc.* **2011**, *1091*, 1091.
[82] P. Kopola, R. Sliz, S. Guillerez, M. Ylikunnari, D. Cheyns, M. Välimäki, M. Tuomikoski, J. Hast, G. Jabbour, R. Myllylä, A. Maaninen, *Sol. Energy Mater. Sol. Cells* **2011**, *95*, 1344.
[83] T. T. Larsen-Olsen, R. R. Søndergaard, K. Norrman, M. Jørgensen, F. C. Krebs, *Energy Environ. Sci.* **2012**, *5*, 9467.
[84] S. H. Eom, S. Senthilarasu, P. Uthirakumar, S. C. Yoon, J. Lim, C. Lee, H. S. Lim, J. Lee, S.-H. Lee, *Org. Electron.* **2009**, *10*, 536.
[85] M. Neophytou, F. Hermerschmidt, A. Savva, E. Georgiou, S. A. Choulis, *Appl. Phys. Lett.* **2012**, *101*, 193302.
[86] M. Cherrington, T. C. Claypole, D. Deganello, I. Mabbett, T. Watson, D. Worsley, *J. Mater. Chem.* **2011**, *21*, 7562.
[87] F. Guo, X. Zhu, K. Forberich, J. Krantz, T. Stubhan, M. Salinas, M. Halik, S. Spallek, B. Butz, E. Spiecker, T. Ameri, N. Li, P. Kubis, D. M. Guldi, G. J. Matt, C. J. Brabec, *Adv. Energy Mater.* **2013**, *3*, 1062.
[88] J. Krantz, M. Richter, S. Spallek, E. Spiecker, C. J. Brabec, *Adv. Funct. Mater.* **2011**, *21*, 4784.
[89] J.-S. Yu, G. H. Jung, J. Jo, J.-S. Kim, J. W. Kim, S.-W. Kwak, J.-L. Lee, I. Kim, D. Kim, *Sol. Energy Mater. Sol. Cells* **2013**, *109*, 142.
[90] R. R. Søndergaard, N. Espinosa, M. Jørgensen, F. C. Krebs, *Energy Environ. Sci.* **2014**, *3*, 1006.
[91] P. Sommer-Larsen, M. Jørgensen, R. R. Søndergaard, M. Hösel, F. C. Krebs, *Energy Technol.* **2013**, *1*, 15.
[92] N. Espinosa, F. O. Lenzmann, S. Ryley, D. Angmo, M. Hösel, R. R. Søndergaard, D. Huss, S. Dafinger, S. Gritsch, J. M. Kroon, M. Jørgensen, F. C. Krebs, *J. Mater. Chem. A* **2013**, *1*, 7037.
[93] G. A. dos Reis Benatto, B. Roth, M. V. Madsen, M. Hösel, R. R. Søndergaard, M. Jørgensen, F. C. Krebs, *Adv. Energy Mater.* **2014**, DOI 10.1002/aenm.201400732.
[94] N. Espinosa, R. García-Valverde, A. Urbina, F. C. Krebs, *Sol. Energy Mater. Sol. Cells* **2011**, *95*, 1293.
[95] R. Søndergaard, M. Hösel, D. Angmo, T. T. Larsen-Olsen, F. C. Krebs, *Mater. Today* **2012**, *15*, 36.
[96] J. E. Carlé, T. R. Andersen, M. Helgesen, E. Bundgaard, M. Jørgensen, F. C. Krebs, *Sol. Energy Mater. Sol. Cells* **2013**, *108*, 126.
[97] H. F. Dam, F. C. Krebs, *Sol. Energy Mater. Sol. Cells* **2012**, *97*, 191.
[98] J. E. Carlé, M. Helgesen, M. V. Madsen, E. Bundgaard, F. C. Krebs, *J. Mater. Chem. C* **2014**, *2*, 1290.
[99] S. Yan, J. Krantz, K. Forberich, C. Pflaum, C. J. Brabec, *J. Appl. Phys.* **2013**, *113*, 154303.
[100] J. E. Carlé, M. Helgesen, N. K. Zawacka, M. V. Madsen, E. Bundgaard, F. C. Krebs, *J. Polym. Sci. B Polym. Phys.* **2014**, *52*, 893.
[101] M. Helgesen, J. E. Carlé, F. C. Krebs, *Adv. Energy Mater.* **2013**, *3*, 1664.
[102] T. R. Andersen, H. F. Dam, B. Andreasen, M. Hösel, M. V. Madsen, S. A. Gevorgyan, R. R. Søndergaard, M. Jørgensen, F. C. Krebs, *Sol. Energy Mater. Sol. Cells* **2014**, *120*, 735.
[103] T. R. Andersen, H. F. Dam, M. Hösel, M. Helgesen, J. E. Carlé, T. T. Larsen-Olsen, S. A. Gevorgyan, J. W. Andreasen, J. Adams, N. Li, F. Machui, G. D. Spyropoulos, T. Ameri, N. Lemaître, M. Legros, A. Scheel, D. Gaiser, K. Kreul, S. Berny, O. R. Lozman, S. Nordman, M. Välimäki, M. Vilkman, R. R. Søndergaard, M. Jørgensen, C. J. Brabec, F. C. Krebs, *Energy Environ. Sci.* **2014**, *7*, 2725.
[104] N. Espinosa, M. Hösel, M. Jørgensen, F. C. Krebs, *Energy Environ. Sci.* **2014**, *3*, 855.
[105] J. Idígoras, E. Guillen, F. J. Ramos, J. A. Anta, M. K. Nazeeruddin, S. Ahmad, *J. Mater. Chem. A* **2014**, *2*, 3175.
[106] Y. Kato, M.-C. Jung, M. V. Lee, Y. Qi, *Org. Electron.* **2014**, *15*, 721.

Carbon: The Ultimate Electrode Choice for Widely Distributed Polymer Solar Cells

*Gisele A. dos Reis Benatto, Bérenger Roth, Morten V. Madsen, Markus Hösel, Roar R. Søndergaard, Mikkel Jørgensen, and Frederik C. Krebs**

As mass-produced, low-cost organic electronics enter our everyday lives, so does the waste from them. The challenges associated with end-of-life management must be addressed by careful design and carbon-based electrodes are central to these developments. Here, the reproducible production of vacuum-, indium tin oxide (ITO)-, and silver-free solar cells in a fully packaged form using only roll-to-roll processing is reported. Replacing silver with carbon as electrode material significantly lowers the manufacturing cost and makes the organic photovoltaic (OPV) modules environmentally safe while retaining their flexibility, active area efficiency, and stability. The substitution of silver with carbon does not affect the roll-to-roll manufacturing of the modules and allows for the same fast printing and coating. The use of carbon as electrode material is one step closer to the wide release of low-cost plastic solar cells and opens the door to new possible applications where silver recycling is not manageable.

1. Introduction

The vision of organic electronics being a very low-cost mass-produced commodity has several implications when it comes to the sustainability and environmental impact. When compared to alternative technologies, their fast and facile manufacture using little material and processes that use little energy does offer the possibility for a low environmental impact. However, some components used to manufacture polymer solar cells have been shown to impact the level of sustainability negatively unless special precautions are taken.[1–4] A process leading to a complex device such as a polymer solar cell module may be optimized with respect to the amounts of materials used, the speed of manufacture, and the energy used.[5,6] Interestingly the case for both polymer solar cells and organic electronics in general is exceptionally strong as it allows for optimization in all senses (low cost, flexibility, light weight, energy payback time for organic photovoltaics). Some of the ingredients however are mandatory in some device architectures and when such ingredients have a negative environmental impact it becomes difficult to realize the potential of the technology unless the application grants an easy way of handling the potential environmental danger. A very good example is the use of silver metal electrodes in fully printed/coated polymer solar cells.[6] The high conductivity of silver has enabled devices that are as efficient as indium tin oxide (ITO) based semitransparent electrodes used in the past (see **Figure 1**) while fortuitously also enabling a much faster manufacture than is possible with ITO-based electrodes. In addition to imparting a high cost to the device silver also has a massive environmental impact, cannot be disposed of without special care, and cannot be distributed widely in nature without potentially doing more harm than good.[7,8] The use of silver in organic electronics is fortunately not unmanageable as was shown in a recent study where a silver-based polymer solar cell power plant could be operated and the silver efficiently recovered and recycled with several benefits (lower cost, shorter energy payback time, lower environmental impact).[8] The particular case, however, also presented the interesting boundary condition that the location of the polymer solar cells containing the silver is known at all times from manufacture, through installation to operation and decommissioning.[9] In such a case the use of silver was found to be fully justified and, in addition, making only reduced claims on the available silver resources if considered on a very large scale.[10] For consumer electronics based on very low-cost technology it is likely that the large scale implies that a huge number of discrete products will be characteristic of the application and as a consequence the distribution is likely to be vast. The environmental responsibility that the consumer feels when disposing of the product cannot be assumed to be sufficient. The environmentally responsible assumption is that the consumer will not always dispose the product correctly, which means that unwanted discharge into the environment will take place. The technology should therefore be developed in a form where environmental impact is eliminated or reduced to a level enabling full or partial recycling of the plastic materials, landfill, or incineration without harmful emission beyond CO_2.

Figure 1 shows the freeOPV platform that was conceived as a generic OPV module enabling development of processes, processing, testing of new materials and also importantly the

G. A. dos Reis Benatto, B. Roth, Dr. M. V. Madsen, Dr. M. Hösel, Dr. R. R. Søndergaard, Dr. M. Jørgensen, Prof. F. C. Krebs
Department of Energy Conversion and Storage
Technical University of Denmark
Frederiksborgvej 399, DK-4000 Roskilde, Denmark
E-mail: frkr@dtu.dk

DOI: 10.1002/aenm.201400732

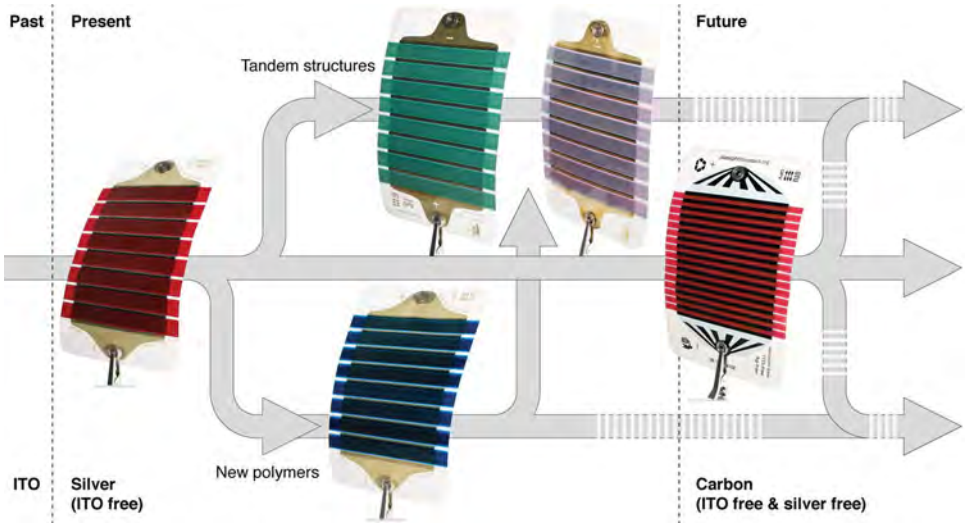

Figure 1. An illustration of the evolution of the freeOPV platform from its initial form based on slanted silver grids and poly(3-hexylthiophene):phenyl-C_{61}-butyric acid methyl ester (P3HT:PCBM) as the active materials to encompass novel polymer active materials and present complex multilayer architectures such as the tandem freeOPV. This work demonstrates printed carbon electrodes for consumer electronics with low environmental impact.

free distribution of OPVs to anybody with an interest.[11–13] The largest success of freeOPV has been its free distribution to school children and the majority of the distribution has been for teaching purposes especially in the recent context of the massive open online courses (MOOCs) where the freeOPV was used as part of the course material.[14] The massive demand on the freeOPV in its original silver-based form, tandem form and carbon-based form is shown in **Figure 2**. The demography of freeOPV is of some interest as it shows how a possible future organic electronics product is likely to distribute in the world and it is first of all clear that it presents a more or less global distribution to all continents and thus certainly demands management of its end-of-life through product design. Our motivation was thus to create a new version of freeOPV that can be disposed as regular plastic waste while at the same time maintaining the performance and functionality as a teaching tool and this is what we show in this report.

2. Results and Discussion

The silver-based freeOPV employs state-of-the-art printed grid electrode structures comprising a ±5° slant to minimize comb line cross-overs that often lead to a shunt.[6] The silver grid lines enable a low sheet resistivity of the silver poly(3,4-ethylenedioxythiophene):polystyrene sulfonate (PEDOT:PSS) composite electrode and enable cell dimensions in the direction of charge transport of 9–15 mm with current densities in the range of 6–12 mA cm^{-2}. In the case of a silver-free version relying on PEDOT:PSS alone the cell dimension is diminished somewhat and the optical transparency compromised.[7] Earlier demonstrations showed that cell dimensions of 1–2 mm were possible without loss using PEDOT:PSS[15] alone and these were also used in the case of the OE-A demonstrator in 2011[16] where carbon was also reported as a printed electrode.[7,17] However the packaging and operational stability proved to be

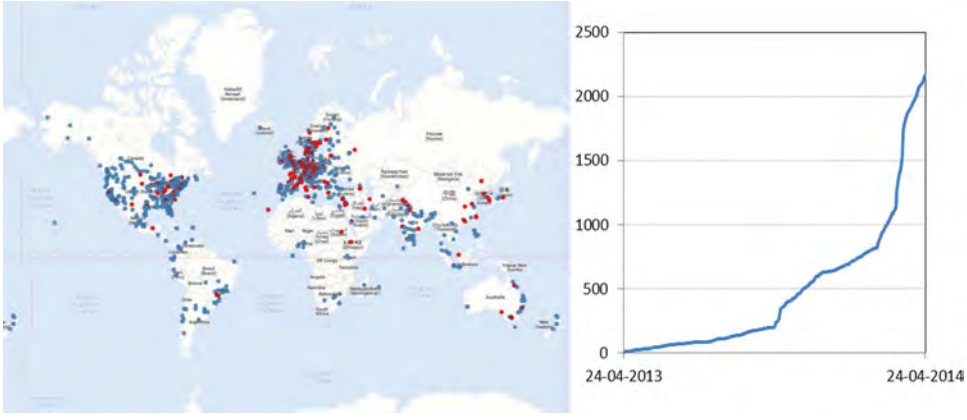

Figure 2. The world map showing the demography of single junction and tandem freeOPV modules with silver (red dots) and carbon (blue dots) based freeOPV (left). The graph shows the number of freeOPV shipped during the first year of the freeOPV initiative (right).

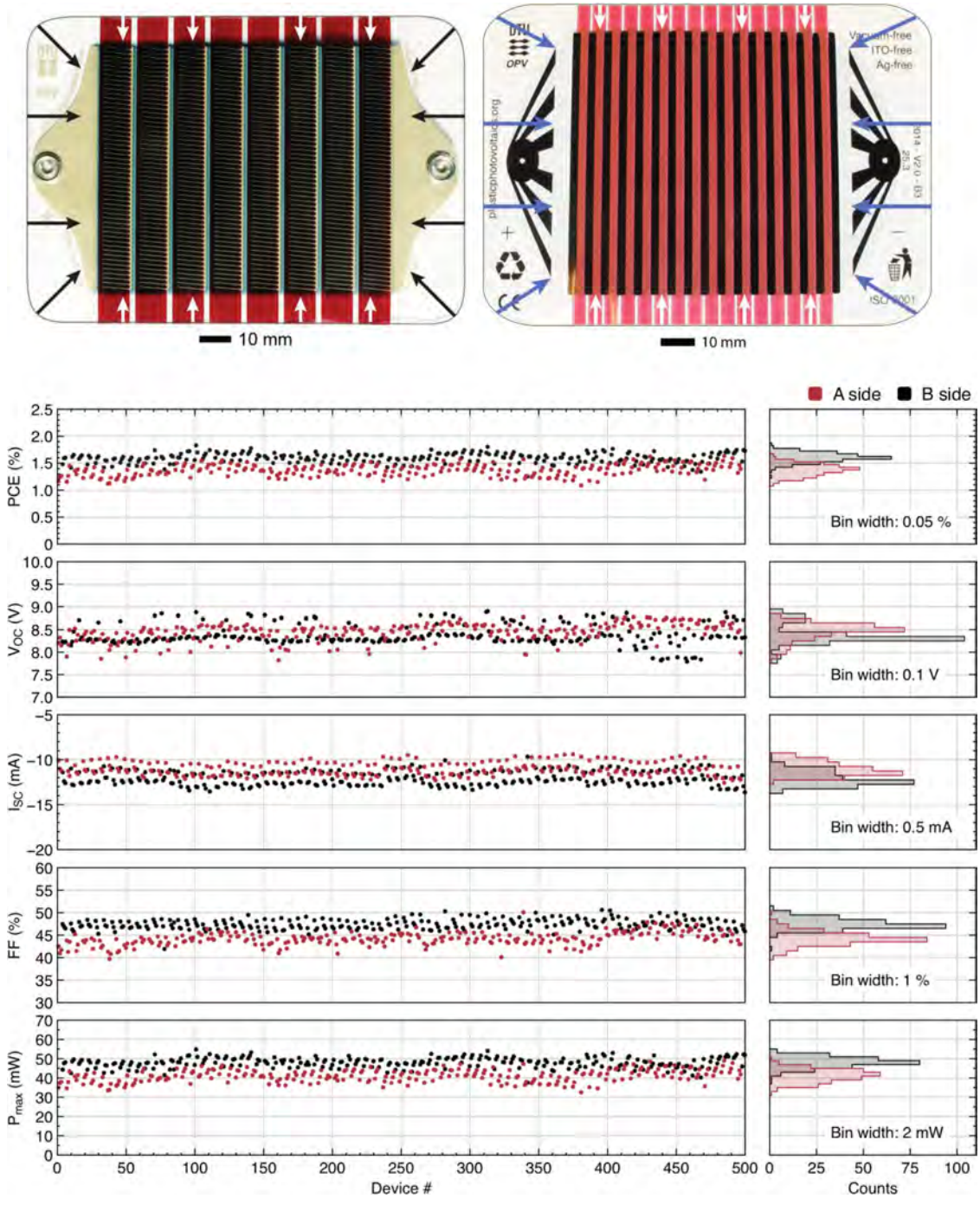

Figure 3. Top: Comparison of the diffusion path into the silver and carbon based freeOPV. The arrows show the diffusion pathways from the edges to the solar cell. Bottom: The reproducibility of 500 modules (250 A-side, 250 B-side) is shown with respect to the photovoltaic parameters and is also presented in a histogram (right) to highlight the distinct differences between the two sides of the web but also the relatively narrow distribution of performance.

challenging. In order to make an efficient edge seal and extract the current out of the cell based on a thin PEDOT:PSS layer alone, a new approach was sought. In the silver based freeOPV a thin (<250 nm) flexo-printed silver electrode is employed that enables a good edge seal.[12] Printed carbon does not enable this, as it provides a diffusion path into the device especially for oxygen. We thus employ a thin PEDOT:PSS layer as the bus-bar and use this as the edge seal as seen in **Figure 3**. The printed carbon extraction lines do not extend all the way to the device area and enable similar performance to freeOPV with highly reproducible performance as shown for 500 modules (Figure 3) comprised in 83 printed motifs. The web width employed in the experiments was 305 mm and two modules were processed simultaneously (referred to as the A-side and the B-side). There

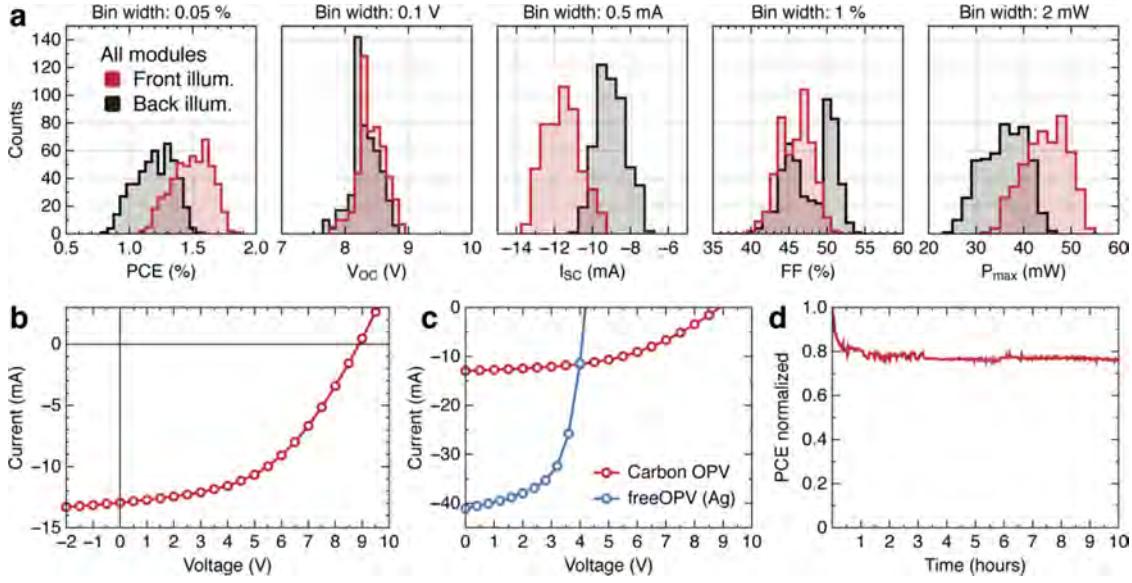

Figure 4. a) Front-versus-back illumination of 500 modules shown as histograms with the bin width quoted on top of each graph. b) A typical IV-curve of the carbon OPV module is shown along with a comparison of the original Ag-based freeOPV (c). d) Lifetime curve recorded under ISOS-L-2 conditions.[13]

are differences between the two sides in addition to experimental variation due to experiments with slightly different gap widths (evident as a clear repeating pattern for every three modules). We employed the same wet thickness for both the front and back PEDOT:PSS implying that the optical path from the front and back was similar and thus enabled bi-facial operation as shown in **Figure 4** and **Table 1**. The back PEDOT:PSS ink has a slightly higher solid content reducing the transparency somewhat leading to a slightly lower current and consequently a higher fill factor as expected. The general performance over the active area was very similar to freeOPV based on silver electrodes, but a sacrifice was of course made in the module power which for carbon based freeOPV was around 50 mW whereas the module power for silver based freeOPV typically is 100 mW. This is due to the poorer geometric fill factor which is a consequence of the larger number of cells (16 versus 8). In terms of sustainability and cost, the carbon-based free OPV is superior to silver-based freeOPV and the performance in terms of power conversion efficiency on the active area and the operational stability is similar, as shown in Figure 4, with the only difference being that carbon-based OPV does not support exposure to liquid water near to the contacts.

3. Conclusions

We have accomplished the reproducible production of vacuum-, ITO-, and silver-free solar cells in a fully packaged form using only roll-to-roll processing. We showed that the replacement of silver with carbon as the electrode material significantly lowers the manufacturing cost and makes the OPV modules environmentally safe while retaining the flexibility, the active area efficiency, and the stability (except liquid water near contacts). Additionally, the substitution of silver with carbon does not affect the roll-to-roll manufacturing of the modules and allows for the same fast printing and coating. The use of carbon as the

Table 1. The photovoltaic parameters for 500 modules including the maximum values. Results from front and back side illumination and from the two different sides of the web are also quoted.

	PCE[a] [%] front	PCE [%] back	V_{OC}[b] [V] front	V_{OC} [V] back	I_{SC}[c] [mA] front	I_{SC} [mA] back	FF[d] [%] front	FF [%] back	P_{max}[e] [mW] front	P_{max} [mW] back
Average	1.49	1.20	8.41	8.31	11.57	9.01	45.86	47.85	44.67	35.90
Standard deviation	0.15	0.15	0.21	0.22	0.92	0.78	2.11	3.11	4.55	4.55
Maximum	1.83	1.54	8.91	8.80	13.6	10.81	50.67	53.74	54.96	46.19
	PCE [%] A side	PCE [%] B side	V_{OC} [V] A side	V_{OC} [V] B side	I_{SC} [mA] A side	I_{SC} [mA] B side	FF [%] A side	FF [%] B side	P_{max} [mW] A side	P_{max} [mW] B side
Average	1.37	1.60	8.45	8.37	11.02	12.11	44.22	47.51	41.20	48.14
Standard deviation	0.11	0.09	0.20	0.22	0.71	0.76	1.47	1.15	3.22	2.64
Maximum	1.64	1.83	8.78	8.91	12.55	13.6	50.13	50.67	49.15	54.96

[a]Power conversion efficiency; [b]open-circuit voltage; [c]short-circuit current; [d]fill factor; [e]maximum power.

electrode material is one step closer to the wide release of low-cost plastic solar cells and opens the door to new possible applications where silver recycling is not manageable. The freeOPV modules with carbon are about one third cheaper than the previous generation that contained silver and can be disposed of in the normal household waste for incineration or in the bin for plastic recycling, thus supporting further the philosophy of sustainable organic electronics. We encourage and welcome any inquiries, scientific or technical studies independent of their nature.[13]

Experimental Section

Materials and Inks: The front PEDOT:PSS was composed of PH1000 from Heraeus diluted with isopropanol (10:3 w/w) and the back PEDOT:PSS was composed of Agfa EL-P-5010 diluted with isopropanol (10:2 w/w). The ZnO ink was composed of nanoparticles dispersed in acetone with a concentration of 56 mg mL^{-1}. The active layer was composed of P3HT (Sepiolid P-200 from BASF) and [60]PCBM (from Merck). Both materials were dissolved at a concentration of 30 mg mL^{-1} in chlorobenzene. The carbon ink was Electrodag PF-407C (from Acheson) that was used as received. The adhesive used for encapsulation was VE110484 from DELO that was used as received. The flexible foil was a 42 micrometer thick barrier material from Amcor with a WVTR of 0.04 g m^{-2} day^{-1} and an OTR of 0.01 cm^3 m^{-2} day^{-1} that was used as both superstrate and back laminate during packaging.

Roll-to-Roll Processing: Four different roll-to-roll (R2R) processing machines were used. The solar cell stack was processed on an inline printing/coating machine with a web width of 305 mm, composed of a unwinder, edge guide, corona treater, flexo printer, slot-die coating unit #1, hot air oven #1 (2 m length), rotary screen printer active, slot-die unit #2, 3 × 1.5 kW IR driers, hot air oven #2 (2 m length), ink jet printer (for barcodes), barcode readers and rewinder. The first PEDOT:PSS layer (Heraeus) was rotary screen printed with a nominal wet thickness of 20 µm, a web speed of 10 m min^{-1}, infrared drying and a hot air oven temperature of 140 °C. A unique barcode was inkjet printed on each motif for later registration and indexing during this first printing step. The ZnO layer was slot die coated at 10 m min^{-1} a nominal wet thickness of 7 µm and dried using both ovens (90 °C and 140 °C). The active layer was coated at 2 m min^{-1} (to ensure thermal annealing of P3HT:PCBM) with a nominal wet thickness of 12 µm having both ovens at 140 °C. The back PEDOT:PSS layer (Agfa) was rotary screen printed at a speed of 4 m min^{-1} with a nominal wet thickness of 20 µm, infrared drying and the hot air oven set to 140 °C. The back carbon electrode was rotary screen printed in two steps. Firstly the text pattern and the extraction lines were printed with a nominal wet thickness of 10 µm at 10 m min^{-1}, IR drying and the hot air oven set to 140 °C. In a secondary printing step the interconnections between the cells were rotary screen printed with a nominal wet thickness of 40 µm at a web speed of 4 m min^{-1} using the same drying conditions. The devices were R2R tested before lamination that was carried out using a R2R UV-laminator operated at 2 m min^{-1} using hard UV lamp power of 2 kW (power rating) and a 350 W (optical output) light-emitting diode (LED) curing lamp. The adhesive was applied to the back barrier foil and the barrier foil carrying the printed solar cell stack was used as the laminate. The roll of fully laminated solar cells was then laser-cut into modules using a R2R laser cutter comprising unwinder, 90 W CO_2 laser cutter and rewinder, and the devices finally contacted using snap-button contacts.

Testing: R2R testing was carried out using a system composed of an unwinder, edge guide, bar code reader, test head and rewinder. Keithley 2400 SMUs were used for all current–voltage characterization. Solar simulation was carried out on a number of solar simulators. Results quoted are from a Steuernagel KHS1200 calibrated to 1000 W m^{-2}. ISOS-L-2[18] measurements were carried out at 85 °C. The active area was accurately measured for one module using ultrafast LBIC[19] whereas the active areas in tables are nominal areas based on the nominal printing/coating overlaps defined by the pattern. Each printed motif has a total of six modules and each side (A and B side) has three slightly different device pattern with small variation in the gap between the cells to test. The periodic variation is clearly seen in Figure 3 where the B side presents the least spread in data. The active area of the device presenting the highest PCE in Table 1 was carefully determined using LBIC and the corresponding PCE corrected for the area was 1.85% as opposed to 1.83% based on the nominally printed area. The values quoted in Table 1 are based on the nominally printed active area and should therefore be viewed as quite accurate even though the exact active area was not established for every module.

Acknowledgements

This work was supported by Energinet.dk (project no. 12144), the Eurotech Universities Alliance project "Interface science for photovoltaics (ISPV)," the Danish Ministry of Science, Innovation and Higher Education under a Sapere Aude Top Scientist grant (no. DFF – 1335–00037A) and an Elite Scientist grant (no. 11–116028).

Received: May 2, 2014
Revised: May 20, 2014
Published online: June 13, 2014

[1] C. J. M. Emmott, A. Urbina, J. Nelson, *Sol. Energy Mater. Sol. Cells* **2012**, *97*, 14.
[2] B. Azzopardi, C. J. M. Emmott, A. Urbina, F. C. Krebs, J. Mutale, J. Nelson, *Energy Environ. Sci.* **2011**, *4*, 3741.
[3] N. Espinosa, R. García-Valverde, A. Urbina, F. C. Krebs, *Sol. Energy Mater. Sol. Cells* **2011**, *95*, 1293.
[4] N. Espinosa, F. C. Krebs, *Sol. Energy Mater. Sol. Cells* **2014**, *120*, 692.
[5] P. Sommer-Larsen, M. Jørgensen, R. R. Søndergaard, M. Hösel, F. C. Krebs, *Energy Technol.* **2013**, *1*, 15.
[6] F. C. Krebs, N. Espinosa, M. Hösel, R. R. Søndergaard, M. Jørgensen, *Adv. Mater.* **2014**, *26*, 29.
[7] N. Espinosa, F. O. Lenzmann, S. Ryley, D. Angmo, M. Hösel, R. R. Søndergaard, D. Huss, S. Dafinger, S. Gritsch, J. M. Kroon, M. Jørgensen, F. C. Krebs, *J. Mater. Chem. A* **2013**, *1*, 7037.
[8] R. R. Søndergaard, N. Espinosa, M. Jørgensen, F. C. Krebs, *Energy Environ. Sci.* **2014**, *7*, 1006.
[9] N. Espinosa, M. Hösel, M. Jørgensen, F. C. Krebs, *Energy Environ. Sci.* **2014**, *7*, 855.
[10] L. Grandell, A. Thorenz, *Renew. Energy* **2014**, *69*, 157.
[11] T. R. Andersen, H. F. Dam, M. Hösel, M. Helgesen, J. E. Carlé, T. T. Larsen-Olsen, S. A. Gevorgyan, J. W. Andreasen, J. Adams, N. Li, F. Machui, G. D Spyropoulos, T. Ameri, N. Lemaître, M. Legros, A. Scheel, D. Gaiser, K. Kreul, S. Berny, O. R. Lozman, S. Nordman, M. Välimäki, M. Vilkman, R. R. Søndergaard, M. Jørgensen, C. J. Brabec, F. C. Krebs, *Energy Environ. Sci.* **2014**, 10.1039/c4ee01223b.
[12] F. C. Krebs, M. Hösel, M. Corazza, B. Roth, M. V. Madsen, S. A. Gevorgyan, R. R. Søndergaard, D. Karg, M. Jørgensen, *Energy Technol.* **2013**, *1*, 378.
[13] FreeOPV samples can be obtained free of charge by submitting a postal address and registering at the www.plasticphotovoltaics.org website (accessed April 2014).
[14] The course is available for free enrolment on the Coursera website. https://www.coursera.org/course/opv (accessed April 2014).
[15] Y. Galagan, B. Zimmermann, E. W. C. Coenen, M. Jørgensen, D. M. Tanenbaum, F. C. Krebs, H. Gorter, S. Sabik, L. H. Slooff, S. C. Veenstra, J. M. Kroon, R. Andriessen, *Adv. Energy Mater.* **2012**, *2*, 103.

[16] F. C. Krebs, J. Fyenbo, D. M. Tanenbaum, S. A. Gevorgyan, R. Andriessen, B. van Remoortere, Y. Galagan, M. Jørgensen, *Energy Environ. Sci.* **2011**, *4*, 4116.
[17] T. T. Larsen-Olsen, R. R. Søndergaard, K. Norrman, M. Jørgensen, F. C. Krebs, *Energy Environ. Sci.* **2012**, *5*, 9467.
[18] M. O. Reese, S. A. Gevorgyan, M. Jørgensen, E. Bundgaard, S. R. Kurtz, D. S. Ginley, D. C. Olson, M. T. Lloyd, P. Morvillo, E. A. Katz, A. Elschner, O. Haillant, T. R. Currier, V. Shrotriya, M. Hermenau, M. Riede, K. R. Kirov, G. Trimmel, T. Rath, O. Inganäs, F. Zhang, M. Andersson, K. Tvingstedt, M. Lira-Cantu, D. Laird, C. McGuiness, S. Gowrisanker, M. Pannone, M. Xiao, J. Hauch, R. Steim, D. M. DeLongchamp, R. Rösch, H. Hoppe, N. Espinosa, A. Urbina, G. Yaman-Uzunoglu, J.-B. Bonekamp, A. J. J. M. van Breemen, C. Girotto, E. Voroshazi, F. C. Krebs, *Sol. Energy Mater. Sol. Cells* **2011**, *95*, 1253.
[19] F. C. Krebs, M. Jørgensen, *Adv. Opt. Mater.* **2014**, *2*, 765.

$f(x+\Delta x)=\sum_{i=0}^{\infty}\frac{(\Delta x)^i}{i!}f^{(i)}(x)$
$\int_a^b$

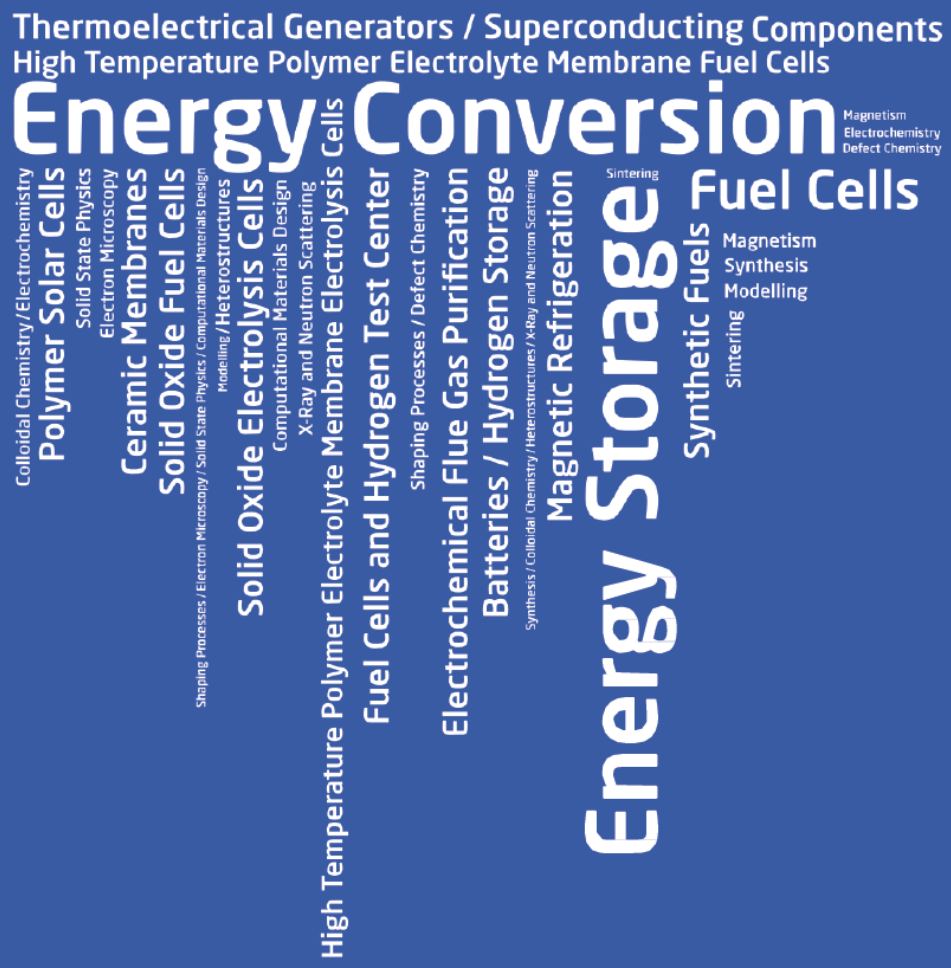

Department of Energy Conversion and Storage
Technical University of Denmark
Risø Campus
Frederiksborgvej 399
4000 Roskilde
Denmark
www.ecs.dtu.dk

ISBN 978-87-92986-60-3